

**IMPROVING THE PERFORMANCE OF
CAVITY-BACKED ANTENNAS
BY USING PASSIVE SCATTERERS**

THESIS

Joseph S. Zaren, Captain, USAF

AFIT/GE/ENG/94D-34

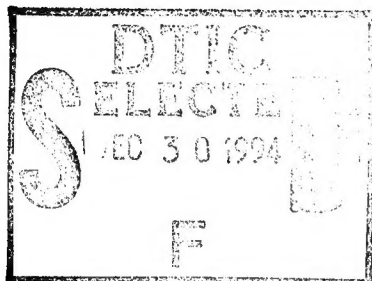
This document has been reviewed
for public release and its
distribution is unlimited.

**DEPARTMENT OF THE AIR FORCE
AIR UNIVERSITY
AIR FORCE INSTITUTE OF TECHNOLOGY**

Wright-Patterson Air Force Base, Ohio

19941228 110

AFIT/GE/ENG/94D-34



Accession For	
NTIS GRA&I	<input checked="" type="checkbox"/>
DTIC TAB	<input type="checkbox"/>
Unannounced	<input type="checkbox"/>
Justification	
By _____	
Distribution/	
Availability Codes	
Dist	Avail and/or Special
A-1	

**IMPROVING THE PERFORMANCE OF
CAVITY-BACKED ANTENNAS
BY USING PASSIVE SCATTERERS**

THESIS

Joseph S. Zaren, Captain, USAF

AFIT/GE/ENG/94D-34

THIS DOCUMENT IS UNCLASSIFIED

Approved for public release; distribution unlimited

"The views expressed in this thesis are those of the author and do not reflect the official policy or position of the Department of Defense or the U.S. Government."

**IMPROVING THE PERFORMANCE OF
CAVITY-BACKED ANTENNAS
BY USING PASSIVE SCATTERERS**

THESIS

**Presented to the Faculty of the School of Engineering
of the Air Force Institute of Technology
Air University
In Partial Fulfillment of the Requirements for the Degree of
Master of Science in Electrical Engineering**

**Joseph S. Zaren, B.S.
Captain, USAF**

December 1994

Preface

The purpose of this study was to explore the viability of improving the performance of cavity-backed antennas. Traditionally antenna cavities are filled with electromagnetic absorber to mitigate interference effects that would otherwise cause the antenna radiation pattern to vary widely at different frequencies. The approach used in this research was to replace the absorber with dielectric slabs, some of which contained arrays of dipoles. The results, based on radiation pattern cuts from seven cavity configurations integrated with a log periodic trapezoid wire antenna, were somewhat inconclusive. Additional research is recommended.

This thesis research was made even more rewarding because of the opportunity it provided to work with numerous individuals that were consistently helpful, patient, and supportive. I wish to express my sincere appreciation to two of these individuals, my sponsor, Dr. Stephen Schneider, and my advisor, Capt Paul Skinner. Their insight on different ways to approach parts of my research was invaluable. In addition, I also wish to thank Dr. Terzouli and Capt Joe Sacchini for serving on my Committee and providing helpful feedback throughout this effort. The assistance I recieved from Bob Lindsay was extremely helpful during the test phase. Finally, I wish to thank my wife for her understanding, support, and energetic assistance over the last few months.

Joseph S. Zaren

Table of Contents

	Page
Preface	ii
List of Figures	v
List of Tables	ix
Abstract	x
 I. Problem Definition	 1-1
1.1 Problem Definition	1-1
1.2 Justification of Research	1-1
 II. Literature Review.	 2-1
 III. Approach	 3-1
3.1 Modifications to and Dimensions of the Cavity	3-1
3.2 Definition of Frequency Selective Surfaces	3-4
3.3 Tools Used to Model the Cavity	3-5
3.4 Choice of Antennas to Use in Testing	3-7
3.5 Test Approach	3-7
 IV. Detailed Approach to Cavity Design	 4-1
4.1 Identification of Cavity Parameters	4-1
4.2 Modeling Capabilities of Design Tools & Their Associated Outputs	4-3
4.3 Fundamental FSS Behavior Relating to Design Process	4-5
4.4 Implications of Foster's Reactance Theorem for the Cavity Design	4-5
4.5 Design Insights Gained Using the First of Three Modeling Tools: PMM	4-5
4.6 Design Insights Gained Using the Second Tool: Transmission Line Code	4-8
4.7 Design Insights Gained Using the Third Tool: Hoser Code	4-10
 V. Antenna and Feed Design.	 5-1
 VI. Results and Analysis	 6-1
6.1 Absorber-Filled and Dielectric-Filled Cavity Designs	6-2
6.2 One Layer Design	6-4
6.3 Two Layer Design	6-5
6.3.1 The 6.2 & 3.1 GHz Design	6-5
6.3.2 The 6.2 & 2.7 GHz Design	6-6
6.3.3 The 6.2 & 3.7 GHz Design	6-7
6.4 Three Layer Design	6-8

	Page
VII. Conclusions and Recommendations	7-1
Appendix A: Determination of the Normalization Constant Used in Hoser Code	A-1
Appendix B: Source Code for Transmission Line Code	B-1
Appendix C: Equivalent Circuit Parameters Needed For Input to T-Line Code .	C-1
Appendix D: Different DX variations of Actual Fabricated Three Layer Design .	D-1
Appendix E: Antenna Data for Gain Calibration	E-1
Appendix F: Antenna Data for Absorber-Filled Cavity Design	F-1
Appendix G: Antenna Pattern Cuts for Dielectric-Filled Cavity Design . .	G-1
Appendix H: Antenna Pattern Cuts for One Layer Design	H-1
Appendix I: Antenna Pattern Cuts for 6.2 & 3.1 GHz Two Layer Design .	I-1
Appendix J: Antenna Pattern Cuts for 6.2 & 2.7 GHz Two Layer Design .	J-1
Appendix K: Antenna Pattern Cuts for 6.2 & 3.7 GHz Two Layer Design .	K-1
Appendix L: Antenna Pattern Cuts for 12.4, 7.4, & 3.1 GHz Three Layer Design	L-1
Bibliography	BIB-1
Vita	V-1

List of Figures

Figure	Page
Fig. 2-1 Archimedean spiral antenna	2-1
Fig. 2-2 Equiangular spiral antenna	2-1
Fig. 2-3 A cavity-backed Archimedean spiral antenna	2-2
Fig. 2-4 Square spiral	2-3
Fig. 2-5 Octagonal spiral	2-3
Fig. 2-6 Side view of spiral antenna	2-4
Fig. 2-7 Side view of two split tapered coaxial baluns	2-4
Fig. 3-1 Typical elements used in frequency selective surfaces	3-4
Fig. 4-1 Example of Hoser Code Output for One Array Case	4-17
Fig. 4-2(a & b) PMM Code Output For Baseline 6.2 GHz Design With $X = 0.25\lambda$	4-18
Fig. 4-3(a & b) PMM Code Output For 6.2 GHz Design With $X = 0.15\lambda$.	4-19
Fig. 4-4(a & b) PMM Code Output For 6.2 GHz Design With $X = 0.35\lambda$.	4-20
Fig. 4-5(a & b) PMM Code Output For 6.2 GHz Design With $DZ = 0.65\lambda$	4-21
Fig. 4-6(a & b) PMM Code Output For 6.2 GHz Design With $DZ = 0.75\lambda$	4-22
Fig. 4-7(a & b) PMM Code Output For 6.2 GHz Design With $L = 0.55\lambda$.	4-23
Fig. 4-8(a & b) PMM Code Output For 6.2 GHz Design With $L = 0.69\lambda$.	4-24
Fig. 4-9(a & b) PMM Code Output For 6.2 GHz Design With $W = 0.025\lambda$.	4-25
Fig. 4-10(a & b) PMM Code Output For 6.2 GHz Design With $W = 0.100\lambda$	4-26
Fig. 4-11(a & b) PMM Code Output For 6.2 GHz Design With $DY = 0.15\lambda$	4-27
Fig. 4-12(a & b) PMM Code Output For 6.2 GHz Design With $DY = 0.35\lambda$	4-28

Fig. 4-13(a & b) PMM Code Output For 6.2 GHz Design With Skewed Grid	4-29
Fig. 4-14(a & b) PMM Code Output For First Two Layer Design . . .	4-30
Fig. 4-15(a & b) PMM Code Output For Second Two Layer Design . . .	4-31
Fig. 4-16(a & b) PMM Code Output For Third Two Layer Design . . .	4-32
Fig. 4-17(a & b) PMM Code Outpt For Fourth Two Layer Design . . .	4-33
Fig. 4-18(a & b) PMM Code Output For Three Layer Design . . .	4-34
Fig. 4-19(a & b) PMM Code Output For Four Layer Design . . .	4-35
Fig. 4-20(a & b) Transmission Line Code Output For One Layer Design . . .	4-36
Fig. 4-21(a & b) Transmission Line Code Output For First Two Layer Design . . .	4-37
Fig. 4-22(a & b) Transmission Line Code Output For Second Two Layer Design . . .	4-38
Fig. 4-23(a & b) Transmission Line Code Output For Four Layer Design . . .	4-39
Fig. 4-24 Effect of Varying The X Parameter in Hoser Code For One Layer . . .	4-40
Fig. 4-25 Effect of Varying The DZ Parameter in Hoser Code For One Layer . . .	4-41
Fig. 4-26 Effect of Varying The L Parameter in The Hoser Code For One Layer . . .	4-42
Fig. 4-27 Effect of Varying The R Parameter in The Hoser Code For One Layer . . .	4-43
Fig. 4-28 Hoser Code Output For The Baseline One Layer Three Array Design . . .	4-44
Fig. 4-29 Effect of Adding More Arrays To The Baseline Design . . .	4-45
Fig. 4-30 Effect of Varying DY In The Baseline Design . . .	4-46
Fig. 4-31 Best Two Layer Design As Predicted By The Hoser Code . . .	4-47
Fig. 4-32 Hoser Code Output Associated With An Alternative Two Layer Design . . .	4-48
Fig. 4-33 (a,b,c,d,&e) The Five Scattering Layers Used In Testing . . .	4-49
Fig. 4-34 Hoser Code Output Associated With A Third Two Layer Design . . .	4-50

	Page
Fig. 4-35 Hoser Code Output Associated With The Best Three Layer Design .	4-51
Fig. 5-1 Log Periodic Antenna Designed for 2.3 - 16.0 GHz . . .	5-3
Fig. 6-1 VSWR vs. Frequency For Absorber-Filled Cavity . . .	6-10
Fig. 6-2 VSWR vs. Frequency For Dielectric-Filled Cavity . . .	6-11
Fig. 6-3 Time Domain Plot Containing Reflection Information For Dielectric-Filled Cavity	6-12
Fig. 6-4 Gain vs. Frequency For Absorber-Filled Cavity	6-13
Fig. 6-5 Gain vs. Frequency For Dielectric-Filled Cavity	6-14
Fig. 6-6 Beamwidth and Squint vs Frequency For Absorber-Filled Cavity .	6-15
Fig. 6-7 Beamwidth and Squint vs Frequency For Dielectric-Filled Cavity .	6-16
Fig. 6-8 Normal Incidence Gain vs. Frequency For 3.1 GHz Design .	6-17
Fig. 6-9 Peak Gain vs. Frequency For 3.1 GHz Design	6-18
Fig. 6-10 Beamwidth and Squint vs Frequency For 3.1 GHz Design .	6-19
Fig. 6-11 VSWR vs Frequency For 3.1 GHz Design	6-20
Fig. 6-12 Time Domain Plot Containing Reflection Information For 3.1 GHz Design	6-21
Fig. 6-13 Normal Incidence Gain vs. Frequency For 6.2 & 3.1 GHz Design .	6-22
Fig. 6-14 Peak Gain vs. Frequency For 6.2 & 3.1 GHz Design . . .	6-23
Fig. 6-15 Beamwidth and Squint vs. Frequency For 6.2 & 3.1 GHz Design .	6-24
Fig. 6-16 VSWR vs. Frequency for 6.2 & 3.1 GHz Design	6-25
Fig. 6-17 Normal Incidence Gain vs. Frequency For 6.2 & 2.7 GHz Design .	6-26
Fig. 6-18 Peak Gain vs. Frequency For 6.2 & 2.7 GHz Design . . .	6-27
Fig. 6-19 Hoser Code Output For 6.2 & 2.7 GHz Design	6-28

	Page
Fig. 6-20 Beamwidth & Squint vs. Frequency For 6.2 & 2.7 GHz Design .	6-29
Fig. 6-21 VSWR vs Frequency For 6.2 & 2.7 GHz Design . . .	6-30
Fig. 6-22 Time Domain Plot Containing Reflection Information For 6.2 & 2.7 GHz Design	6-31
Fig. 6-23 Normal Incidence Gain vs. Frequency For 6.2 & 3.7 GHz Design	6-32
Fig. 6-24 Peak Gain vs. Frequency For 6.2 & 3.7 GHz Design . . .	6-33
Fig. 6-25 Hoser Code Output For 6.2 & 3.7 GHz Design	6-34
Fig. 6-26 Beamwidth & Squint vs. Frequency For 6.2 & 3.7 GHz Design .	6-35
Fig. 6-27 VSWR vs. Frequency For 6.2 & 3.7 GHz Design	6-36
Fig. 6-28 Time Domain Plot Containing Reflection Information For 6.2 & 3.7 GHz Design	6-37
Fig. 6-29 Comparison of Normal Incidence Gains For Two Layer Designs .	6-38
Fig. 6-30 Comparison of Peak Gains For Two Layer Designs	6-39
Fig. 6-31 Hoser Code Output For Three Layer Design	6-40
Fig. 6-32 Normal Incidence Gain vs. Frequency For Three Layer Design .	6-41
Fig. 6-33 Peak Gain vs. Frequency For Three Layer Design	6-42
Fig. 6-34 Beamwidth & Squint vs. Frequency Using Three Layer Design .	6-43
Fig. 6-35 VSWR vs. Frequency For Three Layer Design	6-44

List of Tables

Table	Page
3.1 Identification of the Cavity's Layers and Its Electrical Length at each Frequency	3-3
4.1 Identification of Cavity Layers	4-1
4.2 Summary of Modeling Capability of Design Tools	4-2
4.3 Effect of Varying Dipole Length and Interelement Separation	4-5
4.4 Summary of Designs of Fabricated Cavity Layers	4-8
5.1 Summary of Log Periodic Trapezoid Wire Antenna Design	5-1

Abstract

The purpose of this study was to explore the viability of improving the performance of cavity-backed antennas. Traditionally antenna cavities are filled with electromagnetic absorber to mitigate interference effects that would otherwise cause the antenna radiation pattern to vary widely at different frequencies. The approach used in this research was to replace the absorber with dielectric slabs, some of which contained arrays of dipoles. These dipole arrays were modeled as frequency selective selective surfaces using two periodic moment method based computer programs and one transmission line program. A systematic study was performed that identified the effect of changing the dipole array parameters on prospective cavity designs.

Seven different cavity configurations were tested using a log periodic trapezoid wire antenna system designed to support 2.3 - 12.4 GHz. Cavity configurations using one, two, and three layers of dipole arrays were tested and compared to both absorber-filled and dielectric-filled cavity configurations. The results were inconclusive because even though some two layer designs and one three layer design had better gain almost entirely throughout the 2 - 12 GHz region, the gain of the baseline absorber-filled and dielectric-filled cavities varied widely over this bandwidth. No cavity configuration provided an extended 3 dB bandwidth. Additional research is recommended.

IMPROVING THE PERFORMANCE OF CAVITY-BACKED ANTENNAS BY USING PASSIVE SCATTERERS

1. Problem Definition

1.1 Problem Definition

The objective of this research is to improve the performance of broadband antennas that use an electromagnetic absorber-filled cavity to obtain a unidirectional radiation pattern. This pattern is perpendicular to the plane containing the radiating elements of the antenna. In addition, it exists on the free space side (non-cavity-backed side) of the antenna.

Examples of these types of antennas include the bowtie antenna, the spiral antenna, and many different log periodic types.

1.2 Justification for Research

Cavity-backed spiral antennas are used extensively in critical military communications systems. Most notably, they are used in aircraft, ship, and ground-based radar warning systems. They are also used in electronic warfare systems.

By designing a more sensitive spiral antenna, the range at which these systems operate would increase. For example, doubling the gain of the spiral antenna used in an aircraft's radar warning system would double the range at which enemy radar would be detected.

Realizing the implications for improved performance of mission essential military communication systems like radar warning ones, the Active Electromagnetic Countermeasures Branch of the Wright Laboratory Avionics Directorate at Wright - Patterson Air Force Base in Dayton, Ohio has sponsored this research.

This research into the use of passive scatterers to improve the performance of cavity-backed spiral antennas has potential application to the civilian sector as well. One example of such an application is their use in commercial interferometric direction finding systems. Since this research is in a dual-use technology area, an area in which the potential for applying technology extends into the commercial sector in addition to its use to satisfy a military objective, the potential civilian sector benefits offer additional justification for this research.

2. Literature Review

Four main assets of spiral antennas were noted by Laxtapi and Mittra in 1967 [12]. First, they provide good performance over a very broad frequency band (up to 20:1). Up until the development of the log periodic and spiral antennas in the late 1950s and early 1960s such broadband antenna performance was unobtainable. Second, they provide wide angular coverage, typically about a 75 degree -3 dB to -3 dB beamwidth. Third, multi-arm spirals, those with more than two arms, provide a direction finding capability. This capability exists because the spiral antenna's pattern switching property can be controlled by using different feeding techniques [14]. Fourth, they provide circular or elliptical polarization depending on the feed network. Knott *et al.* identified yet another positive attribute of spiral antennas -- that they can be made to conform to a surface [10]. For example, conformal spiral antennas can be mounted flush against an aircraft's fuselage, which has both aerodynamic and radar cross section reduction benefits.

There are two major categories of spiral antennas -- Archimedean and equiangular as shown below in Figures 2-1 and 2-2. Both consist of three components -- the spiral arms, the balun (feed), and the antenna backing, usually a cavity.

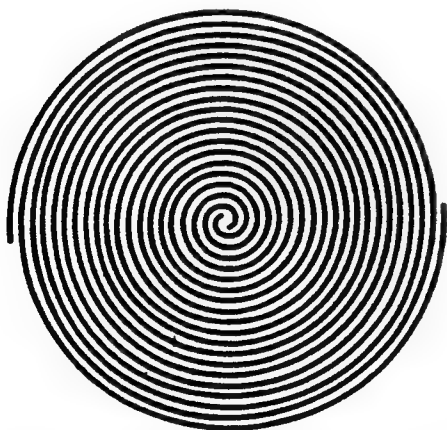


Figure 2-1 Archimedean spiral antenna [17]

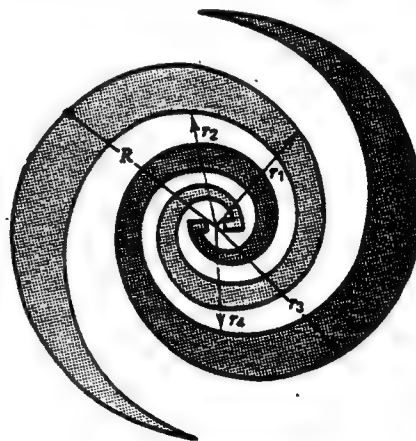


Figure 2-2 Equiangular spiral antenna [23]

Figure 2-3 shows how these three components are integrated into a functional Archimedean spiral antenna. The spiral arms of both categories of planar spiral antennas can be described geometrically. For one arm of an Archimedean spiral, described by Curtis in 1960 [2]:

$$r = c + a \cdot \phi \quad (1.1)$$

where

r = radial distance from the origin to any point on the spiral

c, a = constants

ϕ = polar angle in the plane of the spiral.

For the equiangular spiral, also known as the log periodic spiral, described by Dyson in 1959 [3]:

$$r = \exp[a \cdot \phi] \quad (1.2)$$

where

r = radial distance from origin to any point on the spiral

a = the constant angle formed between a tangent to the curve at any point and a line to the origin at that point

ϕ = polar angle in plane of the spiral.

From these two equations, it is important to note that the distance from the origin to any point on the spiral increases as the variables a and ϕ increase. These equations are consistent with Figures 2-1 and 2-2.

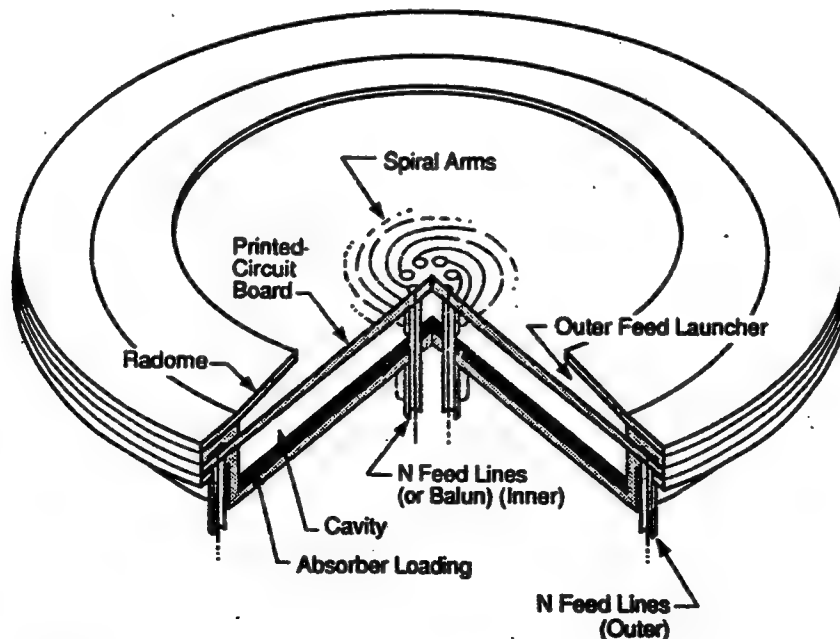


Figure 2-3 A cavity-backed Archimedean spiral antenna [10]. Note the spiral arms, balun, and cavity.

The effect of different spiral arm shaping has been studied extensively by Ransom [21], Nakano *et al.* [19], and Kraft [11]. In fact, as Figures 1-4 and 1-5 indicate, recent shapes included in the spiral antenna category may in fact be quite different geometrically, though analogous operationally, compared to the traditional Archimedean or equiangular designs. Most recently, Kraft in 1990 demonstrated that proper choice of the arm shape could improve the crosspolarization discrimination of the antenna by more than 15 dB when compared to a traditional Archimedean or equiangular designs. Though he achieved a significant improvement in crosspolarization discrimination, he did not identify any associated increase in the antenna gain.

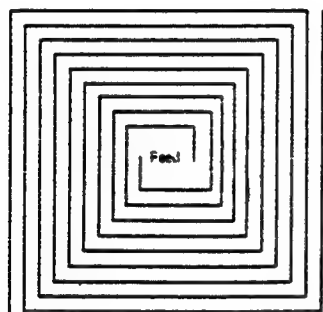


Figure 2-4 Square spiral [14]

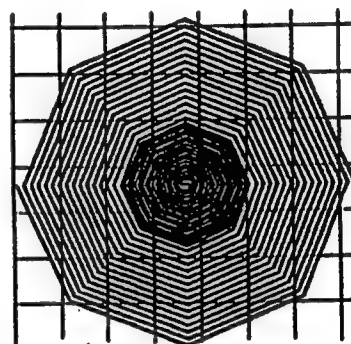


Figure 2-5 Octagonal spiral

[16]

As with the design of spiral arms, the design of the balun, which is the second component of the spiral antenna, has been researched more extensively than the design of the spiral's cavity. There are two types of broadband baluns [16]. The first type, the Marchand balun, is shown in Figure 1-6. In this case, a tapered twin line is used to feed the spiral antenna over frequency bands as large as 13:1. The second type, the taper balun shown in Figure 1-7, is simpler, more cost effective, and accommodates even larger bandwidths, up to 100:1, but can result in pattern squint of about 15 degrees.

This research seeks to improve cavity-backed antenna performance by redesigning the cavity. This implies that any further improvements in either spiral arm design or balun

design could be integrated with an improved cavity design to further optimize antenna performance.

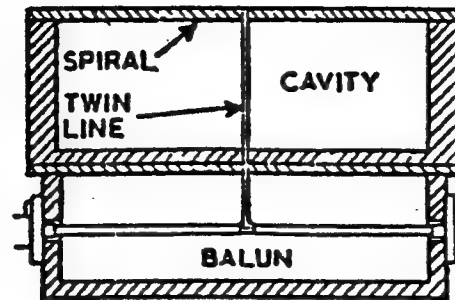


Figure 2-6 Side view of spiral antenna using a Marchand balun to couple energy from the source to the radiating arms of the antenna [16].

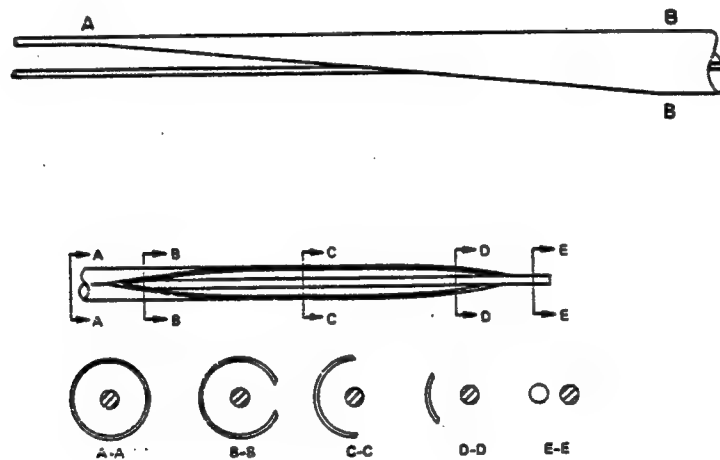


Figure 2-7 Side view of two split tapered coaxial baluns [22] [14].

Unlike the extensive research into arm shaping and, to a lesser extent, feed networks for spiral antennas, there has been very little research published relating to the cavity design. In reference to the planar spiral antenna, Morgan observed in 1987 that "the design of this type of antenna, and in particular its cavity, is left to empirical methods based on intuitive reasoning, generally followed by a number of iterations to achieve an acceptable performance" [15:7]. Nevertheless, four approaches for backing a spiral

antenna are described in published literature. Up until now, these approaches have led to either broadband low gain performance or narrowband medium gain performance. None offer the potential of broadband medium gain performance comparable to what might be possible by filling the cavity with the appropriate frequency selective surfaces. Without any backing, the spiral antenna would radiate in the two opposite directions that are perpendicular to the plane of the spiral. Therefore, to obtain the desired unidirectional beam, one of these four approaches is used:

1. leave cavity empty
2. fill cavity with absorber
3. load cavity with dielectric against the walls
in the form of a picture frame
4. use plane conductor rather than a cavity.

First consider the approach of leaving the cavity empty. When the cavity's depth is an odd multiple of a quarter wavelength, constructive interference will occur and result in increased gain. However, the consequence of this is the loss of the spiral antenna's broadband performance. This is due to the destructive interference that will occur when the cavity's depth is a multiple of a half wavelength. In 1963 Howell noted these "detrimental effects of the reflected wave when using cavities" [8:5].

Now consider the second approach of filling the cavity with a material that absorbs electromagnetic waves. This method reduces any interference-causing reflected waves because the waves radiated into the cavity are greatly attenuated by the lossy material in the cavity. This results in a more constant radiation pattern, though at a nominal gain that is at times less than, and at other times more than, that obtained with an empty cavity at selected frequencies [20].

Next consider the third approach of loading the cavity with a dielectric material against its walls in the form of a picture frame. Morgan used this approach to address the problem of absorbing low frequency reflections from the unloaded ends of spiral arms for a reduced aperture spiral antenna [16]. This approach is usually not applicable to normal

aperture spiral antennas with end loading since the reflected energy from the ends of the spiral arms is typically negligible.

Now consider the final approach of backing the spiral antenna with a tightly spaced conducting plane reflector. Most recently, Holzheimer and Hollaway in 1993 concluded "certain applications ... that allow for pattern degradation, gain variations, and varying axial ratio by providing low element profiles" can be appropriately addressed by adopting this backing approach [7:455]. Though they examined the performance over a 6:1 frequency range, they presented results only for one frequency near the center of the range. The authors provided insufficient data to allow the reviewer to assess actual performance towards the limits of the frequency range.

In addition, in 1986 Nakano *et al.* analyzed a truncated spiral with a conducting plane reflector one quarter of a wavelength behind the plane of the spiral [19]. They obtained a good gain, 8.5 dBi, but only over a very narrow 1.2:1 bandwidth. This gain was about 4.0 dB greater than that of a corresponding isolated spiral antenna, with no backing, radiating over the same frequency band. This improved performance at the cost of introducing resonant behavior is consistent with the physics of constructive and destructive wave interference.

This concept of interference forms the basis for the use of passive scatterers, modeled as frequency selective surfaces to potentially improve the performance of cavity-backed antennas. One of the main applications of frequency selective surfaces is their use in protective domes for antennas. Going one step further, Wheeler [24] patented an antenna system that uses frequency selective surfaces to create a reflector antenna with a construction that is substantially open to permit the passage of wind but closed to the passage of electromagnetic waves at selected frequencies. Furthermore, Munk [18] patented designs that use frequency selective surfaces to obtain either a high or low reflection coefficient over a narrow bandwidth substantially independent of angle of incidence of the incident wave. While both of these patents hint at the possibility of

designing an improved antenna cavity using frequency selective surfaces, no documented research exists yet that investigates this possibility.

3. Approach

This chapter will provide an overview of the approach used to try to improve the performance of cavity-backed antennas. It will be divided into five sections. First, the modification to the antenna's cavity, including the rationale used to determine the cavity's dimension, will be addressed. Second, frequency selective surfaces (FSSs) will be defined to lay the foundation for understanding the modeling techniques used. More detailed insight into the use of FSSs to reflect radiation at selected frequencies will occur in the next chapter. Third, the three tools used to model the cavity will be identified. Again, more in depth coverage of these tools and the results they predicted for different cases will occur in the next chapter. Fourth, the antenna used to test the scatterer-filled cavity will be described. The fifth and final section will outline the testing approach.

3.1 Modifications to and Dimensions of the Cavity

In this research, the approach used to try to improve the performance of absorber-filled cavity-backed broadband antennas was to modify their cavities. Recall that the traditional practice of filling a cavity with absorber is done to attenuate the energy radiated into the cavity so that neither destructive nor constructive interference from energy being reflected from the its bottom influences the radiation pattern on the free space side of the antenna. By using a different approach and not filling the cavity with absorber, one might be able to achieve a continuous state of constructive interference over a wide bandwidth at the plane containing the antenna.

To achieve this goal and hence realize the improved performance promised by radiating almost all the energy in the free space direction, one could place a perfect electric conductor (PEC) a constant electrical distance of $\lambda/4$ below the antenna's plane and adjusted its physical distance as the frequency changed. Under these conditions,

constructive interference would then occur because the round trip distance of $\lambda/2$ and the 180 degree phase shift caused by reflection from the PEC would combine to result in a phase shift of 360 degrees.

The approach explored in this report is analogous to the one described above. The main difference is the method used to obtain reflections -- the actual approach relied on scattering from arrays of dipoles that were fixed at specific distances from the antenna's plane rather than relying on reflections from a PEC that moved closer to and farther from the antenna's plane as the frequency increased or decreased.

The ideal design would contain an infinite number of infinitely thin slabs that each had such a sharp resonance that they would perfectly reflect the radiation from the antenna when their distance below the antenna's plane was $\lambda/4$, yet allow all radiation having a lower frequency to pass through the slab without any perturbation.

In contrast, the actual design consisted of 17 layers of dielectric slabs each having a relative dielectric constant of 2.5 and a thickness of 50 mils (1.27 mm). The slab parameters were chosen based on availability and cost. One of the advantages of using slabs of the same thickness was that they could easily be interchanged. This was conducive to easily exploring the effects of varying the distance from the antenna's plane to those slabs containing scatterers. Not every slab contained scatterers. The main reason for this was because of the difficulty in achieving a high Q for a single reflecting surface. Without this very sharp resonance, it was not possible to obtain a quick roll off of the reflection coefficient to allow for electromagnetic waves having a slightly lower frequency to penetrate the slab and get reflected at the $\lambda/4$ distance needed to obtain constructive interference. The second reason each slab did not contain scatterers was that the model used to optimize the design could not model this case.

As indicated in Table 3.1, these 17 layers provided the potential for perfect reflection for discrete frequencies ranging from 2.2 to 12.4 GHz. This table also identifies

the electrical length of the 2.5 inch long by 2.5 inch wide cavity. The electrical length was based on the relative dielectric constant being 2.5 and the use of equation 3.1.

The frequency corresponding to a $\lambda/4$ distance from the plane of the antenna for each 1.27 mm thick slab was obtained by using the following equation:

$$f = c/(\lambda \cdot \sqrt{e_r}) \quad (3.1)$$

f = frequency

c = speed of light

$e_r = 2.5$ = dielectric constant of slabs

λ = wavelength = $4 \cdot$ distance from the slab to the antenna's plane

The cavity, which did not contain any backing, was 2 inches deep, which equates to $\lambda/4$ at 1.48 GHz in air and 0.93 GHz when e_r equals 2.5. These cavity dimensions were chosen to house an antenna that would support frequencies as low as 2.25 GHz. The cavity was placed at the center of an 18 inch by 18 inch groundplane. Both the groundplane and cavity were metal.

Table 3.1
Identification of the Cavity's Layers
and Its Electrical Length at each Frequency

Freq GHz	λ in $E_r=2.5$ cm	$\lambda/4$ distance cm	2.5" Electrical Length λ
12.45	1.525	0.38125	4.16
9.34	2.031	0.50775	3.13
7.47	2.540	0.63500	2.50
6.22	3.050	0.7625	2.08
5.33	3.560	0.8900	1.78
4.67	4.063	1.01575	1.56
4.14	4.583	1.14575	1.39
3.73	5.087	1.27175	1.25
3.39	5.597	1.39925	1.13
3.11	6.101	1.52525	1.04
2.87	6.611	1.65275	0.96
2.667	7.114	1.7785	0.89
2.49	7.620	1.9050	0.83
2.33	8.143	2.03575	0.78

3.2 Definition of Frequency Selective Surfaces

The layers of scatterers that replaced the traditional absorber in the antenna's cavity can, to a certain degree, be modeled as layers of frequency selective surfaces (FSSs). These surfaces can be used to obtain high levels of reflection at their resonant frequency while permitting transmission of other frequencies. They are analogous to filters in communication theory.

Physically, FSSs are arrays of elements arranged periodically such that the dimensions of one element and its location referenced to its neighboring elements on the Y axis and Z axis are all that are needed to describe the surface when it lies in the Y-Z plane. The elements can vary from simple dipoles to any complex arbitrary shape. Examples of the more commonly used elements are shown in Figure 3-1. Only one type of element was used in this research -- unloaded dipoles. Though this precluded the design of cavities for circularly polarized antennas, it still allowed for good proof of concept research aimed at improving the performance of linearly polarized cavity-backed antennas. In addition, it was consistent with the modeling constraints imposed by the final tool used to optimize the design, the Hoser code.

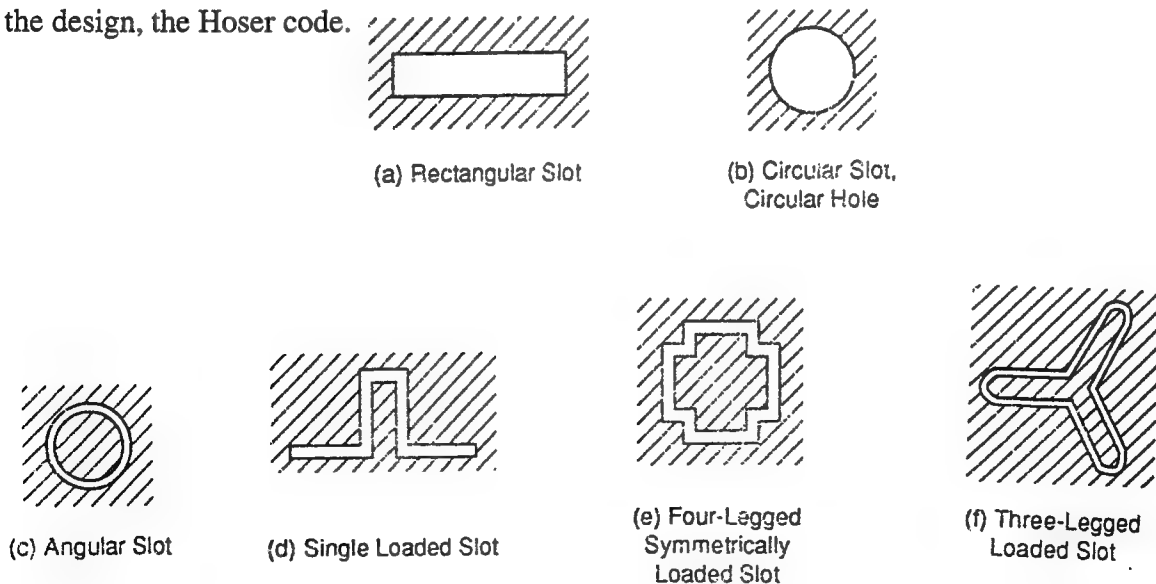


Figure 3-1 Typical elements used in frequency selective surfaces [10].

Computer models which exist for FSS analysis fall within one of three categories. These first two categories are the infinite by infinite case and the finite by infinite case. Consider a FSS in the Y-Z plane. In the first case, the reference element repeats itself forever in the z direction with each element separated by a constant distance, dz . In addition, there are an infinite number of these arrays of periodic z -directed elements each at a constant separation distance, dy , from each other. By comparison, in the finite by infinite case, there are only a finite number of z -directed arrays that contain an infinite number of elements separated by dz . The logical extension of this, and the only physically realizable case of course, is when the number of z -directed arrays is finite and the number of elements in each of these arrays is finite.

3.3 Computer Codes Used to Model the Cavity

Three computer codes were used to model the scatterer-filled cavity. The first two codes assumed the cavity's dielectric slabs that contained scatterers would be modeled by the infinite by infinite case. These codes were used to gain a better understanding of the behavior of single and multiple layer FSS cavity designs as certain parameters were modified.

To benefit from using FSS analysis methods, the layers of scatterers within the cavity were modeled as distinct FSSs. One may question the validity of doing so based on the dimensions of the cavity and corresponding electrical lengths identified in Table 3.1, but given the computer resources necessary to analyze these as layers of scatterers via the brute force finite element method, this approach seemed quite logical.

The periodic moment method was used to analyze the cavity layers that were treated as FSSs. The method is based on a plane wave expansion theory that allows each infinite array of scatterers to be represented as one element -- the reference element. As the name implies, this method is a special application of the moment method that relies on Floquet's Theorem to define periodic basis functions. The end result is a double

summation which requires careful determination of mode structure to lead to efficient convergence.

The Ohio State University's (OSU's) PMM code [6] was the first of three codes used to model the cavity layers. This robust code was used because it analyzed infinite by infinite arrays and because it was readily available. It was used to gain insight into fundamental FSS design concepts that will be identified in the next chapter.

The second code modeled the slabs as infinite by infinite FSS arrays which were represented as series LC circuits (lumped elements) that shunted a transmission line at distances from its port that corresponded to the array's distance from the plane of the antenna. Though the OSU PMM code provided the capability to model an FSS using transmission line techniques, the self-developed code listed in Appendix B was used. This code is based on the theory of small reflections. It was used for two reasons. First, it provided accurate results much more quickly than by using the rigorous periodic moment method approach of the OSU PMM code. Second, it modeled stacks of FSS layers that were located anywhere within the cavity. This overcame the OSU PMM code's restriction that the dz term remain constant.

This transmission line approach is based on the theory that a single infinite by infinite FSS array can be modeled by a lossless impedance -- one having a purely reactive component (that is capacitive below resonance and inductive above it) -- shunted across a transmission line. The equivalent impedance consists of a lumped capacitance and inductance and can be obtained by using the rigorous OSU PMM code. For example, the equivalent transmission line representation of two infinite by infinite FSSs separated by a distance " d " consists of the reactance associated with the first FSS shunted across a transmission line followed a distance " d " later by the reactance associated with the second FSS shunted across this transmission line.

Unlike the first two codes that could not model finite by infinite FSS arrays, the third code used to analyze the cavity, known as the Hoser code [9], relied on PMM theory

to do just that -- model a finite number of infinitely long dipole arrays. This code was used because it more accurately represented the 2.5 square inch slabs and because of its availability. Like the OSU PMM code, it placed a restriction, though less of one, on the dz parameter. It required all the dz terms, which represented the distance between elements in one array, to be multiples of each other. This made the code most suitable to modeling FSS layers that resonated at frequencies which were multiples of each other.

With all three codes, the approach used to optimize potential cavity designs remained the same -- to identify the relevant parameters and determine methods to tailor them in order to control the phase at the antenna's plane. A more detailed review of the design process to include the effects of parameter changes will occur in the next chapter.

3.4 Choice of Antenna to Use in Testing

Initially this research focused on improving the performance of cavity-backed spiral antennas. These types of antennas produce circularly polarized waves which would require using FSS layers of loaded crossed dipoles. These elements could not be modeled by the Hoser code. For that reason and because the concept of using arrays of scatterers could still be explored using simple dipoles, an antenna that produced linearly polarized waves was chosen for testing purposes. The design of this antenna, a log periodic trapezoid wire antenna, will be discussed in more detail in Chapter 5.

3.5 Test Approach

This section will identify what data was collected and why, the dimensions and location of the test chamber, and will conclude with a list of the equipment used and its configuration and calibration.

The objective of the testing was to obtain radiation patterns and VSWR plots for different cavity configurations at various frequencies. These objectives were met by using the same feed, antenna, mounting structure, and test facility for each measurement so that

valid comparisons of results were possible. Results from each cavity design were compared to two baseline cases. The first baseline design consisted of filling the cavity with standard AN-75 absorber whereas the second design used 17 blank dielectric slabs. The absorber-filled cavity contained 2 inches of absorber sandwiched between the antenna and one dielectric slab containing copper tape on its outside surface. Copper tape was placed on the outside surface, the one visible from the rear of the cavity, of the deepest dielectric slab in every design. This was done to prevent radiation from passing beyond that point and interfering with the measurements.

The first of the two types of data collected for each cavity design, the Voltage Standing Wave Ratio (VSWR), was measured using an HP8720 Network Analyzer. This was done to obtain insight into how much energy was actually reaching the antenna. Additional insight into where reflections occurred in the process of coupling this energy from the source to the antenna was obtained by using the HP8720 to transform the data from the frequency to the time domain. This VSWR data was important because the bandwidth over which an antenna maintains a VSWR below two, the 2:1 VSWR bandwidth, is a standard criteria used to judge antenna performance.

The second category of collected data was a set of radiation pattern cuts at selected frequencies. This data was essential to collect and analyze because it provided insight into the antenna gain at different frequencies and at different angles. From this data one can determine the -3 dB to -3 dB beamwidth at a given frequency and, with a collection of these pattern cuts at different frequencies, one can determine the bandwidth over which acceptable gain is achieved for a desired antenna orientation.

All testing occurred at the AFIT Anechoic Chamber, which was approximately 8.3 feet wide, 7.9 feet high, and 12 feet deep and covered with both 17 inch pyramidal absorber and wedge absorber. It was open on one end. The transmitting horn antenna used to measure the test antenna was located approximately 3 feet from this open end. The antenna pedestal upon which the antenna was mounted was located approximately 3.2

feet from the rear of the chamber. This made the distance from the test pedestal to the transmitting antenna about 12 feet, which made this a far field calculation. The antenna was mounted on a the pedestal so that its height from the base of the chamber to its center point was 43 inches compared to a height of 38 inches for the transmitting horn antenna.

As mentioned previously, the HP8720 Network Analyzer and an associated calibration kit along with the appropriate cables and a printer were all that was needed to take frequency and time domain reflection data such as VSWR.

To obtain radiation pattern cuts the following equipment was used:

1. Hewlett-Packard (HP) 8349B Microwave Amplifier
2. HP9000 236 Computer with associated antenna measurement support software
3. Model 855C Newport (pedestal) Controller
4. HP8510B Network Analyzer
5. HP8515 Test Set
6. HP7470 Plotter
7. American Electronics Laboratories (AEL)Horn Antenna
8. Peripheral Cables

Essentially the HP9000 computer controlled the other equipment so that the user could follow a menu driven program to obtain the radiation patterns at frequencies between 2 and 20 GHz.

As seen from the radiation pattern cuts in the later Appendices, the scale listed on the radiation patterns using this configuration is in dB, not dBi. To convert them to meaningful values, it was necessary to take calibration measurements using an antenna with known gain characteristics as a function of frequency. This was done using an AEL Model H-1498 Horn Antenna. With the absolute gain value now known for a frequency, meaningful dBi values could be obtained by adding the appropriate calibration factor to the measured data. These calibration factors for frequencies used in this research are included in Appendix E.

4. Detailed Approach to Cavity Design

This chapter complements Section 1 of Chapter 3 by providing detailed information relating to the design of the scatterer-filled cavity. The purpose of this chapter is to:

- a. identify the parameters involved in the cavity design
- b. identify which of these are variables in each of the design tools
- c. identify basic FSS behavior and use the design tools to verify these concepts
- d. identify Foster's Reactance Theorem and show that it implies it is impossible to achieve the desired phase response when using one or more infinite by infinite FSSs
- e. identify the effect of different parameters using the different codes
- f. identify and provide rationale for the choice of parameters used in the fabricated designs.

4.1 Identification of Cavity Parameters

The parameters associated with the cavity design fall into three major categories -- the locations of the slabs, the dielectric constants of the slabs, and the layout of the scatterers, if any, on each slab.

The slabs were stacked on top of each other within the cavity so their 1.27 mm thickness determined their locations. Recall the design frequencies for the FSSs on each slab was therefore based on the multiples of 1.27 mm equating to the distance of $\lambda/4$ below the plane of the antenna. This uniform thickness allowed for easy exploration of design variations by interchanging the slabs. As indicated in Table 4.1 this thickness allowed the use of up to 10 layers of scatterers to try to obtain good phase performance over the 3-13 GHz range. Note as well that by using slabs of uniform thickness, fabrication of these slabs was simplified.

Table 4.1
Identification of Cavity Layers

Layer	Distance from the Plane of the Antenna	Freq of $\lambda/4$ Depth
	<i>cm</i>	<i>GHz</i>
1	.127	37.35
2	.254	18.67
3	.381	12.45
4	.508	9.34
5	.635	7.47
6	.762	6.22
7	.889	5.33
8	1.016	4.67
9	1.143	4.14
10	1.270	3.73
11	1.397	3.39
12	1.524	3.11
13	1.651	2.87
14	1.778	2.67
15	1.905	2.49
16	2.032	2.33
17	2.159	2.19

The slabs were made by Taconic Plastics in Petersburg, New York. The slab material, known as TLX, had a dielectric constant of 2.51 and a loss tangent of 0.0017. Had these dielectric constants not been uniform, the reflections due to impedance mismatches would have resulted in degraded performance. Though a larger dielectric constant would have increased the electrical length of the cavity and hence improved the validity of the modeling techniques used, 2.5 was chosen because this value is typically used as a substrate upon which elements are etched.

To simplify the description of the variables associated with the layout of the scatterers on the slabs, consider the case of a dielectric slab in the Y-Z plane that contains only one z-directed dipole array. To completely describe it, one would first specify the element geometry. This could be a simple dipole as used in this research or any arbitrarily

shaped design. Second, one would specify the separation distance, dz , between the centers of adjacent elements parallel to the z axis. Third, one would identify the origin in the Y - Z plane and identify the y and z distances from the origin to the center of the closest element.

By introducing multiple z -directed arrays, one must identify their uniform separation distance from adjacent z -directed arrays, dy , and also identify if the arrays are skewed (reference Figure 4-13(a) for an example of a skewed geometry).

4.2 Modeling Capabilities of Design Tools & Their Associated Outputs

Recall from Chapter 3 Section 3, that three codes were used to model the slabs as frequency selective surfaces. Both the OSU PMM code and transmission line code modeled the geometry of a YZ plane having along the y axis an infinite number of infinitely long z -directed elements. The Hoser code allowed the number of infinitely long z -directed elements to be finite.

Table 4.2 on the next page identifies the capability of each of these codes to model the cavity using the parameters discussed in section 4.1.

Table 4.2

Summary of Modeling Capability of Design Tools

<u>PARAMETER</u>	<u>OSU PMM</u>	<u>T-Line</u>	<u>Hoser Code</u>
Slab Location	IC1	Y	IC1
Dielectric const	Y	Y	EM
Element geometry	Y	Y	R1
Element dz	Y1	Y	Y2
Array dy	Y	Y	Y
Skewed arrays	Y	Y	Y
Finite number of z-directed infinitely long arrays	N	N	Y

Y = can fully model			
IC1 = is indirectly constrained by dz			
EM = requires easy modification to source code			
R1 = models loaded and unloaded dipole arrays			
Y1 = dz must remain constant for multiple layers			
Y2 = dz s must be multiples of each other for multiple layers			
N = can not model			

The value of the lumped capacitances and inductances needed as inputs to the transmission line code are obtained by using the rigorous OSU PMM code for single layer FSS geometries.

Both the OSU PMM code and the transmission line code provide the magnitude and phase of the reflection coefficient as their output. For the finite by infinite case, the Hoser code provides the real and imaginary components of the backscattered field normalized by the maximum backscattered field associated with a single infinite array of always resonant dipoles located at the phase reference point.

This output from the Hoser code does not trace directly to the magnitude and phase of the reflection coefficient. The detailed derivation of this constant is included as Appendix A. A qualitative overview of the derivation follows. It begins with the equation of the electric field scattered from an infinite line array of z -directed dipoles written in terms of the incident field and the array's self impedance. Then, imposing the constraint that forbids grating lobes, and by relating Hankel functions that have an imaginary argument to the modified Bessel function of the second kind, the self impedance is rewritten in terms of its real and imaginary components. At this point, one can revisit the equation for the scattered electric field from the array and, assuming the dipoles are resonant, obtain an expression for the scattered electric field that is independent of its self impedance but dependent on the incident field and a Hankel function having the wavenumber and ρ in its argument. The normalization constant is then realized by considering the large argument form of the Hankel function.

Reference Figure 4-1 (all figures are listed at the end of this chapter -- starting on page 4-16) for an example of the output for the Hoser code for the basic case of one infinite string of dipoles. The important concept is that a positive real component of the normalized electric field implies the existence of a backscattered field. When a backscattered field does occur, it is desirable to obtain as constant a phase response as possible. This implies the points on the real-imaginary plane corresponding to different frequencies should be as close to each other as possible. In the case of Figure 4-1 the Hoser code predicts the resonant frequency of this one infinite z -directed array is 9.0 GHz. This assumes the array is in free space. After dividing this by the square root of the dielectric constant to account for the fact the this array is not in free space, the code predicts a resonance at 5.7 GHz, only 0.5 GHz below what PMM predicts based on the case of using an infinite number of these same z -directed arrays separated by $\lambda/4$ along the y axis in the Y - Z plane.

4.3 Fundamental FSS Behavior Relating to Design Process

Ideally each layer in the cavity would have a very narrow resonance at its design frequency. Earlier research conducted at OSU showed that increasing dy , the distance between the infinite arrays of z -directed elements, narrows the resonant bandwidth. Given the 2.5 inch diameter of the cavity, wider separation of arrays could lead to less total number of z -directed arrays.

4.4 Implications of Foster's Reactance Theorem for the Cavity Design

Foster's Reactance Theorem states the slope of the reactance or susceptance for a loss-free one port network is always positive [4]. One important consequence of this is that all poles and zeros of the reactance or susceptance function for a loss free one port network are simple. Furthermore, these poles and zeros must alternate as the frequency is increased or decreased [5]. Therefore, for the case of an arbitrary number of lossless infinite by infinite arrays of elements excited by plane waves of varying frequencies, it is impossible to achieve a constant phase response. Though this does not bode well for the design of a cavity that can offer broadband performance, one must remember that the actual design is based on a finite 2.5 square inch cavity dimension and the elements do contain some loss.

4.5 Design Insights Gained Using the First of Three Modeling Tools: OSU PMM

A systematic approach using each of the three tools was used to identify the effect of changing the different parameters identified in section 4.1. Starting with the OSU

PMM code, these effects will be explored by beginning with the simplest case of one infinite by infinite array and then progressing to designs using up to four layers.

For this basic one array case the baseline output is shown in Figure 4-2(a&b). Note the geometry is described pictorially in part (a) of this figure. The design uses a nonskewed grid layout, a relative dielectric constant of 2.5 everywhere, a phase reference point at the plane of the antenna and, as with all the PMM runs, three modes per element. The design has the following geometry:

distance from antenna's plane = 0.76 cm (0.25λ at 12.4 GHz for $\epsilon_r=2.5$)

$dz =$ 2.14 cm (0.70λ)

dipole length = 1.89 cm (0.62λ)

dipole radius = 1.53 cm (0.05λ)

Distance from phase reference point, which is the plane of the antenna; x :

Figure 4-3(a&b) demonstrates $x = 0.15\lambda$

Figure 4-4(a&b) demonstrates $x = 0.35\lambda$

Interelement Separation; dz :

Figure 4-5(a&b) demonstrates $dz = 0.65\lambda$

Figure 4-6(a&b) demonstrates $dz = 0.75\lambda$

Dipole Length; L :

Figure 4-7(a&b) demonstrates $L = 0.55\lambda$

Figure 4-8(a&b) demonstrates $L = 0.69\lambda$

Dipole Width; w :

Figure 4-9(a&b) demonstrates $w = 0.025\lambda$

Figure 4-10(a&b) demonstrates $w = 0.100\lambda$

Array Separation; dy :

Figure 4-11(a&b) demonstrates $dy = 0.15\lambda$

Figure 4-12(a&b) demonstrates $dy = 0.35\lambda$

Grid:

Figure 4-13 demonstrates skewed grid version of baseline design

By analyzing the magnitude plots as each of the parameters is changed, one may conclude that, for a given single layer FSS geometry, one may sharpen the resonance by taking the following steps: increasing dz (until it is on the order of one wavelength), keeping L near its $\lambda/2$ value, decreasing the dipole's width, or by increasing dy .

The effect of varying the five parameters on the phase of the reflection coefficient is of primary concern for this research. As expected from Foster's Reactance Theorem, the slope of the reflection coefficient's phase remains negative in each case.

Before addressing the case of the two layer design, note the results of Table 4.3 which identifies the effect of varying the dipole length and the interelement separation, dz , for the layer corresponding to 2.38 GHz. Observe that grating lobes become a problem when the dz parameter exceeds a value equal to one wavelength since they occur at or below the designed resonant frequency.

Table 4.3

EFFECT OF VARYING DIPOLE LENGTH AND INTERELEMENT SEPARATION

Dipole Length in terms of λ	dz in λ	Resonant Freq in GHz	First Appearance of Grating Lobe in GHz
.65	1.0	2.29	2.4
	0.7	2.38	3.5
.62	1.24	2.19	2.0
	1.1	2.24	2.2
	1.0	2.35	2.4
	0.9	2.43	2.7
	0.8	2.49	3.1
	0.7	2.49	3.5
	1.1	2.43	2.2
.55	1.0	2.46	2.4
	0.9	2.60	2.7
	0.8	2.69	3.1
	0.7	2.74	3.5
	0.6	2.71	4.1
	1.5	2.81	1.6
	1.0	2.63	2.4
.50	0.9	2.72	2.7
	0.8	2.85	3.1
	0.7	2.93	3.5
	0.6	2.96	4.1
	0.55	2.92	4.5
	0.8	3.01	3.1
	0.7	3.14	3.5
.45	0.6	3.21	4.1
	0.5	3.17	4.9
.38	1.0	3.49	2.4
	0.7	3.46	3.5
	0.6	3.61	4.1
	0.5	3.68	4.9
	0.4	3.50	6.2

Now consider the case of using two layers of infinite by infinite arrays. Four different designs were explored. The constraint that the interelement distance dz remain constant implied that this parameter was equal to a value dictated by the lowest frequency array. Another implication of this dz constraint was that grating lobes were likely to arise since these appear when dz is on the order of one wavelength. These grating lobes are indicated by the T1 annotation in Figures 4-14 through 4-19. As expected from the insight provided by Foster's Reactance theorem, the phase performance of these designs is just terrible. Note that as additional layers are added, another pole and zero are introduced with the expected results indicated in the following figures.

	Fig.(14(a&b))	Fig.(15(a&b))	Fig.(16(a&b))	Fig.(17(a&b))
Top Layer				
x	0.38 cm	0.38	0.38	0.51
dz	1.42 cm	1.78	2.14	2.14
L	0.85 cm	0.82	0.75	1.01
w	0.076 cm	0.076	0.076	0.076
dy	0.38 cm	0.38	0.38	0.51
<hr/>				
Bottom Layer				
x	0.51	0.64	0.76	0.76
dz	1.42	1.78	2.14	2.14
L	1.26	1.57	1.89	1.81
w	0.102	0.127	0.153	0.153
dy	0.51	0.64	0.76	0.76
<hr/>				

Again, for the three and four layer designs in Figures 4-18(a&b) and 4-19(a&b), note the implications of Foster's Reactance Theorem -- that there are phase reversals between the zeros that correspond to the design frequencies.

4.6 Design Insights Gained Using the Second Tool: Transmission Line Code

Recall from Chapter 3 Section 3, this code relies on the equivalent circuit LC parameters obtained from the OSU PMM code (when it is run to model a single infinite by infinite case) to model both single and multiple arrays. A copy of the source code listing is included in Appendix B. It is based on the theory of small reflections as described by E.F. Knott [10]. Though it still only modeled the case of infinite by infinite arrays as did the OSU PMM code, it added value to the design process for two reasons. First, without the OSU PMM code's constraint that dz remain constant, one could model more realistic multilayer cavity designs. Second, the run time was dramatically reduced. For example, a three layer design run in PMM ranging over 80 different frequency points required about 30 minutes on a 486DX2 66MHz computer with 8 Meg of RAM whereas this transmission line code took less than a minute.

First consider the basic one layer infinite by infinite case examined in the previous OSU PMM section. Based on obtaining the values of $L=3188$ pH, $C1=.205$ pF, and $C2=.01076$ pF from PMM, note how well Figure 4-20(a&b), which is based on this transmission line model, compares to the OSU PMM output in Figure 4-2(a&b).

Next consider two different two layer cases. The first one in Figure 4-21(a&b) corresponds to the layers modeled by the OSU PMM code in Figure 4-16(a&b). Note that the comparisons are good up until the grating lobes appear. The second two layer case shown in Figure 4-22(a&b) is designed for the same frequencies but uses a smaller more realistic value of dz for the top layer to emphasize the fact that in this code the interelement separations can indeed be different for each layer. Comparing these two designs, one can see that the magnitude of the reflection coefficient is almost 0 dB at the design frequencies. However, in both designs, the phase plots imply poor performance at the antenna's plane, which is the phase reference point.

Now consider a four layer case. Figure 4-23(a&b) corresponds to the design modeled by the OSU PMM code in Figure 4-19(a&b). In this case, the agreement of the magnitude performance is poor even at frequencies below which grating lobes occur. Also note the effect of Foster's Reactance Theorem can be seen by the phase reversals at about 8.3 GHz and 11 GHz, which is between the zeros at the design frequencies of 12.4, 9.3 and 7.4 GHz.

Numerous other runs were made using this transmission line code to achieve as constant a phase response as possible. Appendix C contains a listing of the values the OSU PMM code provided for the equivalent circuits associated with many different single layer designs.

4.7 Design Insights Gained Using the Third Tool: Hoser Code

Being able to consider a finite number of z-directed dipole arrays with this code provided much more realistic modeling capability compared to the previous two codes that modeled doubly infinite periodic cases..

Much of the emphasis in terms of identifying a promising design was placed on exploring two layer designs using the 12.4 and 6.2 GHz layers. There were two reasons for this. First, considering the electrical length of the cavity, results at the higher frequencies were more consistent with the infinite array assumption inherent in the Hoser code when compared to other lower frequency designs. Recall the dz restriction in this code, that they must be multiples of each other, meant that the 12.4 and 6.2 layer design was the best two layer design available when using electrical length as the criteria. Second, after obtaining a promising design using these two frequencies, it would be advantageous to explore inserting a third layer designed for resonance at 3.1 GHz. The potential third layer for designs other than those starting with the 12.4 GHz or 9.3 GHz layer required

the third layer to resonate at a frequency that would exceed the 2.3 GHz lower limit of the antenna's capabilities.

Examples of outputs from this code will be reviewed as follows. First, these examples will provide insight into the effect of changing the parameters for the two different one layer cases below. After this, the best two layer designs will be identified. Following this, the actual layer designs that were fabricated will be identified. In addition, their predicted performance (using the Hoser code) when combined in different ways will be identified.

First, consider the one layer case below. Note that the frequencies range from 2 to 23 GHz. This is because the Hoser code assumed the relative dielectric constant was unity. By dividing the frequency on the output plots by 1.58, the square root of the dielectric constant used, one can convert these frequencies to their true value in the cavity.

One layer case with one array:

<i>Distance from phase reference point;</i>	Figure 4-24
<i>Interelement Separation, dz;</i>	Figure 4-25
<i>Dipole length;</i>	Figure 4-26
<i>Dipole radius;</i>	Figure 4-27

One layer case with more than one array:

<i>Baseline design;</i>	Figure 4-28
<i>Number of z directed Arrays;</i>	Figure 4-29
<i>Array Separation, dy;</i>	Figure 4-30

One can draw the following conclusions from Figures 4-24 through 4-27 for the one layer case with one array. First, from Figure 4-24 one observes that a slight counterclockwise rotation of the plot can be realized by increasing the distance from the phase reference point. This is in agreement with the concept that a layer containing scatterers will provide constructive interference at the antenna's plane when the layer's

depth equates to $\lambda/4$. From Figure 4-25 one observes the resonant frequency can be decreased slightly by decreasing the interelement spacing. As expected, Figure 4-26 shows that a dipole of length 0.55λ resonates at a lower frequency than a shorter dipole of length 0.45λ . From Figure 4-27 one observes that the dipole radius has very little effect on the resonance of the array; there is just a slight increase in resonant frequency as the radius decreases.

One can draw the following conclusions from Figures 4-28 through 4-30 for the one layer case with more than one dipole array. First, from Figure 4-29 one observes that increasing the number of z-directed arrays does not significantly change the shape of the curve but does scale it in proportion to the number of arrays used. Second, from Figure 4-30 one observes that increasing the separation between adjacent z-directed arrays again does not significantly change the shape of the curve but instead has the effect of scaling it, increasing the curve as dy increases. This is consistent with what was observed with the OSU PMM code -- that increasing dy sharpens the resonance.

The two designs that looked most promising after exploring numerous two layer possibilities are included in Figure 4-31 and Figure 4-32. The first figure outlines a design using scatterers on the layers corresponding to the 6.2 and 3.1 GHz layers of the cavity. Note how the frequencies are grouped together between 8-14 GHz, which scales to 5-9 GHz after dividing by the 1.58 dielectric normalization factor. In addition, frequencies from about 7-17 GHz unscaled, 4.4-10.8 GHz scaled, exhibit a positive real component of the normalized backscattered field. The second figure outlines a design using scatterers on the layers corresponding to 12.4 and 6.2 GHz. The frequencies containing a positive real component of the backscattered normalized field range between 7-15.5 GHz unscaled, 4.4-9.8 GHz scaled, with a small loop occurring between 11-14 GHz unscaled, 7-8.9 GHz scaled. The parameters associated with these two designs are listed in Table 4.4 which

describes the fabricated designs of all the cavity layers that contain scatterers. These five layers are pictured in Figure 4-33.

Table 4.4
SUMMARY OF DESIGNS OF FABRICATED CAVITY LAYERS

Design Freq GHz	# of Arrays	# Dipoles per Array	Dipole Radius cm	Dipole Length cm	DZ cm	Locations of z-directed Arrays on y axis cm
12.4	1	7	.066	.0764	0.844	0
6.2	2	4	.100	1.515	1.590	± 0.46
6.2	5	3	.066	1.515	1.590	0, ± 0.76 , ± 1.52
3.1	5	2	.100	2.870	3.035	0, ± 0.76 , ± 1.52
3.1	7	2	.100	2.870	3.035	0, ± 0.76 , ± 1.52 , ± 2.28

Included in Figure 4-34 is the output associated with the a 12.4 and 6.2 GHz two layer design that shared the same electrical lengths as the best 6.2 and 3.1 GHz design. Frequencies from 15 to at least 23 GHz unscaled, 9.5 to 14.5 GHz scaled, have an associated positive real component of the normalized backscattered field.

Included in Figure 4-35 is the output associated with the best three layer design possible using the layers corresponding to the first, third, and fifth entries in Table 4.4. The effect of varying the locations of these slabs within the cavity can be seen from the Hoser Code outputs included in Appendix D.

The final designs all shared one concept -- that the number of dipole arrays per layer increases as the layers progress deeper into the cavity. This makes sense when one recalls that the scatterers on a layer do not have the ideal extremely narrow resonance characteristics desired. So instead of reflecting well only at their design frequency they

scatter incident waves over a range of frequencies. By having the same number of arrays in each layer, the low frequency waves would be greatly affected by the upper layers (both on the way down and again on the way back).

Baseline One Layer (6.22GHz) One Array Example

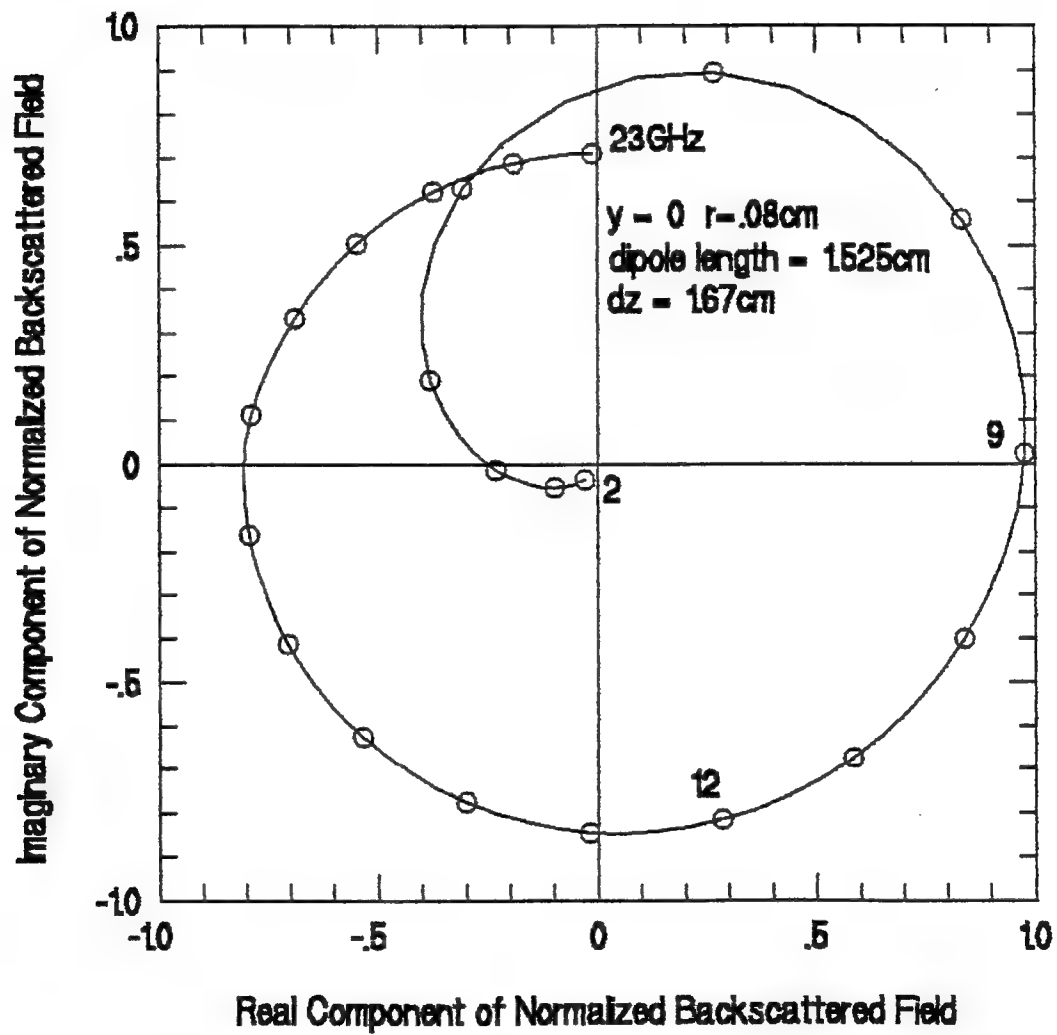
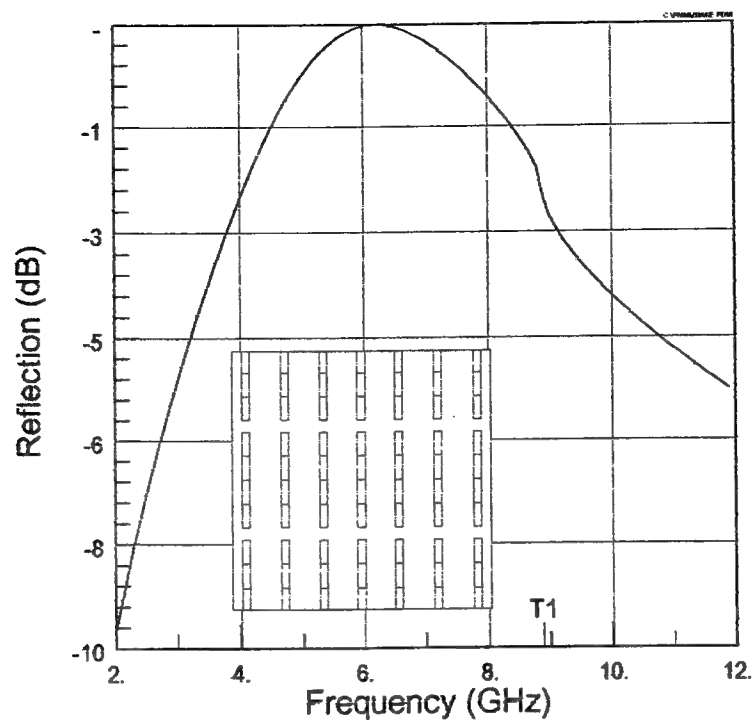


Figure 4-1 Example of Hoser Code Output For One Array Case

6.2 GHz Design With $X=0.25\lambda$



6.2 GHz Design With $X = 0.25\lambda$

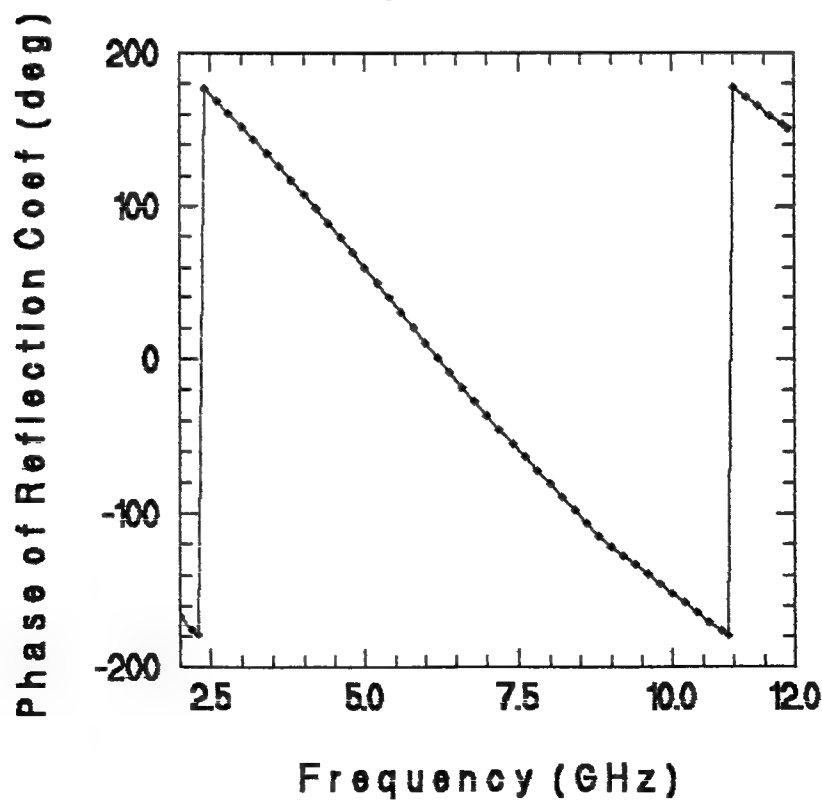
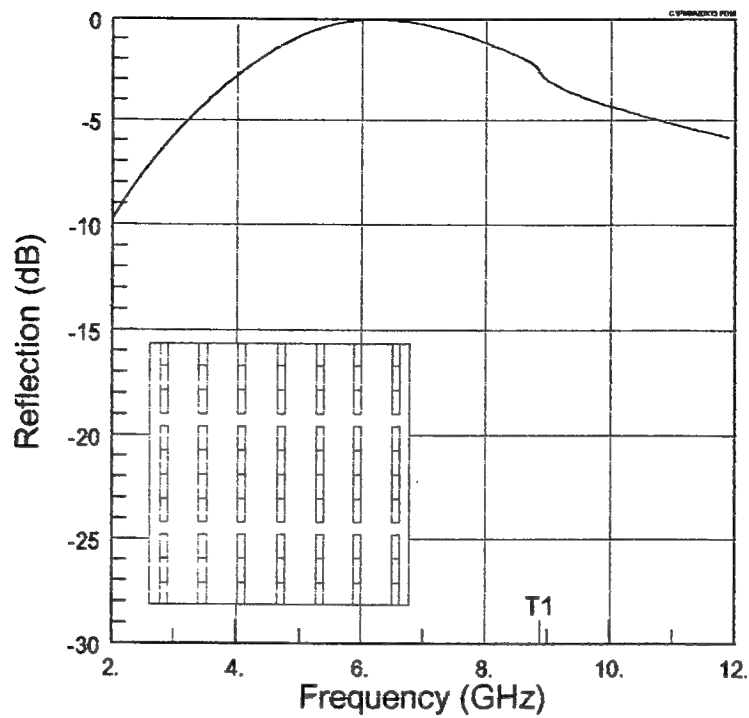


Figure 4-2 (a&b) PMM Code Output For Baseline 6.2 GHz Design With $X = 0.25\lambda$

6.2 GHz Design With $X=0.15\lambda$



6.2 GHz Design With $X = 0.15\lambda$

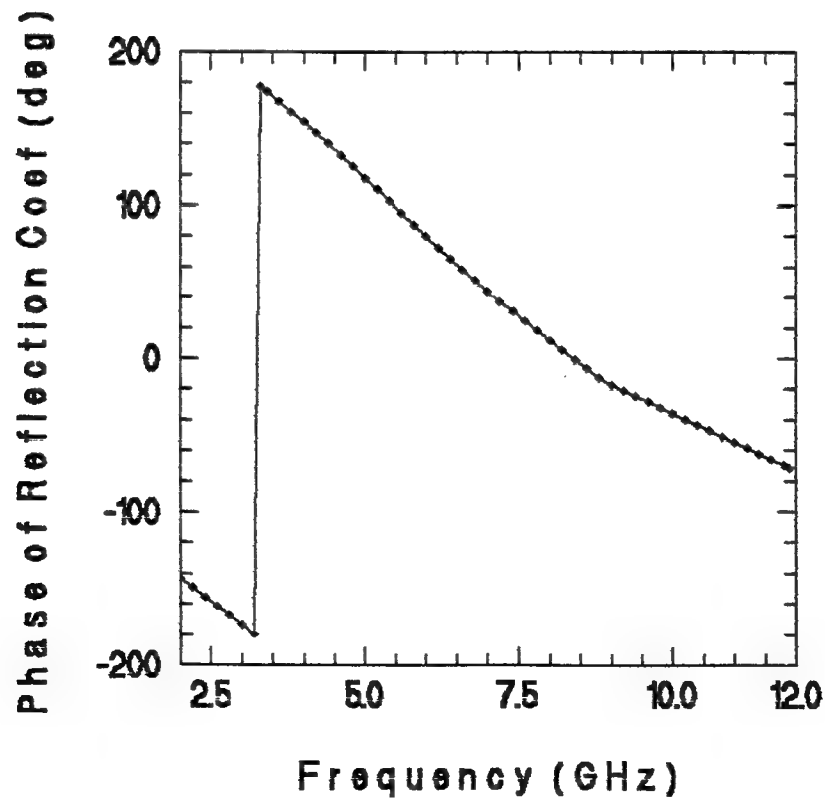


Figure 4-3 (a&b) PMM Code Output For 6.2 GHz Design With $X = 0.15\lambda$

6.2 GHz Design With $X=0.35 \text{ Lambda}$

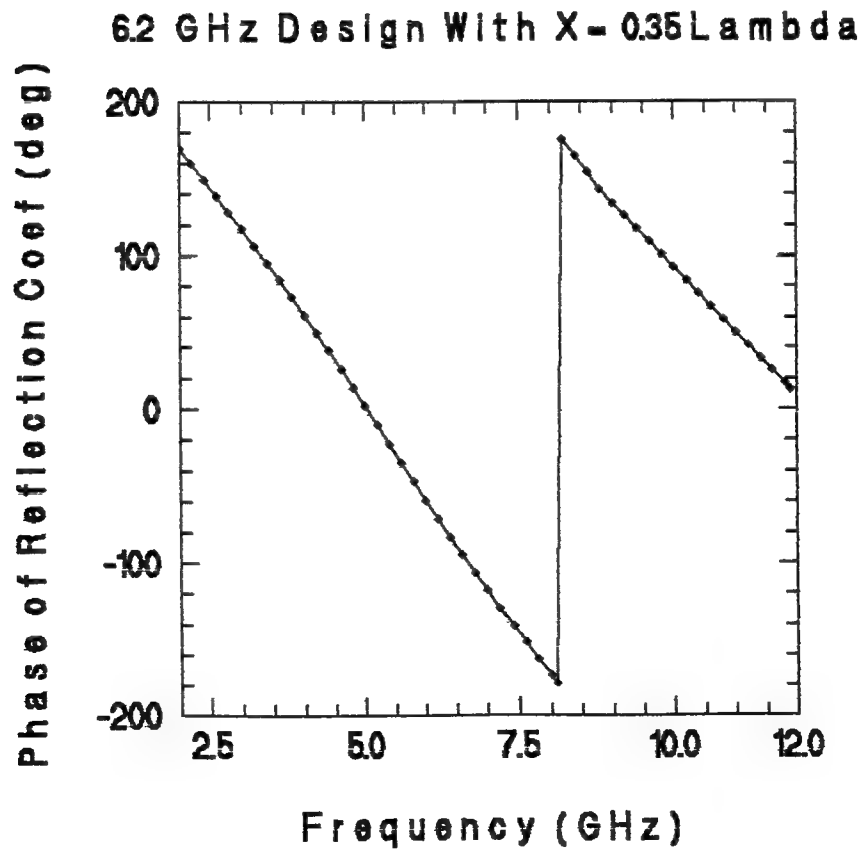
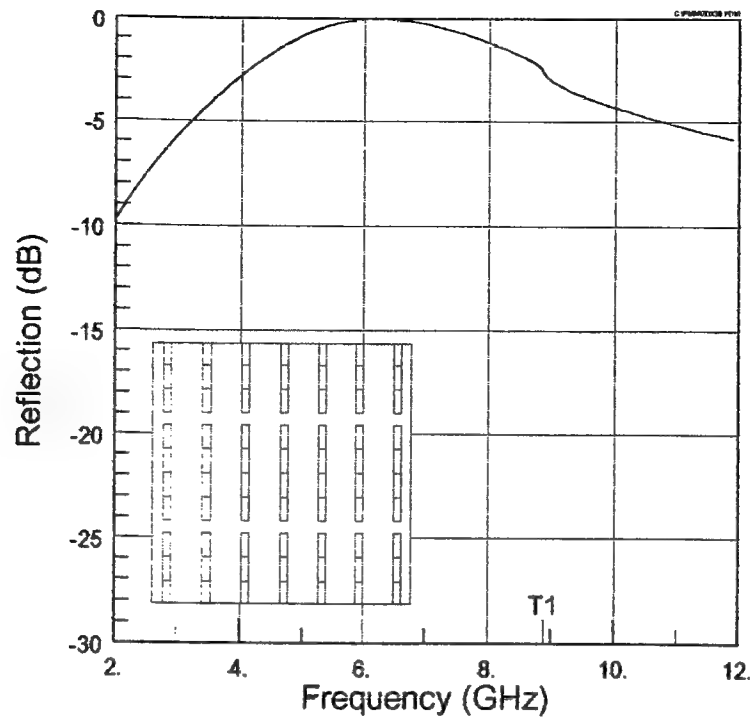
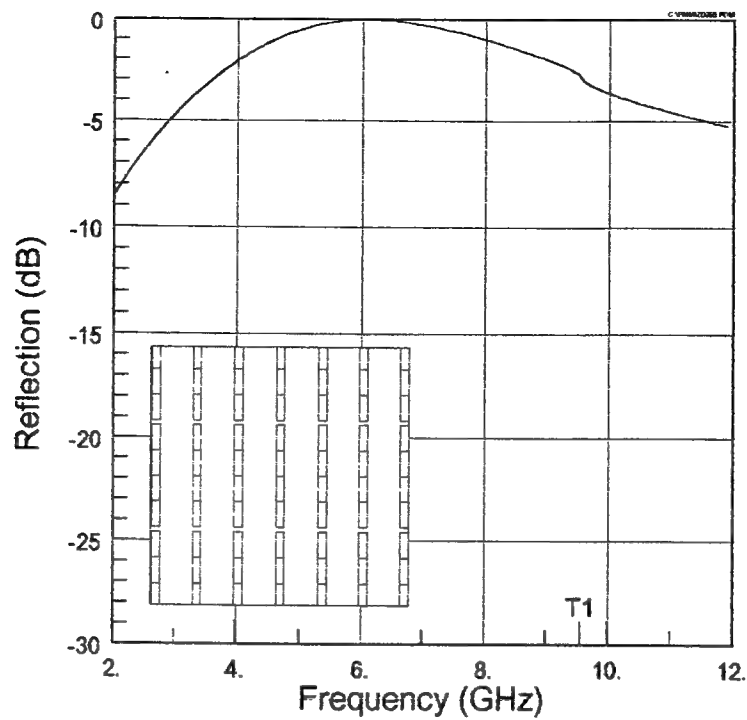


Figure 4-4 (a&b) PMM Code Output For 6.2 GHz Design With $X = 0.35\lambda$

6.2 GHz Design With $DZ = 0.65 \text{ Lambda}$



6.2 GHz Design With $DZ = 0.65 \text{ Lambda}$

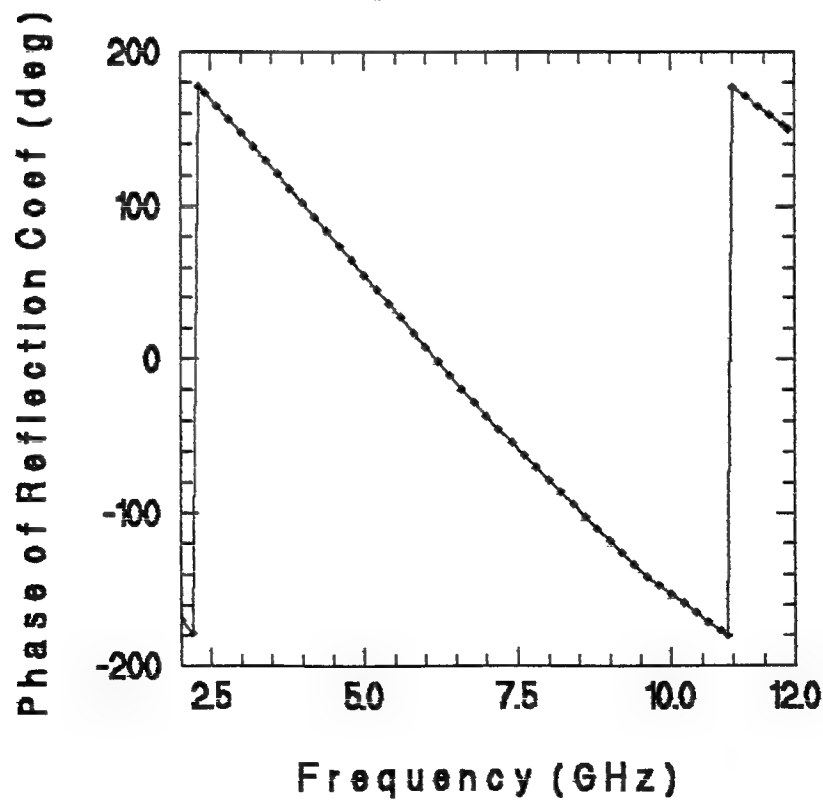
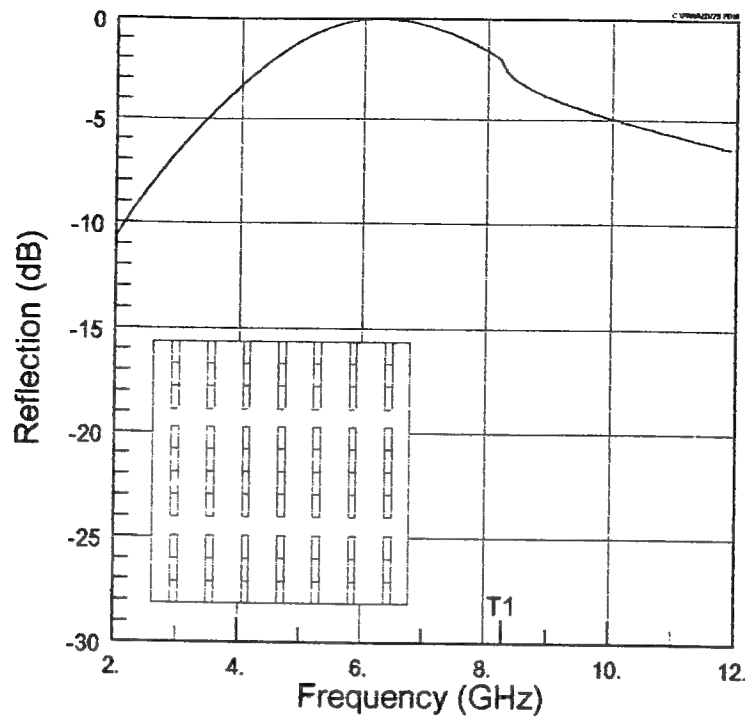


Figure 4-5 (a&b) PMM Code Output For 6.2 GHz Design With $DZ = 0.65\lambda$

6.2 GHz Design With $DZ = 0.75 \text{ Lambda}$



6.2 GHz Design With $DZ = 0.75 \text{ Lambda}$

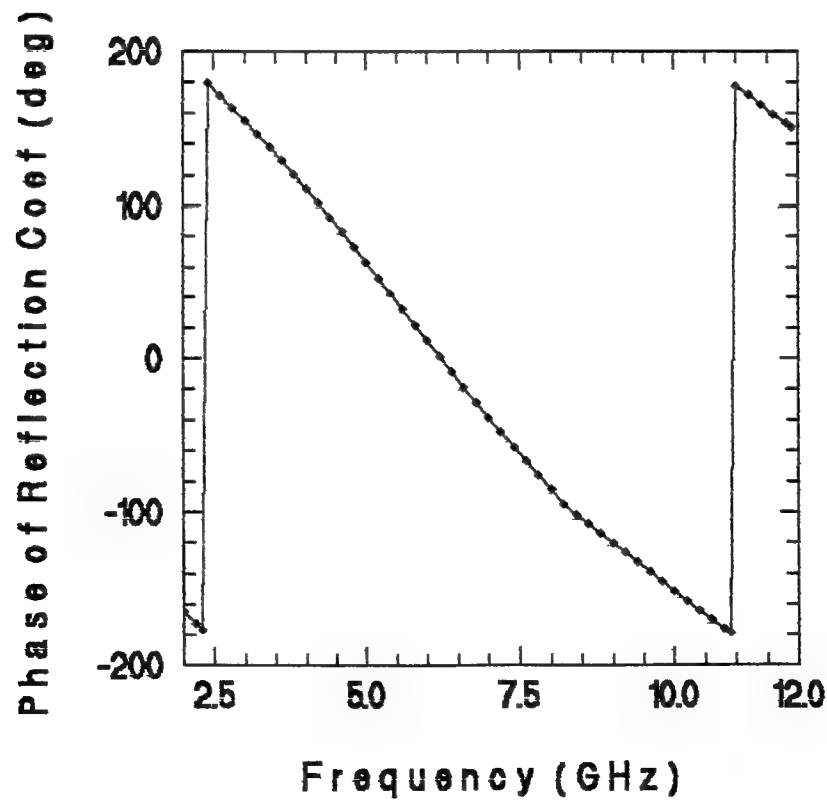
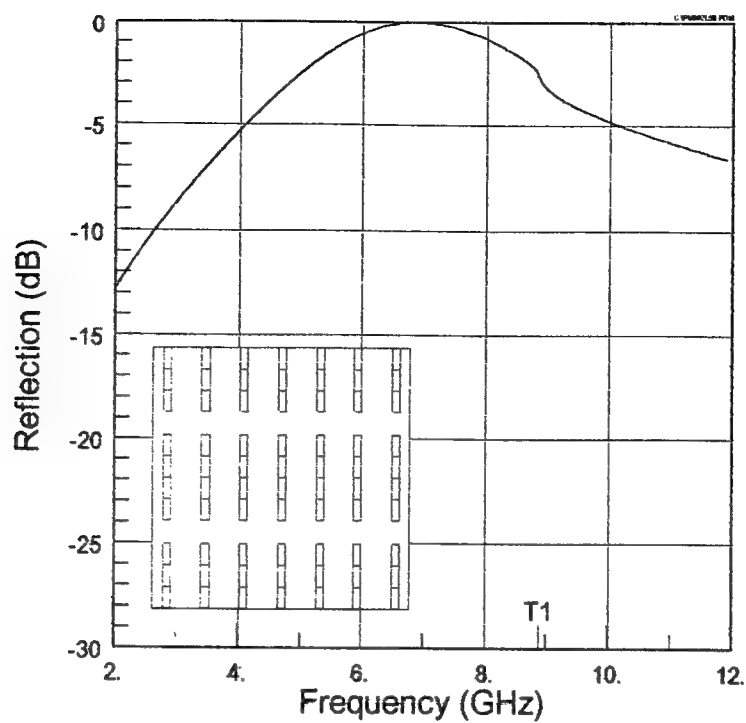


Figure 4-6 (a&b) PMM Code Output For 6.2 GHz Design With $DZ = 0.75\lambda$

6.2 GHz Design With $L = 0.55 \text{ Lambda}$



6.2 GHz Design With $L = 0.55 \text{ Lambda}$

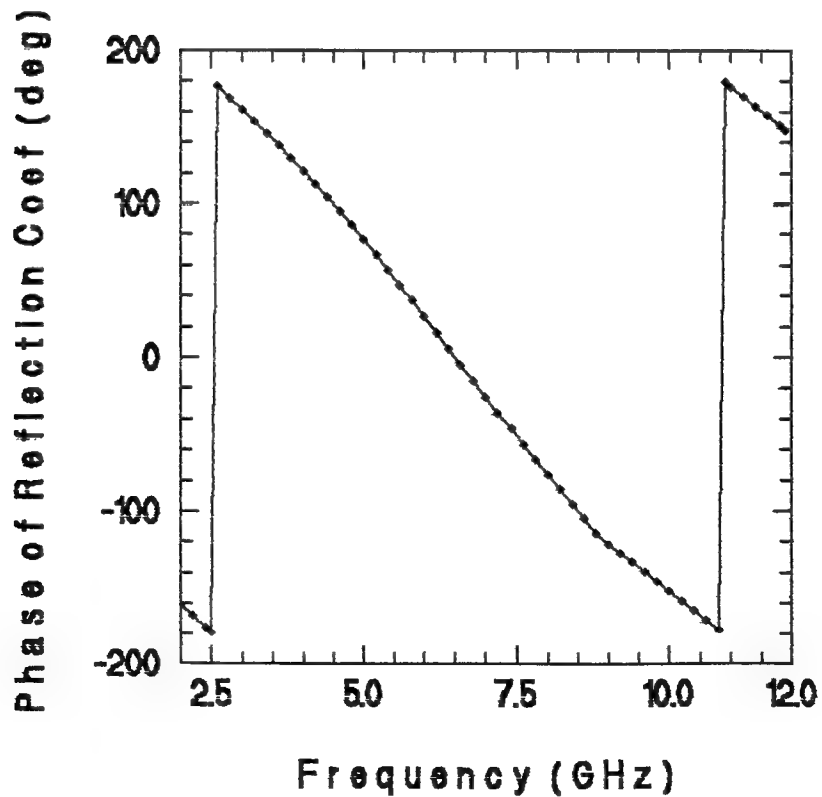
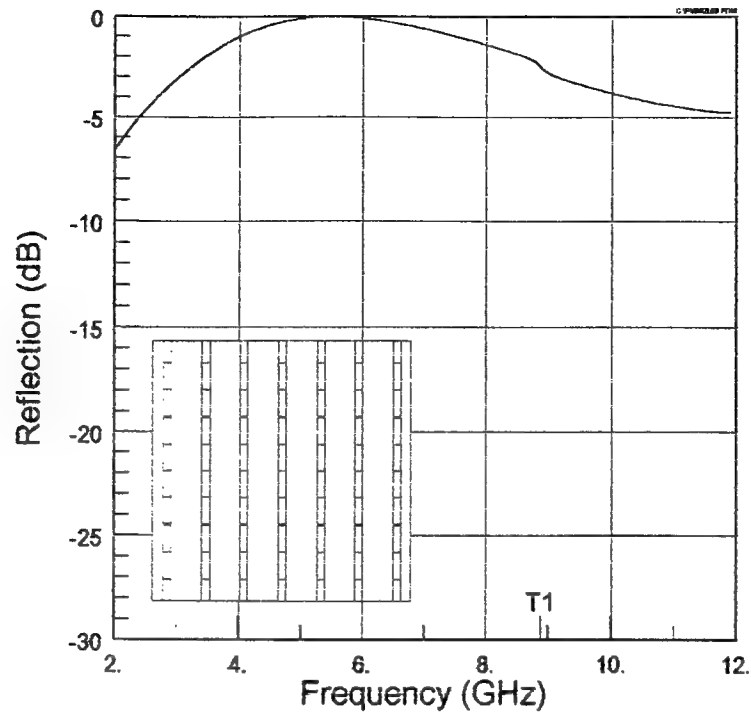


Figure 4-7 (a&b) PMM Code Output For 6.2 GHz Design With $L = 0.55\lambda$

6.2 GHz Design With $L = 0.69 \text{ Lambda}$



6.2 GHz Design With $L = 0.69 \text{ Lambda}$

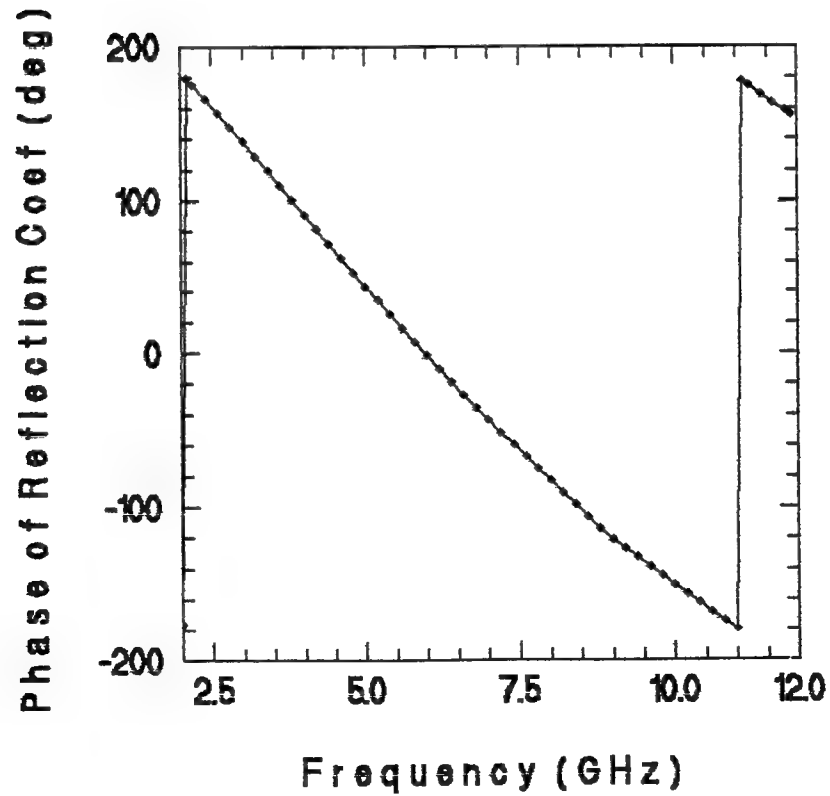
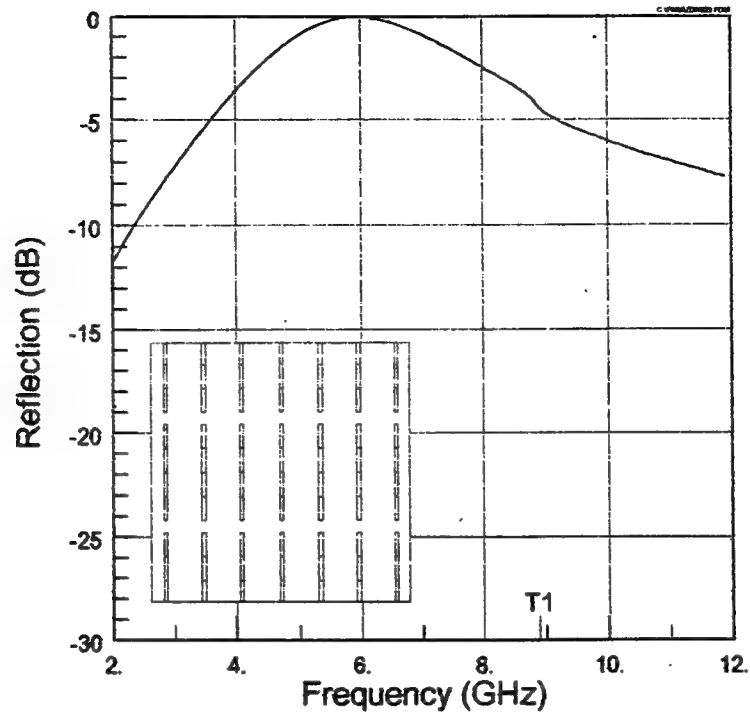


Figure 4-8 (a&b) PMM Code Output For 6.2 GHz Design With $L = 0.69\lambda$

6.2 GHz Design With $W = 0.025 \text{ Lambda}$



62 GHz Design With $W = 0.025 \text{ Lambda}$

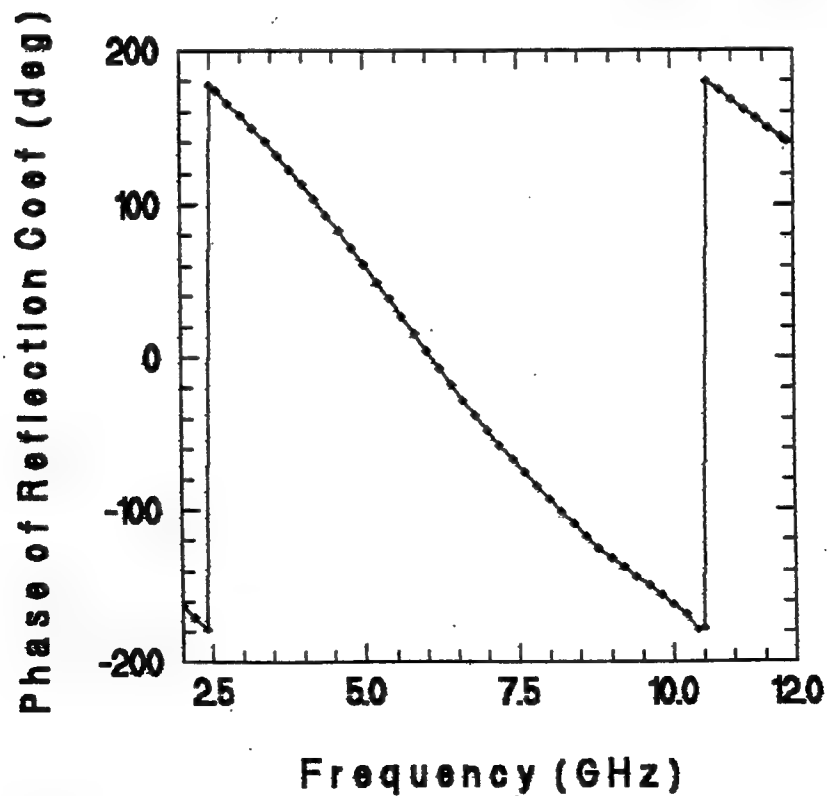
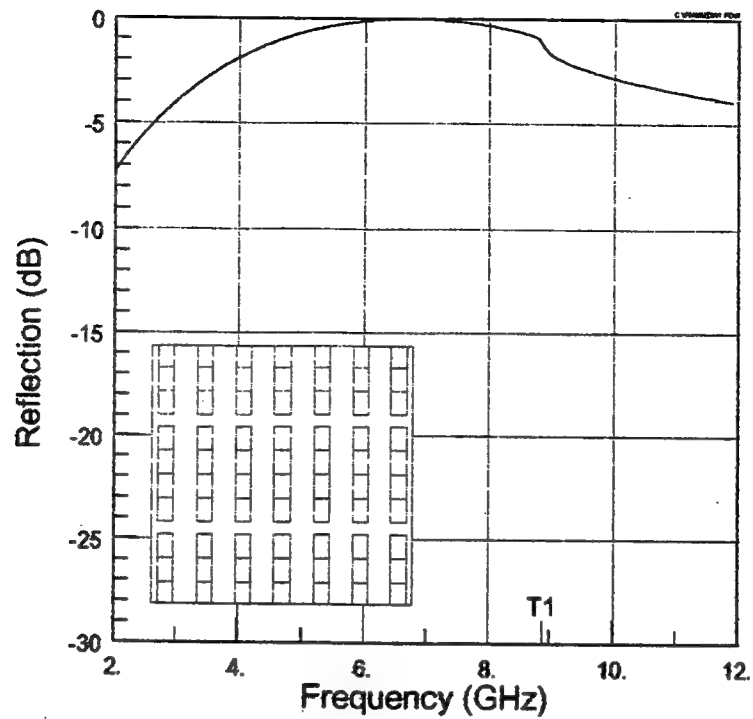


Figure 4-9 (a&b) PMM Code Output For 6.2 GHz Design With $W = 0.025 \lambda$

6.2 GHz Design With $W = 0.1 \text{ Lambda}$



6.2 GHz Design With $W = 0.1 \text{ Lambda}$

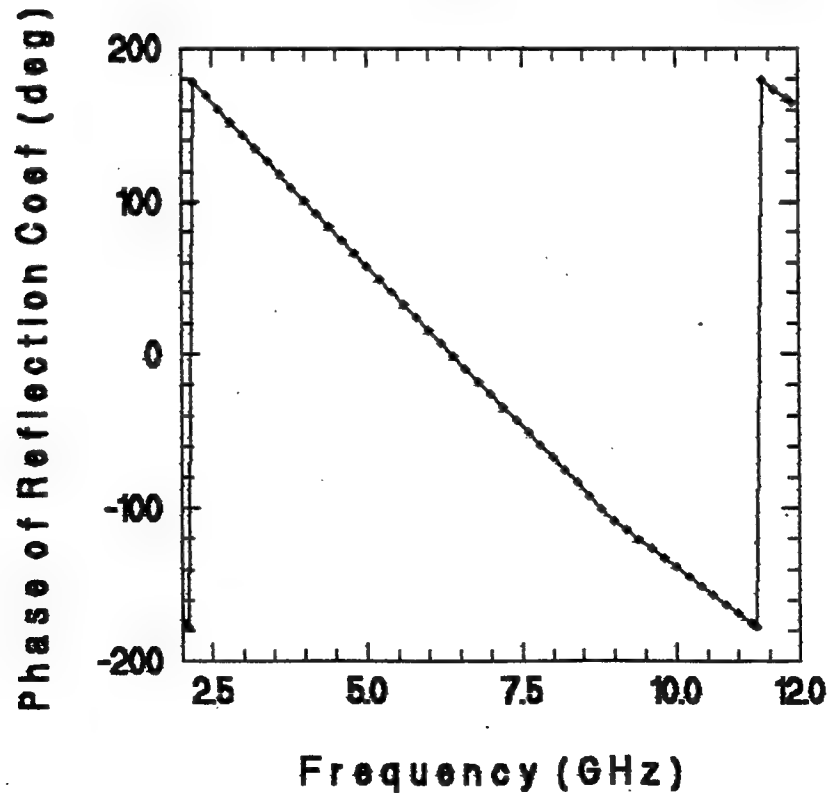
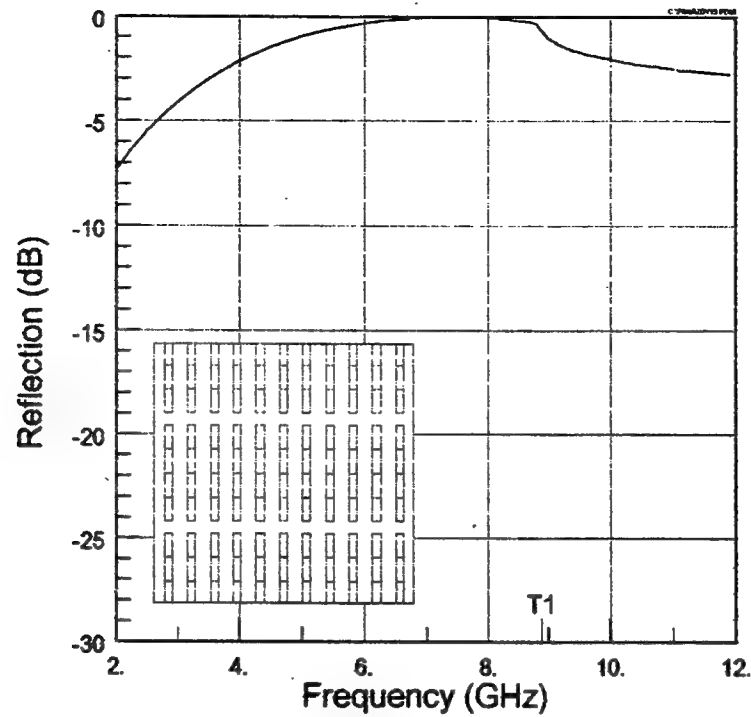


Figure 4-10 (a&b) PMM Code Output For 6.2 GHz Design With $W = 0.1\lambda$

6.2 GHz Design With $DY = 0.15 \text{ Lambda}$



6.2 GHz Design With $DY = 0.15 \text{ Lambda}$

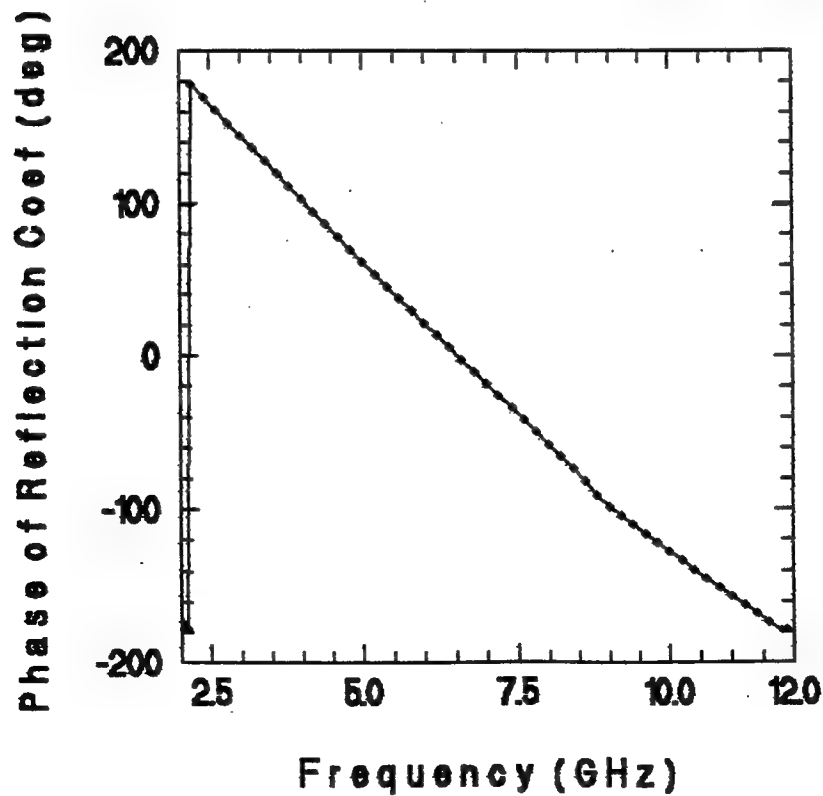
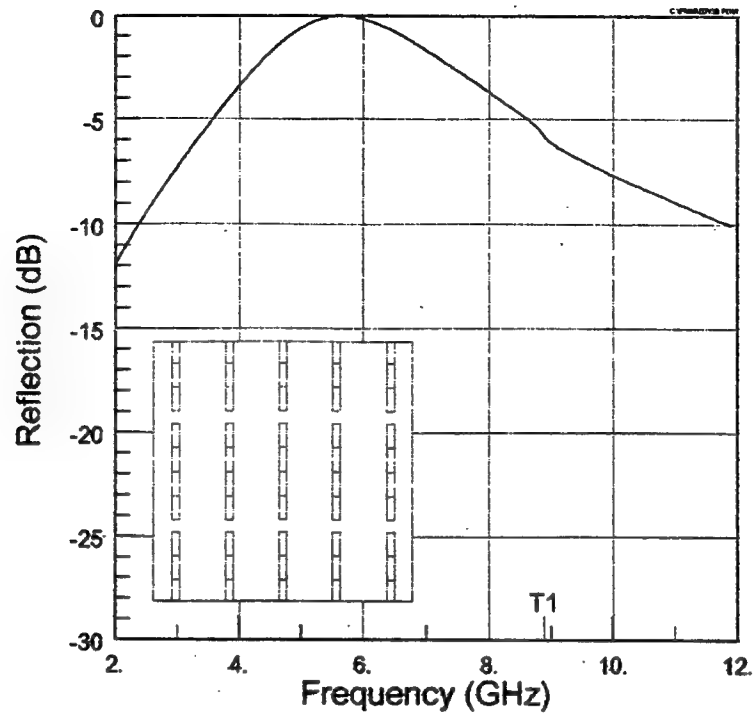


Figure 4-11 (a&b) PMM Code Output For 6.2 GHz Design With $DY = 0.15\lambda$

6.2 GHz Design With $DY = 0.35 \text{ Lambda}$



6.2 GHz Design With $DY = 0.35 \text{ Lambda}$

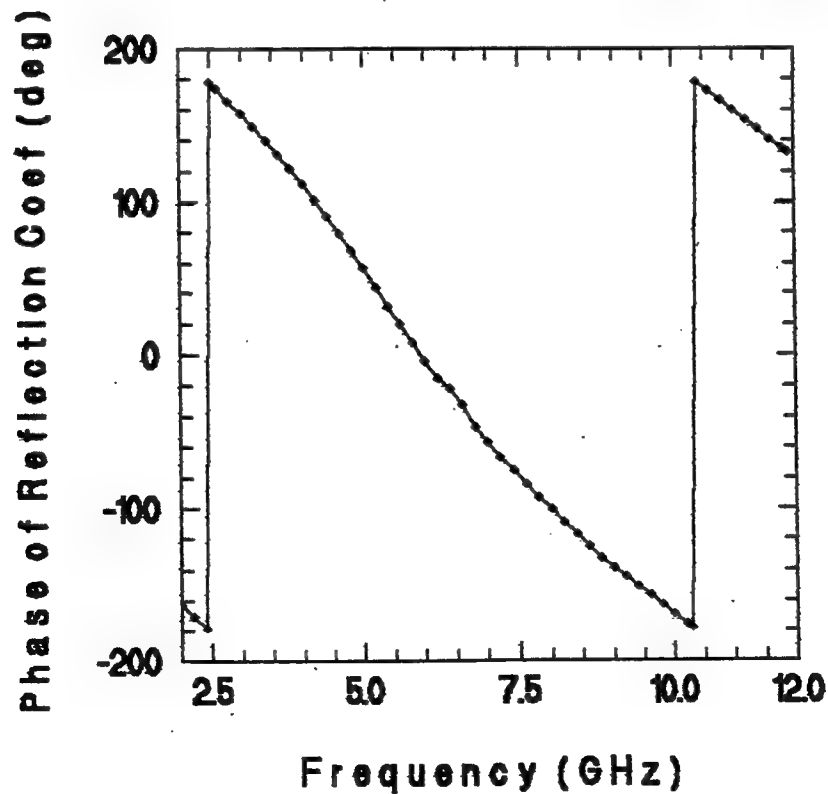
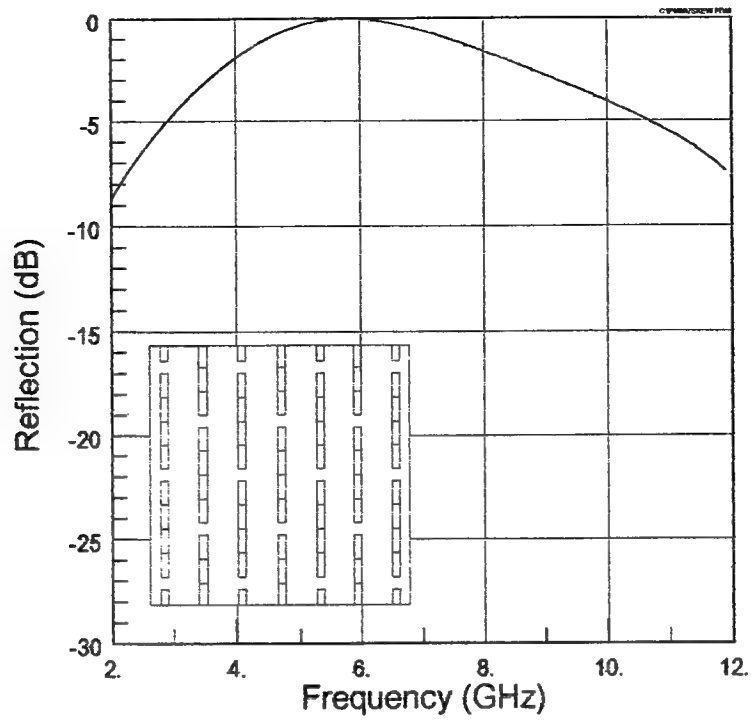


Figure 4-12 (a&b) PMM Code Output For 6.2 GHz Design With $DY = 0.35\lambda$

6.2 GHz Design With $X=0.25$ Lambda and Skewed Grid



6.2 GHz Design With Skewed Grid

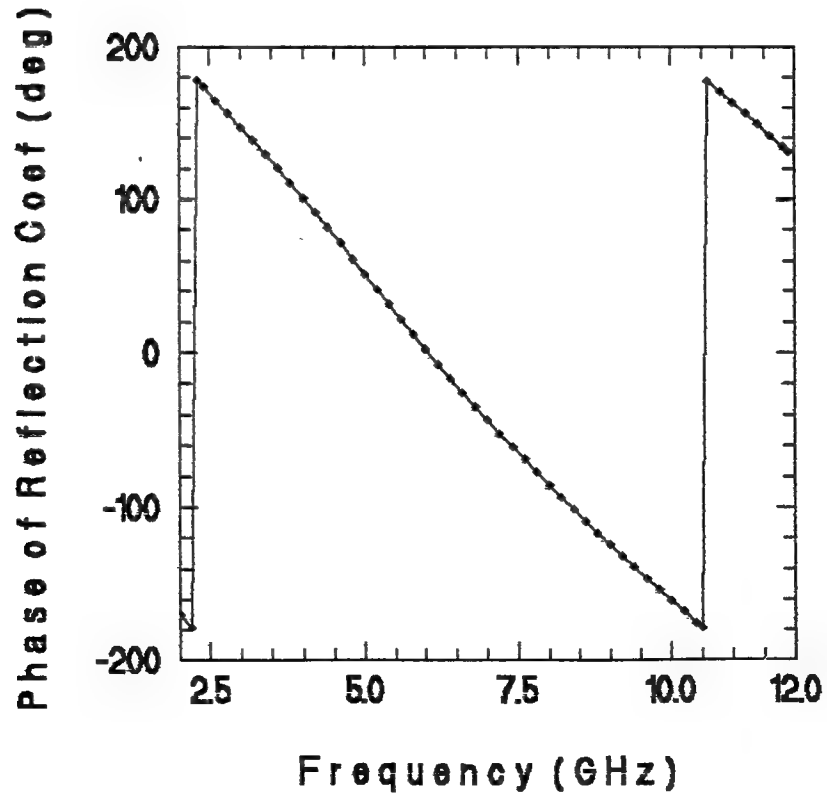
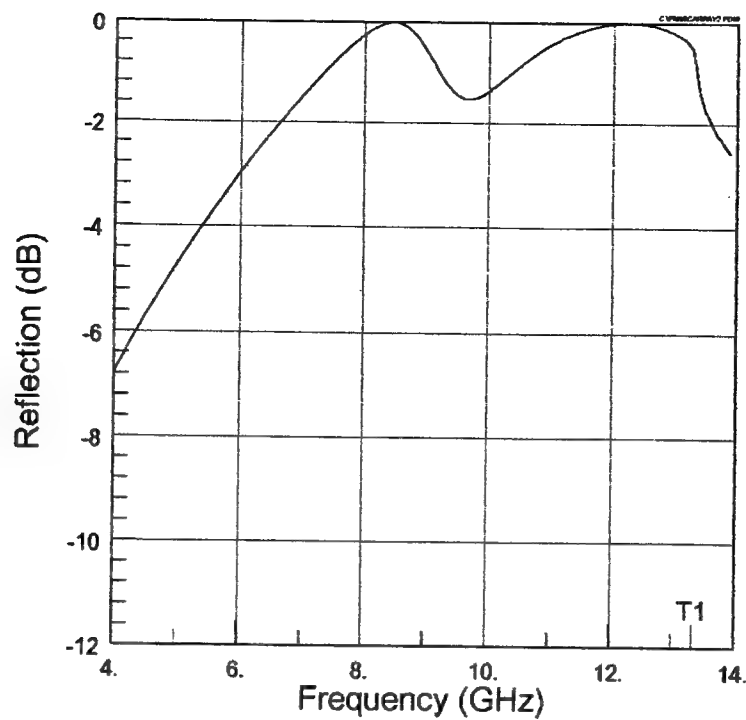


Figure 4-13 (a&b) PMM Code Output For 6.2 GHz Design With Skewed Grid

2 Layer Design (12.4,9.3GHz); Dz=1.4217cm



2 Layer Design (12.4, 9.3GHz); DZ=1.42cm

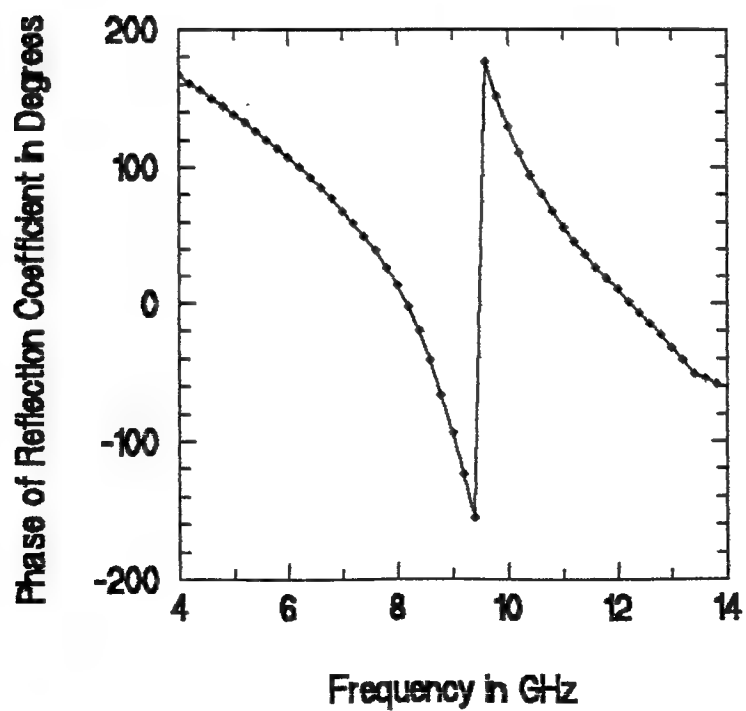
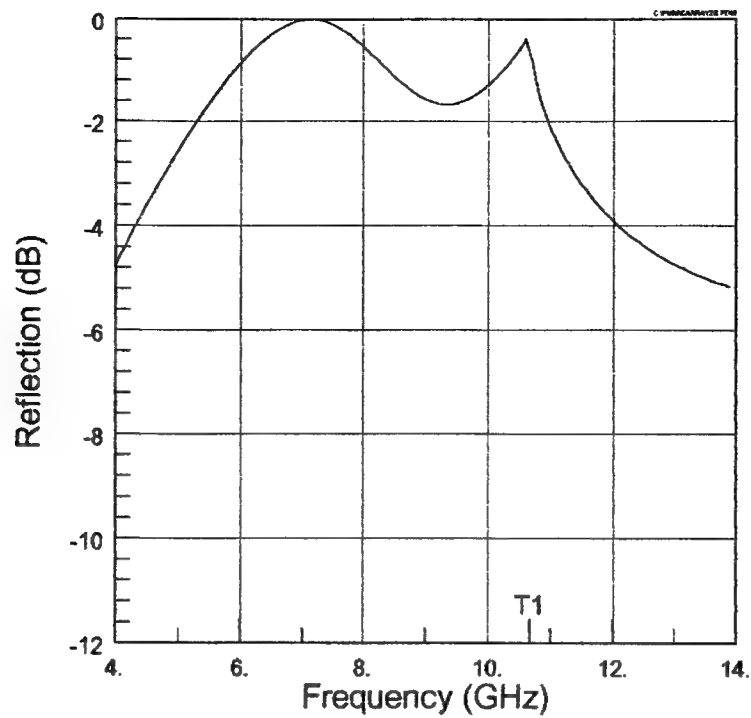


Figure 4-14 (a&b) PMM Code Output For First Two Layer Design

2 Layer Design (12.4, 7.5GHz); Dz = 1.78cm



2 Layer Design (12.4, 7.5GHz); DZ=178cm

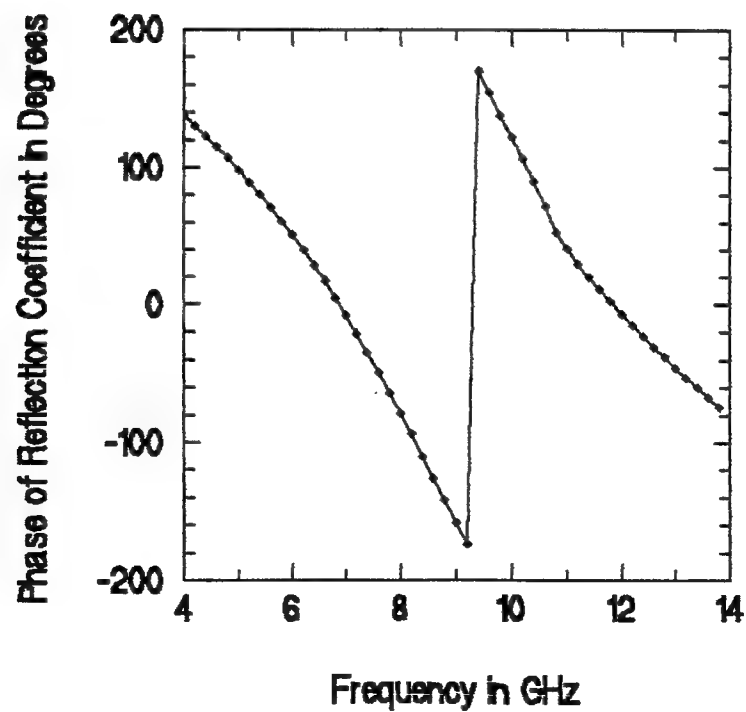
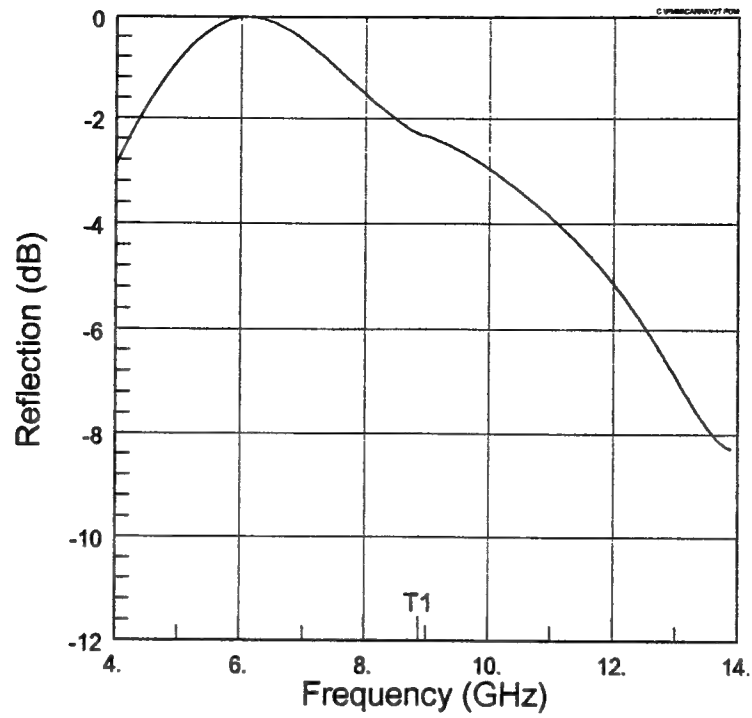


Figure 4-15 (a&b) PMM Code Output For Second Two Layer Design

2 Array Design (12.4, 6.2GHz); Dz =2.135cm



2 Layer Design (12.4, 6.2GHz); DZ= 2.14cm

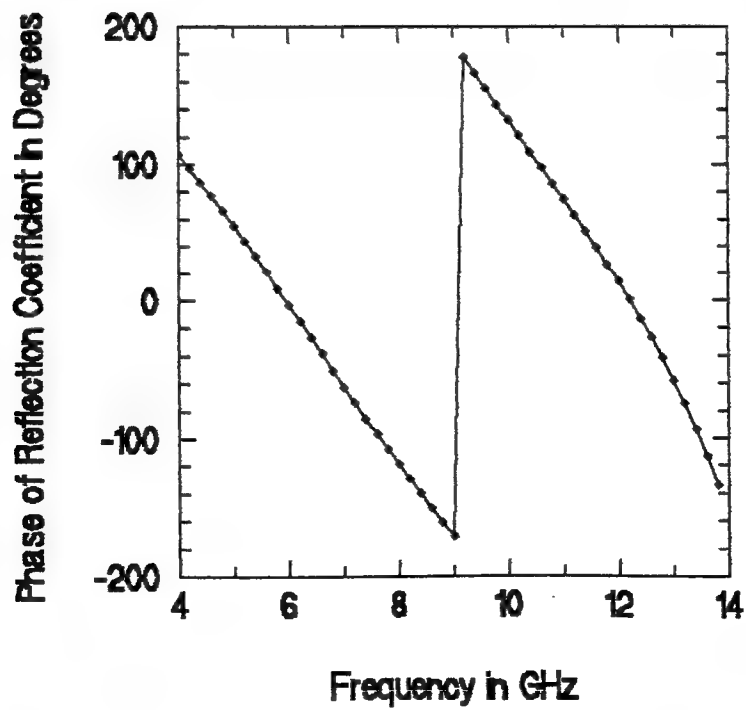
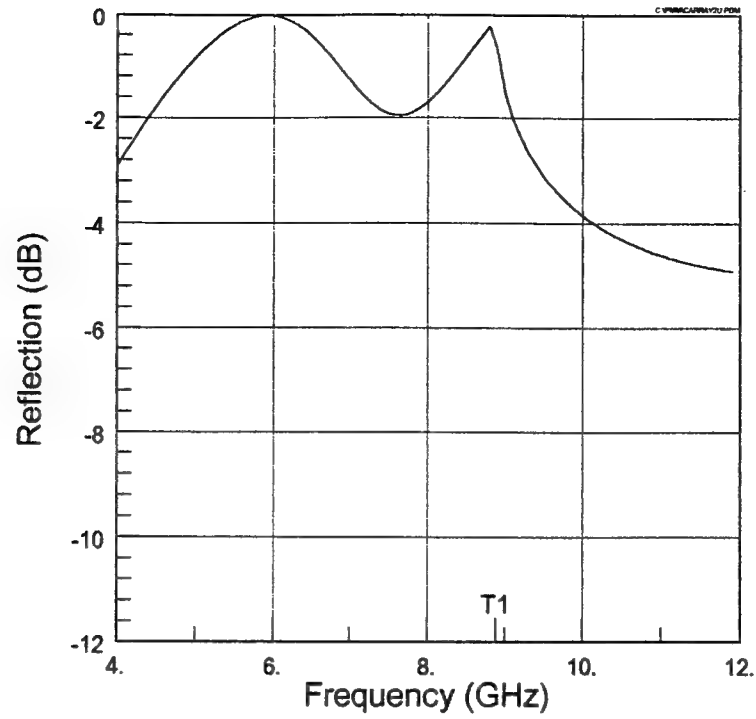


Figure 4-16 (a&b) PMM Code Output For Third Two Layer Design

2 Array Design (9.45, 6.22GHz), Dz=2.14cm



2 Layer Design (9.45, 6.22GHz); DZ=2.14cm

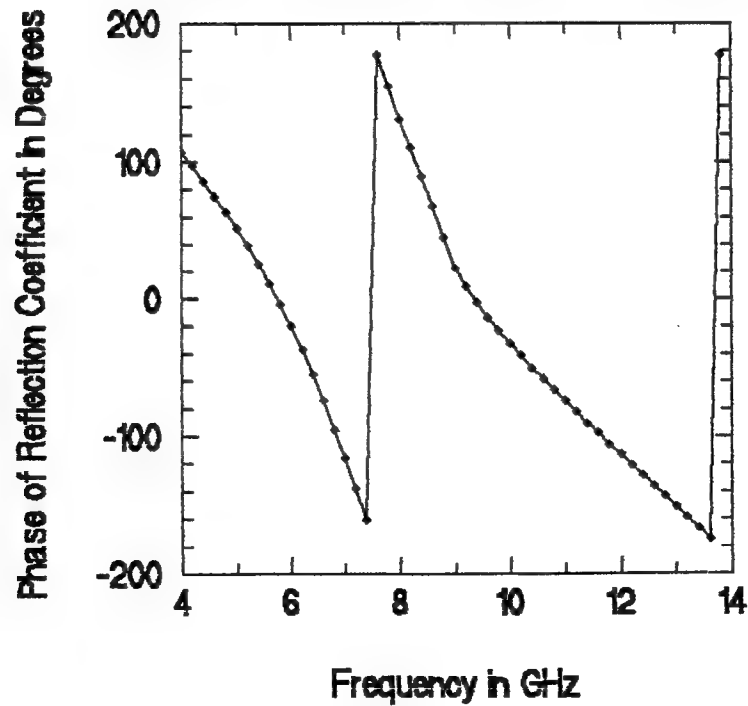
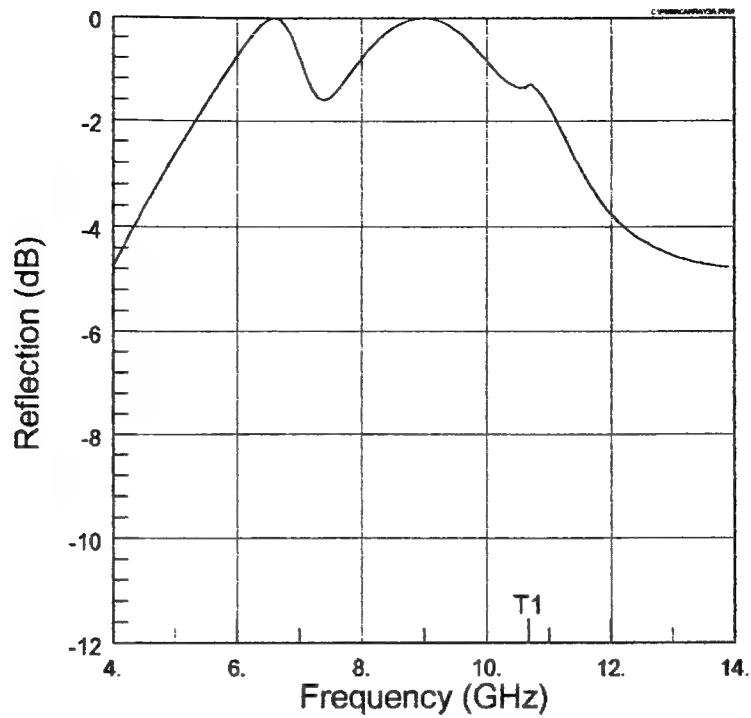


Figure 4-17 (a&b) PMM Code Output For Fourth Two Layer Design

3 Layer Design (12.4, 9.3, 7.5GHz), Dz= 1.78cm



3 Layer Design (12.4, 9.4, 7.5GHz), DZ=178cm

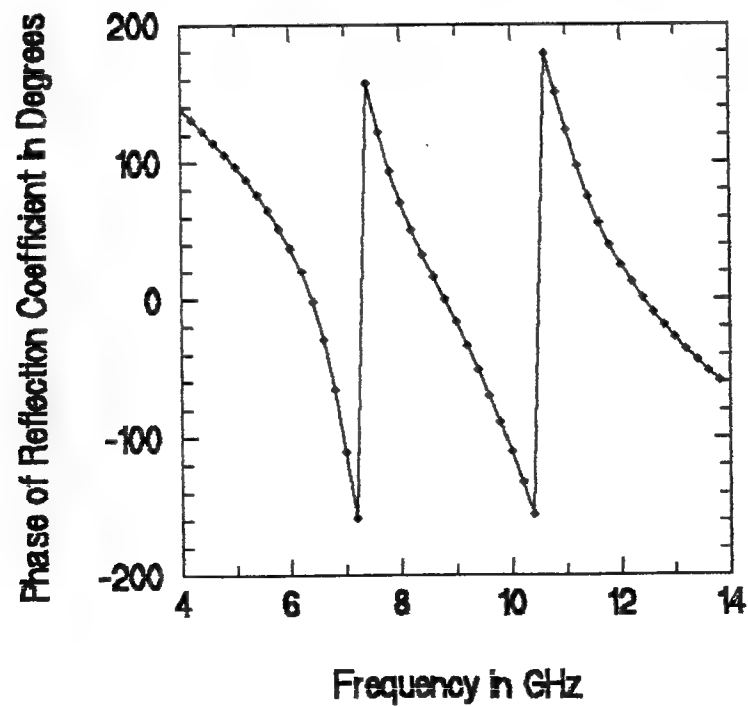
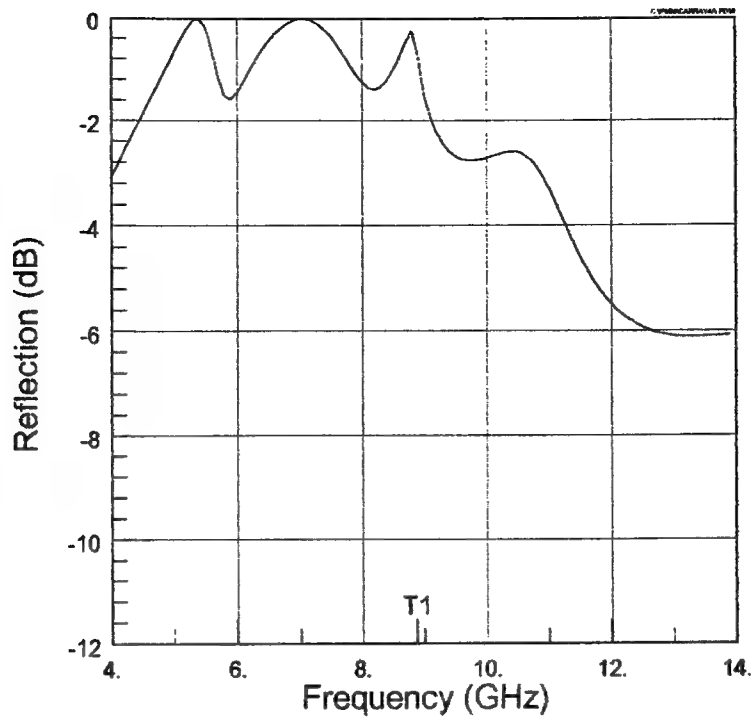


Figure 4-18 (a&b) PMM Code Output For Three Layer Design

4 Layer Design (12.4,9.3,7.4,6.2GHz), Dz = 2.14cm



4 Layer Design (12.4, 9.4, 7.4, 6.2GHz), DZ=2.14cm

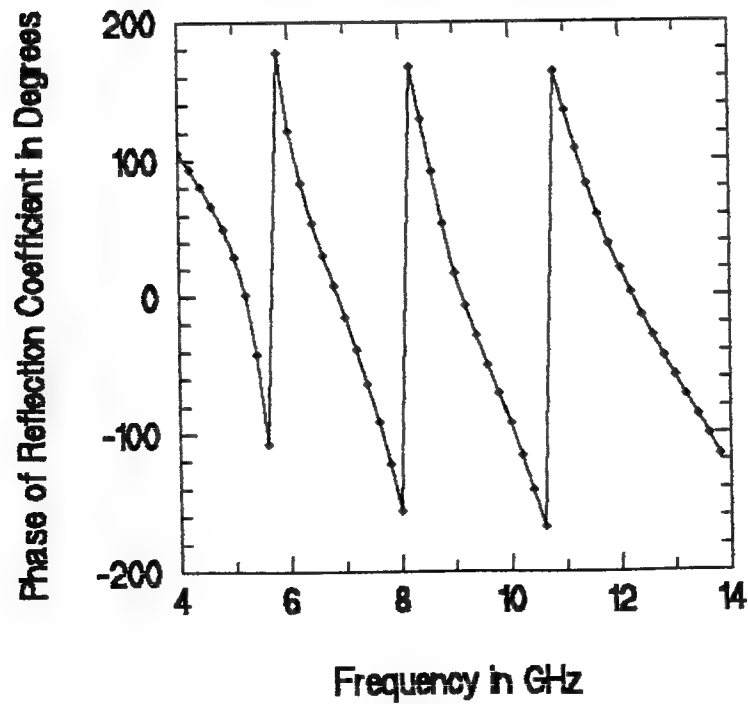
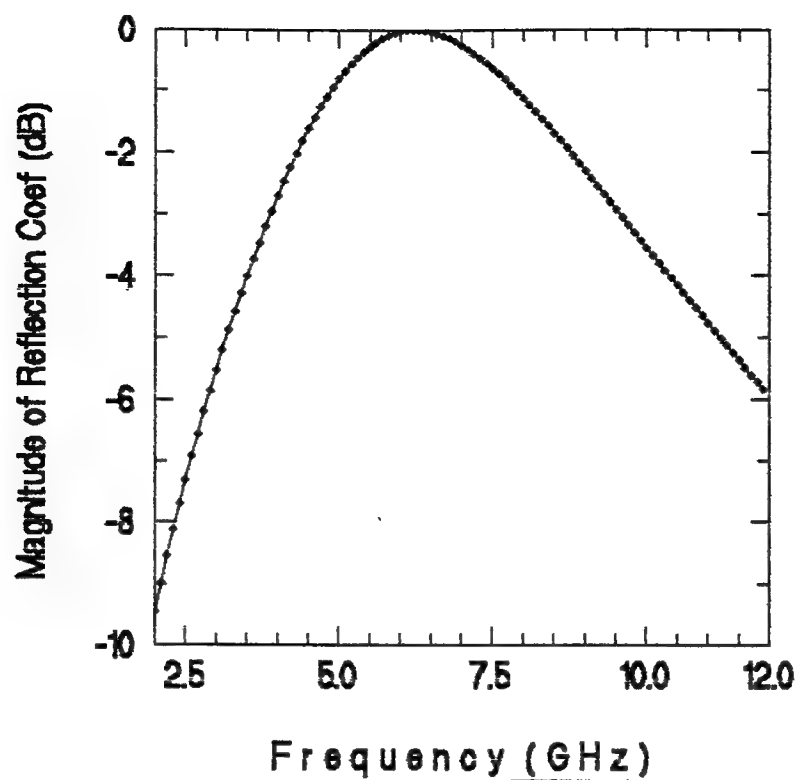


Figure 4-19 (a&b) PMM Code Output For Four Layer Design

T-Line Output For 62 GHz Design In Fig 4-2



T-Line Output For 62 GHz Design In Fig 4-2

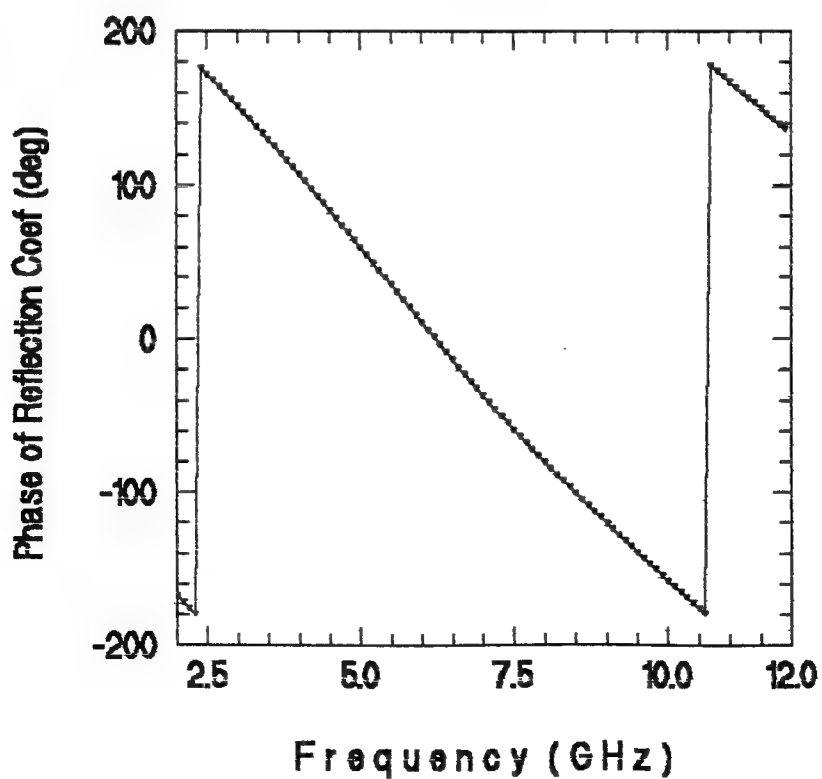
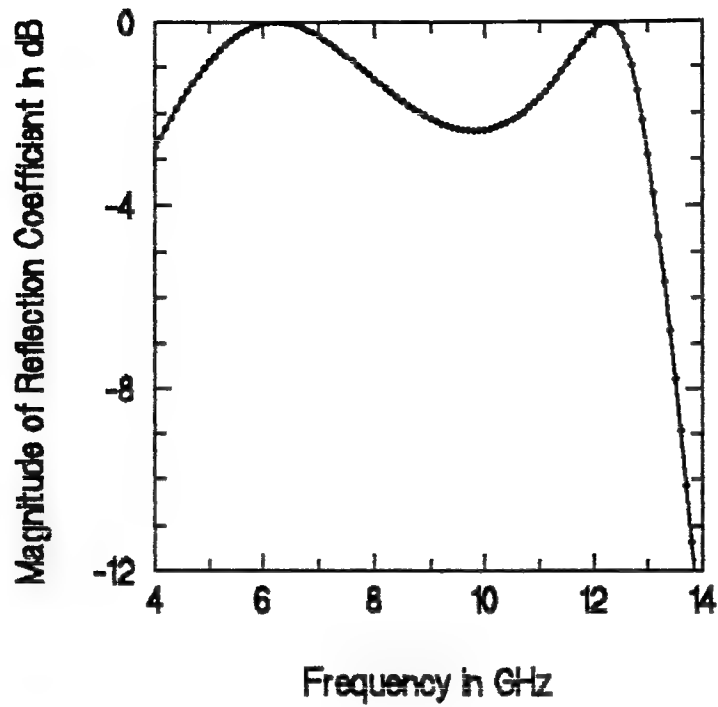


Figure 4-20 (a&b) Transmission Code Output For One Layer Design

T-line 2 layer design (12.4,6.2GHz) with constant $dz=2.14\text{cm}$, $dy=\lambda/4$



T-line 2 layer design (12.4,6.2GHz) but top layer now changed

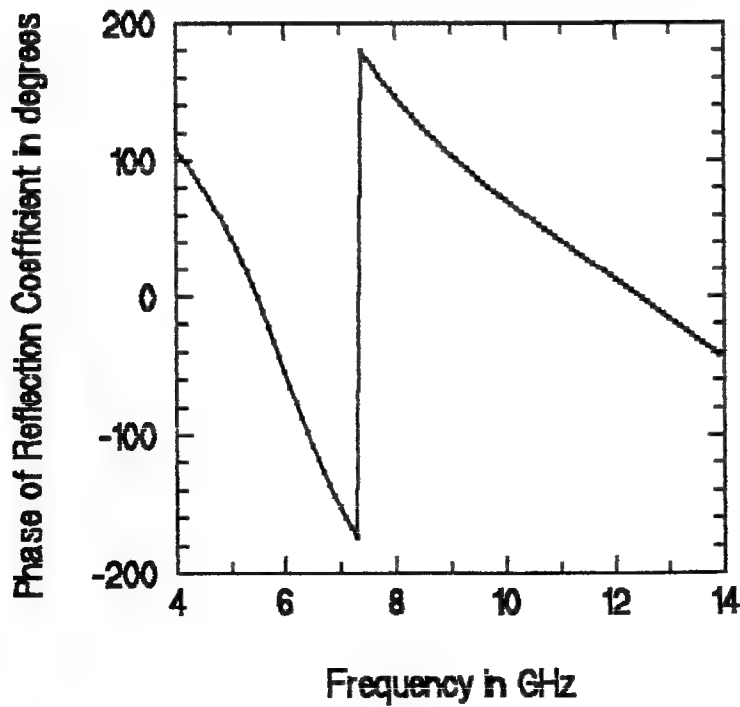
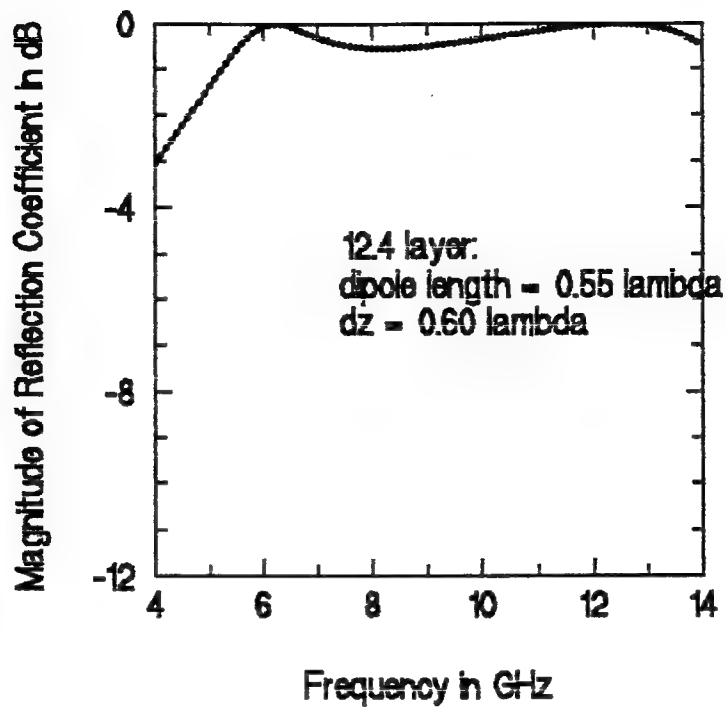


Figure 4-21 (a&b) Transmission Line Code Output For First Two Layer Design

T-line 2 layer design (12.4,6.2GHz) but top layer now changed



T-line 2 layer design (12.4,6.2GHz) with constant dz=2.14cm, dy= lambda/4

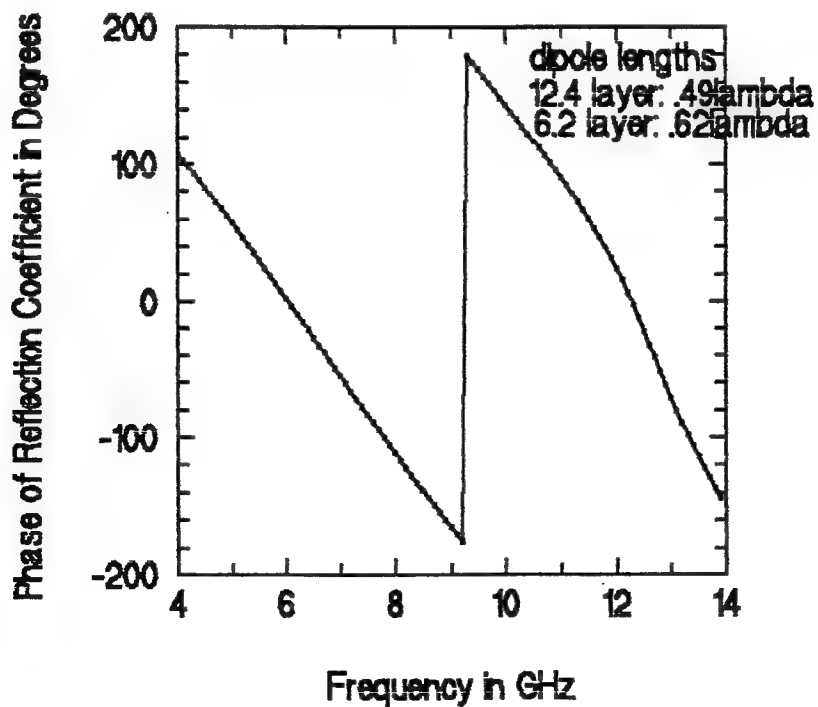


Figure 4-22 (a&b) Transmission Line Code Output For Second Two Layer Design

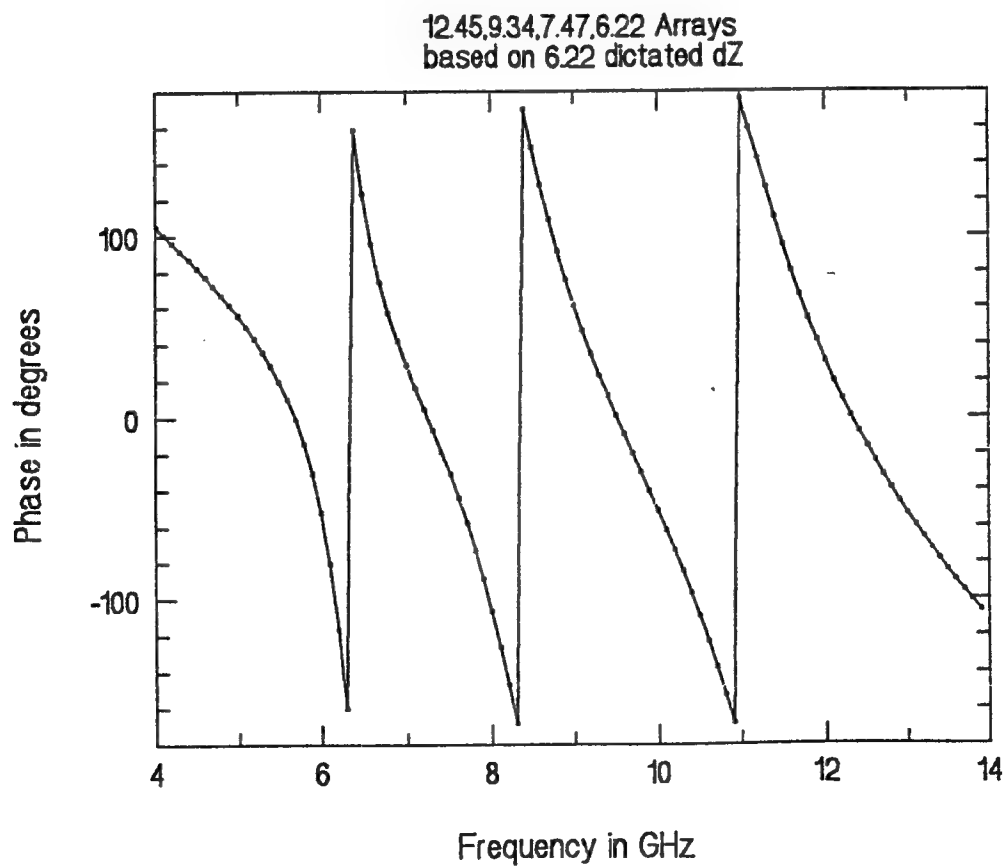
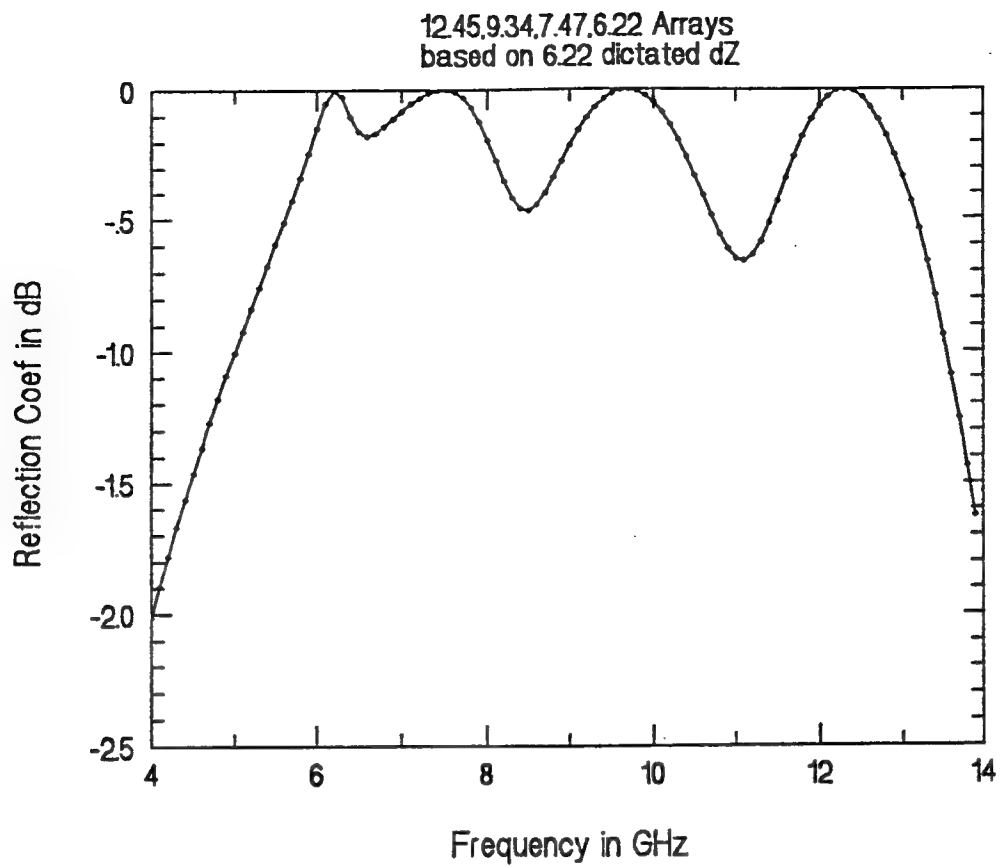


Figure 4-23 (a&b) Transmission Line Code Output For Four Layer Design

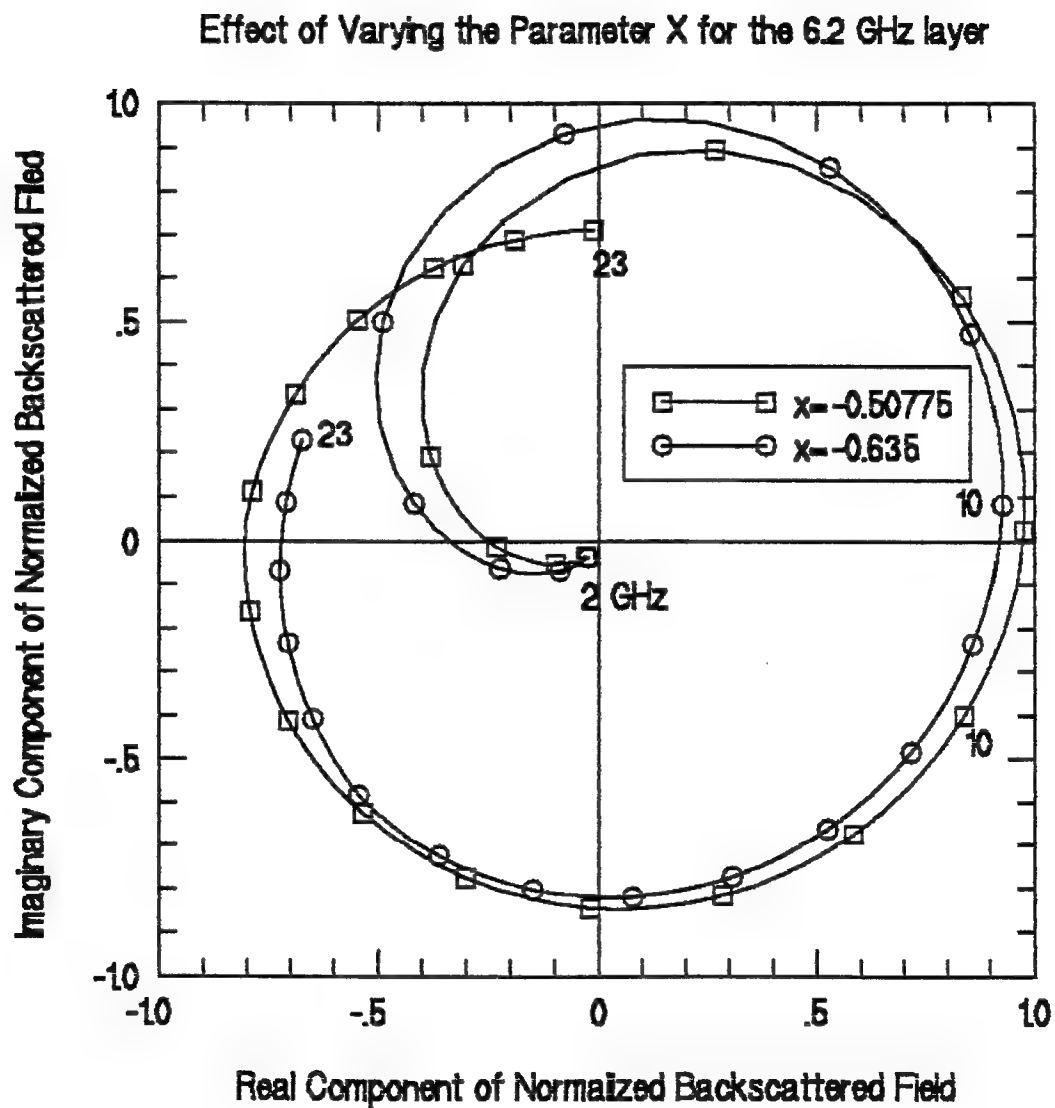


Figure 4-24 The Effect of Varying The X Parameter in The Hoser Code For One Layer

Effect of Varying the Parameter DZ for the 6.2 GHz Layer (one array)

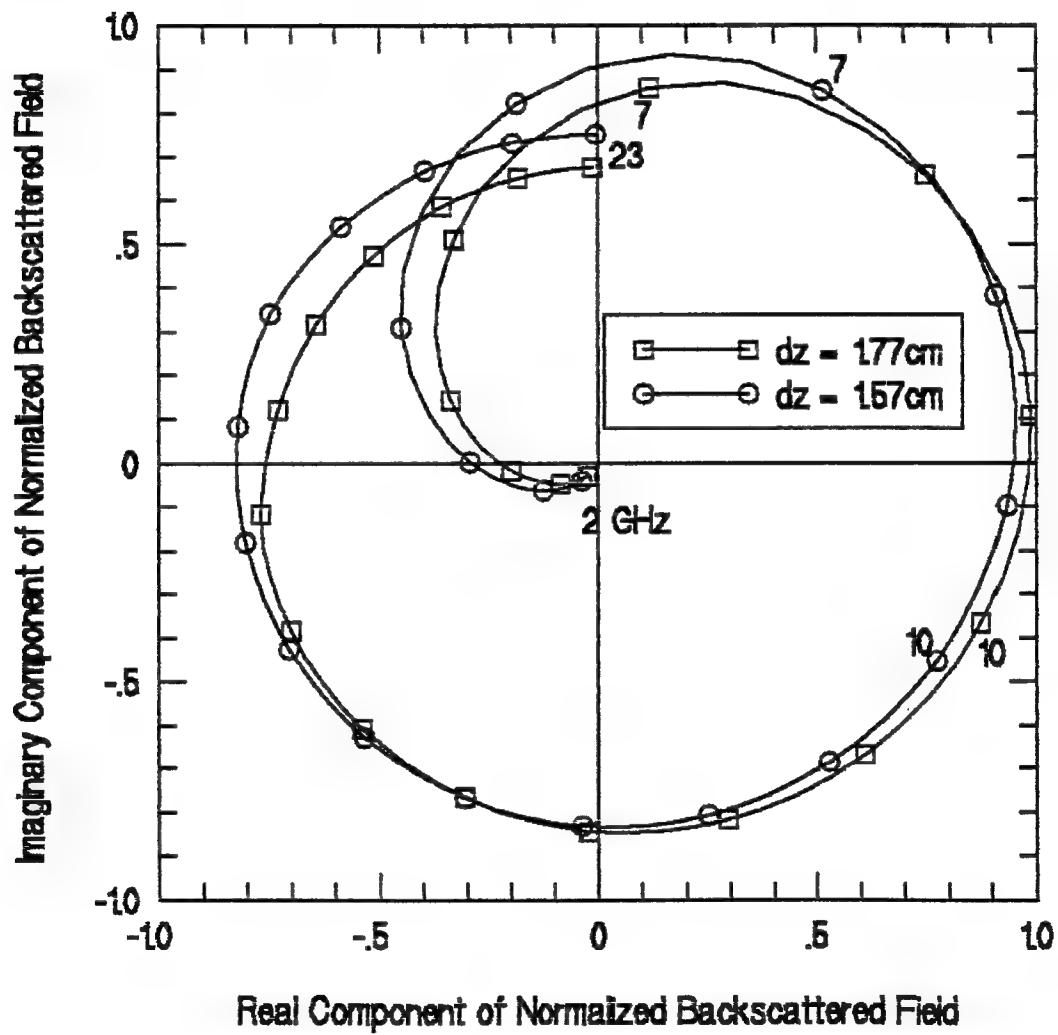


Figure 4-25 The Effect of Varying The DZ Parameter in The Hoser Code For One Layer

Effect of Varying the Parameter of Dipole Length for 6.2 GHz Layer

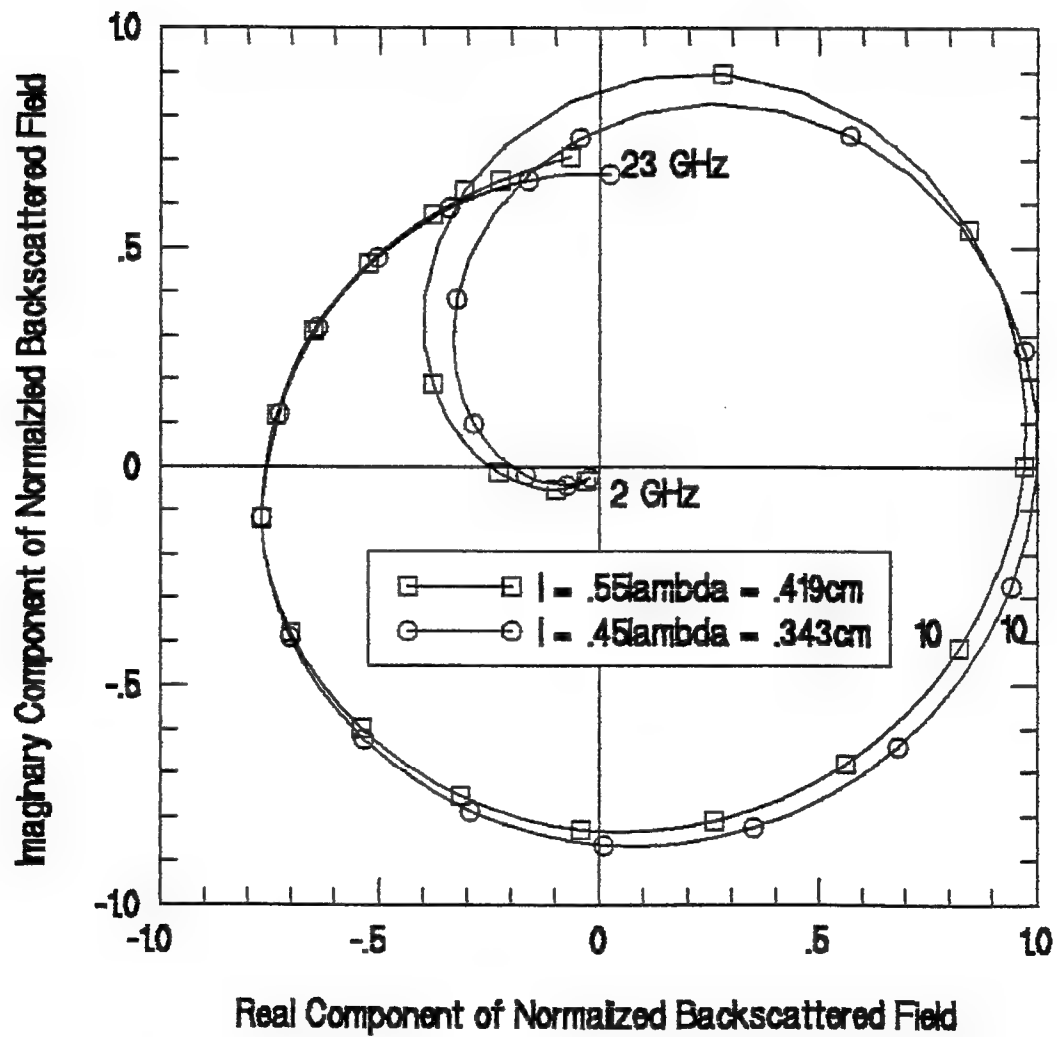


Figure 4-26 The Effect of Varying The L Parameter in The Hoser Code For One Layer

Effect of Varying the Parameter r -radius for the 6.2 GHz Layer

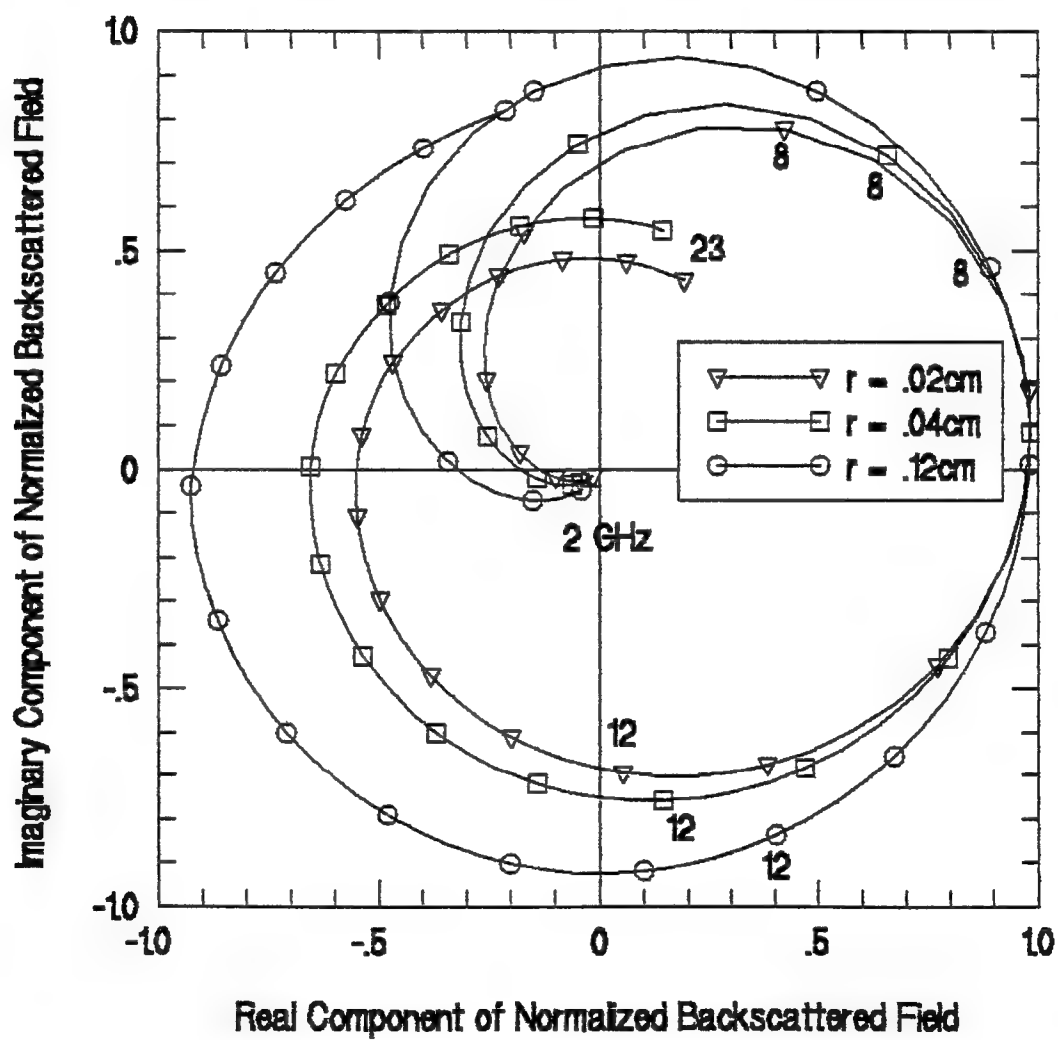


Figure 4-27 The Effect of Varying The R Parameter in The Hoser Code For One Layer

Baseline 6.22 GHz Layer with Three Arrays

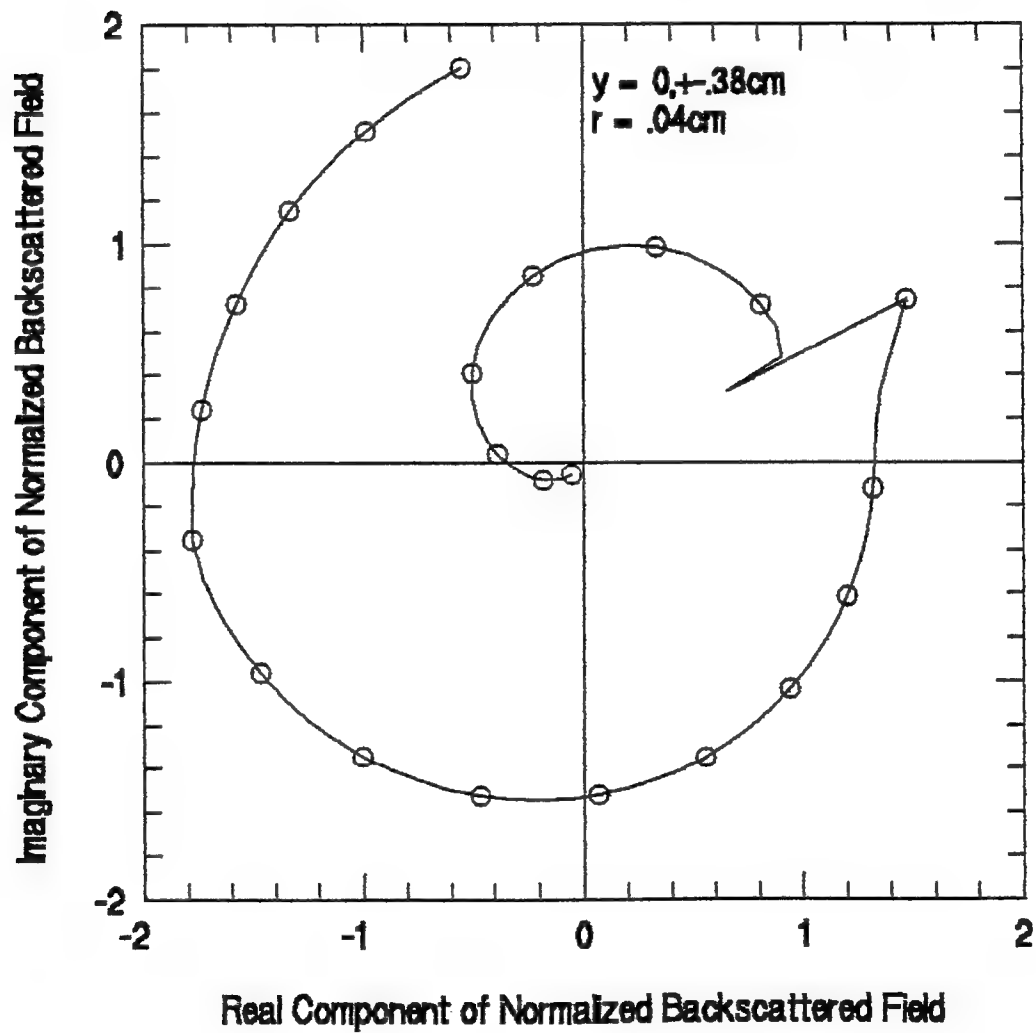


Figure 4-28 The Hoser Code Output For The Baseline One Layer Three Array Design

Effect of Varying Number of Arrays for One Layer Design at 6.22GHz

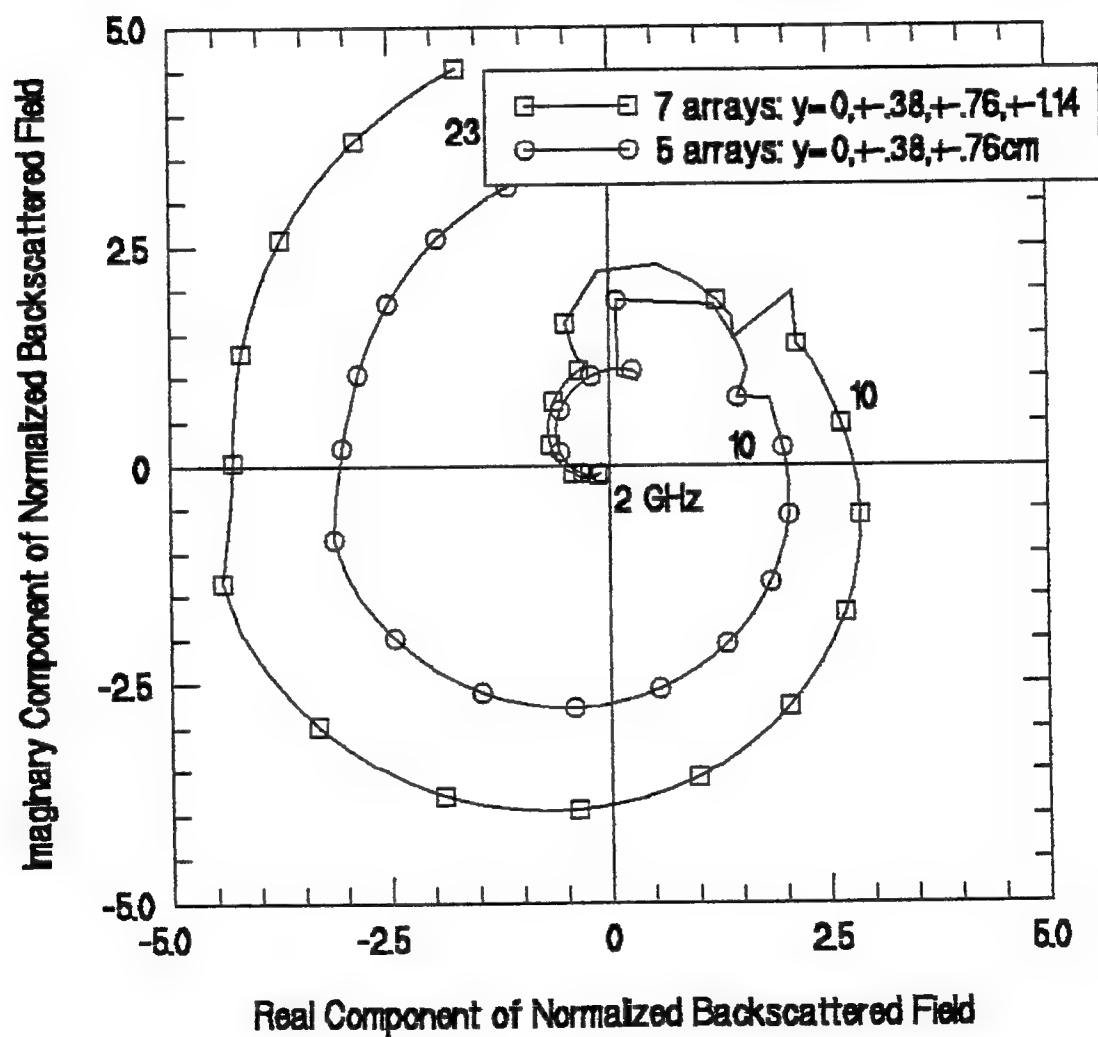


Figure 4-29 The Effect of Adding More Arrays To The Baseline Design

Effect of Varying DY for One Layer Design at 6.22 GHz with Three Arrays

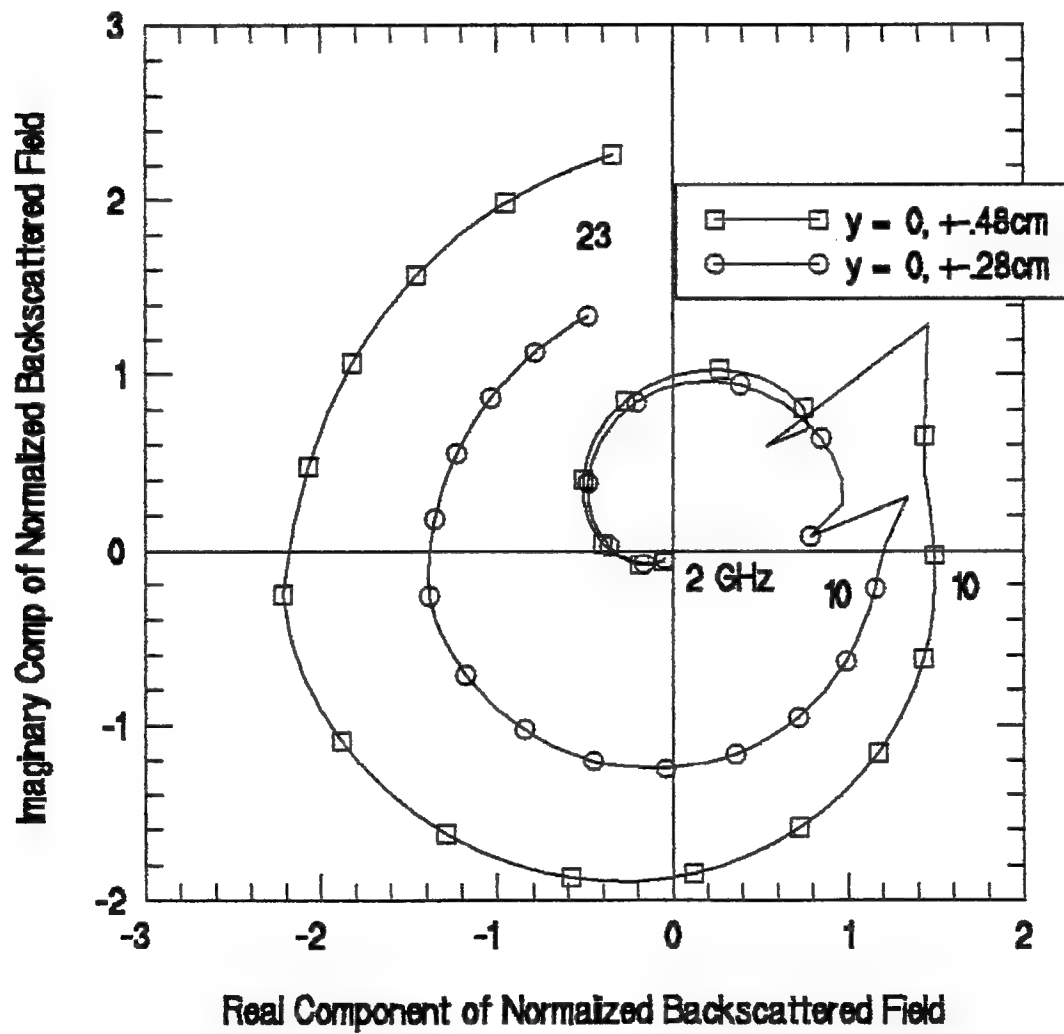


Figure 4-30 The Effect of Varying DY In The Baseline Design

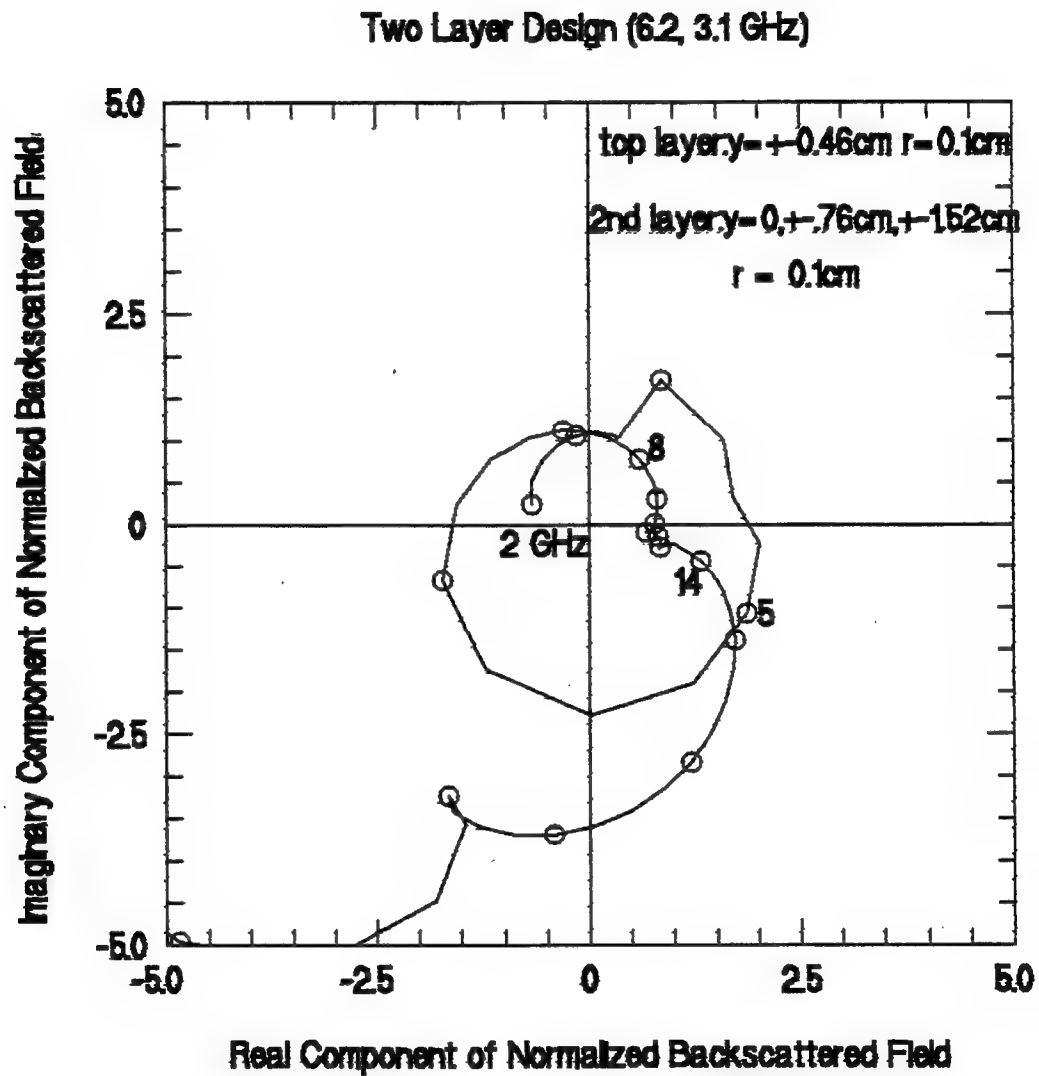


Figure 4-31 The Best Two Layer Design As Predicted By The Hoser Code

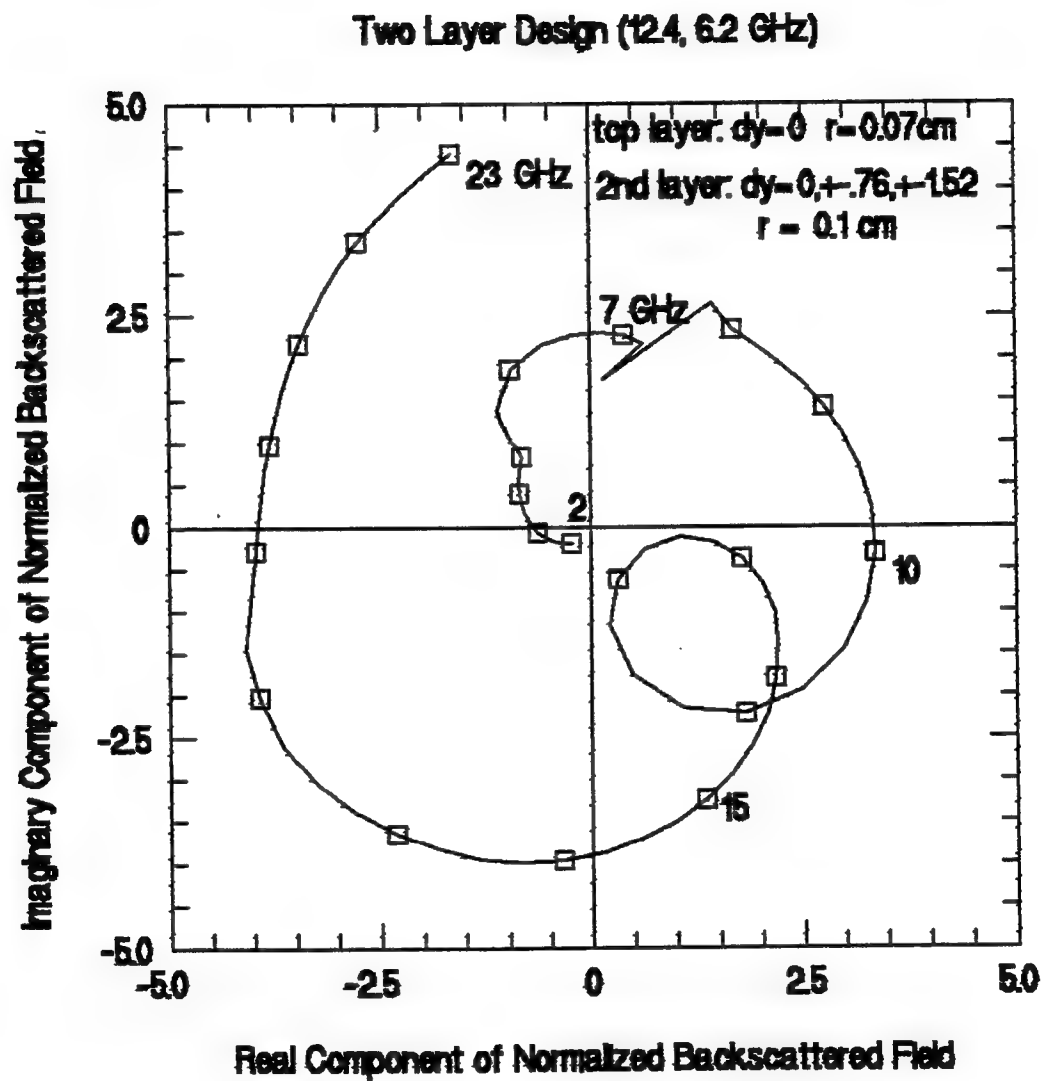


Figure 4-32 The Hoser Code Output Associated With An Alternative Two Layer Design

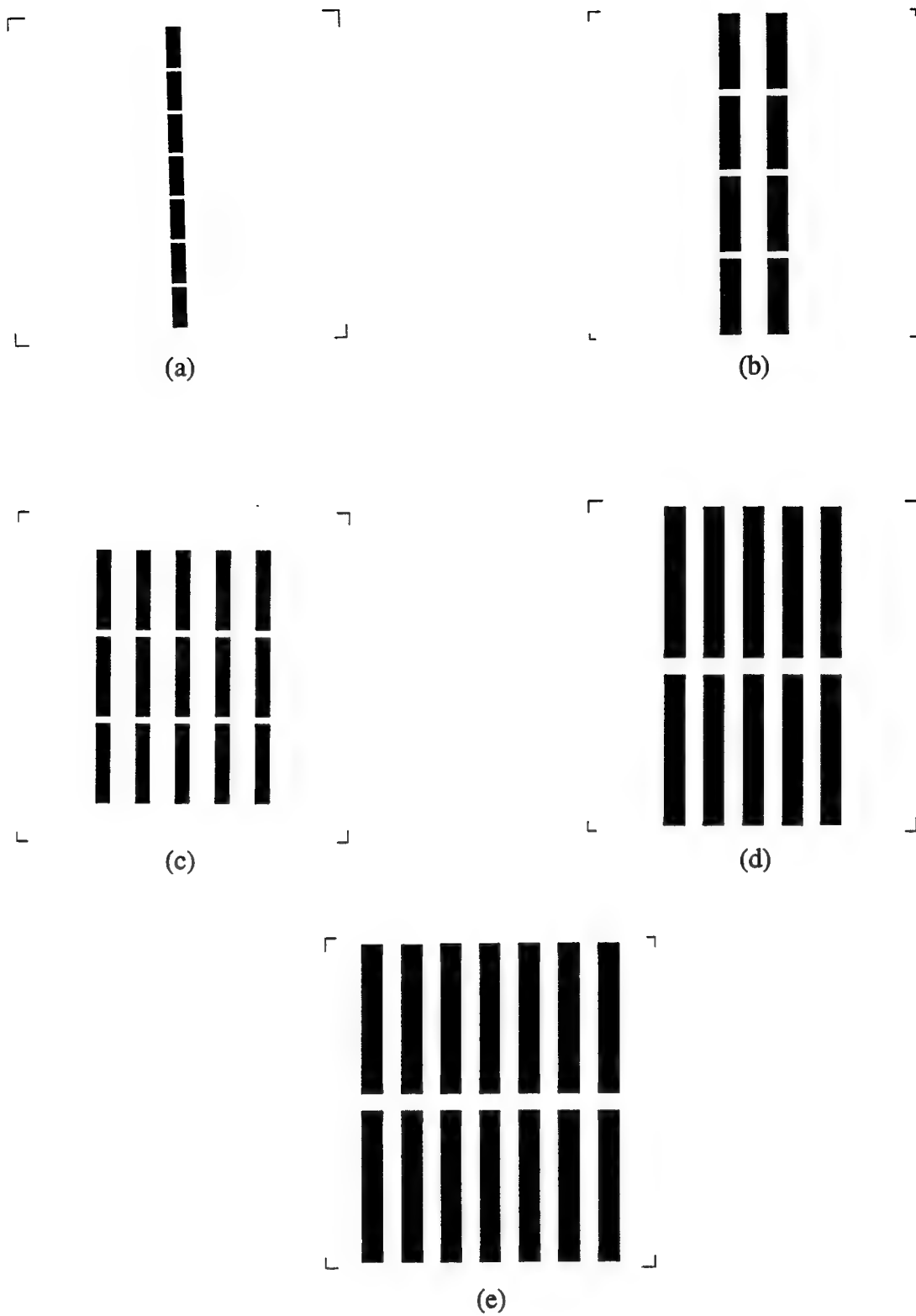


Figure 4-33 The Five Fabricated Slabs Containing Scatterers; (a) corresponds to the first entry in Table 4.4 whereas (e) corresponds to the final entry in Table 4.4

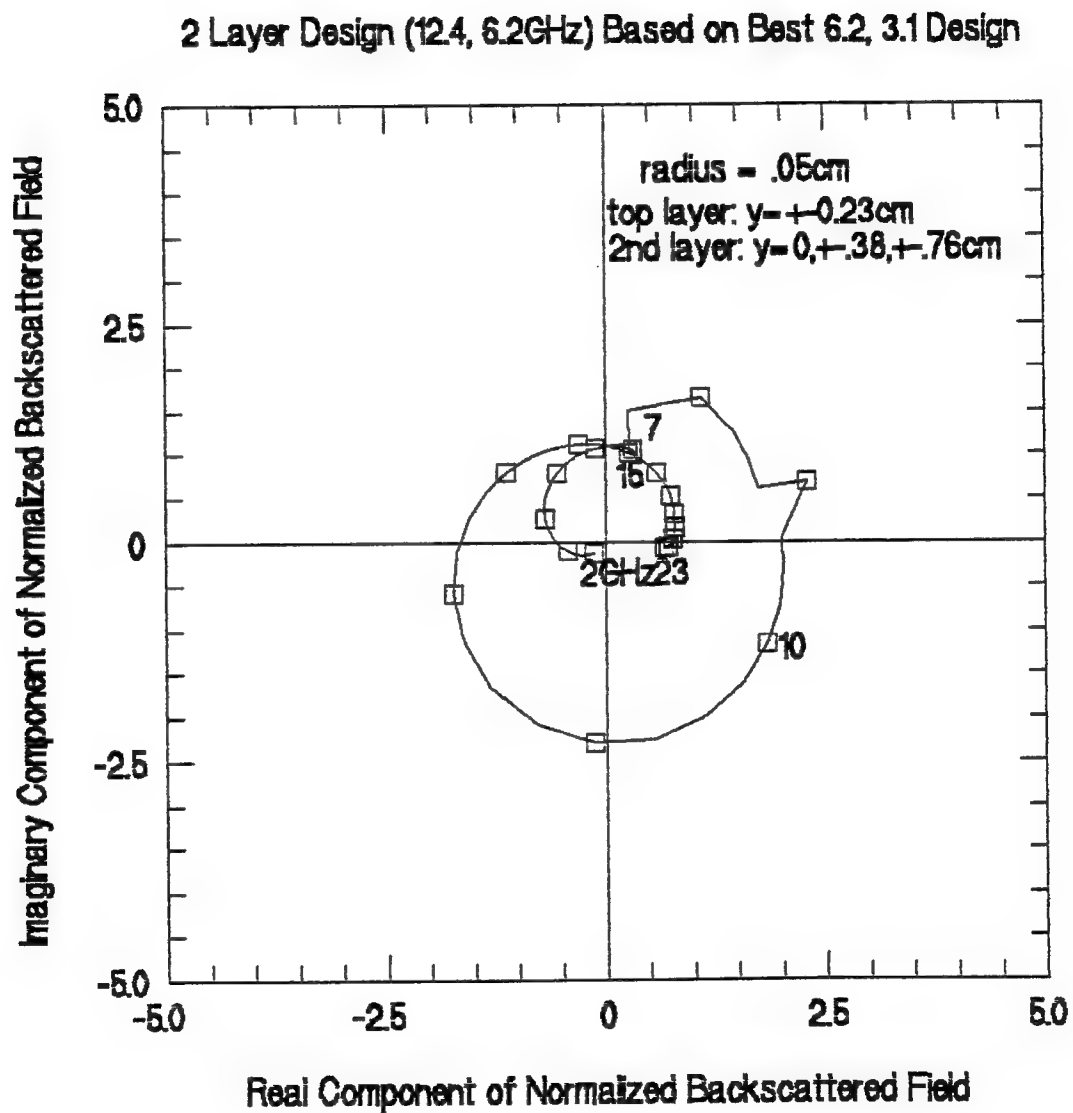


Figure 4-34 The Hoser Code Output Associated With A Third Two Layer Design

The Hoser Code Output Associated With The Best Three Layer Design

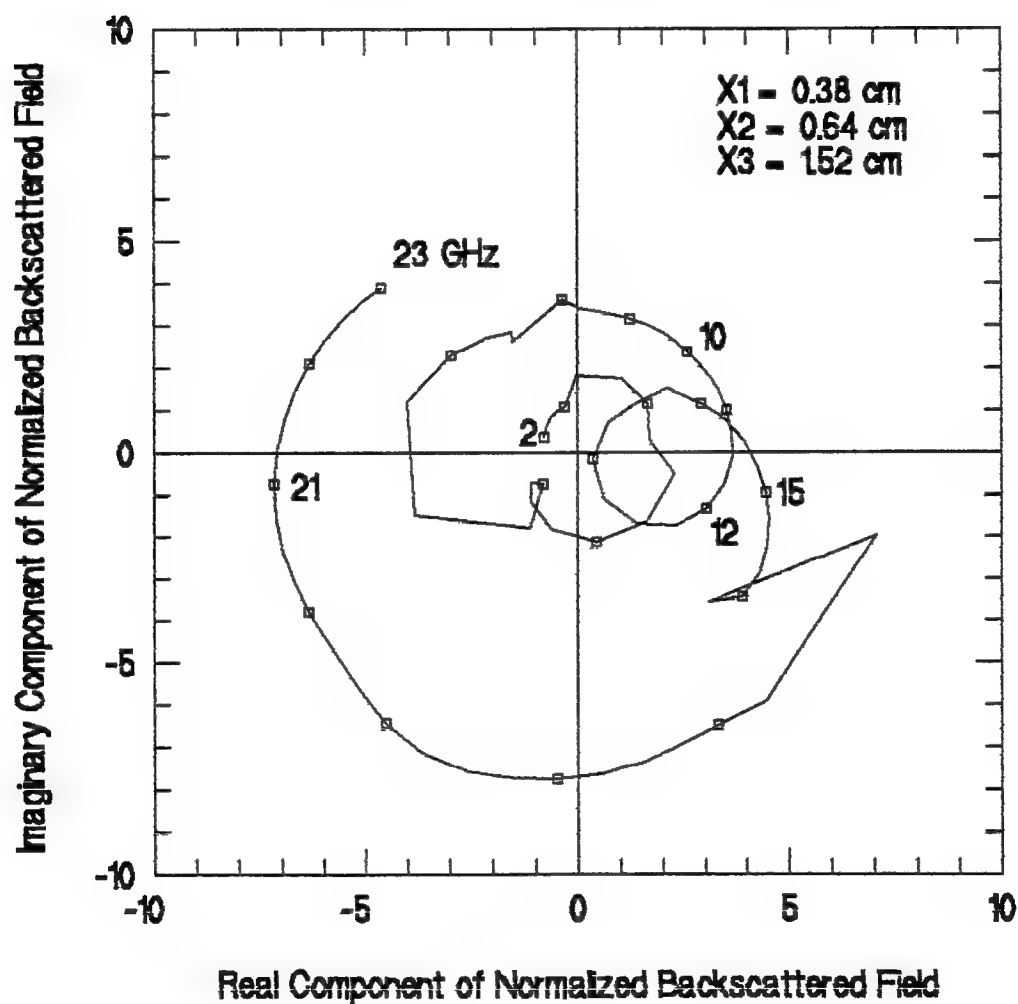


Figure 4-35 The Hoser Code Output Associated With The Best Three Layer Design

5. Antenna & Feed Design

The log periodic trapezoid wire antenna used for testing is pictured in Figure 5-1. This antenna was chosen rather than a spiral antenna due to polarization considerations, for linearly polarized waves were desired. The antenna was placed at the top of the cavity such that its radiating elements were parallel to the z directed arrays of scatterers in the cavity.

The design approach for the log periodic antennas involved assuming the dielectric constant to be the average of air and the substrate material. This resulted in a value of 1.75. Then an iterative approach was used based on the method of keeping the ratios of the distances between adjacent pairs of dipoles the same as the ratio of the length of adjacent dipoles[1]. The results of this method are included in the table below where the ratio described above is 1.215 and dx is the separation between adjacent elements.

Table (5.1)
Summary Of Log Periodic Trapezoid Wire Design

Dipole length <i>cm</i>	DX <i>cm</i>	Distance from feed <i>cm</i>	Resonant Freq. of of Dipole, GHz
0.700		0.25	16.2
0.8505	.1	0.35	13.33
1.033	.1215	0.4715	10.93
1.2556	.1476	0.6191	9.03
1.5255	.1794	0.7985	7.43
1.8534	.2179	1.0164	6.12
2.2520	.2648	1.2812	5.04
2.7361	.3217	1.6029	4.14
3.324	.3909	1.9938	3.41
4.039	.4749	2.4687	2.81
4.907	.5770	3.0450	2.31

Note from Table 5.1 that this antenna has resonances associated with each dipole. Therefore these resonances must be taken into consideration along with the resonances of the cavity when the radiation pattern results are analyzed.

Since soldering and unsoldering the feed lines to the antenna feed points tended to ruin the antenna after a while (the first antenna lasted 5 soldering-unsoldering cycles), two extra antennas sharing the same dimensions were fabricated.

The third integral part of the antenna besides the cavity and the radiating antenna itself is the feed network. The objective in feeding the antenna was to achieve a constant 180 degree phase shift between the two feed ports of the antenna. In an attempt to achieve this, the input signal carried by a 50 ohm cable was fed into a hybrid device, with a 100 ohm input impedance, that divided the input signal into two signals that were 180 degrees out of phase at the two exit ports. The specified lower and upper frequency limits on the hybrid were 2 and 12.4 GHz respectively. Then two semi-rigid RG58 A/U type coaxial cables of identical electrical length (ideally) with a characteristic impedance of 50 ohms and an outer diameter of 0.2 inches were run from the output ports of the hybrid, through the center of the bottom of the cavity, and up to the antenna's two feed points. The outer conductors of these two cables were shorted together to prevent floating and the exposed inner conductor of each cable was then soldered to one of the antenna's feed points. An area just large enough for the cables to pass through was drilled out of each dielectric slab. Except for the two array dielectric slab in which the dipoles were offset from the centerline, this meant that the center dipole array elements were drilled through. The hybrid and coaxial cables were placed behind the 18 inch by 18 inch metal groundplane, the antenna support unit, that housed the cavity in its center. The hybrid unit, about a 0.3 inches thick, 3 inches wide, and 6 inches long, rested on the hardware that mounted the antenna support unit to the pedestal.

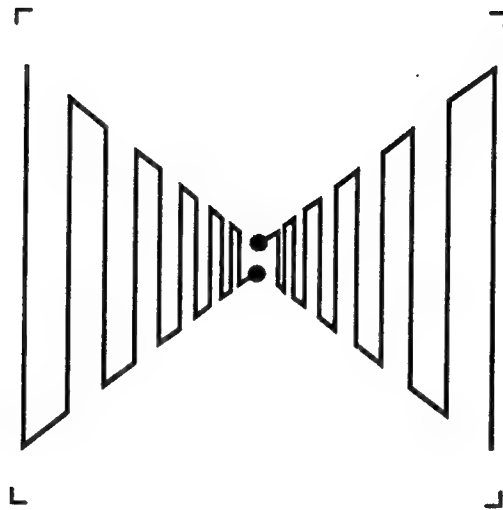


Figure 5-1: Log Periodic Antenna Designed for 2.3 - 16.0 GHz

Chapter 6: Results and Analysis

Five different cavity designs were tested to assess the viability of improving the performance of a cavity-backed log periodic trapezoid wire antenna by modifying its cavity. One design used scatterers just on one dielectric slab, the next three designs used scatterers on two dielectric slabs, and the fifth design used scatterers on three dielectric slabs. Results from these five designs provide sufficient data to conclude that increased gain compared to the traditional absorber-filled cavity design is achievable over certain frequencies by modifying the cavity as done here.

Besides results from the five designs mentioned above, results were obtained for two baseline cases that served as the criteria against which to judge the performance of each cavity design. Recall from Chapter 3 Section 5 that these were the absorber-filled and dielectric-filled cavities. The reader is referred to that section for a review of the test approach.

Measurement errors in the pattern cut and VSWR measurements were small. The peak gain values from the radiation pattern cuts were provided by the test equipment. However, it was necessary to read data points off the pattern cut plots for the normal incidence gain, the bandwidth, and the number of degrees away from normal incidence that the peak gain occurred, known as the squint. Some error may have been introduced in the calibration procedure due to slight differences between the calibration horn and its specifications and because it appeared the calibration curve consisted of measurements taken at integer frequencies with an assumed linear interpolation between these integer frequencies. Reference Appendix E for the calibration data.

Additional factors also contributed to the differences that will be seen between the measured and predicted results. One factor is that the dielectric slabs were not fully flush against each other and that the final layer containing the copper tape was not always perfectly vertical. Increased spacing between the slabs would imply the resonances should

occur at lower frequencies than originally predicted. In addition, radiation that reached the copper tape covered deepest slab was reflected back towards the antenna causing different types of interference as the frequency varied. More importantly, the Hoser code modeled the dipole arrays as infinite by finite geometries and did not model the metal structure that encased the cavity and served as a semi-infinite ground plane. Nor did it model the effect of the feed structure that ran right through the center of the cavity.

Three other factors also contributed to the differences between predicted and measured results. First, there was diffraction from the perimeter of the antenna's support structure as well as scattering from the imperfections in the AFIT mini-chamber. Second, the log periodic antenna had its own resonance frequencies as noted in Table 5.1. This is the one disadvantage of using this type of antenna compared to a spiral antenna which has what one may consider an extended resonance over its bandwidth. Lastly, some patterns exhibited a large amount of squint due to instances of poor feed network performance. Not only did this shift the peak of the radiation patterns to an off center angle, but it also affected the shape of the radiation patterns to a certain extent.

The remaining portion of this chapter will present both radiation pattern cut and VSWR data for each of the seven cavity designs integrated with the feed and 2.3-16 GHz log periodic trapezoid antenna.

6.1 Absorber-Filled and Dielectric-Filled Cavity Designs

Refer to Figure 6-1 for insight into how the VSWR changes as a function of frequency for the absorber-filled cavity. This figure indicates that little energy was coupled from the source to the antenna until the frequency exceeded about 4.3 GHz. The upper frequency of 12.4 GHz was chosen based on the manufacturer's upper limit specification for the hybrid used in the feed network. In later examples, 20 GHz was used as the upper limit to gain insight into the antenna systems' input impedance performance at higher frequencies.

Now refer to Figure 6-2 for the dielectric-filled cavity. Again, little energy was coupled from the source to the antenna until the frequency exceeded about 4.7 GHz. By transforming the data from this figure into the time domain, as done in Figure 6-3, one can gain insight into the relative magnitude and location of the different sources of reflection. Three main peaks are observed. The first peak corresponds to the source to hybrid connection. The second peak corresponds to a reflection within the hybrid. The third peak corresponds to the hybrid to semi-rigid coaxial connections. Had the x axis of this plot continued beyond 4 ns, the reflection from the semi-rigid coaxial to antenna feed point connection, the solder points, would have been observed.

antenna's feed would have been observed. In later examples this fourth peak is displayed.

Figure 6-4 shows both the peak and normal incidence gain values as a function of frequency for the absorber-filled cavity. These values were obtained from the pattern cuts included in Appendix F. Unfortunately, neither the peak nor normal incidence gain is very constant as a function of frequency. This may be due to the interaction of the fields reflected from the cavity with the fields radiating from the antenna which itself is resonant at the specific frequencies listed in Table 5.1. Note the peak and normal incidence gain coincide for only three of the eleven measurements. This condition of not having the peak gain equal to the normal incidence gain, known as squint, is mainly due to the antenna arms not being fed 180 degrees out of phase. Any inhomogeneities in the absorber would also have contributed to the squint.

Figure 6-5 shows the normal incidence and peak gain values as a function of frequency for the dielectric-filled cavity. In this case squint is less of a problem since it occurs in only three of the eleven measured frequencies. The peak and normal incidence gain of the dielectric-filled cavity design exceeded that of the absorber-filled cavity case at all frequencies except near 4 GHz. Refer to Appendix G for the actual pattern cuts associated with this design.

Using an absorber-filled cavity resulted in a -3 dB to -3 dB beamwidth of about 45 degrees from 2-12 GHz as indicated in Figure 6-6. This figure also provides insight into the specific amount of squint observed. Compared to the absorber-filled cavity, the dielectric-filled cavity's design beamwidth was much less consistent, as seen from Figure 6-7. The largest bandwidth was 80 degrees at 12 GHz.

In summary, neither the dielectric-filled nor the absorber-filled cavity designs performed well over the 2-12 GHz band.

6.2 One Layer Design

In this design, the slab containing five dipole arrays, as identified in Figure 4-33(d) and by the fourth entry in Table 4.4, was used as the twelfth of the seventeen layers (where layer one corresponds to the slab closest to the antenna's plane). All sixteen other layers were dielectric slabs without scatterers. The twelfth layer corresponds to a distance below the antenna's plane of $\lambda/4$ at 3.1 GHz. Though good performance, in terms of constant normal incidence gain over extended bandwidths, was not expected, measurements were taken with this design to see if results would show peaks in the gain at multiples of the 3.1 GHz design frequency. In addition, this design was tested because it formed the lowest frequency layer for the best predicted two layer design and, as such, could prove valuable in its analysis.

Figures 6-8 and 6-9 summarize the normal incidence and peak gain as a function of frequency. Data from the pattern cuts in Appendix H was used to create these two figures. Both gains were best at 3.5, 7 and 9 GHz. Surprisingly, both gains at 3 GHz were less than -13 dBi. The only relatively constant gain was the peak gain between 9-11 GHz which exceeded 1.3 dBi by as much as 1.1 dB.

From Figure 6-10 which summarizes this design's beamwidth and squint, note the beamwidth remains relatively constant at about 25 degrees for frequencies above 8 GHz.

Figures 6-11 and 6-12 correspond to the VSWR and time domain reflection data respectively for this one layer design. The VSWR performance is poor until about 6 GHz, slightly worse than the absorber or dielectric-filled cavity. The frequency range on this plot extends out to almost 20 GHz, revealing that the feed worked well even beyond the 12.4 GHz upper limit specification of the hybrid. The time domain data extends out far enough this time to show that the largest average reflection is from the initial source to hybrid connection followed by the reflection from the semi-rigid coaxial to antenna feed point connection.

In summary, this design performed poorly over the 2-12 GHz band.

6.3 Two Layer Designs

Three two layer designs were tested. The designs differed only in the placement of one dielectric slab within the cavity. The deeper scattering layer was chosen to be moved both up and down within the cavity rather than the top layer. One could just have easily demonstrated the sensitivity of the antenna to slight cavity configuration changes by varying the top layer. The objective for this testing was to provide insight into how sensitive antenna performance would be to slight changes in cavity configuration and to gain insight into whether the types of trends observed agreed with those predicted by the Hoser code.

6.3.1 The 6.2 & 3.1 GHz Design. The first two layer run used the same geometry as was used to obtain the best predicted Hoser code output shown in Figure 4-31. The dielectric slabs with two and five dipole arrays identified in Figure 4-33 (b & d) were used as the sixth and twelfth layers of the seventeen layers used in the cavity. The normal incidence and peak gain values as a function of frequency are shown in Figures 6-13 and 6-14 which are based on the pattern cuts included as Appendix I.

Referencing Figure 4-31 one observes that the Hoser code predicted this cavity configuration would contribute constructively to the antenna's radiation pattern at frequencies between 5 and 10 GHz (obtained by dividing 8 and 16 GHz by the square root of the dielectric constant). The actual gain values were no more consistent nor impressively high in this region compared to frequencies outside of this range, implying poor agreement between the model and actual results.

Examining this design's performance at 6.0 GHz one observes that the two dipole arrays used to provide resonance at 6.2 GHz did not perform well at 6.0 GHz. However, by increasing the frequency by 1 GHz, the gain increased by 8.5 dB. If one were to attribute this improved performance at 7.0 GHz to the scatterers on the sixth layer and recall that the one layer case designed for 3.1 GHz exhibited improved performance at 3.5 GHz, one could conclude that the actual resonant frequency of the layers containing scatterers is about 15% higher than expected.

As indicated in Figure 6-15 the beamwidth averaged about 42 degrees. It was more constant compared to the beamwidth of the one layer 3.1 GHz design.

From examining the VSWR of this design as shown in Figure 6-16, one sees that it remained below two only for frequencies above about 6.8 GHz. This was worse than either the absorber-filled or dielectric-filled cavity cases but consistent in the sense that the VSWR was much better at the higher frequencies than the lower frequencies.

6.3.2 The 6.2 & 2.7 GHz Design. This design used the same scatterers as in the previous two layer design except that now the slab containing the five dipole arrays was used as the fourteenth layer rather than the twelfth layer. The normal incidence and peak gain values as a function of frequency are shown in Figures 6-17 and 6-18. These figures are based on the pattern cuts included in Appendix J. Surprisingly, except for a slight dip near 2, 3.5, and 8 GHz, this design provided gains typically exceeding 0 dBi, with a peak of 7

dBi at 2.25 GHz. However, this performance is still poor because the gain does not vary less than 3 dB over any significant bandwidth.

The Hoser code output associated with this cavity configuration is shown in Figure 6-19. It predicts the most constructive interference near 2.7 and 7.6 GHz (4.2 and 12 GHz divided by the square root of the slabs' dielectric constant). Whereas the gain at 2.7 GHz exceeds 0 dBi, the gain at 7.5 GHz is less than -3 dBi.

Figure 6-20 provides beamwidth and squint values as a function of frequency for this design. The bandwidth at frequencies below 7.5 GHz exceeds 50 degrees, peaking at a full 105 degrees at 5.75 GHz.

The VSWR as a function of frequency is provided in Figure 6-21. This design has a VSWR less than two for frequencies exceeding 4.6 GHz, similar to the results obtained for the dielectric-filled cavity design. Note that the frequency range on this plot extends out to almost 20 GHz, revealing that the feed worked well even beyond the 12.4 GHz upper limit specification of the hybrid.

Consistent with results from previous cavity designs, the time domain plot in Figure 6-22 reveals that, on average, the largest source of reflections is from the source to hybrid connection followed by the return from the coaxial to antenna feed point connection.

6.3.3 The 6.2 & 3.7 GHz Design. This design used the same scatterers as in the previous two layer design except that now the slab containing the five dipole arrays was used as the tenth layer rather than the fourteenth layer. Figures 6-23 and 6-24 provide normal incidence and peak gain values as a function of frequency. These figures are based upon the data obtained from the pattern cuts included in Appendix K. As with each design to this point, there was no extended bandwidth over which the gain fluctuated by less than 3 dB. This design's most constant frequency range at normal incidence was from 6 to 7.25 GHz where the gain averaged about -0.8 dBi.

The Hoser code output associated with this cavity configuration is provided in Figure 6-25. Unlike the output associated with the 6.2 & 3.1 GHz design in Figure 4-30, this output predicts rather poor performance since there is no condensed grouping of frequencies that share a position on or near the positive part of the x axis. Instead, this output predicts that the cavity will provide constructive interference at the antenna's plane at 3.3, 5.8 and 12 GHz. At 6 GHz, the gain is about 0 dBi with a 55 degree beamwidth, which is better than most but not all normal incidence gain values. Interestingly, at 12 GHz the antenna provided its peak gain, 6.7 dBi, with zero squint and a 23 degree -3 dB to -3 dB beamwidth. Based on the fact that the frequencies predicted by the Hoser code to yield the best results with earlier designs did not consistently agree with the measured results, one can conclude that this agreement at 12 GHz is a coincidence.

Figure 6-26 provides the beamwidth and squint as a function of frequency for this design. As with the last design, there is one instance in which the beamwidth exceeds 100 degrees; it is 115 degrees at 6.3 GHz.

The VSWR information contained in Figure 6-27 is consistent with earlier measurements in that the VSWR is very poor for low frequencies but remains below 2 for frequencies above about 8 GHz.

Again, the time domain plot in Figure 6-28 reveals that, on average, the most significant source of reflections is the source to hybrid connection.

Comparing the gains of these three two layer designs, as done in Figures 6-29 and 6-30, one can see that the 6.2 & 2.7 GHz design provides the most consistent gain as a function of frequency and it provides the best gain at frequencies up until 6 GHz, though at frequencies lower than 4.6 GHz the VSWR unfortunately exceeds two.

6.4 Three Layer Design

The Hoser code predicted that the best design using the slabs etched with 1, 5, and 7 dipole arrays, identified in Figure 4-33 (a), (c), (e), corresponded to placing these three slabs at the third, fifth, and twelfth layers of the cavity, respectively. From this configuration's Hoser code output predicted in Figure 6-31, one expects the cavity to provide constructive interference in the antenna's plane mainly in the 7-9.5 GHz range (obtained by dividing 11 and 15 GHz by the square root of the slabs' dielectric constant). By reviewing the measured gain information in Figures 6-32 and 6-33 (which are based on the pattern cuts included in Appendix L), one can conclude that the performance between 7-9.5 GHz is not particularly better than the performance over similar bandwidths elsewhere. In addition, the normal incidence gain figure shows that the magnitude of the maximum and minimum gains have increased slightly compared to the one and two layer designs. Though the peak gain varied much less than the normal incidence gain, it still lacked the consistency that characterizes a good antenna.

Figure 6-34 provides insight into how the beamwidth and squint vary with frequency for this design. The best beamwidth occurs in the 6-7 GHz region, peaking at 75 degrees at 6.5 GHz.

The VSWR information in Figure 6-35 again implies that little power will be coupled to the antenna until frequencies exceed about 6.8 GHz. Therefore, even if the radiation patterns provided good gain and beamwidth results at frequencies below 8 GHz, the antenna system would be inefficient.

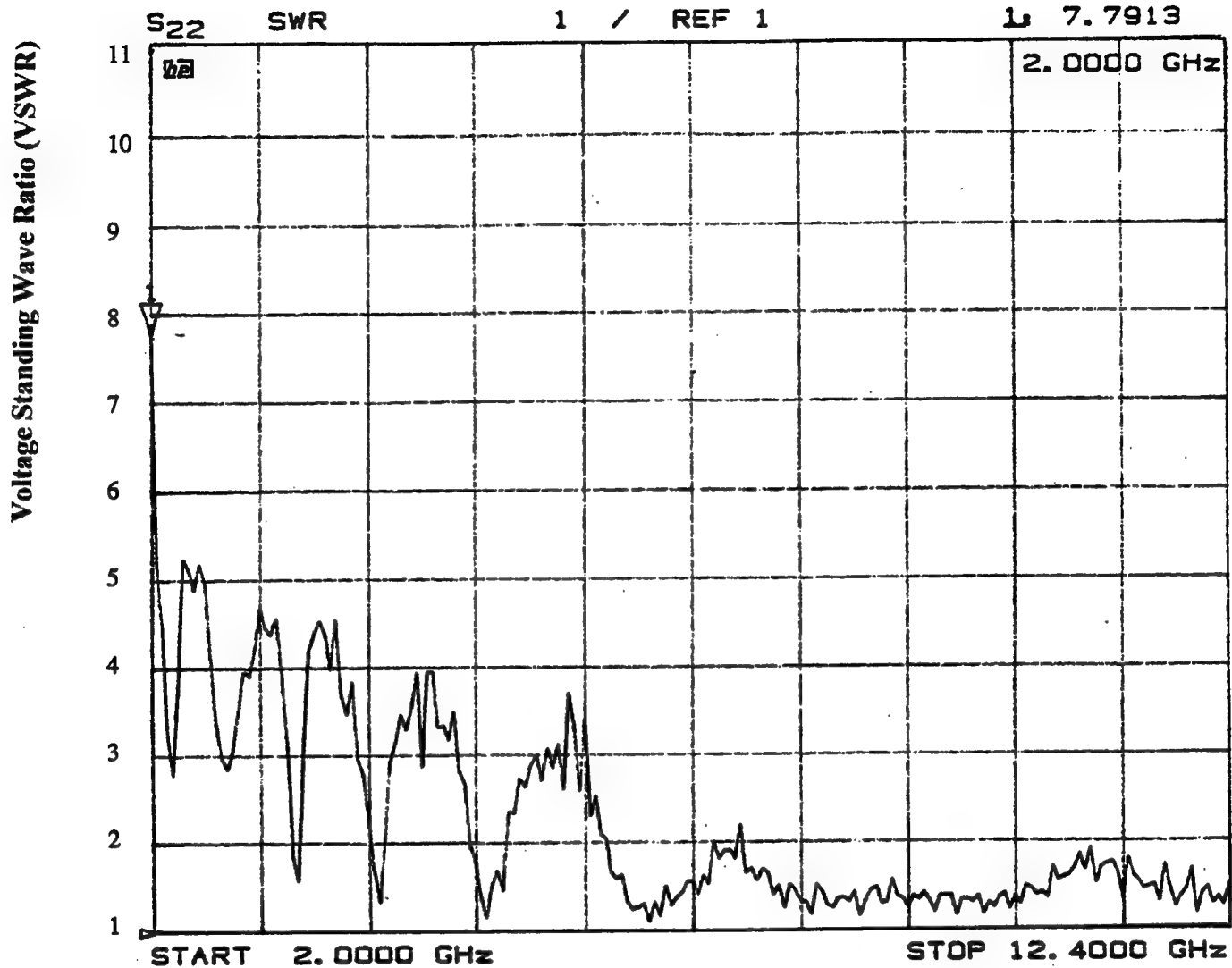


Figure 6-1 VSWR vs. Frequency For Absorber-Filled Cavity

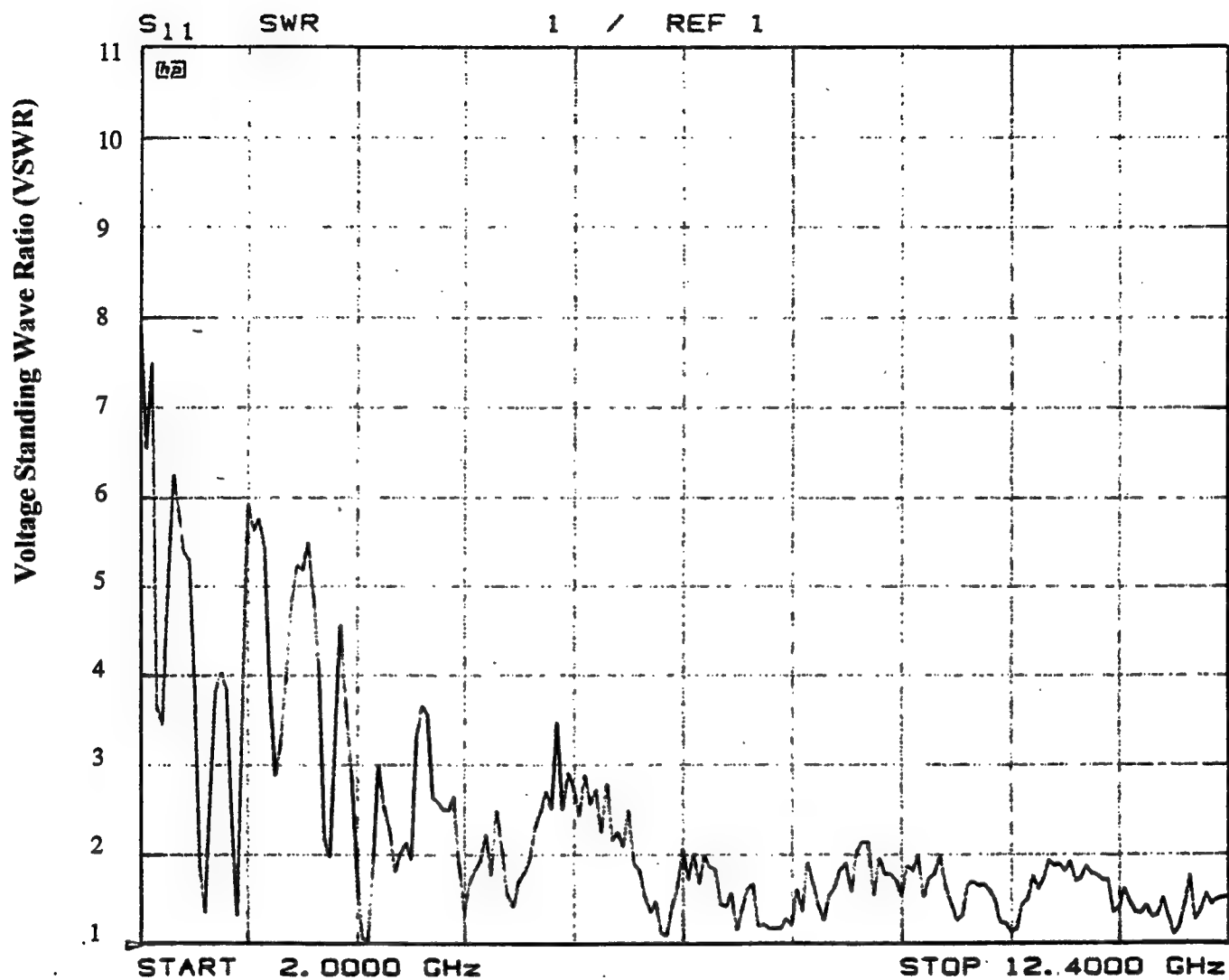


Figure 6-2 VSWR vs. Frequency For Dielectric-Filled Cavity

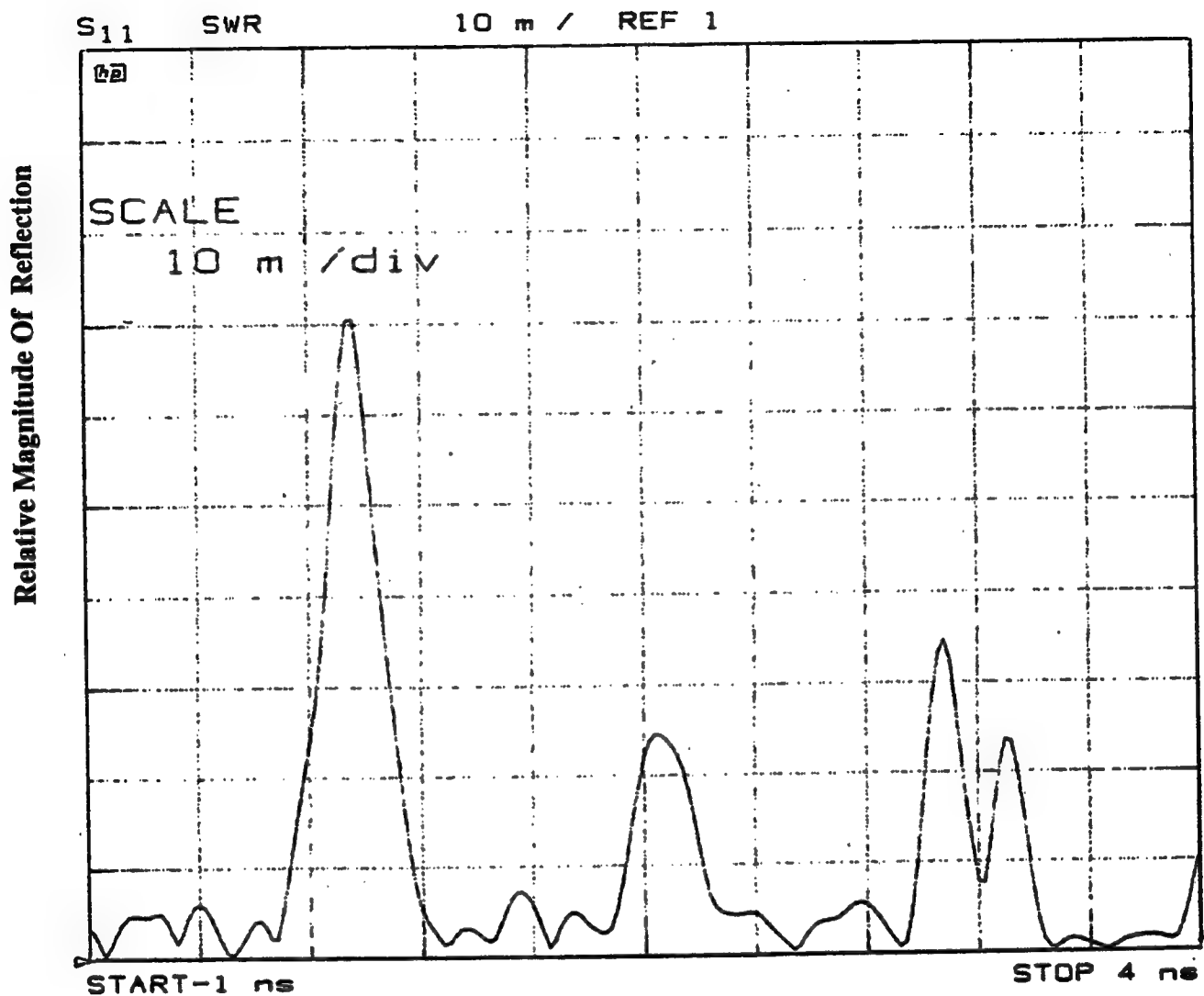


Figure 6-3 Time Domain Plot Containing Reflection Information For Dielectric-Filled Cavity

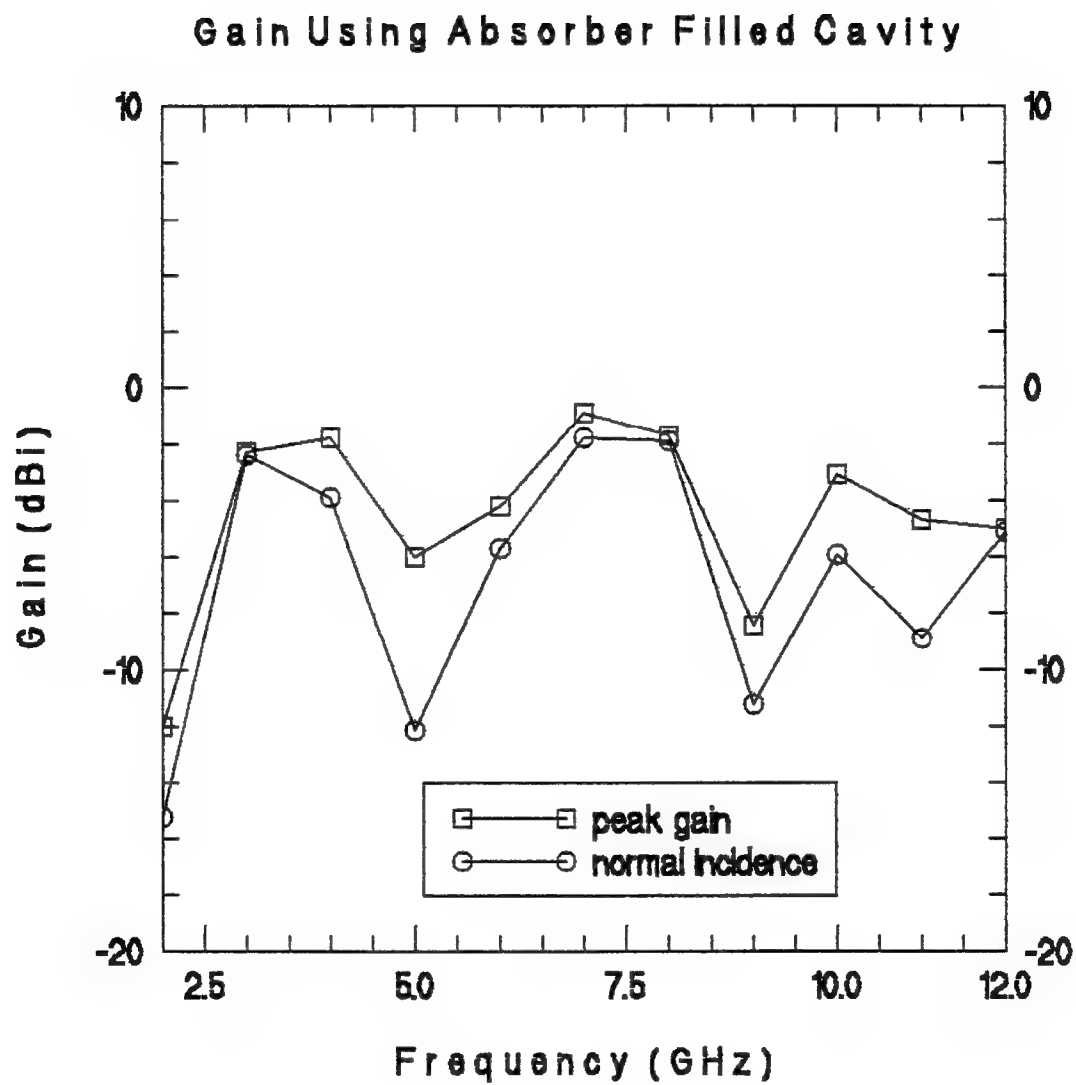


Figure 6-4 Gain vs. Frequency For Absorber-Filled Cavity

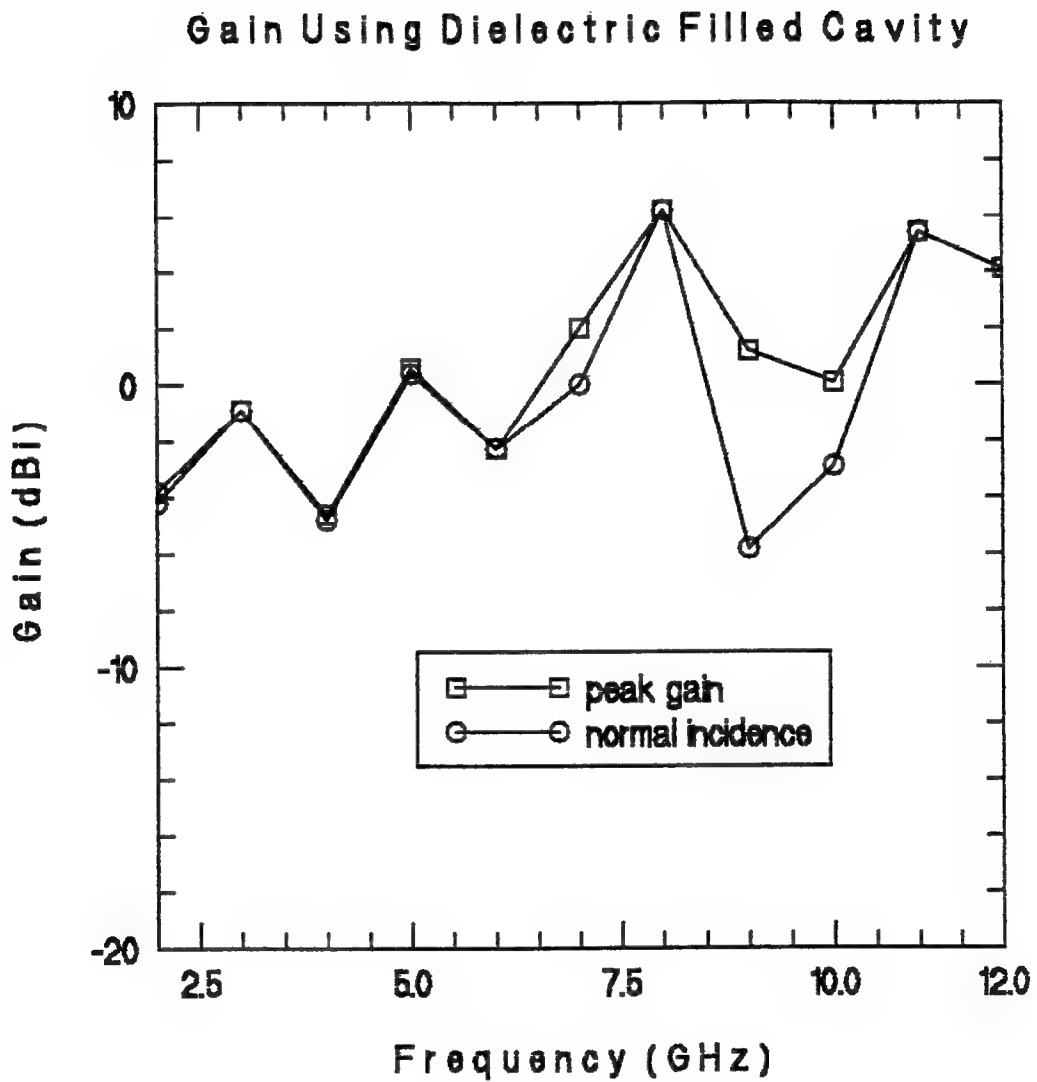


Figure 6-5 Gain vs. Frequency For Dielectric-Filled Cavity

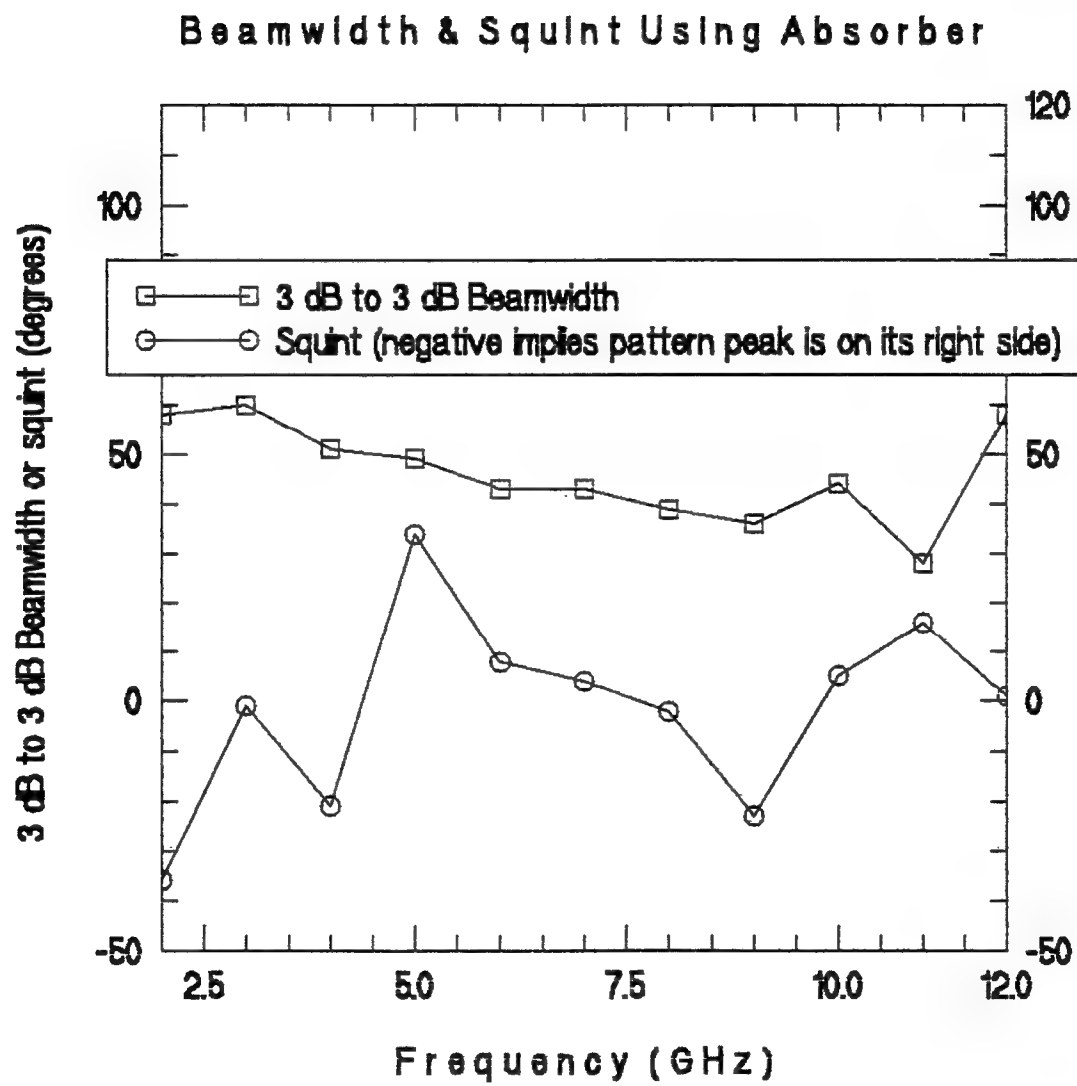


Figure 6-6 Beamwidth and Squint vs. Frequency For Absorber-Filled Cavity

Beamwidth & Squint Using 17 Dielectric Slabs

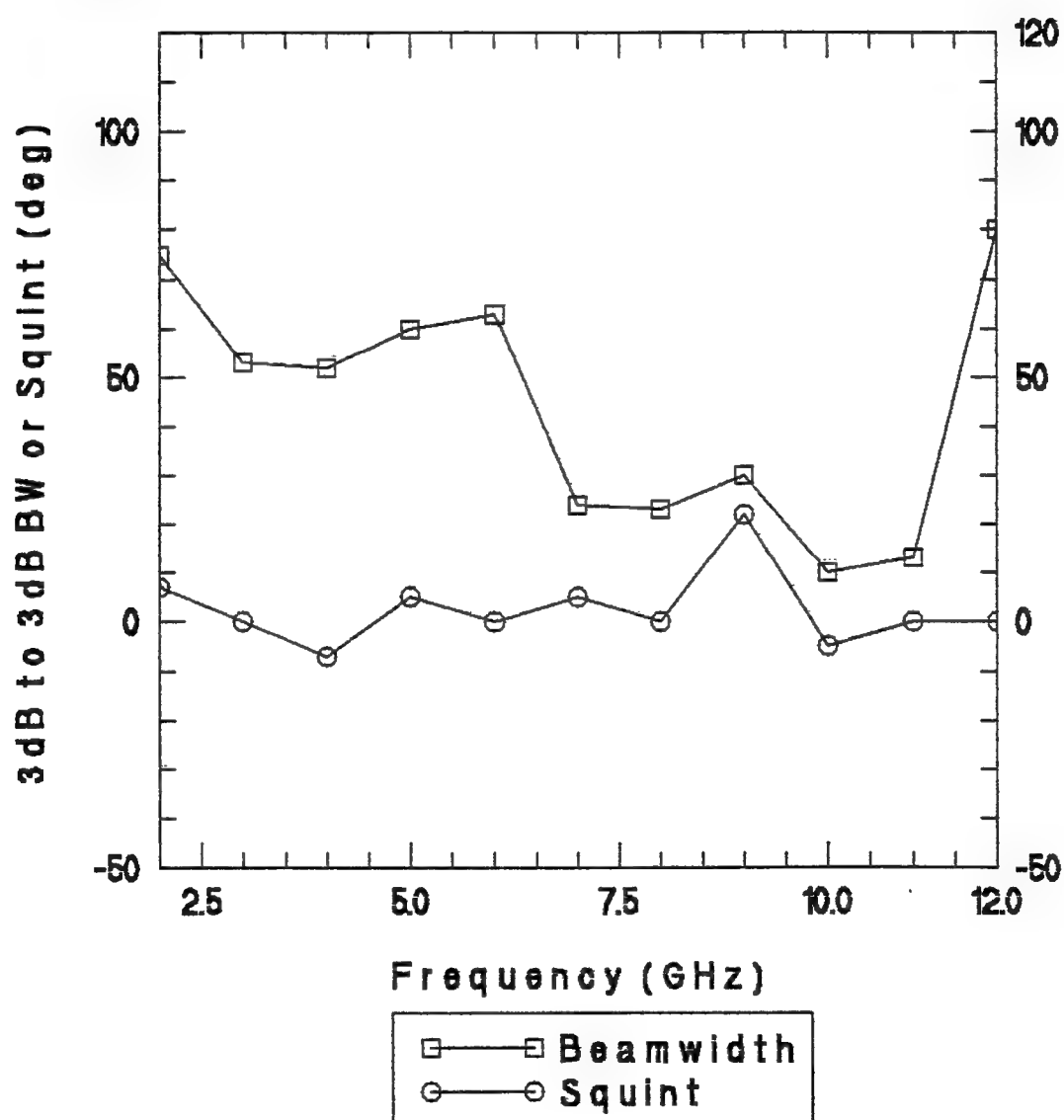


Figure 6-7 Beamwidth and Squint vs. Frequency For Dielectric-Filled Cavity

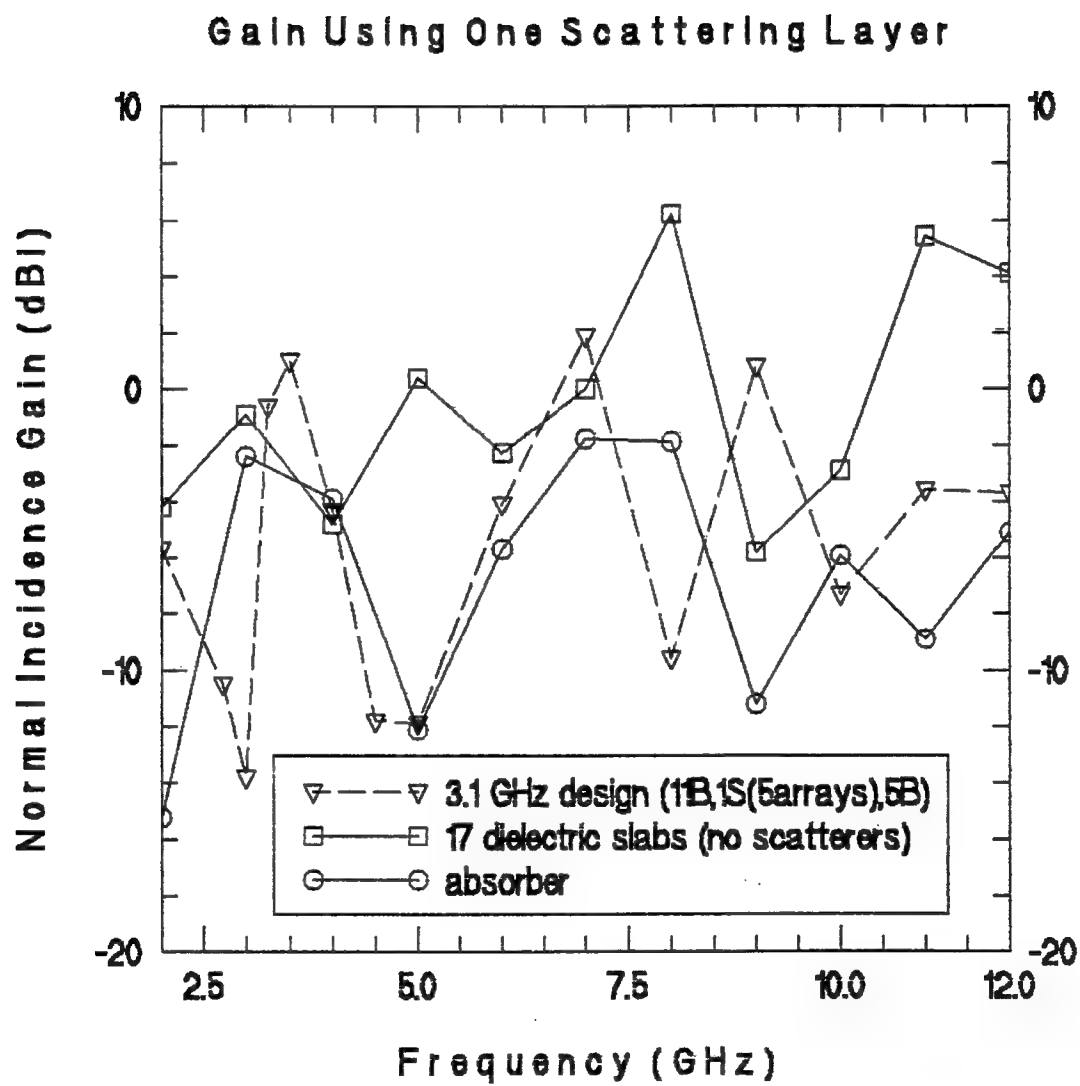


Figure 6-8 Normal Incidence Gain vs. Frequency For 3.1 GHz Design

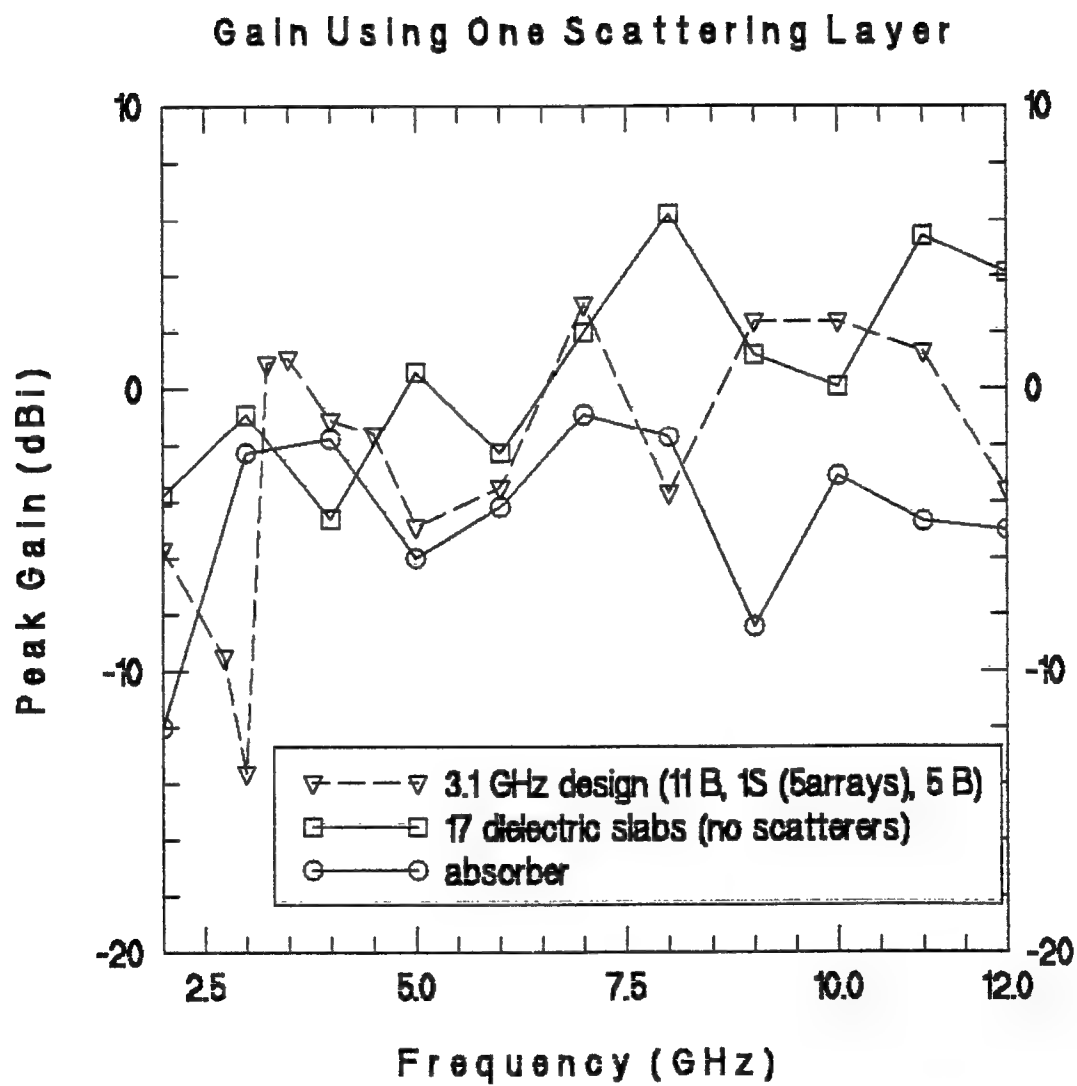


Figure 6-9 Peak Gain vs Frequency For 3.1 GHz Design

Beamwidth & Squint Using 3.1 GHz Design

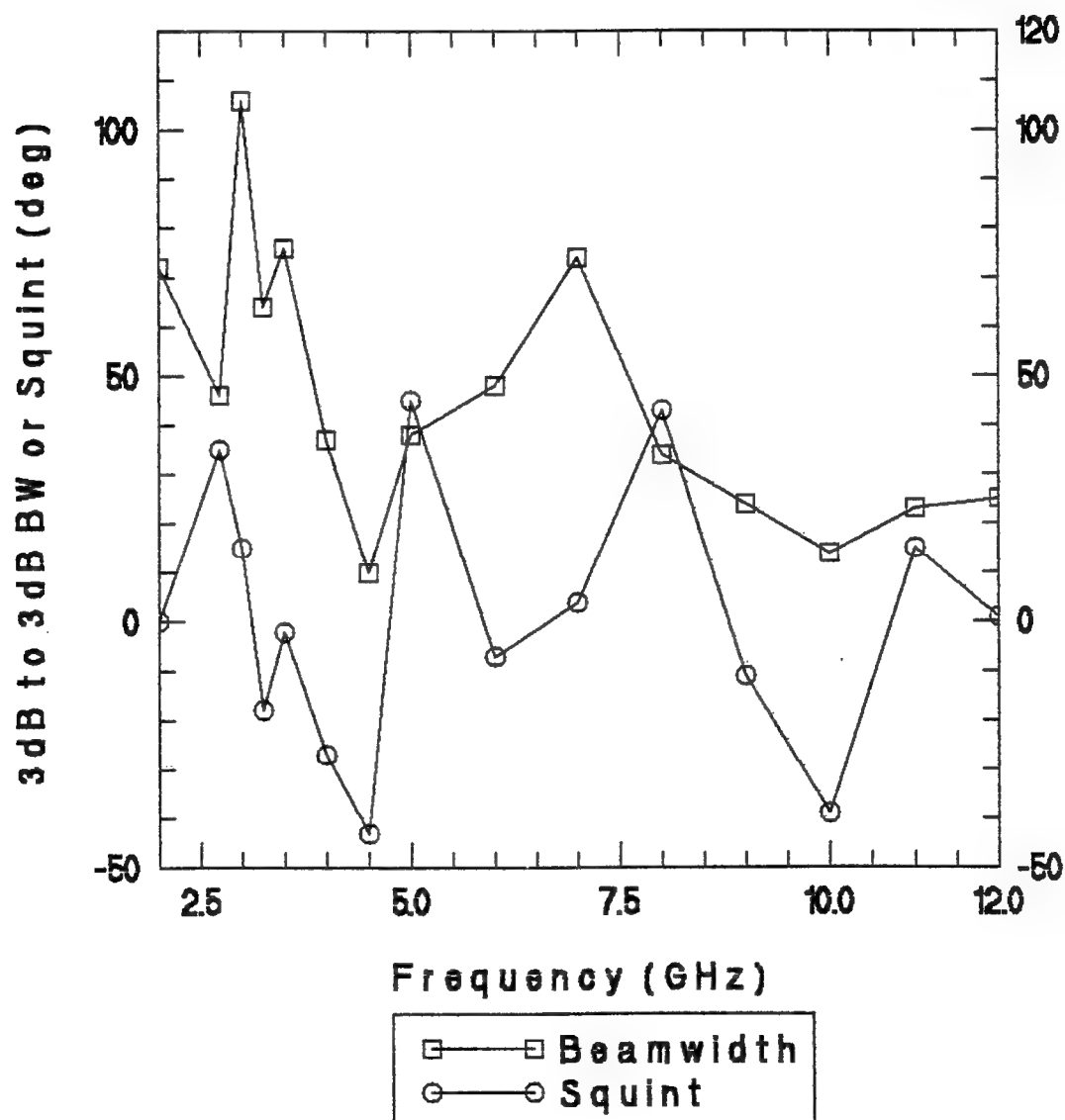


Figure 6-10 Beamwidth and Squint vs. Frequency For 3.1 GHz Design

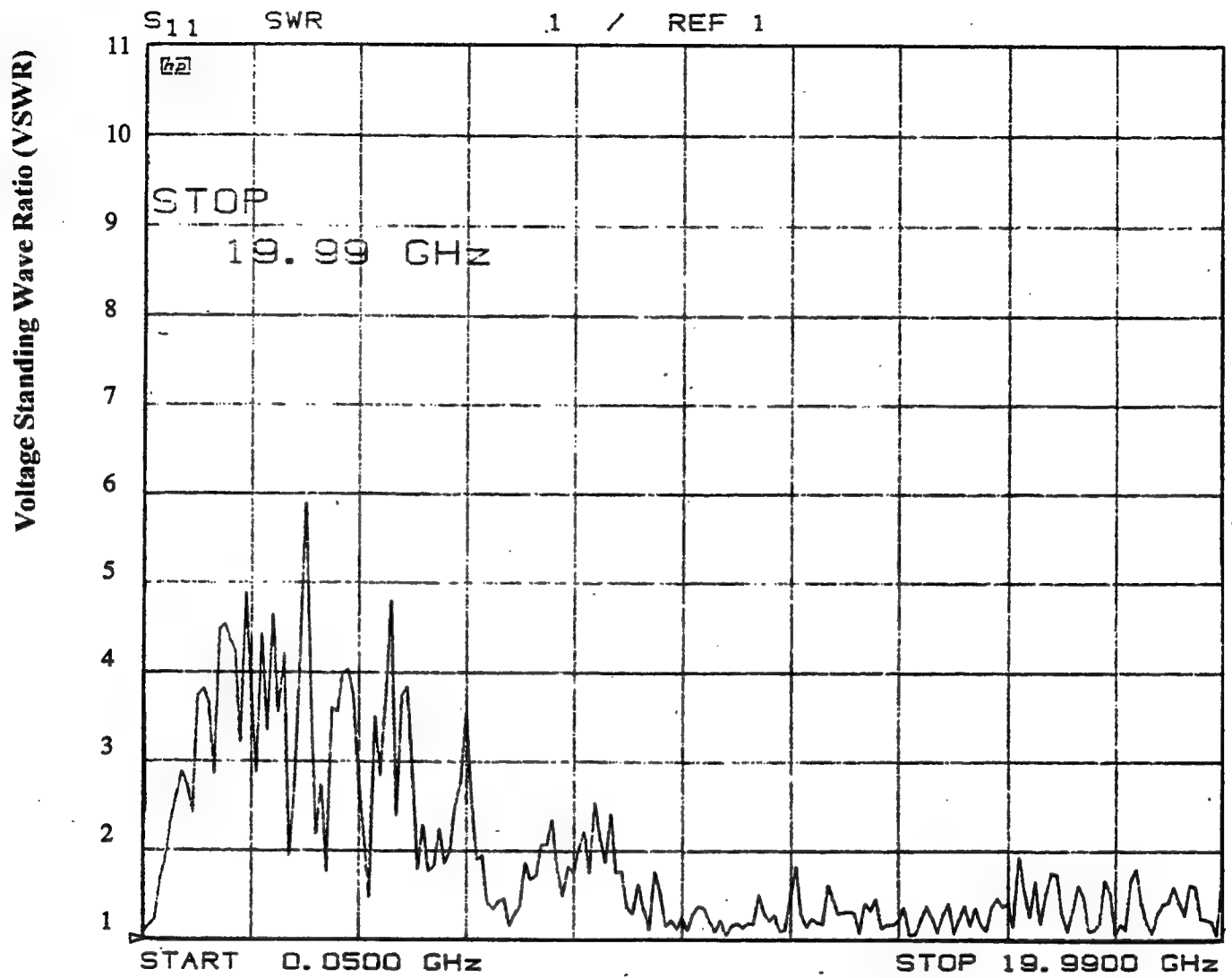


Figure 6-11 VSWR vs Frequency For 3.1 GHz Design

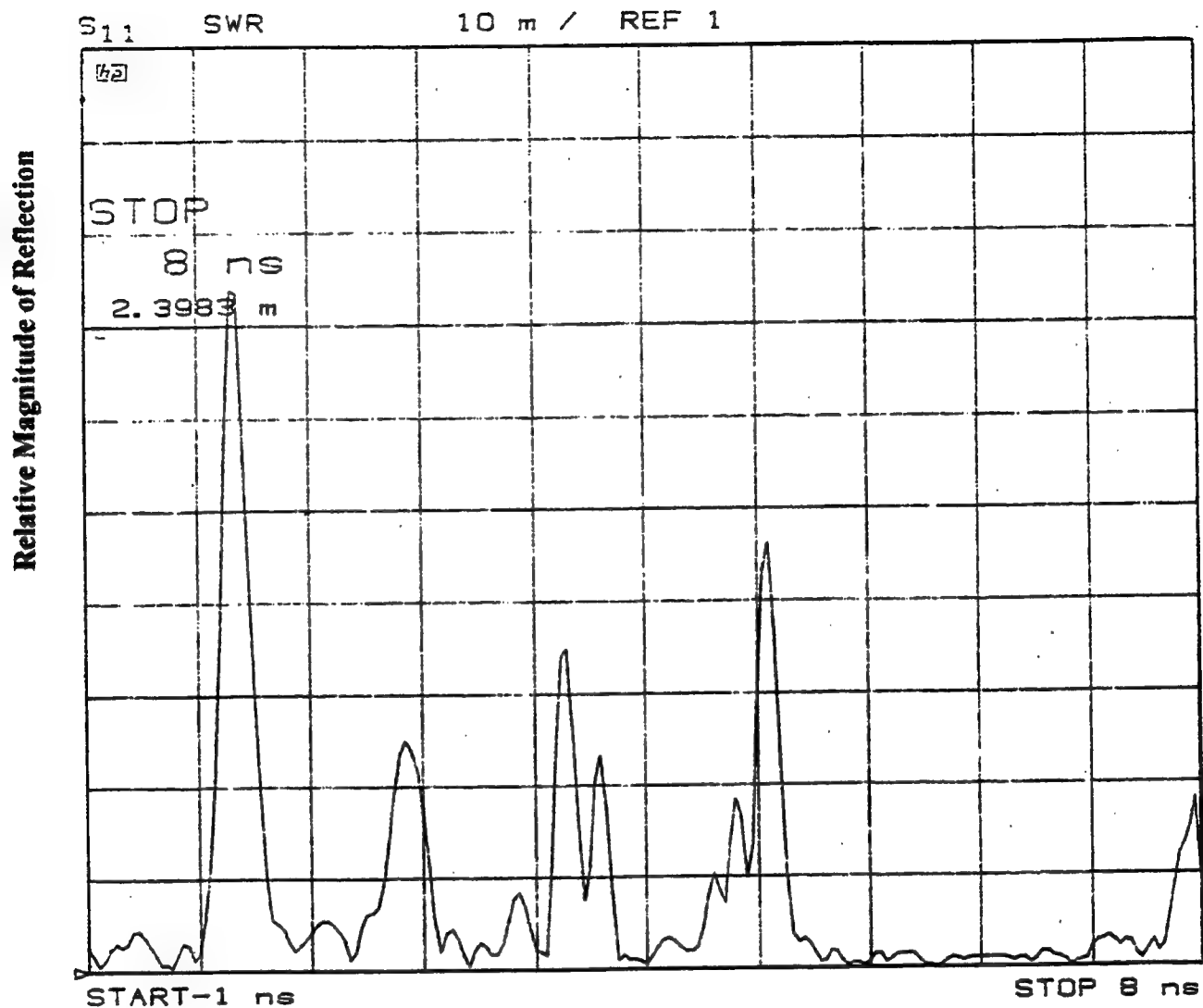


Figure 6-12 Time Domain Plot Containing Reflection Information For 3.1 GHz Design

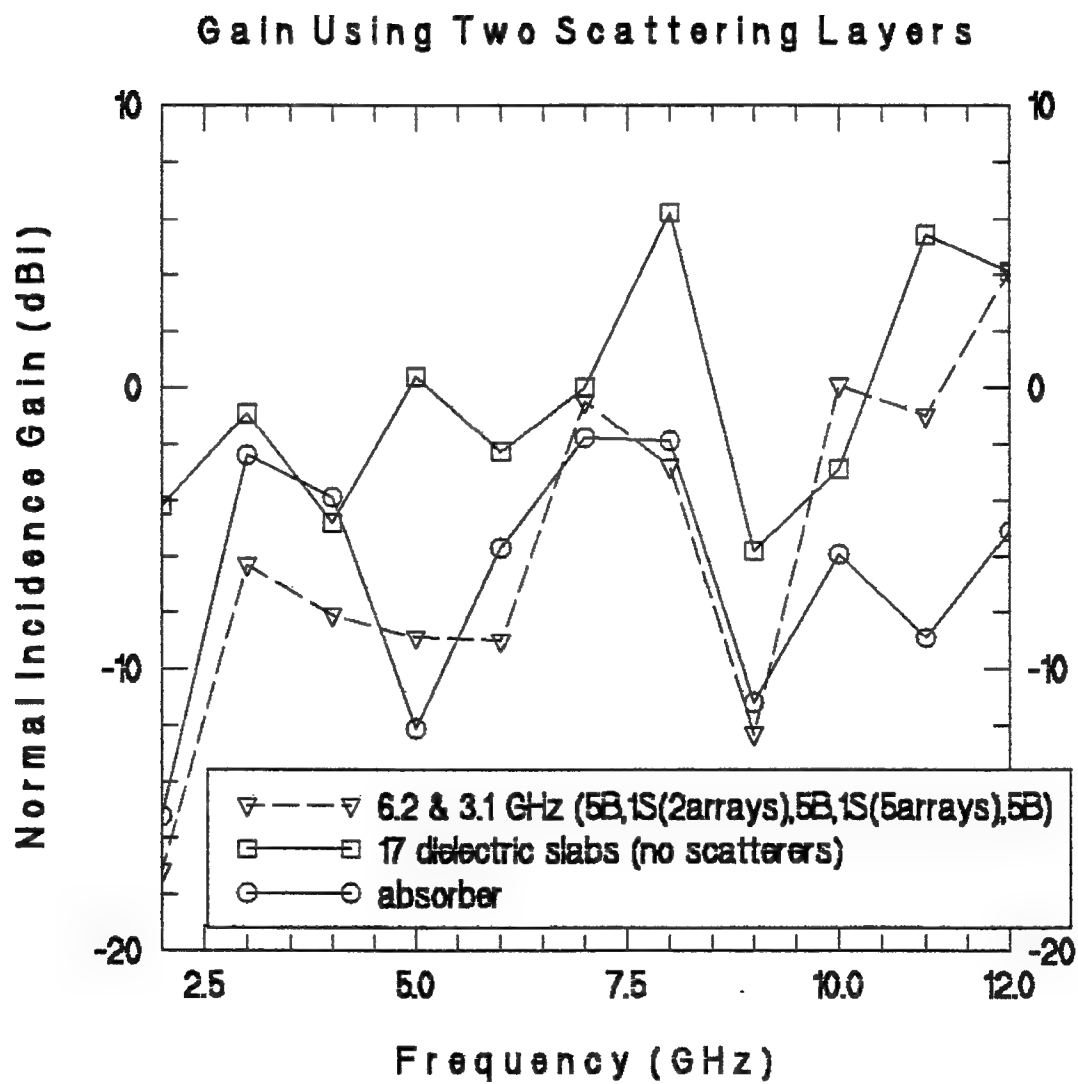


Figure 6-13 Normal Incidence Gain vs. Frequency For 6.2 and 3.1 GHz Design

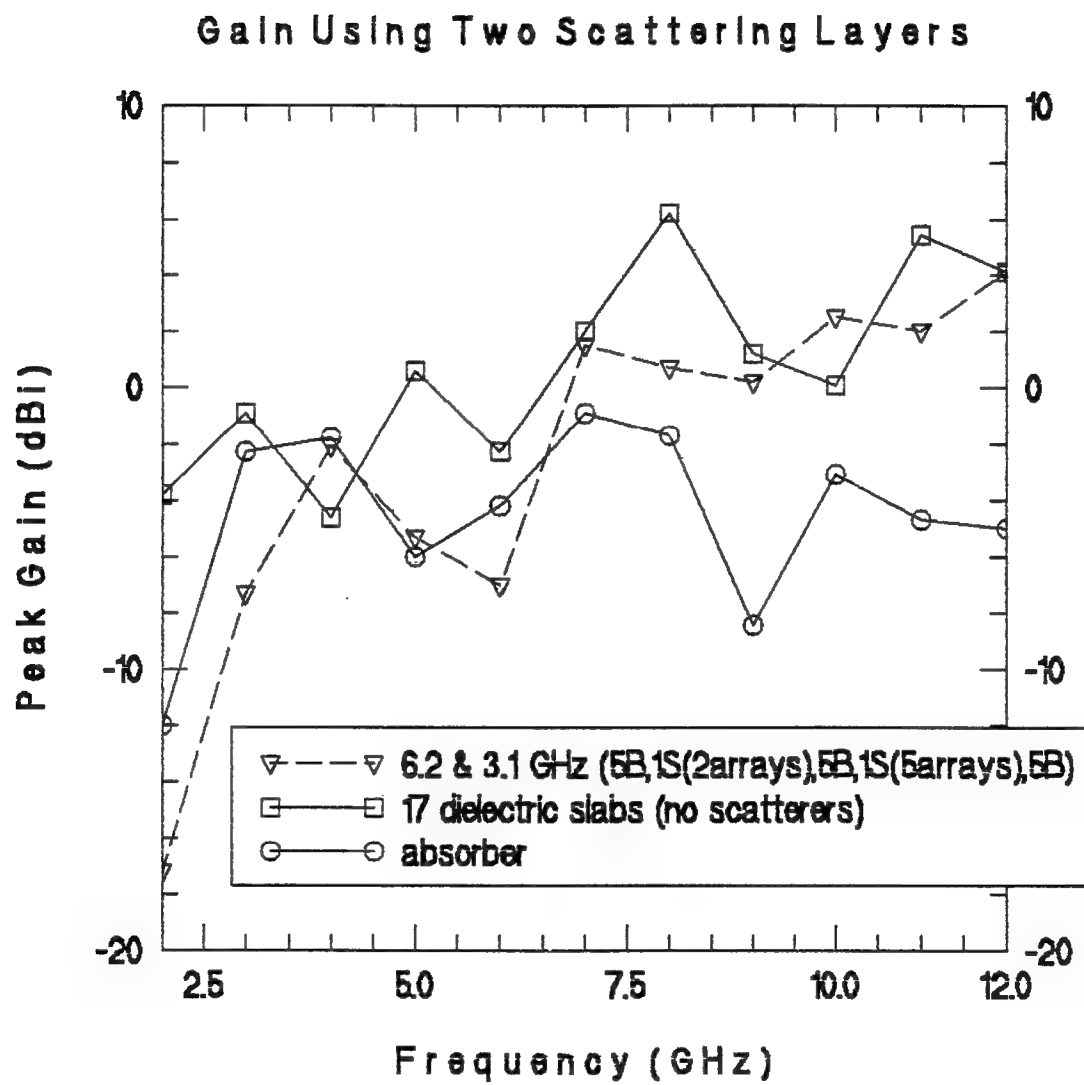


Figure 6-14 Peak Gain vs. Frequency For 6.2 & 3.1 GHz Design

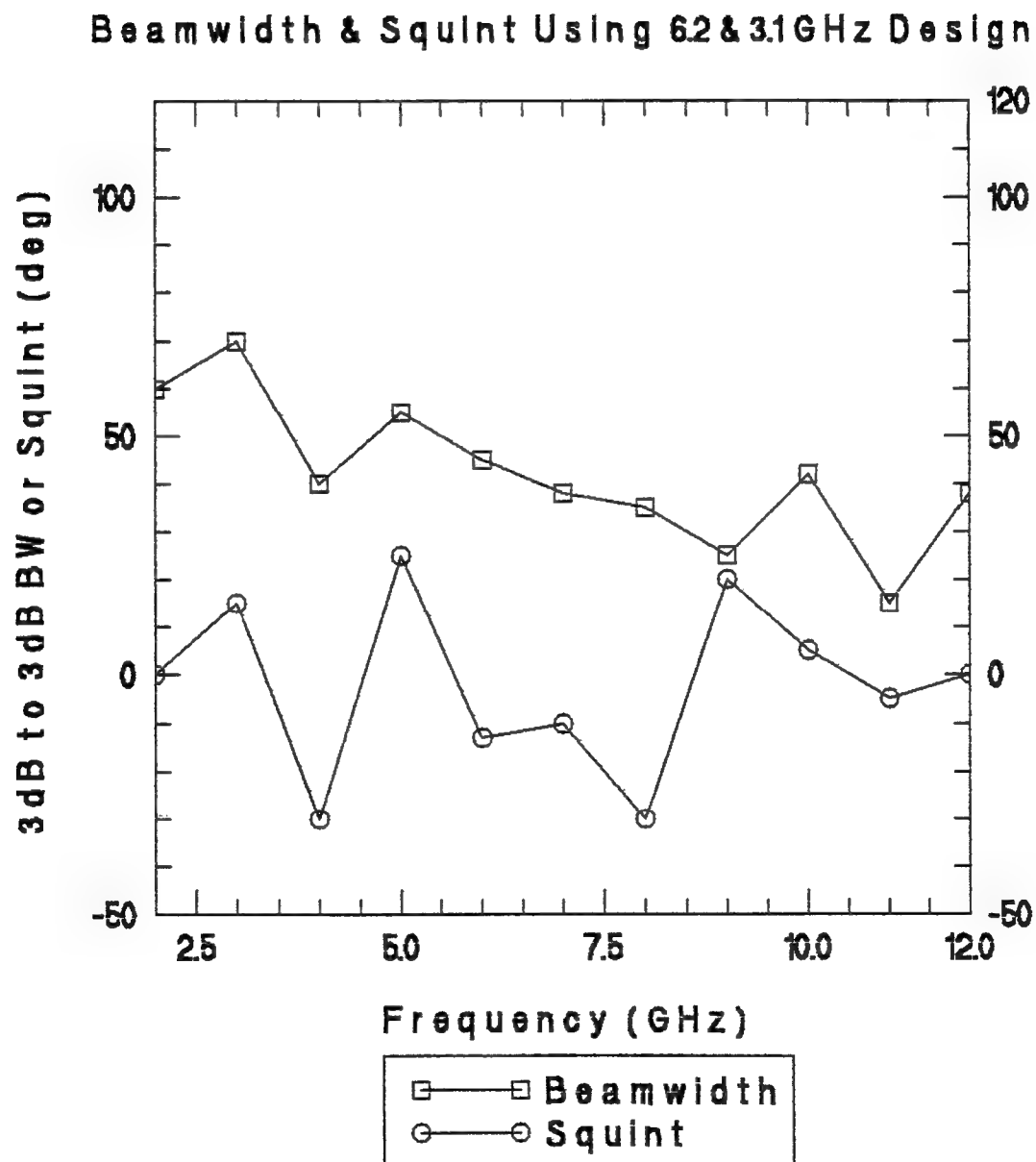


Figure 6-15 Beamwidth and Squint vs Frequency For 6.2 & 3.1 GHz Design

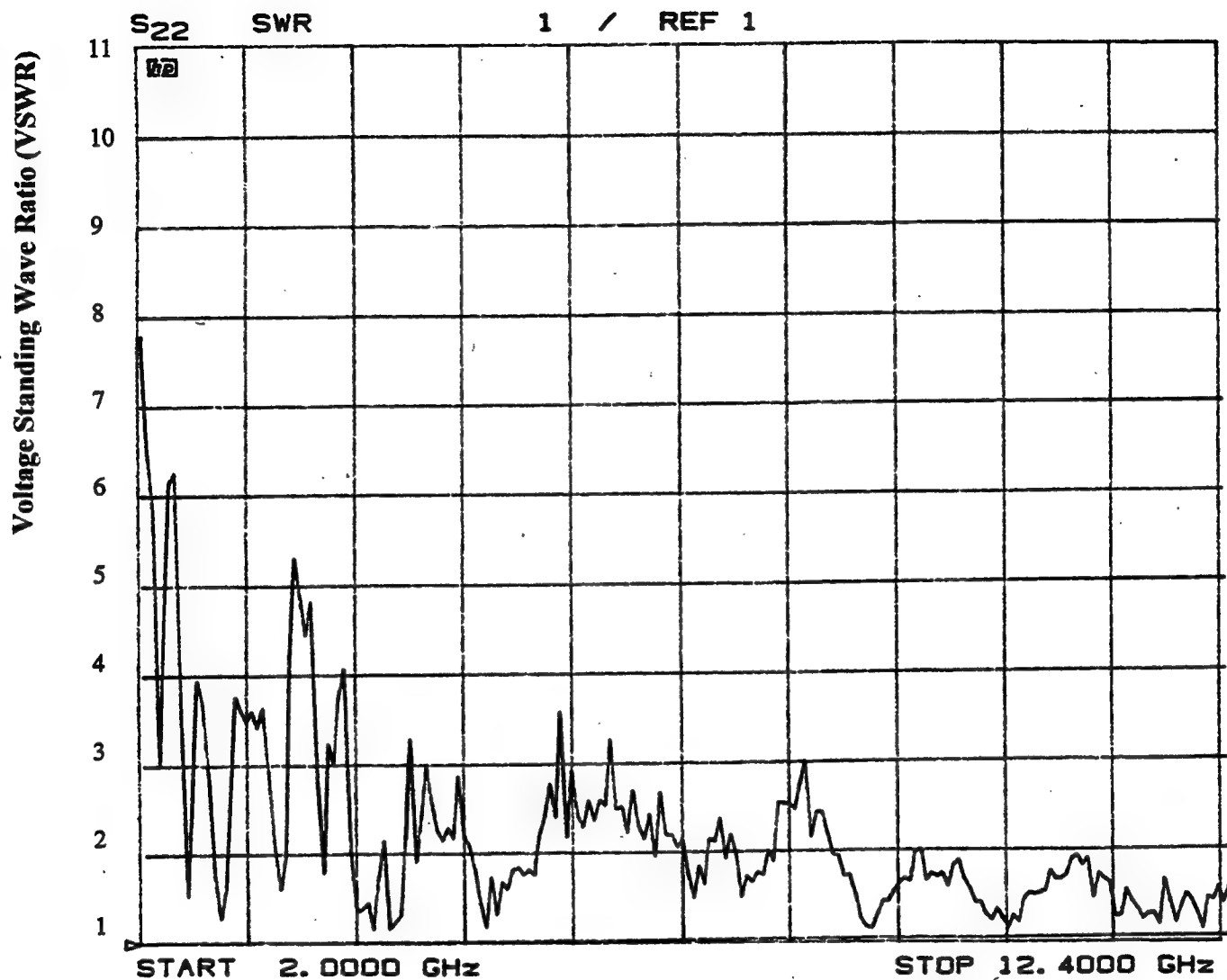


Figure 6-16 VSWR vs Frequency For 6.2 & 3.1 GHz Design

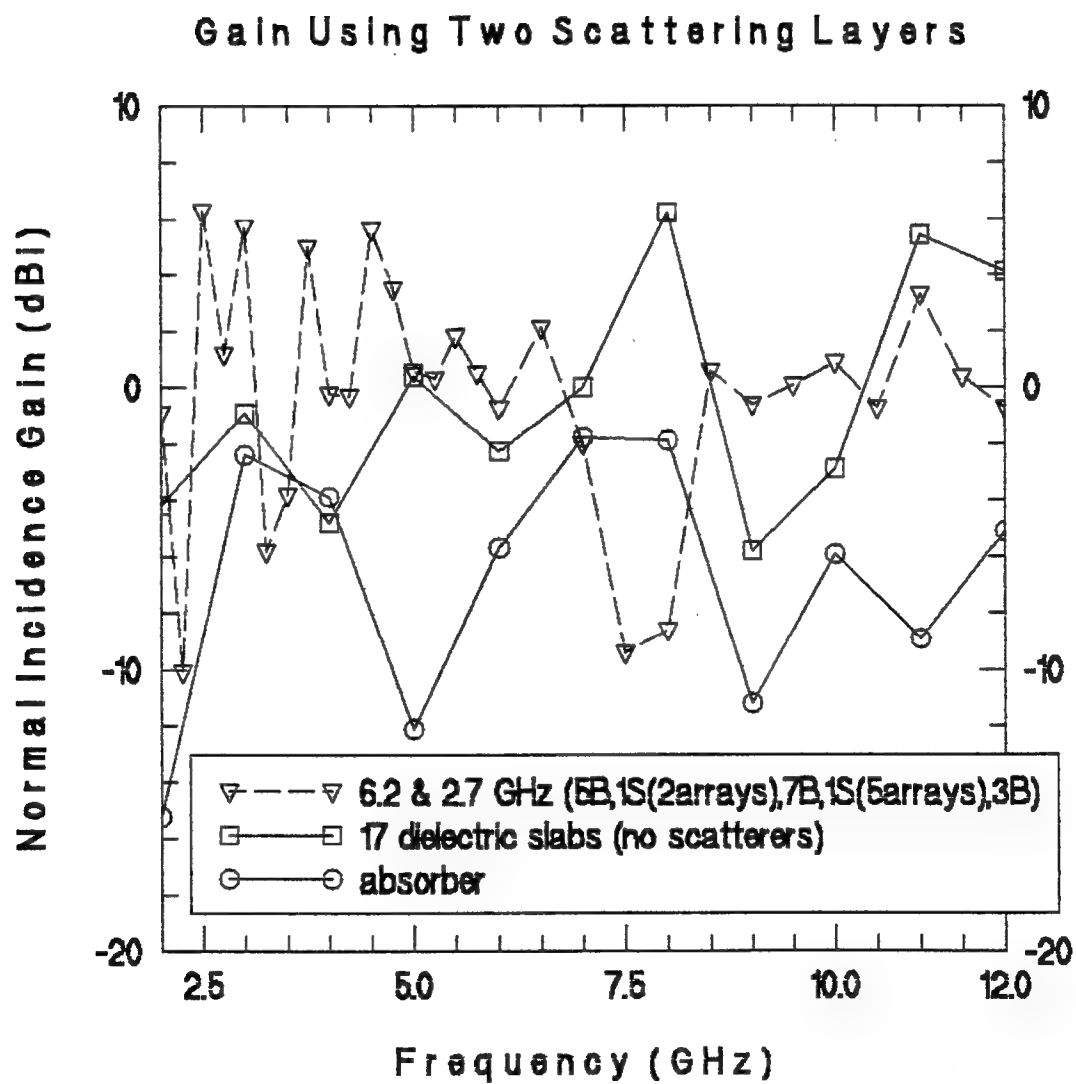


Figure 6-17 Normal Incidence Gain vs. Frequency For 6.2 & 2.7 GHz Design

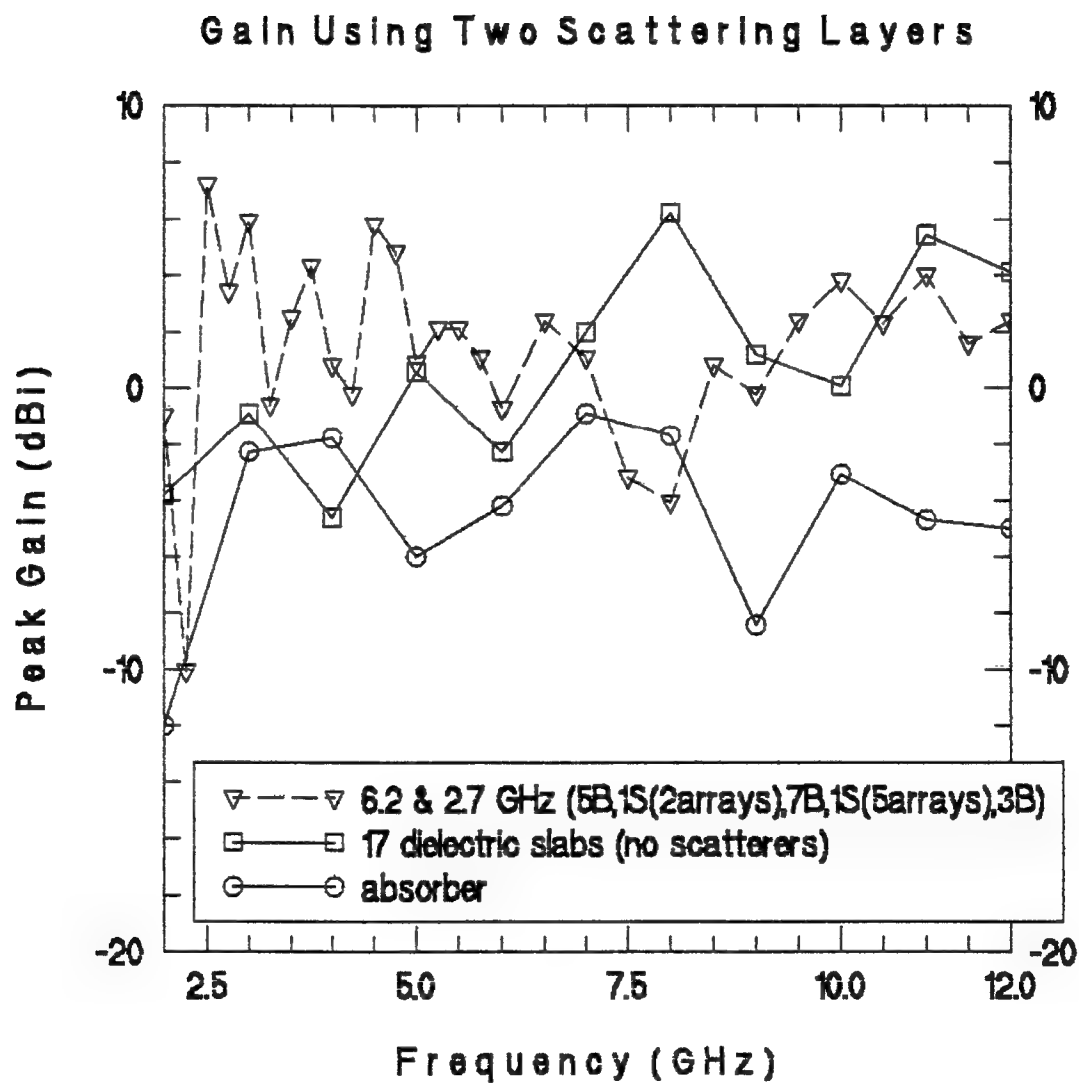


Figure 6-18 Peak Gain vs. Frequency For 6.2 & 2.7 GHz Design

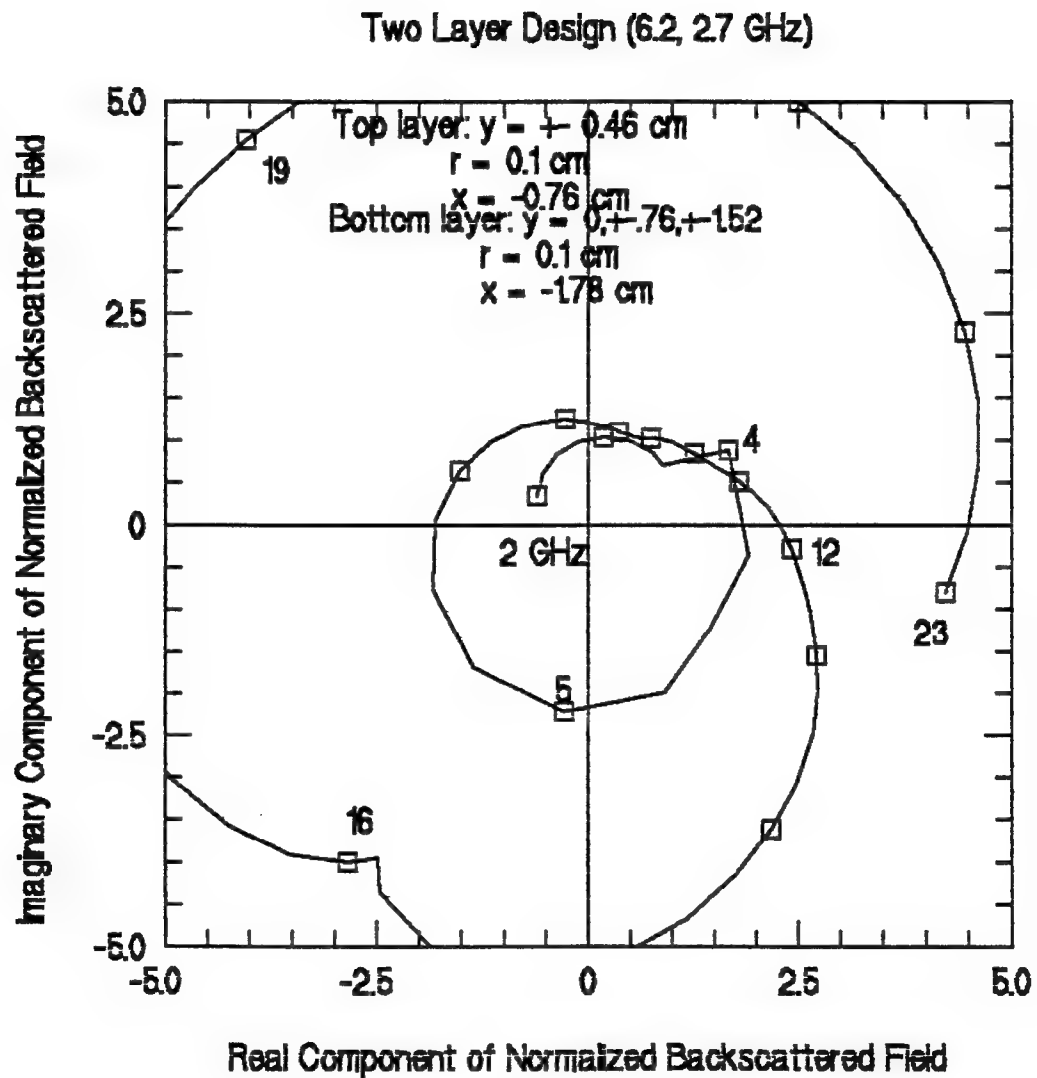


Figure 6-19 Hoser Code Output For 6.2 & 2.7 GHz Design

Beamwidth & Squint Using 6.2 & 2.7 GHz Design

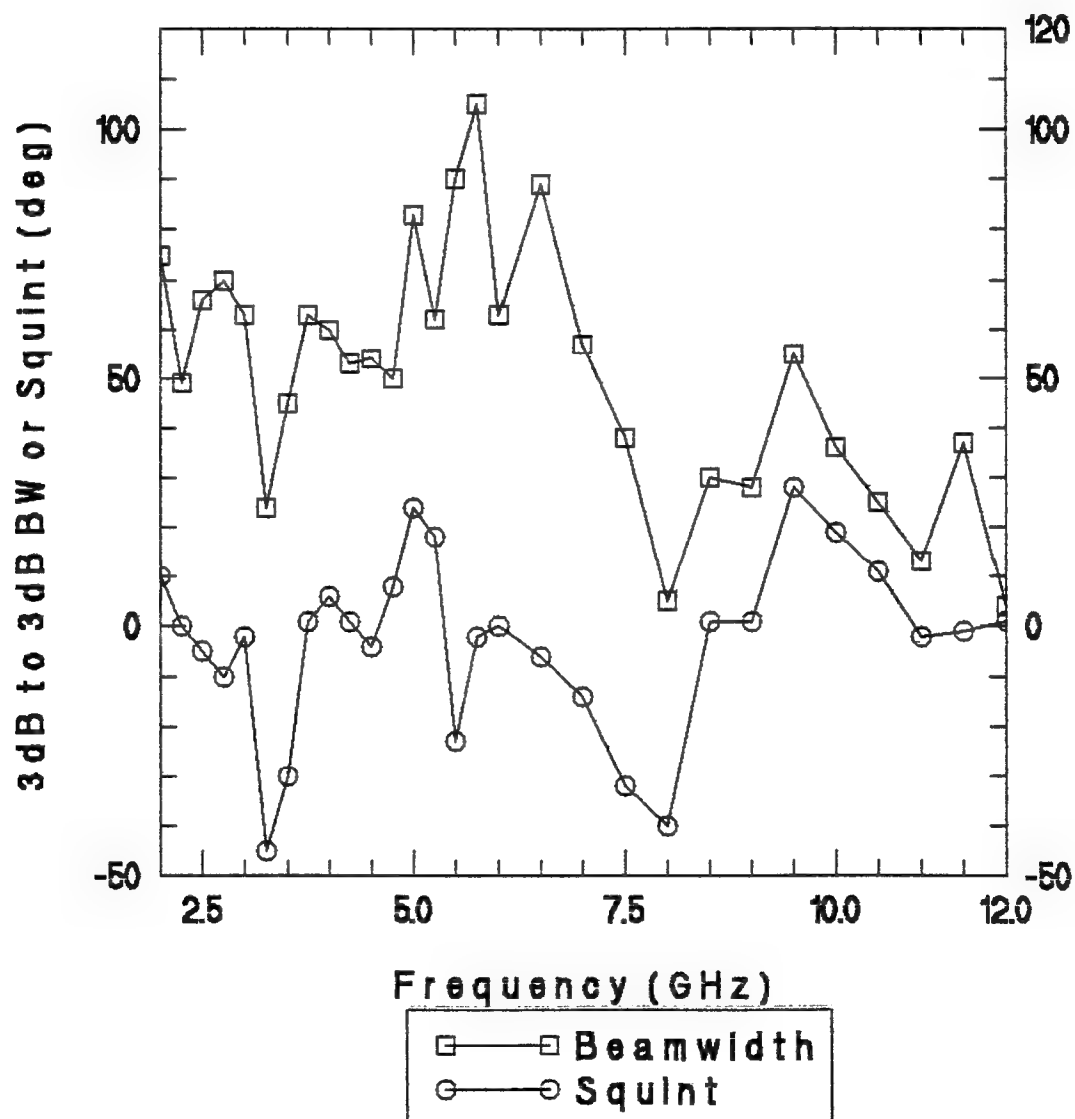


Figure 6-20 Beamwidth & Squint vs Frequency For 6.2 & 2.7 GHz Design

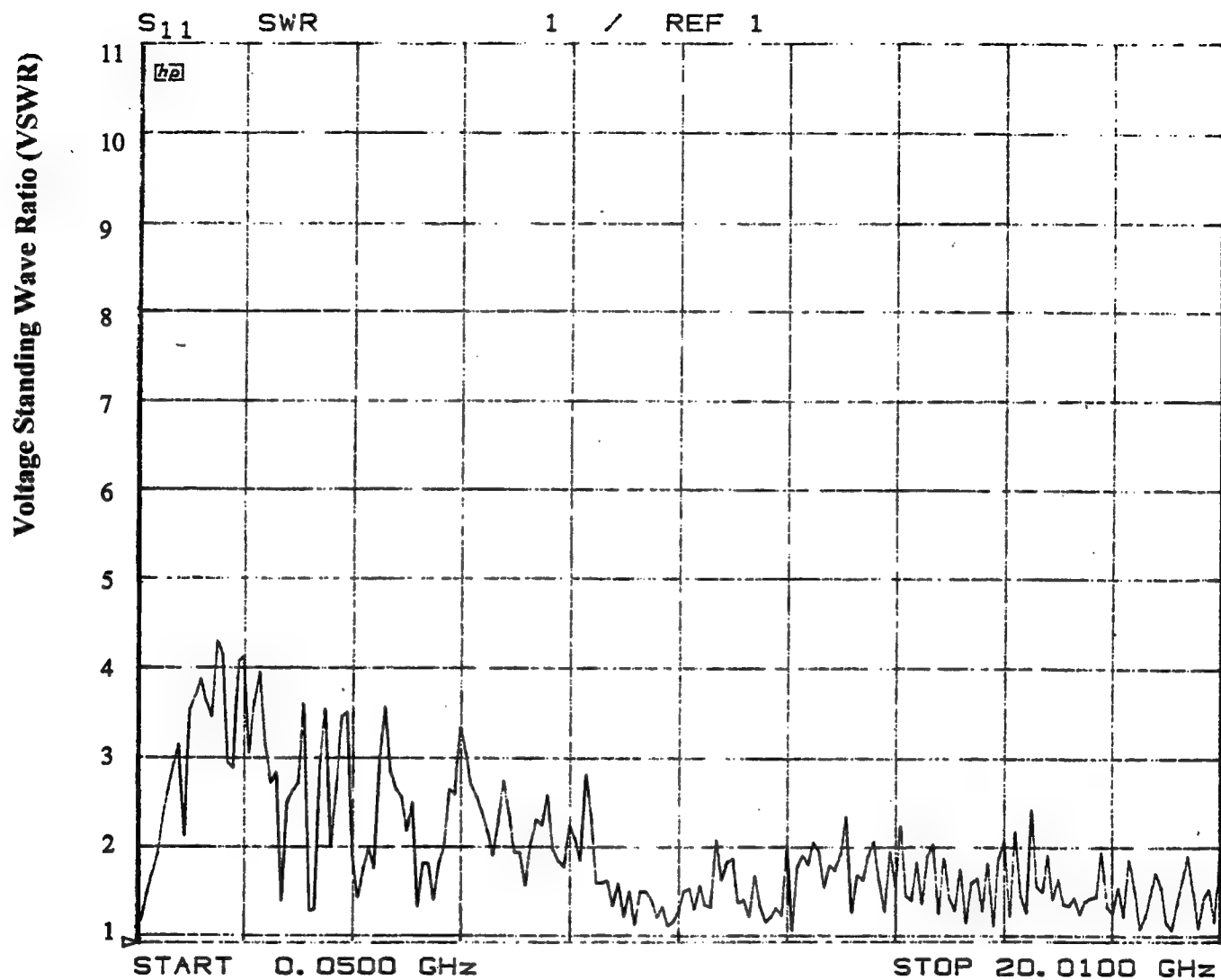


Figure 6-21 VSWR vs Frequency For 6.2 & 2.7 GHz Design

Relative Magnitude of Reflection

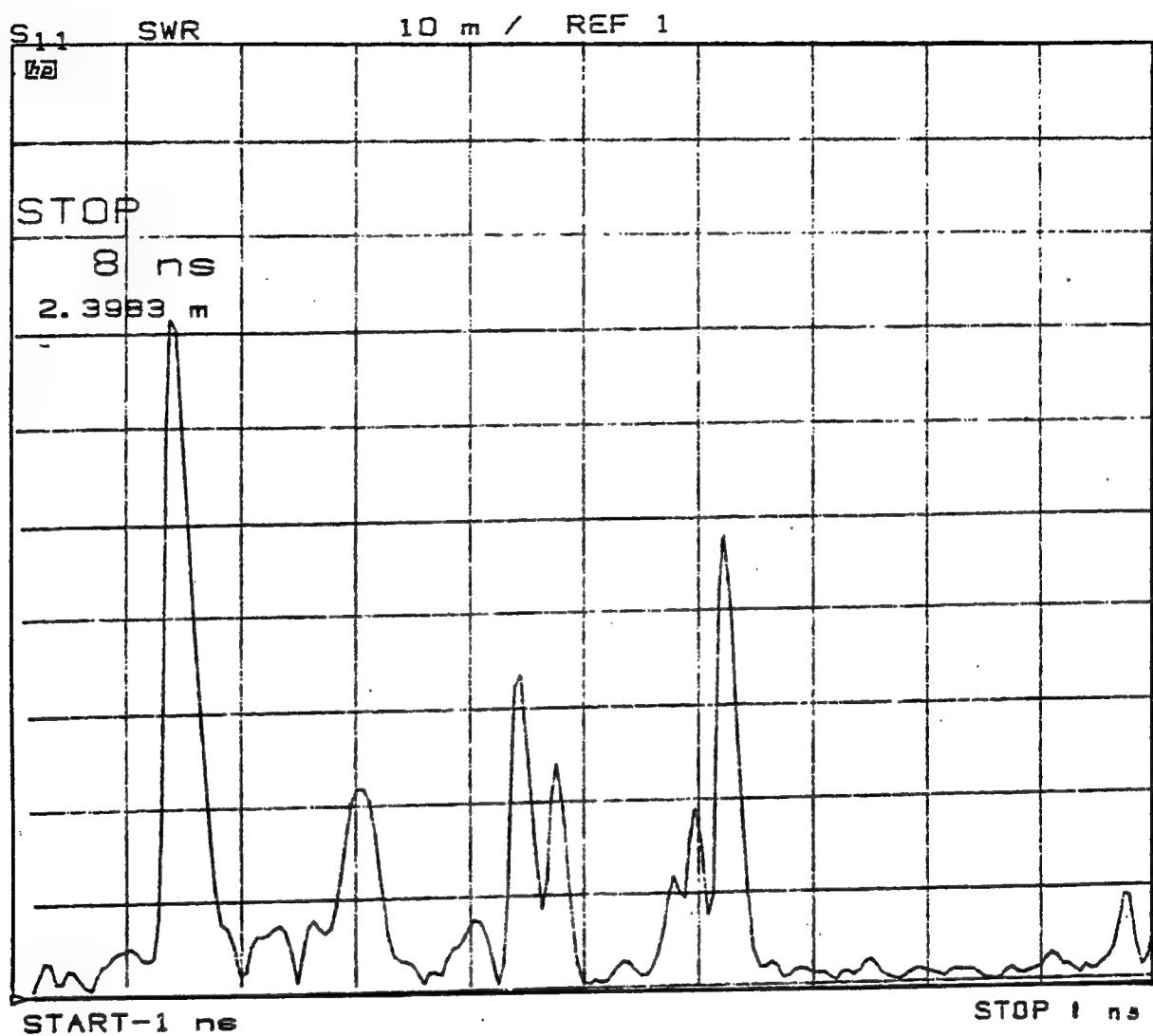


Figure 6-22 Time Domain Plot Containing Information For 6.2 & 2.7 GHz Design

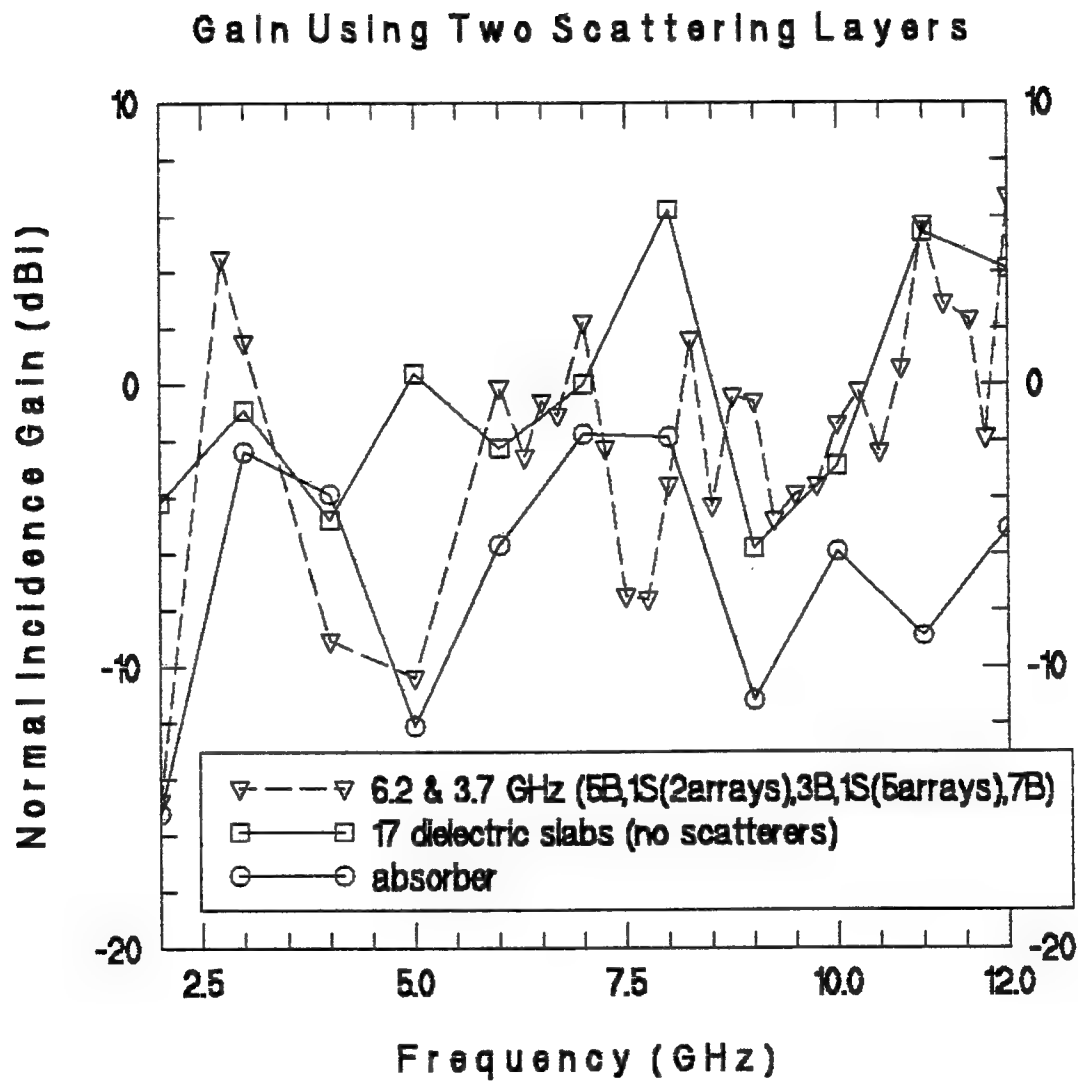


Figure 6-23 Normal Incidence Gain vs. Frequency For 6.2 & 3.7 GHz Design

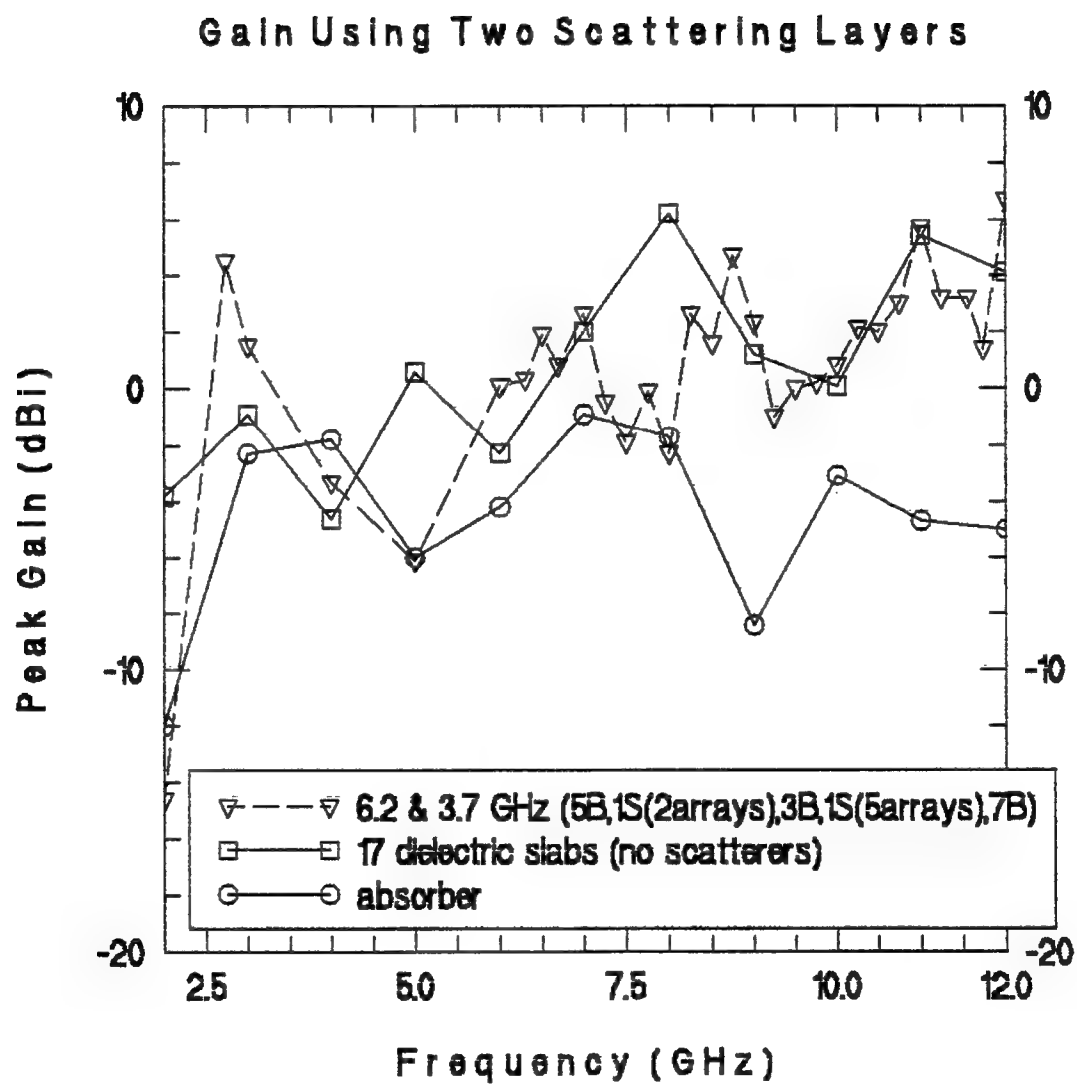


Figure 6-24 Peak Gain vs Frequency For 6.2 & 3.7 GHz Design

Two Layer Design (6.2, 3.7 GHz)

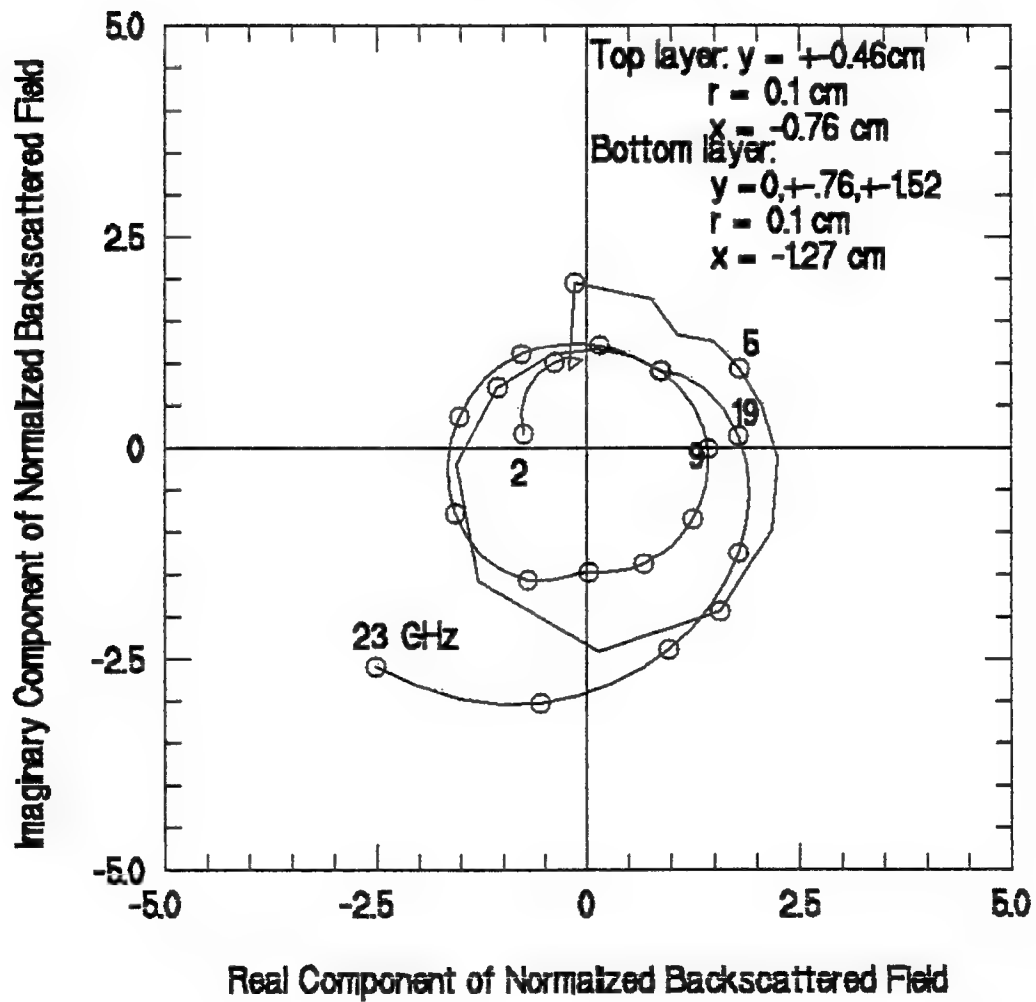


Figure 6-25 Hoser Code Output For 6.2 & 3.7 GHz Design

Beamwidth & Squint Using 6.2 & 3.7 GHz Design

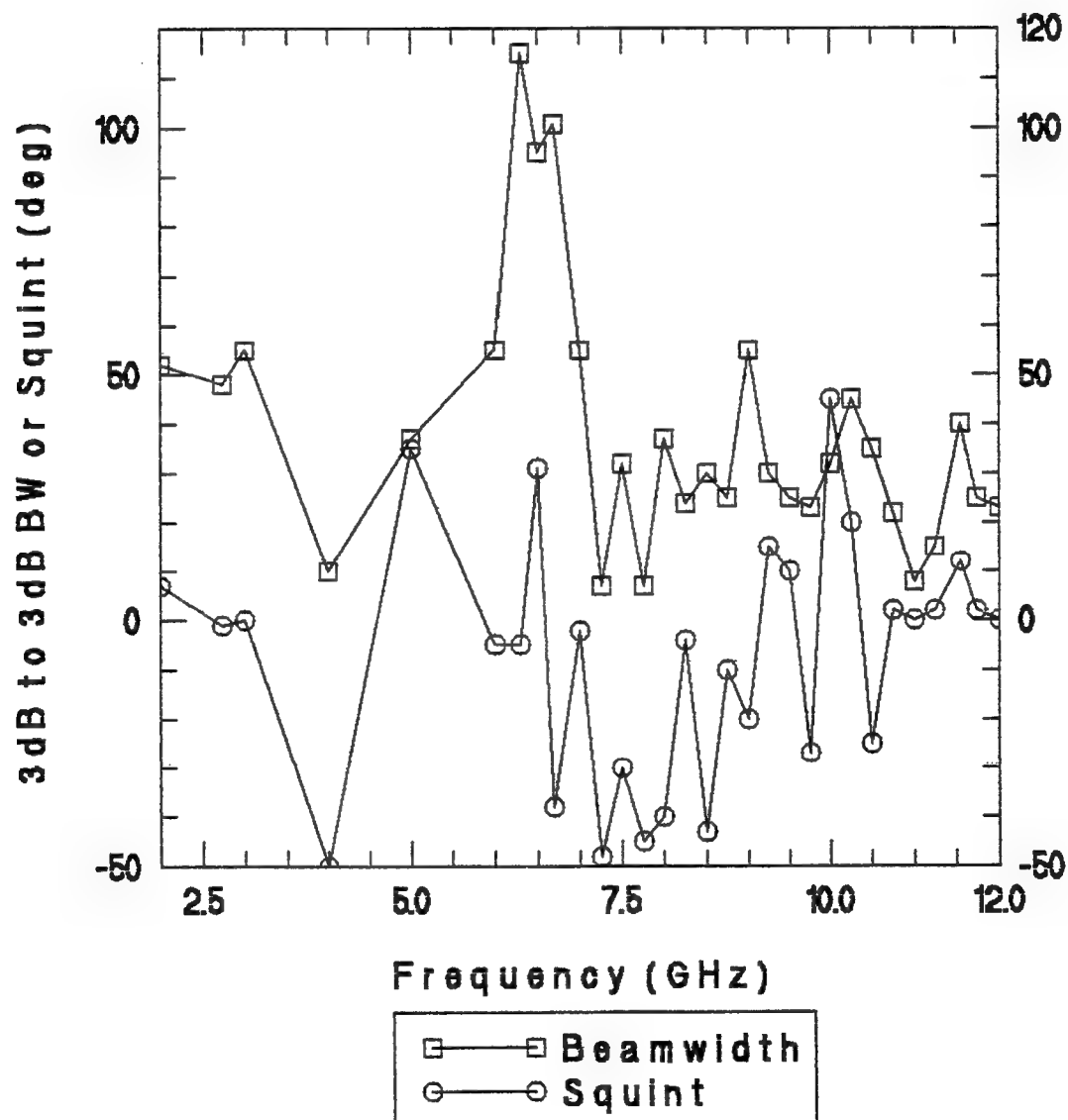


Figure 6-26 Beamwidth & Squint vs. Frequency For 6.2 & 3.7 GHz Design

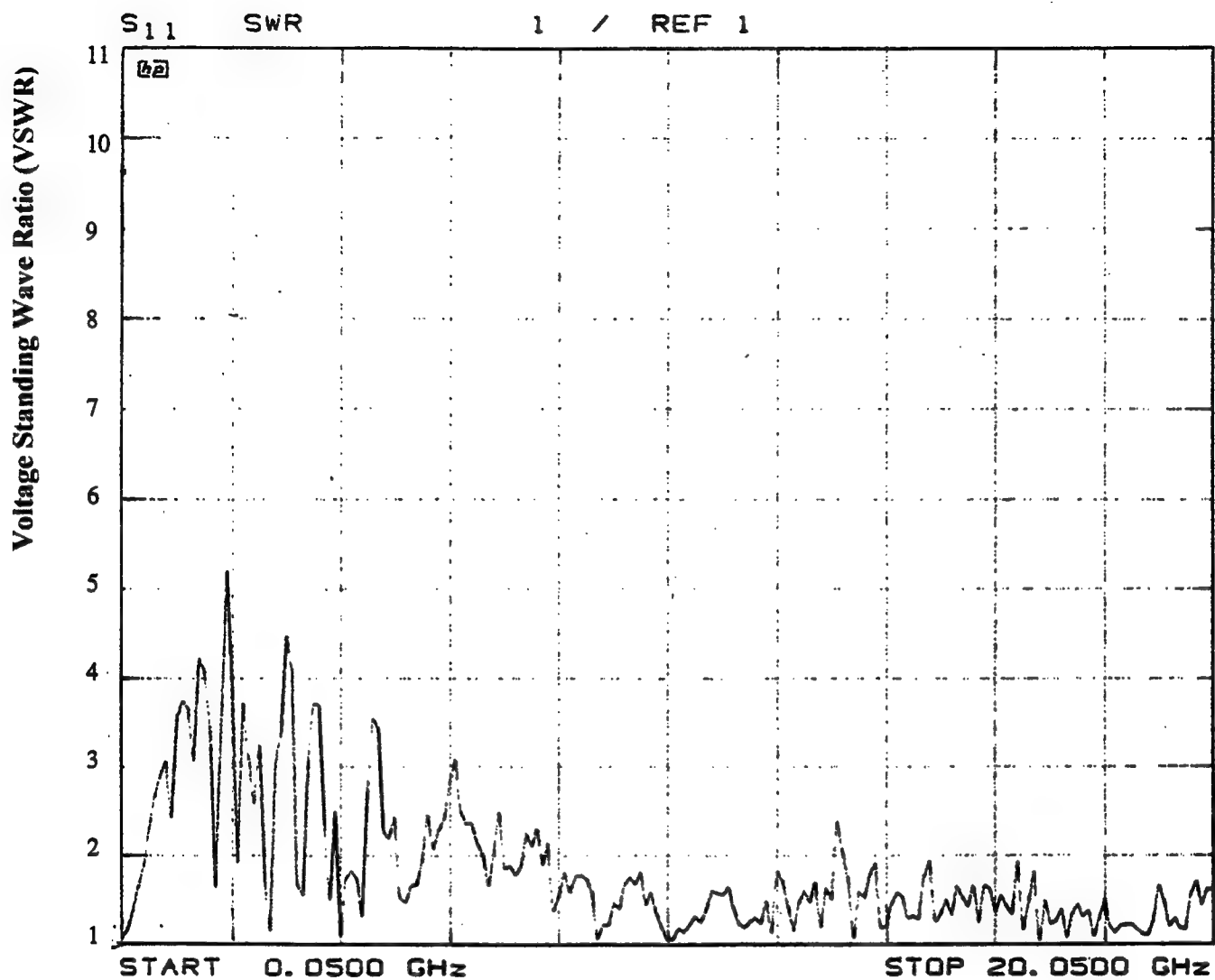


Figure 6-27 VSWR vs Frequency For 6.2 & 3.7 GHz Design

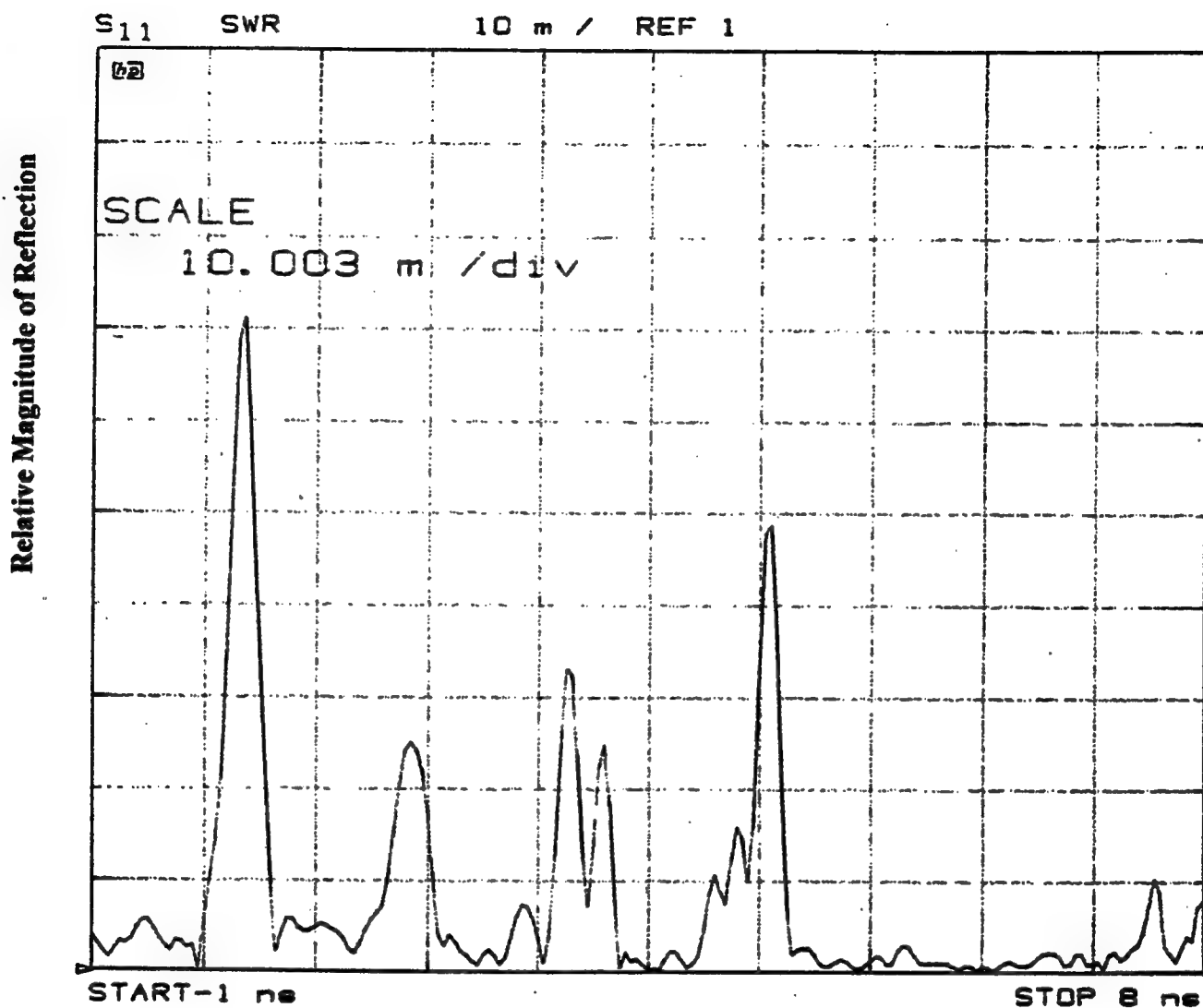


Figure 6-28 Time Domain Plot Containing Reflection Information For 6.2 & 3.7 GHz Design

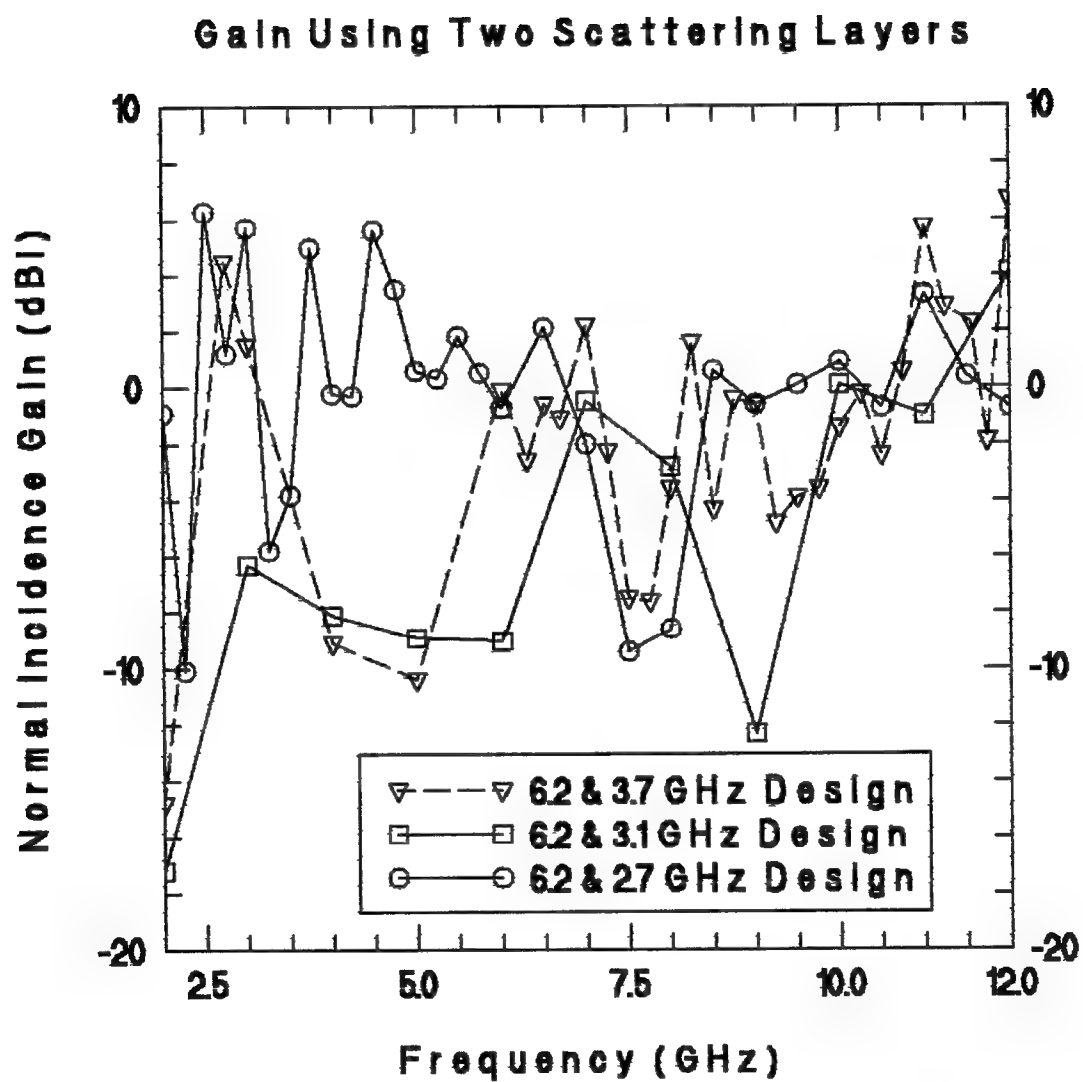


Figure 6-29 Comparison Of Normal Incidence Gain For Two Layer Designs

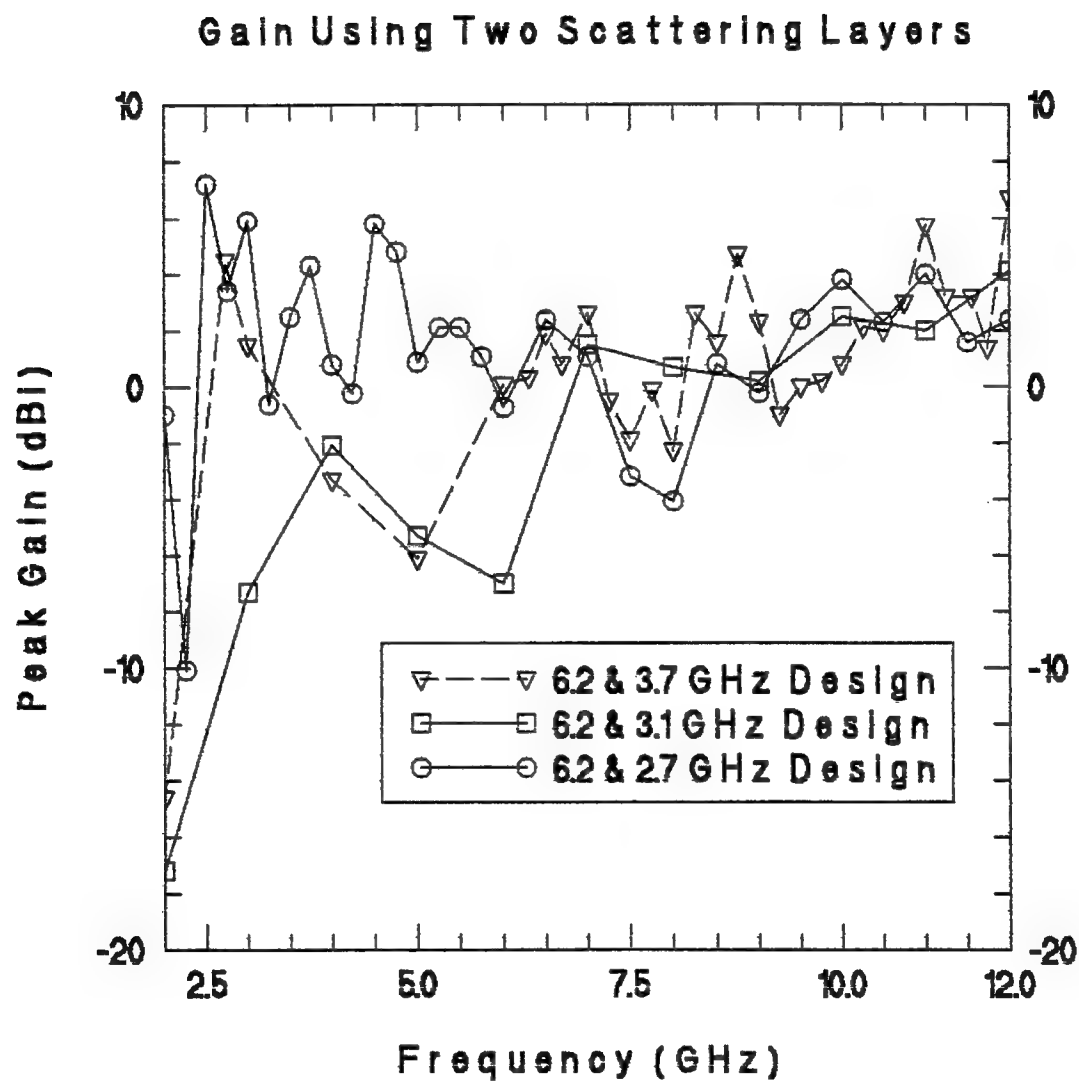


Figure 6-30 Comparison of Peak Gains For Two Layer Design

Three Layer Design Using 1, 5, and 7 Dipole Arrays (12.4, 7.5, 3.1 GHz)

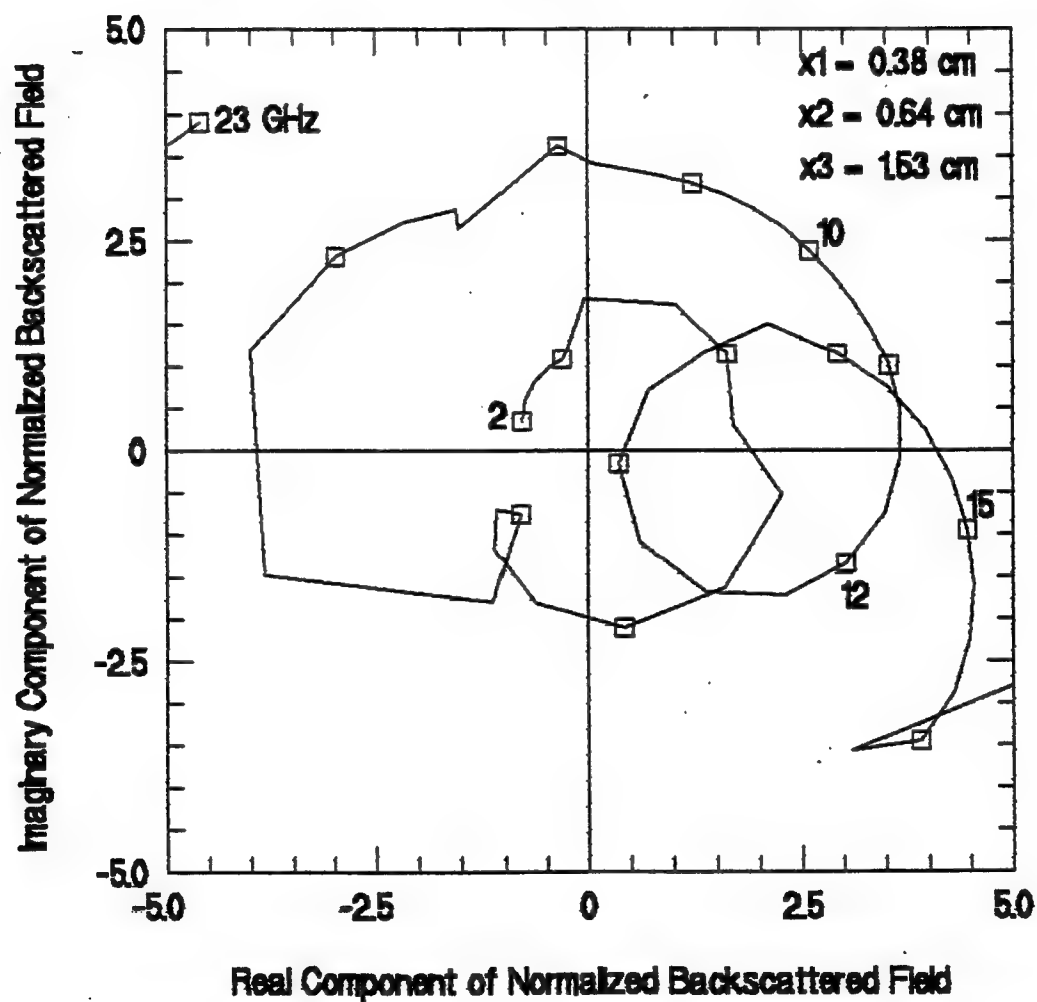


Figure 6-31 Hoser Code Output For Three Layer Design

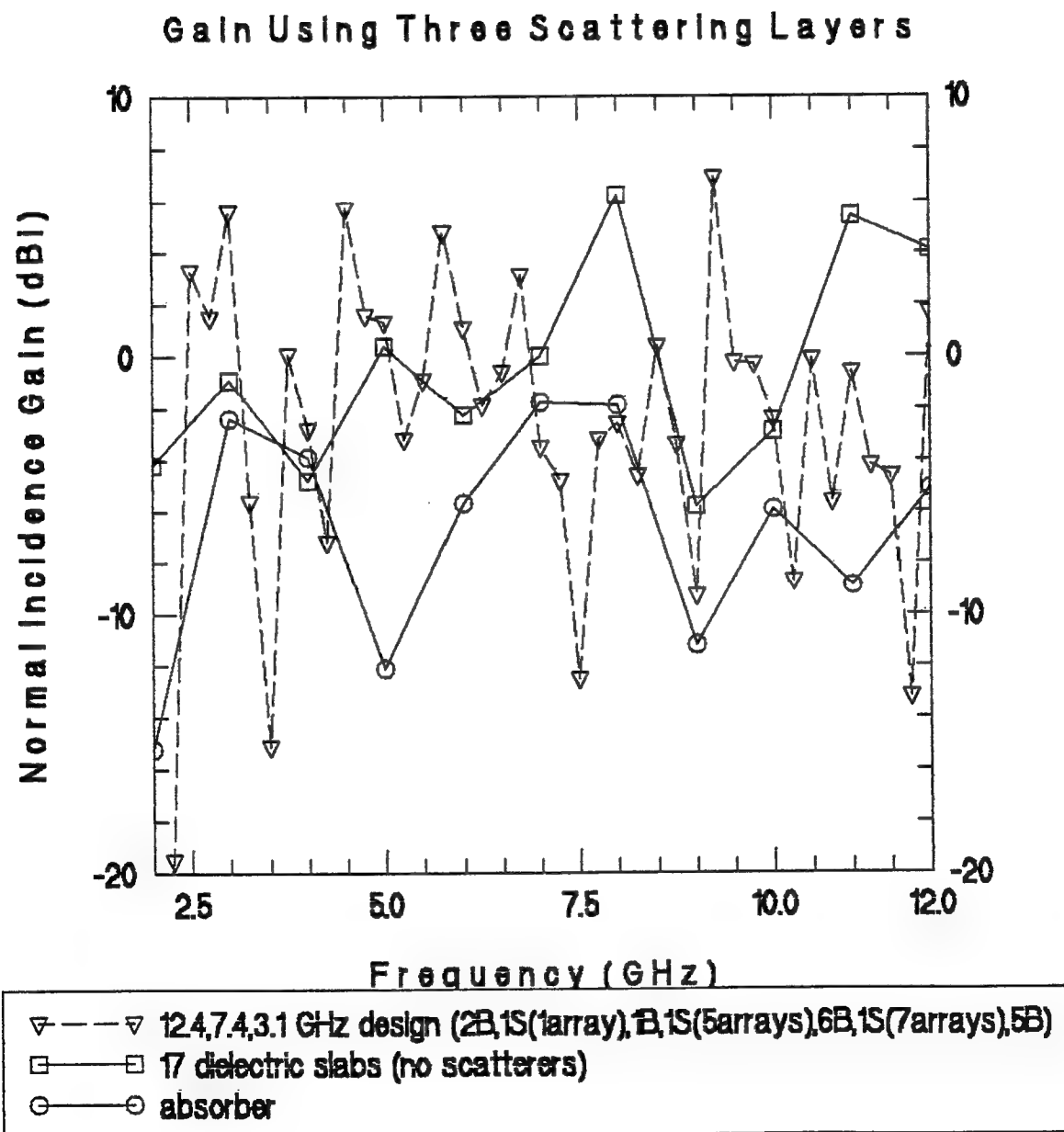


Figure 6-32 Normal Incidence Gain vs. Frequency For Three Layer Design

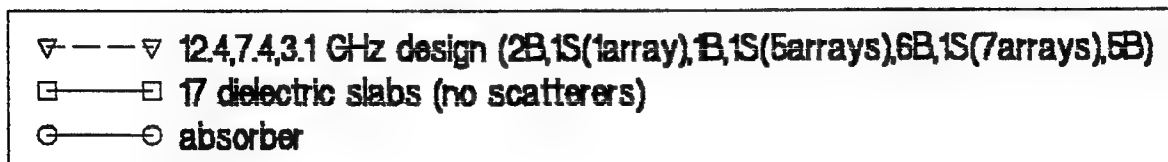
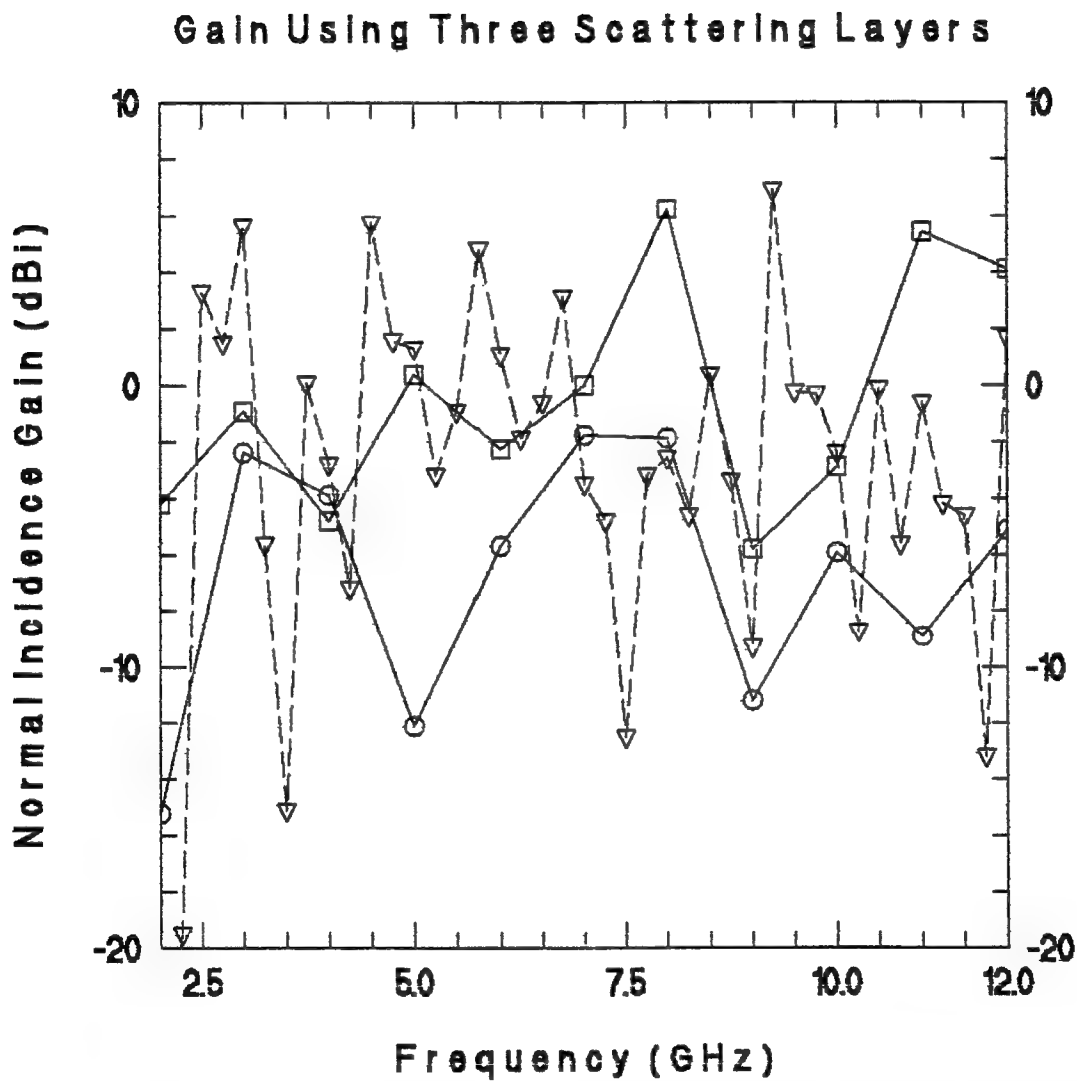


Figure 6-33 Peak Gain vs Frequency For Three Layer Design

Beamwidth & Squint Using 124,74,3.1GHz Design

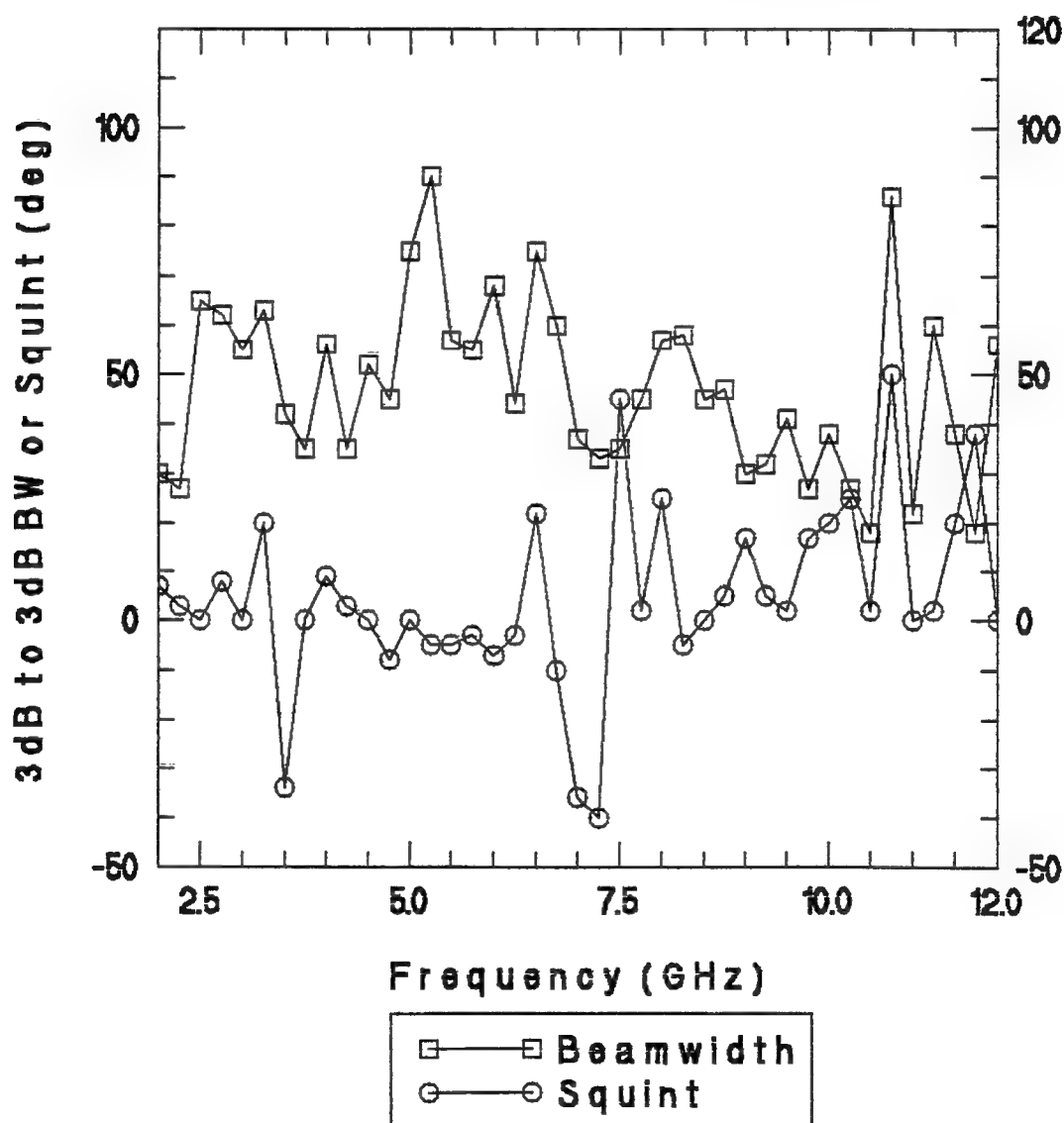


Figure 6-34 Bandwidth & Squint vs. Frequency For Three Layer Design

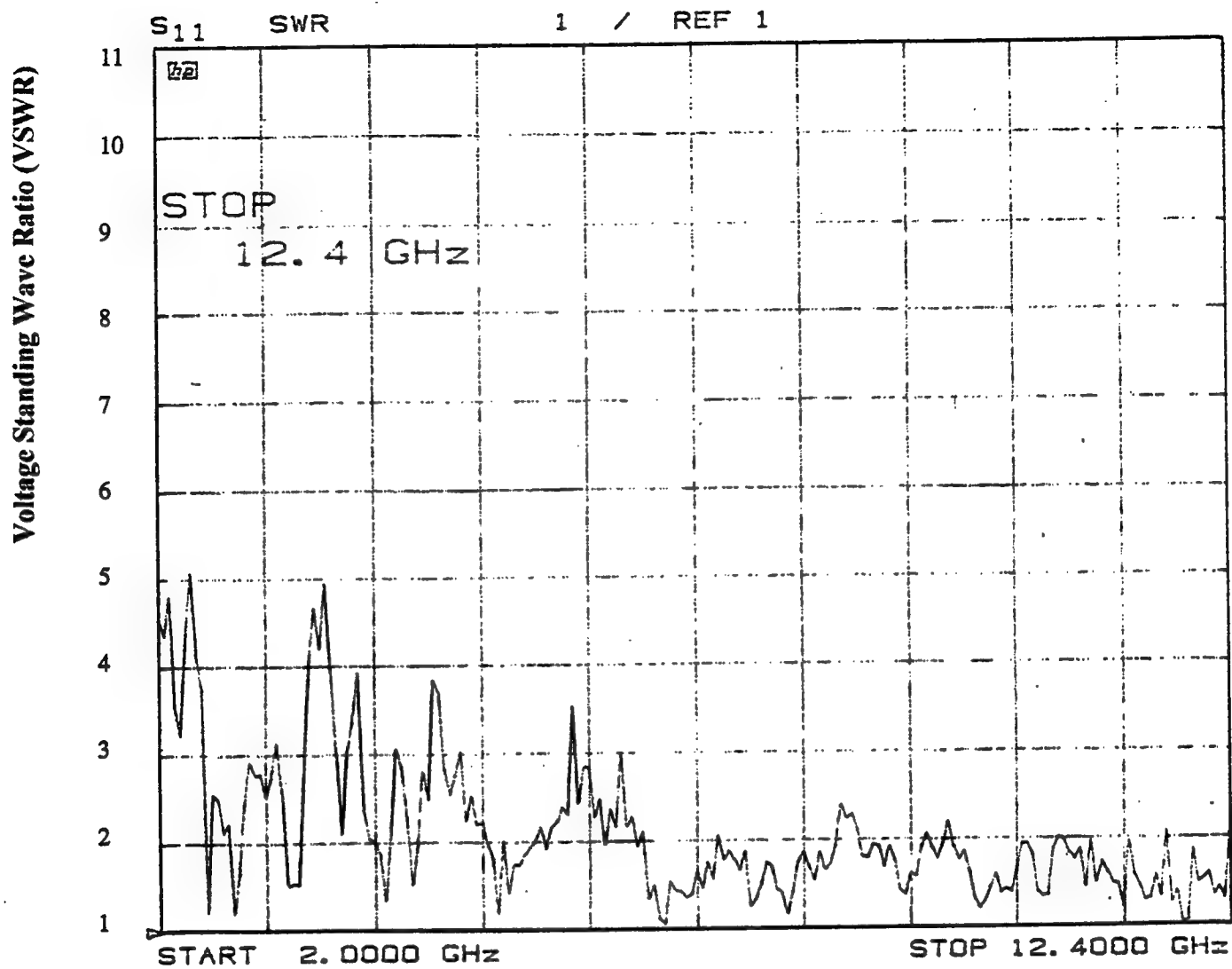


Figure 6-35 VSWR vs. Frequency For Three Layer Design

7. Conclusions and Recommendations

The results of replacing the absorber with scatterers in a cavity-backed log periodic trapezoid wire antenna were inconclusive. This inconclusiveness was mainly due to the atypical gain characteristics of the absorber-filled cavity design. Rather than providing a relatively constant gain as a function of frequency, as expected, this design's gain fluctuated by as much as 8 dB over the 2-12 GHz band. The question that must be asked is how could one expect to achieve good performance using scatterers in the cavity if the traditional absorber-filled design was unable to produce respectable results.

If one were to attribute the poor performance of the absorber-filled case to the feed set-up, and then assume it equally affected results using other cavity designs, then some of the results can be made to look good by judging performance solely on how the antenna's gain compared to the absorber-filled antenna's gain. Referencing Figures 6-18, 6-24, and 6-33, one observes that the 6.2 & 2.7 GHz and 6.2 & 3.7 GHz two layer designs and the one three layer design all had peak gains that exceeded that of the absorber-filled case at virtually every frequency.

On the other hand, if one uses the standard criteria to judge antenna performance - that is, its normal incidence gain and the bandwidth over which it remains within 3 dB of its peak -- then the clear conclusion from the results in Chapter 6 is that using scatterers rather than absorber in the cavity of cavity-backed antennas can result in moderate improvements in the gain but only over some narrow 3 dB bandwidths that could not be predicted very accurately with the modeling approaches used in this research.

Further investigation into engineering a method of harnessing the energy that an absorber-filled cavity-backed antenna radiates into its cavity is warranted. First, to avoid the resonances associated with the log periodic antenna, it is recommended that a spiral antenna be used in any further research. Second, to obtain better correlation between

predicted and actual results, it is recommended that the modeling techniques consider the effect of the cavity's side walls and the copper tape on the deepest dielectric slab.

In addition, future testing to evaluate possible cavity designs should begin with the validation of the performance of the traditional absorber-filled cavity design over its designed bandwidth.

APPENDIX A: Determination of the Normalization Constant Used In The Hoser Code

Note: This appendix was extracted from the report titled "On Edge Absorbers In General" which is listed as reference 17 in the bibliography. References and figure numbers in this appendix therefore refer to those cited in the original report.

Determination of a Normalization Constant for an Infinite \hat{z} -Directed Line Array of Dipoles

For some time now the Ohio State University ElectroScience Laboratory has been studying the scattering from finite arrays of dipoles by modelling the array as a finite collection of dipoles strings which are infinitely periodic in one direction. Hughes [5] first considered \hat{z} directed dipoles that are infinitely periodic in z . In this Appendix a normalization constant for the scattered field is presented to help understand these results. This is the first attempt to formulate an approach similar to the use of the Smith Chart in doubly infinite periodic surfaces.

Consider the far zone \hat{z} directed scattered field from an infinite line array of \hat{z} directed dipoles. The terminals of the reference dipole and the phase reference point are located at the origin.

$$E_z^{scat} = -\frac{\omega\mu}{4D_z} I_o s_\rho^2 H_o^{(2)}(\beta s_\rho \rho) P^{scat}(n=0) \quad (A.1)$$

Recall that the current in Equation (A.1) is just the voltage induced in the reference element divided by the self impedance of the array, i.e.:

$$I_o = \frac{V^{ind}}{Z^{1,1}} = \frac{(\vec{E}^{inc} \cdot \hat{z}) P^{tran}(n=0)}{Z^{1,1}} = \frac{E_o P^{tran}(n=0)}{Z^{1,1}} \quad (A.2)$$

By applying Equation (A.2) to (A.1) the scattered field may be written in terms of the incident field and the self impedance.

$$E_z^{scat} = -\left[\frac{\omega\mu}{4D_z} s_\rho^2 P^{scat}(n=0) P^{tran}(n=0) \right] \frac{E_o H_o^{(2)}(\beta s_\rho \rho)}{Z^{1,1}} \quad (A.3)$$

*While it is impossible to be in the far zone of an infinitely periodic array, the far zone here is just the principle cylindrical wave emanating from the string array.

The self impedance of the dipole array string is given in [5] as:

$$Z^{1,1} = \frac{\omega\mu}{4D_z} \sum_{n=-\infty}^{\infty} \tau_\rho^2 H_o^{(2)}(\beta\tau_\rho a) P^{scat}(n) P^{tran}(n) \quad (A.4)$$

where the term τ_ρ is given as:

$$\tau_\rho = \sqrt{1 - \tau_z^2} = \sqrt{1 - (s_z + \frac{n\lambda}{D_z})^2} \quad (A.5)$$

A careful inspection of Equation (A.5) reveals that, for no grating lobes, τ_ρ is only real for the $n = 0$ term. All other values of n result in τ_ρ becoming imaginary, i.e.:

$$\tau_\rho = \begin{cases} s_\rho & = \sqrt{1 - s_z^2} & n = 0 \\ -j|\tau_\rho| & = -j\sqrt{\tau_z^2 - 1} & n \neq 0 \end{cases} \quad (A.6)$$

In Equation (A.6) the negative root is chosen to satisfy the radiation condition. Using these results in Equation (A.4) yields:

$$\begin{aligned} Z^{1,1} &= \frac{\omega\mu}{4D_z} s_\rho^2 H_o^{(2)}(\beta a s_\rho) P^{scat}(n=0) P^{tran}(n=0) \\ &+ \frac{\omega\mu}{4D_z} \sum_{\substack{n=-\infty \\ (n \neq 0)}}^{\infty} \tau_\rho^2 H_o^{(2)}(-j\beta a |\tau_\rho|) P^{scat}(n) P^{tran}(n) \end{aligned} \quad (A.7)$$

The Hankel function of an imaginary argument may be written in terms of modified Bessel functions of the second kind[6].

$$K_\nu(u) = \frac{\pi}{2} (-j)^{\nu+1} H_\nu^{(2)}(-ju) \quad (A.8)$$

The modified Bessel Function of the second kind is real for real arguments [6], therefore all terms $n \neq 0$ in the self impedance are purely imaginary. Using Equation (A.8) in Equation (A.7) gives the self impedance in real and imaginary terms.

$$\begin{aligned} Z^{1,1} &= \frac{\omega\mu}{4D_z} s_\rho^2 J_o(\beta a s_\rho) P^{scat}(n=0) P^{tran}(n=0) \\ &- j \frac{\omega\mu}{4D_z} s_\rho^2 \widehat{N_o}(\beta a s_\rho) P^{scat}(n=0) P^{tran}(n=0) \\ &+ j \frac{\omega\mu}{2\pi D_z} \sum_{\substack{n=-\infty \\ (n \neq 0)}}^{\infty} \tau_\rho^2 K_o(\beta a |\tau_\rho|) P^{scat}(n) P^{tran}(n) \end{aligned} \quad (A.9)$$

The bracketed term of Equation (A.3) is the real part of the $n = 0$ value of the self impedance for thin dipoles (i.e. $\beta a \simeq 0$). At resonance this term represents the self impedance of the dipole string. Using this fact in Equation (A.3) gives:

$$E_z^{scat} = -\frac{R^{1,1}}{Z^{1,1}} E_o H_o^{(2)}(\beta s_\rho \rho) \quad (A.10)$$

Now, the scattered field at resonance is just

$$E_z^{scat} = -E_0 H_0^{(2)}(\beta s_\rho \rho) \quad (\text{A.11})$$

The normalization presented here makes use of Equation (A.11) by dividing the scattered field of an array by the maximum possible scattered field of a single column of dipoles given at resonance.

The exact normalizing constant is found by considering the large argument form of the Hankel function [6].

$$\lim_{u \rightarrow \infty} H_\nu^{(2)}(u) = \sqrt{\frac{2j}{\pi u}} j^\nu e^{-ju} \quad (\text{A.12})$$

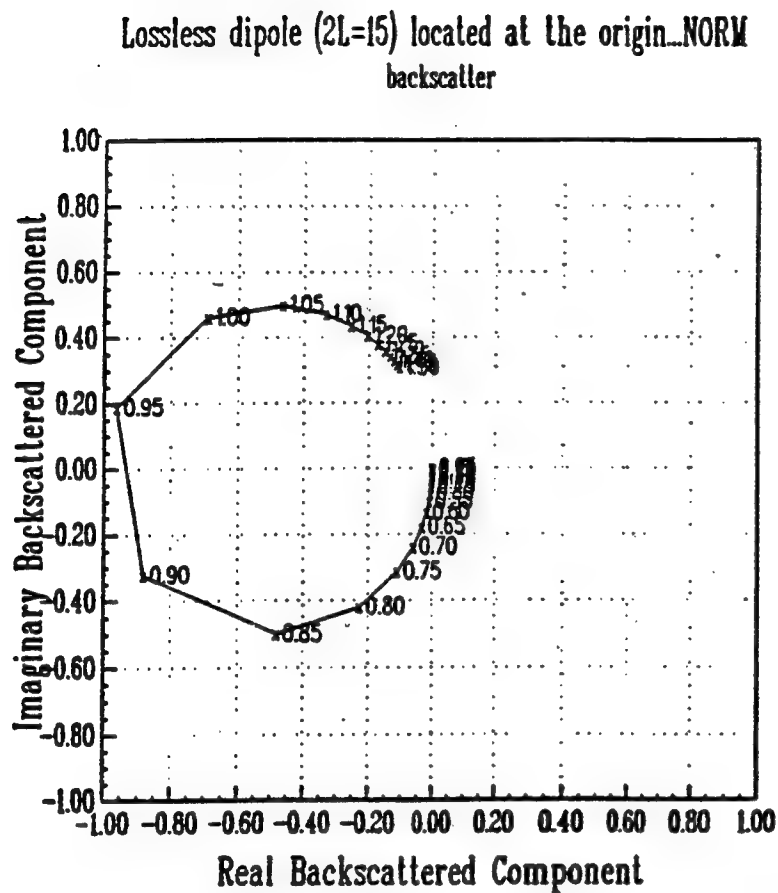
So for the Hankel function of the normalization:

$$\begin{aligned} \lim_{s_\rho \rho \rightarrow \infty} H_0^{(2)}(\beta s_\rho \rho) &= \sqrt{\frac{2j}{\pi \beta s_\rho \rho}} e^{-j\beta s_\rho \rho} \\ &= \sqrt{\frac{j\lambda}{\pi^2}} \left(\frac{e^{-j\beta s_\rho \rho}}{\sqrt{s_\rho \rho}} \right) \end{aligned} \quad (\text{A.13})$$

The term in the parenthesis in Equation (A.13) is just the far zone term which may be omitted. Thus the proposed normalization constant is just:

$$NORM = \sqrt{\frac{j\lambda}{\pi^2}} = \sqrt{\frac{\lambda}{2}} \left(\frac{1+j}{\pi} \right) \quad (\text{A.14})$$

This normalization constant is essentially an always resonant dipole situated at the origin. The beauty of the constant is that it is completely independent of the width of the dipoles in the string. An example of a normalized backscattered field from a dipole string is shown in Figure 20.



Plot Description
x — lossless dipole ($r=0.05$)

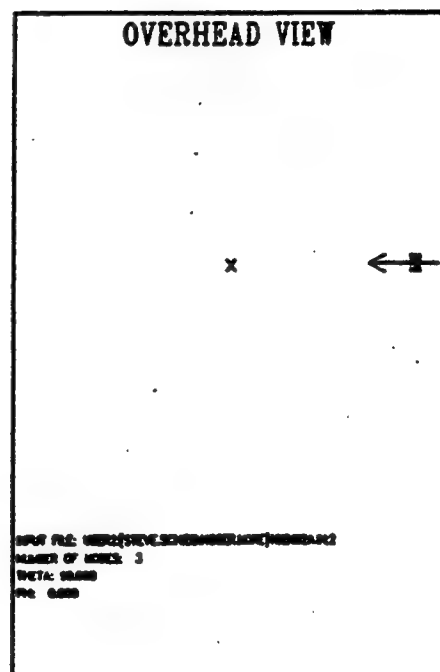


Figure 20: The normalized backscattered field from an infinite string of \hat{z} directed dipoles located at the origin.

APPENDIX B: Source Code For Transmission Line Code

```
c Purpose: To compute the reflection coefficient associated
c with layers of frequency selective surfaces
c
c Assumptions: Normal incidence.
c               Frequency selective surfaces are infinite in 2D
c               planes; these two dimensional planes are parallel
c
c Input:        Lower and upper frequencies
c               - Frequency step size
c               The resistance, inductance, and capacitances associated
c               with the frequency selective surfaces.
c               Number of arrays to model
c               - R,L(ph),C1(pf),C2(pf) values of each of these
c
c Output:       To a file named out.dat: Reflection Coef vs Freq
c               and Phase vs Freq (The phase reference is at the
c               plane of the antenna.)
c
c Restrictions: Source code is set up to support only up to two
c               layers. This can be overcome by modifying the code.
c
c Basis for equations: EENG 627 Class Notes and Section 8.3.3 of
c               Eugene Knott's RCS Text.
c
c Parameter (max=2)
c Dimension XSUBN(max),RIND(max),CAP1(max),CAP2(max),RES(max)
c Complex CAN, CANP1, CBN, CBNP1, CGSUBN, CIMPED1
c Complex CACOEF, CBCOEF, CAS1, CAS2, CBS1, CBS2
c Complex CR
c PI = 3.141592654
c Write (*,*) "Please input the lowest and highest freqs (GHz)"
c Read (*,*) FLGHZ, FHGHZ
c Write (*,*) "Please enter the frequency step size (in GHz)"
c Read (*,*) FSTEP
c istep = (FHGHZ - FLGHZ)/FSTEP
c rstep = (FHGHZ - FLGHZ)/FSTEP
c Write (*,*) "Input the number of periodic arrays to be used"
c Write (*,*) "This number must be less than or equal to",max
c Read (*,*) NUM
c Write (*,*) "Input value of R for the deepest FSS (in ohms)"
c Read (*,*) RES(1)
c R=0.0, L=3187, C1=0.205, C2=0.01076 for example in figure 4-20
c Write (*,*) "Input value of L for the deepest FSS (in pH)"
c Read (*,*) RIND(1)
c Write(*,*) "Input value of C1 for the deepest FSS (in pF)"
c Read(*,*) CAP1(1)
c Write(*,*) "Input value of C2 for the deepest FSS (in pF)"
c Read(*,*) CAP2(1)
```



```

CR = CBNP1/CANP1
A = REAL(CR)
B = AIMAG (CR)
PHASE = ATAN2(B,A)
DEG = PHASE * 180./PI
RC = CABS(CR)
RCDB = 20.0 * ALOG10(RC)
OPEN(unit=22, file="out.dat",status="unknown")
Write(22,*) f, rcdb, deg
F = FLGHZ + M*FSTEP
20  CONTINUE
75  CONTINUE
END
SUBROUTINE FINDZ(RESIST,RL1, CC1, CC2, Freq, CIMPED1)
COMPLEX CIMPED1, CJW, CLC, C1C, CZ1C, C2C
c   Write (*,*)"FINDZ",RL1,CC1,CC2,Freq,CIMPED1
PI = 3.141592654
IF (CC1.gt.0.) THEN
c next line accounts for case when R= real and C2 = zero
  IF(CC2.lt.0.0000000001) CC2 = 0.0000000001
  CJW = (0.,1.) * 2. * PI * Freq
  CLC = CJW * RL1 * 0.001
  C1C = 1./(CJW * CC1 * 0.001)
  CZ1C = CLC + C1C + RESIST
  C2C = 1./(CJW * CC2 * 0.001)
  CIMPED1 = (CZ1C * C2C)/(CZ1C + C2C)
ENDIF
RETURN
END

```

APPENDIX C: Equivalent Circuit Parameters Needed For Input To T-Line Code

SUMMARY OF EQUIVALENT CIRCUIT PARAMETERS PROVIDED BY THE OSU PMM CODE

12.45 GHz / 1.525 cm = λ					Resonant Frequency (GHz)
DY	L(λ)	DZ(λ)	R(ohms)	L(pH)	
$\lambda/2$	0.5	.95	0	9640	12.34
	0.5	.55	0	4420	12.17
$\lambda/4$	0.62	.70	0	1636	12.45
	0.55	.75	.88E-5	2138	>13.4
	0.55	.65	.138E-4	1674	>12.9
	0.54	.9323	0	5347	12.45 (b/o 9.34 dz=0.7 λ)
	0.5	1.1659	.47E-4	8259	12.45 (b/o 7.47 dz=0.7 λ)
	0.5	.55	-.11E-5	1482	>12.9
	0.494	1.4	.5635E-4	12689	12.45 (b/o 6.22 dz=0.7 λ)
$\lambda/3.5$	0.55	.60	0	1836	13.0
$\lambda/3$	0.55	.65	0	2600	12.68
	.60	0	0	2329	12.46
9.34 / 2.031 cm					
$\lambda/2$	0.5	.55	0	5872	9.14
$\lambda/4$	0.62	.70	0	2122	9.34
	0.562	.8754	0	5200	9.34 (b/o 7.47 dz=0.7)
	0.5	1.051	.4922E-4	8454	9.34 (b/o 6.22 dz=0.7)
	0.5	.80	0	4340	10.69
	0.5	.55	.14E-5	1986	10.95
*	0.62	1.24	0	4975	8.01
*	0.62	1.0	0	3734	8.15
*	0.62	.70	0	2192	8.69
*	0.38	.76	0	4945	12.38
*	0.38	.43	0	2116	13.27

Dy	L(λ)	Dz(λ)	R(ohms)	L (pH)	C1 (pF)	C2 (pF)	Resonant Freq (GHz)
$\lambda/6$	0.5	.85	.18E-5	3191	.064	0	10.89
	0.5	.70	.12E-5	1747	.095	0	
	0.5	.55	.31E-5	1064	.149	0	
$\lambda/8$	0.5	.95	.25	3058	.068	0	11.6
	0.5	.70	0	2232	.069	.089	12.79
	0.5	.55	.12E-6	704	.180	0	

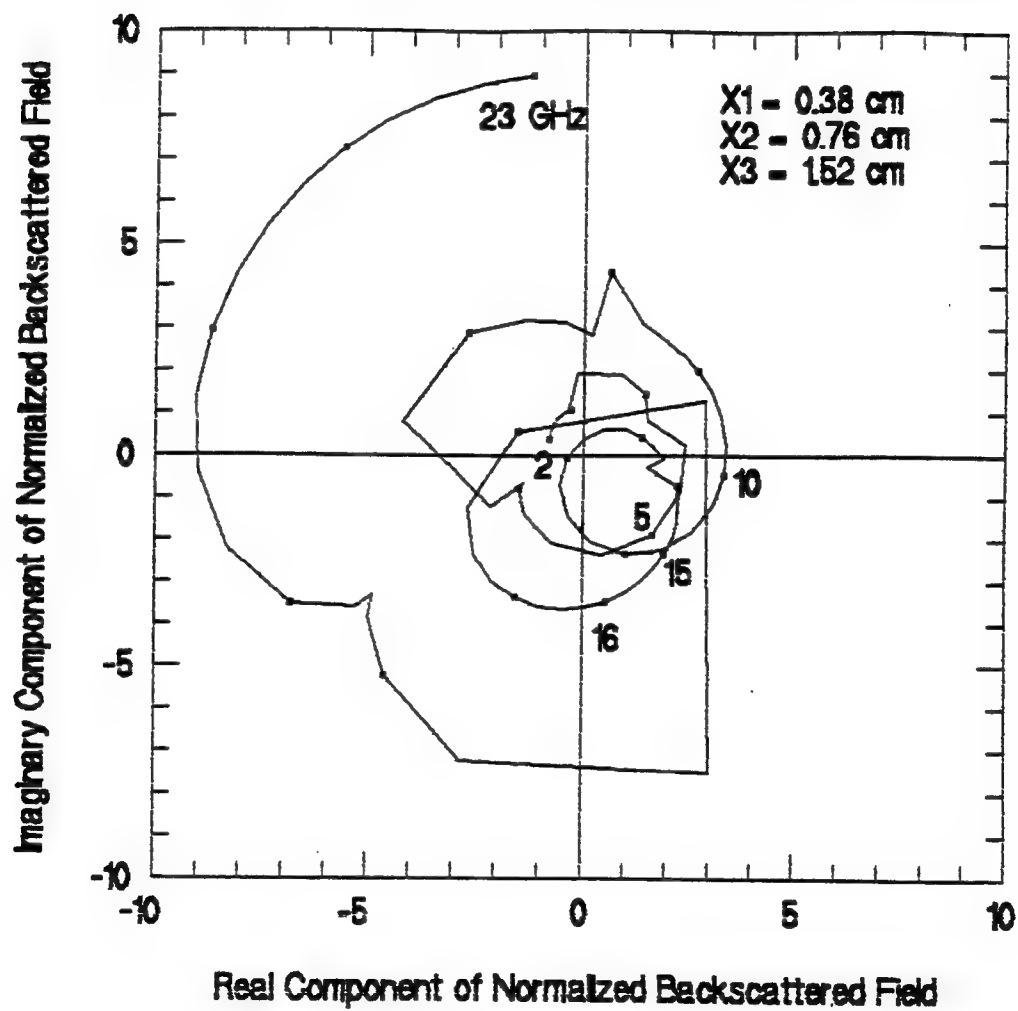
$\lambda/4$	0.62	.70	0	2692	.1686	.007683	7.47
*	0.575	.841	0	5501	.08257	.01474	7.47 (b/o 6.22 dz=0.7)
*	0.62	1.24	0	6212	.09934	.007074	6.41
*	0.62	.70	0	2722	.1928	.007471	6.95
*	0.38	.76	0	6160	.04188	.6865E-5	9.9
*	0.38	.43	0	2635	.08532	.005428	10.61

6.22 GHz/ 3.050 cm					Resonant Frequency (GHz)
DZ	L(λ)	DY	R(ohms)	L (pH)	
$\lambda/2$	0.5	.95	0	19198	.0347
$\lambda/3$	0.5	.95	.39E-4	10940	.0545
$\lambda/3.25$	0.55	1.05	.26E-4	11885	.0598
	0.5	.95	.35E-4	10043	.0580
	0.45	.85	.29E-4	9144	.0520
$\lambda/4$	0.62	.70	0	3188	.2054
	0.5	.55	0	3035	.1569
		.95	.12E-4	8153	.0689
		.99	.23E-4	8810	.064
*	0.62	1.24	0	7480	.1190
*	0.62	.70	0	3290	.2300
*	0.38	.76	0	3824	.2695
*	0.38	.43	0	3717	.1189
$\lambda/8$	0.5	.95	6.4	5631	.09
5.33 / 3.560					
$\lambda/4$	0.62	0.70	0	3728	.2392
*	0.62	1.24	0	8790	.1379
*	0.62	0.70	0	3824	.2695
*	0.38	0.76	0	8653	.05866
*	0.38	0.43	0	3717	.1189
4.67 / 4.063					
$\lambda/4$	0.62	0.70		4314	.2693
*	0.62	1.24	0		
*	0.62	0.70	0	4350	.3086
*	0.38	0.76	0	9899	.1595
*	0.38	0.43	0	4218	.1364

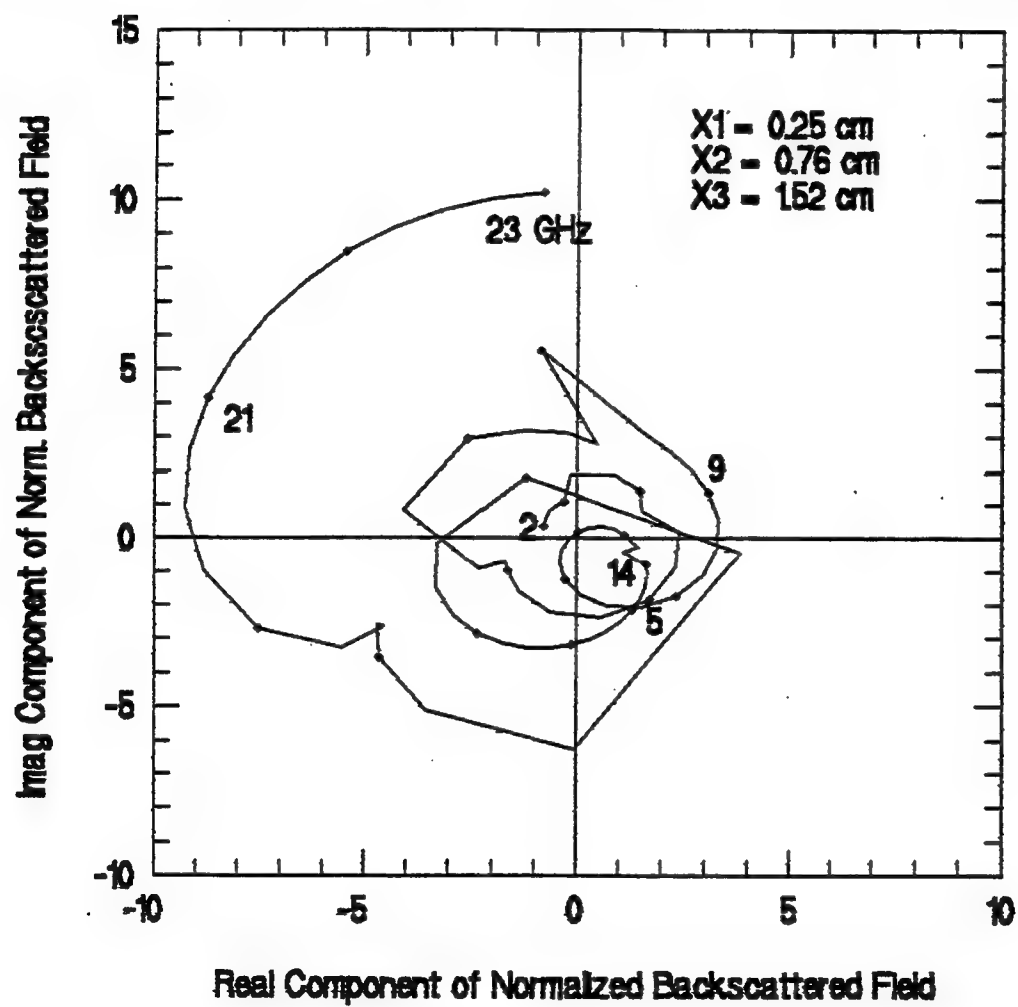
3.73 GHz/ 5.087cm					
DY	L(λ)	DZ(λ)	R	L(pH)	C1(pf)
$\lambda/4$	0.62	0.70	0	5328	.3417
*	0.62	1.24	0	12669	
*	0.62	0.70	0	5483	.3837
*	0.38	0.76	0	12352	.0839
*	0.38	0.43	0	5268	.1712
					.32E-
Resonant Frequency (GHz)					
					3.73&8.77
					3.2&8.77
					3.47&8.44
					4.94
					5.3
2.87/6.611					
$\lambda/4$	0.62	1.24	0	1633	
*	0.62	0.70	0	7139	.4987
*	0.38	0.76	0	15995	.1
*	0.38	0.43	0	6916	.22014
					2.46&6.75
					2.67&6.46
					3.8&6.92
					4.08&8.79
2.33/ 8.143					
$\lambda/4$	0.62	1.24	0	20447	.3102
*	0.62	0.70	0	8810	.619
*	0.38	0.76	0	19917	.133
*	0.38	0.43	0	8385	.2755
					.014
					.0601
					2.00&5.48
					2.17&5.28
					3.09&5.63
					3.31&7.147

APPENDIX D: Different DX Variations Of Actual Fabricated Three Layer Design

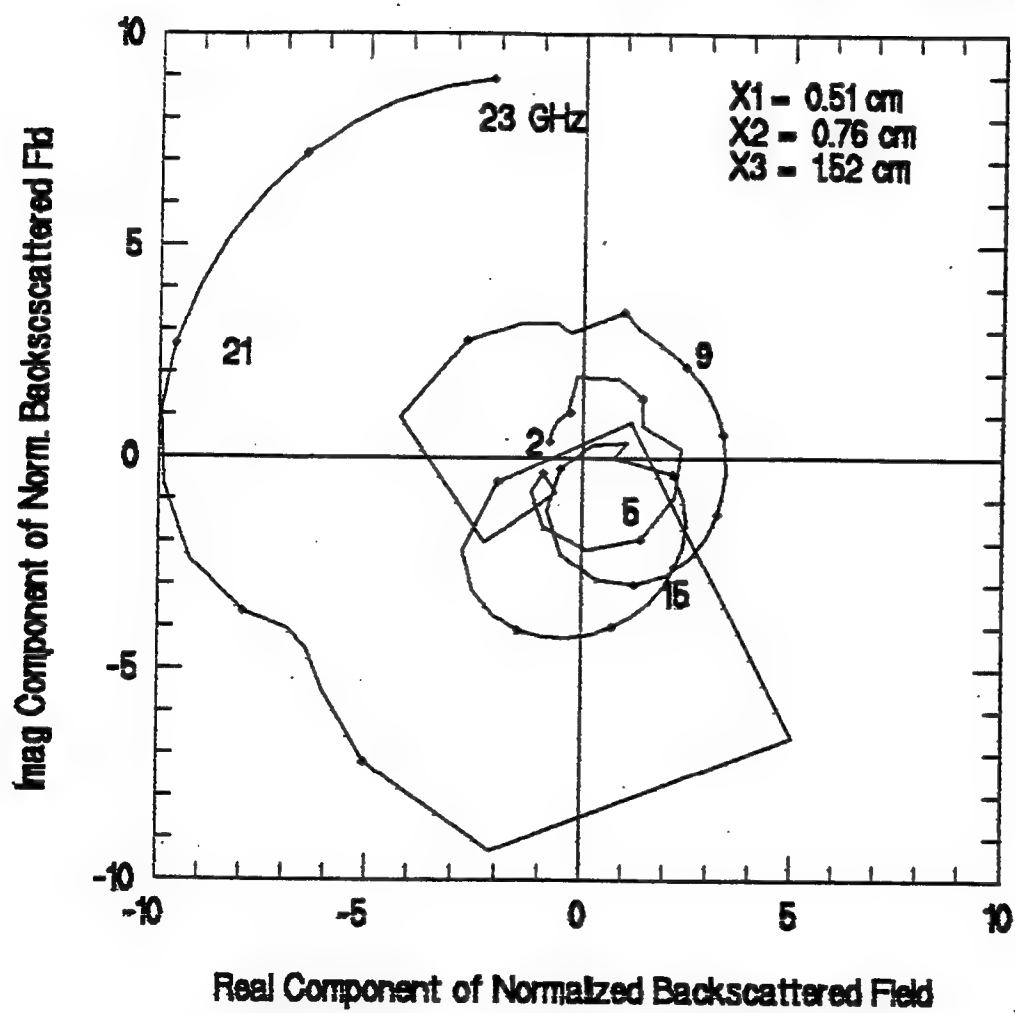
12.4, 6.2, 3.1 GHz design using 1, 5, and 7 arrays respectively



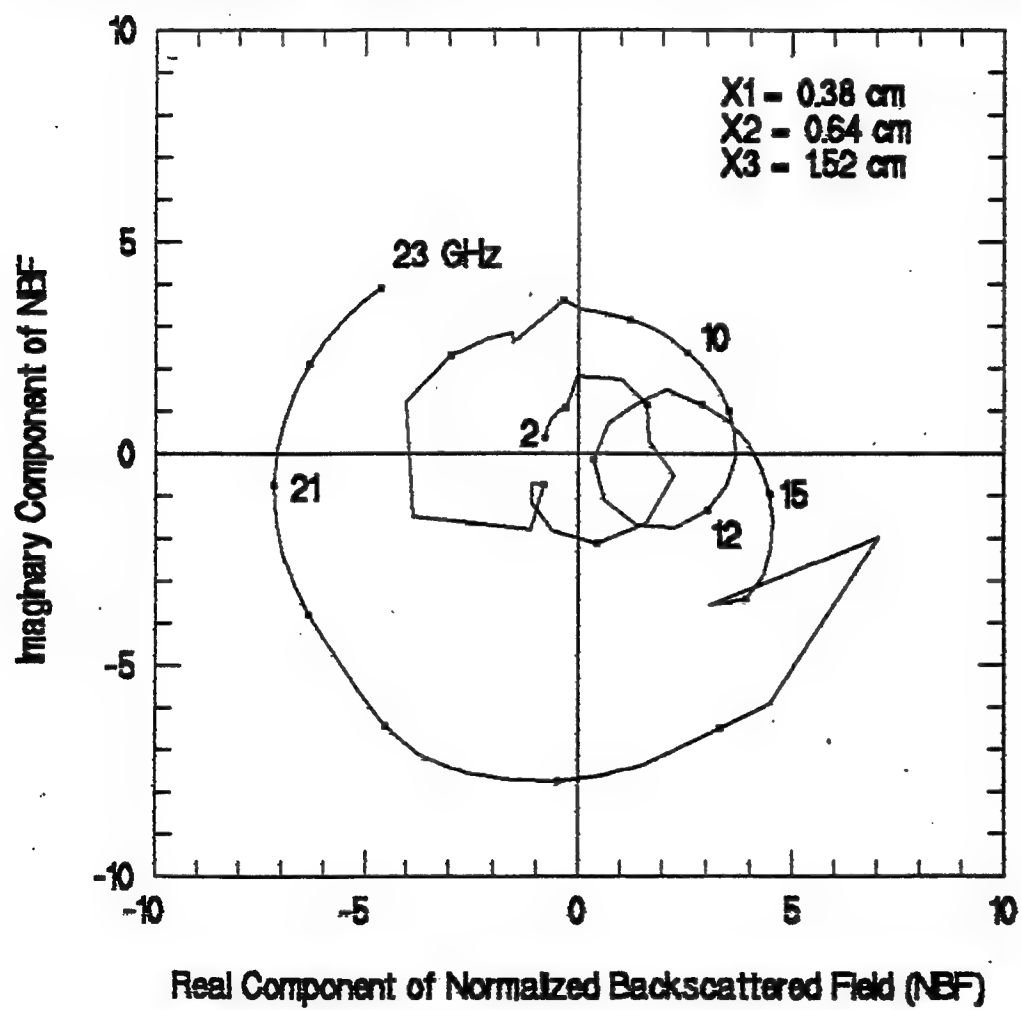
Effect of Decreasing the Distance from the Antenna's Plane To Scattering Layer 1



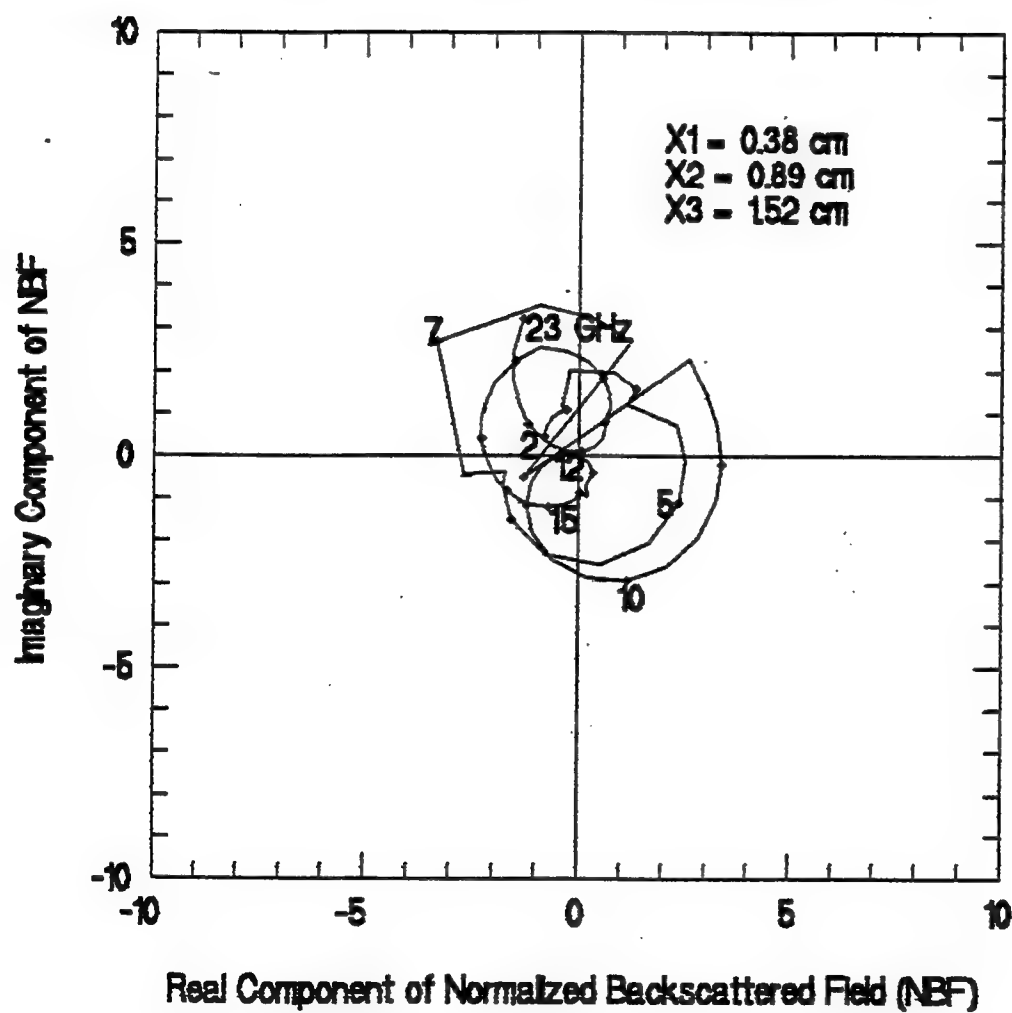
Effect of Increasing the Distance from the Antenna's Plane to Scattering Layer 1



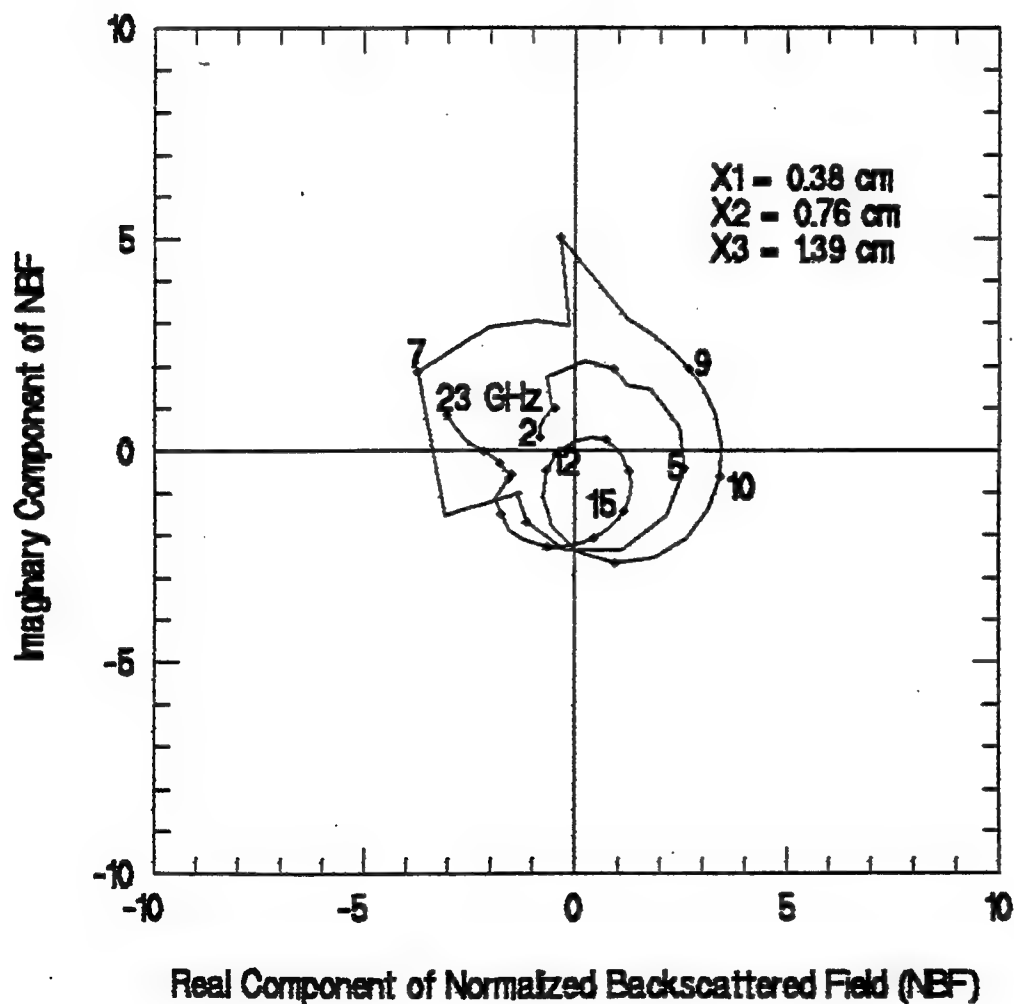
Effect of Decreasing The Distance from the Antenna's Plane to Scattering Layer 2



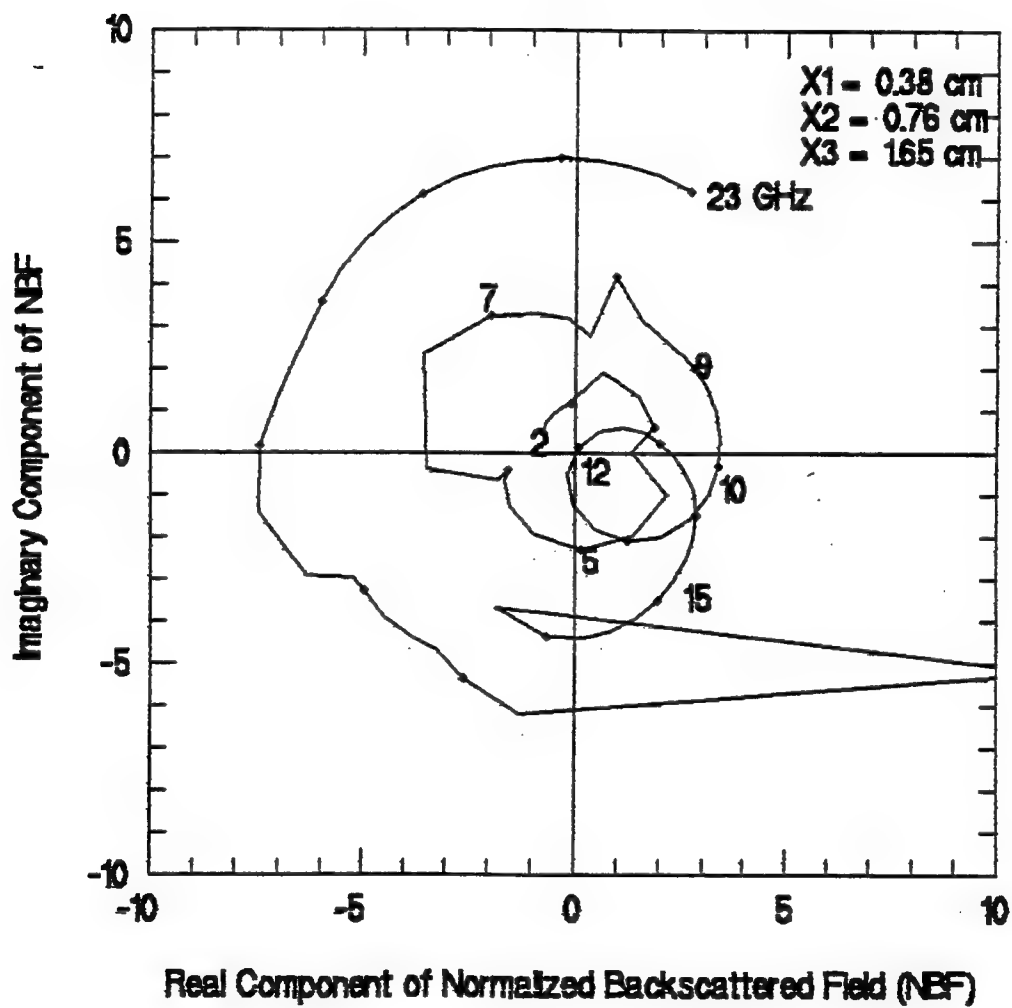
Effect of increasing The Distance from the Antenna's Plane To Scattering Layer 2



Effect of Decreasing The Distance from the Antenna's Plane to Scattering Layer 3



12.4, 6.2, 3.1 design using 1, 5, and 7 arrays respectively



APPENDIX E: Antenna Data for Gain Calibration

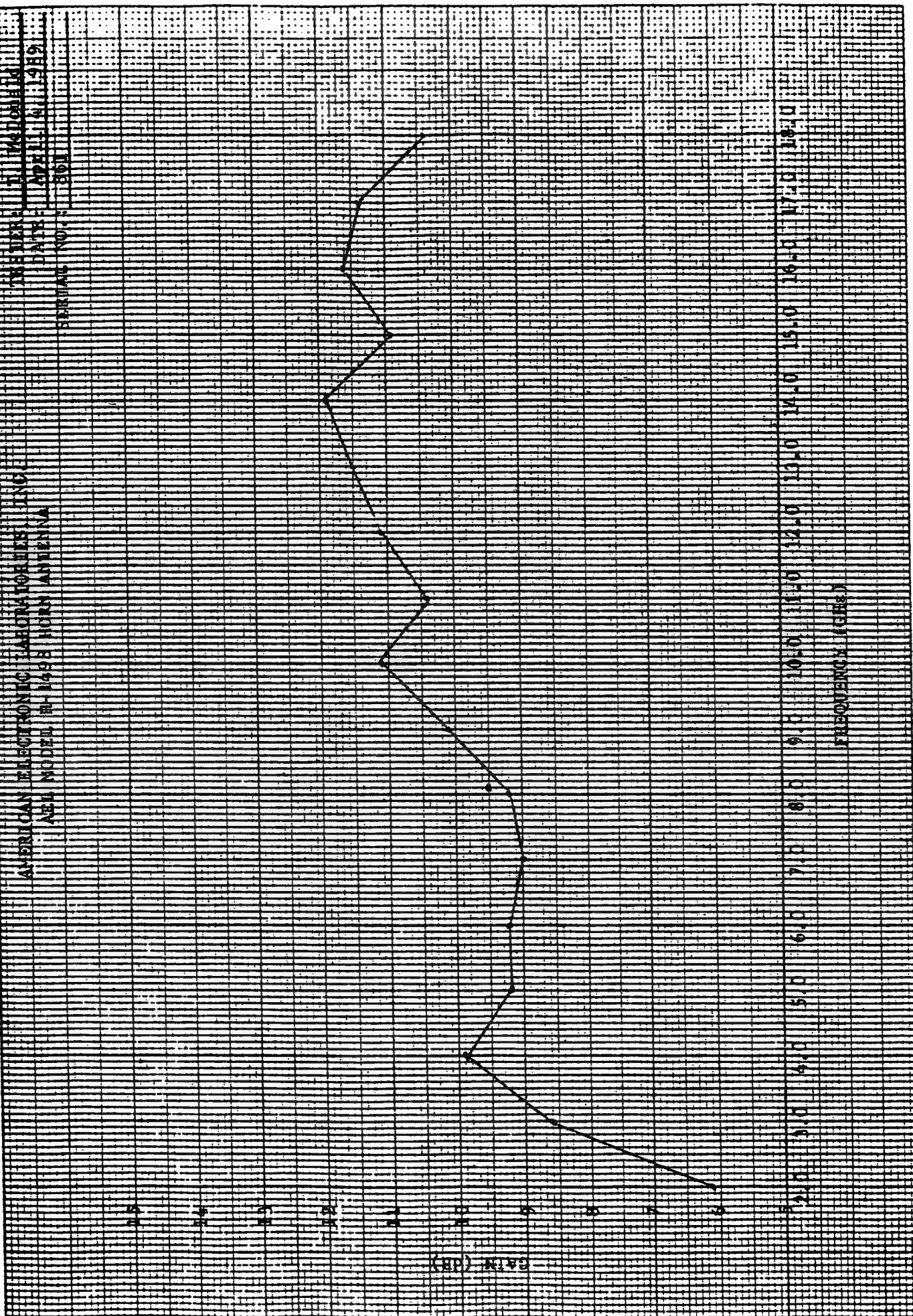
The table below provides insight into the calibration factors used to determine absolute gain values for each different frequency tested. The reference antenna was an American Electronic Laboratories Model H-1498B horn antenna.

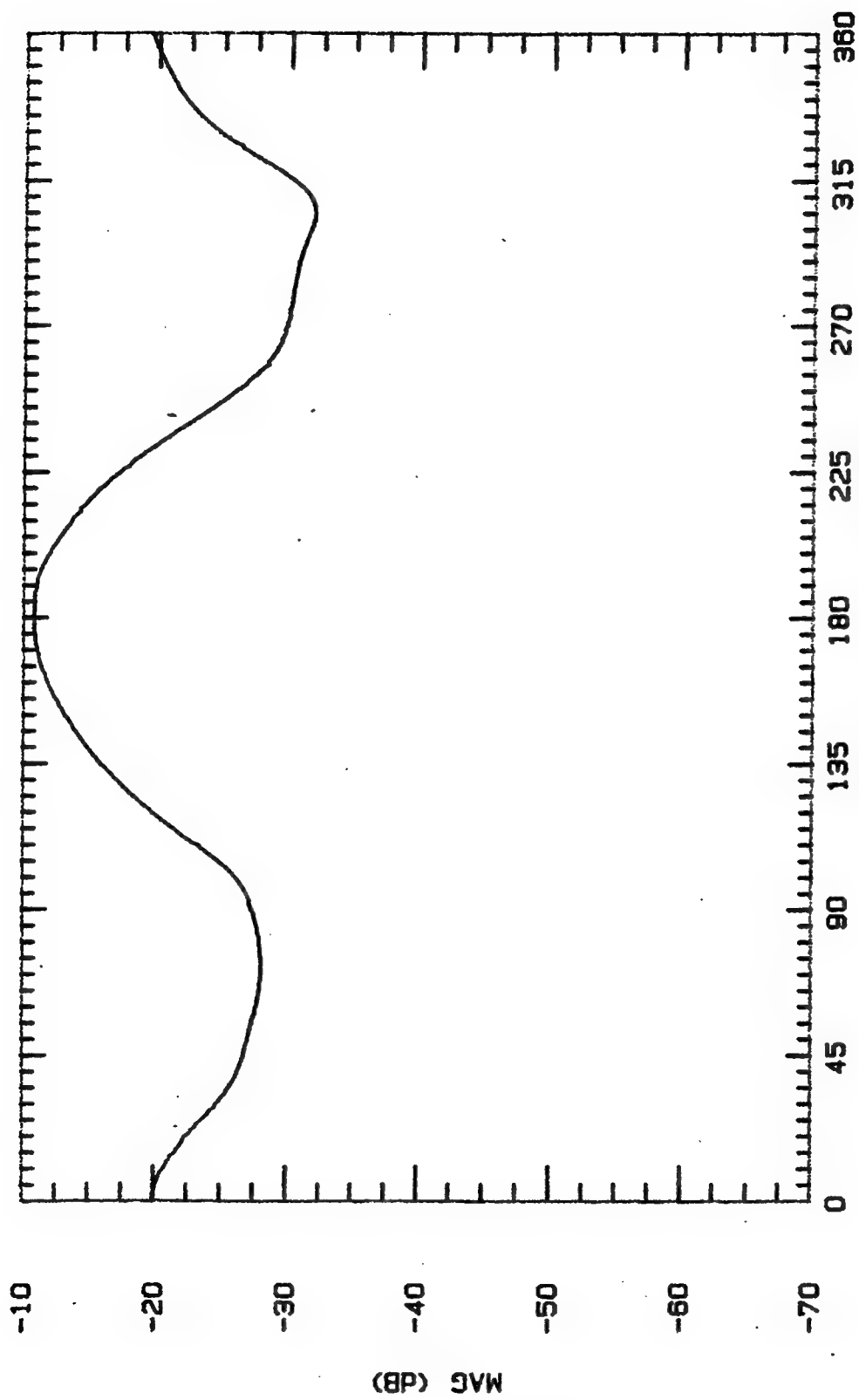
<u>Freq (GHz)</u>	<u>Predicted (dBi)</u>	<u>Measured</u>	<u>Delta</u>
2.00	6.1	-10.7	16.8
2.25	6.3	-10.2	16.5
2.50	7.4	-9.9	17.3
2.75	8.0	-7.5	15.5
3.00	8.6	-9.0	17.6
3.25	8.9	-9.3	18.2
3.50	9.2	-14.2	23.4
3.75	9.6	-13.6	23.2
4.00	9.8	-14.1	23.9
4.25	9.7	-17.2	26.9
4.50	9.5	-16.2	25.7
4.75	9.4	-21.0	30.4
5.00	9.2	-18.7	27.9
5.25	9.2	-20.2	29.4
5.50	9.2	-19.9	29.1
5.75	9.2	-23.9	33.1
6.00	9.2	-26.0	35.2
6.25	9.2	-24.2	33.4
6.50	9.1	-24.1	33.2
6.75	9.0	-23.7	32.7
7.00	9.0	-24.0	33.0
7.25	9.0	-23.7	32.7
7.50	9.1	-24.4	33.5
7.75	9.2	-24.1	31.3
8.00	9.2	-24.0	33.2
8.25	9.4	-26.1	35.5
8.50	9.6	-25.1	34.7
8.75	9.8	-27.8	37.6
9.00	10.1	-27.6	37.7
9.25	10.3	-28.0	38.3
9.50	10.6	-28.5	39.1
9.75	10.8	-27.9	38.7
10.00	11.1	-29.0	40.1
10.25	11.0	-29.0	40.0
10.50	10.7	-29.9	40.6
10.75	10.6	-28.8	39.4
11.00	10.4	-29.0	39.4
11.25	10.6	-28.7	39.3
11.50	10.7	-29.7	40.4
11.75	10.9	-29.7	40.6
12.00	11.1	-31.0	42.1
12.25	11.2	-31.8	42.0
12.40	11.2	-31.8	43.0
12.50	11.3	-33.0	44.3
12.75	11.4	-32.8	44.2
13.00	11.5	-33.2	44.7
16.00	11.6	-36.4	48.0

ASL
700

AMERICAN ELECTRONIC LABORATORIES, INC.
AEL MODEL M-1498 HORN ANTENNA

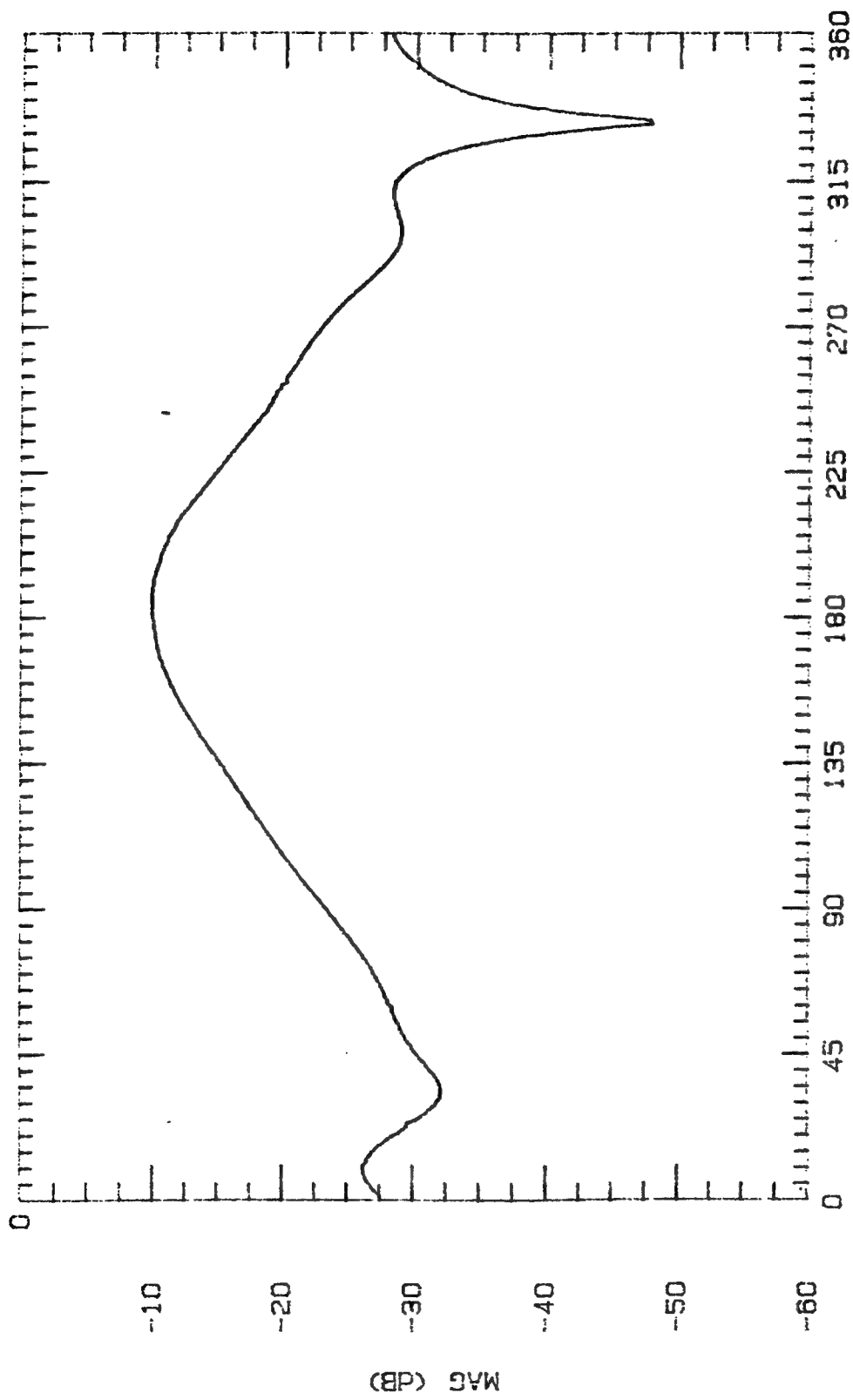
TESTER: J. McTODD
DATE: APRIL 4, 1959
SERIAL NO.: 361





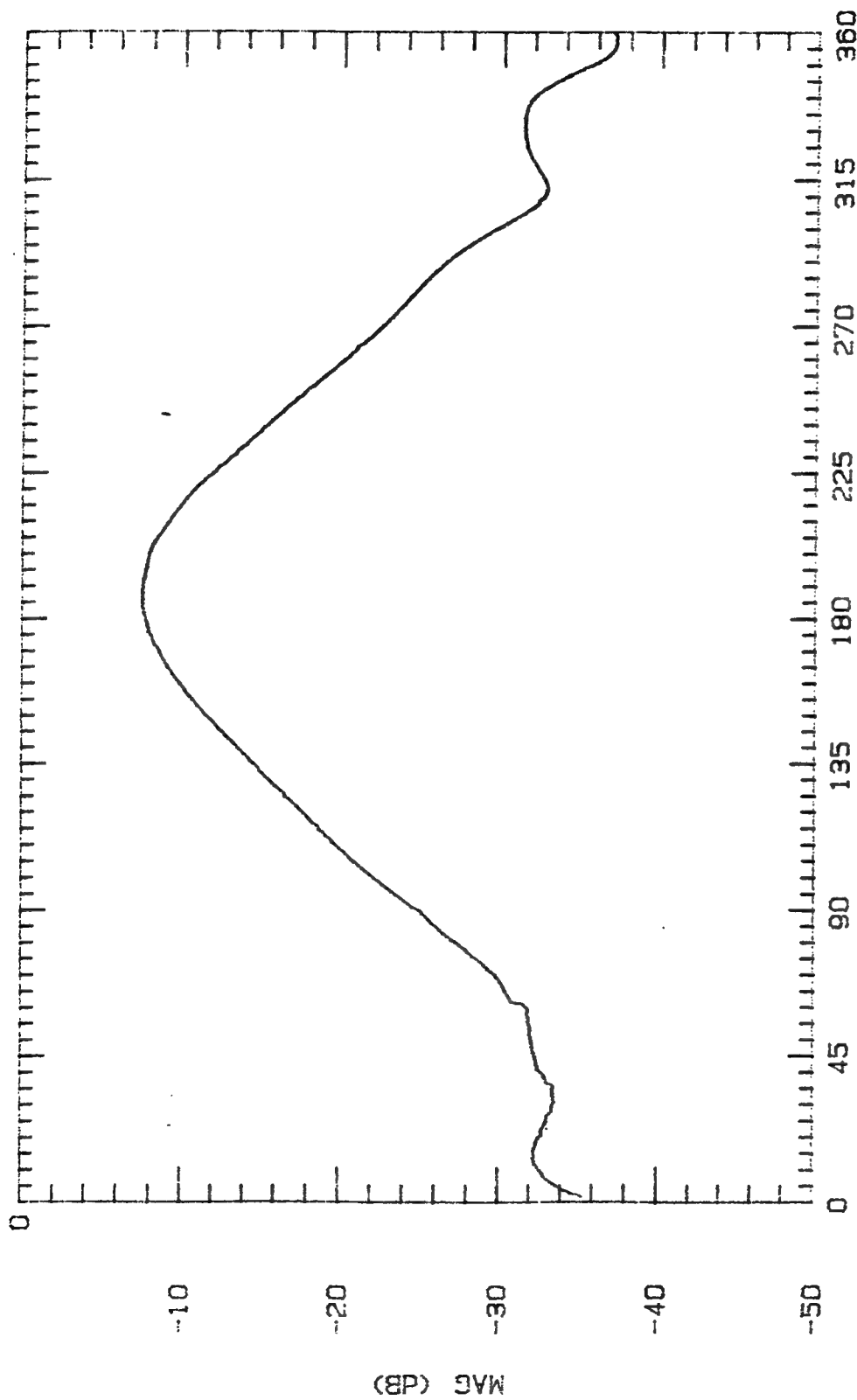
ASPECT ANGLE (DEGREES)

File Name	Frequency	Pattern Type	Date
BH2	2 GHz	E-PLANE	19 OCT



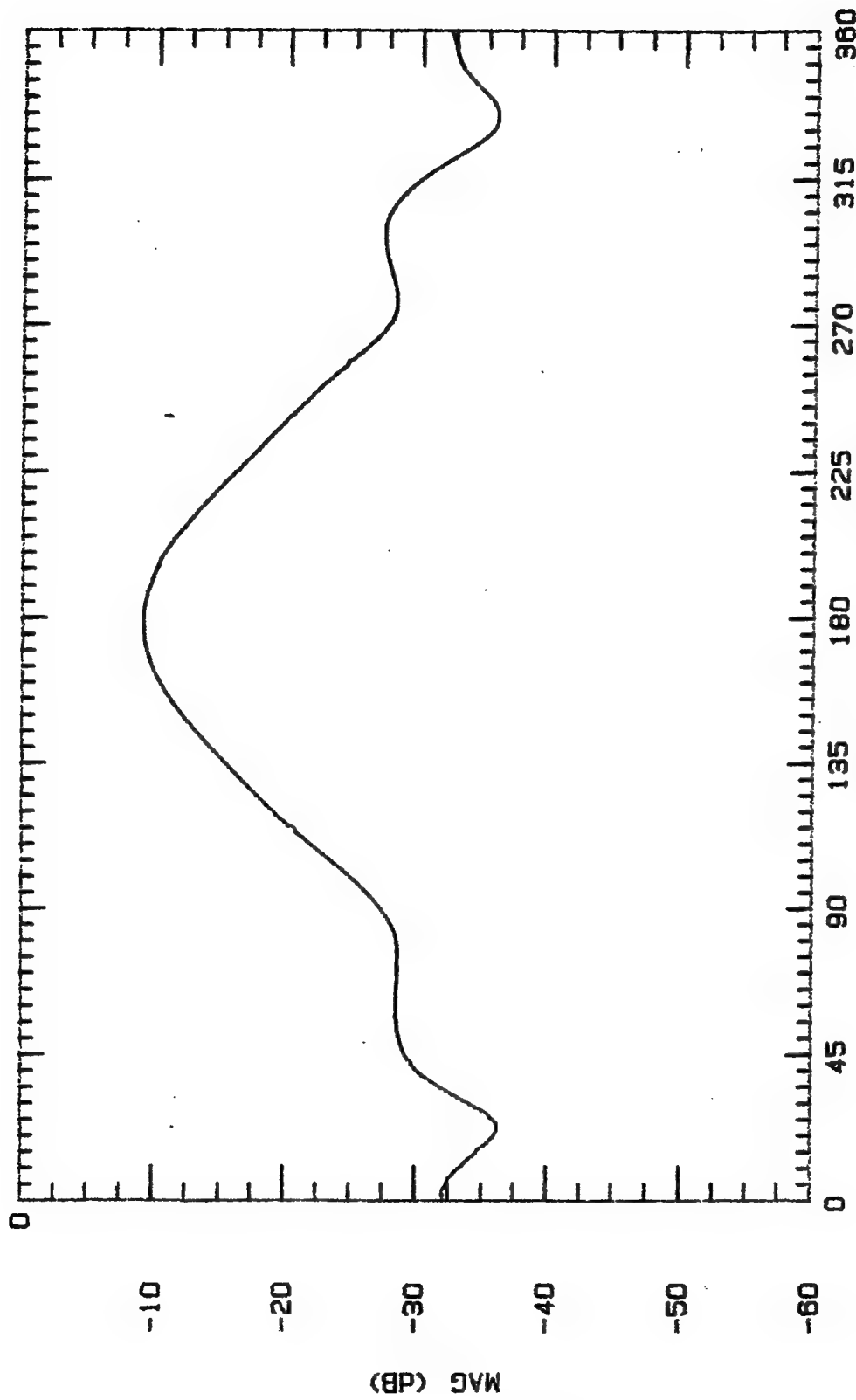
ASPECT ANGLE (DEGREES)

File Name	Frequency	Pattern Type	Date
BH250	2.5 GHz	E-PLANE	1 NOV 94



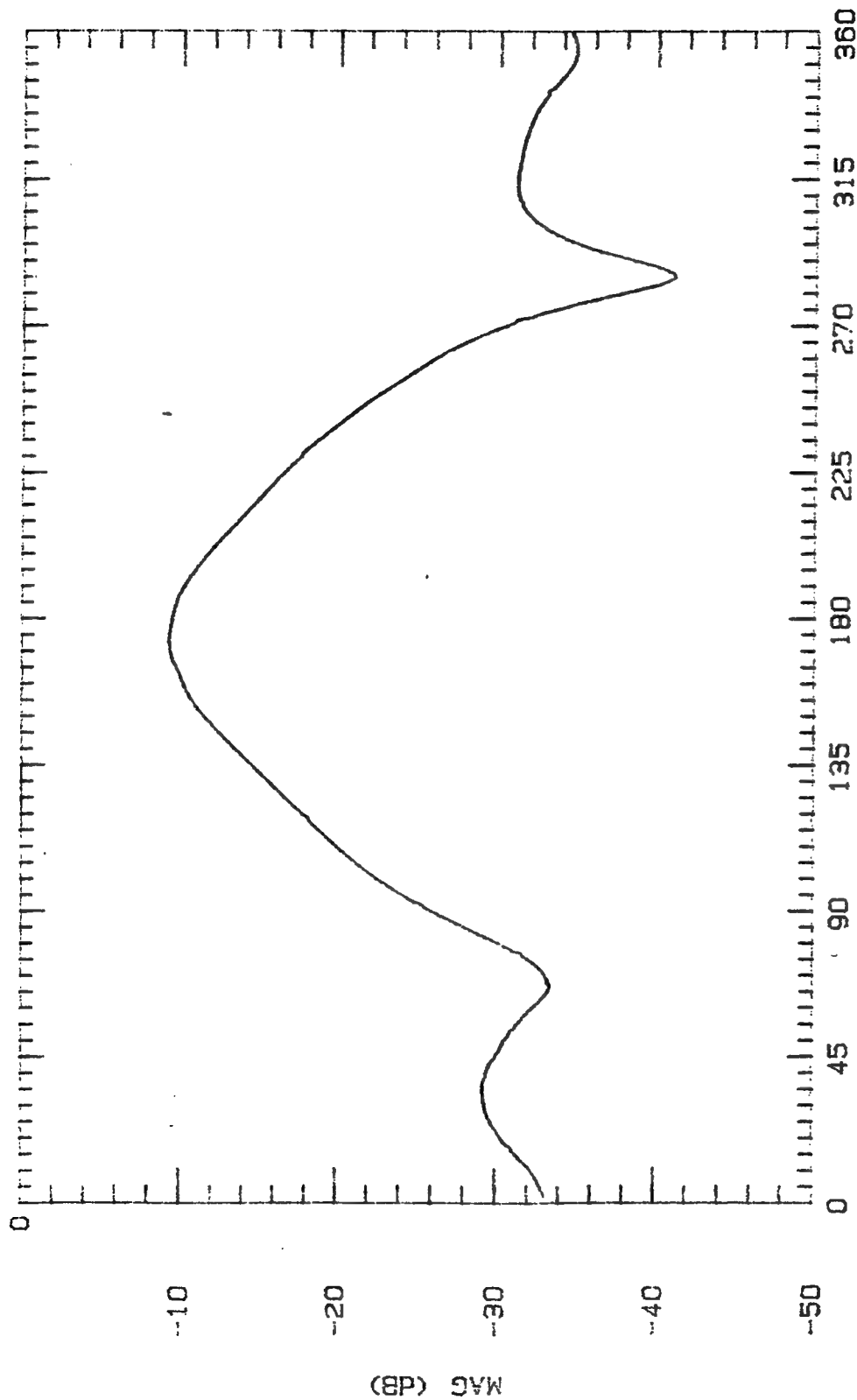
ASPECT ANGLE (DEGREES)

File Name	Frequency	Pattern Type	Date
BH275	2.75 GHz	E-PLANE	1 NOV 94



ASPECT ANGLE (DEGREES)

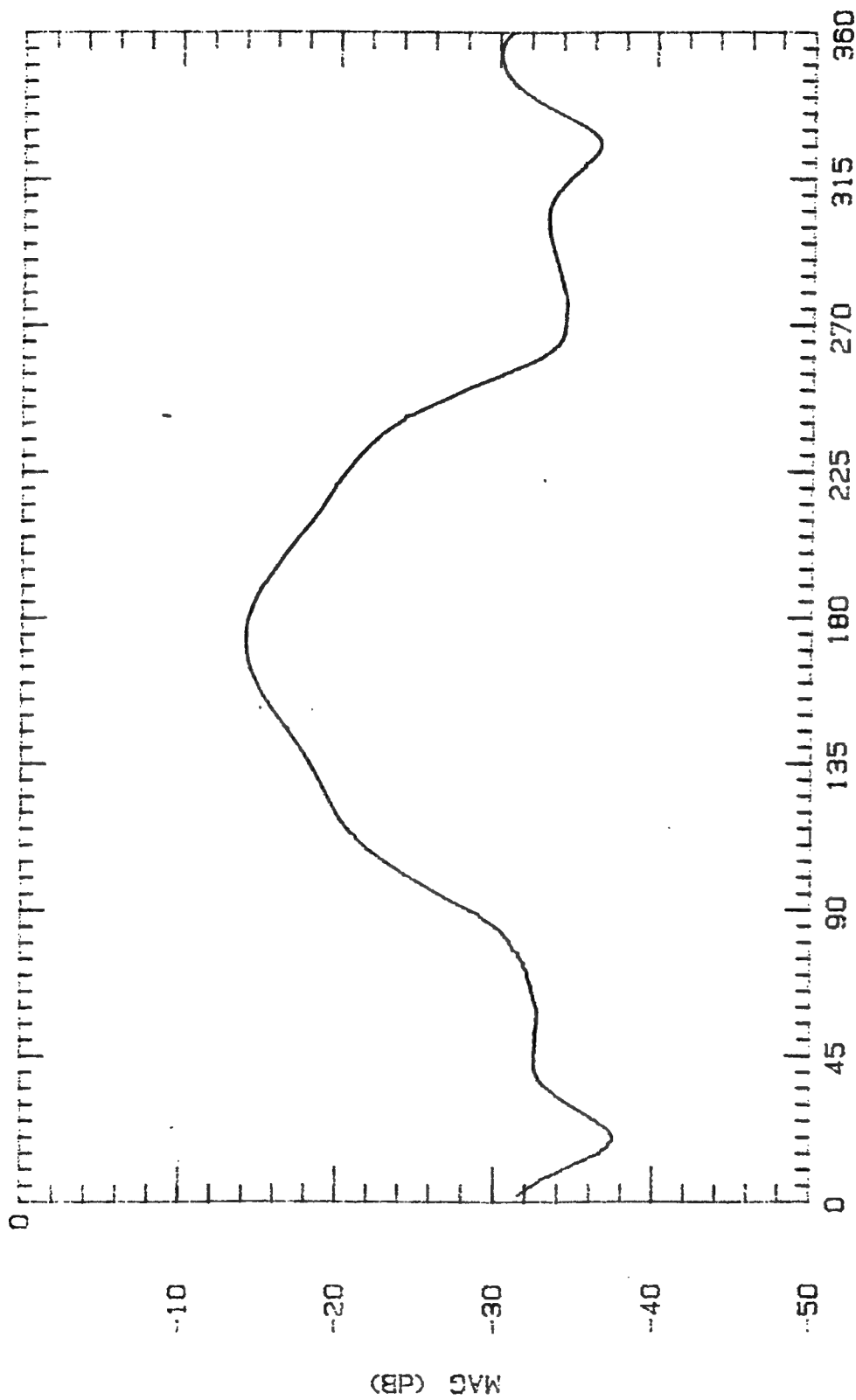
File Name	Frequency	Pattern Type	Date
BH3	3 GHz	E-PLANE	19 OCT



ASPECT ANGLE (DEGREES)

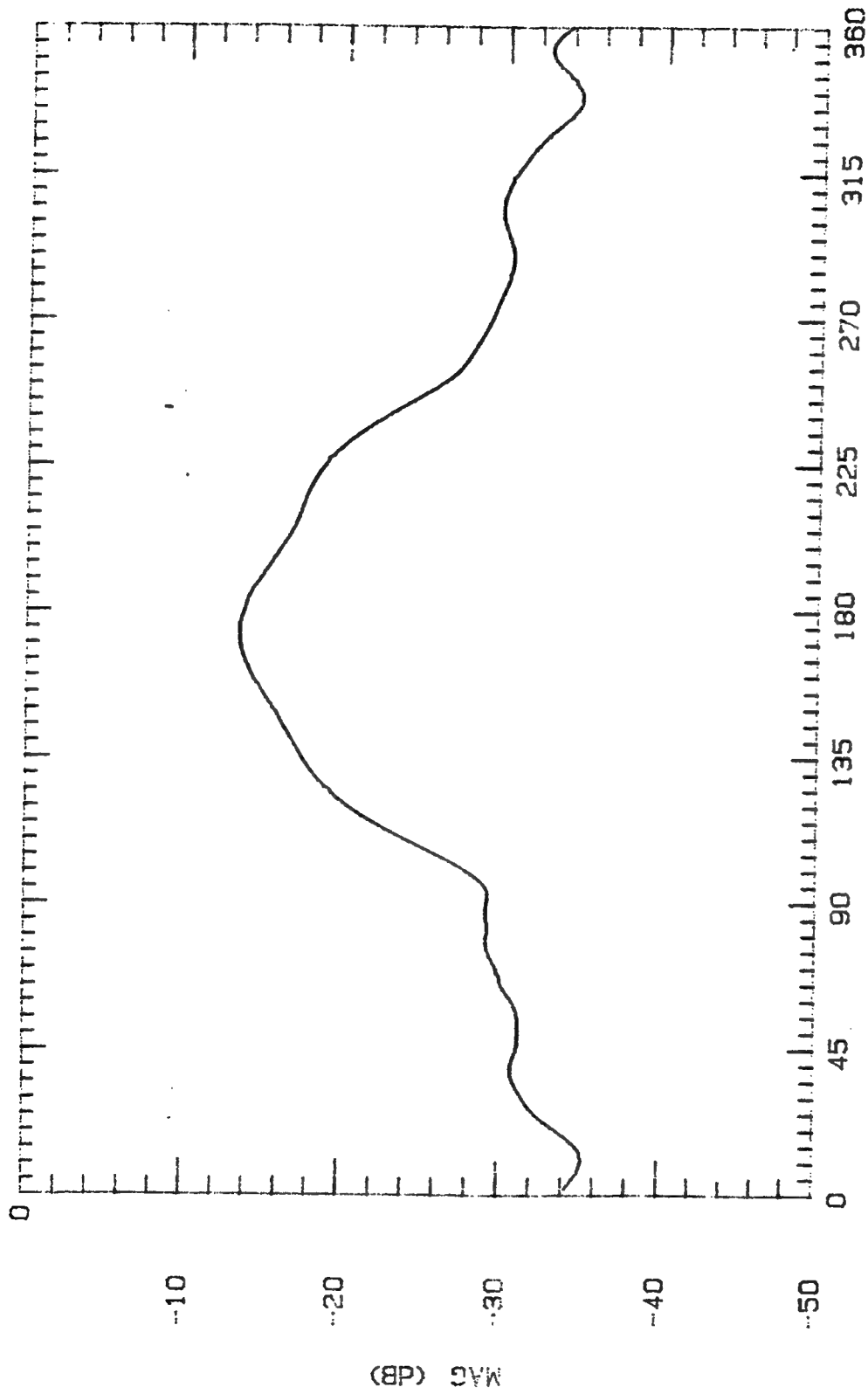
File Name	Frequency	Pattern Type	Date
BH325	3.25 GHz	E-PLANE	1 NOV 94

E-7



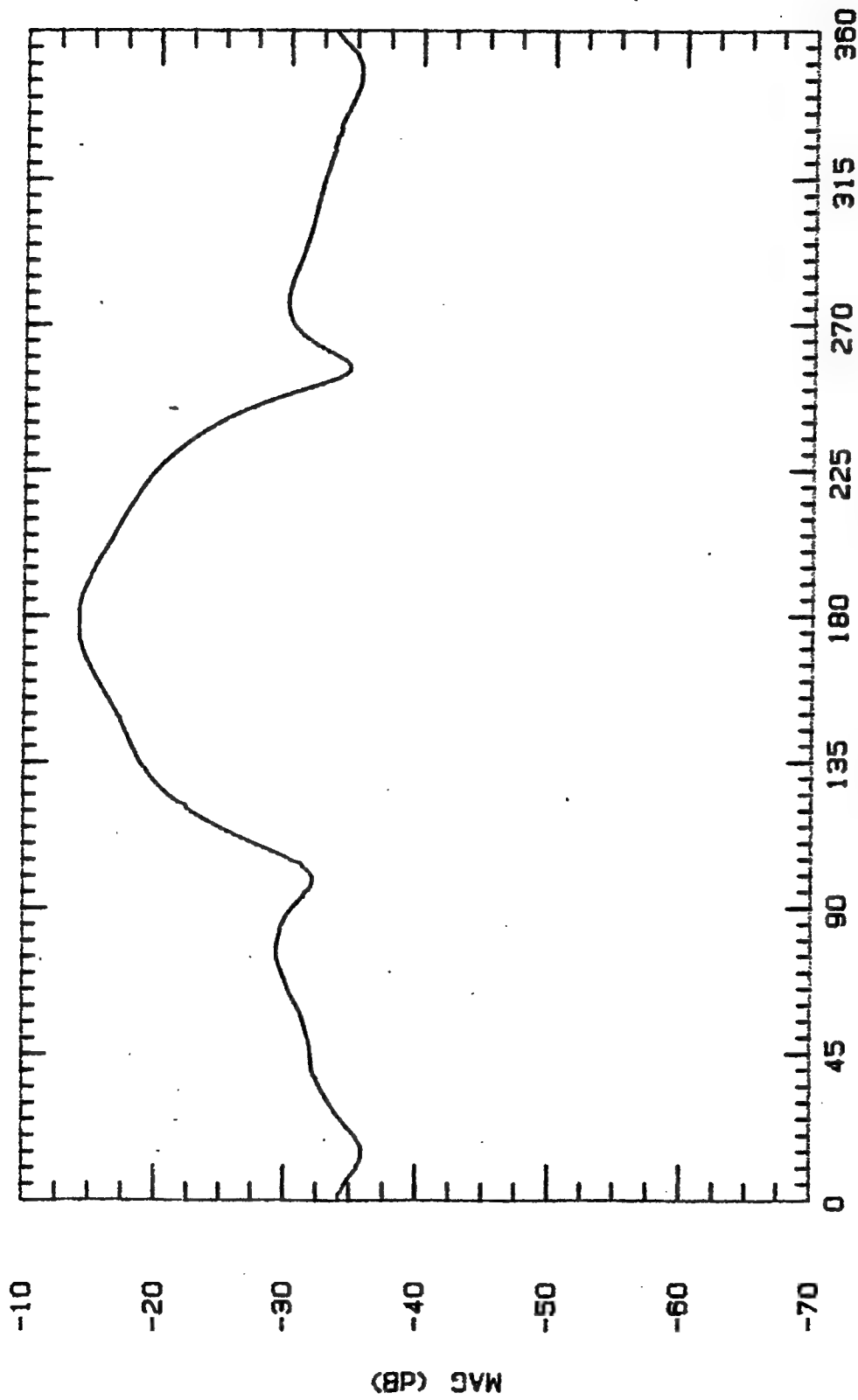
ASPECT ANGLE (DEGREES)

File Name	Frequency	Pattern Type	Date
BH350	3.5 CHz	E-PLANE	1 NOV 94



ASPECT ANGLE (DEGREES)

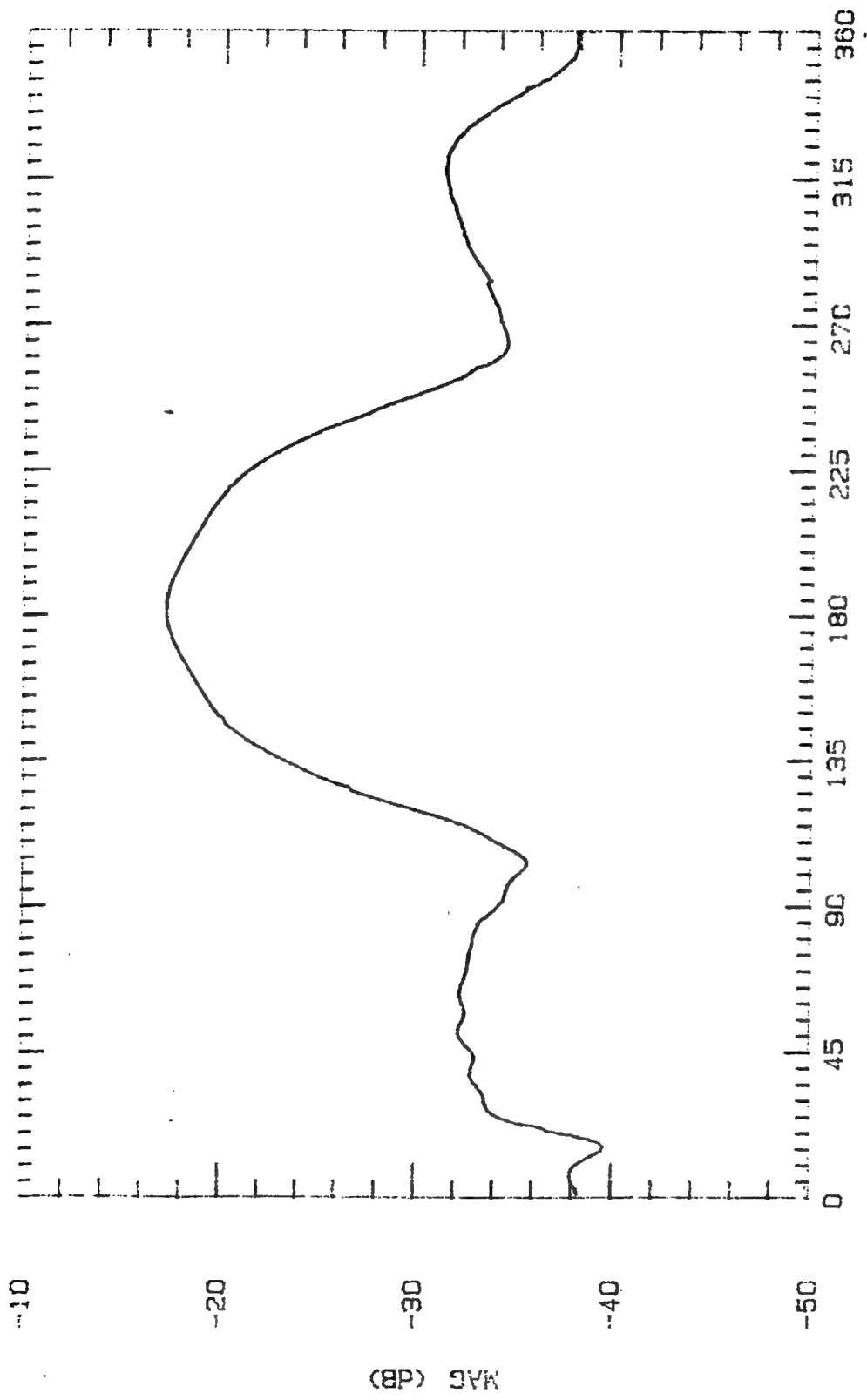
File Name	Frequency	Pattern Type	Data
BH375	3.75 GHz	E-PLANE	1 NOV 94



E - 10

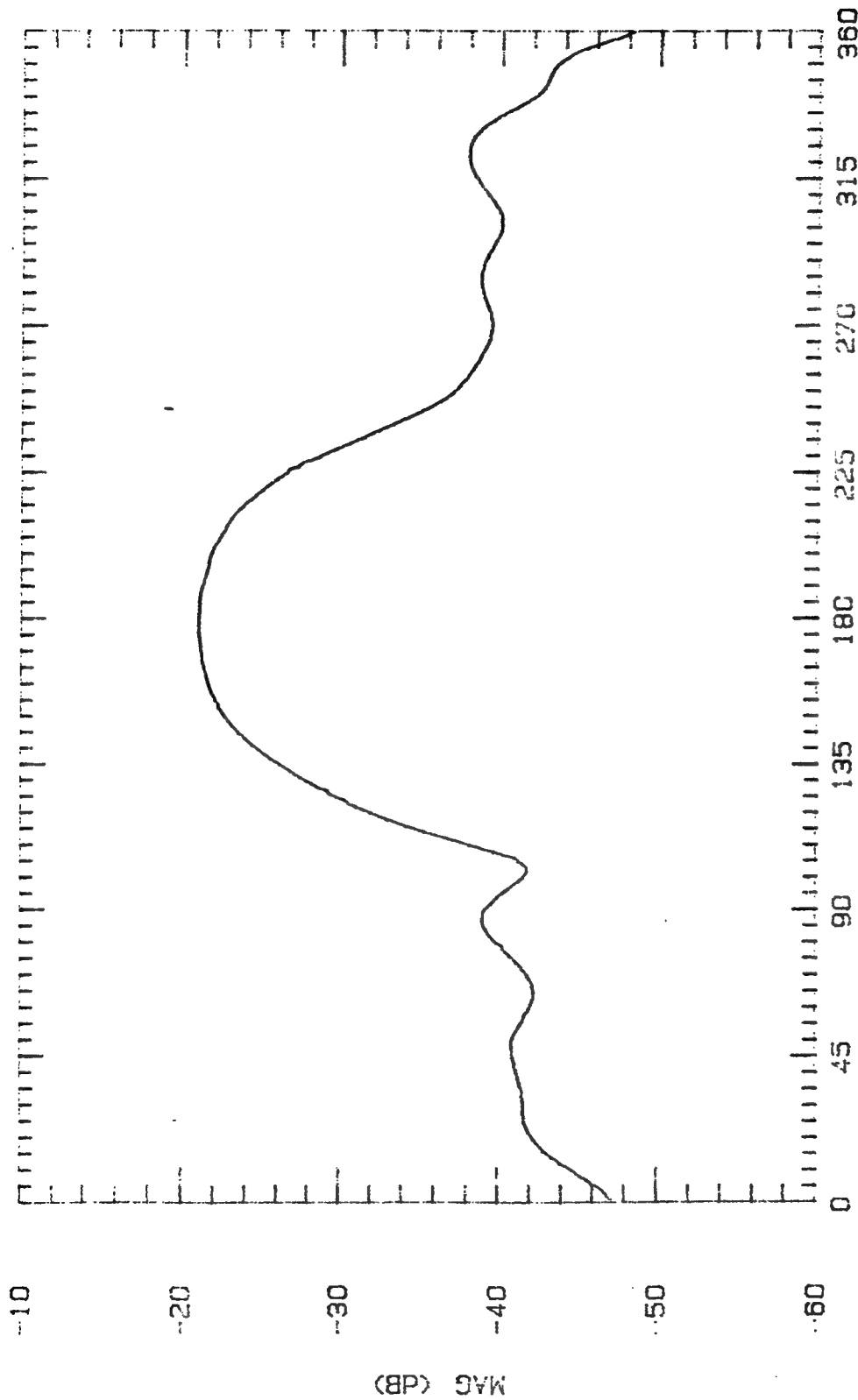
ASPECT ANGLE (DEGREES)

File Name	Frequency	Pattern Type	Date
BH4	4 GHz	E-PLANE	18 OCT



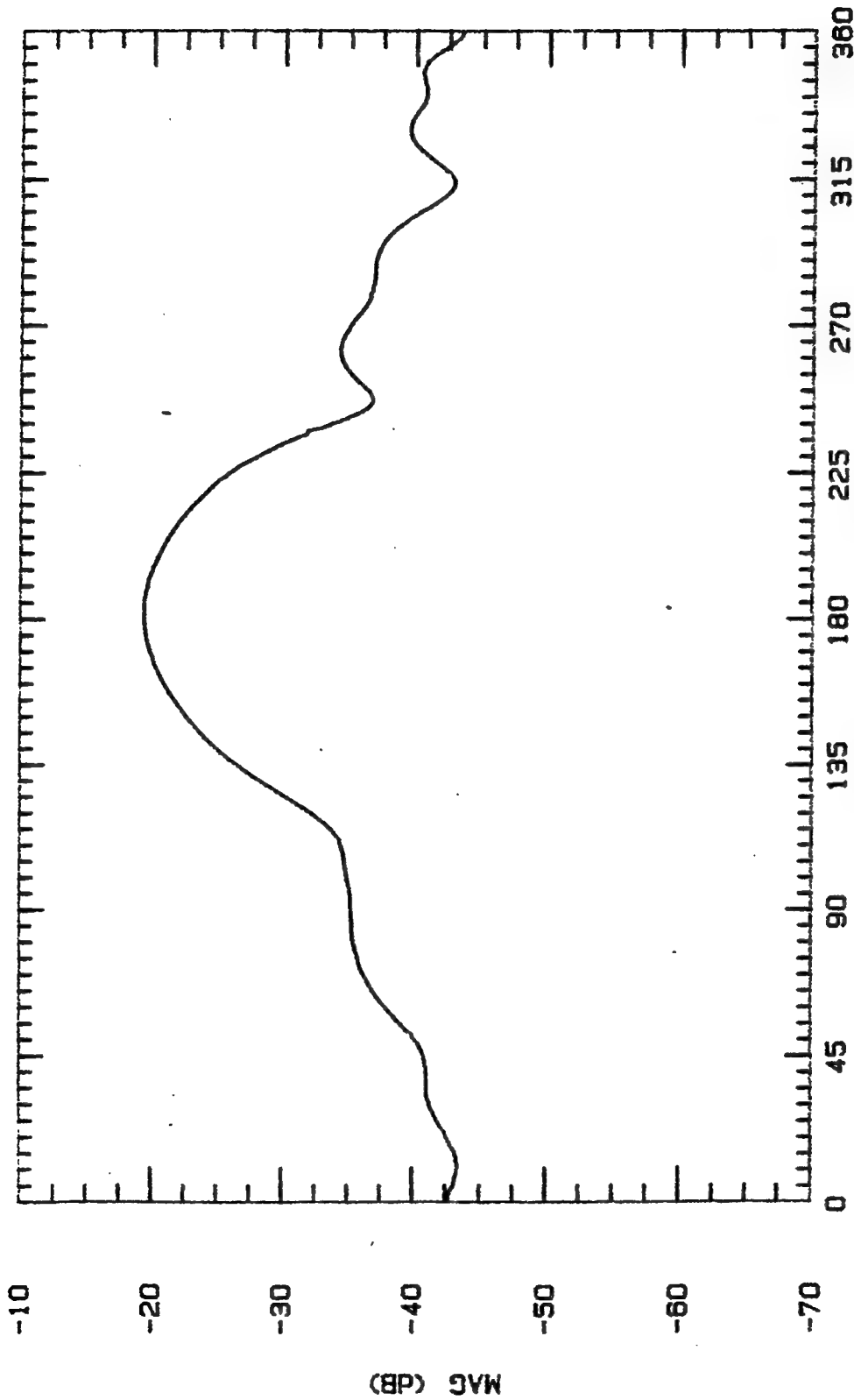
ASPECT ANGLE (DEGREES)

File Name	Frequency	Pattern Type	Date
BH425	4.25 GHz	E-PLANE	1 NOV 94



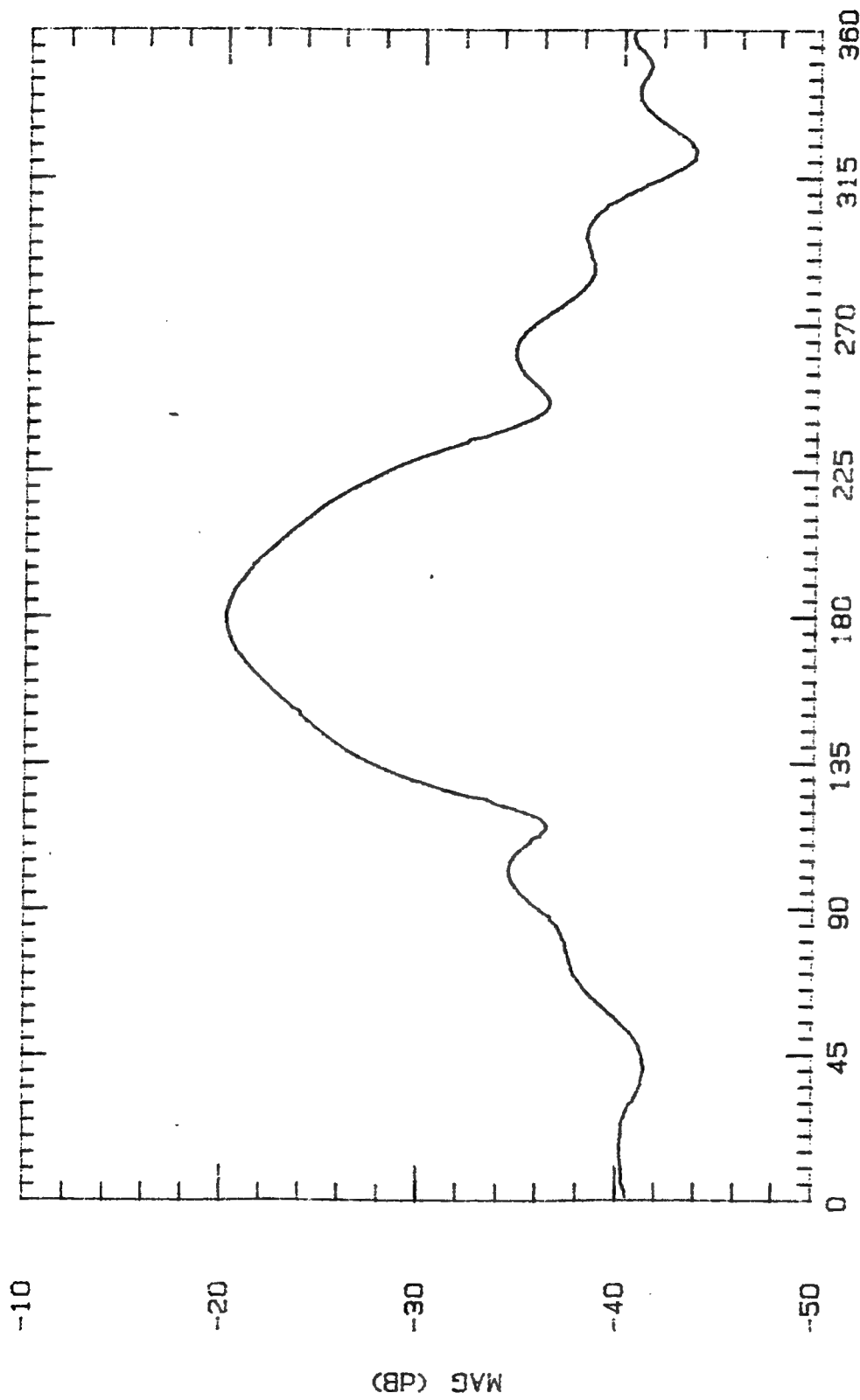
E - 12

File Name	Frequency	Pattern Type	Date
BH475	4.75 GHz	E-PLANE	1 NOV 94



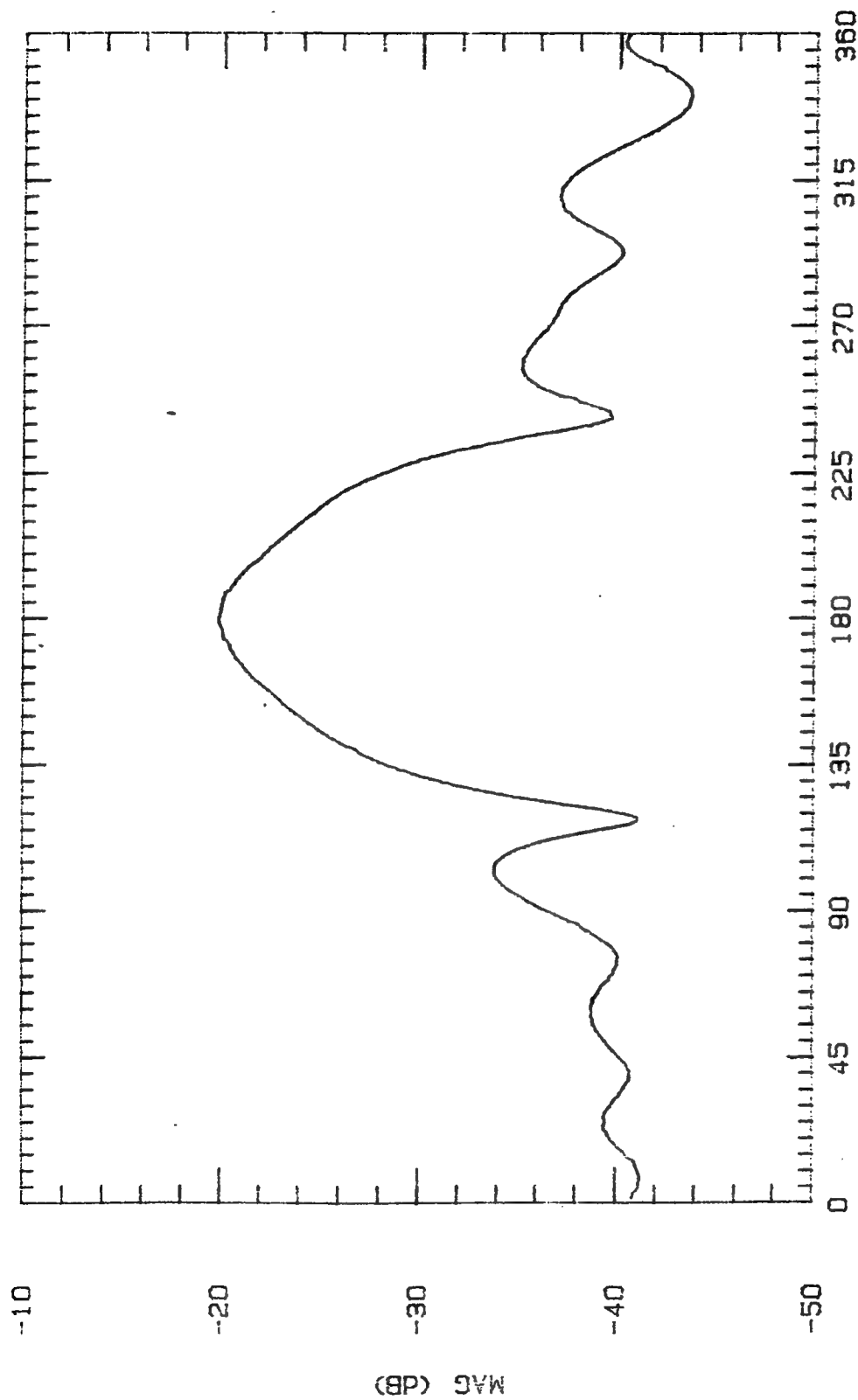
ASPECT ANGLE (DEGREES)

File Name	Frequency	Pattern Type	Date
BH5	5 GHz	E-PLANE	18 OCT



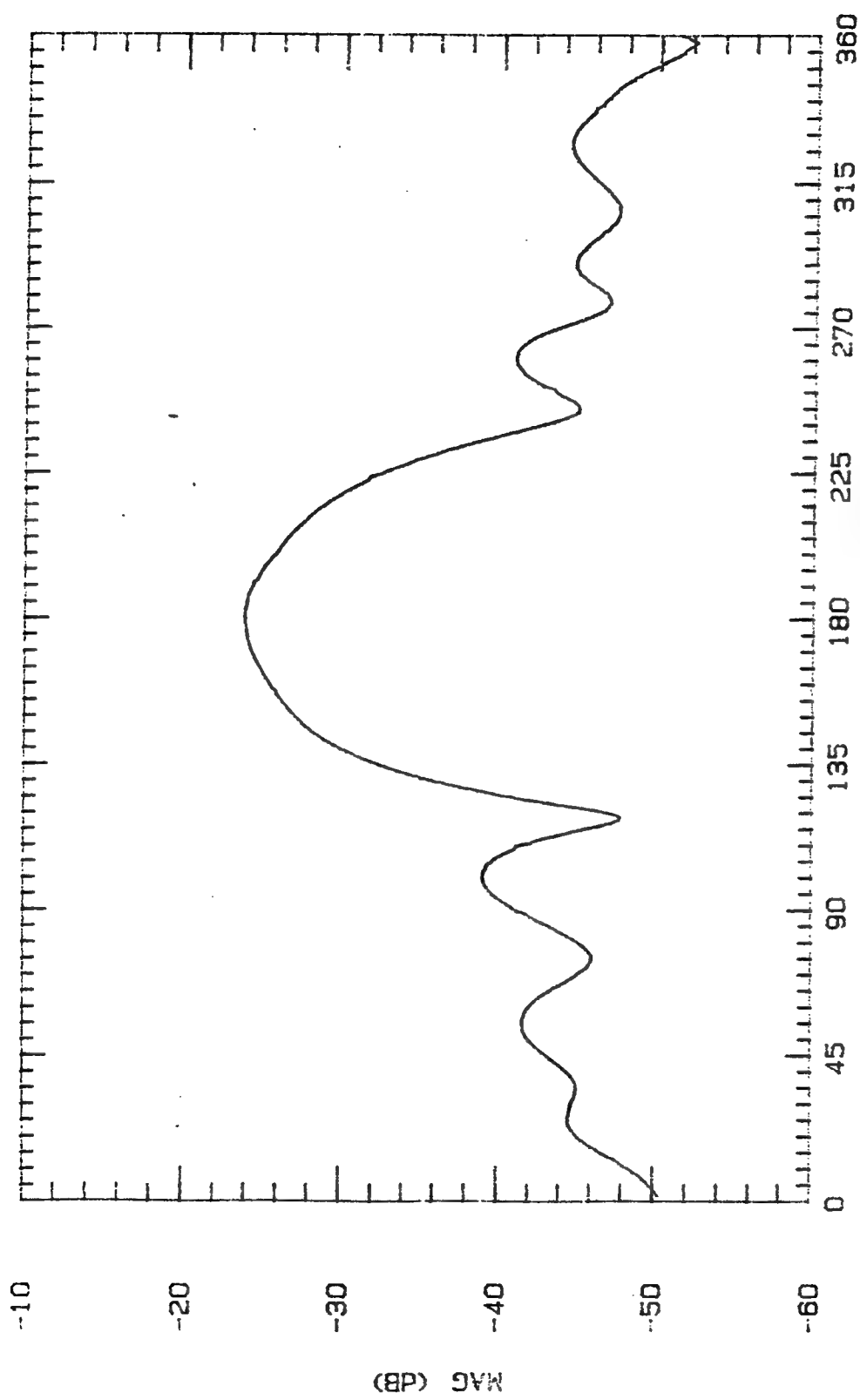
ASPECT ANGLE (DEGREES)

File Name	Frequency	Pattern Type	Data
BH525	5.25 GHz	E-PLANE	1 NOV 94



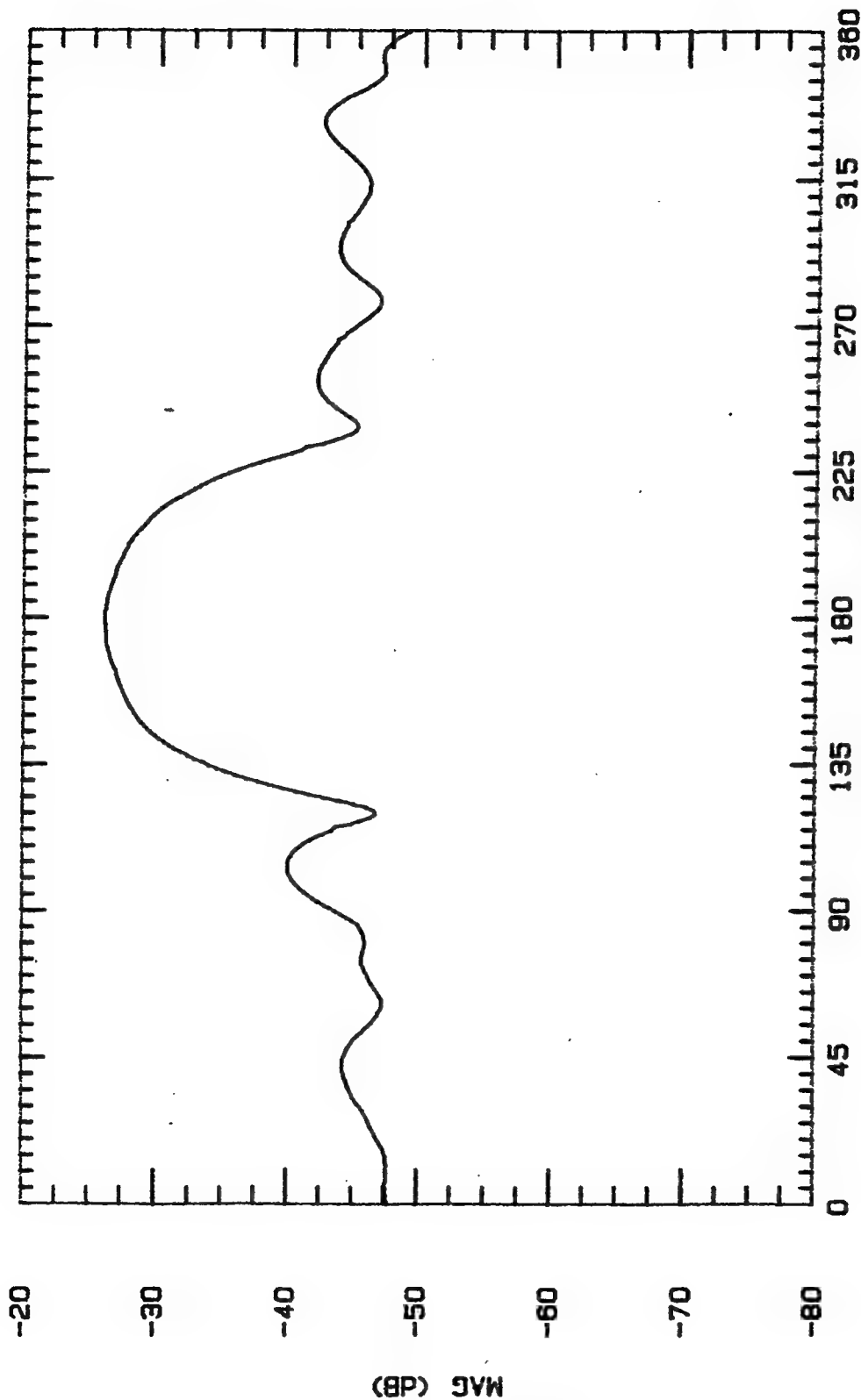
ASPECT ANGLE (DEGREES)

File Name	Frequency	Pattern Type	Date
BH550	5.5 GHz	E-PLANE	1 NOV 94



ASPECT ANGLE (DEGREES)

File Name	Frequency	Pattern Type	Date
BH575	5.75 GHz	E-PLANE	1 NOV 94

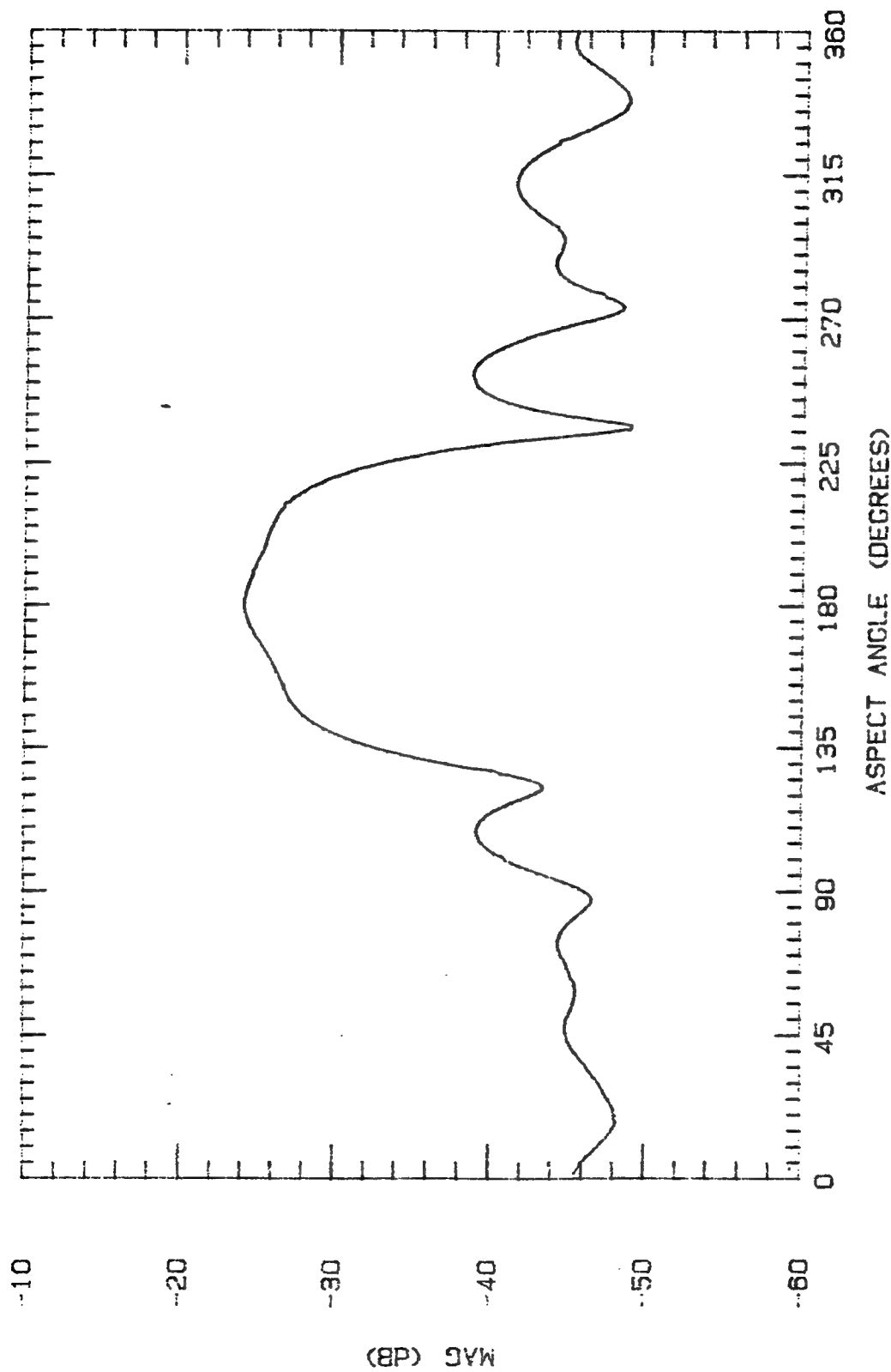


ASPECT ANGLE (DEGREES)

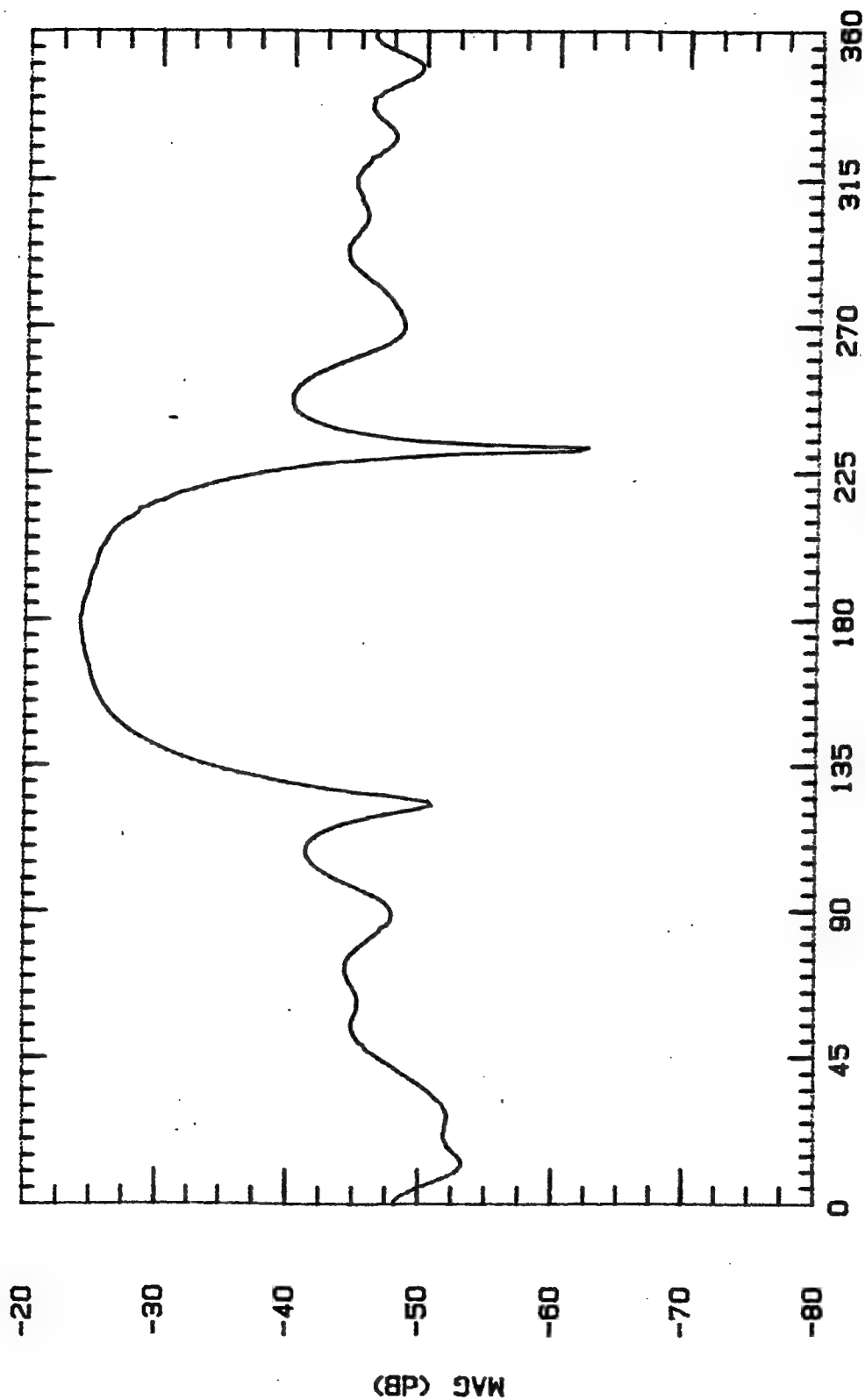
File Name	Frequency	Pattern Type	Date
BH8	8 GHz	E-PLANE	18 OCT 84

(dB) MAC

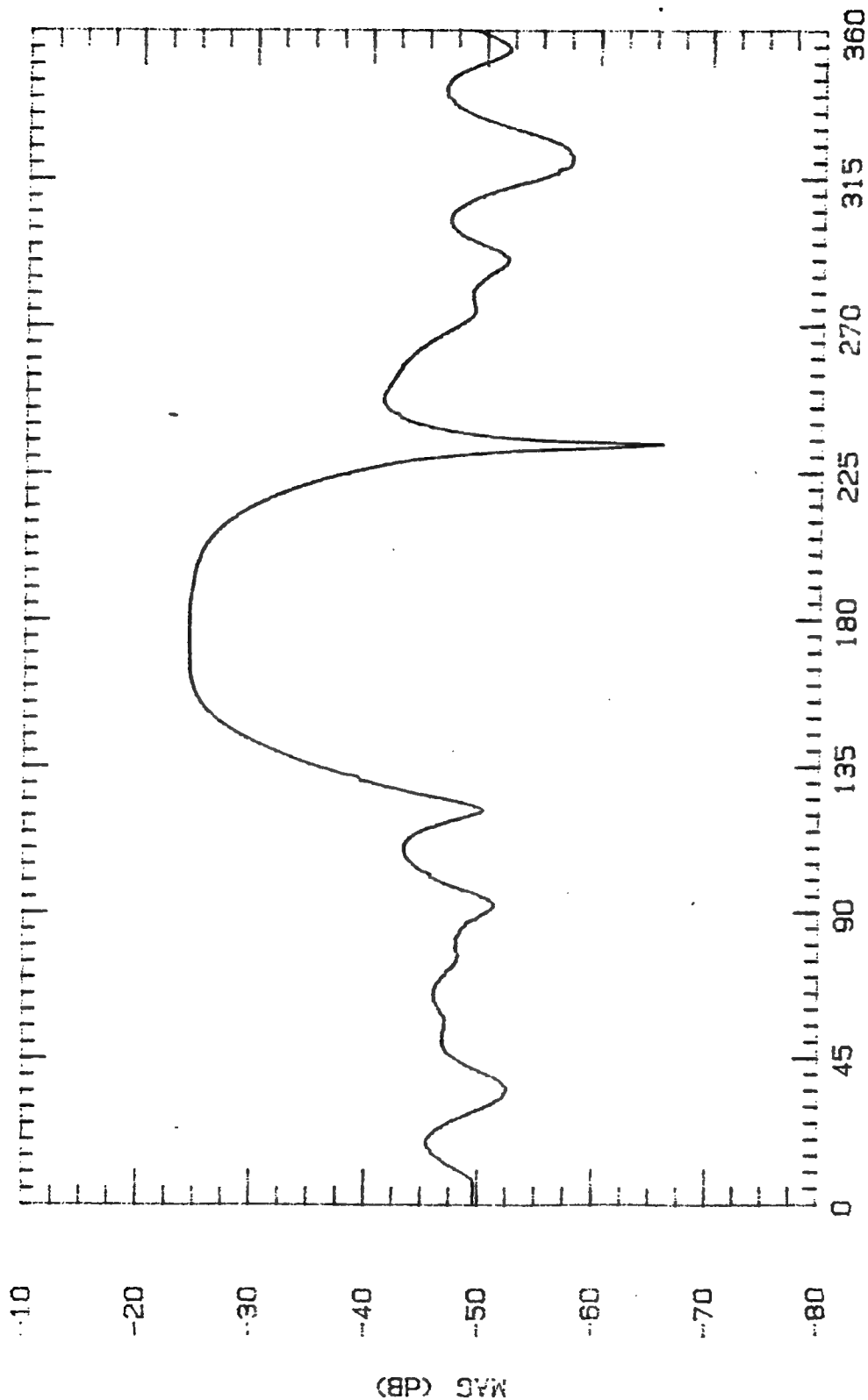
E-17



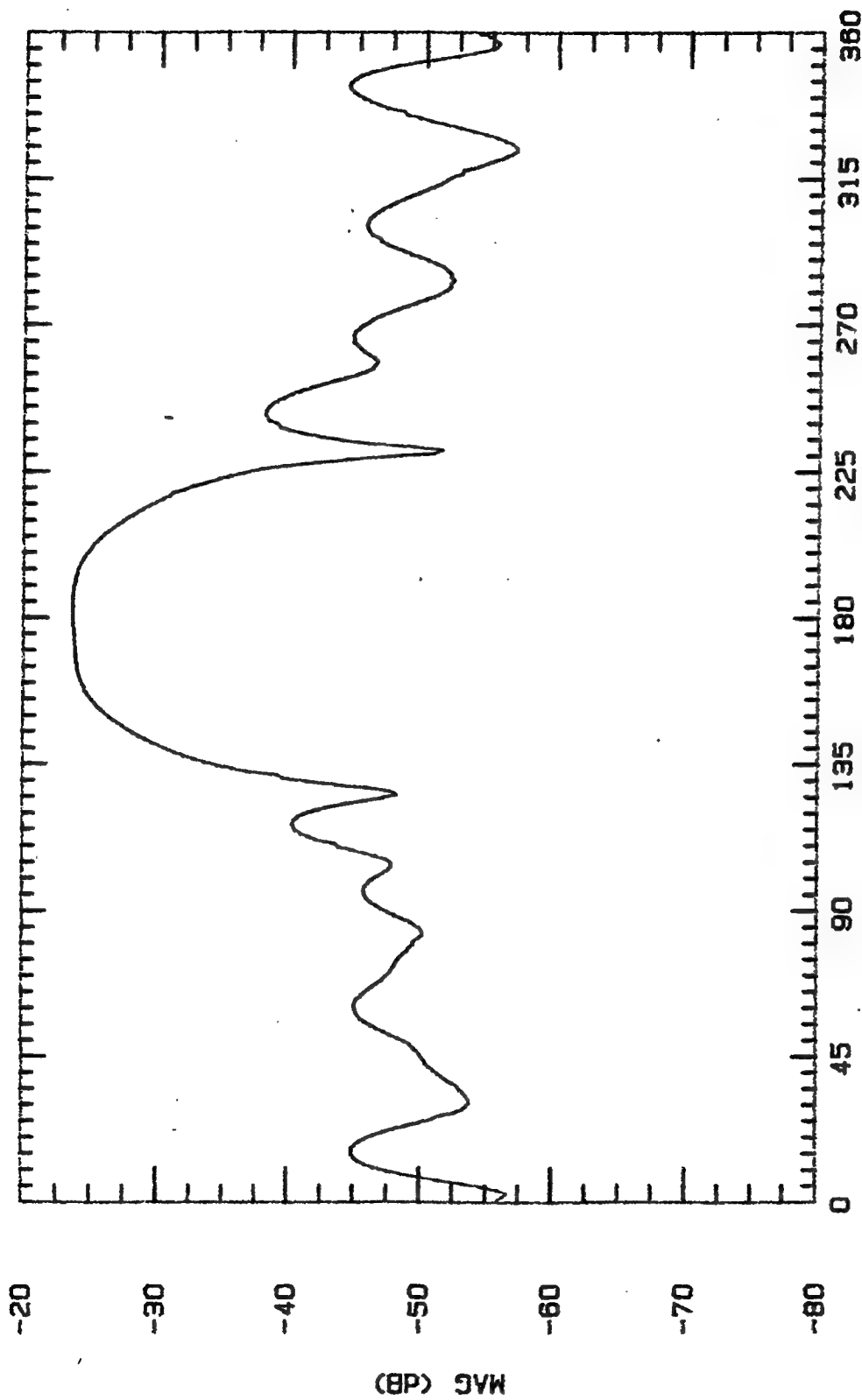
File Name	Frequency	Pattern Type	Date
BH650	6.5 GHz	E-PLANE	1 NOV 94



File Name	Frequency	Pattern Type	Date
BH7	7 GHz	E-PLANE	10 OCT

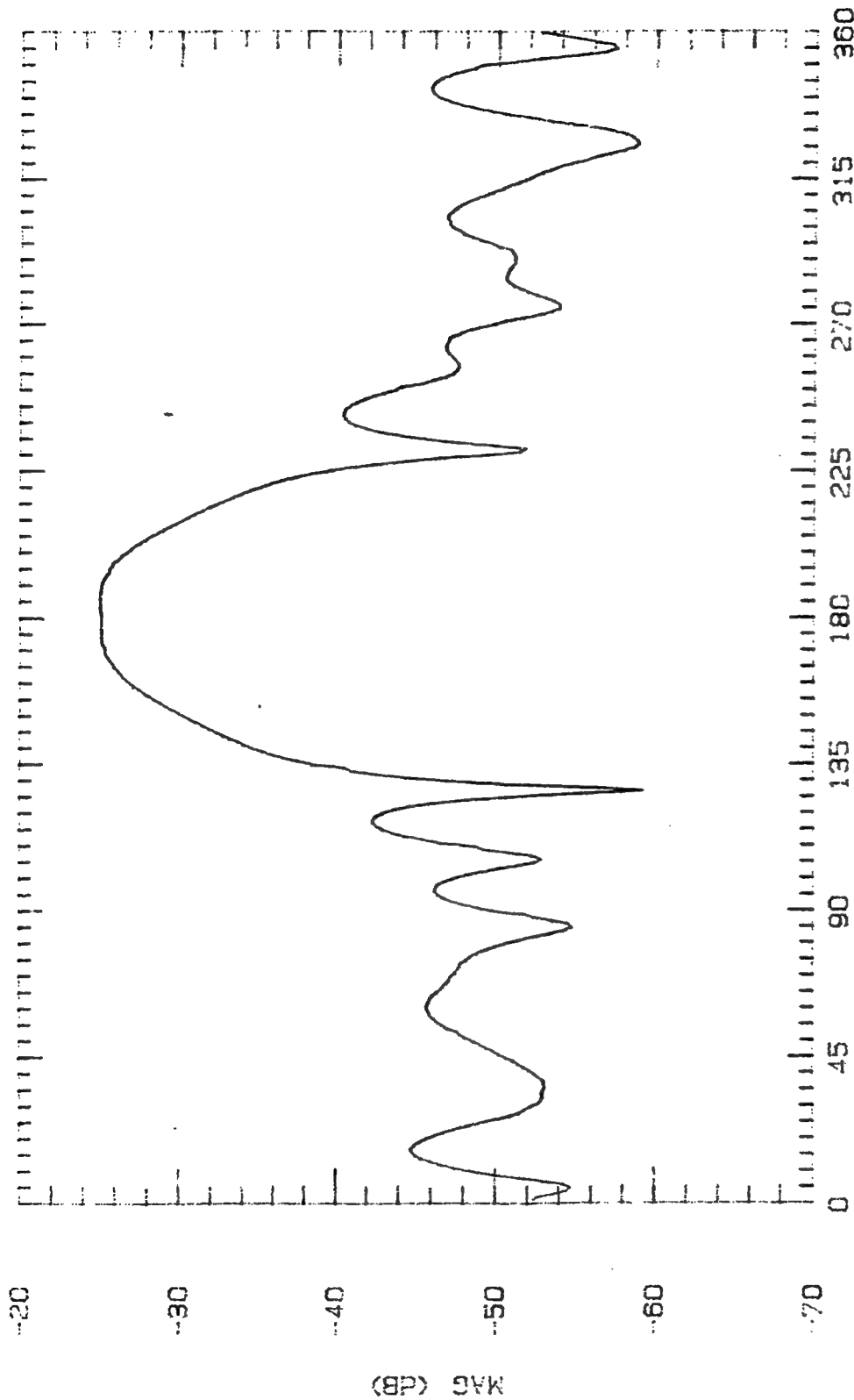


File Name	Frequency	Pattern Type	Date
BH750	7.5 GHz	E-PLANE	1 NOV 94



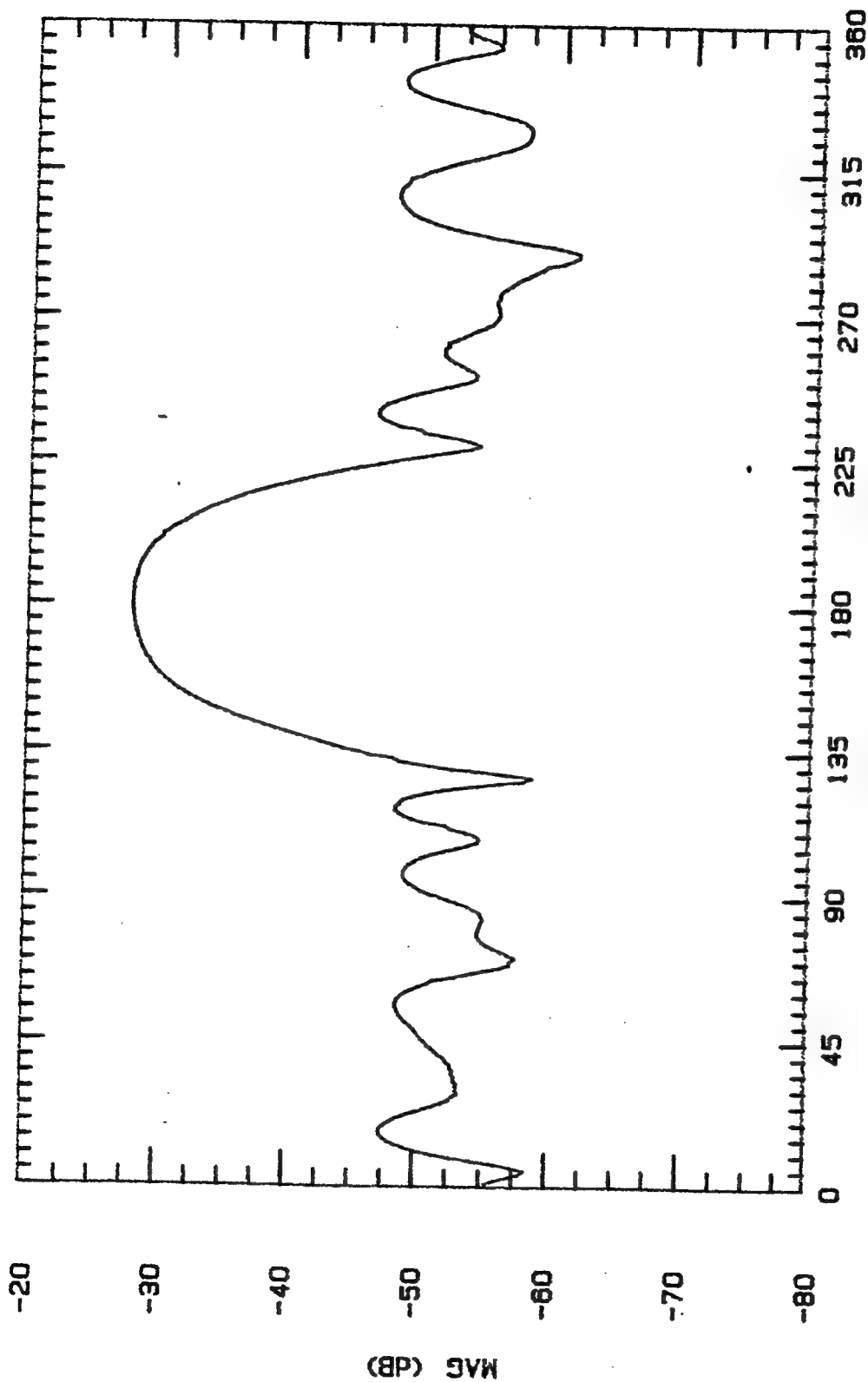
ASPECT ANGLE (DEGREES)

File Name	Frequency	Pattern Type	Date
BHB	8 GHz	E-PLANE	19 OCT 84



ASPECT ANGLE (DEGREES)

File Name	Frequency	Pattern Type	Date
BH050	8.5 GHz	E-PLANE	1 NOV 94



ASPECT ANGLE (DEGREES)

File Name

Frequency

Pattern Type

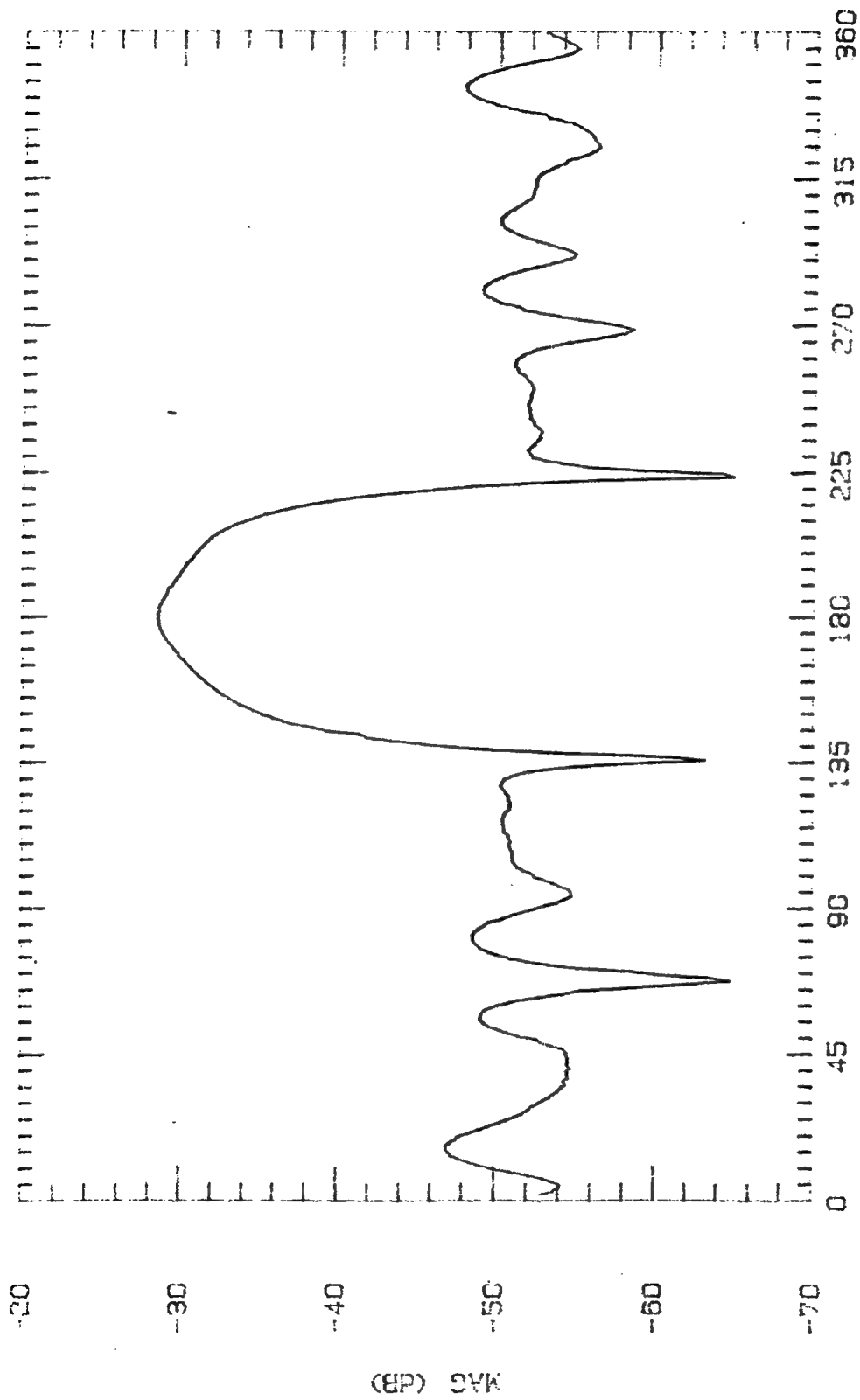
Date

BH9

9 GHz

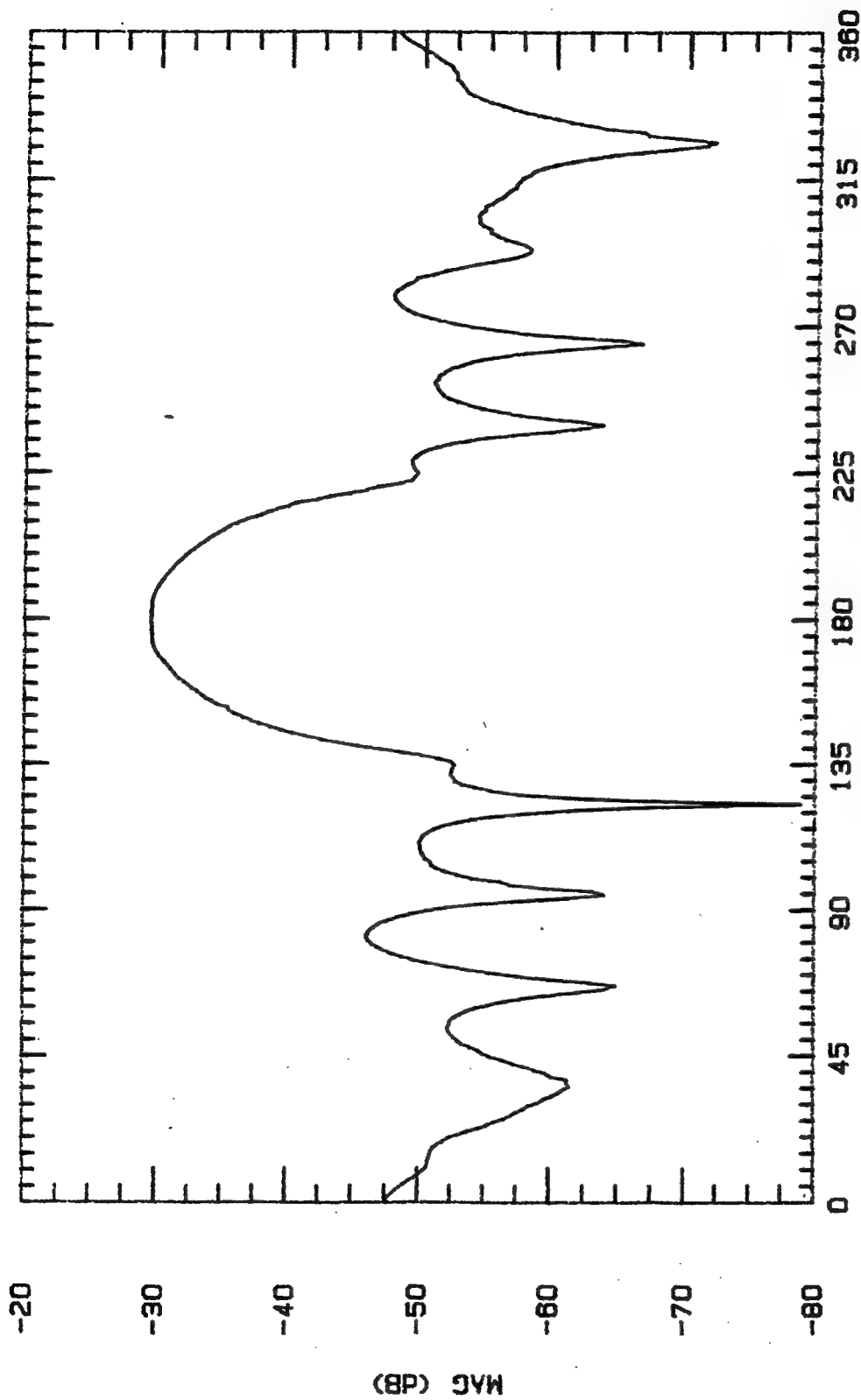
E-PLANE

19 OCT



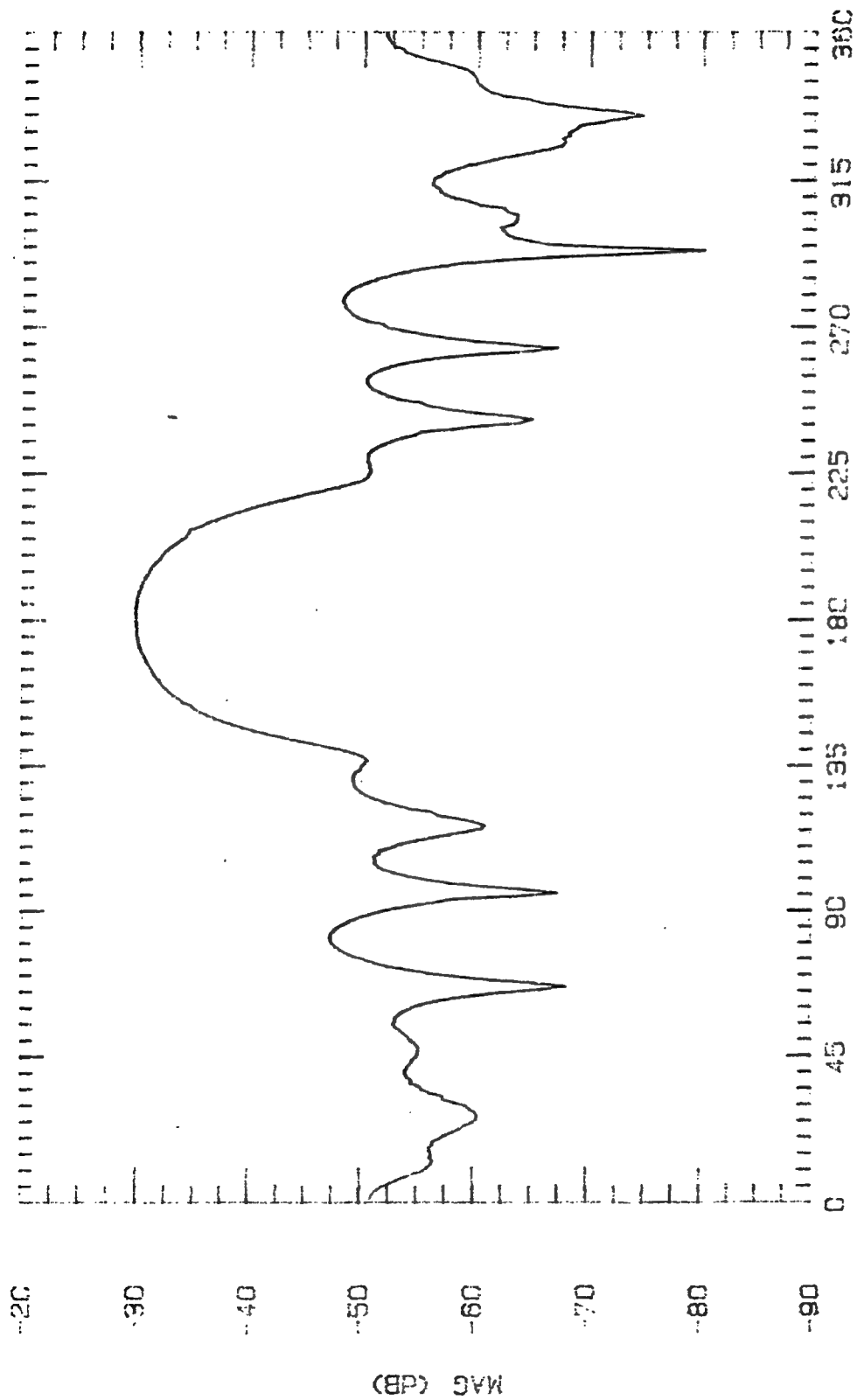
ASPECT ANGLE (DEGREES)

File Name	Frequency	Pattern Type	Data
BH950	9.5 CH ₂	E-PLANE	1 NOV 94

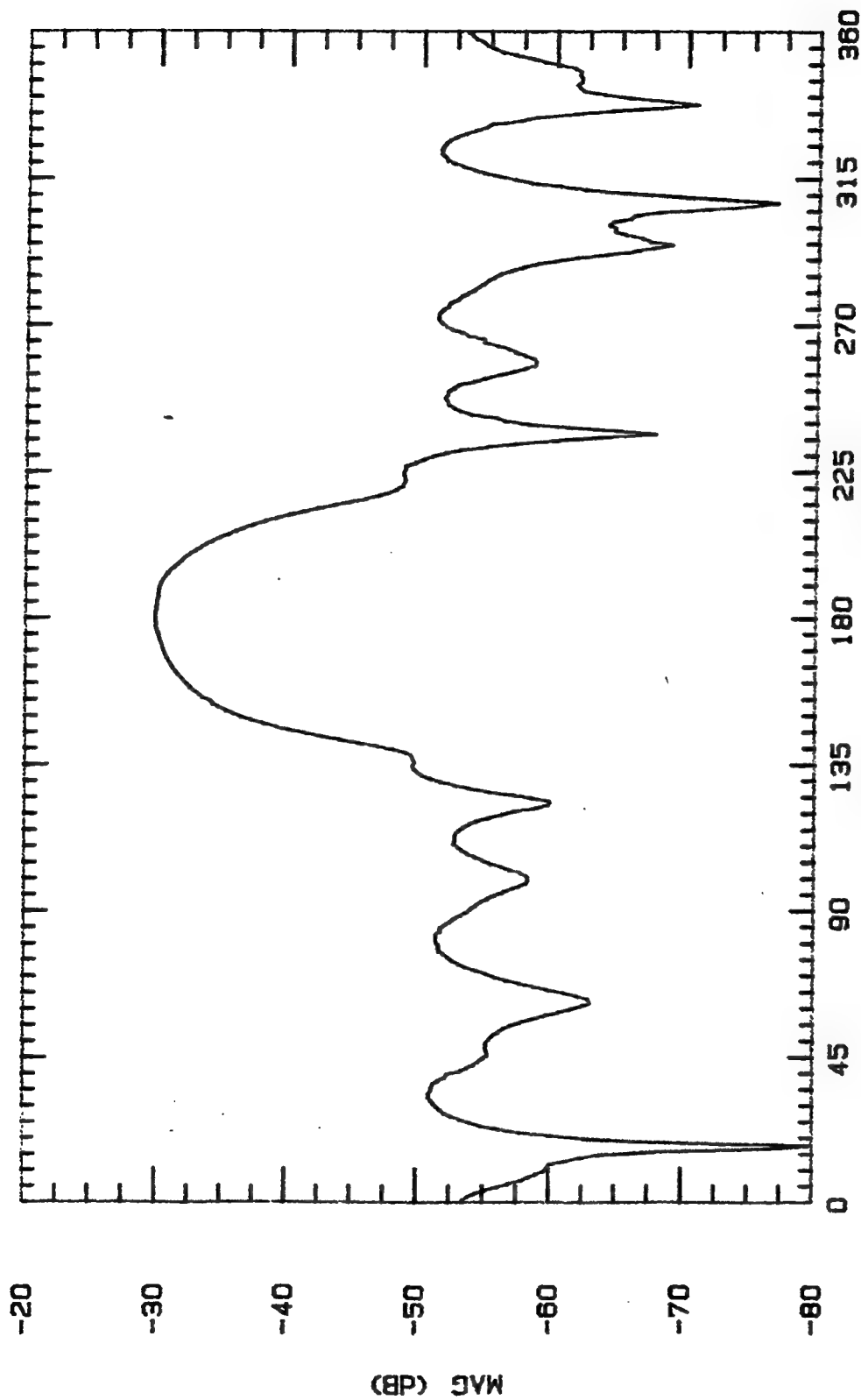


ASPECT ANGLE (DEGREES)

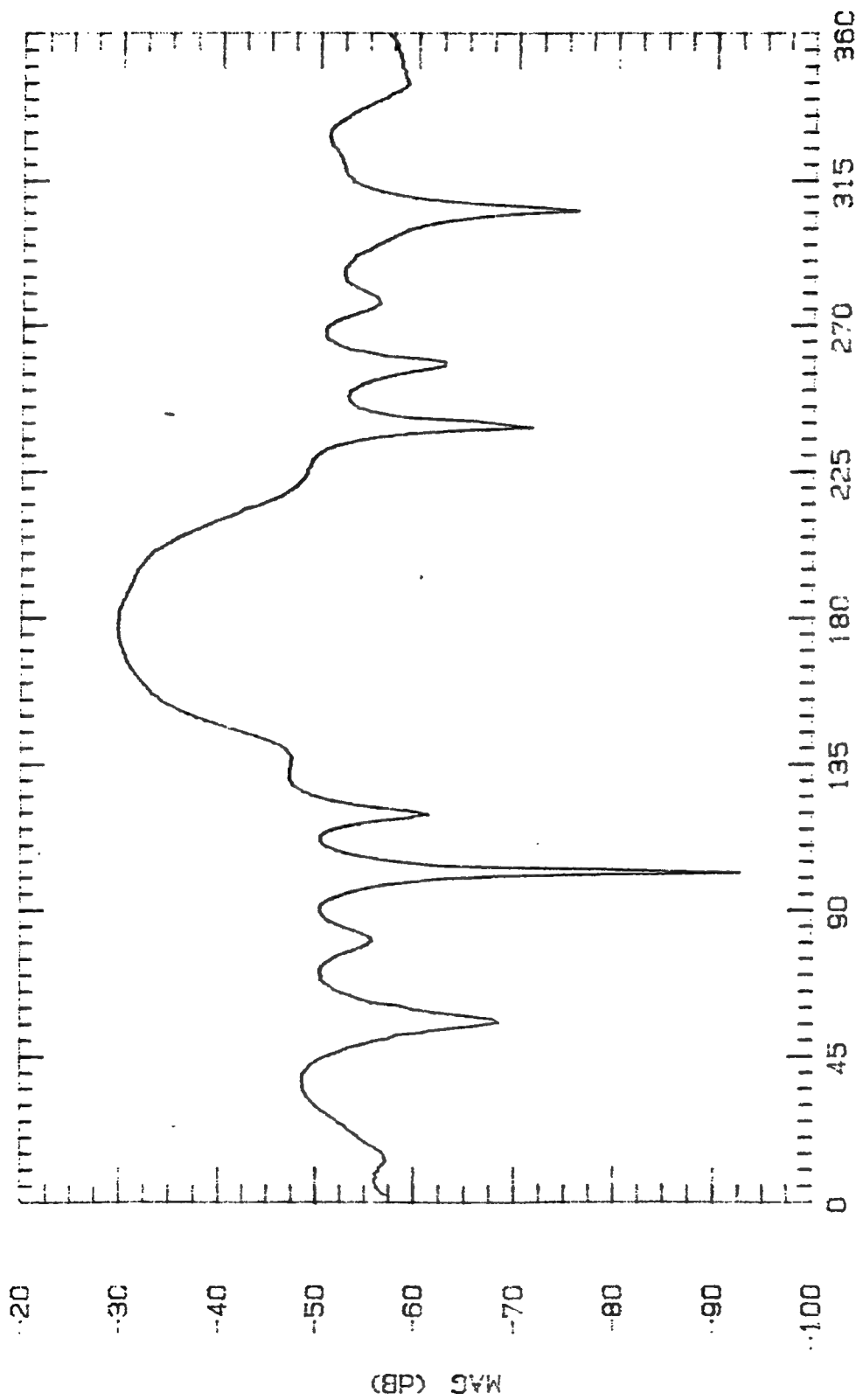
File Name	Frequency	Pattern Type	Date
BH10	10 GHz	E-PLANE	19 OCT 94



File Name	Frequency	Pattern Type	Date
BH105	10.5 CH4	E-PLANE	1 NOV 94

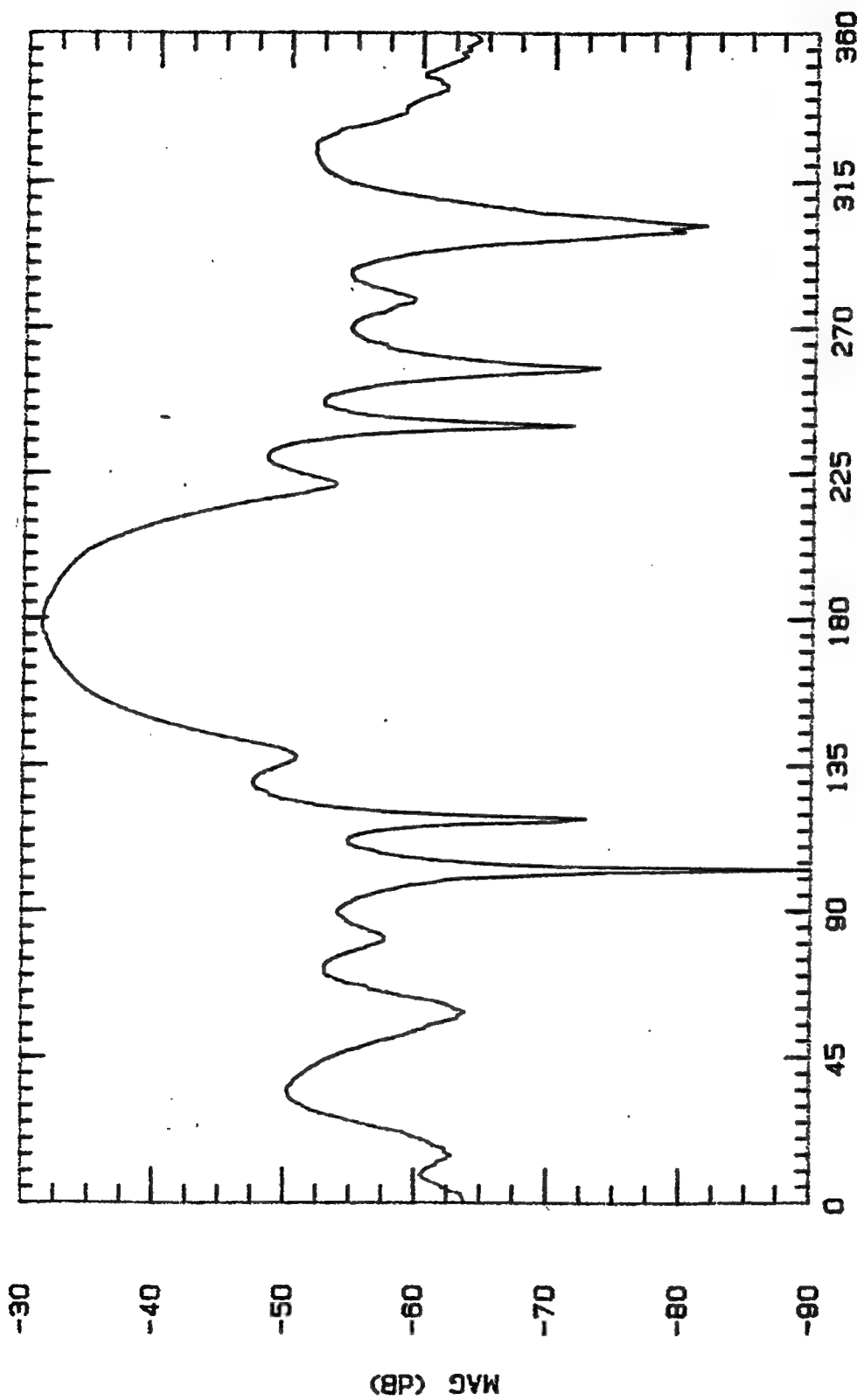


File Name	Frequency	Pattern Type	Date
BH11	11 GHz	E-PLANE	19 OCT

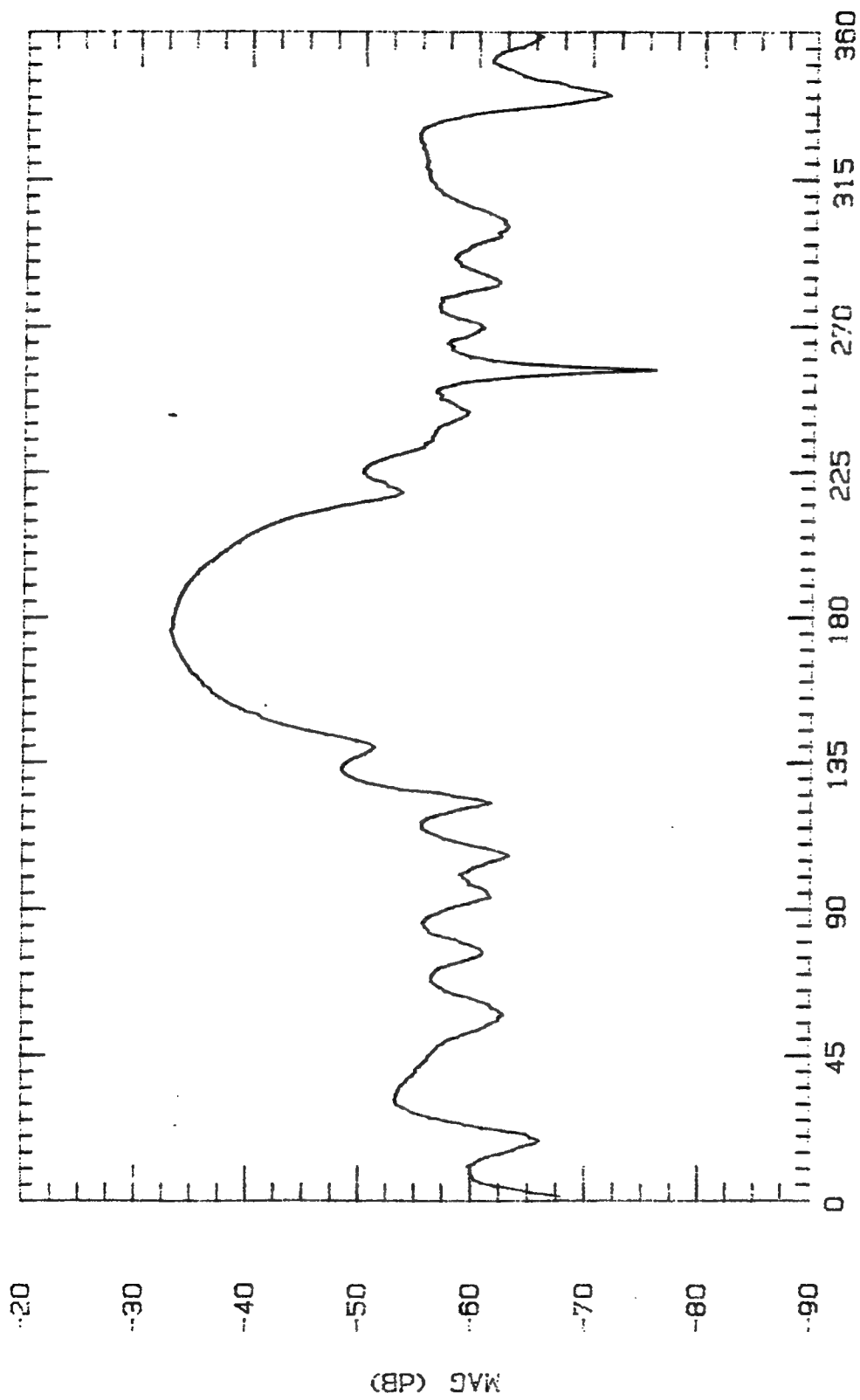


ASPECT ANGLE (DEGREES)

File Name	Frequency	Pattern Type	Date
BH115	11.5 GHz	E-PLANE	1 NOV 94



File Name	Frequency	Pattern Type	Date
BH12	12 GHz	E-PLANE	19 OCT 94

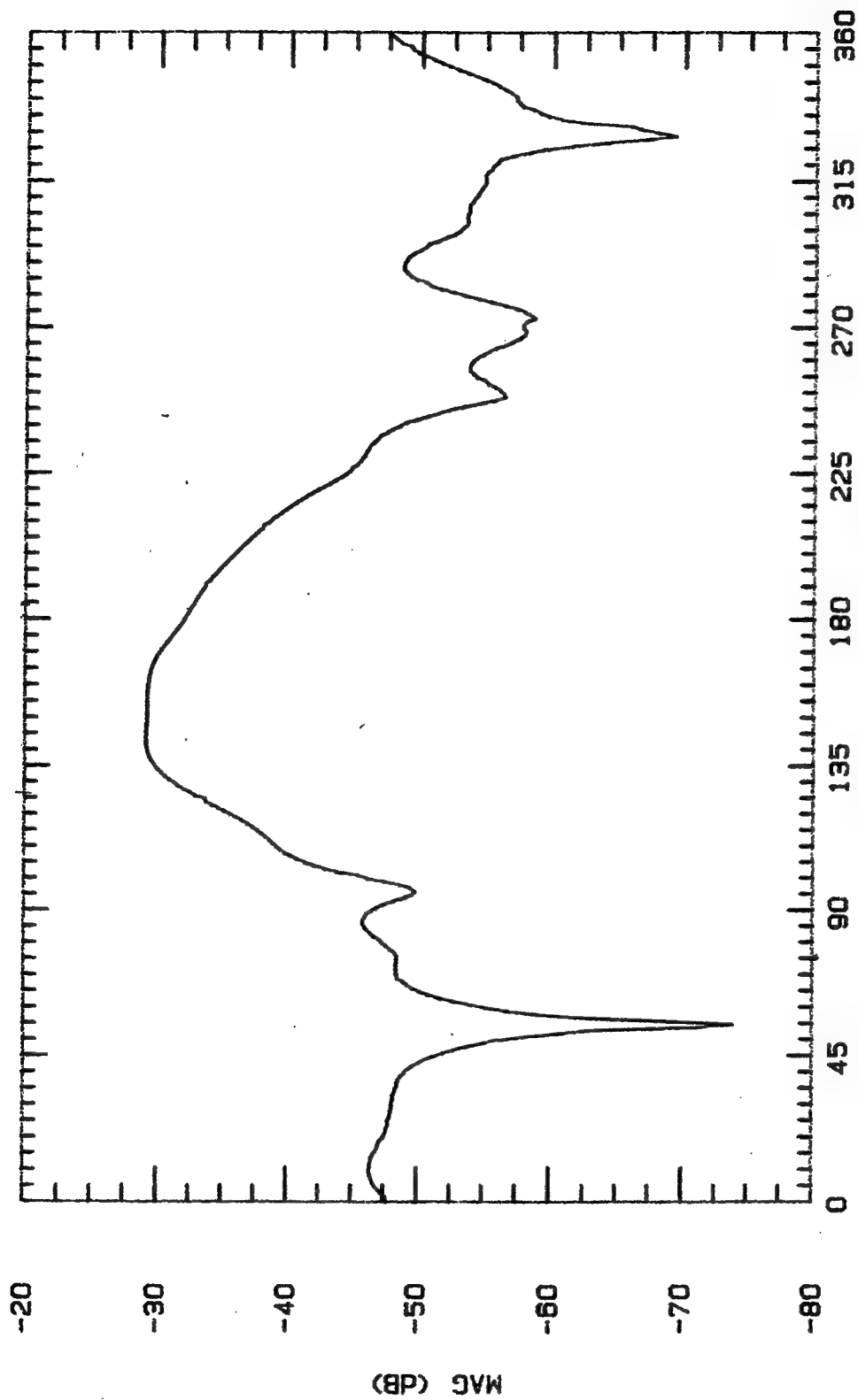


ASPECT ANGLE (DEGREES)

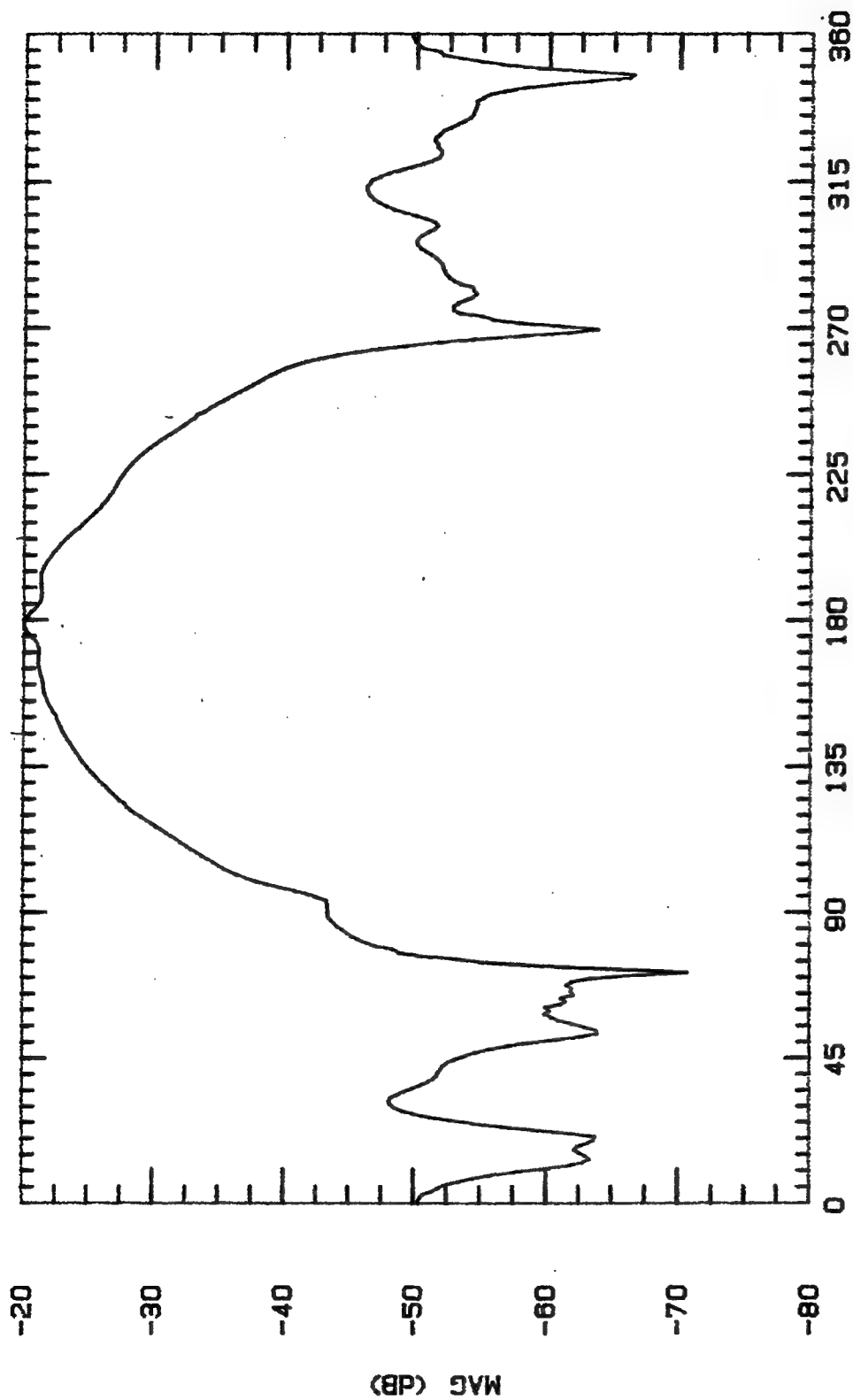
File Name	Frequency	Pattern Type	Date
BH125	12.5 CHz	E-PLANE	1 NOV 94
BH125	12.5 CHz	E-PLANE	1 NOV 94

APPENDIX F: Antenna Pattern Cuts for Absorber-Filled Cavity Design

Freq (GHz)	Normal Gain (dBi)	Max Gain (dBi)	Squint (deg)	Beamwidth (-3dBi to -3dBi) (deg)
-----	-----	-----	-----	-----
2.0	-15.2	-12.0	-36	58
3.0	-2.4	-2.3	-1	60
4.0	-3.9	-1.8	-21	51
5.0	-12.1	-6.0	34	49
6.0	-5.7	-4.2	8	43
7.0	-1.8	-0.9	4	43
8.0	-1.9	-1.7	-2	39
9.0	-11.2	-8.4	-23	36
10.0	-5.9	-3.1	5	44
11.0	-8.9	-4.7	16	28
12.0	-5.1	-5.0	1	58
-----	-----	-----	-----	-----

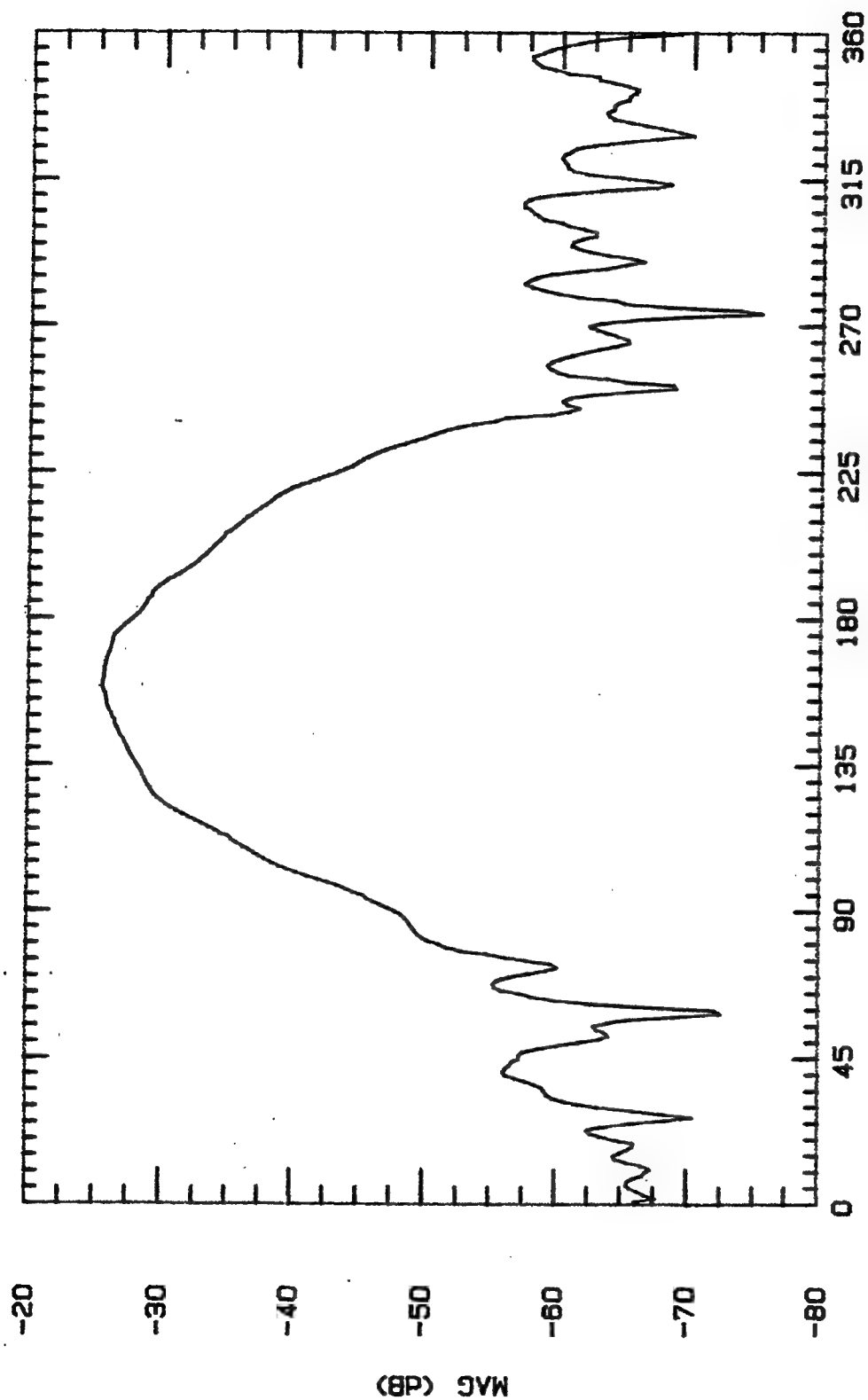


File Name	Frequency	Pattern Type	Date
LPLA2	2 GHz	E-PLANE	18 OCT 94



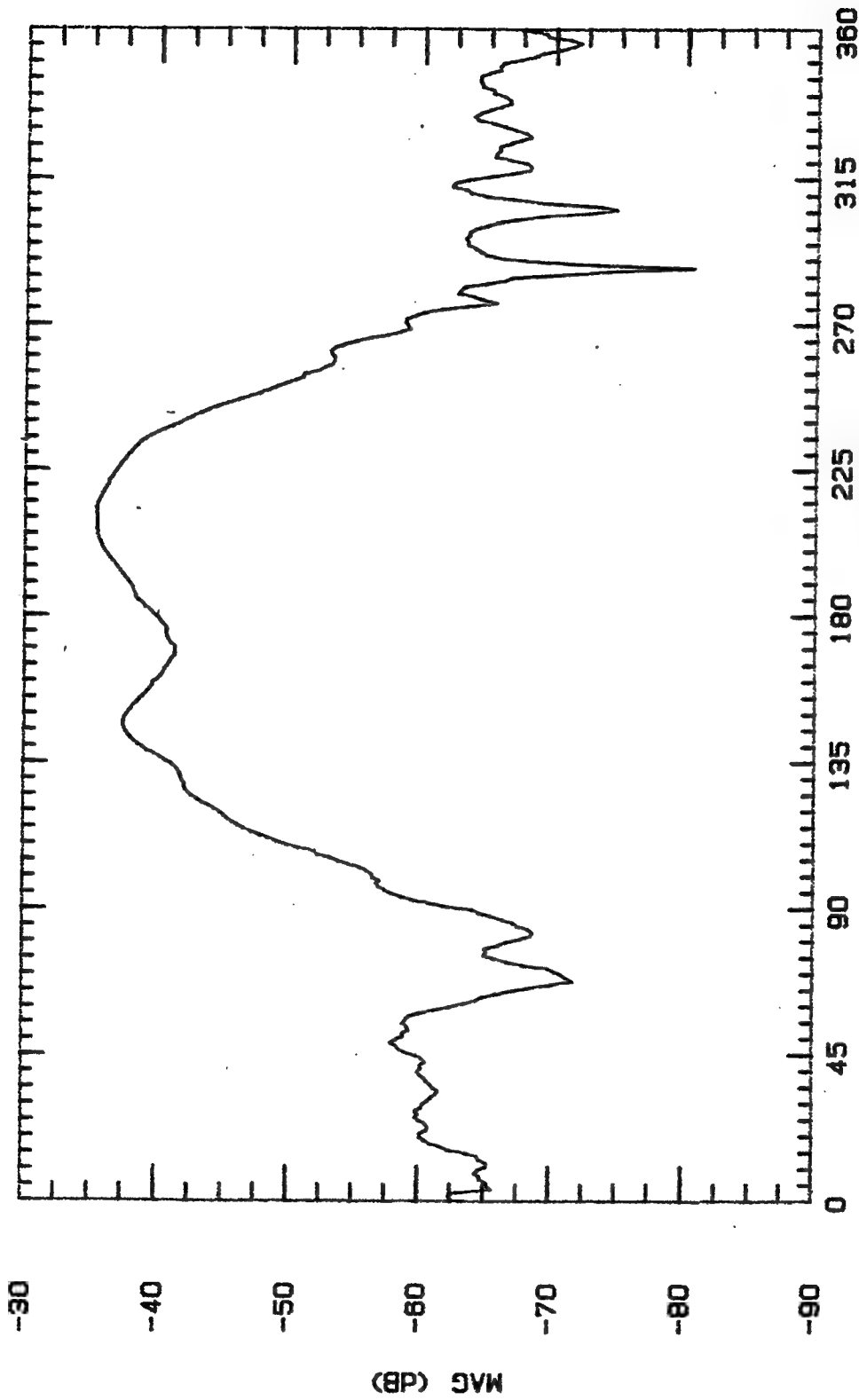
ASPECT ANGLE (DEGREES)

File Name	Frequency	Pattern Type	Date
LPLA3	3 GHz	E-PLANE	19 OCT 94



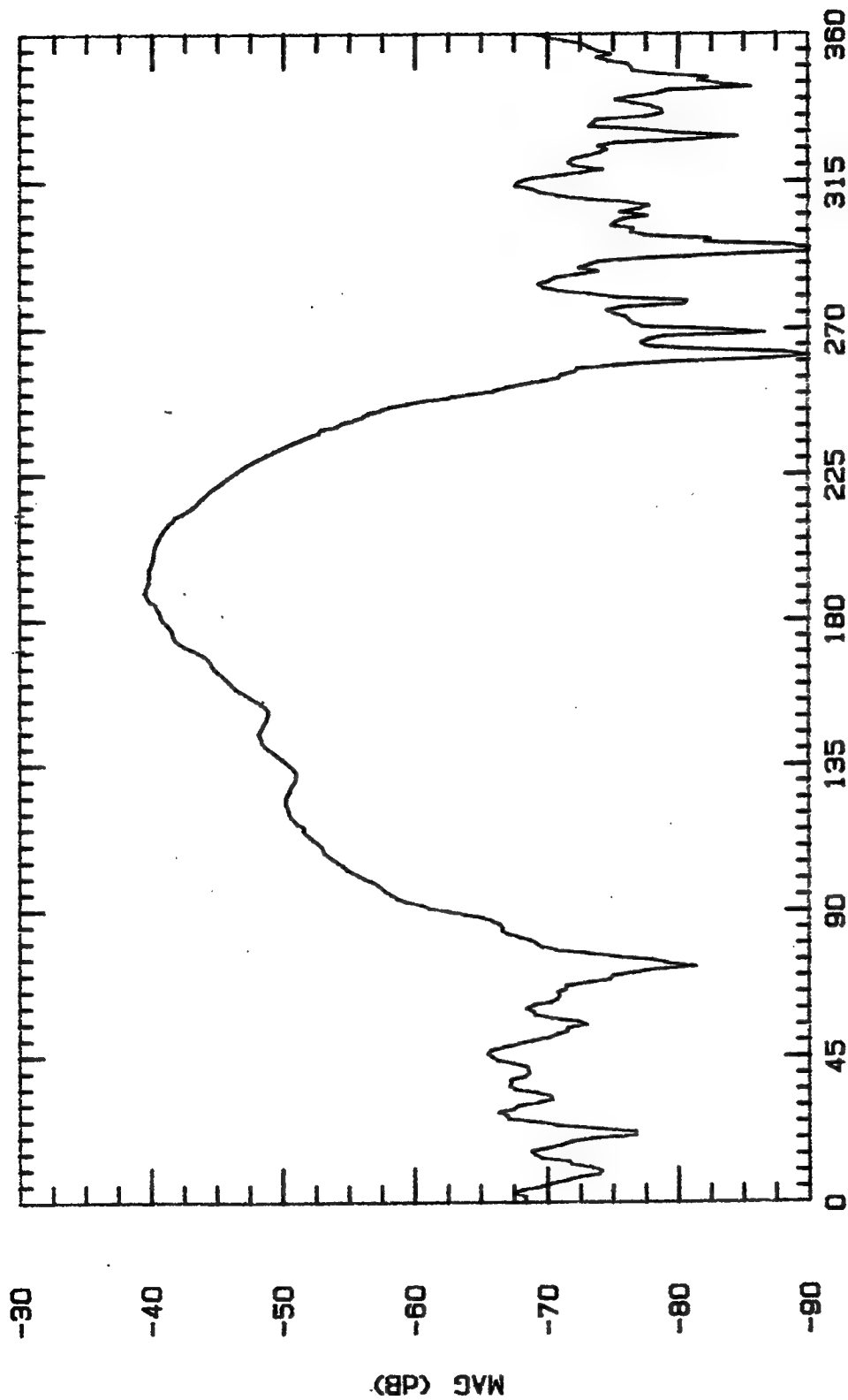
ASPECT ANGLE (DEGREES)

File Name	Frequency	Pattern Type	Date
LPLA4	4 GHz	E-PLANE	18 OCT 94



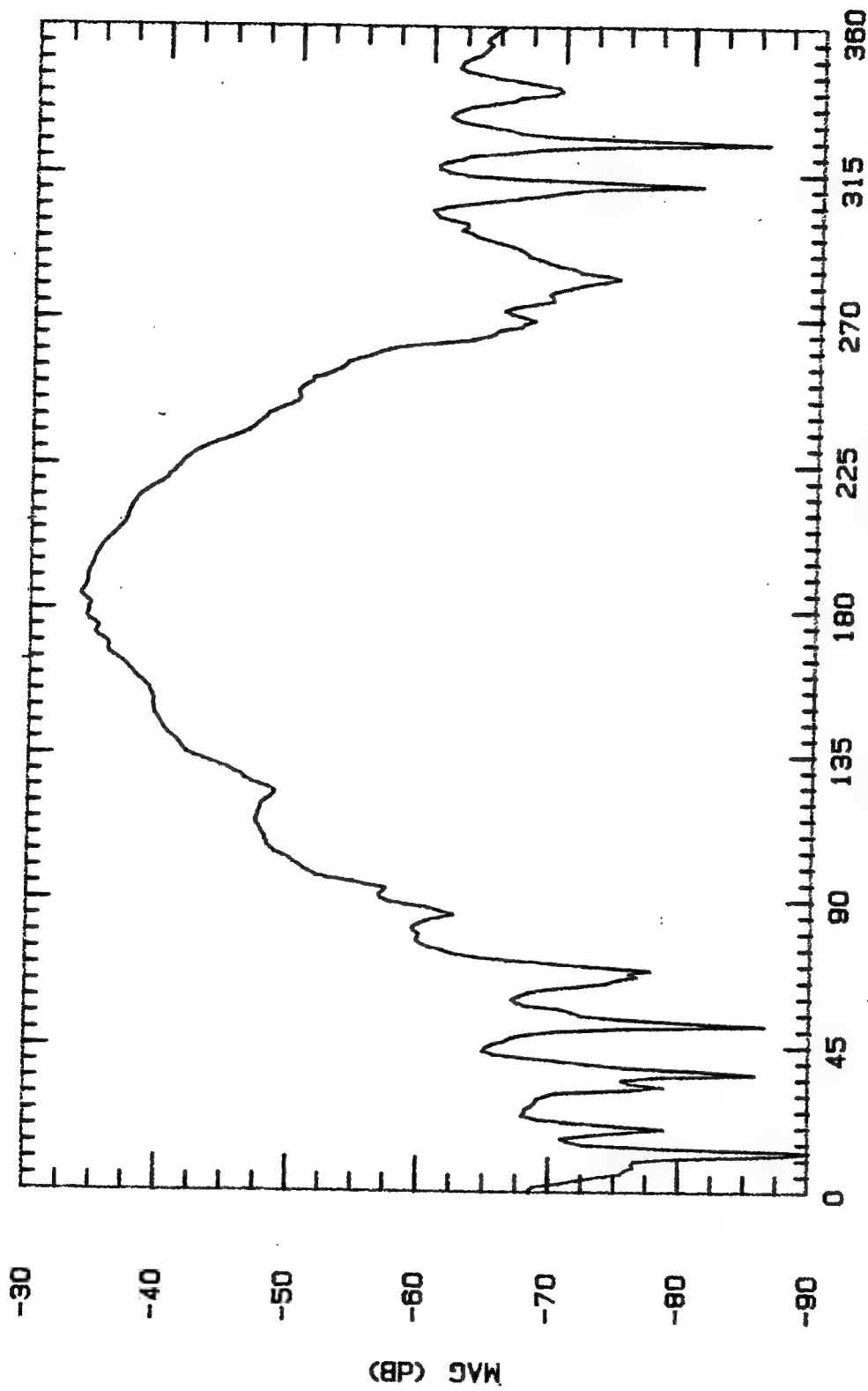
ASPECT ANGLE (DEGREES)

File Name	Frequency	Pattern Type	Date
LPLA5	5 GHz	E-PLANE	19 OCT 94



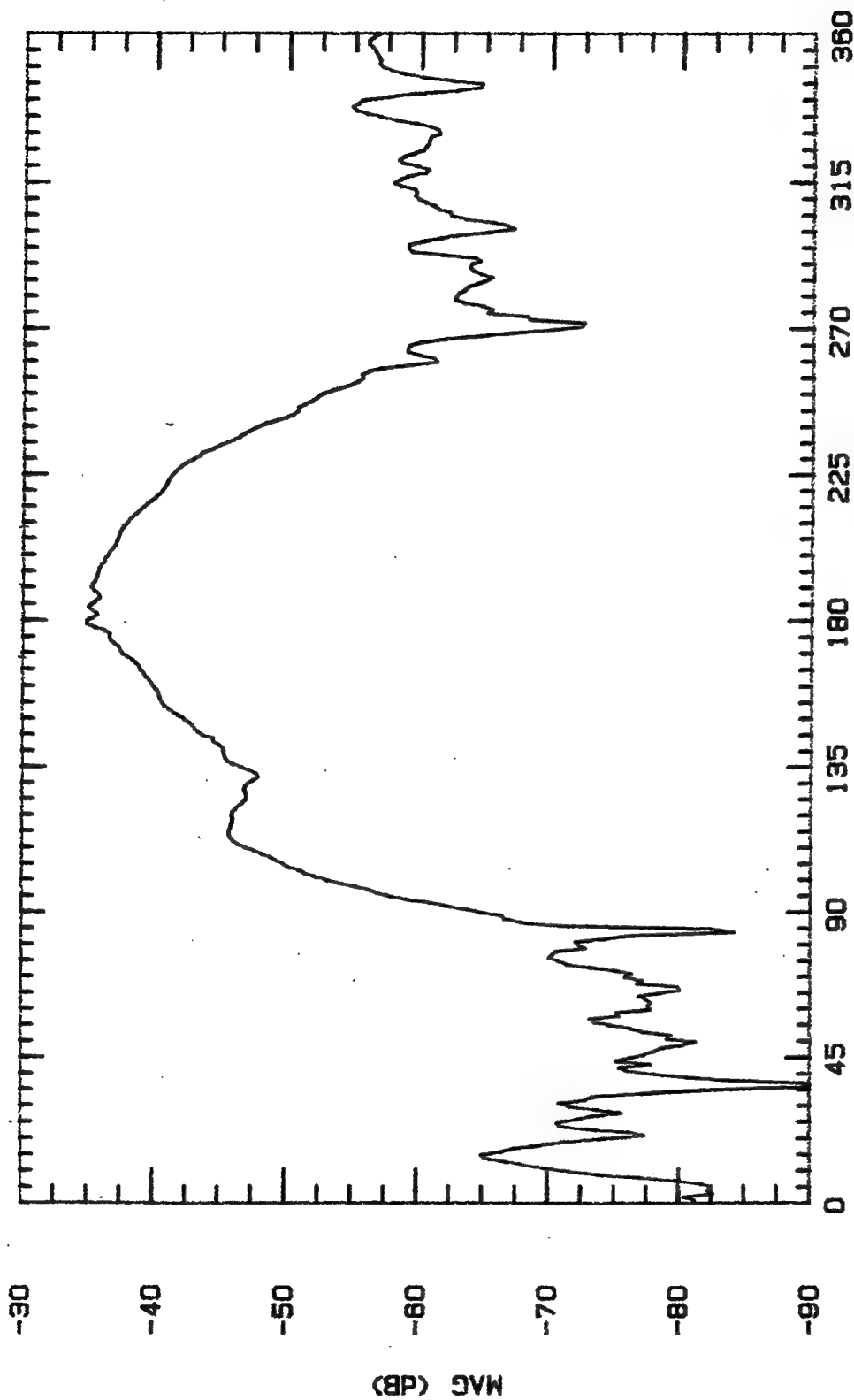
ASPECT ANGLE (DEGREES)

File Name	Frequency	Pattern Type	Date
LPLA8	8 GHz	E-PLANE	18 OCT 94



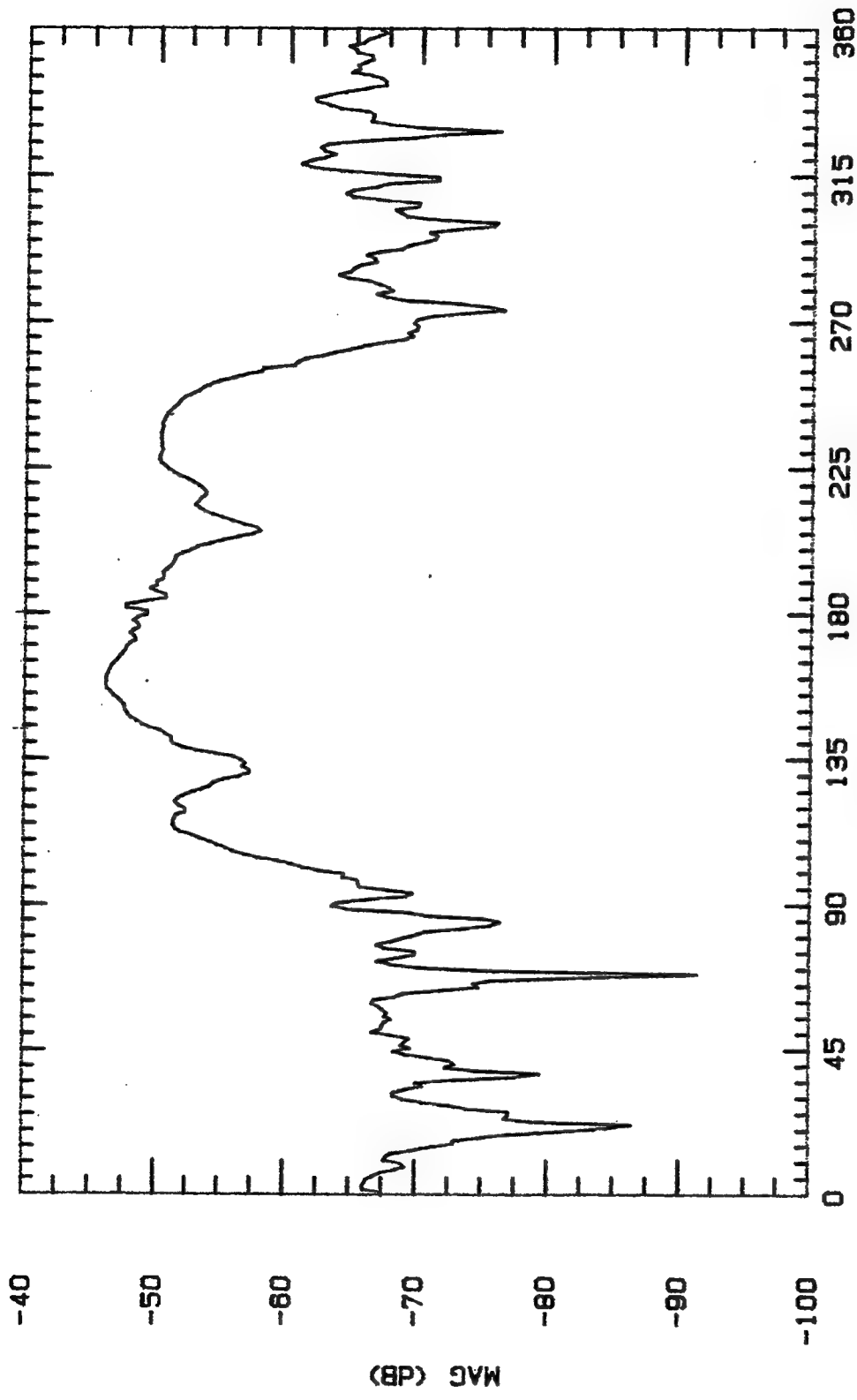
ASPECT ANGLE (DEGREES)

File Name	Frequency	Pattern Type	Date
LPLA7	7 GHz	E-PLANE	18 OCT 94



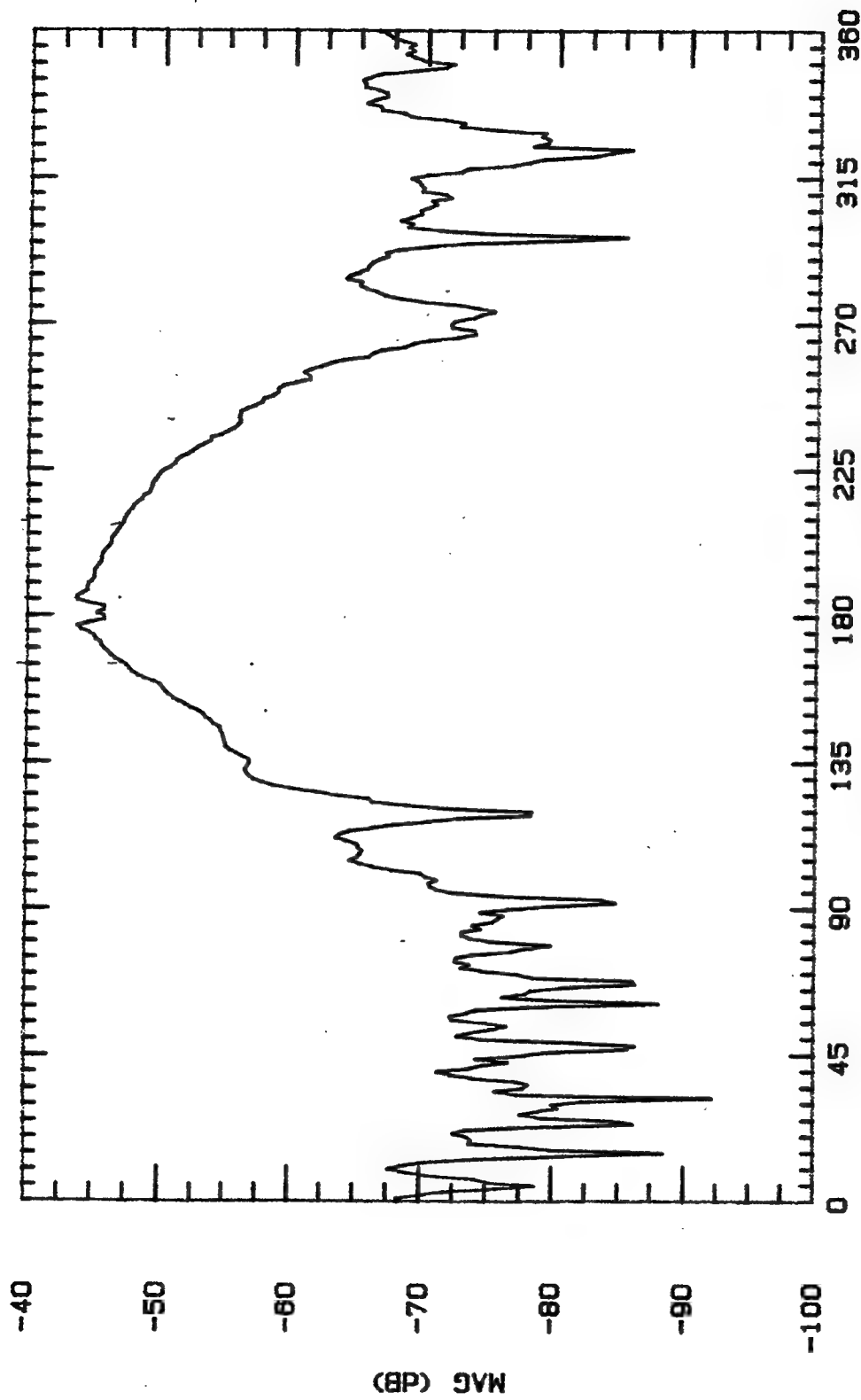
ASPECT ANGLE (DEGREES)

File Name	Frequency	Pattern Type	Date
LPLA8	8 GHz	E-PLANE	18 OCT 94



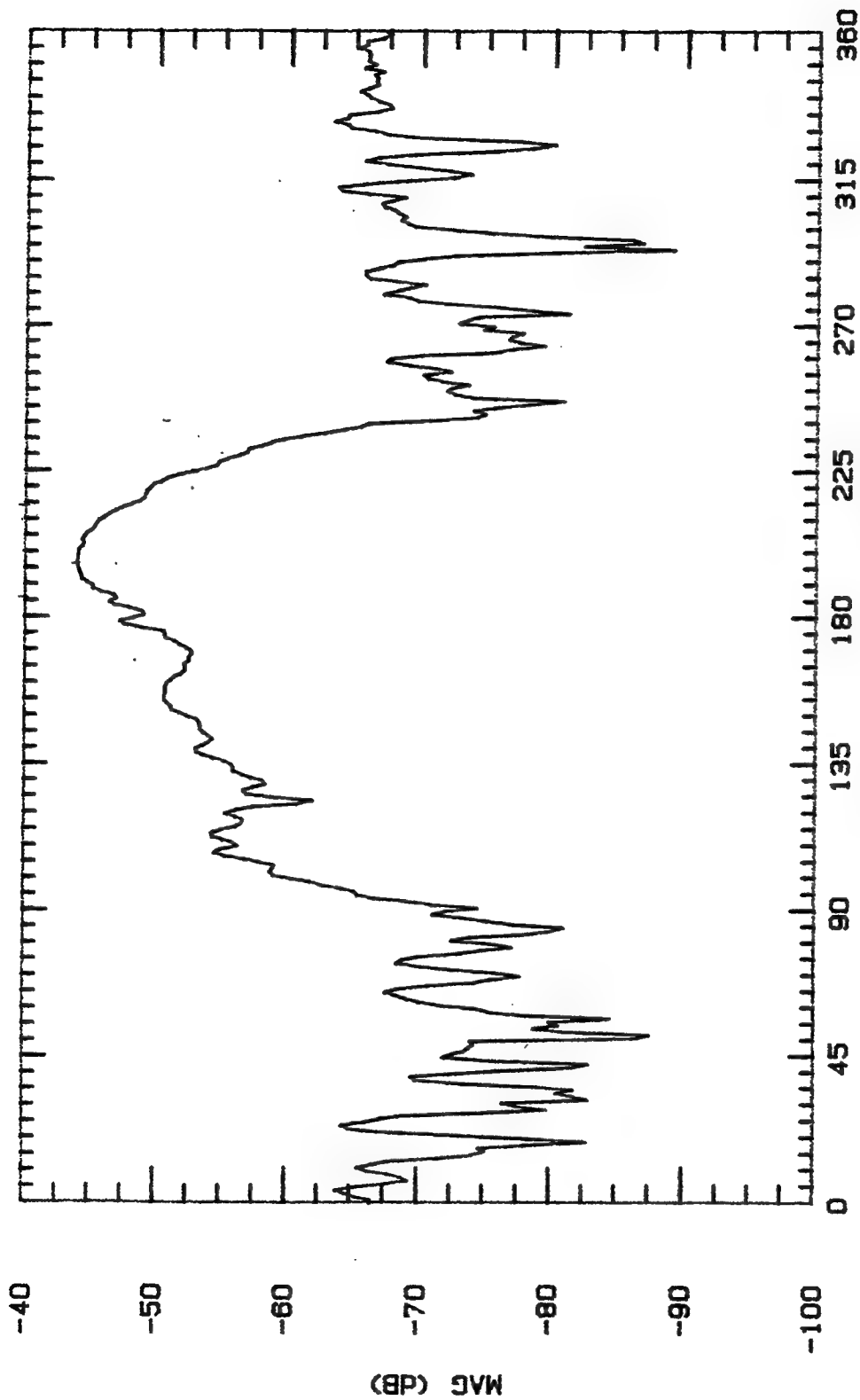
ASPECT ANGLE (DEGREES)

File Name	Frequency	Pattern Type	Date
LPLA9	9 GHz	E-PLANE	19 OCT 94



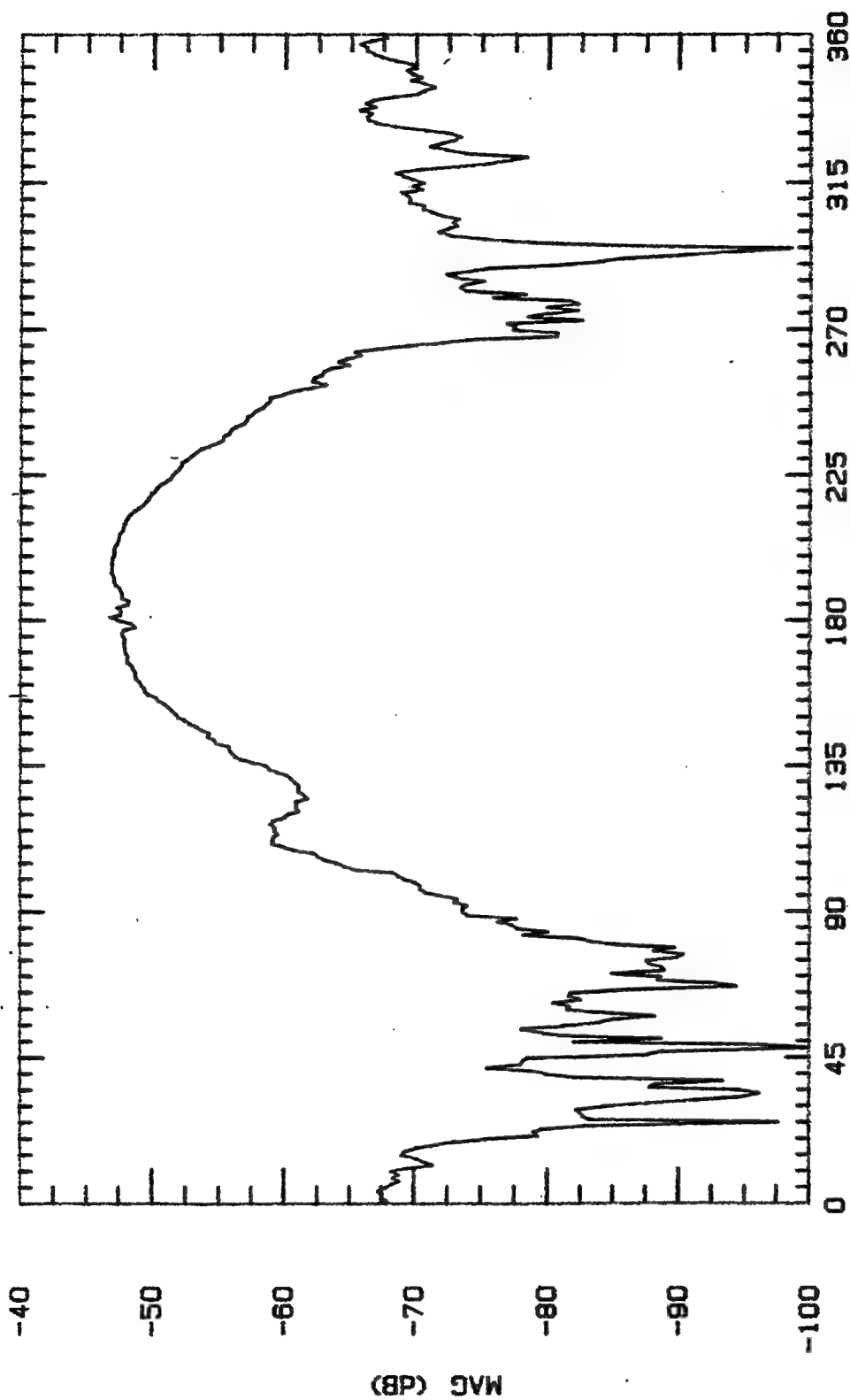
ASPECT ANGLE (DEGREES)

File Name	Frequency	Pattern Type	Data
LPLA10	10 GHz	E-PLANE	18 OCT 84



ASPECT ANGLE (DEGREES)

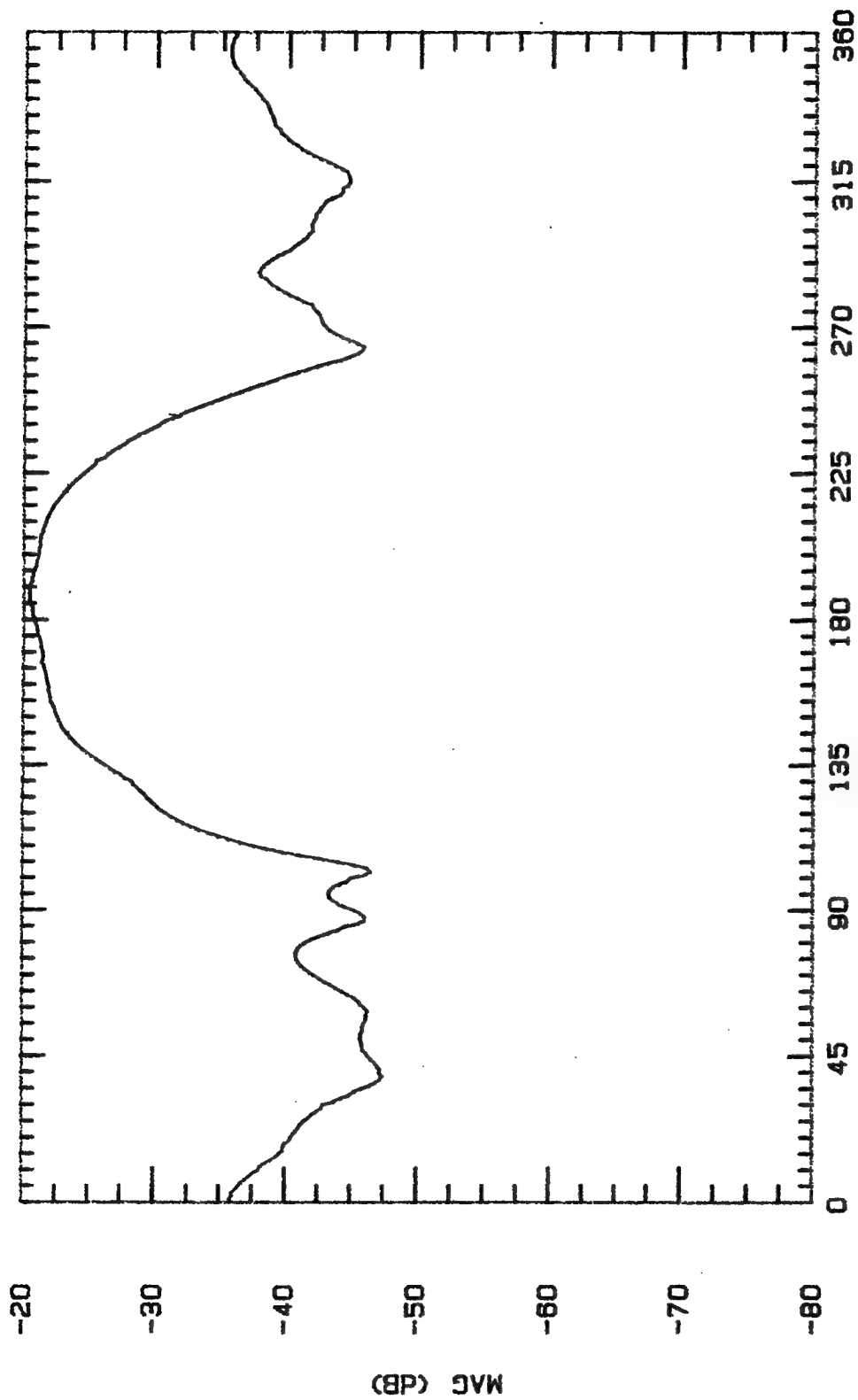
File Name	Frequency	Pattern Type	Date
LPLA11	11 GHz	E-PLANE	19 OCT 84



File Name	Frequency	Pattern Type	Date
LPLA12	12 GHz	E-PLANE	18 OCT 94

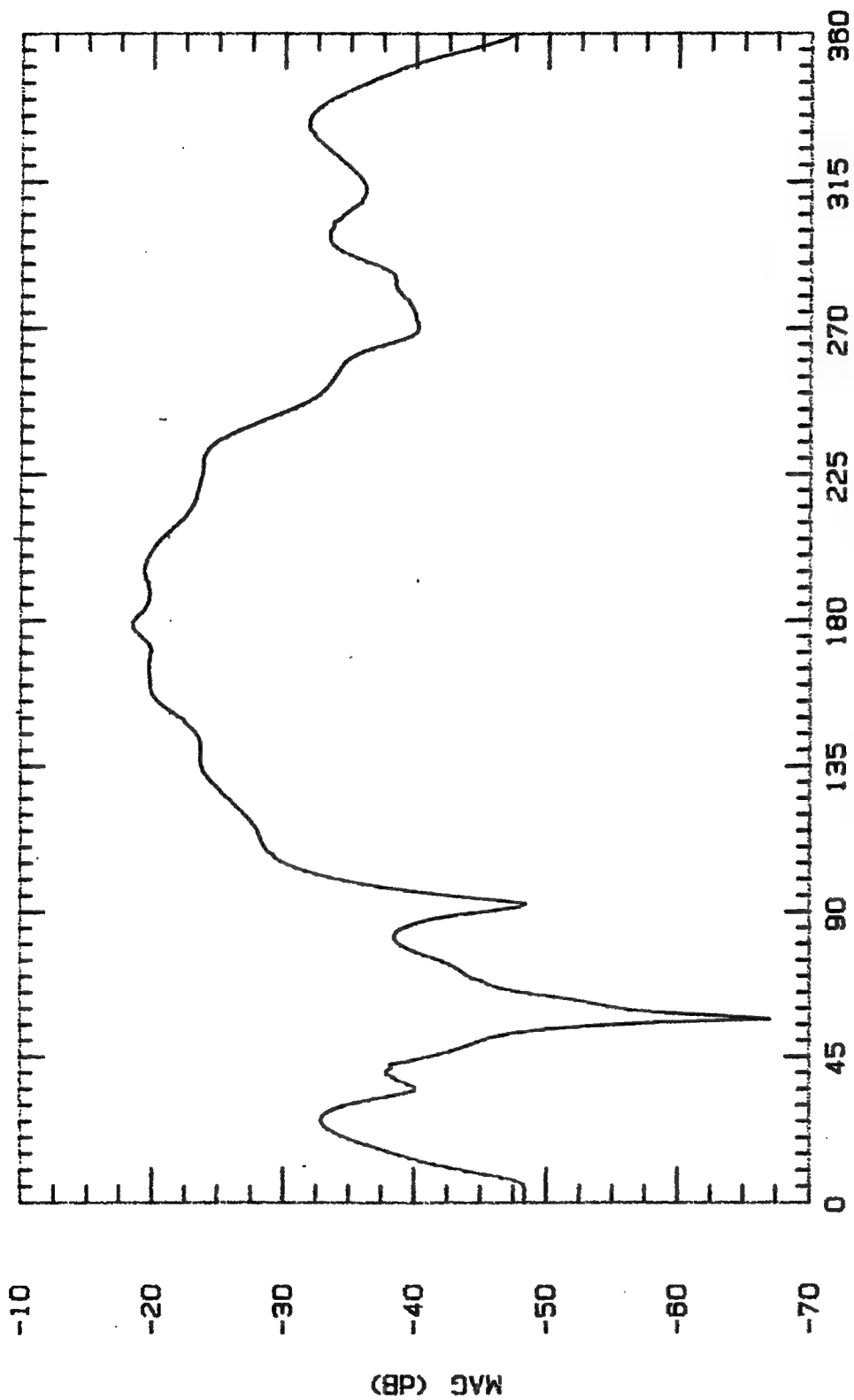
APPENDIX G: Antenna Pattern Cuts For Dielectric-Filled Cavity Design

Freq (GHz)	Normal Gain (dBi)	Max Gain (dBi)	Squint (deg)	Beamwidth (-3dBi to -3dBi) (deg)
-----	-----	-----	-----	-----
2.0	-4.2	-3.8	7	75
3.0	-0.9	-0.9	0	53
4.0	-4.8	-4.6	-7	52
5.0	0.4	0.6	5	60
6.0	-2.3	-2.3	0	63
7.0	0.0	2.0	5	24
8.0	6.2	6.2	0	23
9.0	-5.8	1.2	22	30
10.0	-2.9	0.1	-5	10
11.0	5.4	5.4	0	13
12.0	4.1	4.1	0	80
-----	-----	-----	-----	-----

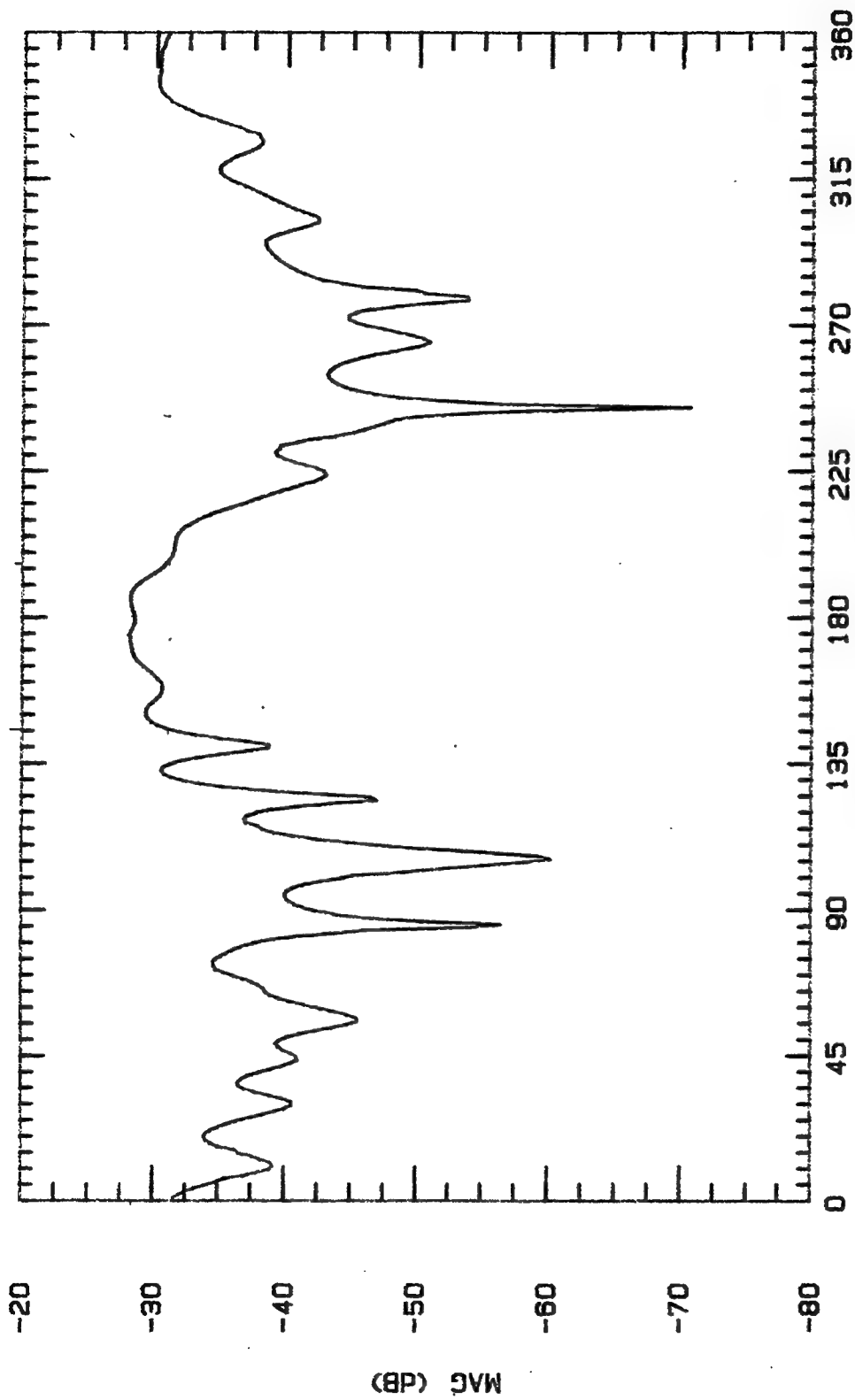


ASPECT ANGLE (DEGREES)

File Name	Frequency	Pattern Type	Date
LPL2NS	2 GHz	E-PLANE	19 OCT

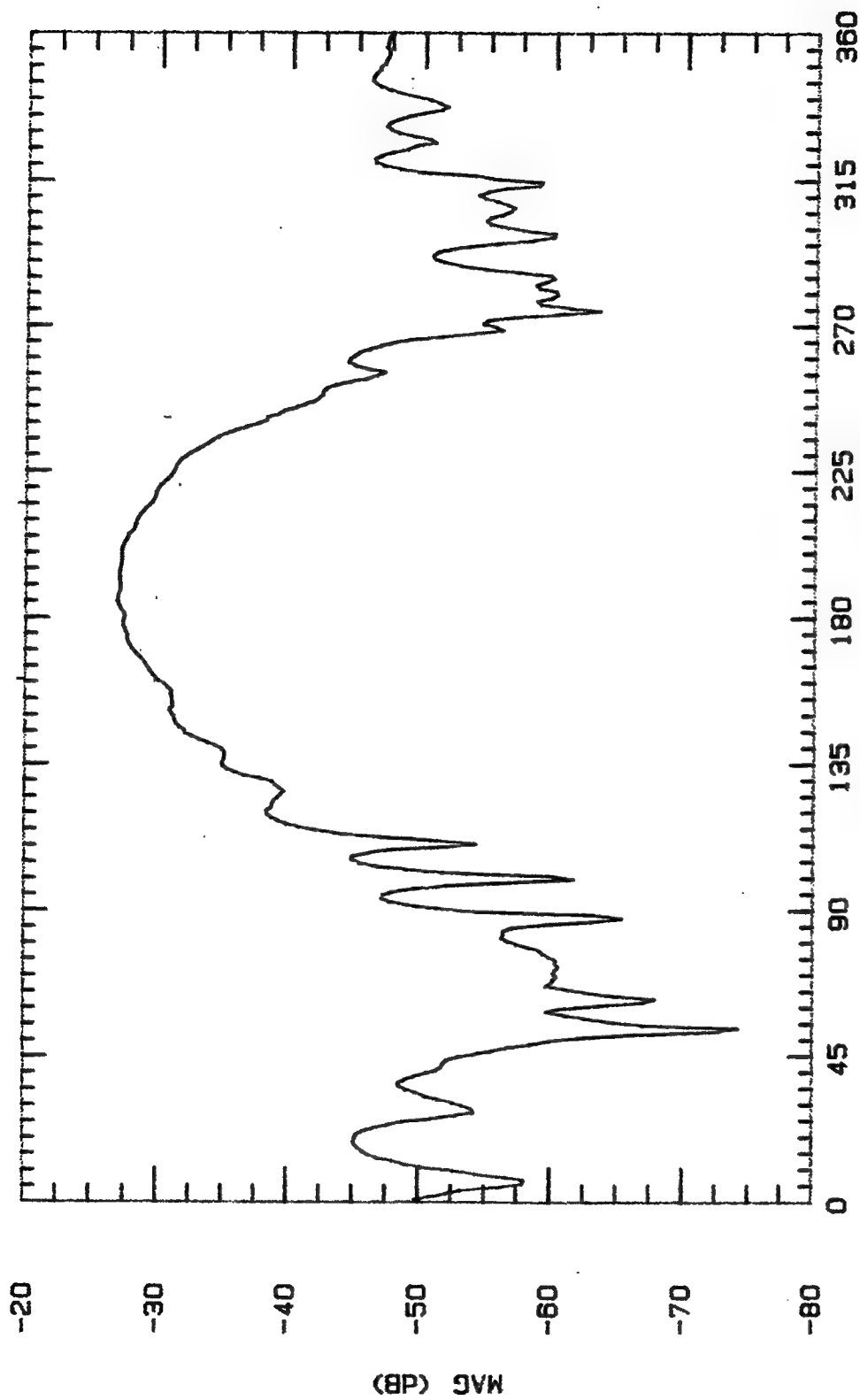


File Name	Frequency	Pattern Type	Date
LPLSNS	3 GHz	E-PLANE	



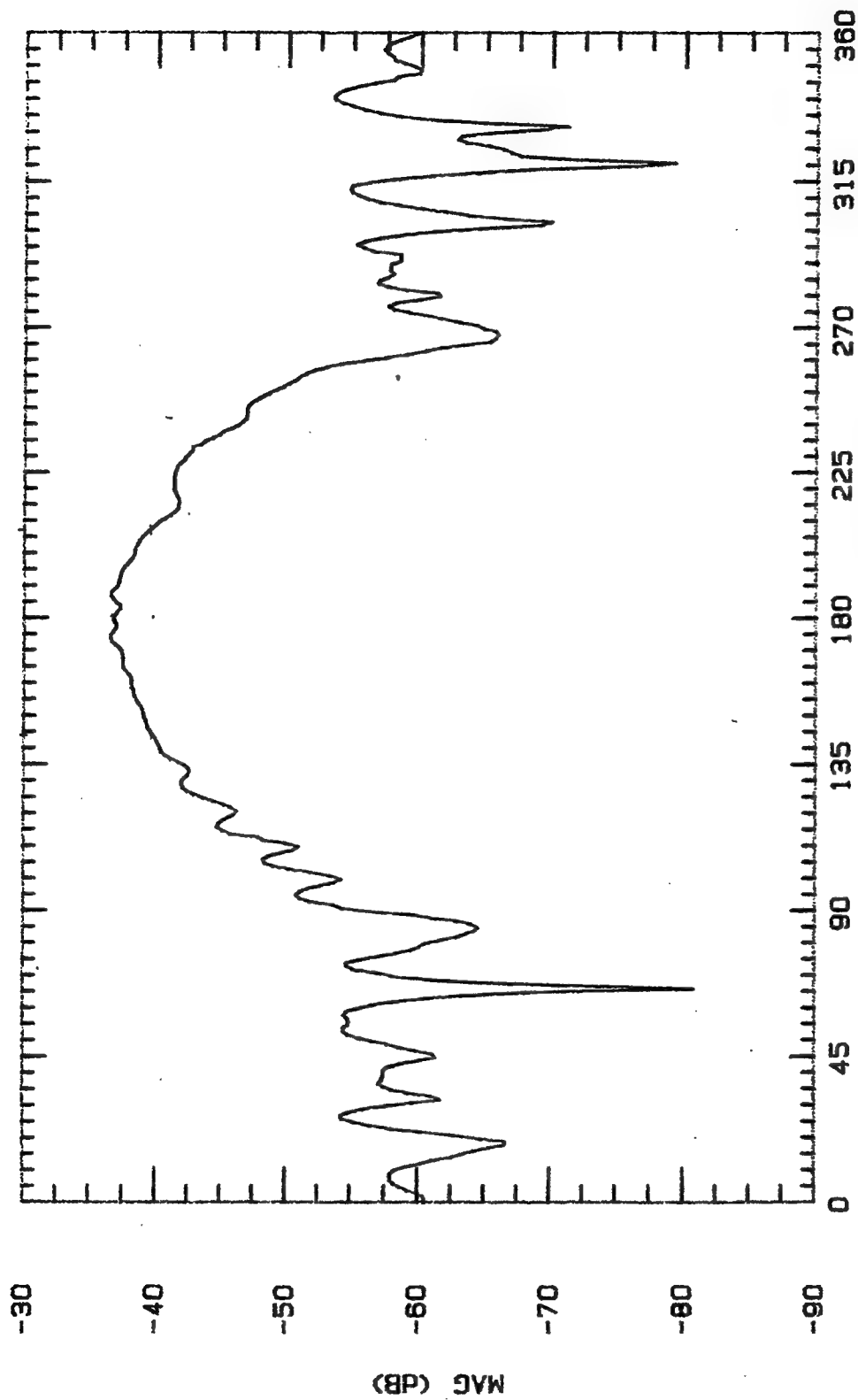
ASPECT ANGLE (DEGREES)

File Name	Frequency	Pattern Type	Date
LPL4NS	4 GHz	E-PLANE	19 OCT



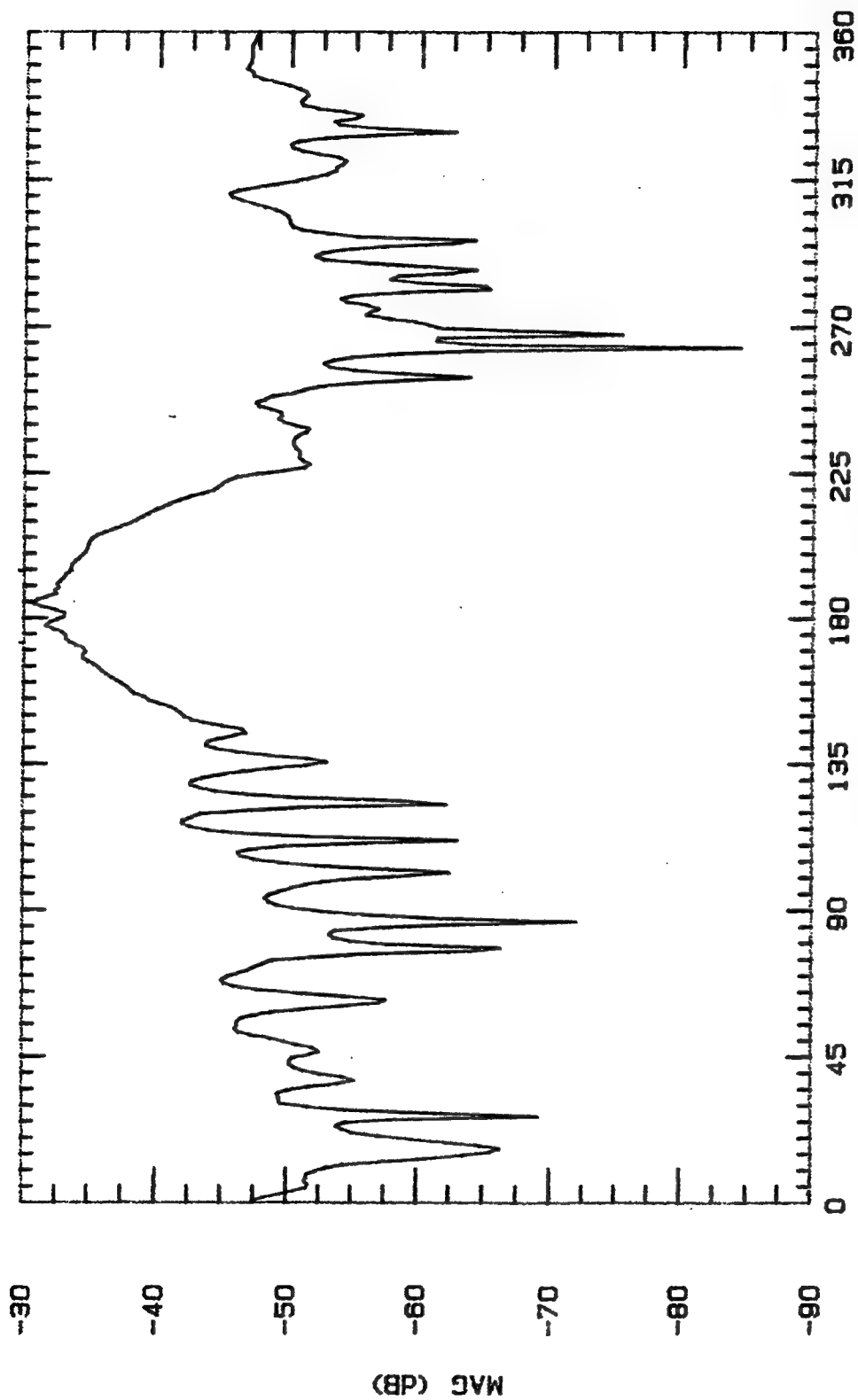
ASPECT ANGLE (DEGREES)

File Name	Frequency	Pattern Type	Date
LPL5NS	5 GHz	E-PLANE	18 OCT



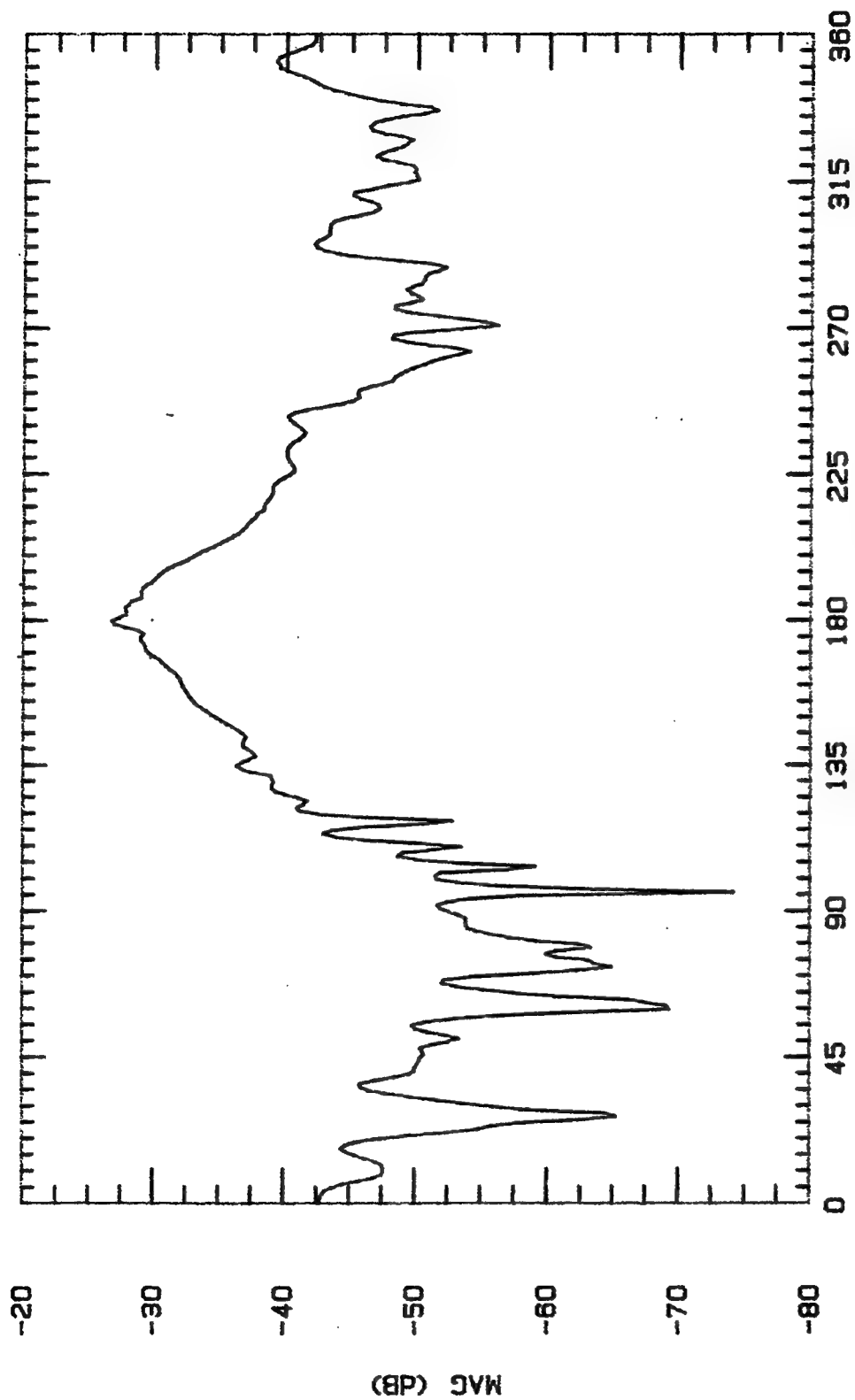
ASPECT ANGLE (DEGREES)

File Name	Frequency	Pattern Type	Date
LPL6NS	8 GHz	E-PLANE	19 OCT

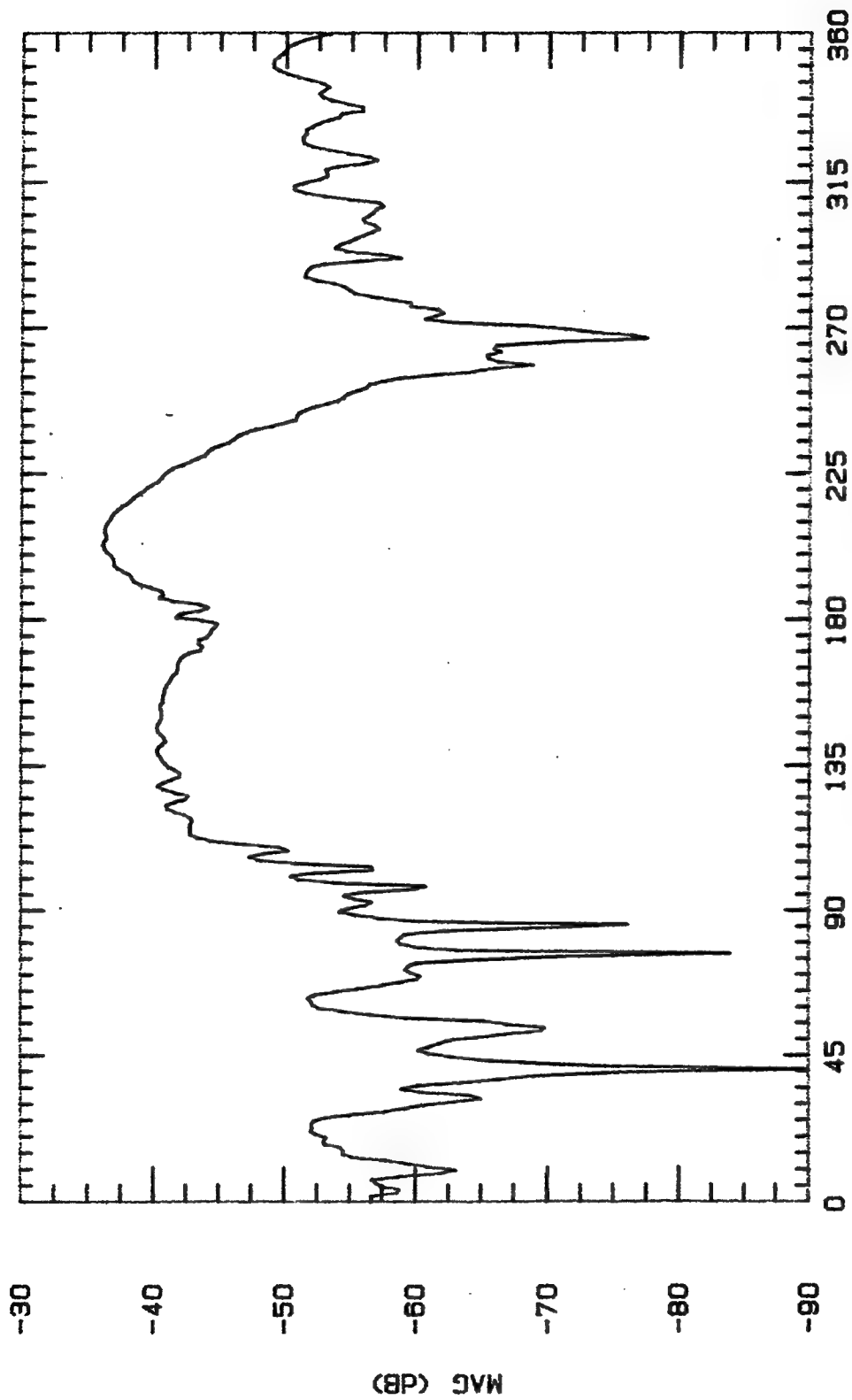


ASPECT ANGLE (DEGREES)

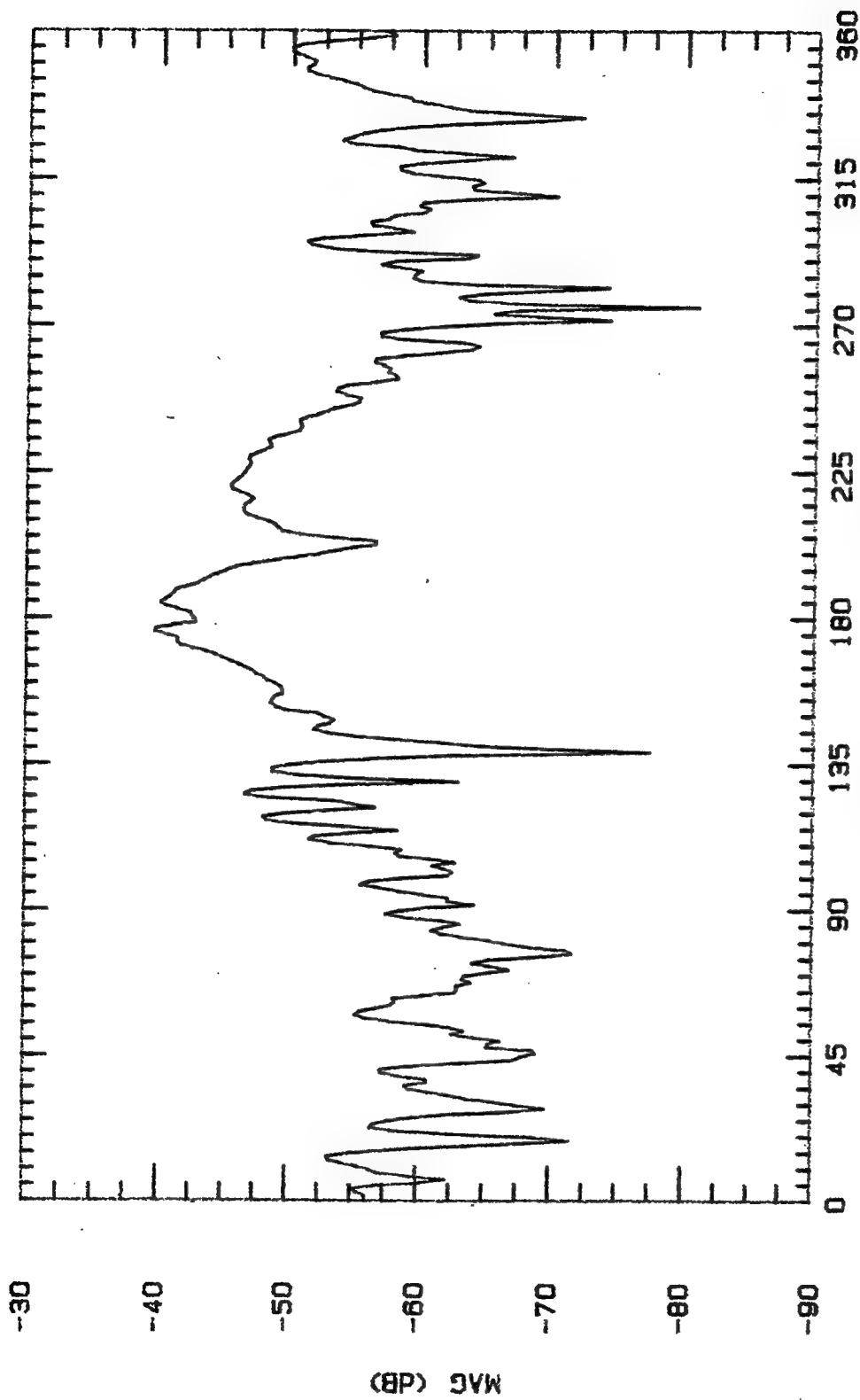
File Name	Frequency	Pattern Type	Date
LPL7NS	7 GHz	E-PLANE	18 OCT



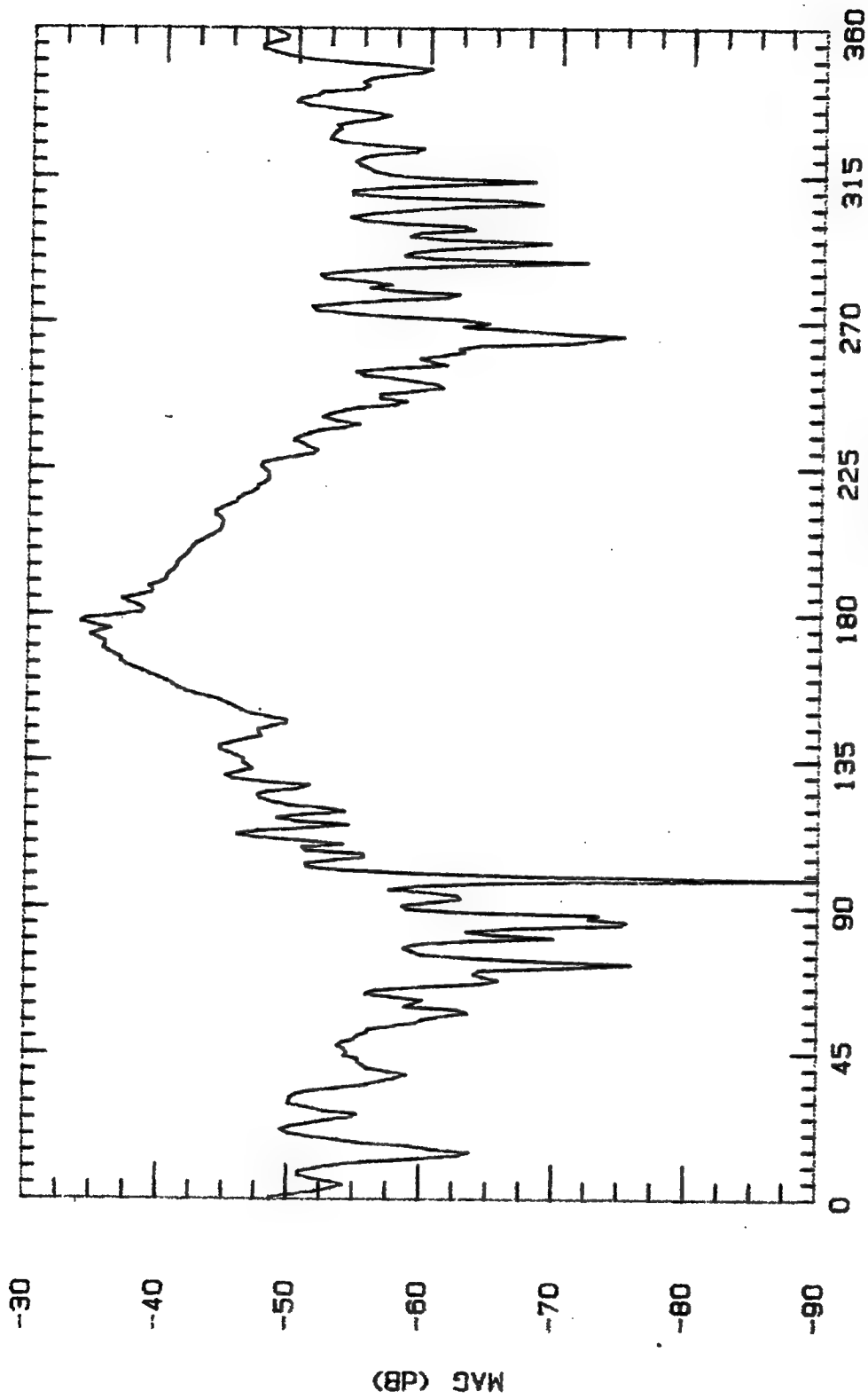
File Name	Frequency	Pattern Type	Date
LPLBNS	8 GHz	E-PLANE	18 OCT



File Name	Frequency	Pattern Type	Date
LPL9NS	9 GHz	E-PLANE	19 OCT

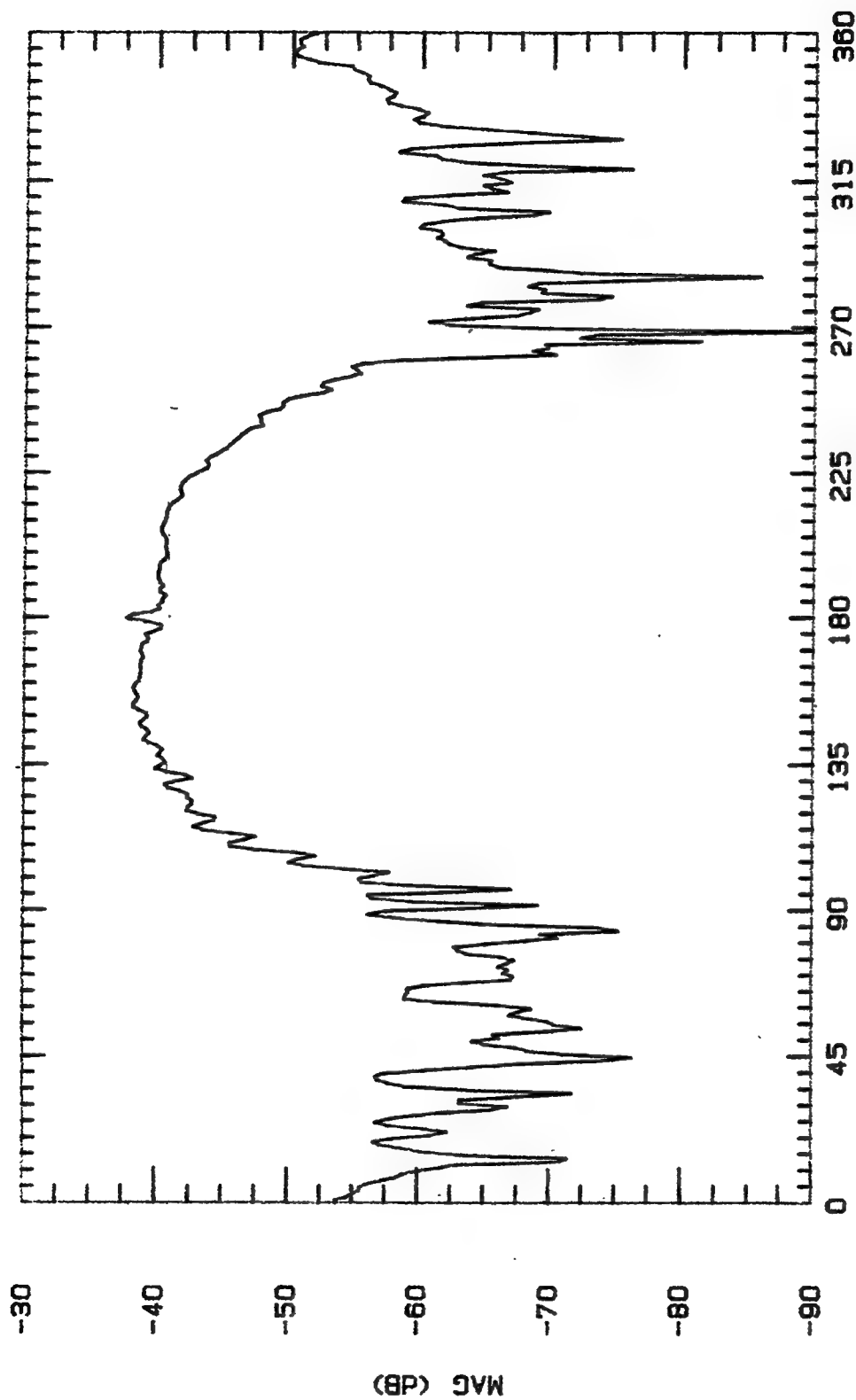


File Name	Frequency	Pattern Type	Date
LPL10NS	10 GHz	E-PLANE	19 OCT



ASPECT ANGLE (DEGREES)

File Name	Frequency	Pattern Type	Date
LPL11NS	11 GHz	E-PLANE	21 oct 94



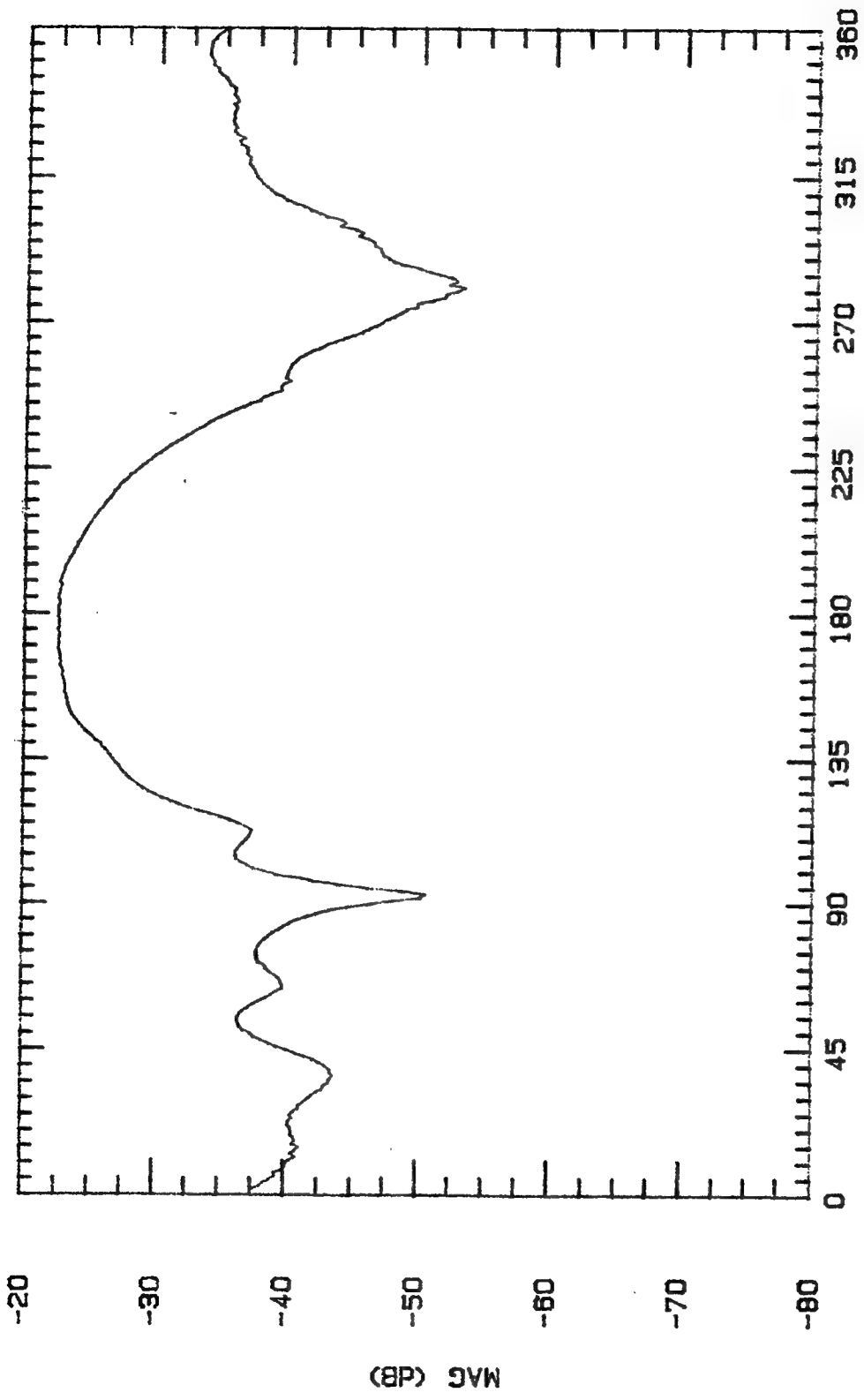
File Name	Frequency	Pattern Type	Date
LPL12NS	12 GHz	E-PLANE	18 OCT

APPENDIX H: Antenna Pattern Cuts For One Layer Design

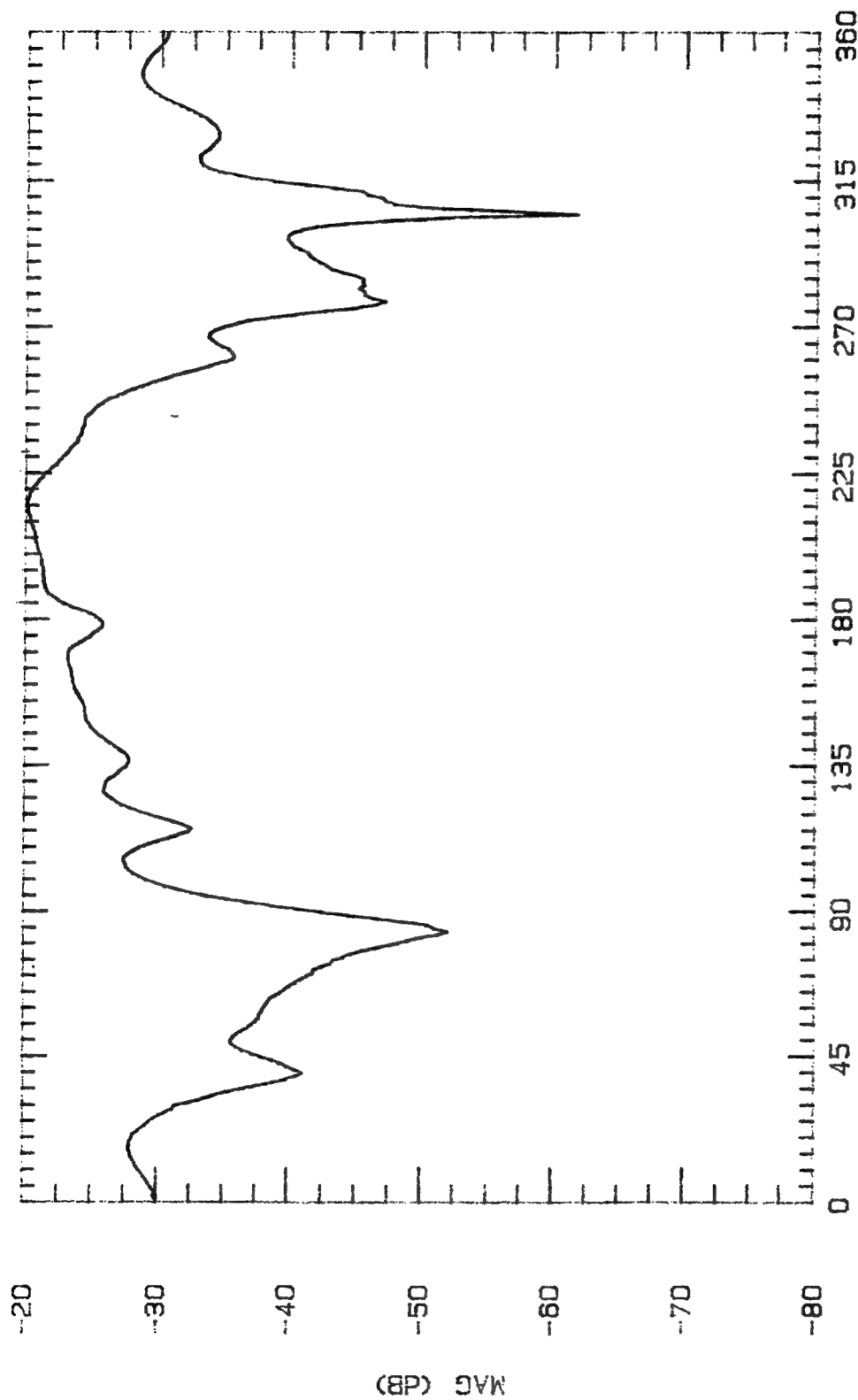
Note the following notation is used to describe the cavity configuration of the different designs listed in the Appendices.

(11 blank dielectric layers, 1 scattering layer with 5 arrays, 5 blank dielectric layers)
(11B, 1S (5 arrays), 5B)

Freq (GHz)	Normal Gain (dBi)	Max Gain (dBi)	Squint (deg)	Beamwidth (-3dBi to -3dBi) (deg)
-----	-----	-----	-----	-----
2.00	-5.7	-5.7	0	72
2.73	-10.5	-9.5	35	46
3.00	-13.8	-13.6	15	106
3.25	-0.6	0.9	-18	64
3.50	1.0	1.1	-2	76
4.00	-4.3	-1.1	-27	37
4.50	-11.8	-1.6	-43	10
5.00	-11.9	-4.9	45	38
6.00	-4.1	-3.5	-7	48
7.00	1.9	3	4	74
8.00	-9.6	-3.7	43	34
9.00	0.8	2.4	-11	24
10.00	-7.3	2.4	-39	14
11.00	-3.6	1.3	15	23
12.00	-3.7	-3.6	1	25
-----	-----	-----	-----	-----

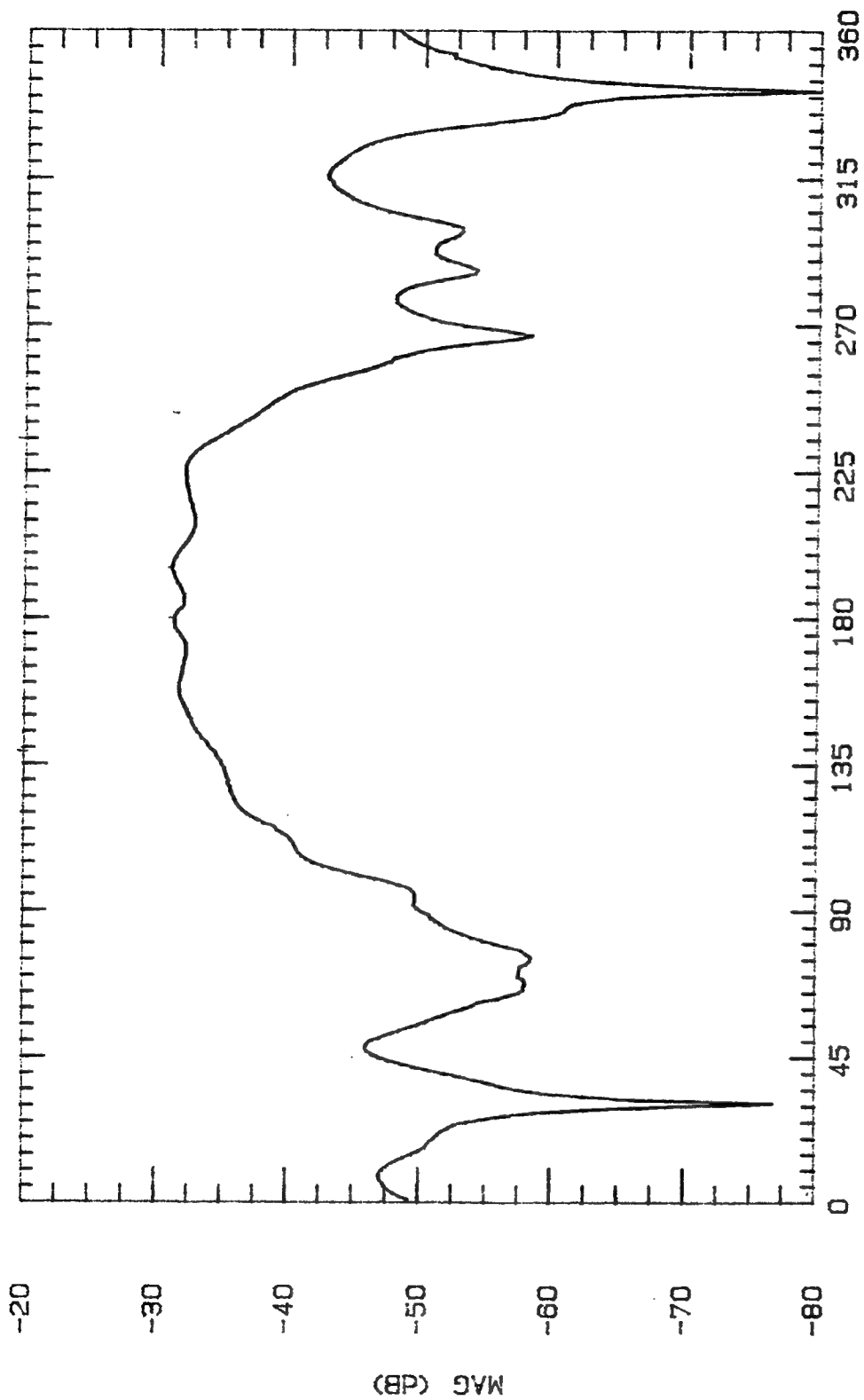


File Name	Frequency	Pattern Type	Date
DLPL200	2 GHz	E-PLANE	28 OCT 94



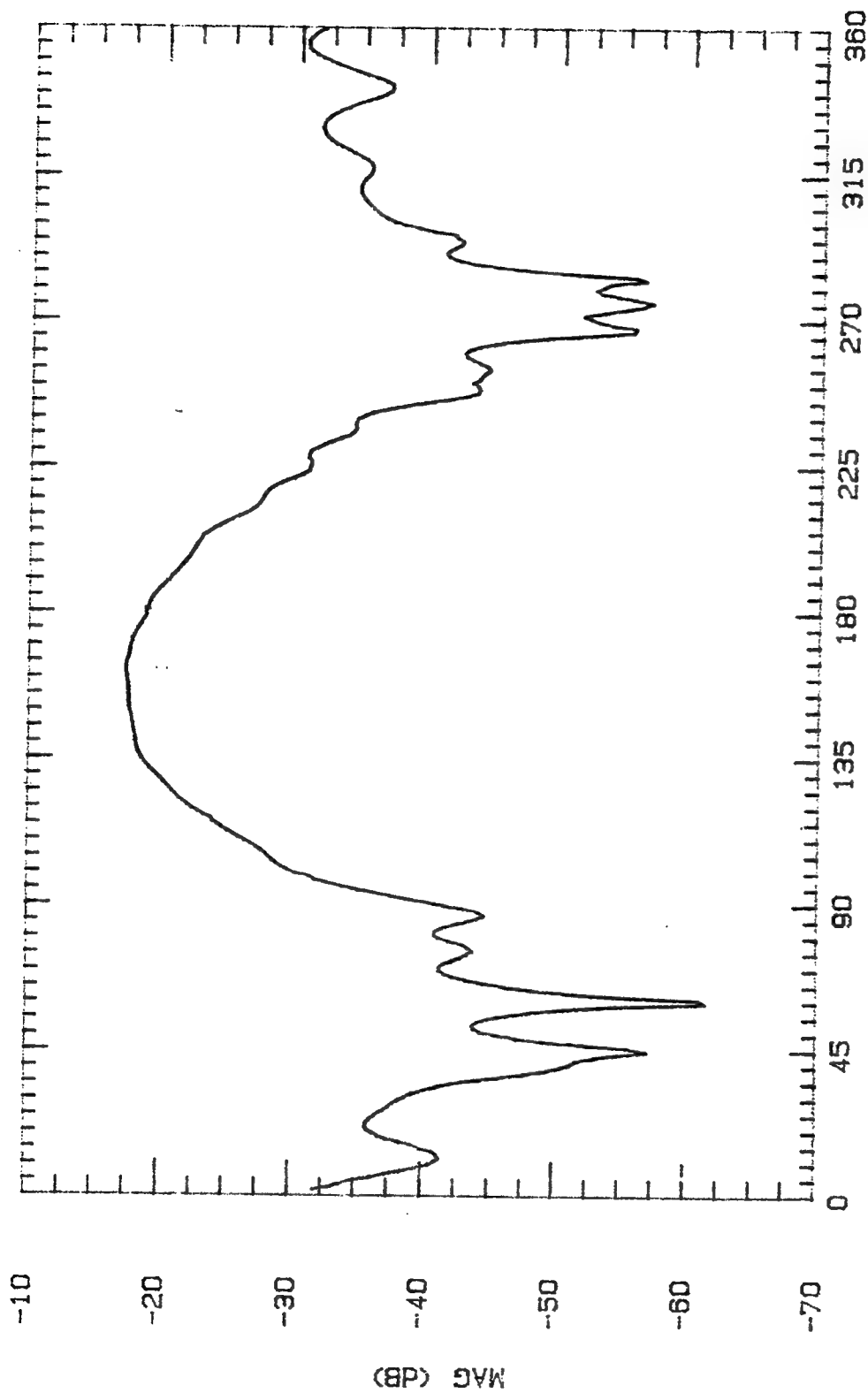
ASPECT ANGLE (DEGREES)

File Name	Frequency	Pattern Type	Date
DLP275	2.75 GHz	E-PLANE	28 OCT 94



ASPECT ANGLE (DEGREES)

File Name	Frequency	Pattern Type	Date
DLPL300	3 GHz	E-PLANE	29 OCT 94



ASPECT ANGLE (DEGREES)

File Name

Frequency

Pattern Type

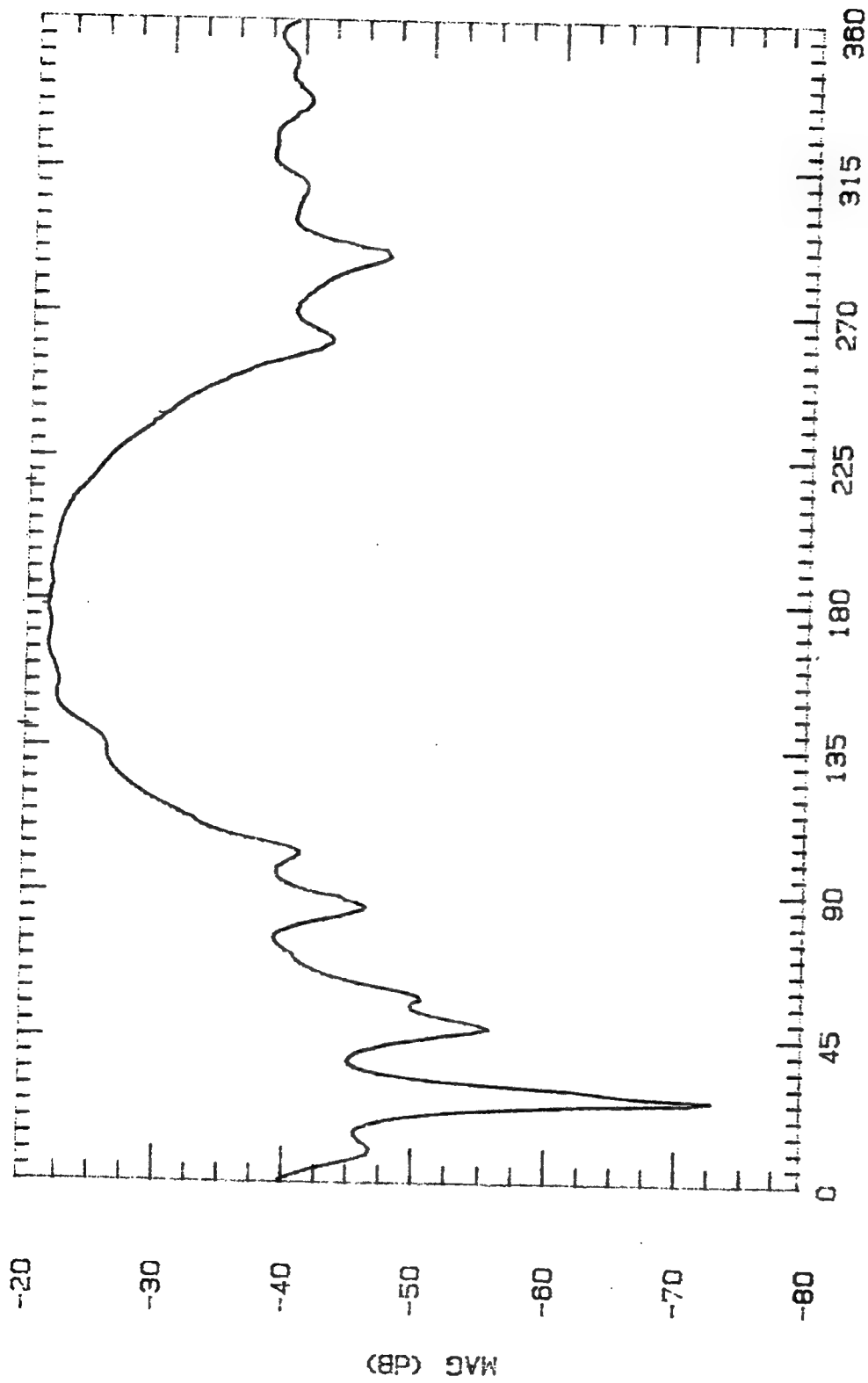
Date

DLPL325

3.25 GHz

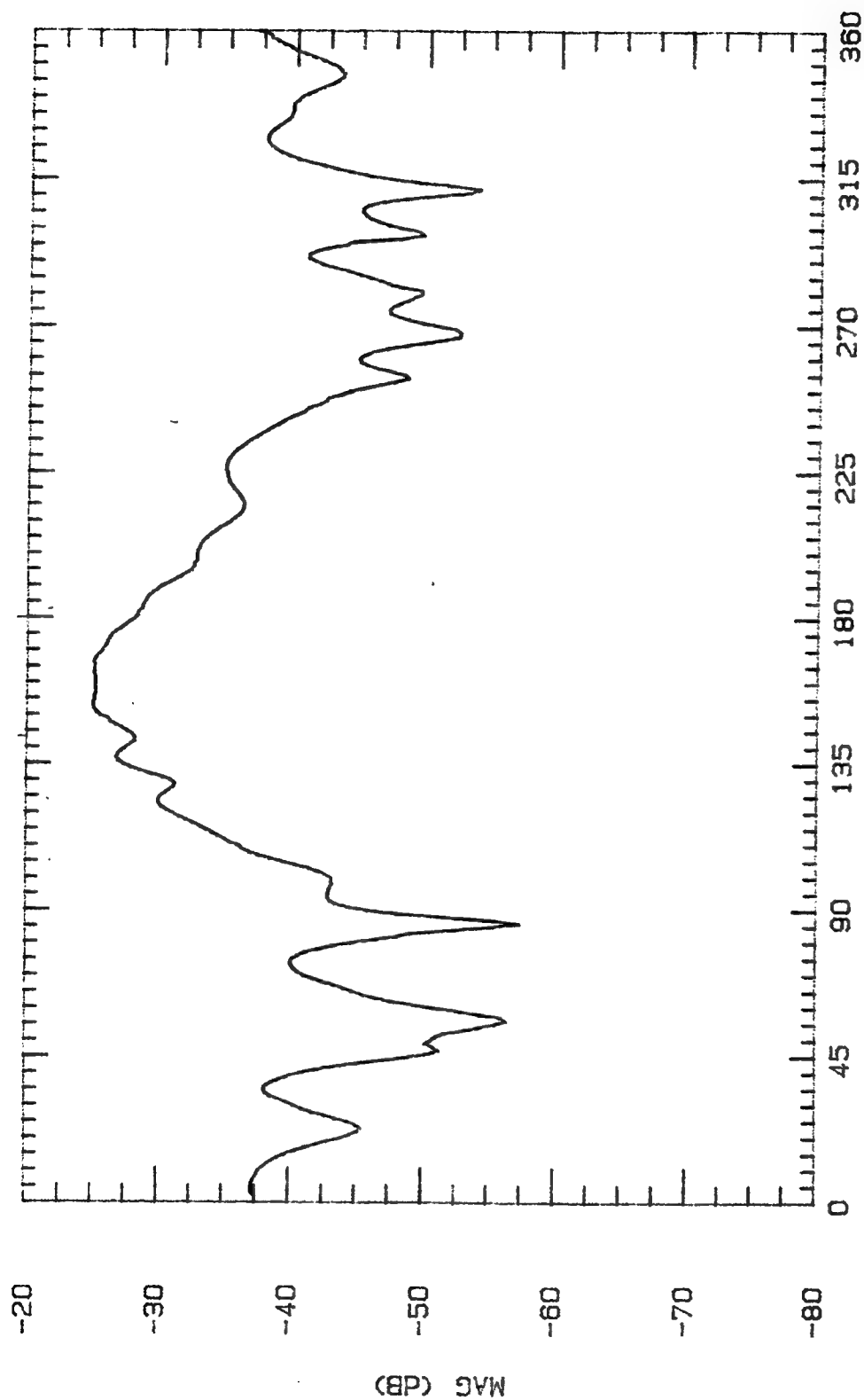
E-PLANE

29 OCT 94

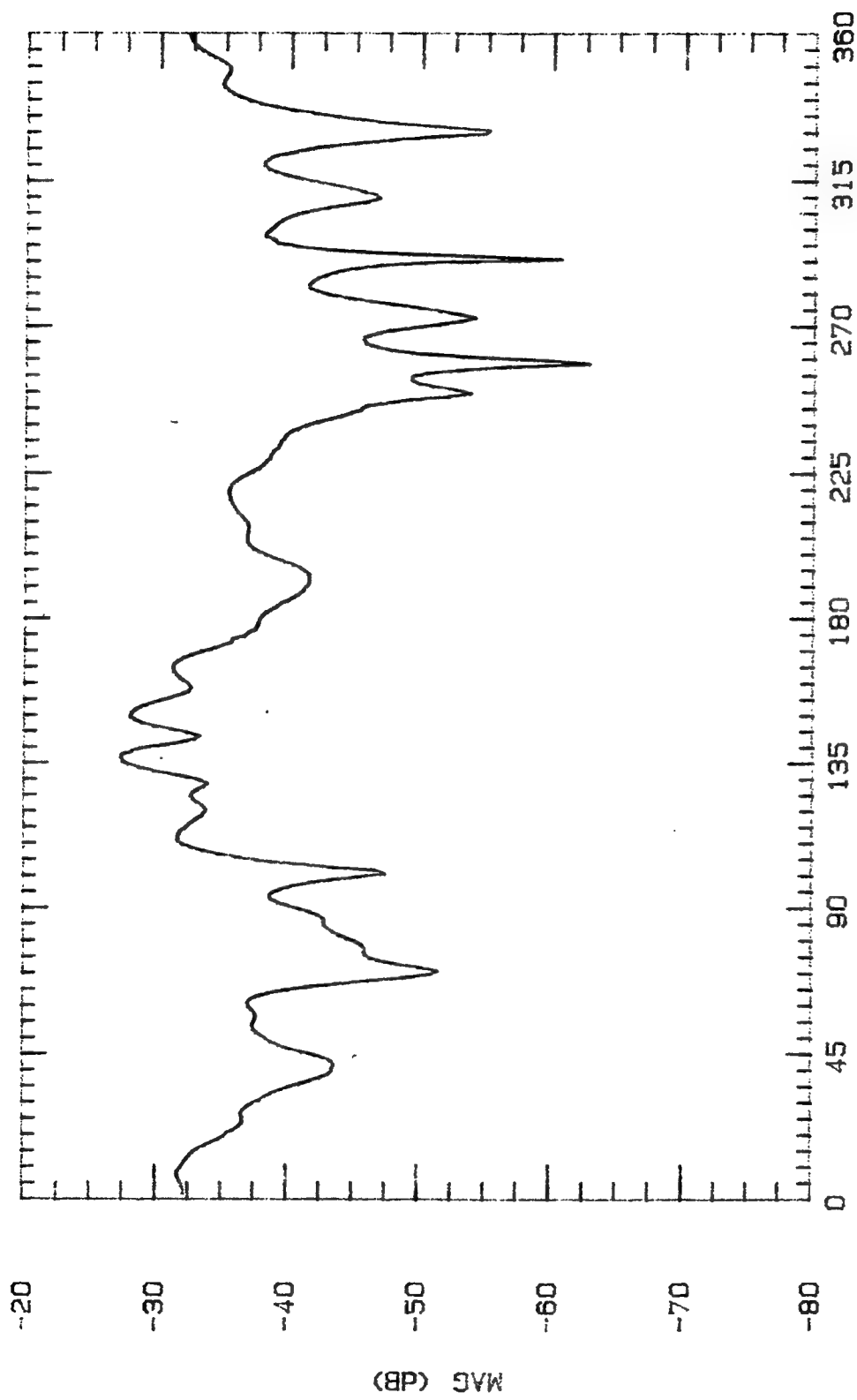


ASPECT ANGLE (DEGREES)

File Name	Frequency	Pattern Type	Date
DLPL350	3.5 GHz	E-PLANE	29 OCT 94

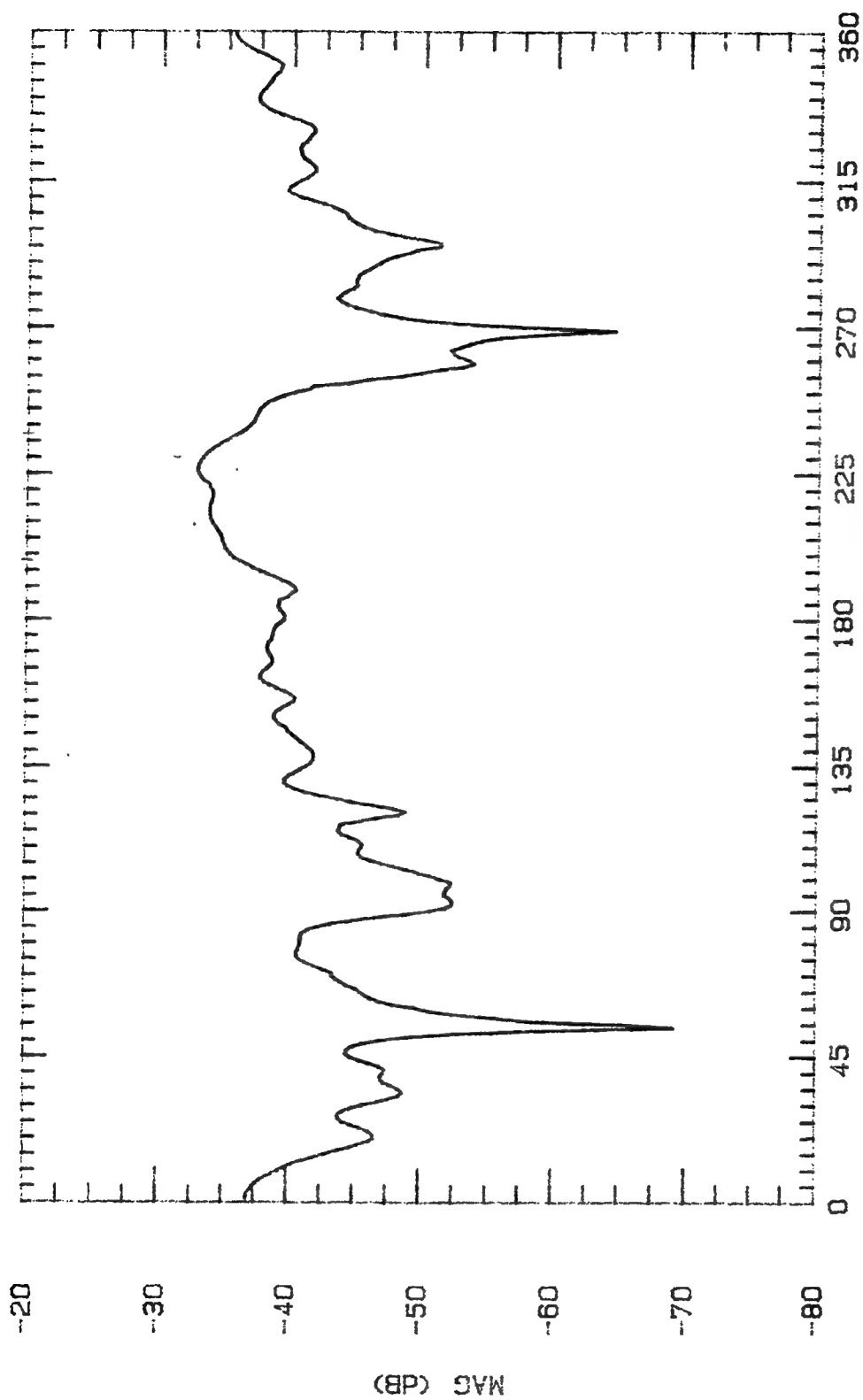


File Name	Frequency	Pattern Type	Date
DLPL400	4 GHz	E-PLANE	28 OCT 94



ASPECT ANGLE (DEGREES)

File Name	Frequency	Pattern Type	Date
DLPL450	4.5 GHz	E-PLANE	28 OCT 94



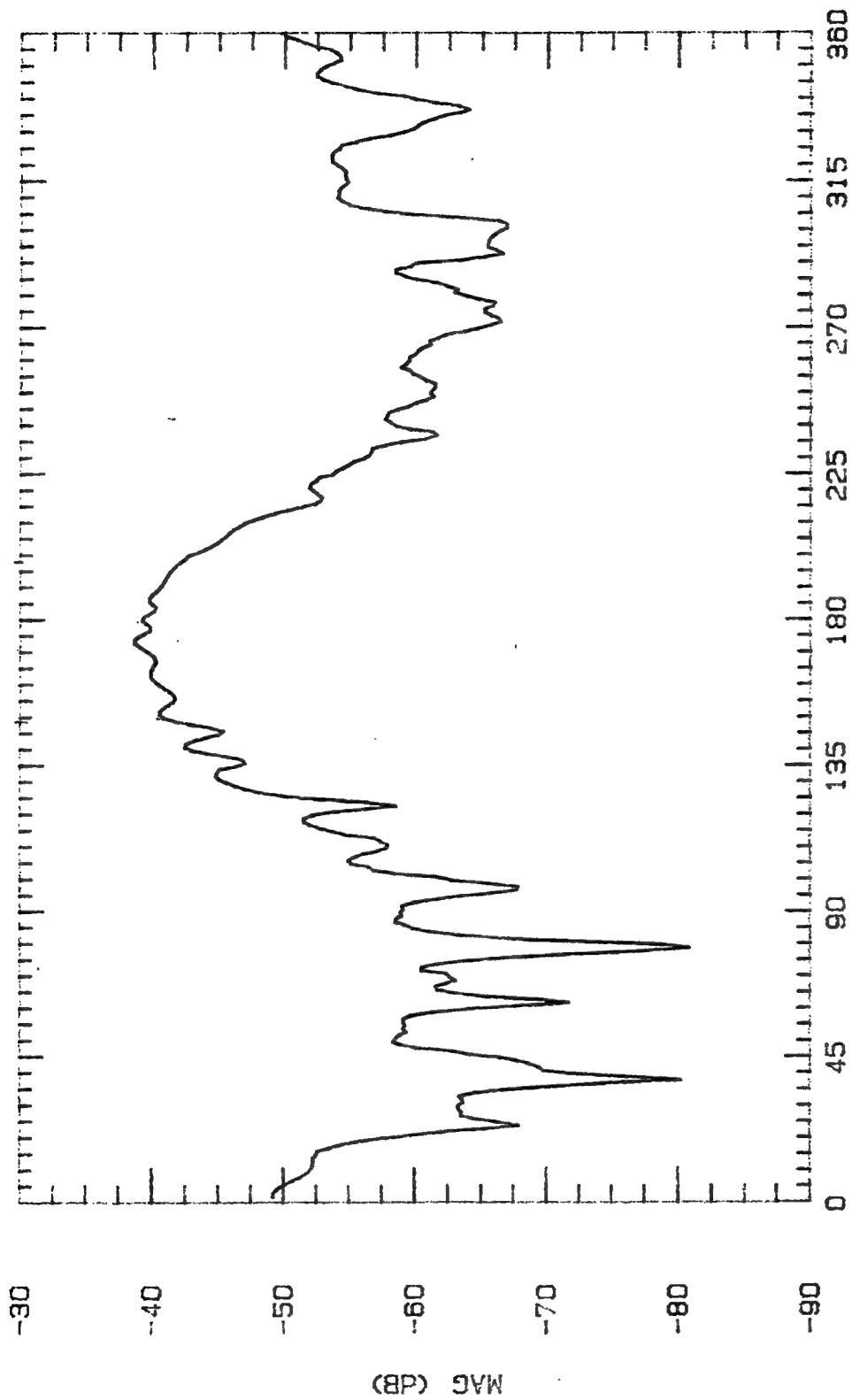
File Name Frequency Pattern Type Date

DLPL500

5 GHz

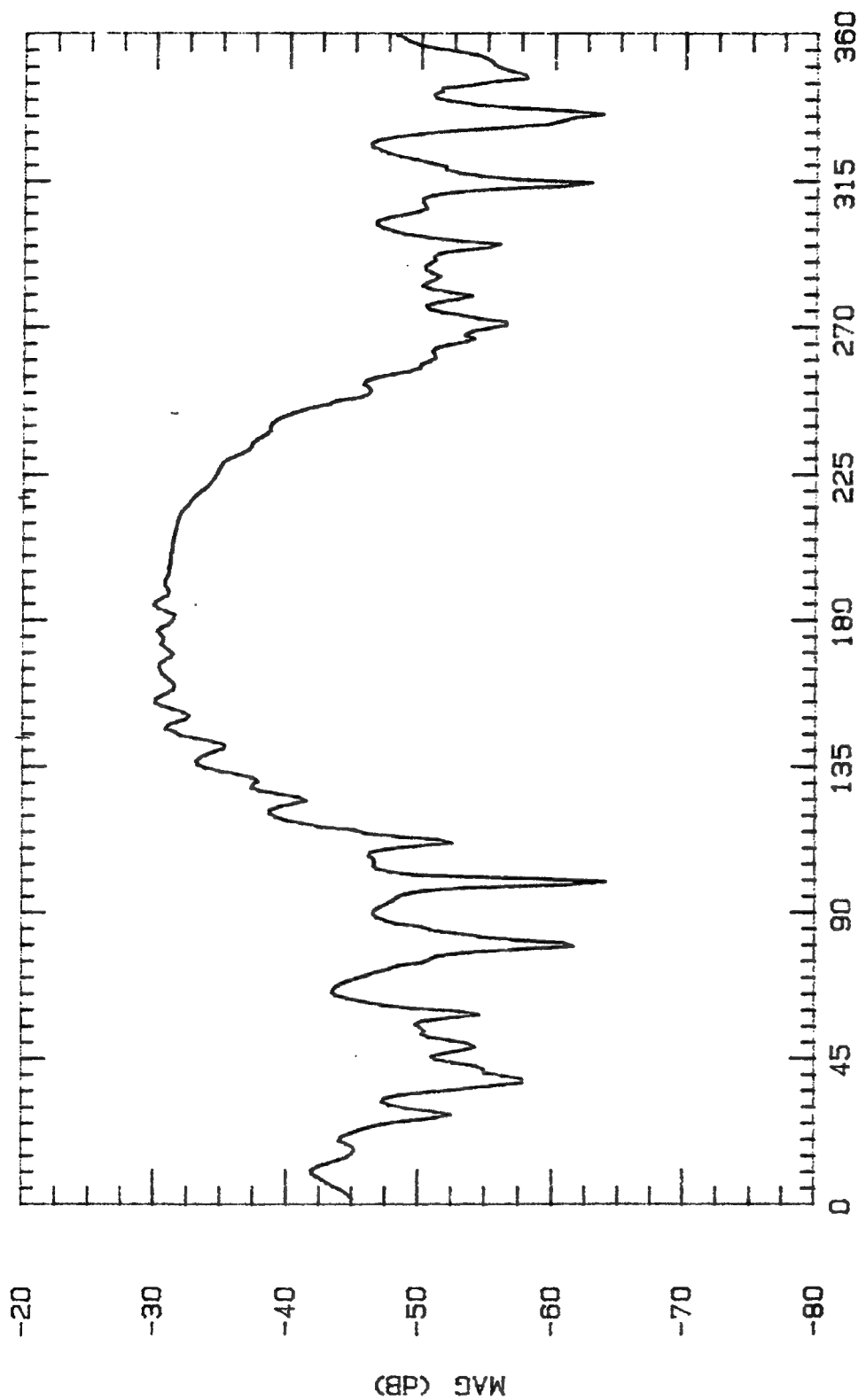
E-PLANE

29 OCT 94



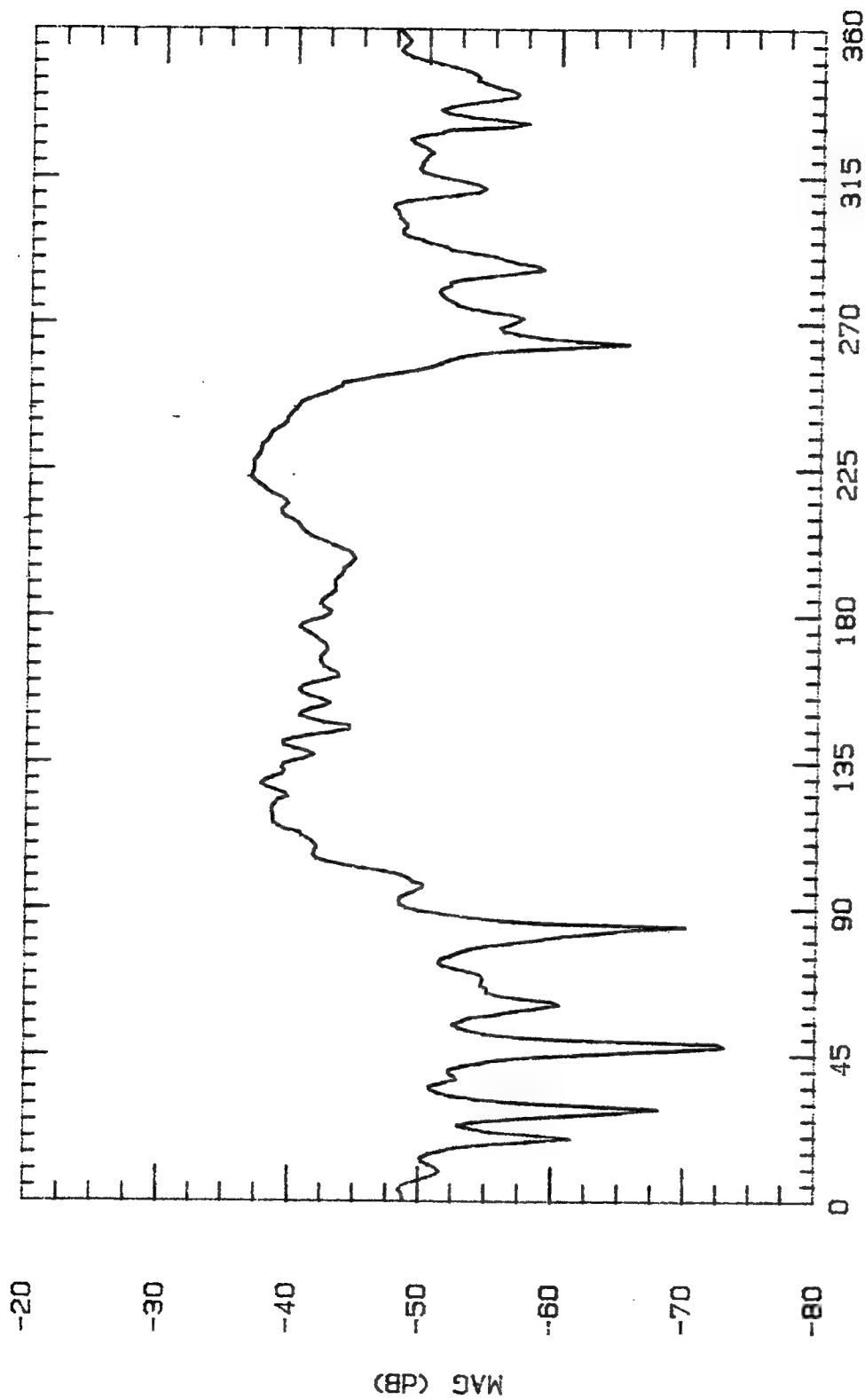
ASPECT ANGLE (DEGREES)

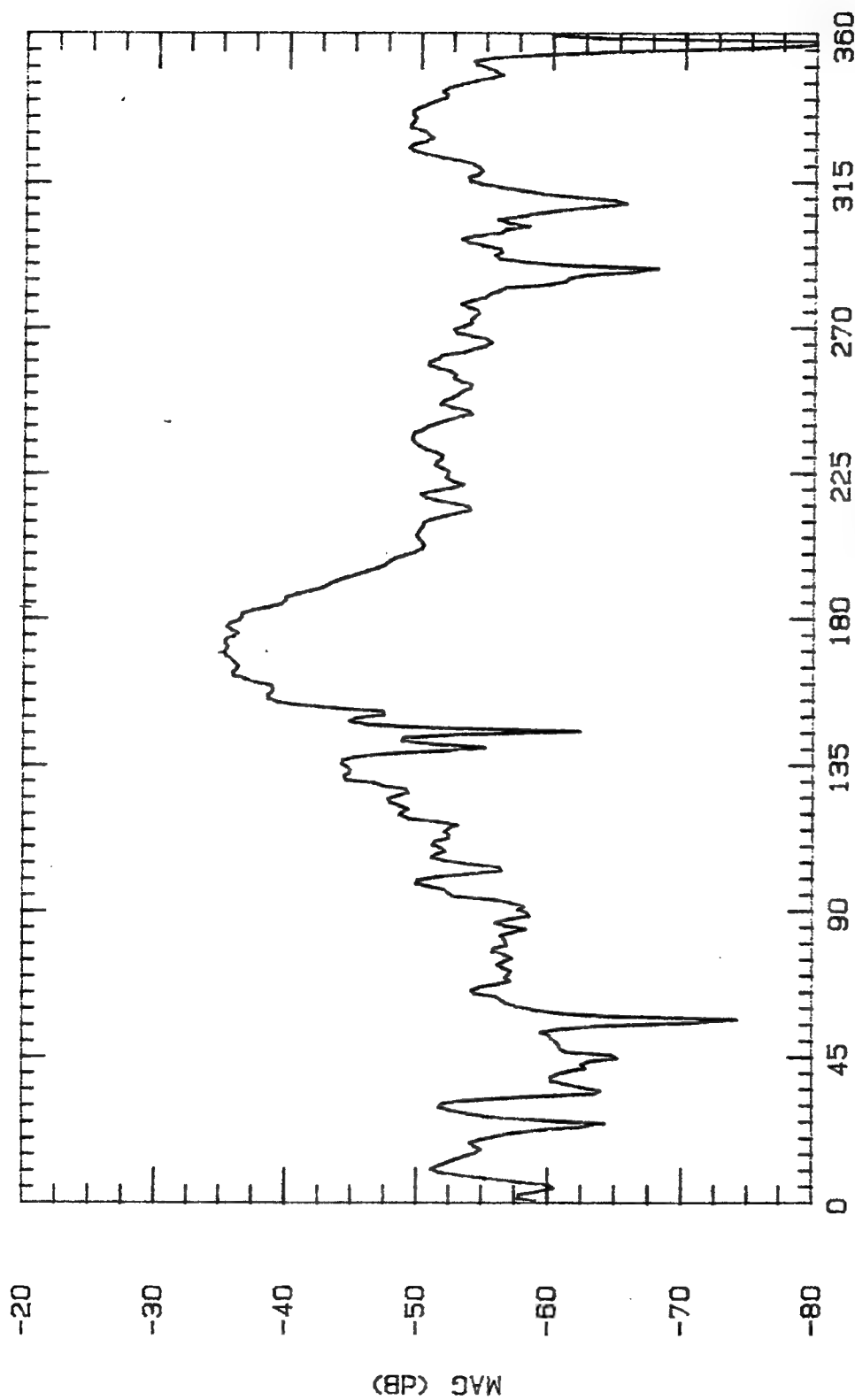
File Name	Frequency	Pattern Type	Date
DLPL800	8 GHz	E-PLANE	29 OCT 94



ASPECT ANGLE (DEGREES)

File Name	Frequency	Pattern Type	Date
DLPL700	7 GHz	E-PLANE	29 OCT 94





ASPECT ANGLE (DEGREES)

File Name

DLP1800

Frequency

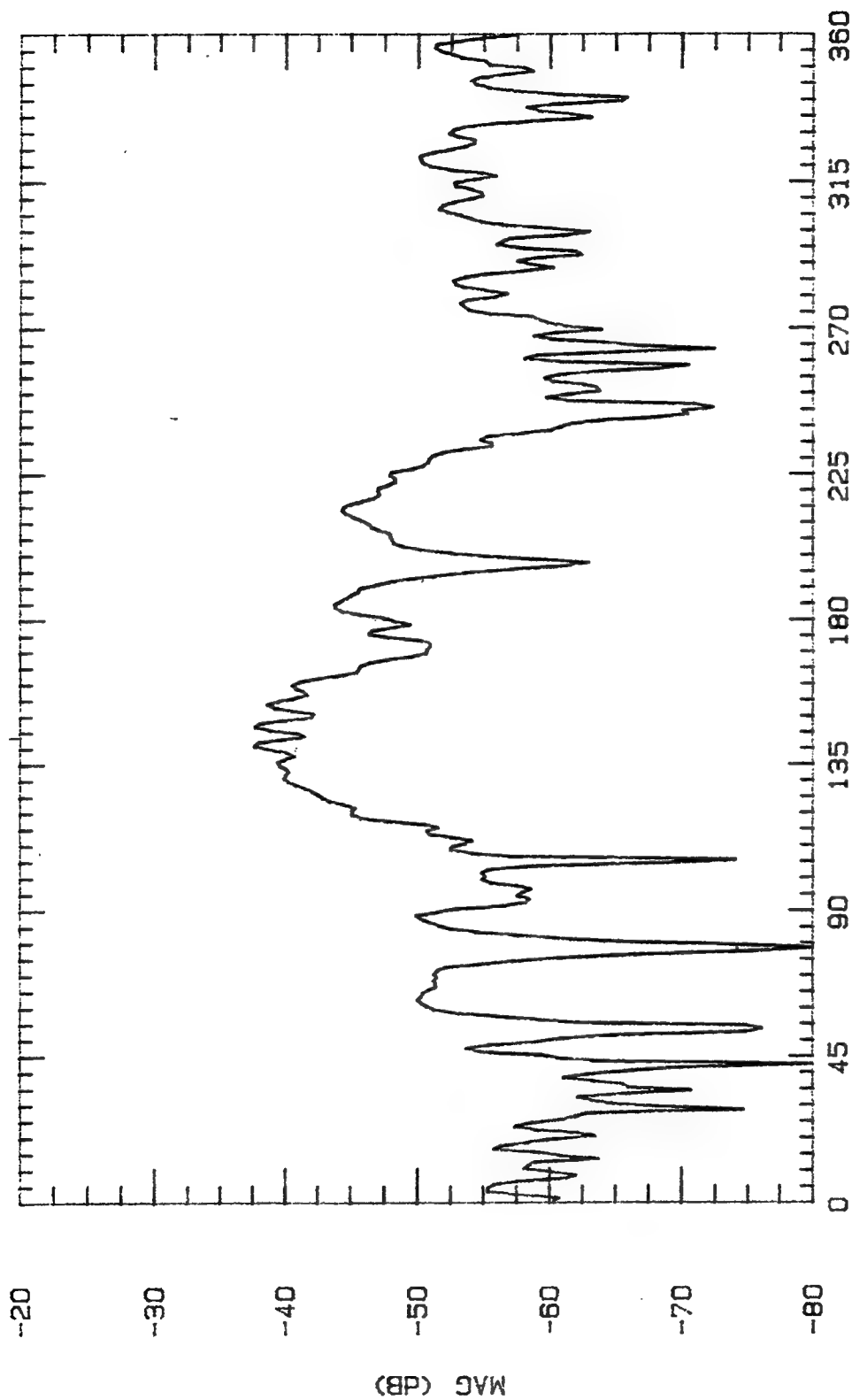
9 GHz

Pattern Type

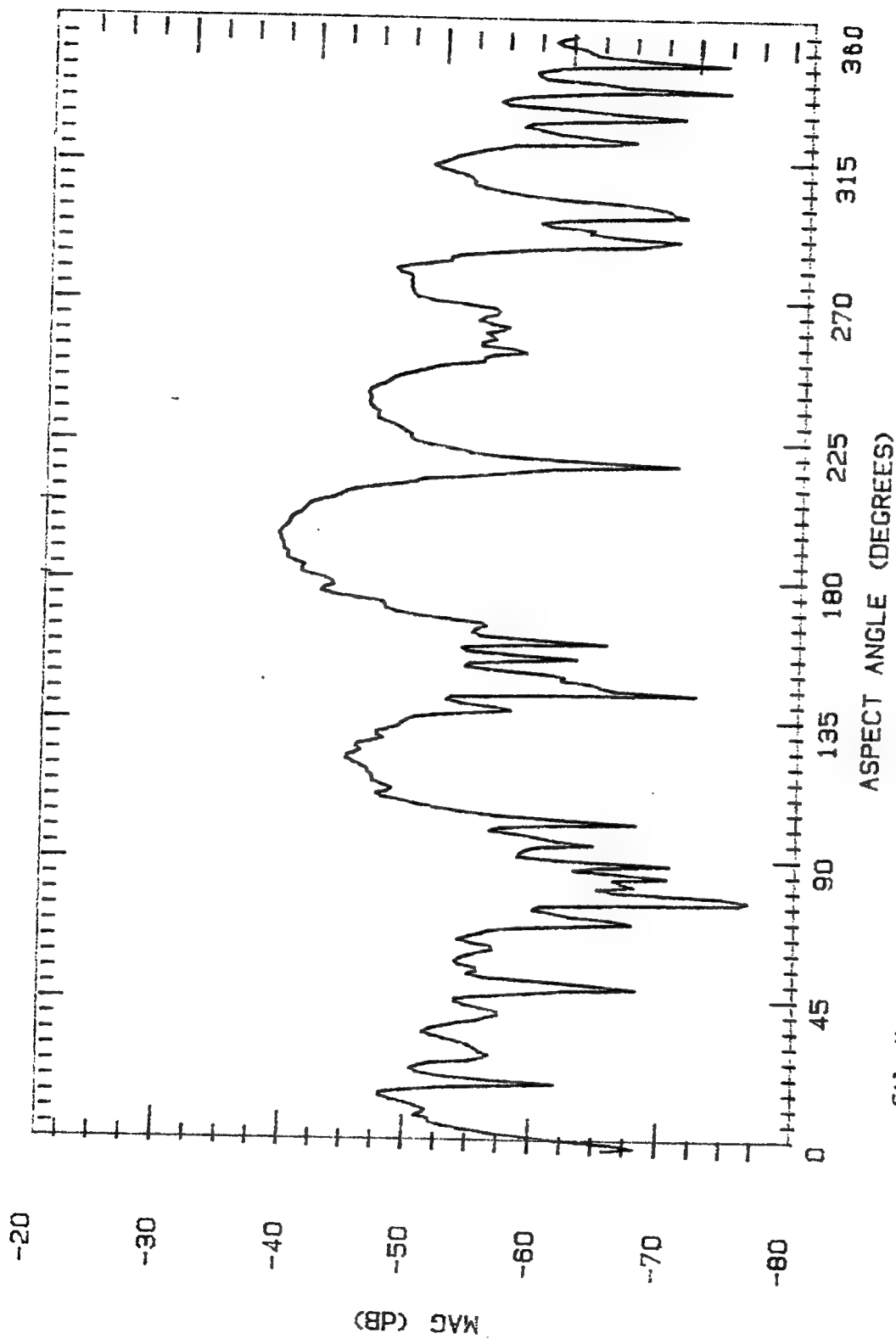
E-PLANE

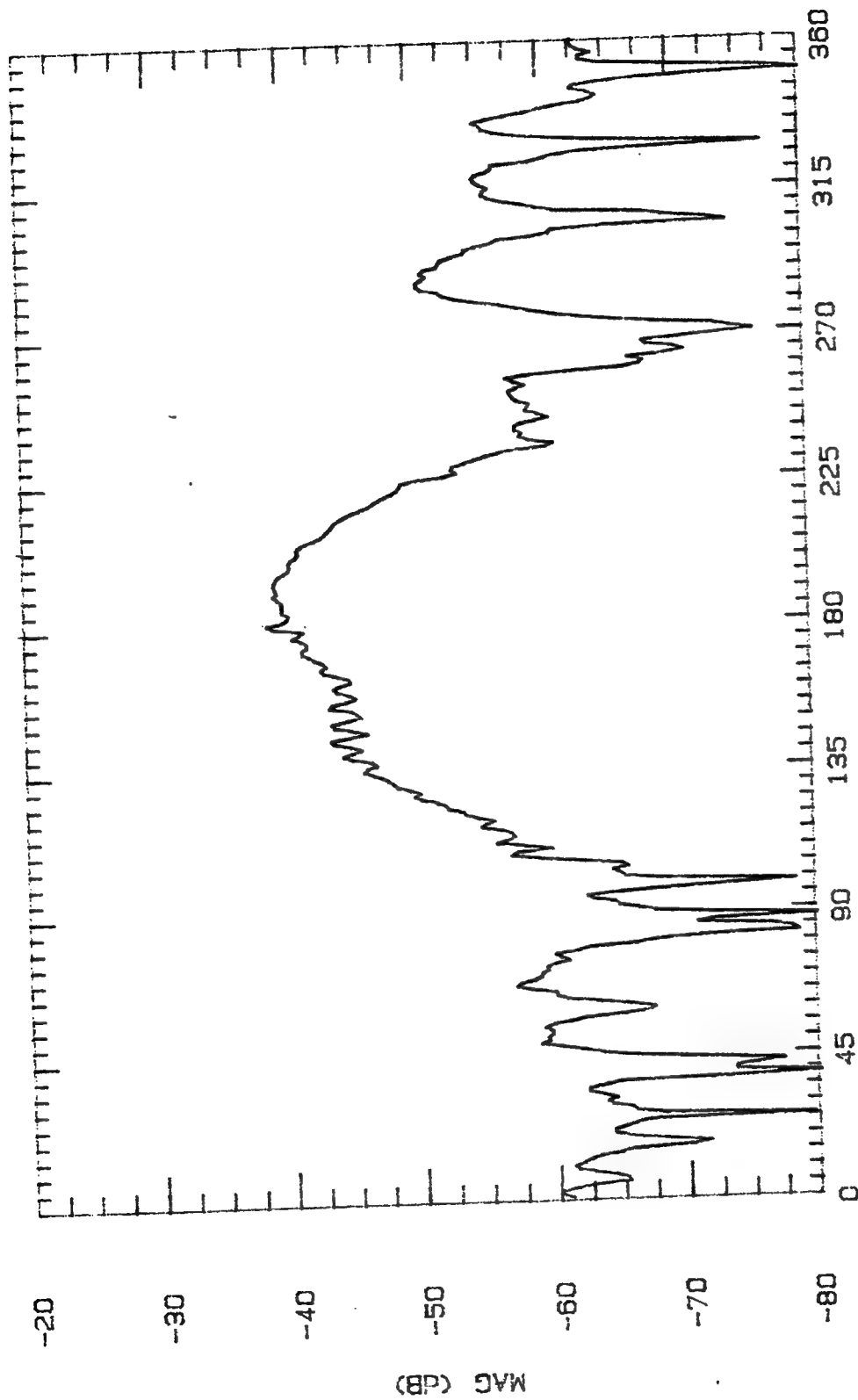
Date

29 OCT 94



File Name	Frequency	Pattern Type	Date
DLPL1000	10 GHz	E-PLANE	29 OCT 94





ASPECT ANGLE (DEGREES)

Data

Pattern Type

Frequency

File Name

29 OCT 94

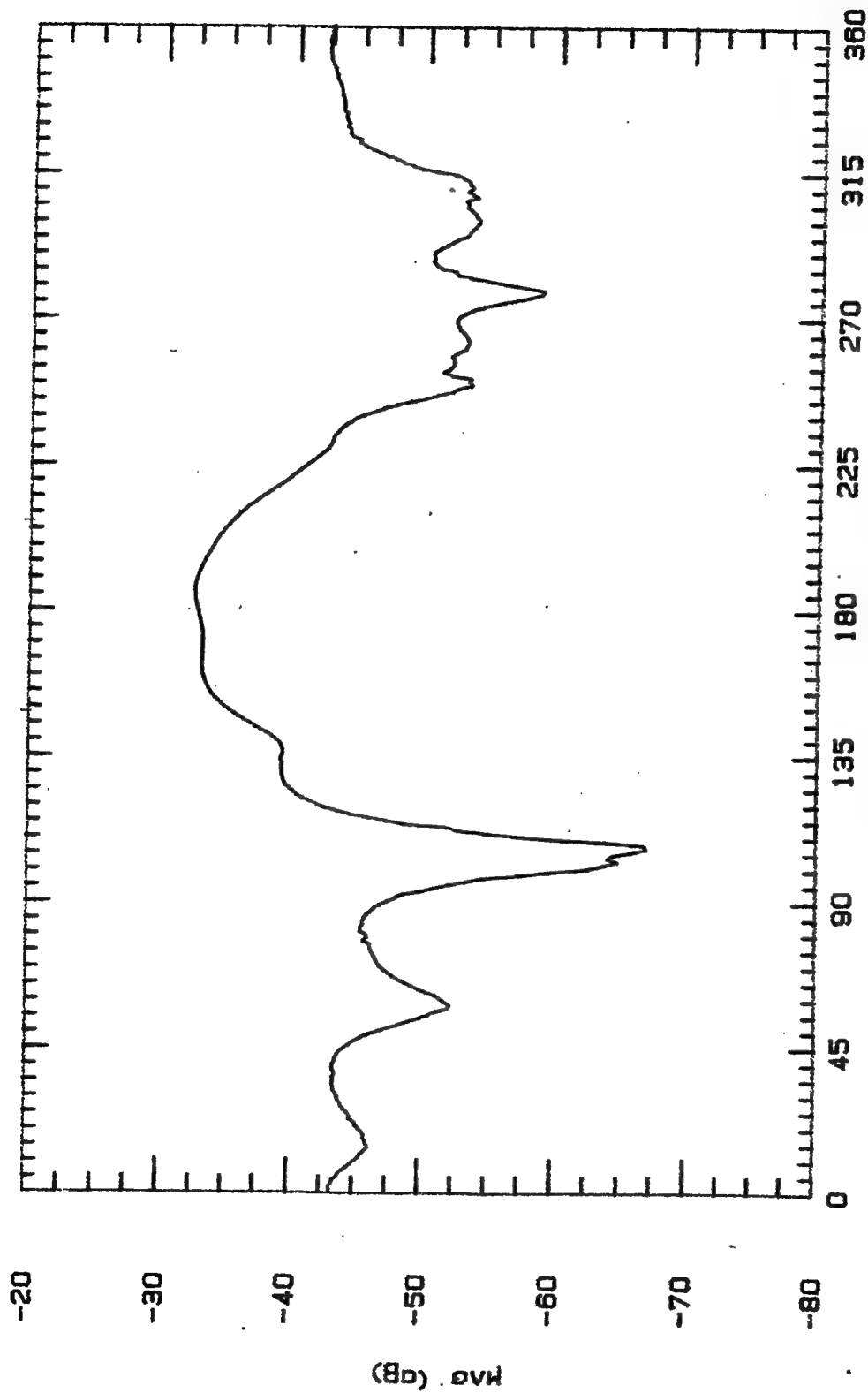
E-PLANE

12 GHz

DLPL1200

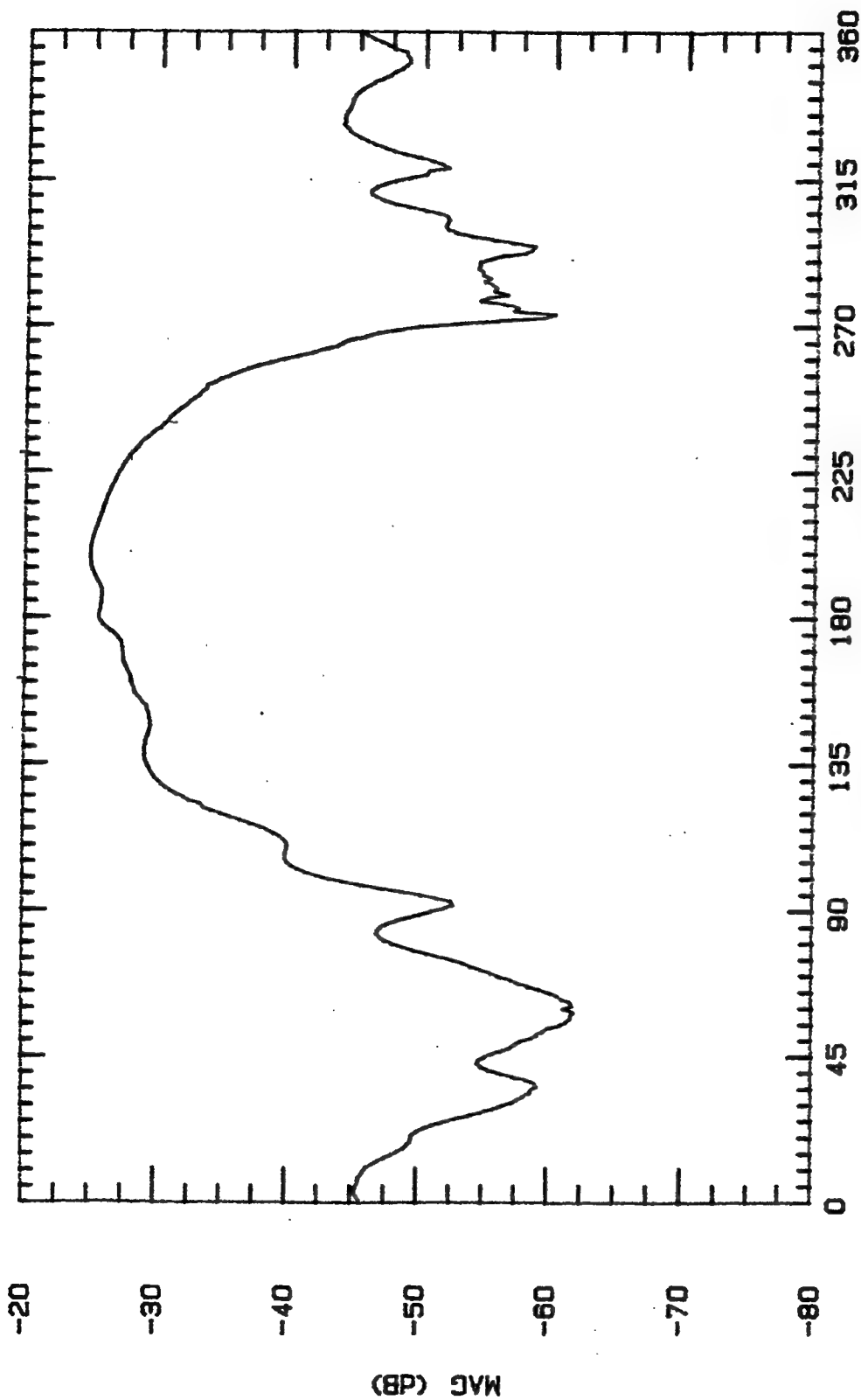
APPENDIX I: Antenna Pattern Cuts For 6.2 & 3.1 GHz Two Layer Design
(5B, 1S, 5B, 1S, 5B)
(6.2(2arrays) & 3.11(5arrays))

Freq (GHz)	Normal Gain (dBi)	Max Gain (dBi)	Squint (deg)	Beamwidth (-3dBi to -3dBi) (deg)
-----	-----	-----	-----	-----
2.0	-17.2	-17.2	0	60
3.0	-6.3	-7.3	15	70
4.0	-8.1	-2.1	-30	40
5.0	-8.9	-5.3	25	55
6.0	-9.0	-7.0	-13	45
7.0	-0.5	1.5	-10	38
8.0	-2.8	0.7	-30	35
9.0	-12.3	0.2	20	25
10.0	0.1	2.5	5	42
11.0	-1.0	2.0	-5	15
12.0	4.1	4.1	0	38
-----	-----	-----	-----	-----



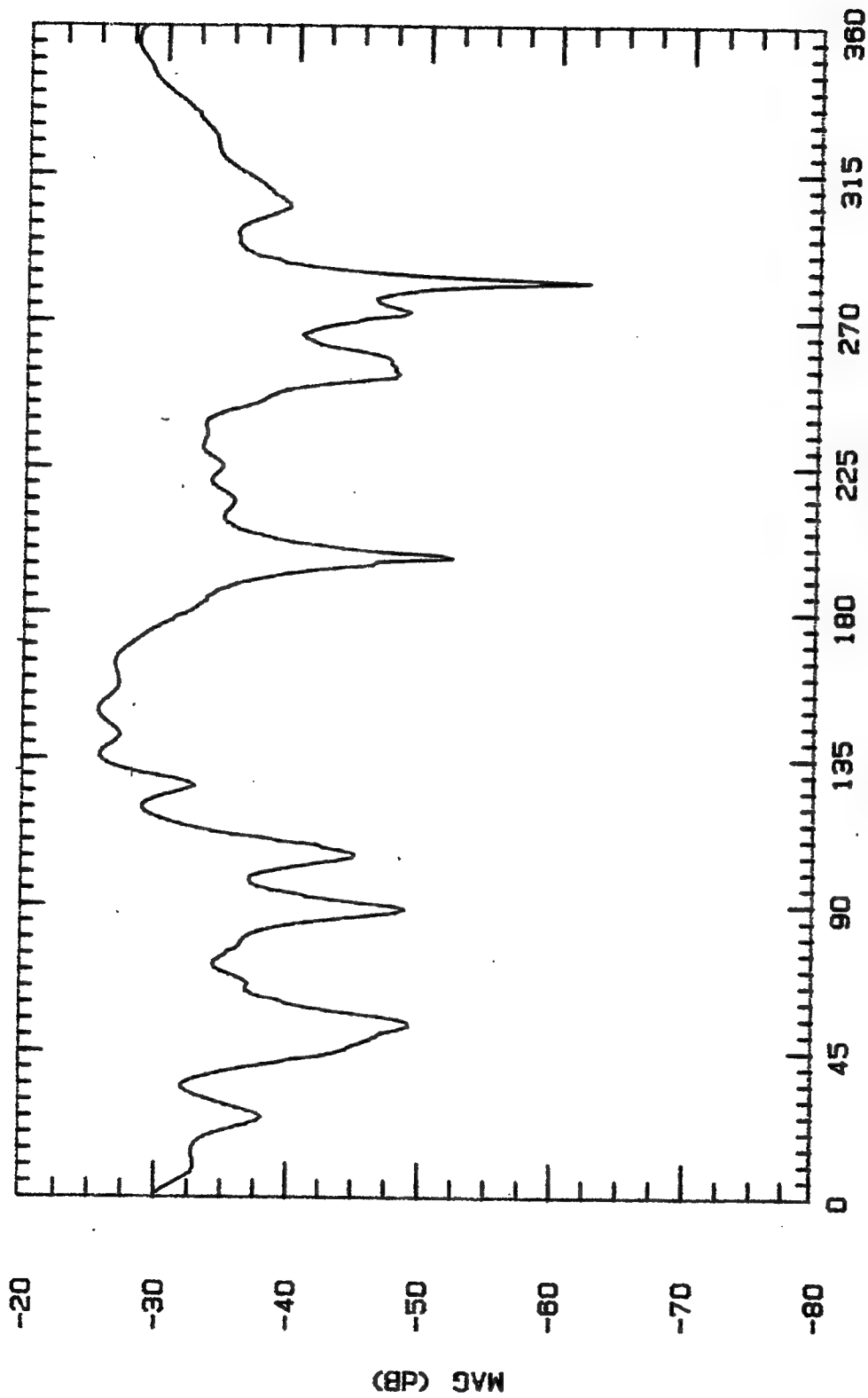
ASPECT ANGLE (DEGREES)

File Name	Frequency	Pattern Type	Date
LPL2	2 GHz	E-PLANE	18 OCT 94



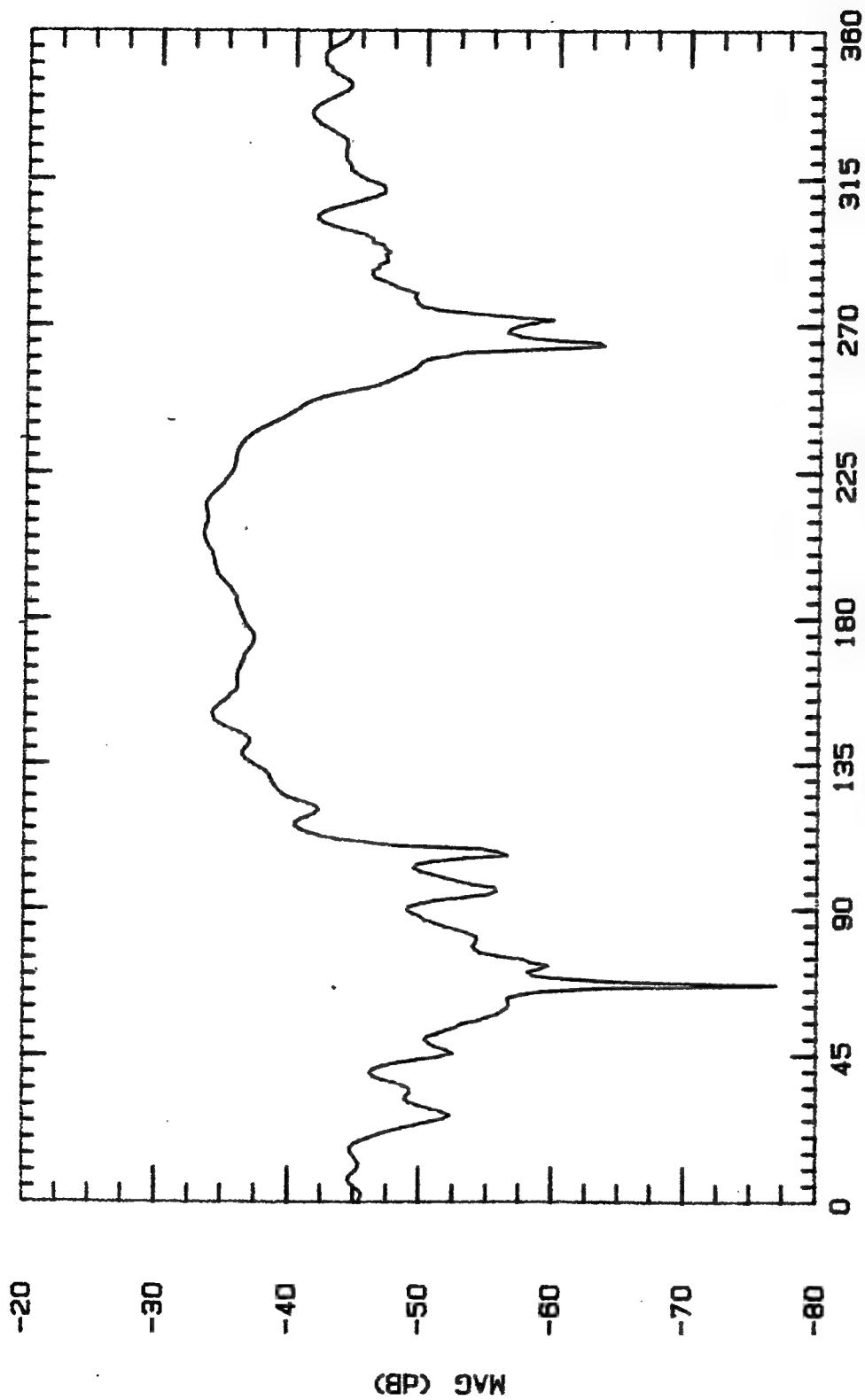
ASPECT ANGLE (DEGREES)

File Name	Frequency	Pattern Type	Date
LPL3	9 GHz	E-PLANE	18 OCT 94



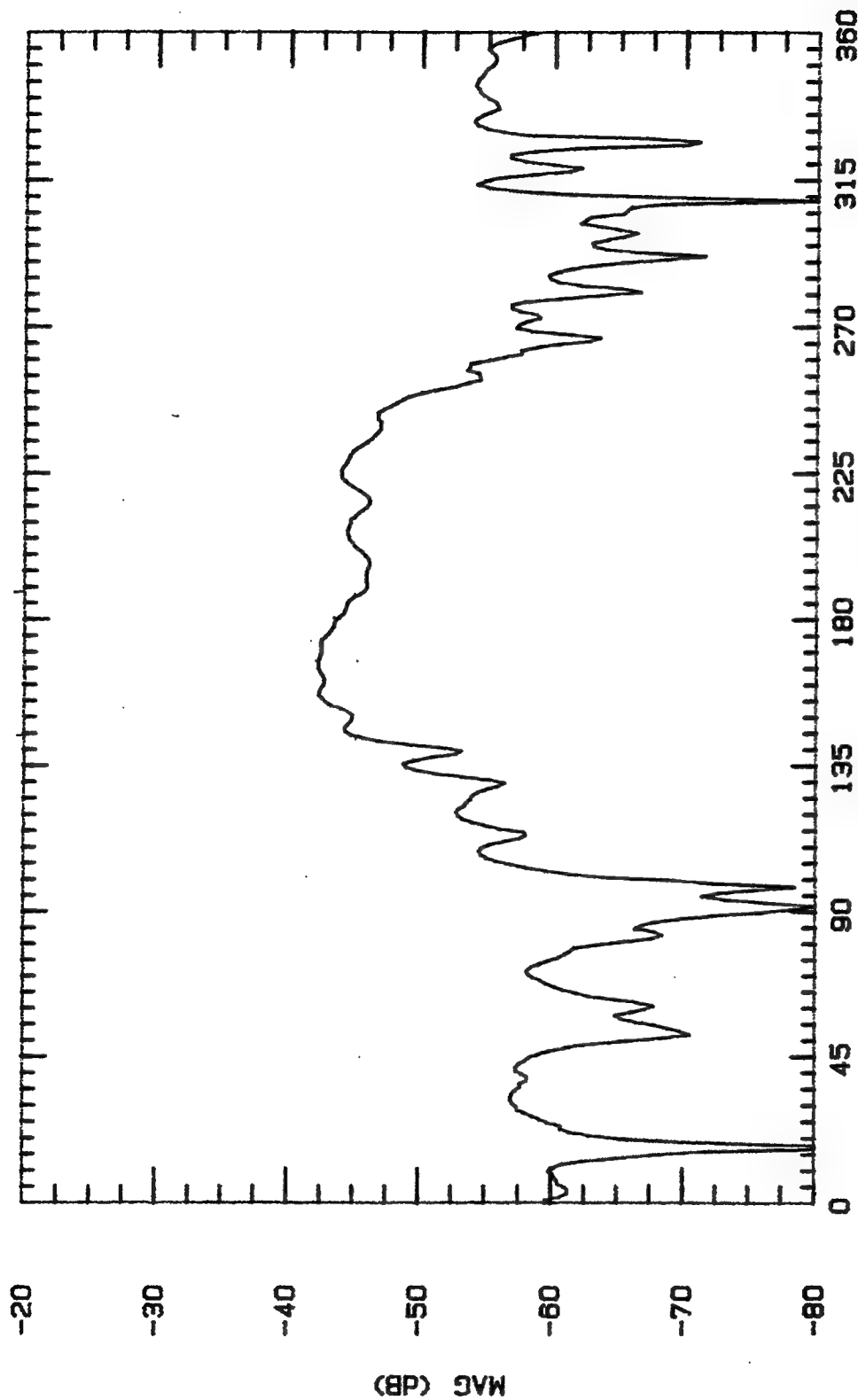
ASPECT ANGLE (DEGREES)

File Name	Frequency	Pattern Type	Date
LPL4	4 GHz	E-PLANE	18 OCT 94



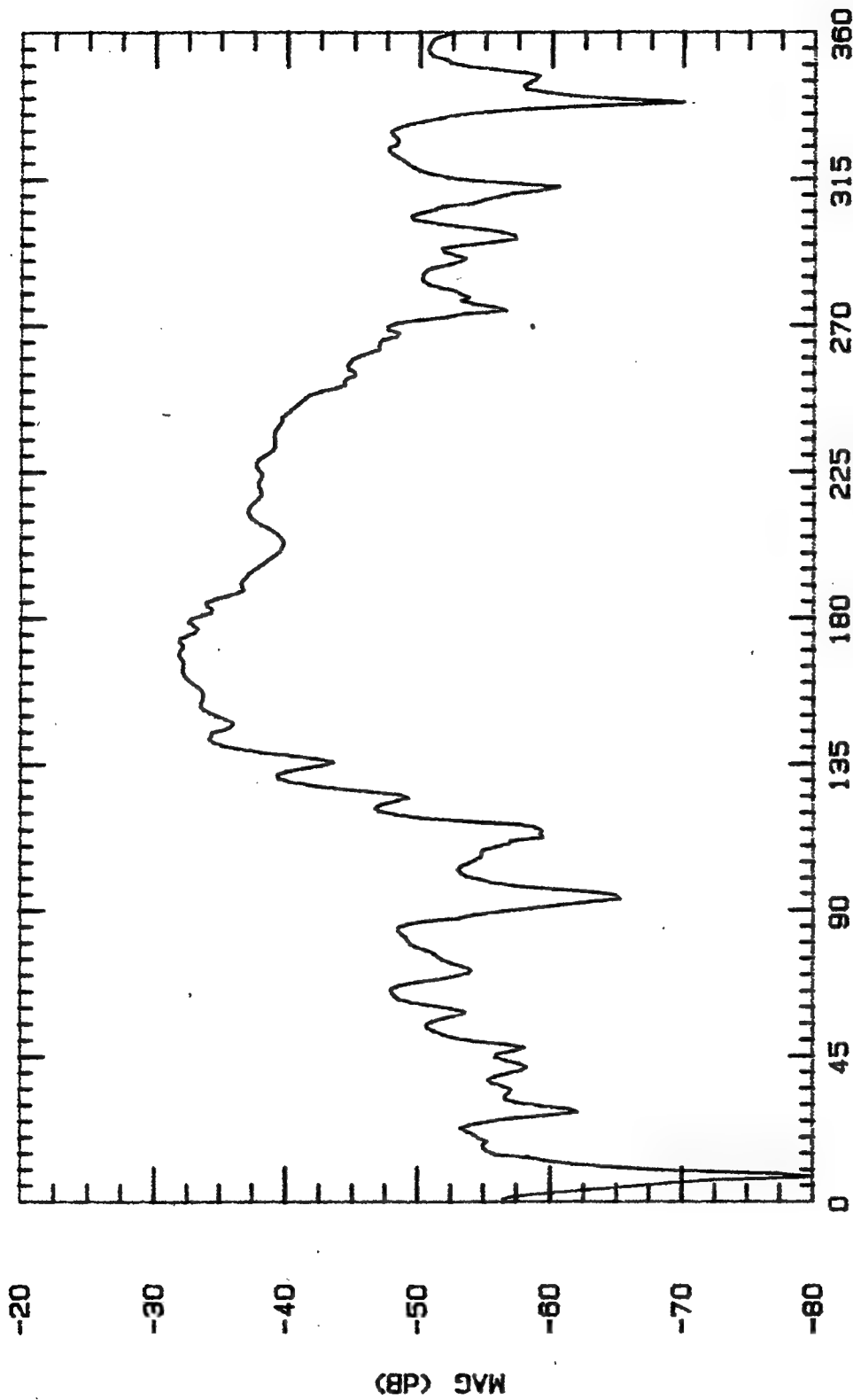
ASPECT ANGLE (DEGREES)

File Name	Frequency	Pattern Type	Date
LPL5	5 GHz	E-PLANE	18 OCT 94



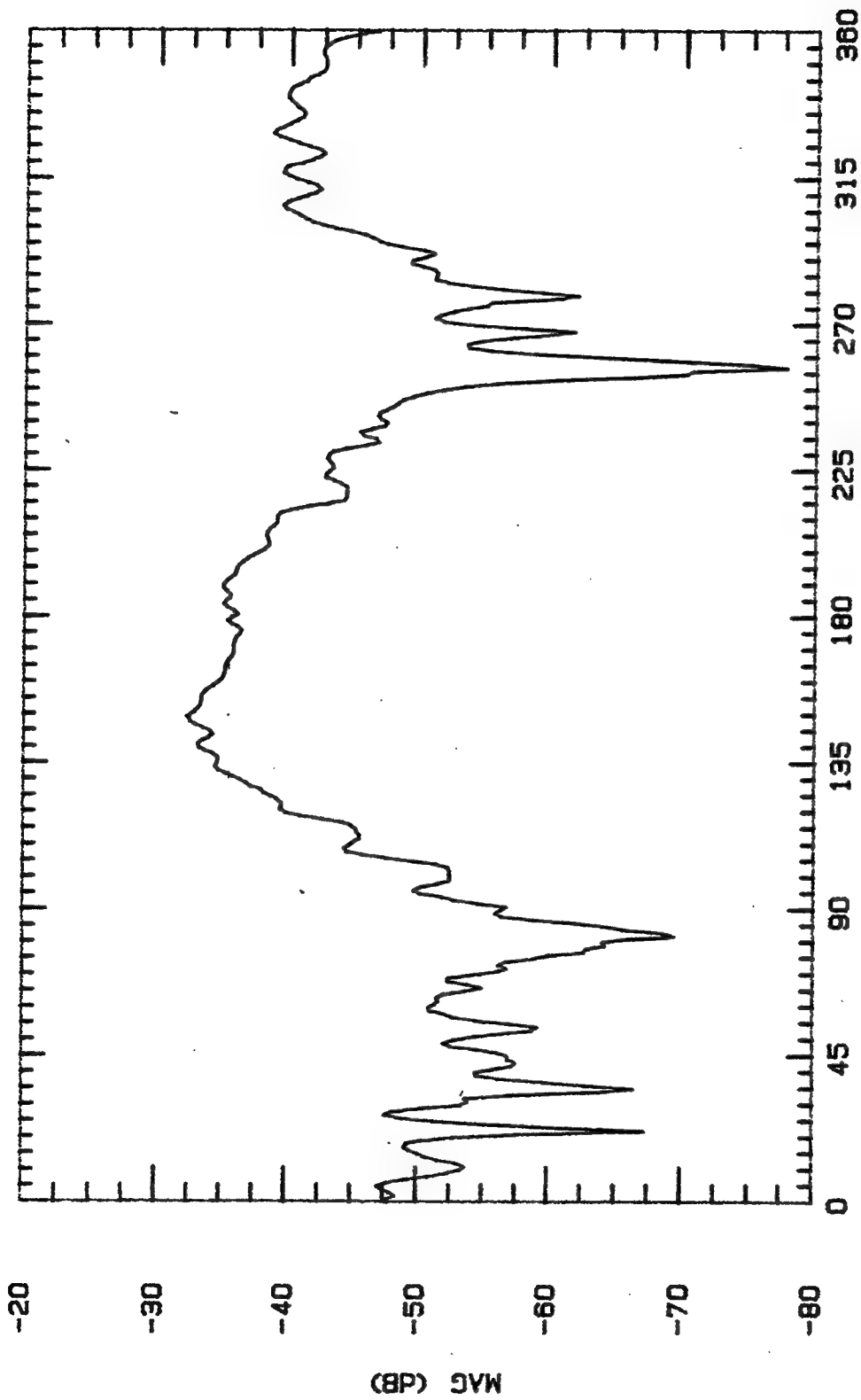
ASPECT ANGLE (DEGREES)

File Name	Frequency	Pattern Type	Date
LPL6	6 GHz	E-PLANE	18 OCT 94



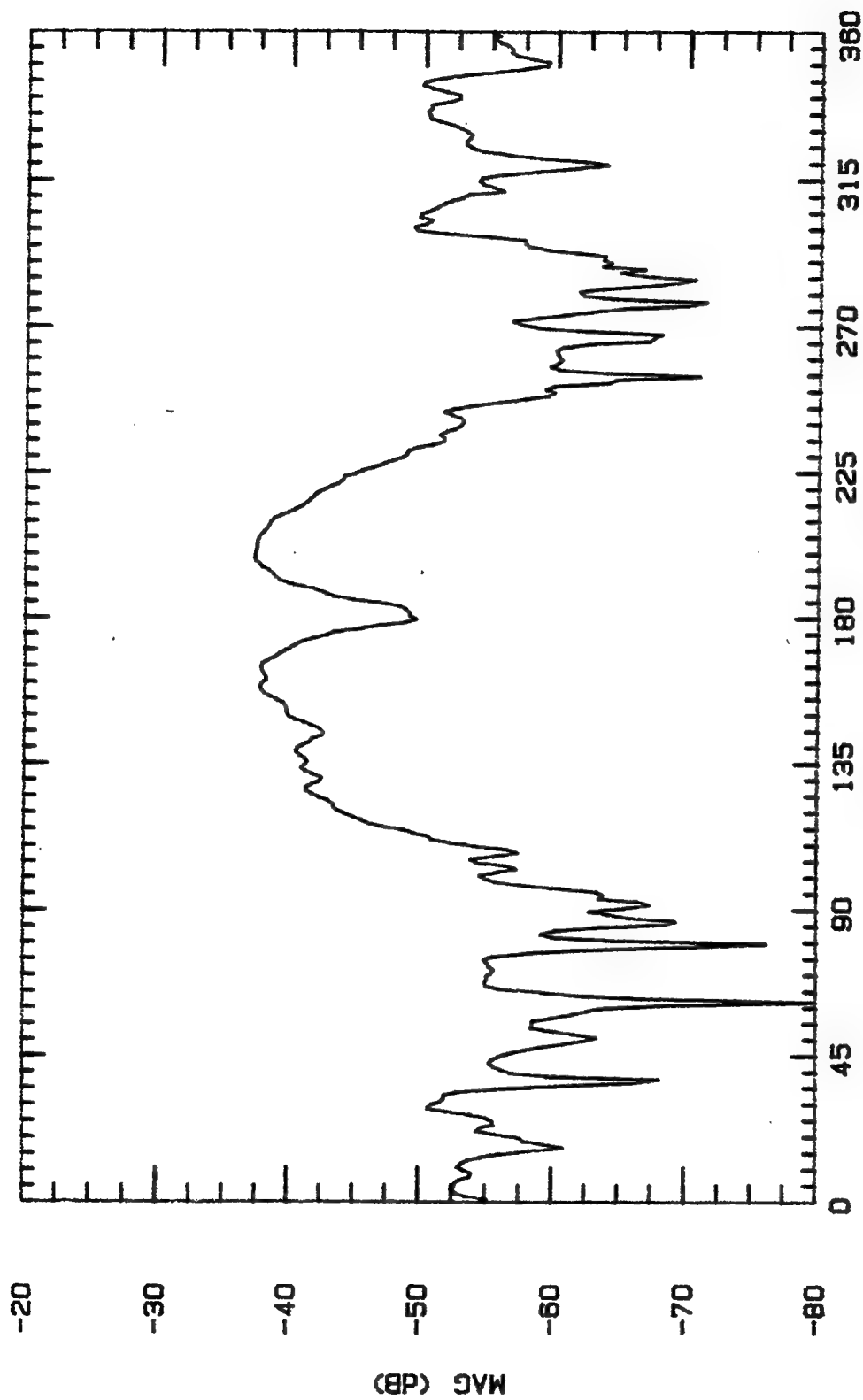
ASPECT ANGLE (DEGREES)

File Name	Frequency	Pattern Type	Date
LPL7	7 GHz	E-PLANE	18 OCT 94



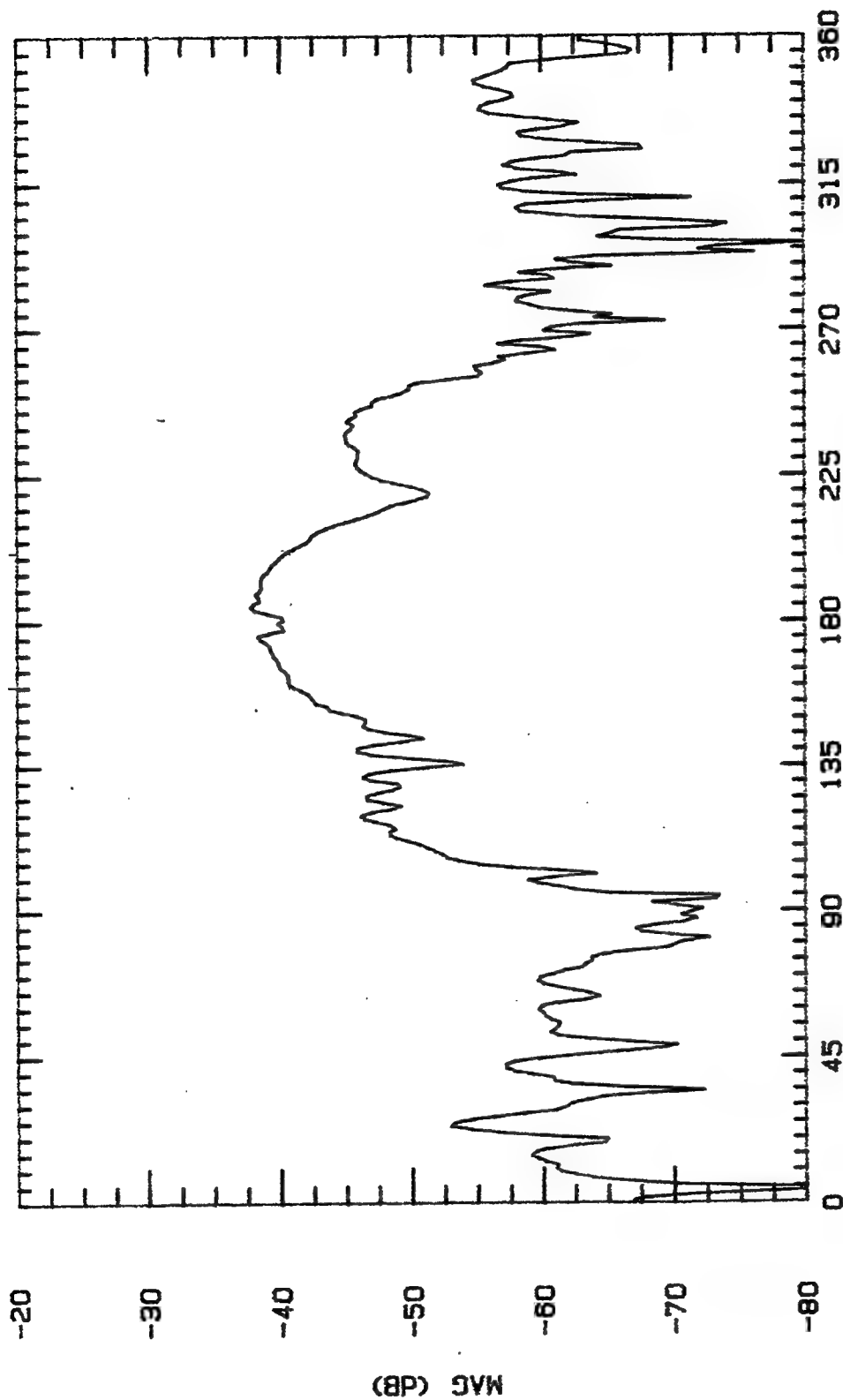
ASPECT ANGLE (DEGREES)

File Name	Frequency	Pattern Type	Date
LPL8	8 GHz	E-PLANE	18 OCT 94



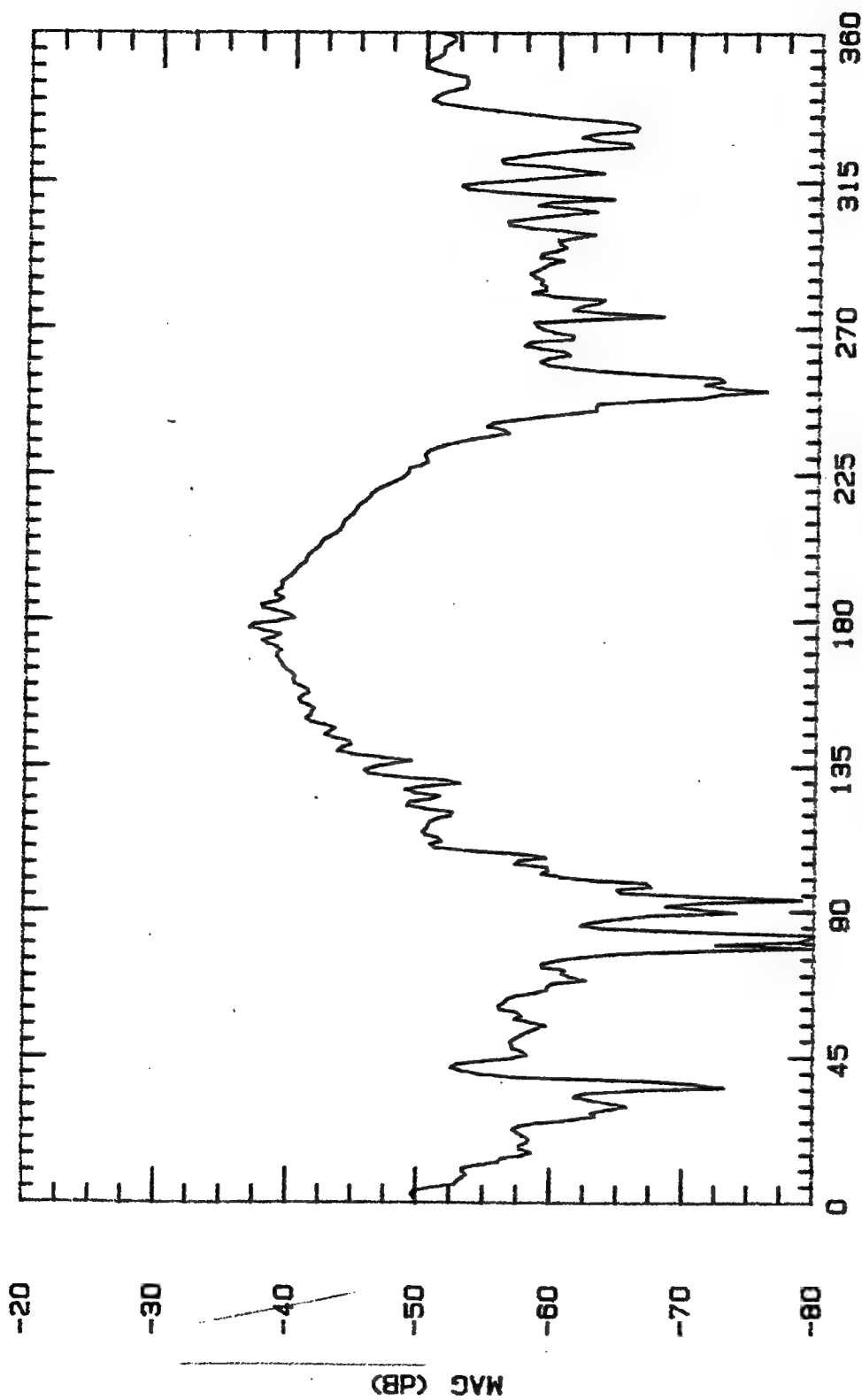
ASPECT ANGLE (DEGREES)

File Name	Frequency	Pattern Type	Date
LPL9A	9 GHz	E-PLANE	18 OCT 94

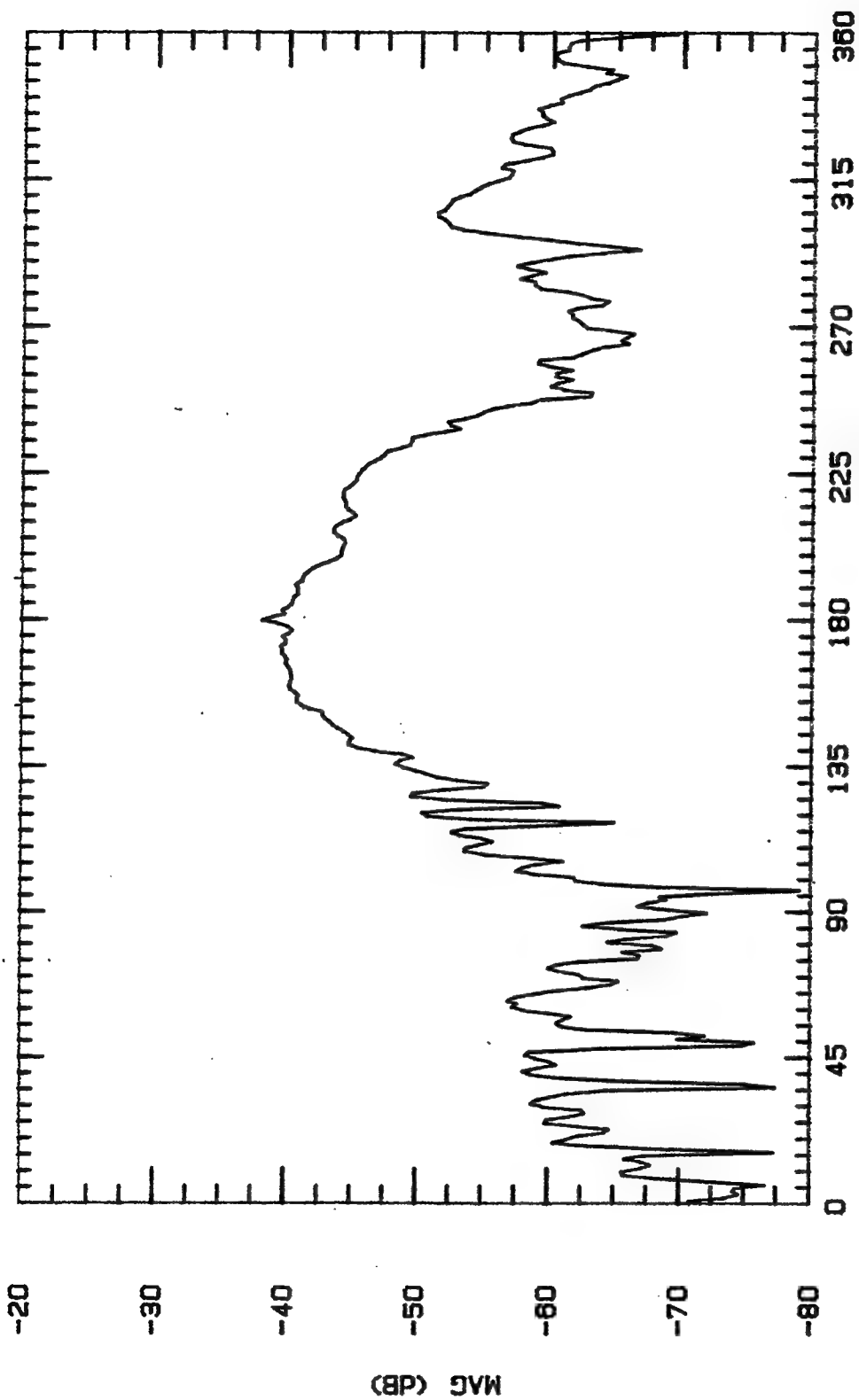


ASPECT ANGLE (DEGREES)

File Name	Frequency	Pattern Type	Date
LPL10	10 GHz	E-PLANE	19 OCT 84



File Name	Frequency	Pattern Type	Date
LPL11	11 GHz	E-PLANE	18 OCT 94

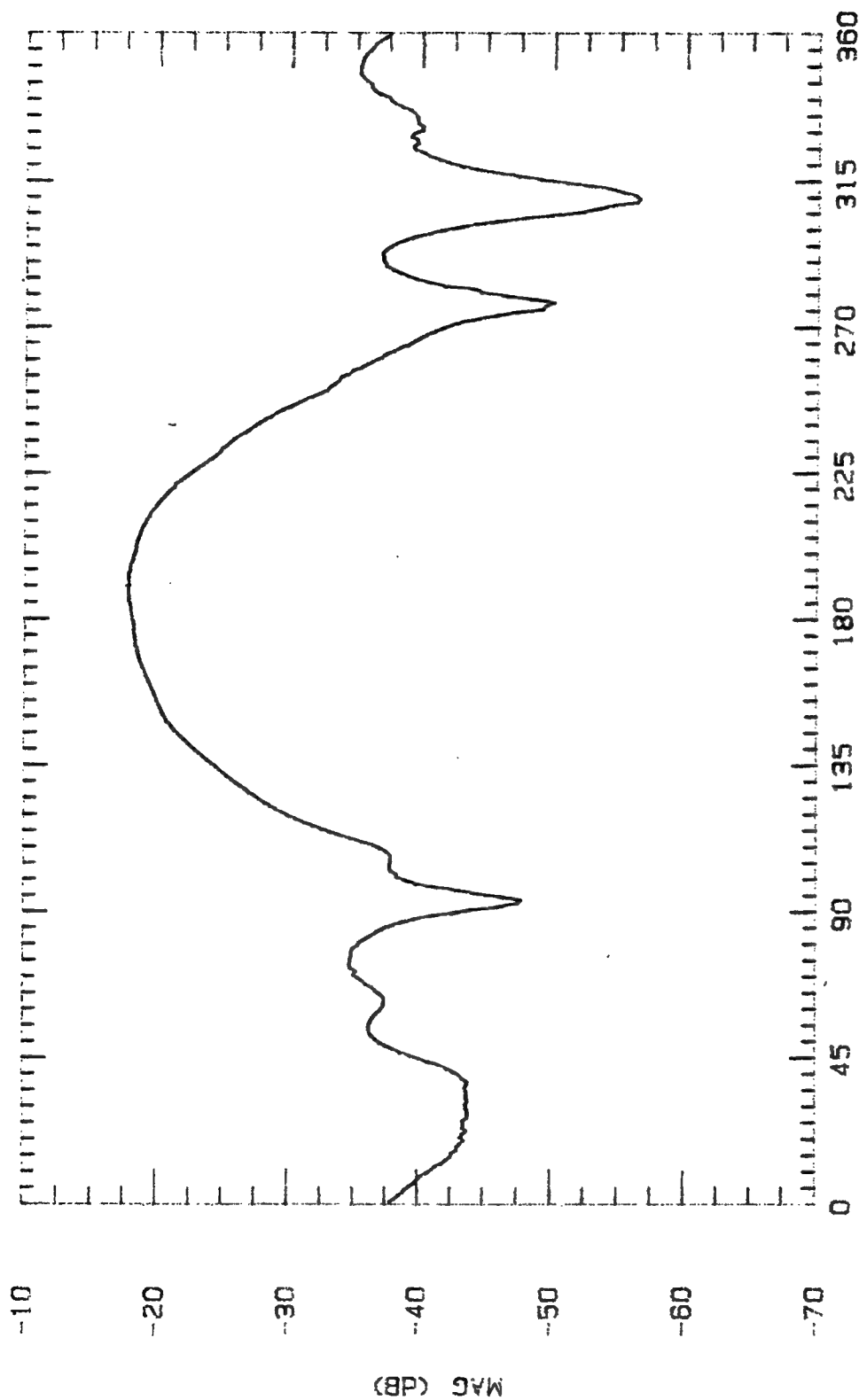


ASPECT ANGLE (DEGREES)

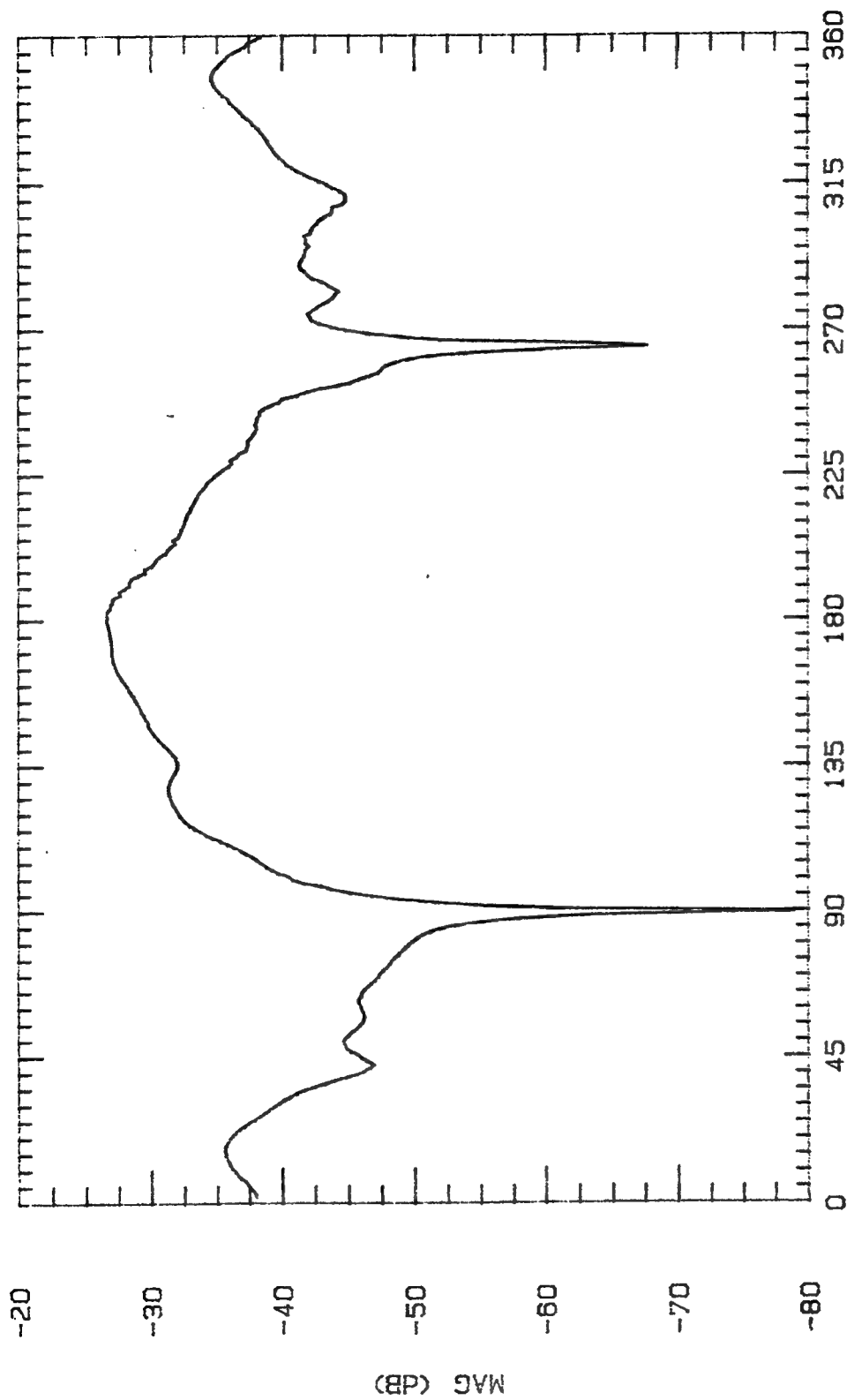
File Name	Frequency	Pattern Type	Date
LPL12	12 GHz	E-PLANE	17 OCT 94

APPENDIX J: Antenna Pattern Cuts For 6.2 & 2.7 GHz Two Layer Design
(5B, 1S (2 arrays), 7B, 1S (5 arrays), 3B)

Freq (GHz)	Normal Gain (dBi)	Max Gain (dBi)	Squint (deg)	Beamwidth (-3dBi to -3dBi) (deg)
-----	-----	-----	-----	-----
2.00	-0.9	-1.0	10	75
2.25	-10.1	-10.1	0	49
2.50	6.3	7.2	-5	66
2.75	1.2	3.4	-10	70
3.00	5.7	5.9	-2	63
3.25	-5.8	-0.6	-45	24
3.50	-3.8	2.5	-30	45
3.75	5.0	4.3	1	63
4.00	-0.2	0.8	6	60
4.25	-0.3	-0.2	1	53
4.50	5.6	5.8	-4	54
4.75	3.5	4.8	8	50
5.00	0.6	0.9	24	83
5.25	0.3	2.1	18	62
5.50	1.8	2.1	-23	90
5.75	0.5	1.1	-2	105
6.00	-0.7	-0.7	0	63
6.50	2.1	2.4	-6	89
7.00	-2.0	1.1	-14	57
7.50	-9.4	-3.2	-32	38
8.00	-8.6	-4.1	-40	5
8.50	0.6	0.8	1	30
9.00	-0.6	-0.2	1	28
9.50	0.1	2.4	28	55
10.00	0.9	3.8	19	36
10.50	-0.7	2.3	11	25
11.00	3.3	4.0	-2	13
11.50	0.4	1.6	-1	37
12.00	-0.7	2.4	1	4
12.40	4.5	4.8	-3	25
13.00	-2.8	2.1	-40	5
16.00	-6.7	-4.4	-30	15
-----	-----	-----	-----	-----

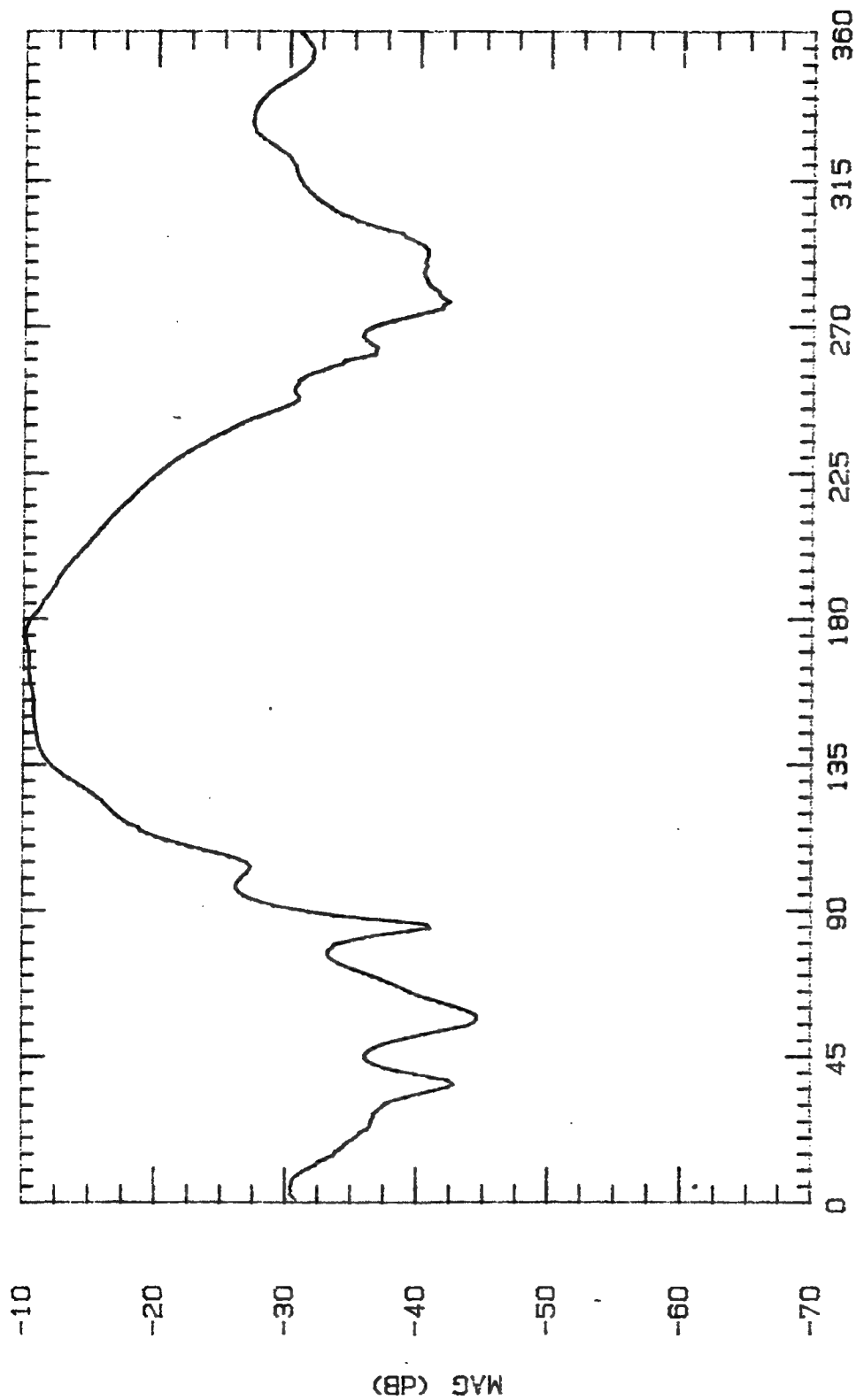


File Name	Frequency	Pattern Type	Date
CLPL200	2 GHz	E-PLANE	28 OCT



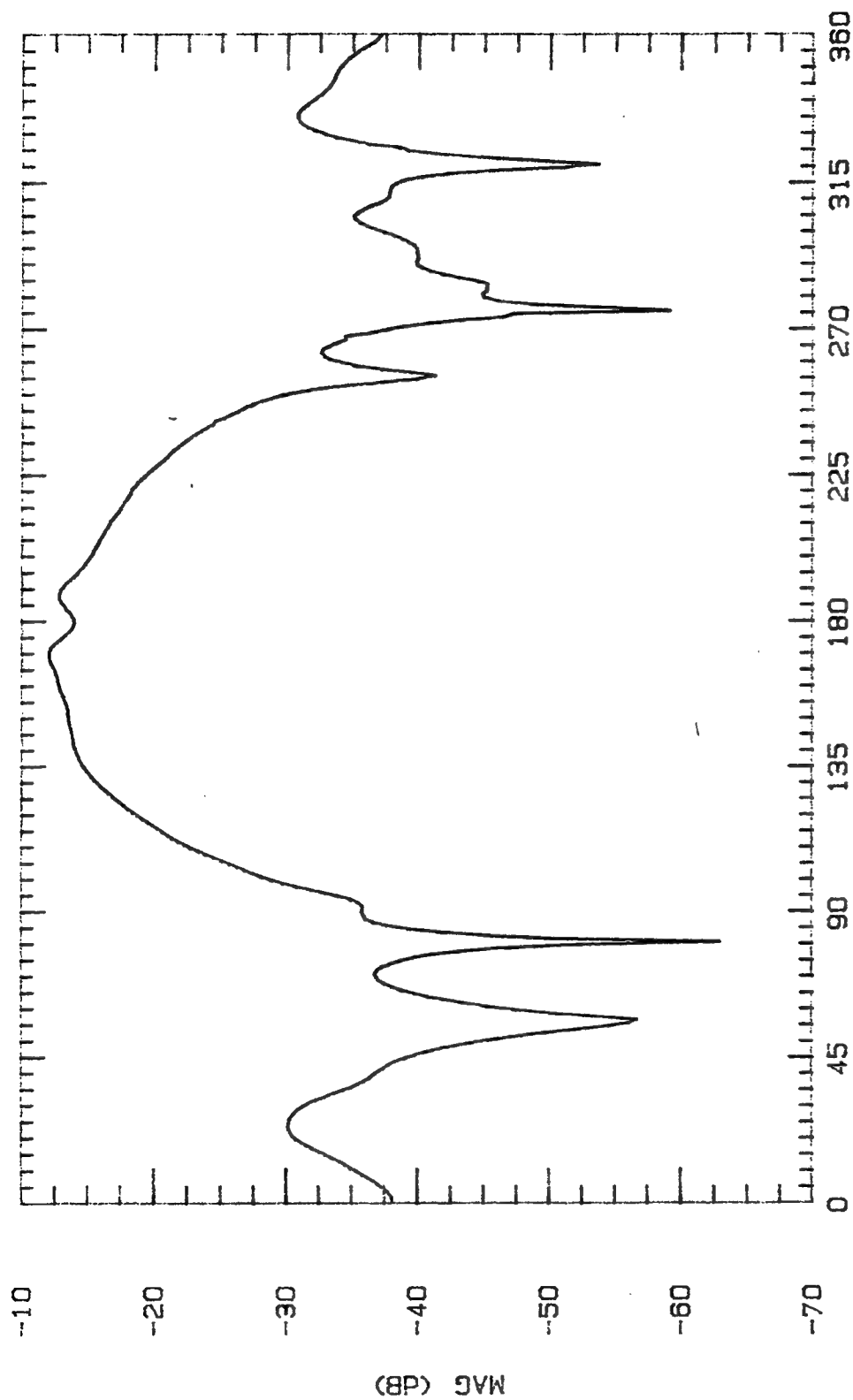
ASPECT ANGLE (DEGREES)

File Name	Frequency	Pattern Type	Date
CLPL225	2.25 GHz	E-PLANE	27 OCT 94



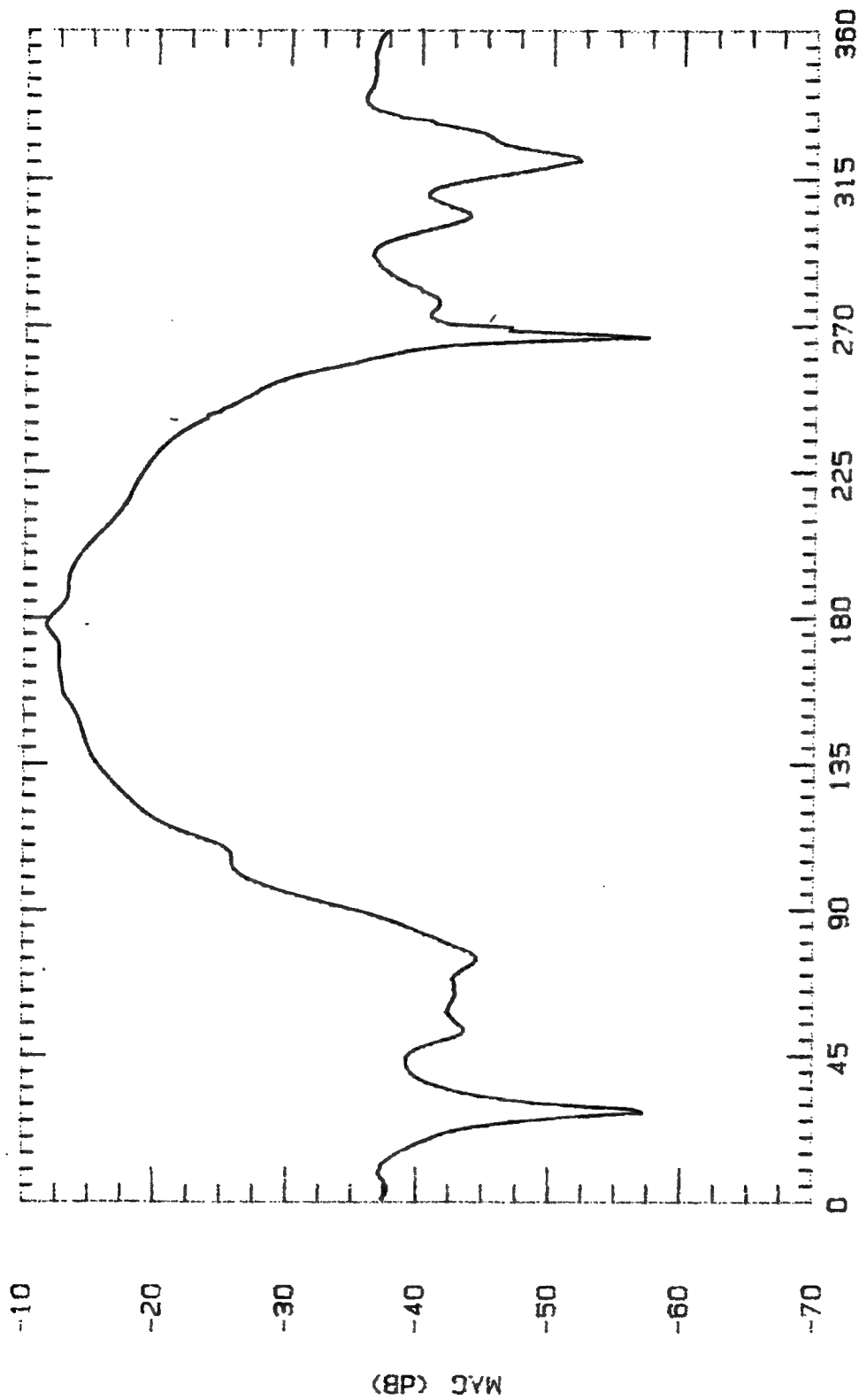
ASPECT ANGLE (DEGREES)

File Name	Frequency	Pattern Type	Date
CLPL250	2.5 GHz	E-PLANE	27 OCT 94



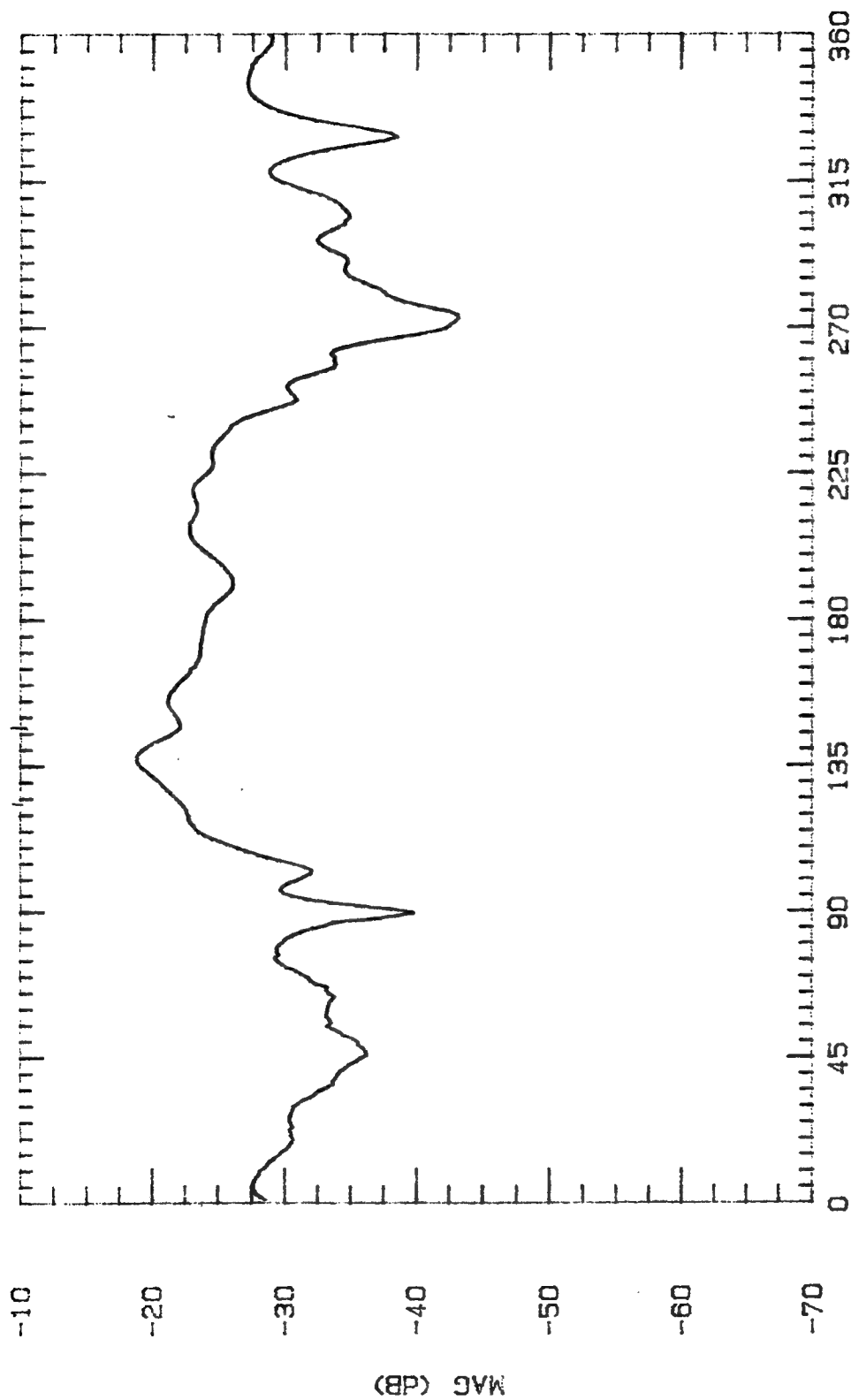
ASPECT ANGLE (DEGREES)

File Name	Frequency	Pattern Type	Date
CLPL275	2.75 GHz	E-PLANE	27 OCT 94

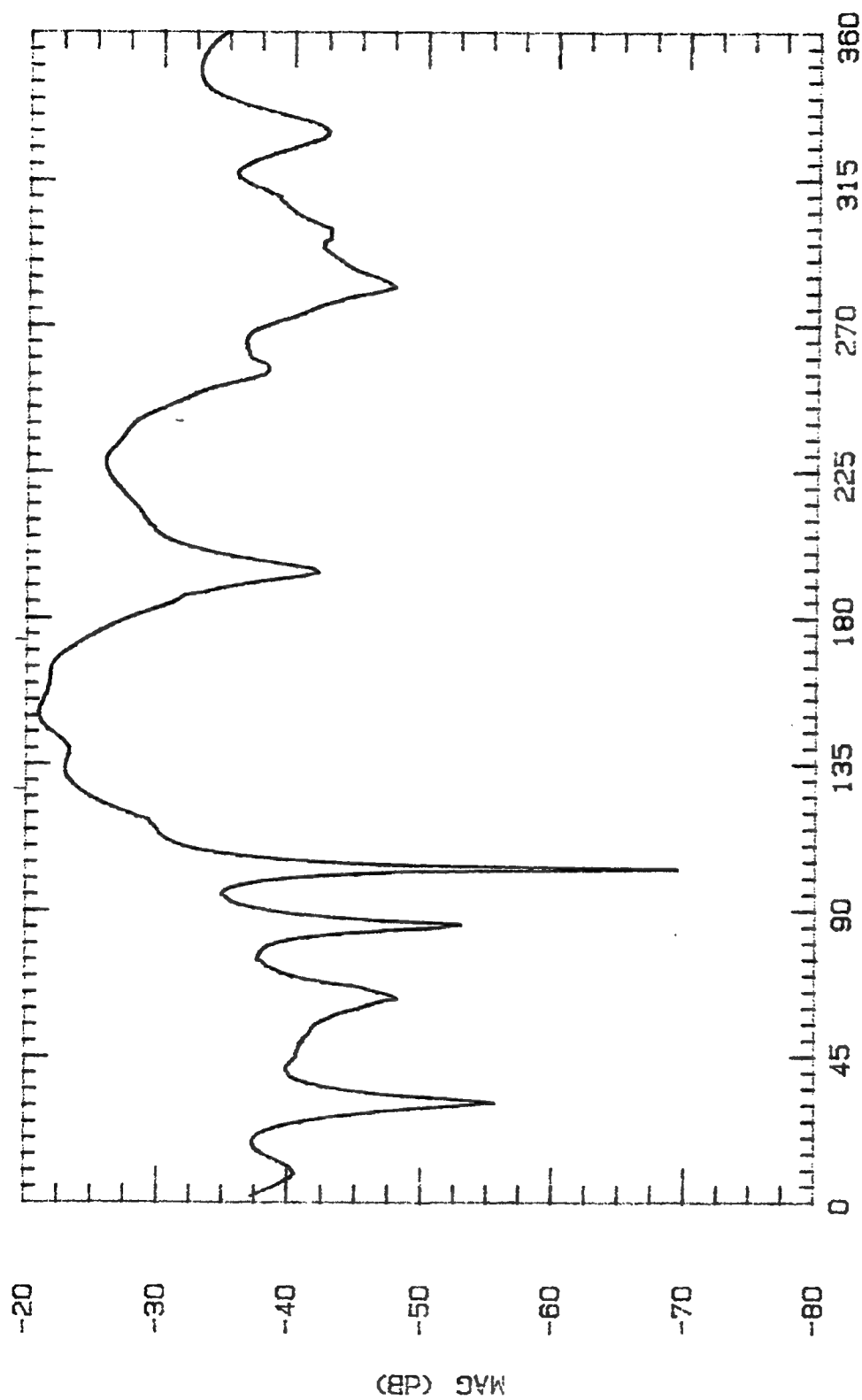


ASPECT ANGLE (DEGREES)

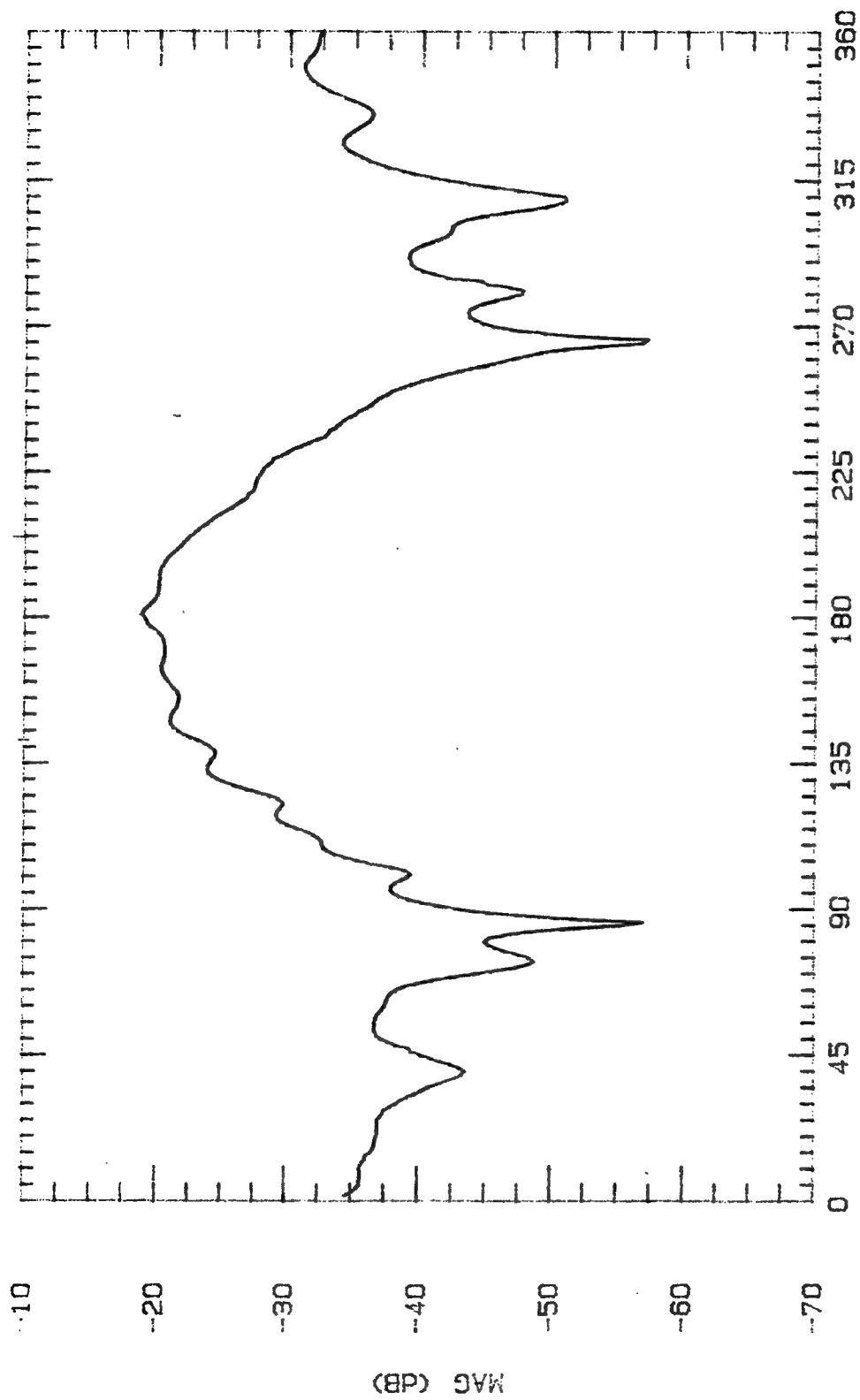
File Name	Frequency	Pattern Type	Date
CLPL300	3 GHz	E-PLANE	28 OCT



File Name	Frequency	Pattern Type	Date
CLPL325	3.25 GHz	E-PLANE	27 OCT 94

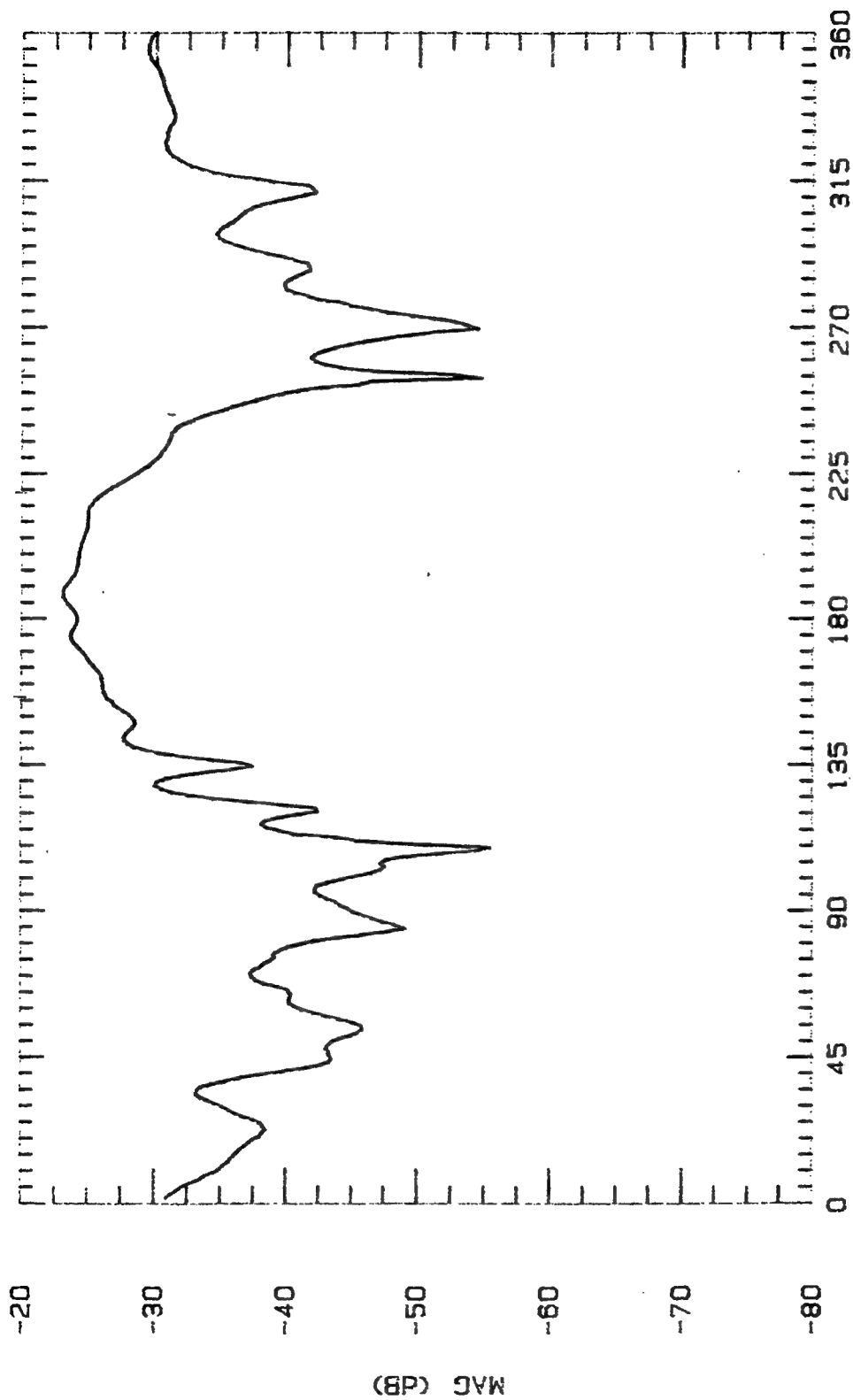


File Name	Frequency	Pattern Type	Date
CLPL350	3.5 GHz	E-PLANE	27 OCT 84



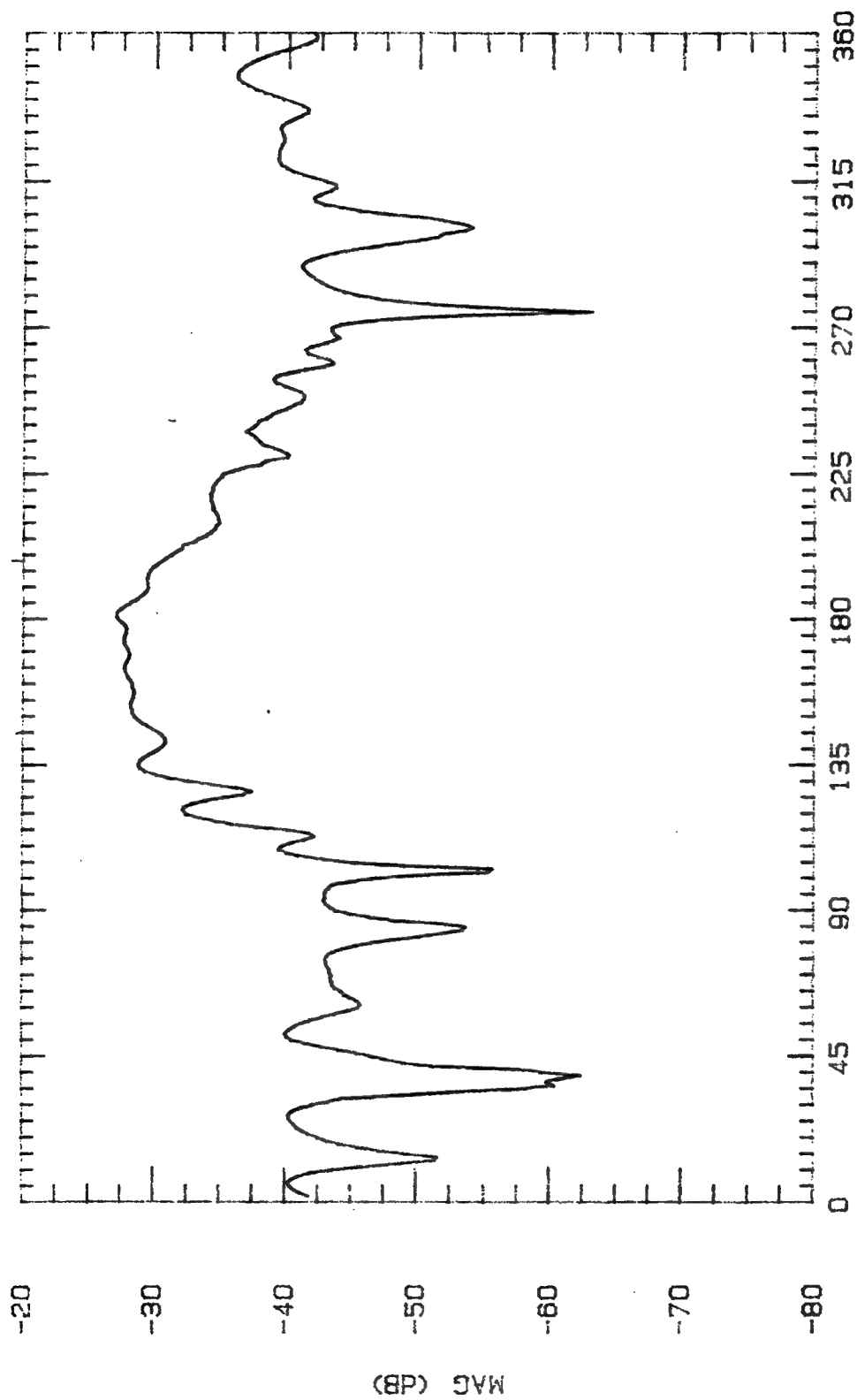
ASPECT ANGLE (DEGREES)

File Name	Frequency	Pattern Type	Date
CLPL375	9.75 GHz	E-PLANE	27 OCT 94

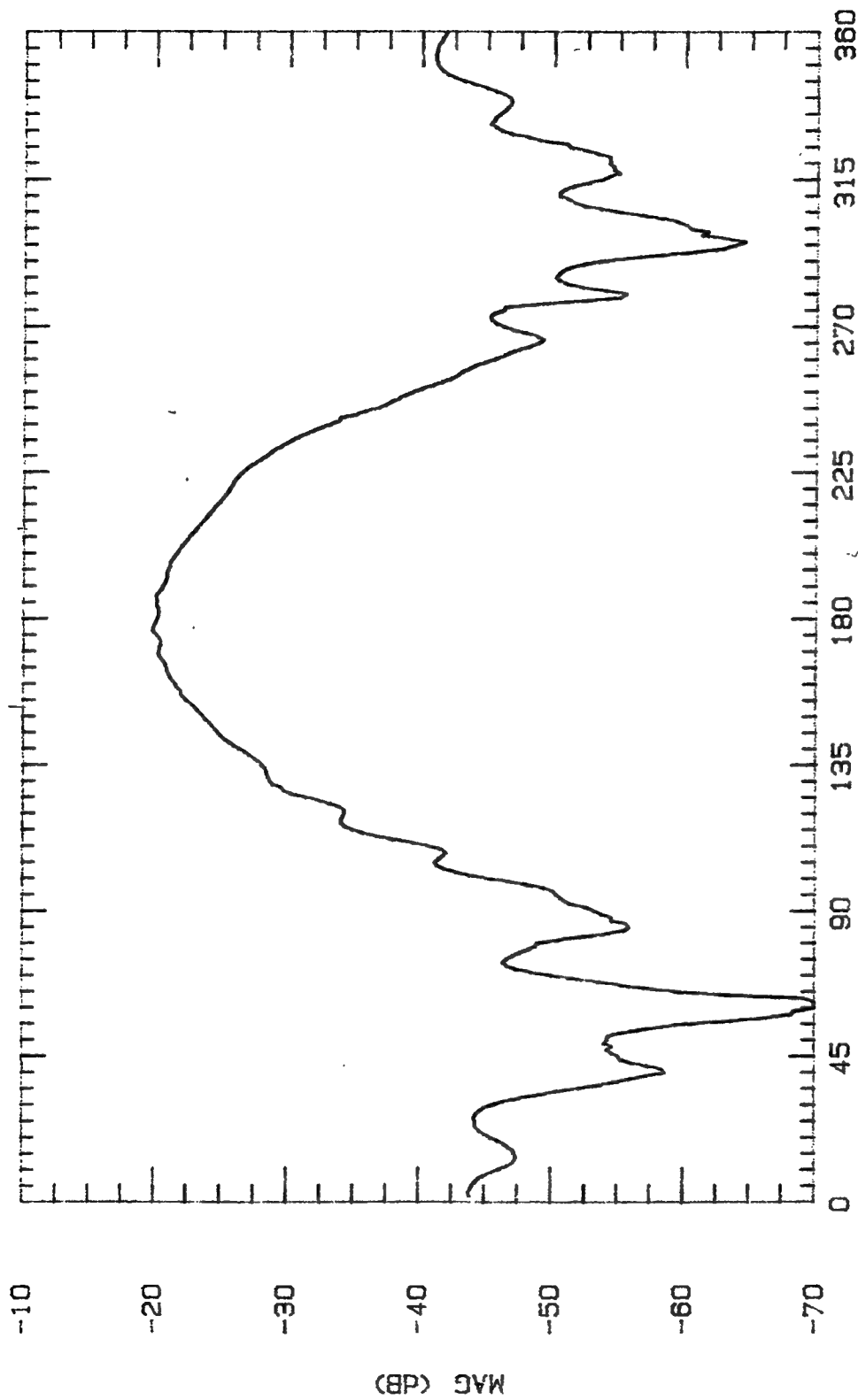


ASPECT ANGLE (DEGREES)

File Name	Frequency	Pattern Type	Date
CLPL400	4 GHz	E-PLANE	28 OCT

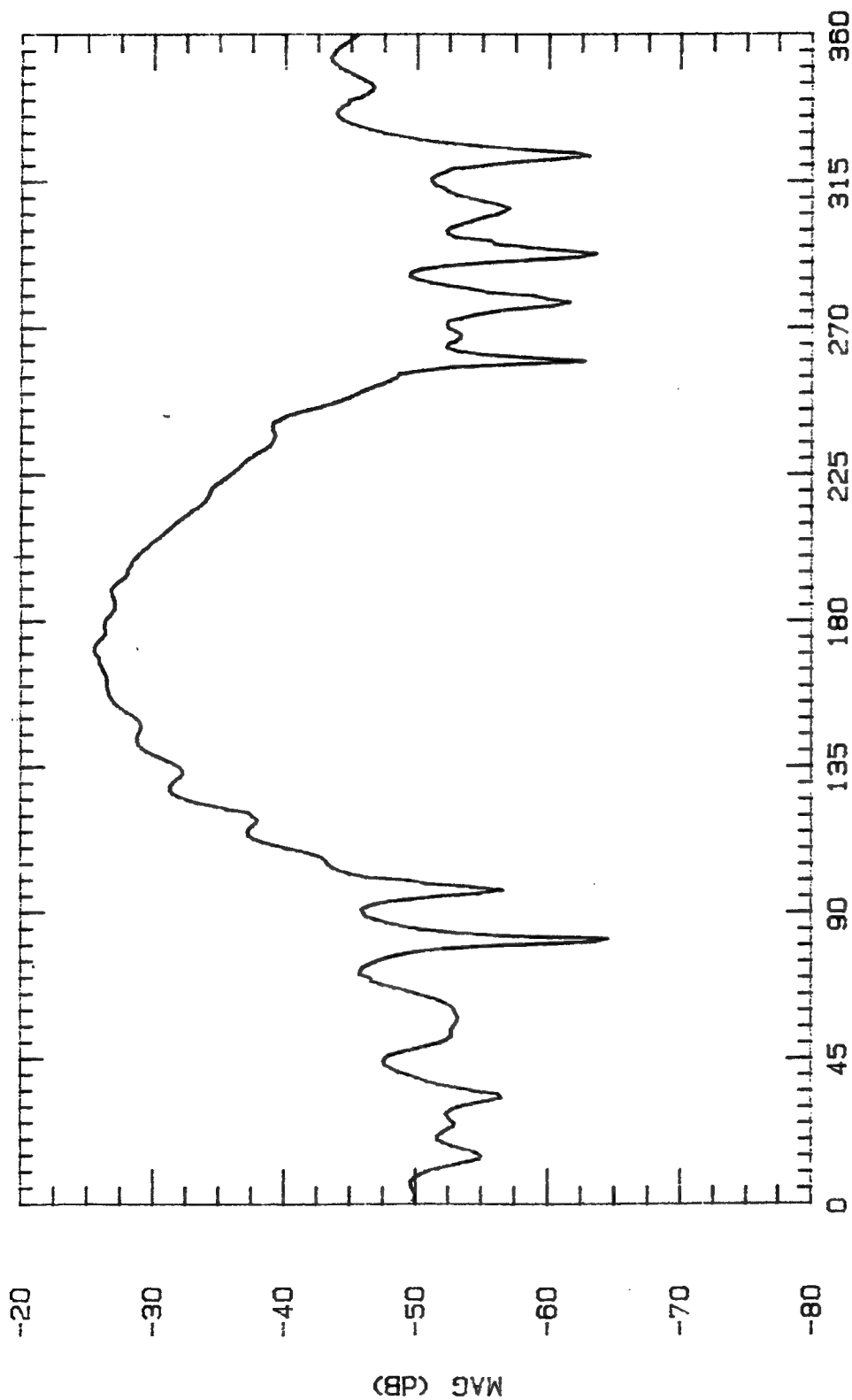


File Name	Frequency	Pattern Type	Date
CLPL425	4.25 GHz	E-PLANE	27 OCT 94



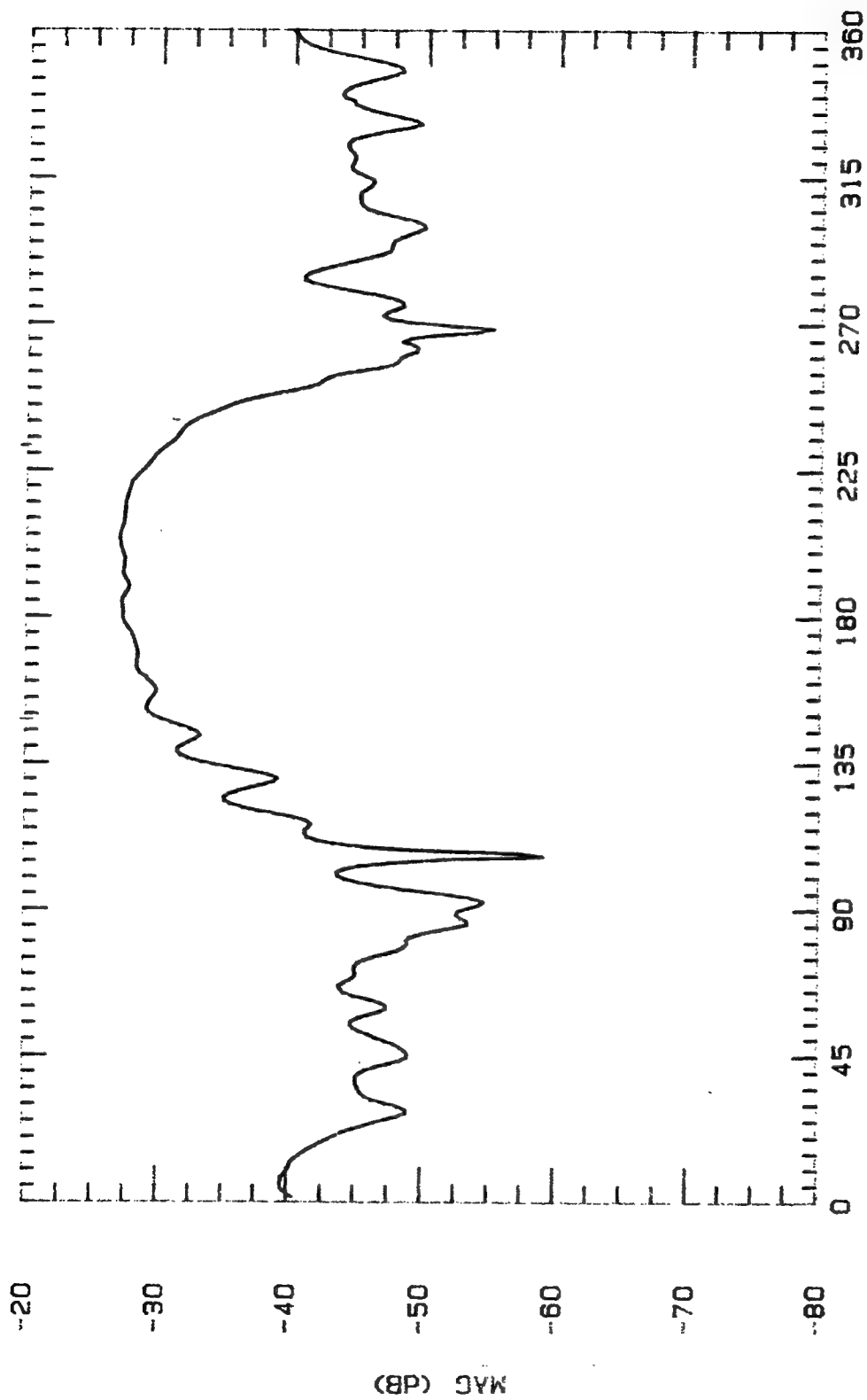
ASPECT ANGLE (DEGREES)

File Name	Frequency	Pattern Type	Date
CLPL45000	4.5 GHz	E-PLANE	27 OCT 94

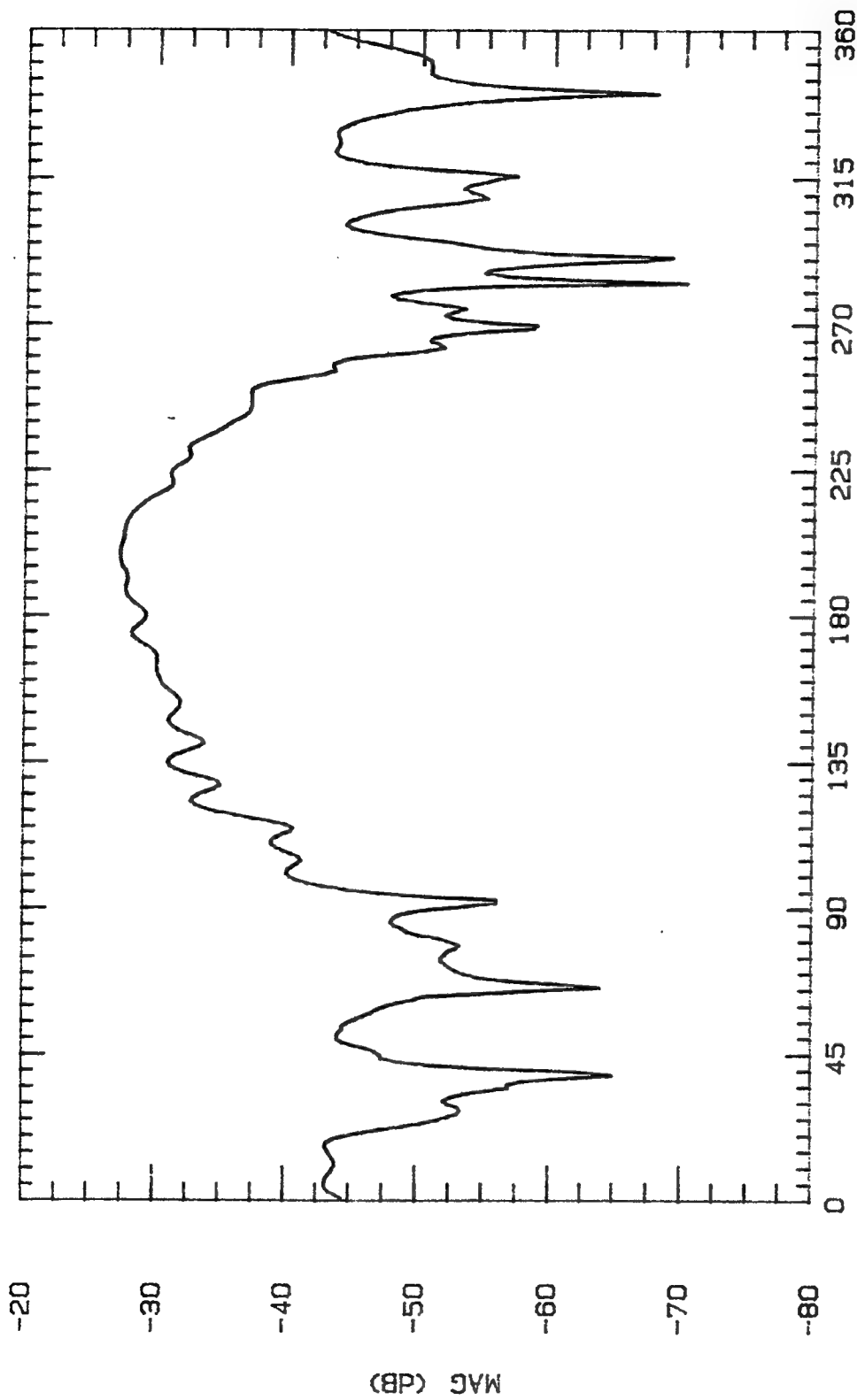


ASPECT ANGLE (DEGREES)

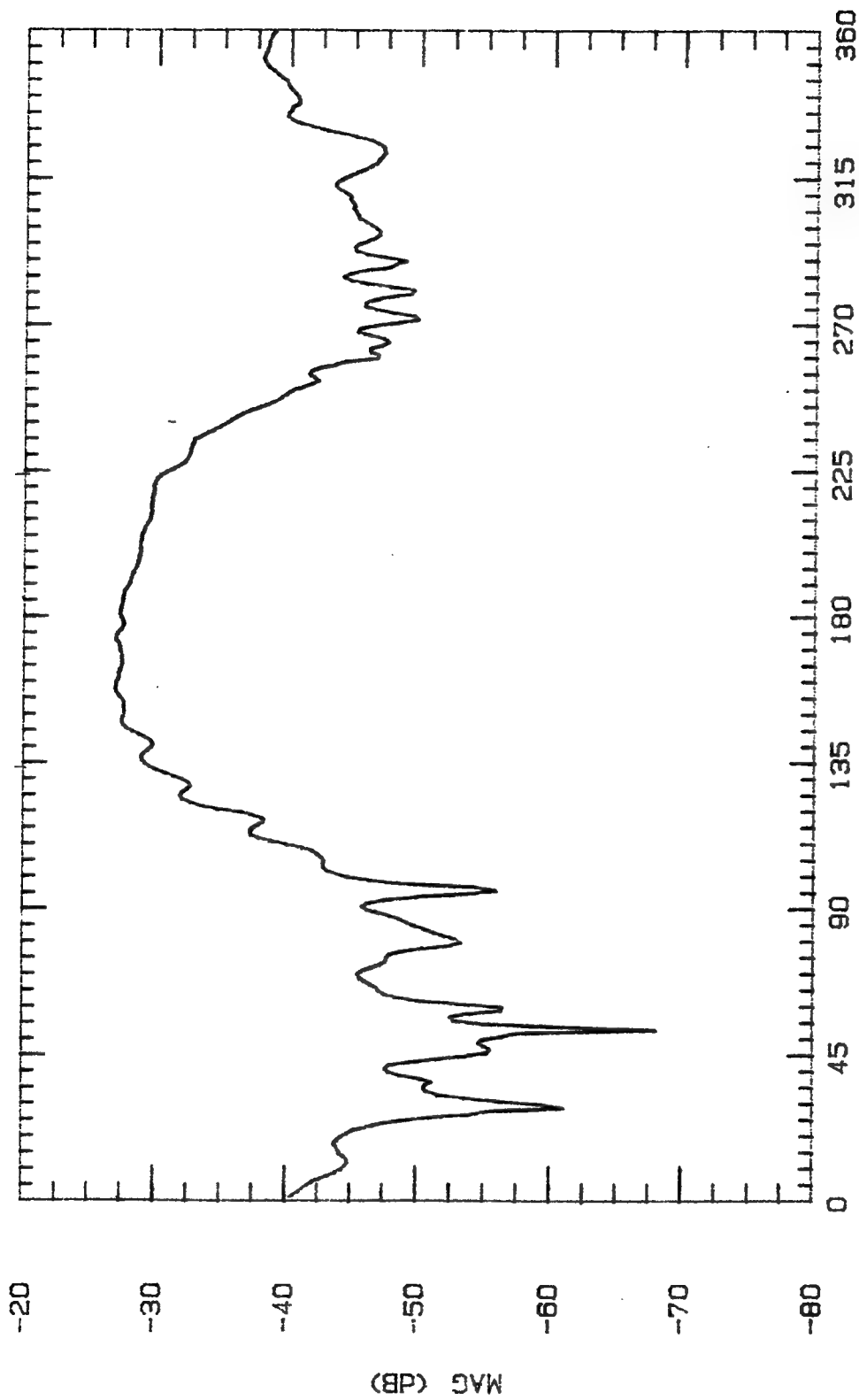
File Name	Frequency	Pattern Type	Date
CLPL475	4.75 GHz	E-PLANE	27 OCT 94



File Name	Frequency	Pattern Type	Date
CLPL500	5 GHz	E-PLANE	28 OCT

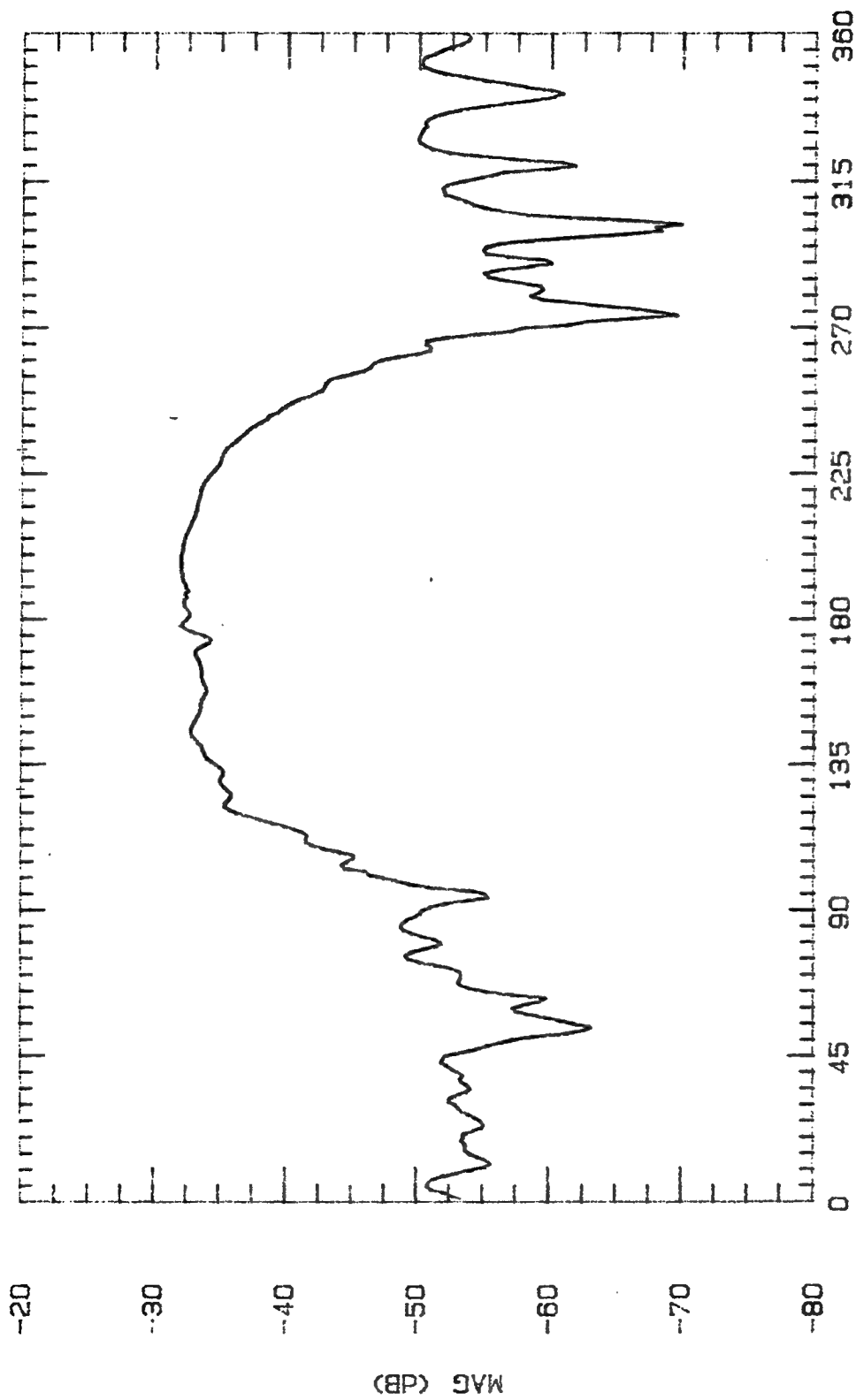


File Name	Frequency	Pattern Type	Date
CLPL525	5.25 GHz	E-PLANE	27 OCT 94



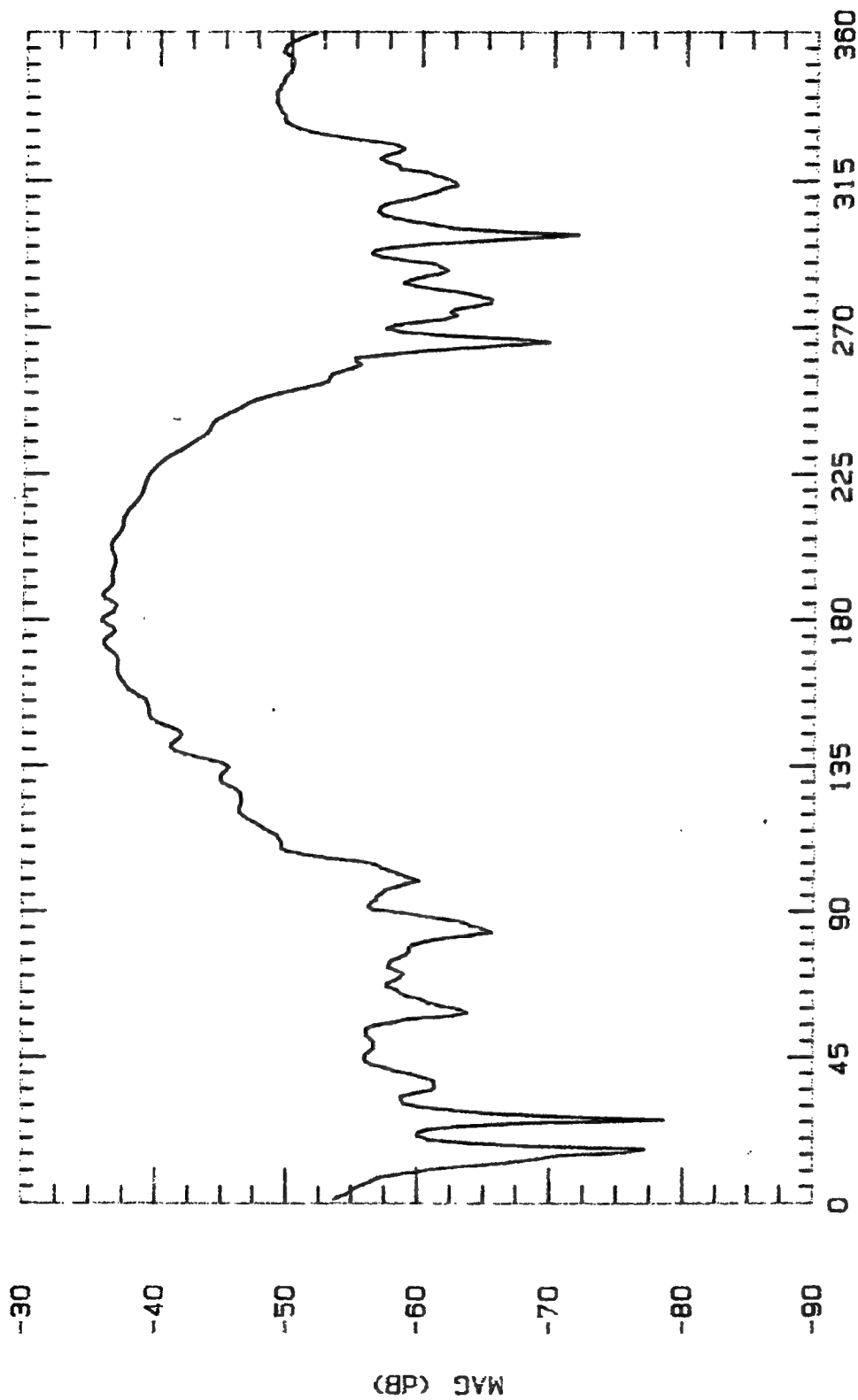
ASPECT ANGLE (DEGREES)

File Name	Frequency	Pattern Type	Date
CLPL550	5.5 GHz	E-PLANE	27 OCT 94

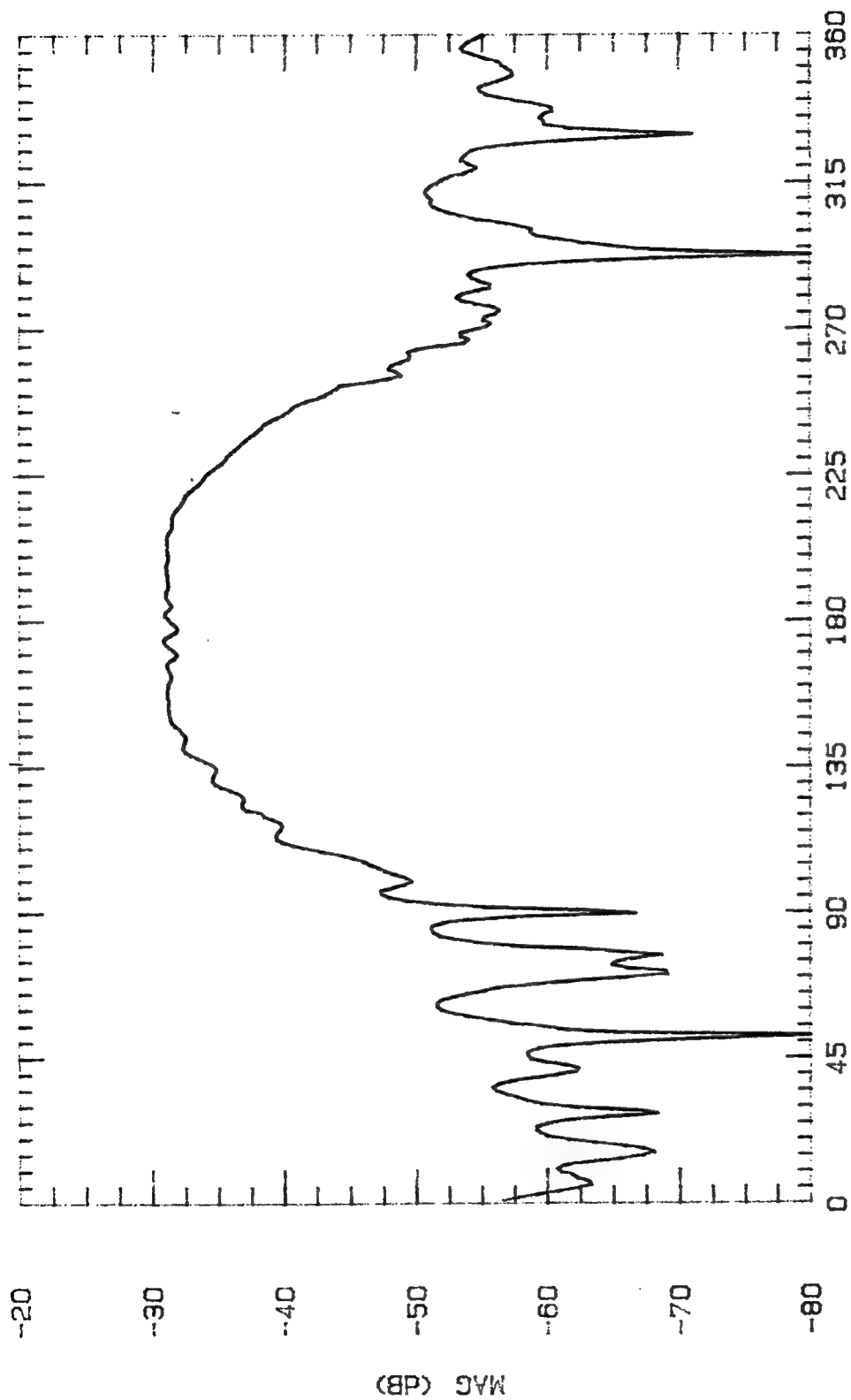


ASPECT ANGLE (DEGREES)

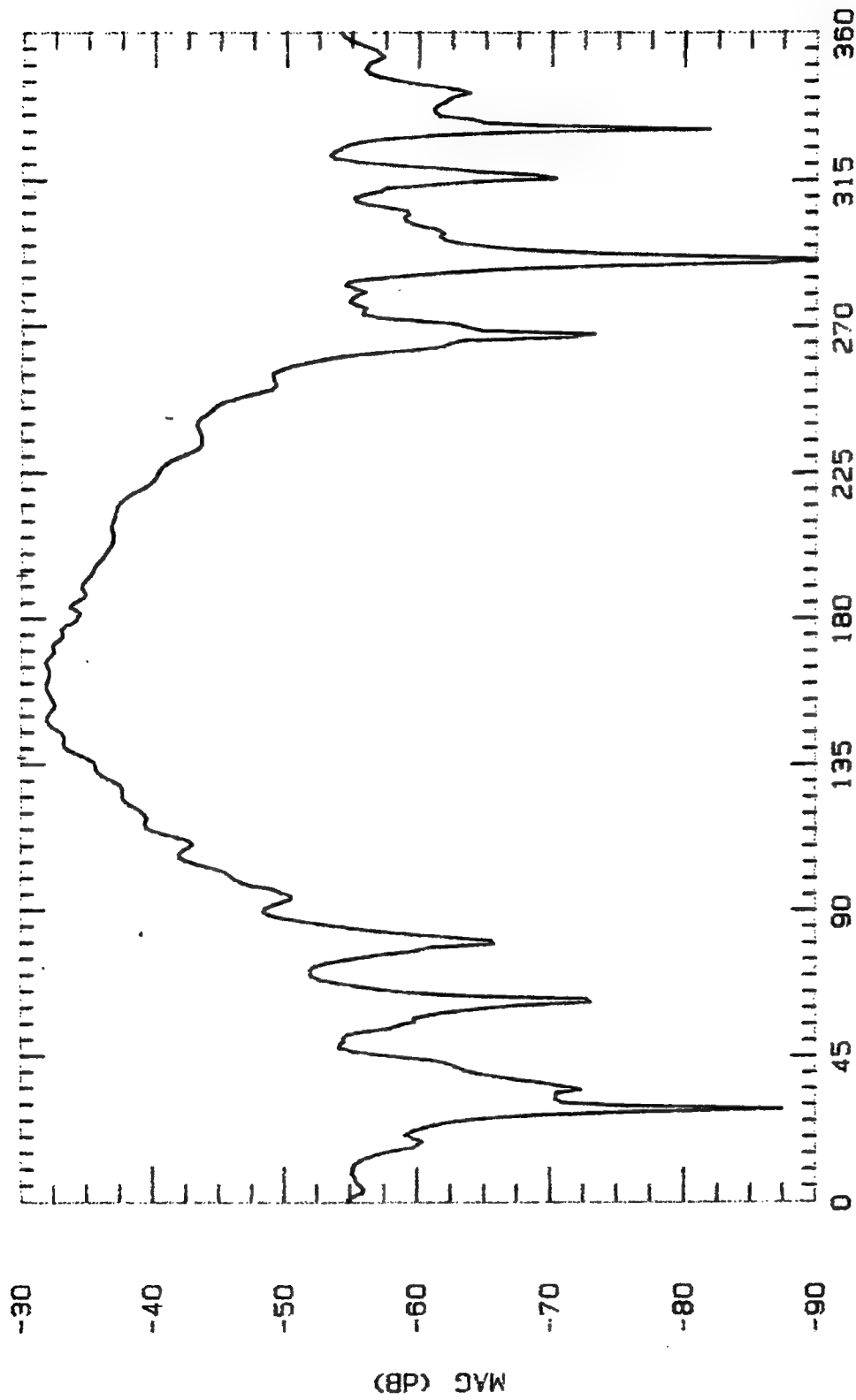
File Name	Frequency	Pattern Type	Date
CLPL575	5.75 GHz	E-PLANE	27 OCT 94



File Name	Frequency	Pattern Type	Date
CLPL800	8 GHz	E-PLANE	28 OCT

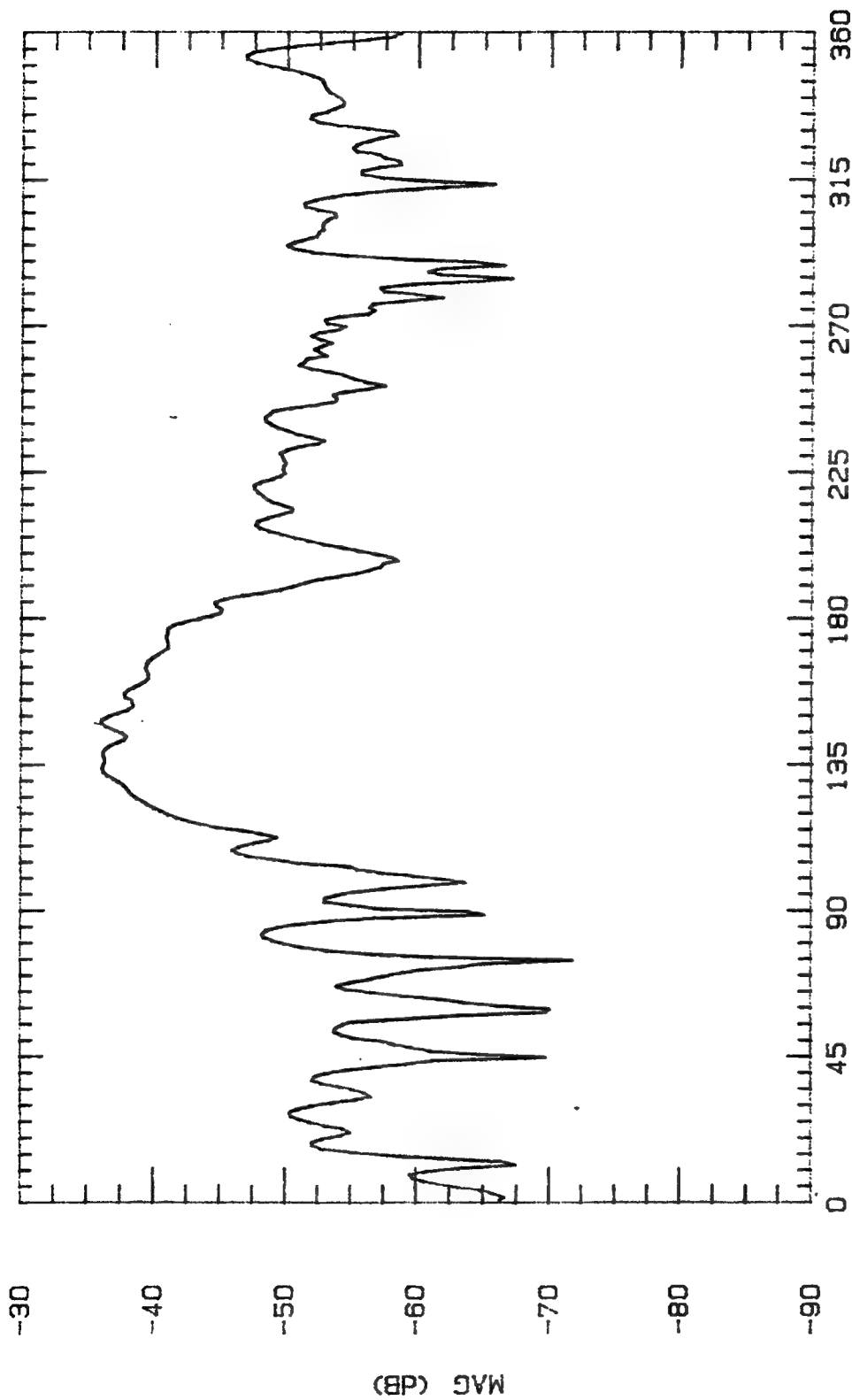


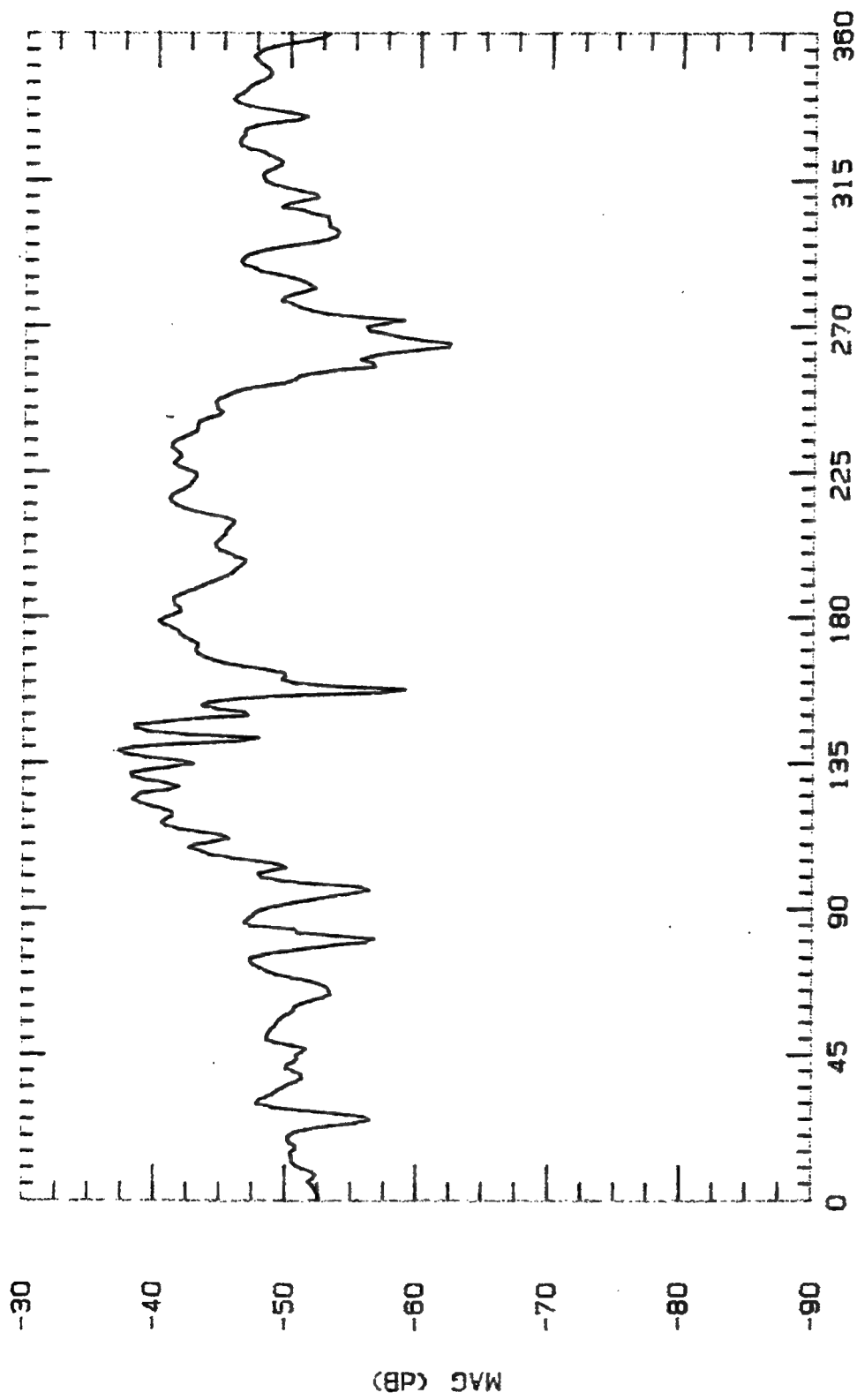
File Name	Frequency	Pattern Type	Date
CLPL850	8.5 GHz	E-PLANE	27 OCT 94



ASPECT ANGLE (DEGREES)

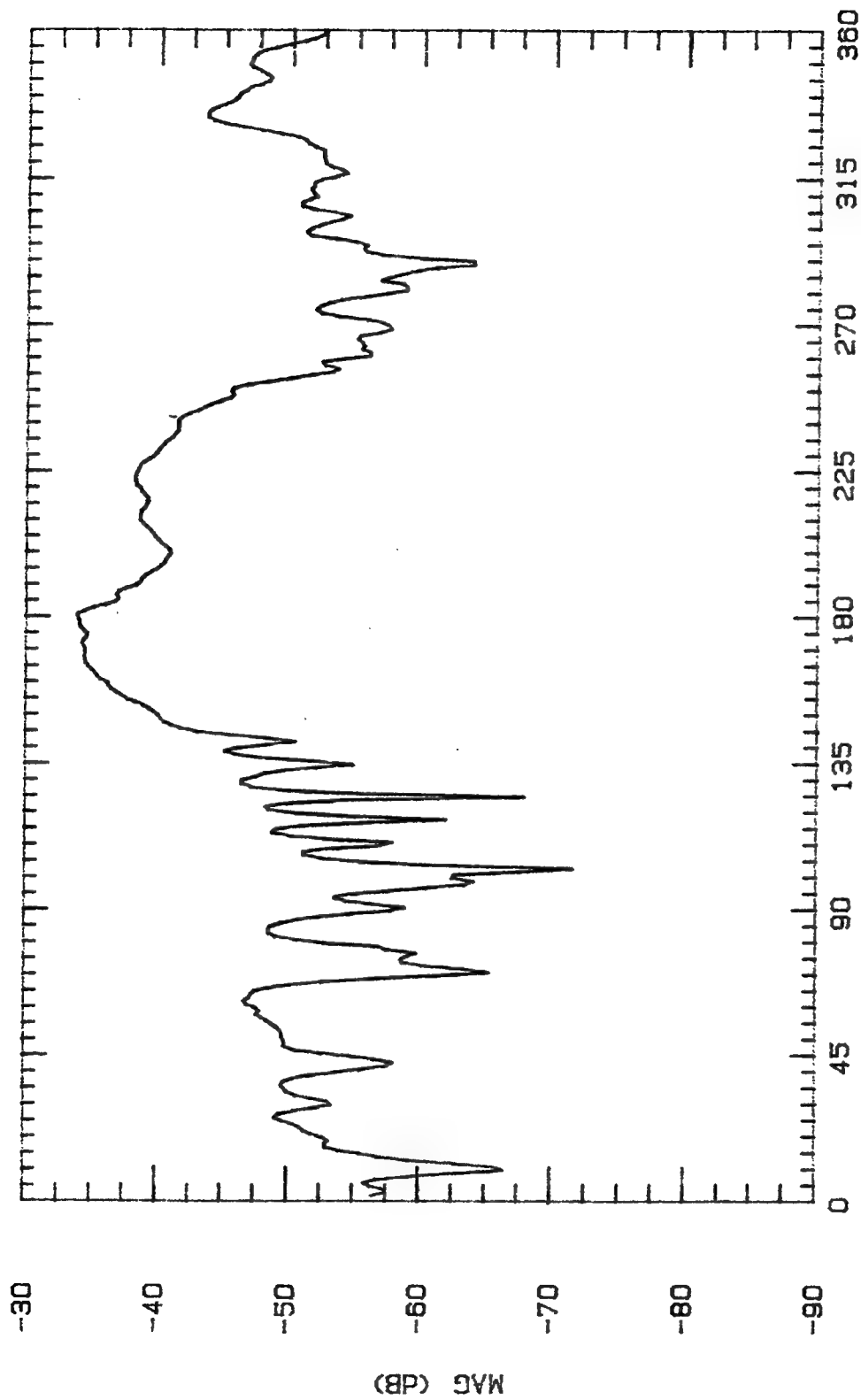
File Name	Frequency	Pattern Type	Date
CLPL700	7 GHz	E-PLANE	28 OCT





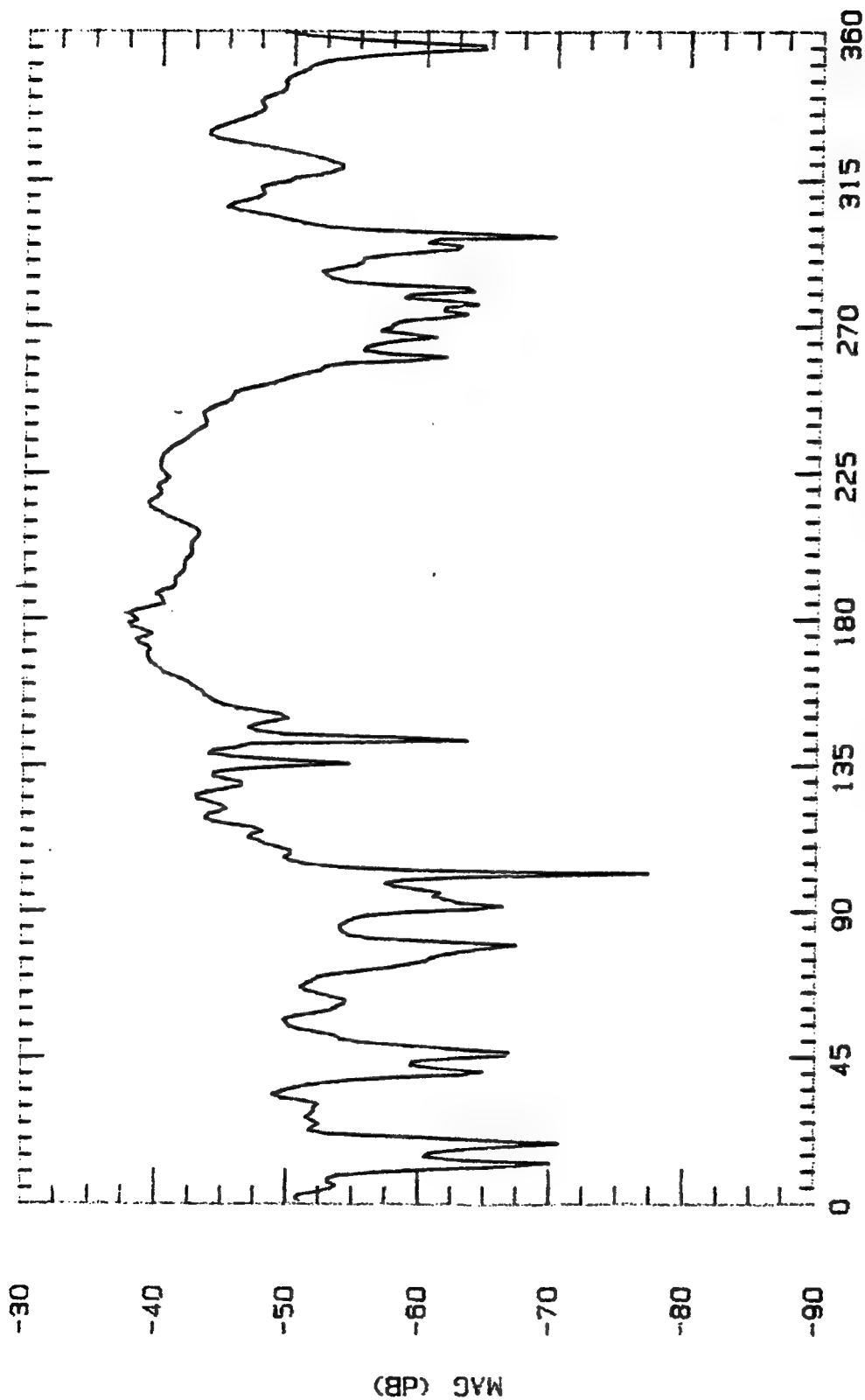
ASPECT ANGLE (DEGREES)

File Name	Frequency	Pattern Type	Date
CLPL800	8 GHz	E-PLANE	28 OCT



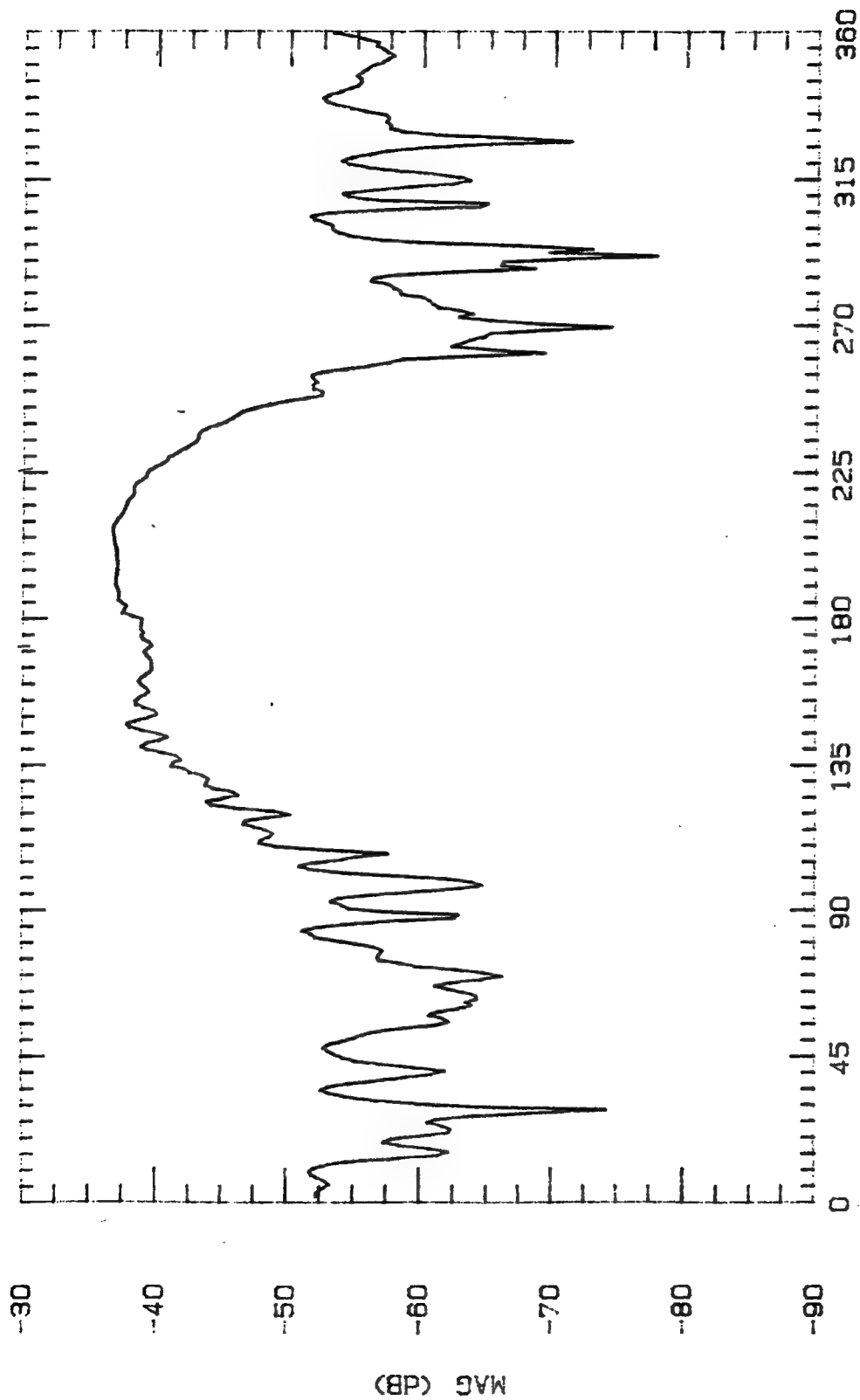
ASPECT ANGLE (DEGREES)

File Name	Frequency	Pattern Type	Date
CLPL850	8.5 GHz	E-PLANE	27 OCT 94



File Name Frequency Pattern Type Date

CLPL900 9 GHz E-PLANE 28 OCT



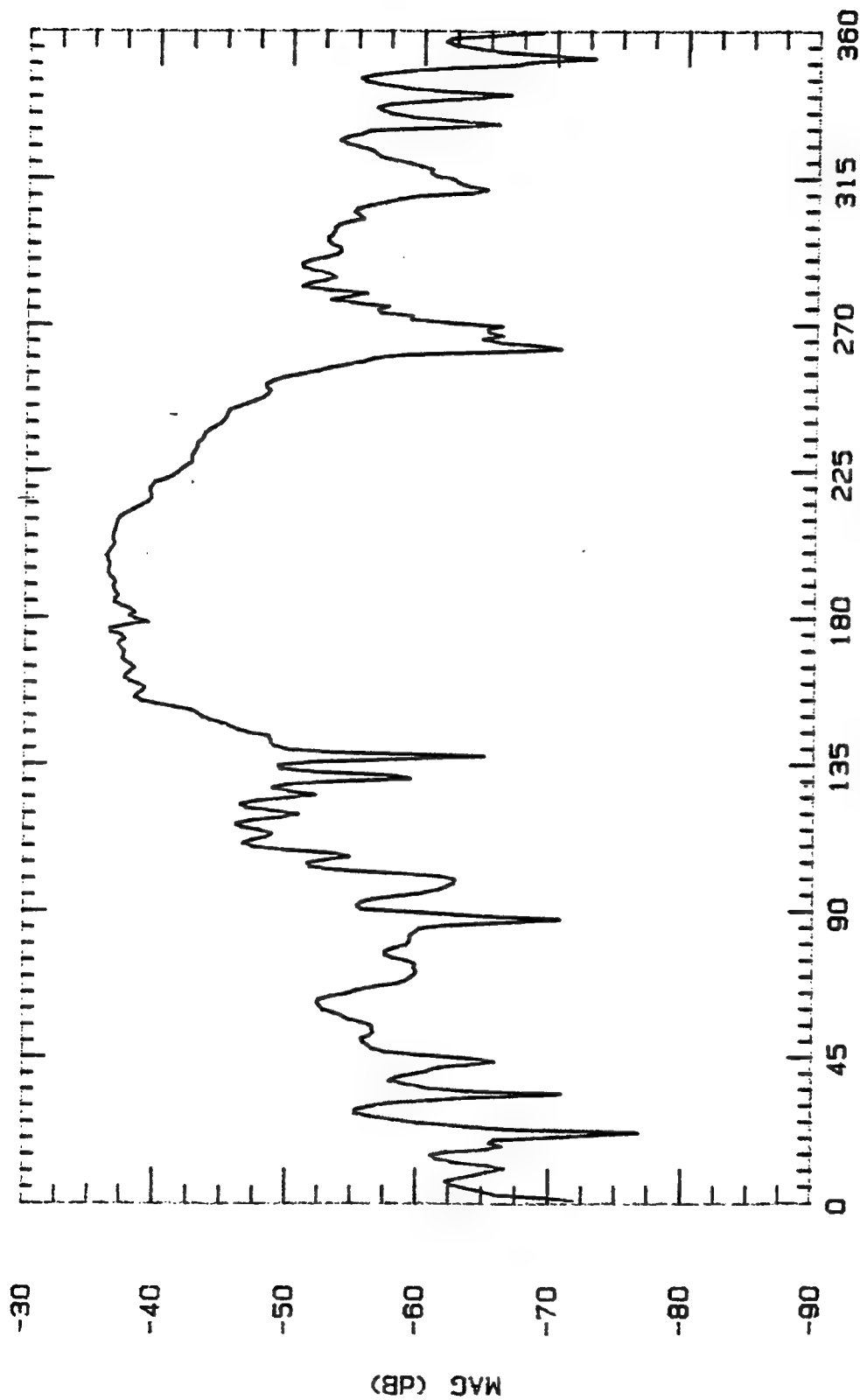
File Name Frequency Pattern Type Date

CLPL950

9.5 GHz

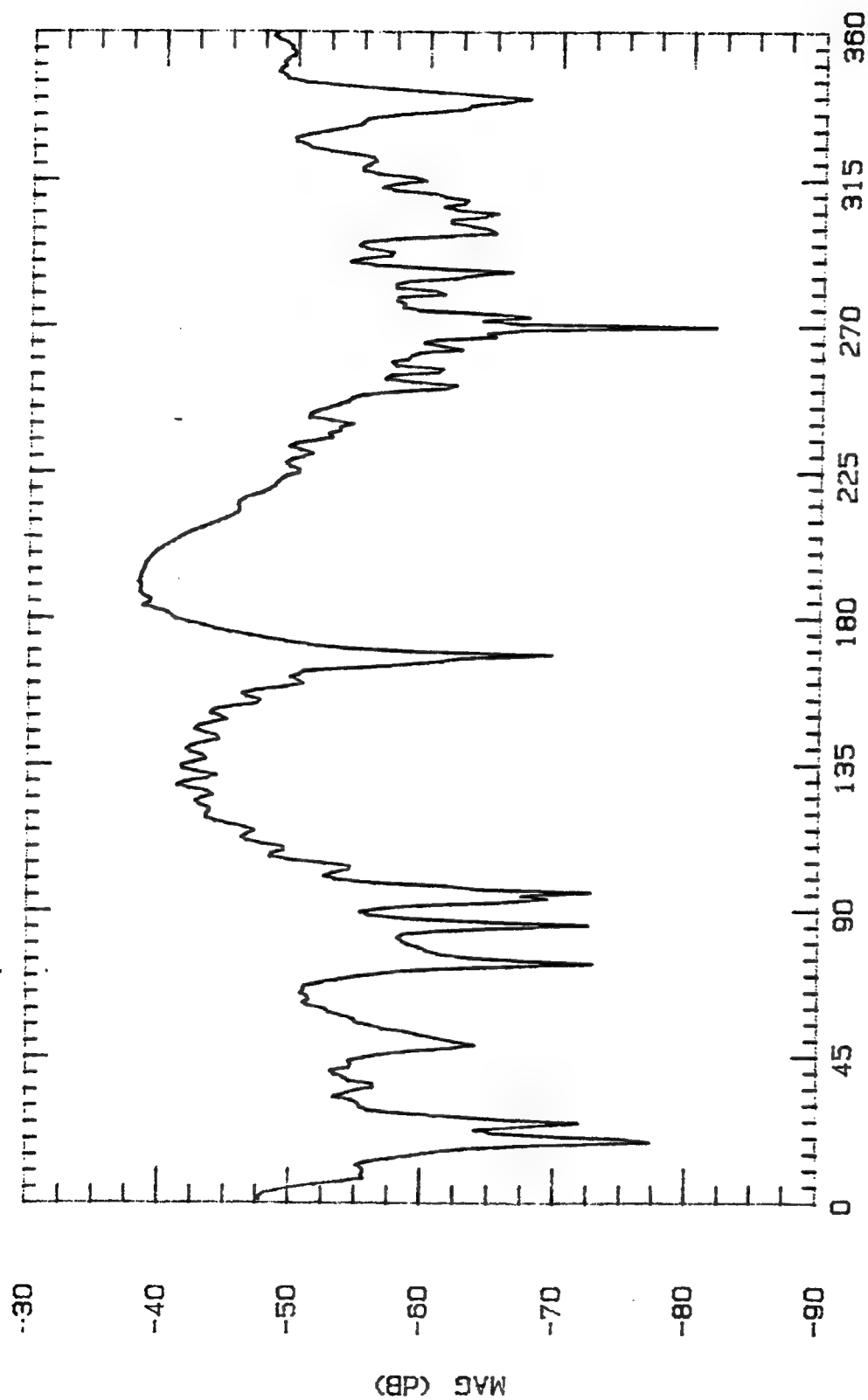
L-PLANE

27 OCT 94

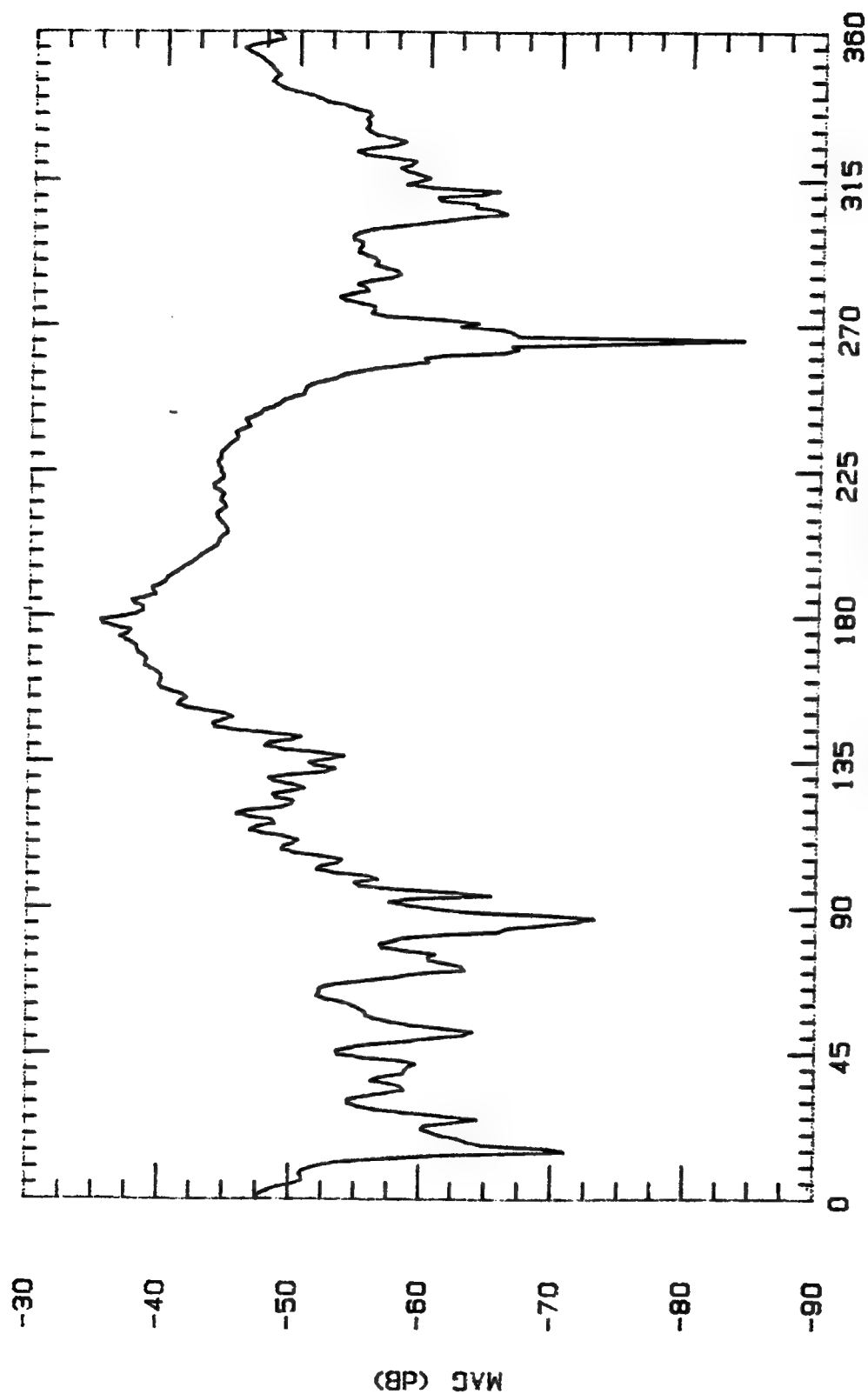


ASPECT ANGLE (DEGREES)

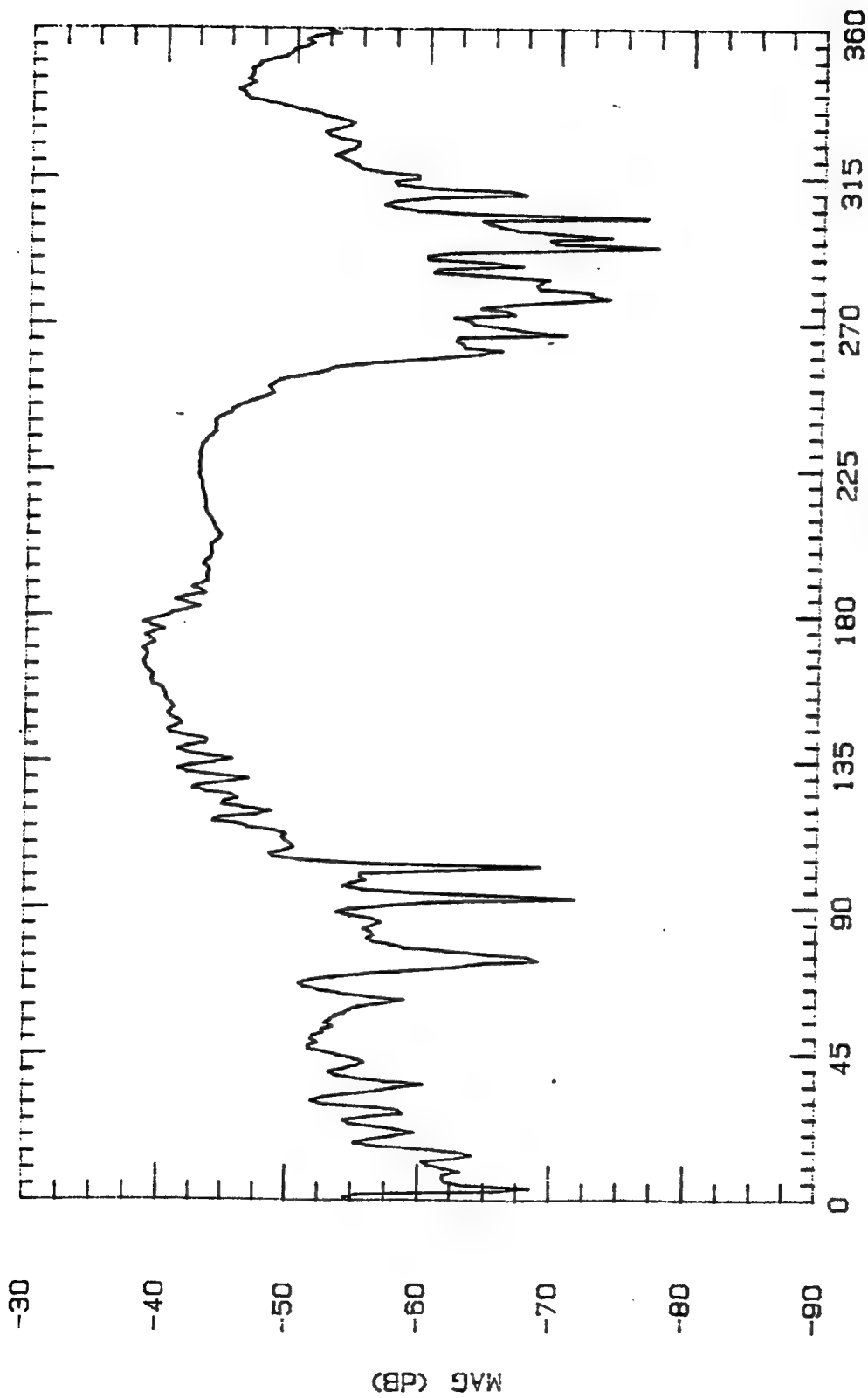
File Name	Frequency	Pattern Type	Date
CLPL1000	10 GHz	E-PLANE	28 OCT



File Name	Frequency	Pattern Type	Date
CLPL1050	10.5 GHz	E-PLANE	27 OCT 94

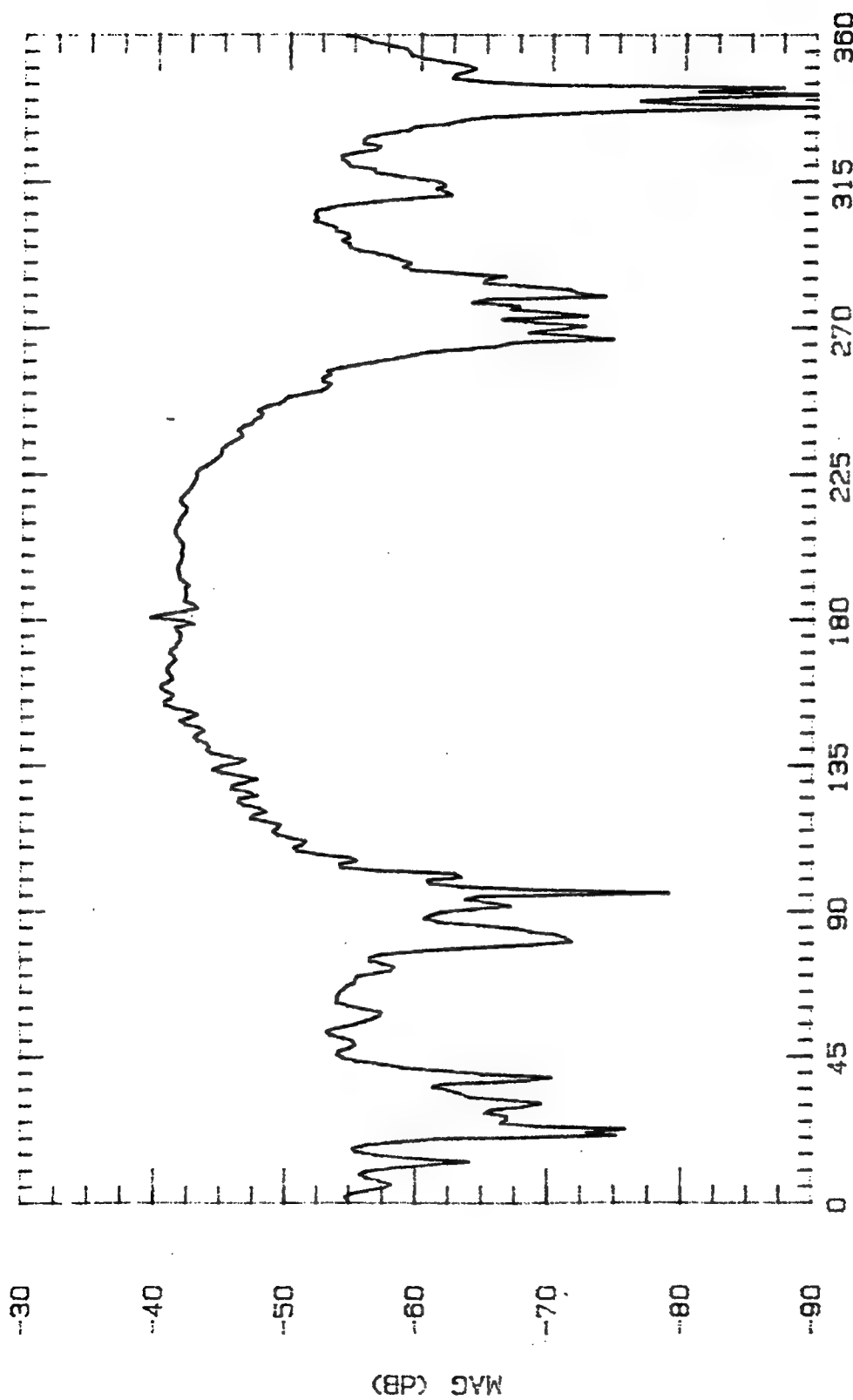


File Name	Frequency	Pattern Type	Date
CLPL1100	11 GHz	E-PLANE	28 OCT



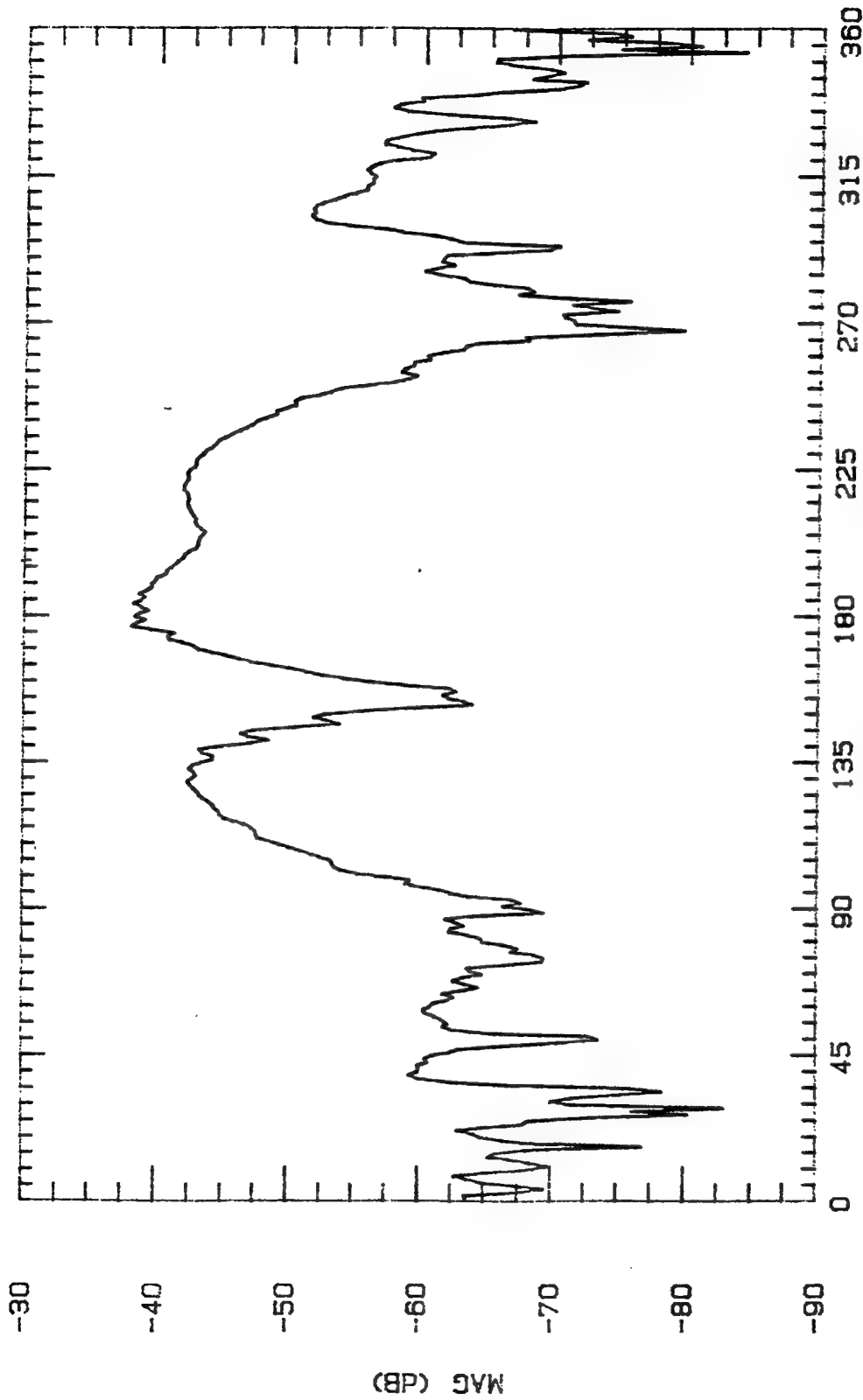
ASPECT ANGLE (DEGREES)

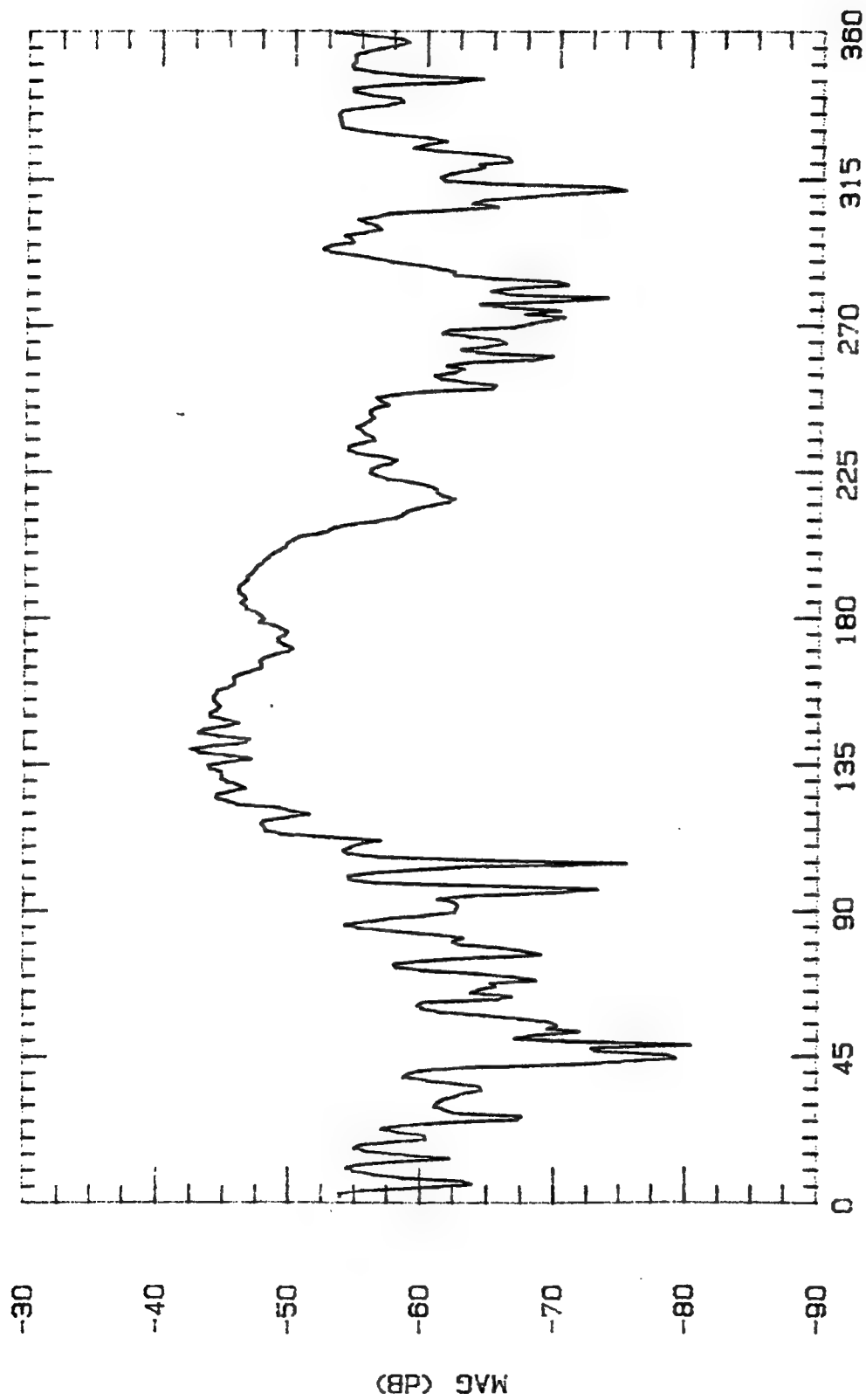
File Name	Frequency	Pattern Type	Date
CLPL1150	11.5 GHz	L-PLANE	27 OCT 94



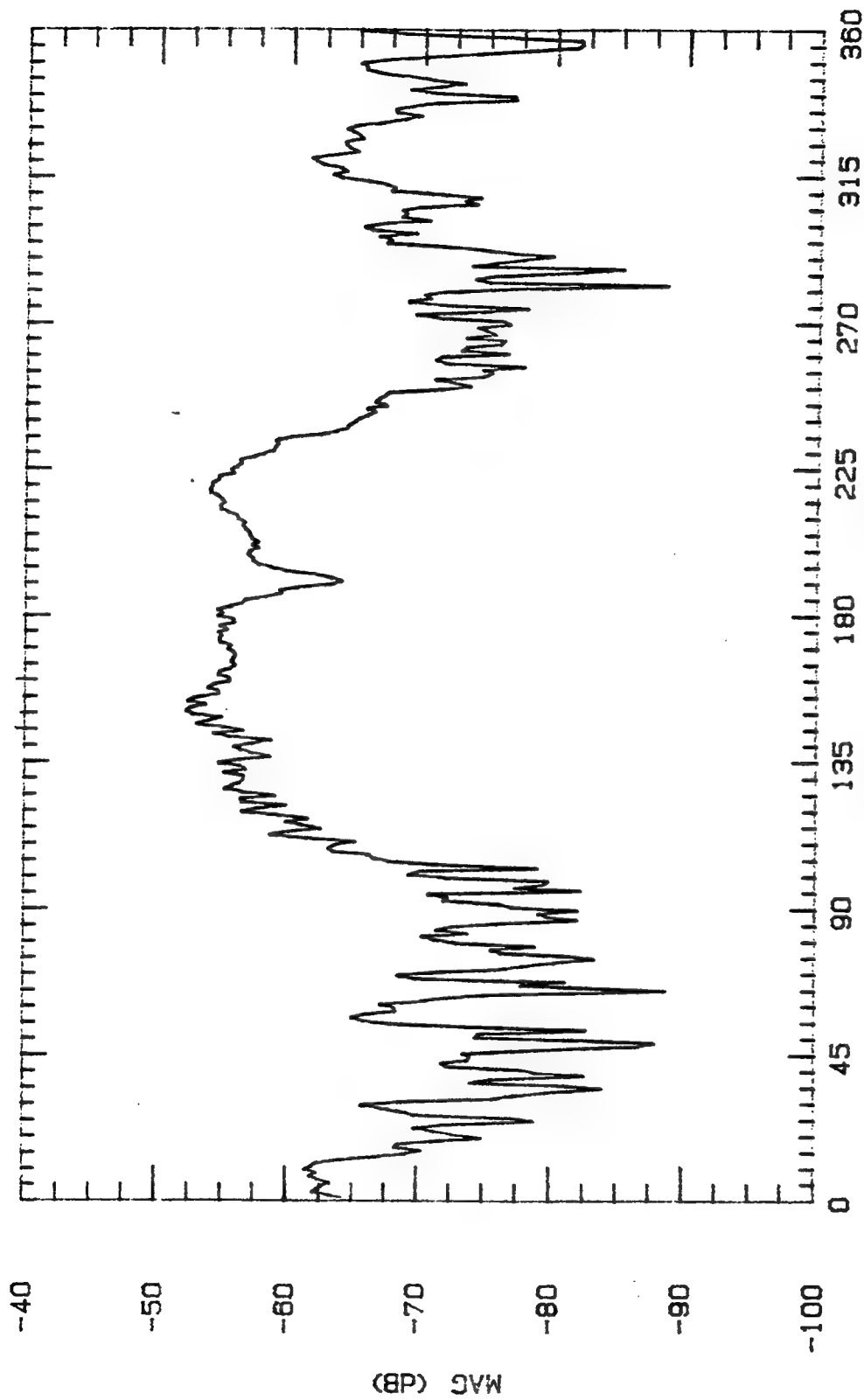
ASPECT ANGLE (DEGREES)

File Name	Frequency	Pattern Type	Data
CLPL1200	12 GHz	E-PLANE	28 OCT





File Name	Frequency	Pattern Type	Date
CLPL1900	19 GHz	L-PLANE	27 OCT 84

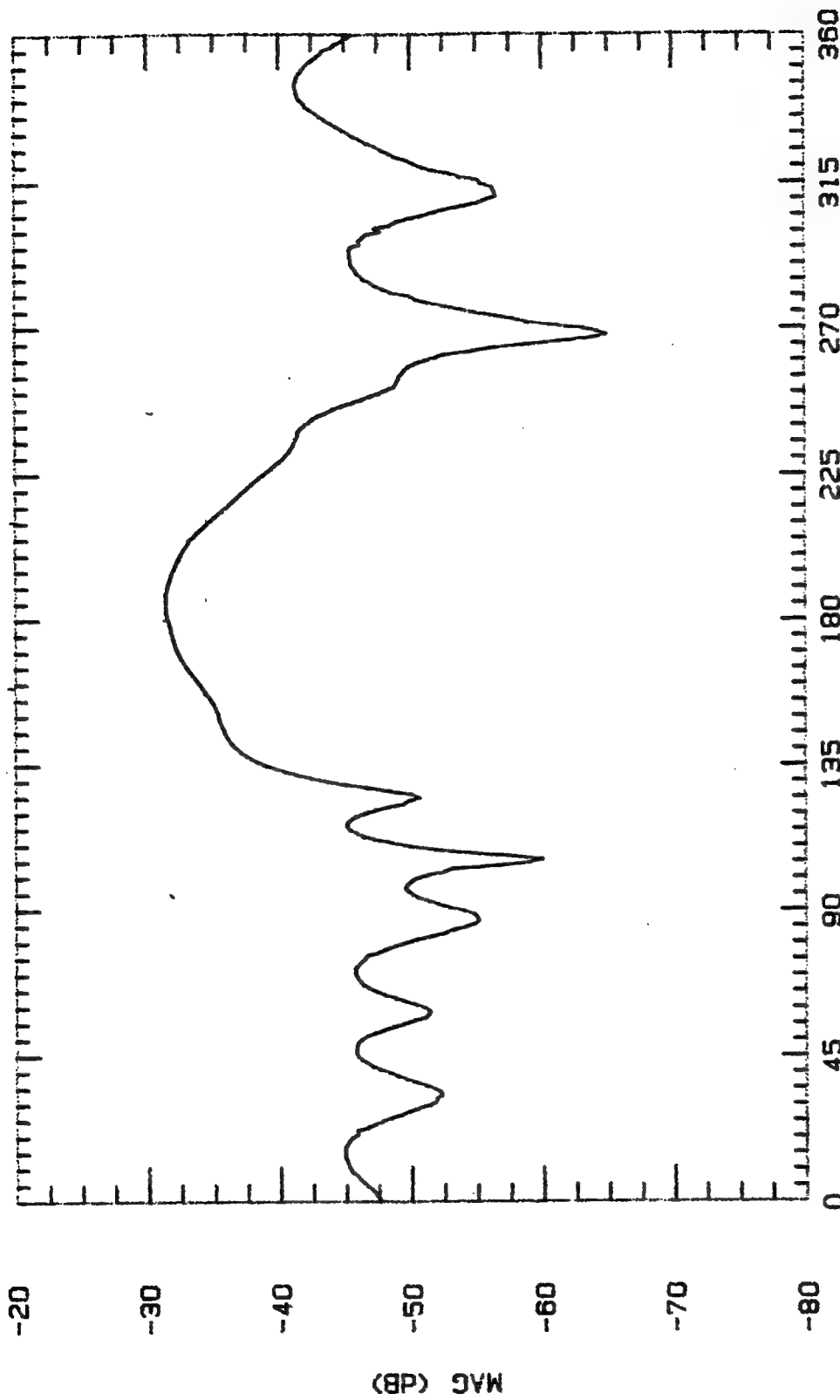


ASPECT ANGLE (DEGREES)

File Name	Frequency	Pattern Type	Date
CLPL1800	18 GHz	E-PLANE	27 OCT 94

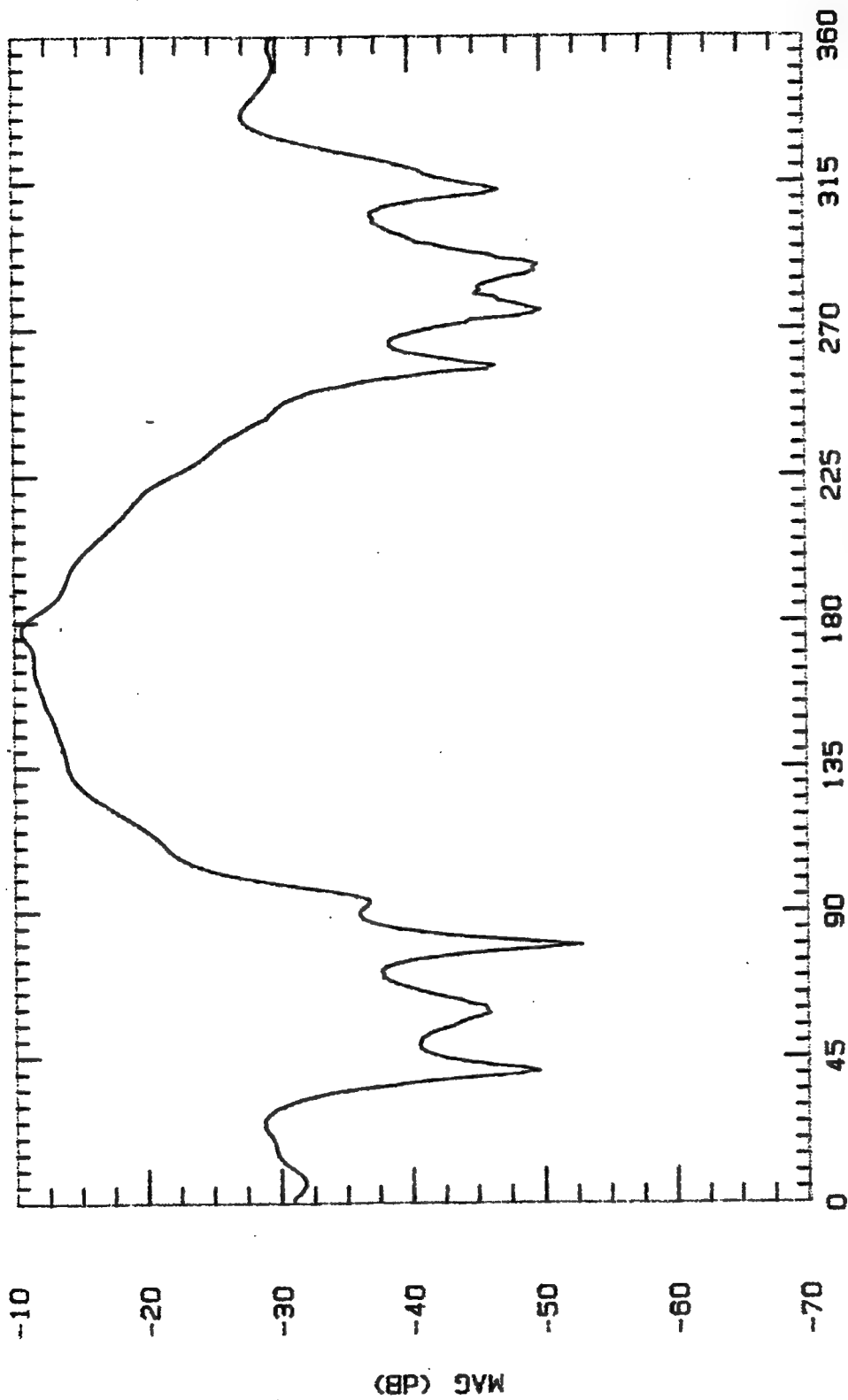
APPENDIX K: Antenna Pattern Cuts For 6.2 & 3.7 GHz Two Layer Design
(5B, 1S, 3B, 1S, 7B)

Freq (GHz)	Normal Gain (dBi)	Max Gain (dBi)	Squint (deg)	Beamwidth (-3dBi to -3dBi) (deg)
-----	-----	-----	-----	-----
2.00	-14.8	-14.6	7	52
2.73	4.5	4.5	-1	48
3.00	1.5	1.5	0	55
4.00	-9.1	-3.3	-50	10
5.00	-10.4	-6.1	35	37
6.00	-0.1	0.1	-5	55
6.30	-2.6	0.3	-5	115
6.50	-0.6	1.9	31	95
6.70	-1.1	0.8	-38	101
7.00	2.2	2.6	-2	55
7.25	-2.3	-0.5	-48	7
7.50	-7.5	-1.9	-30	32
7.75	-7.6	-0.1	-45	7
8.00	-3.6	-2.3	-40	37
8.25	1.6	2.6	-4	24
8.50	-4.3	1.6	-43	30
8.75	-0.4	4.7	-10	25
9.00	-0.6	2.3	-20	55
9.25	-4.8	-1.0	15	30
9.50	-3.9	0	10	25
9.75	-3.6	0.2	-27	23
10.00	-1.4	0.8	45	32
10.25	-0.2	2.1	20	45
10.50	-2.4	2.0	-25	35
10.75	0.6	3.0	2	22
11.00	5.7	5.7	0	8
11.25	2.9	3.2	2	15
11.55	2.3	3.2	12	40
11.75	-1.9	1.4	2	25
12.00	6.7	6.7	0	23
12.40	4.7	5.0	-2	20
12.75	-2.0	3.8	-18	22
13.00	-1.3	3.7	-18	23
-----	-----	-----	-----	-----

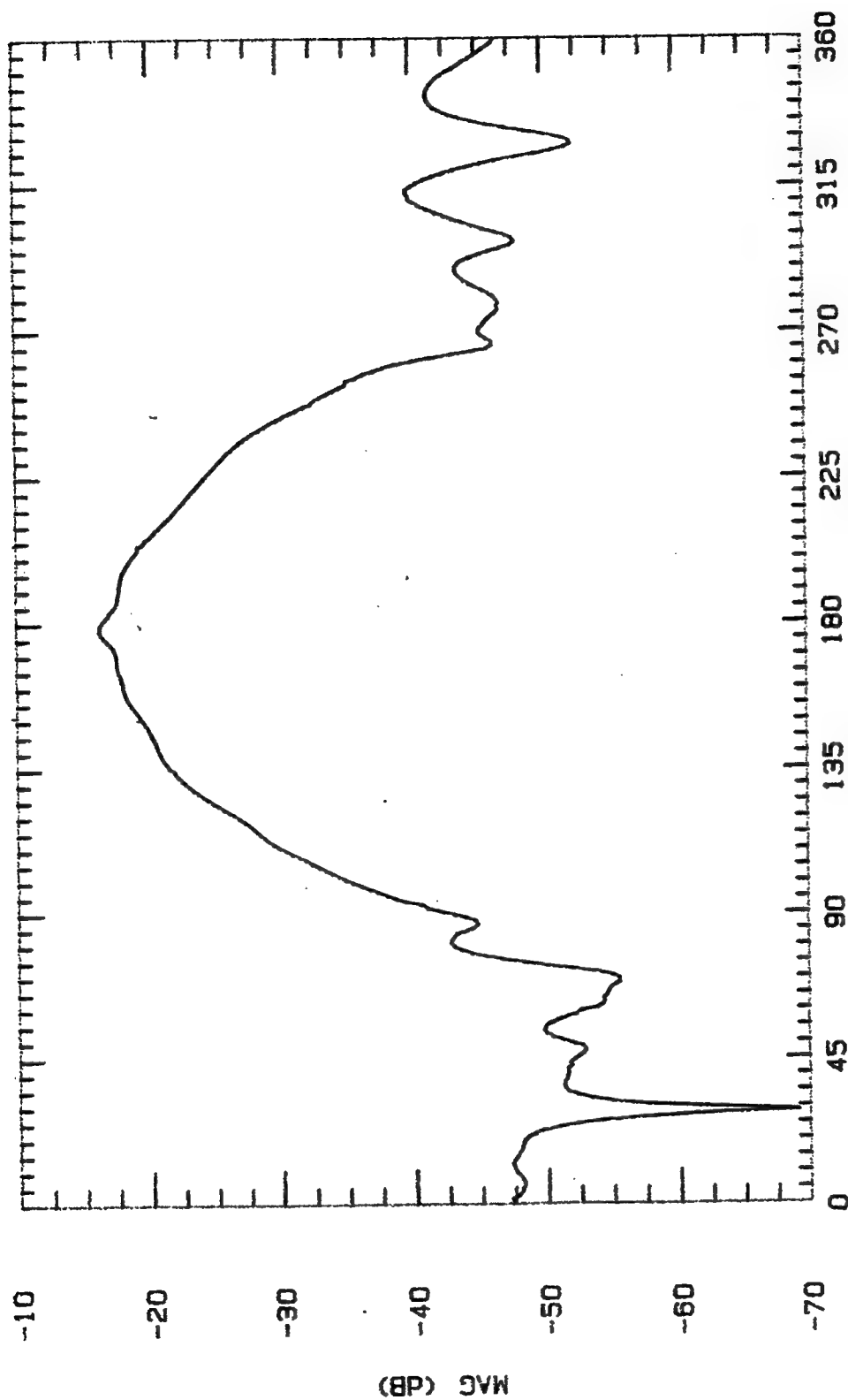


ASPECT ANGLE (DEGREES)

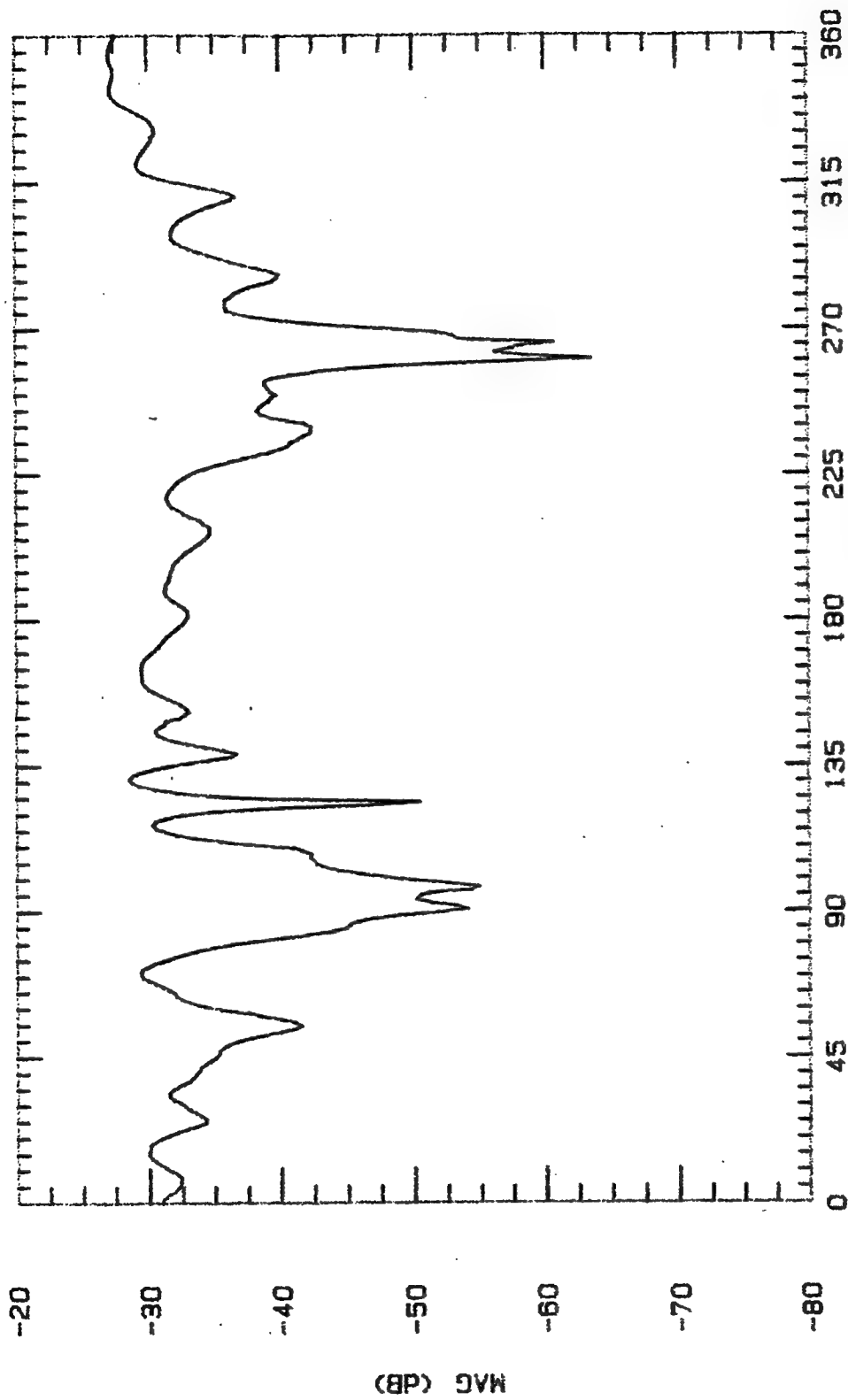
File Name	Frequency	Pattern Type	Date
BLPL200	2 GHz	E-PLANE	25 OCT



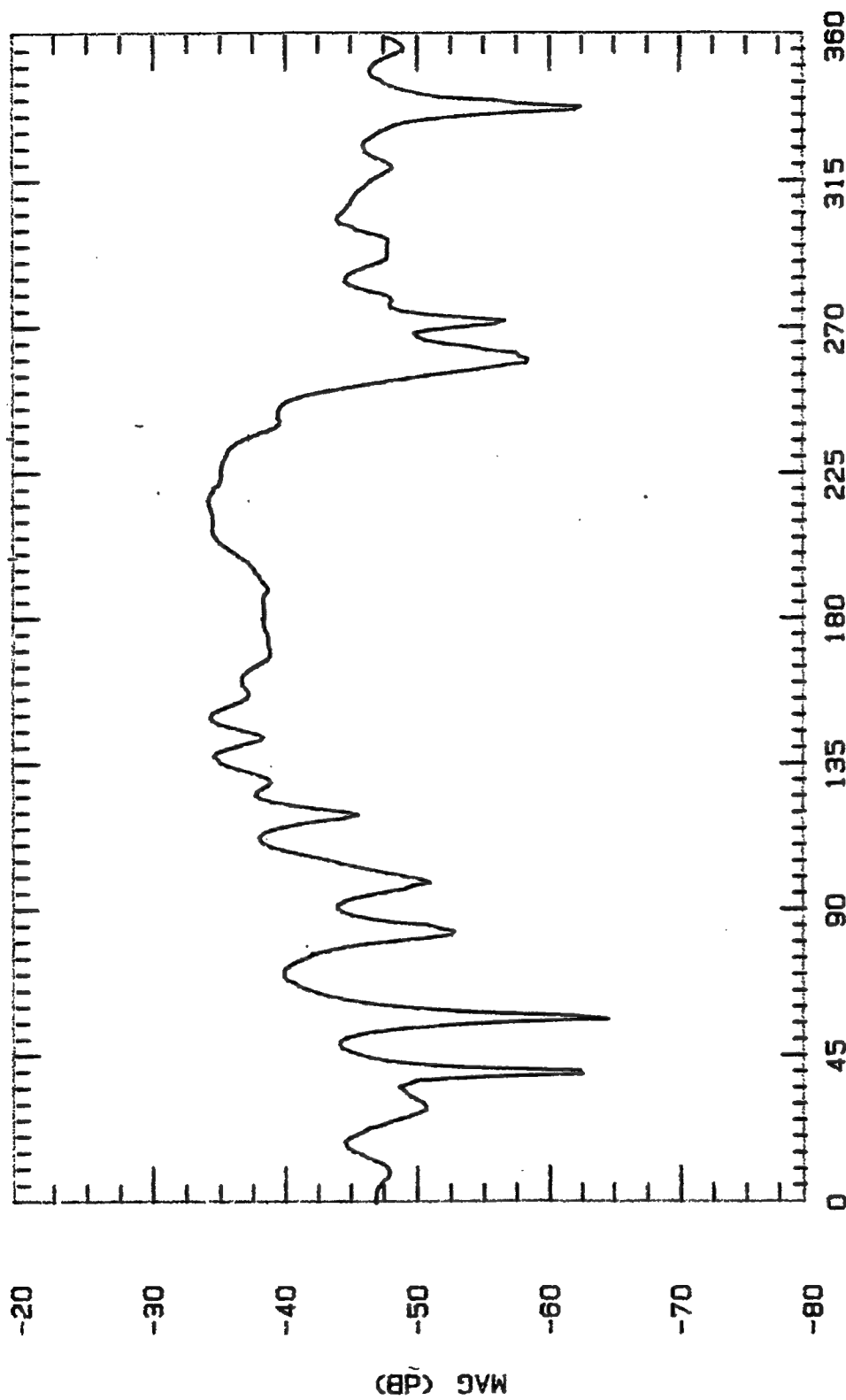
File Name	Frequency	Pattern Type	Date
BLPL273	2.79 GHz	E-PLANE	25 OCT



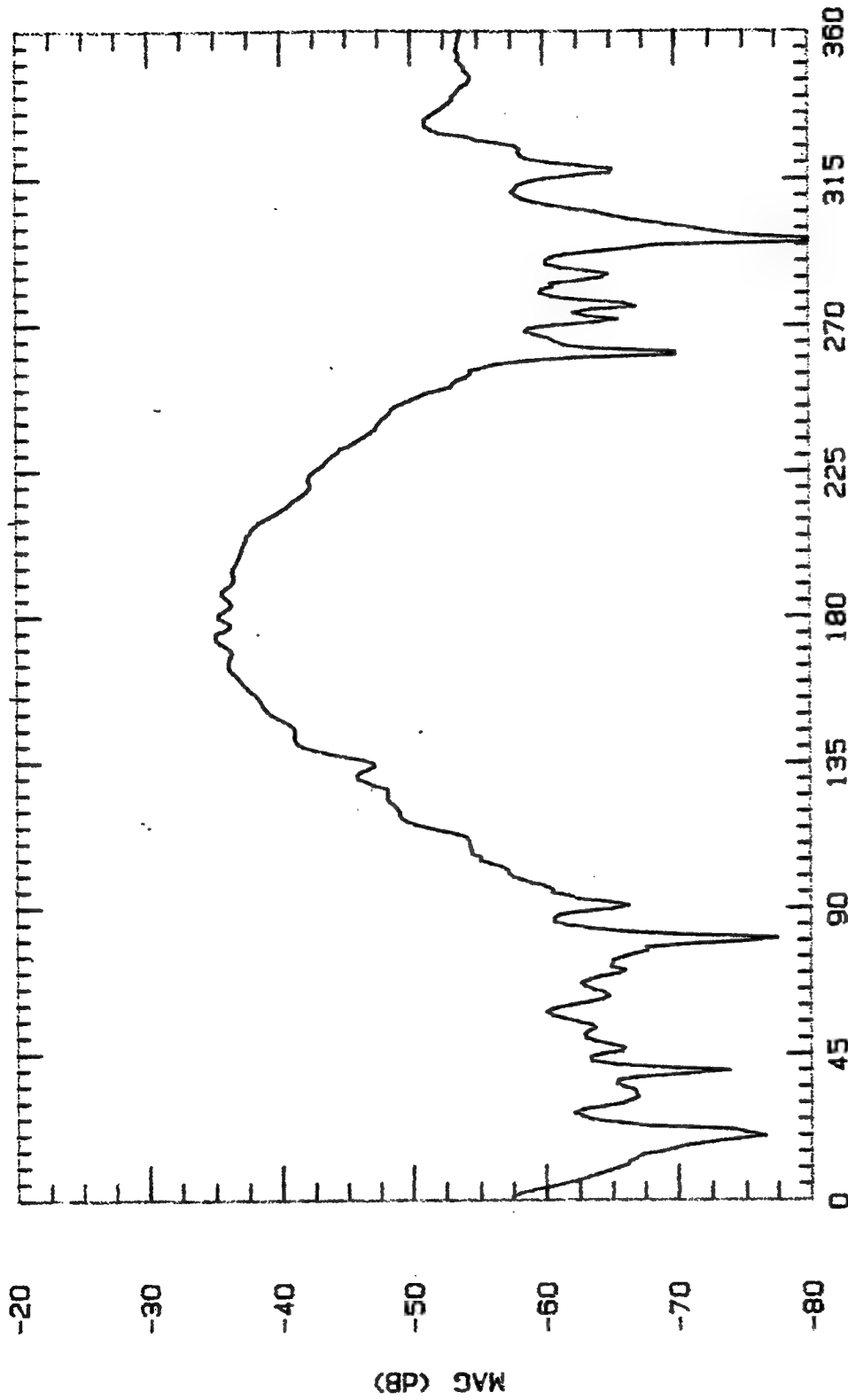
File Name	Frequency	Pattern Type	Date
BLPL300	9 GHz	E-PLANE	25 OCT



File Name	Frequency	Pattern Type	Date
BLPL400	4 GHz	E-PLANE	25 OCT

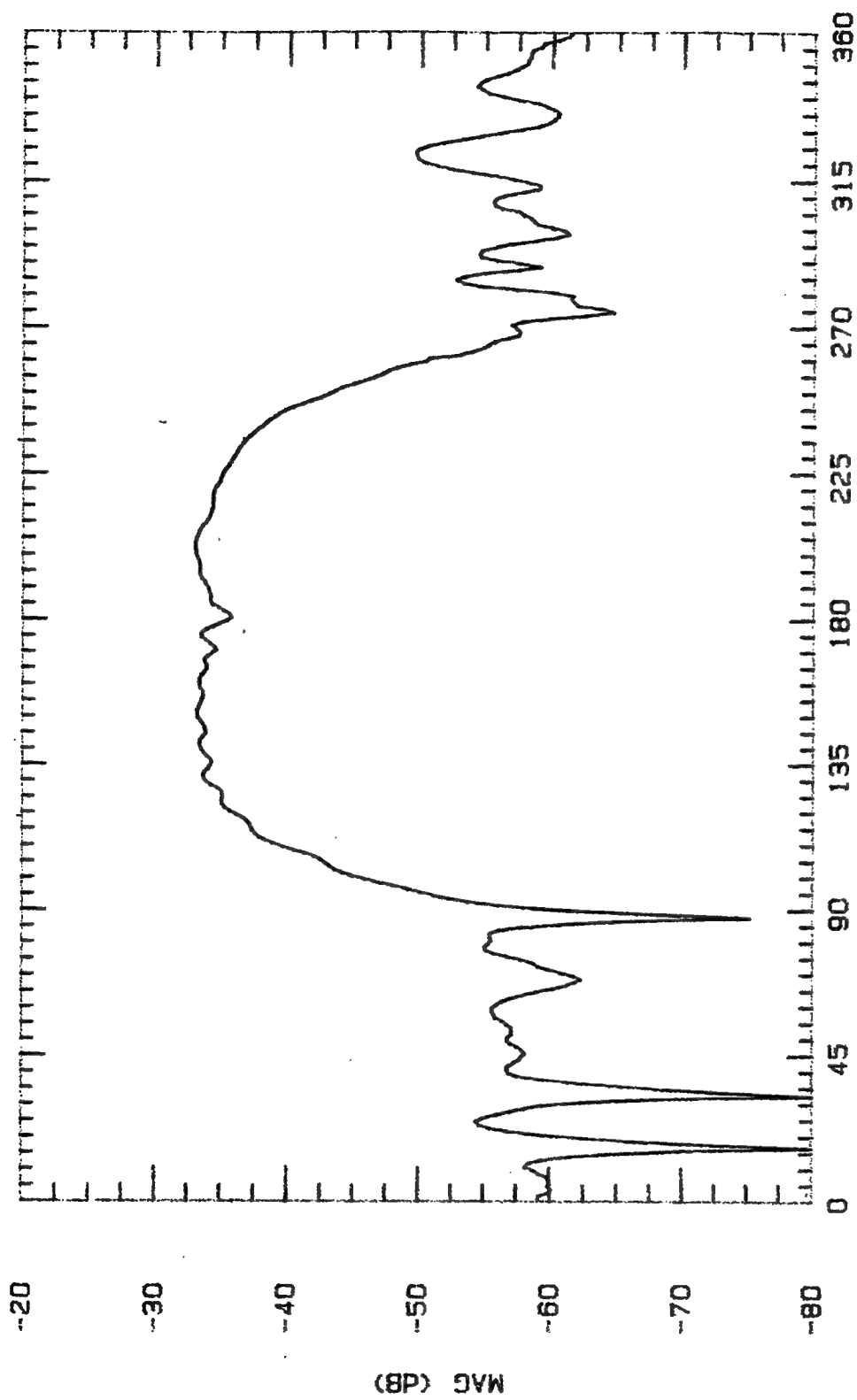


File Name Frequency Pattern Type Date
BLPL500 5 GHz E-PLANE 25 OCT



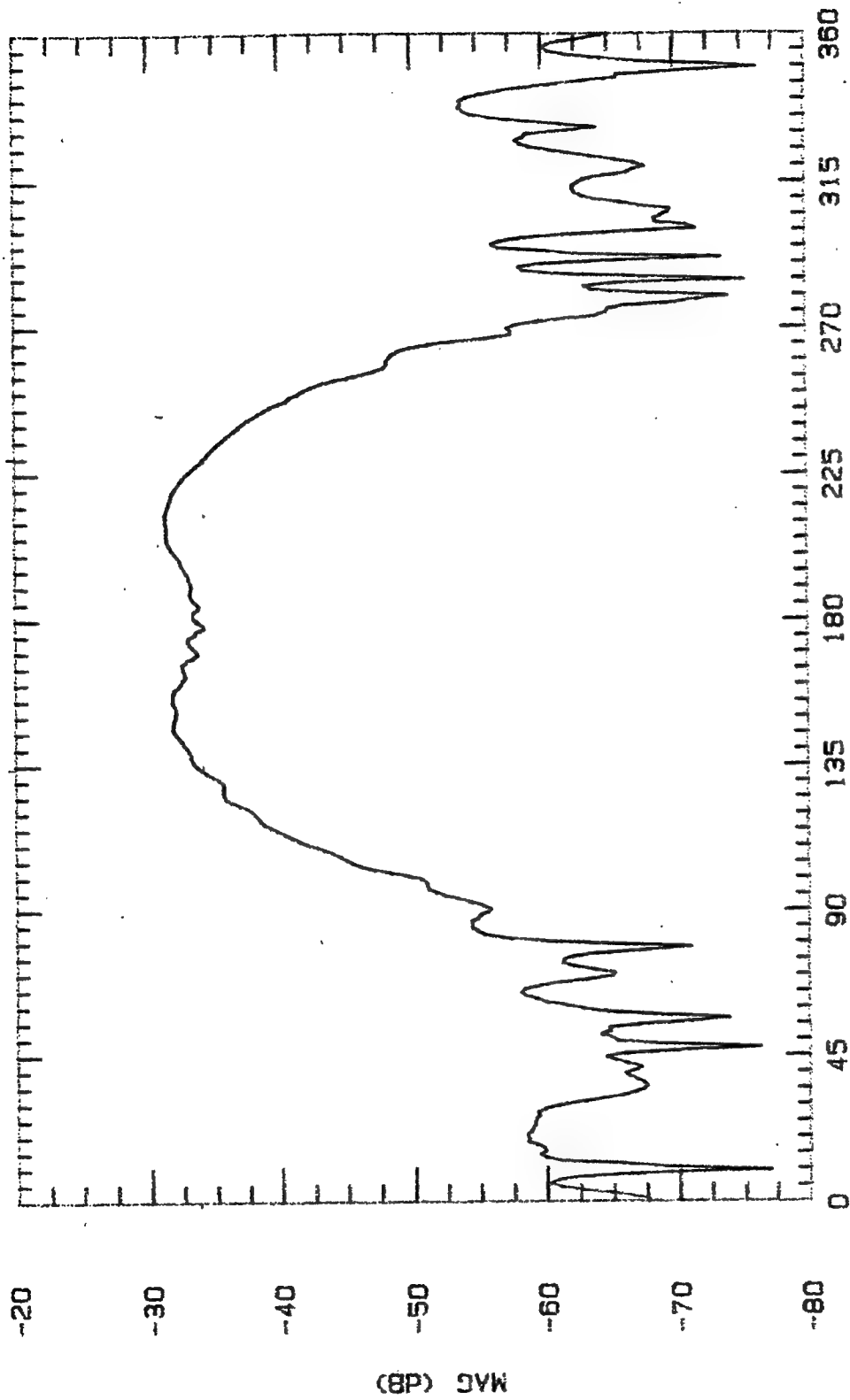
ASPECT ANGLE (DEGREES)

File Name	Frequency	Pattern Type	Date
BLPL800	8 GHz	E-PLANE	25 OCT

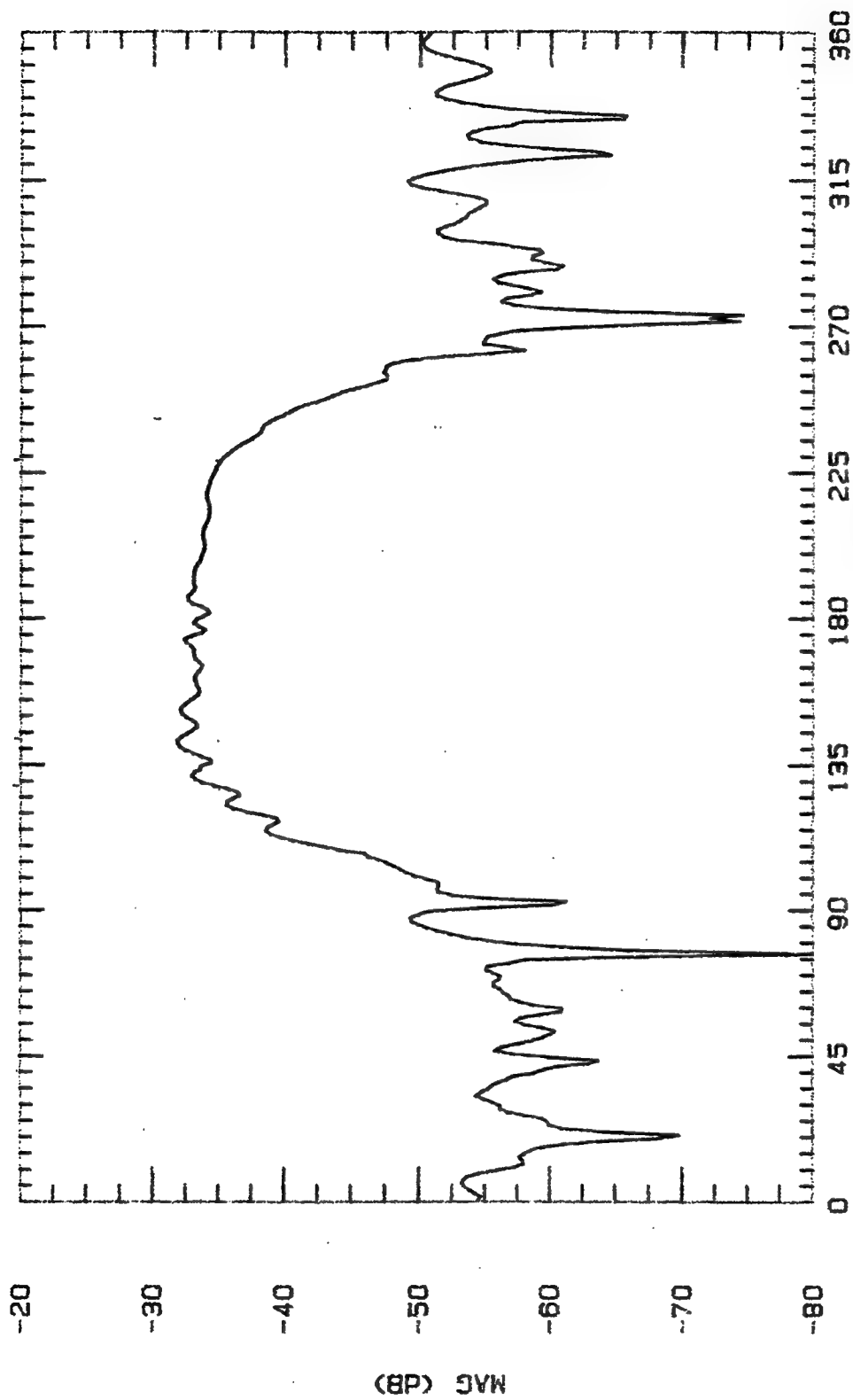


ASPECT ANGLE (DEGREES)

File Name	Frequency	Pattern Type	Date
BLPL630	8.3 GHz	E-PLANE	25 OCT

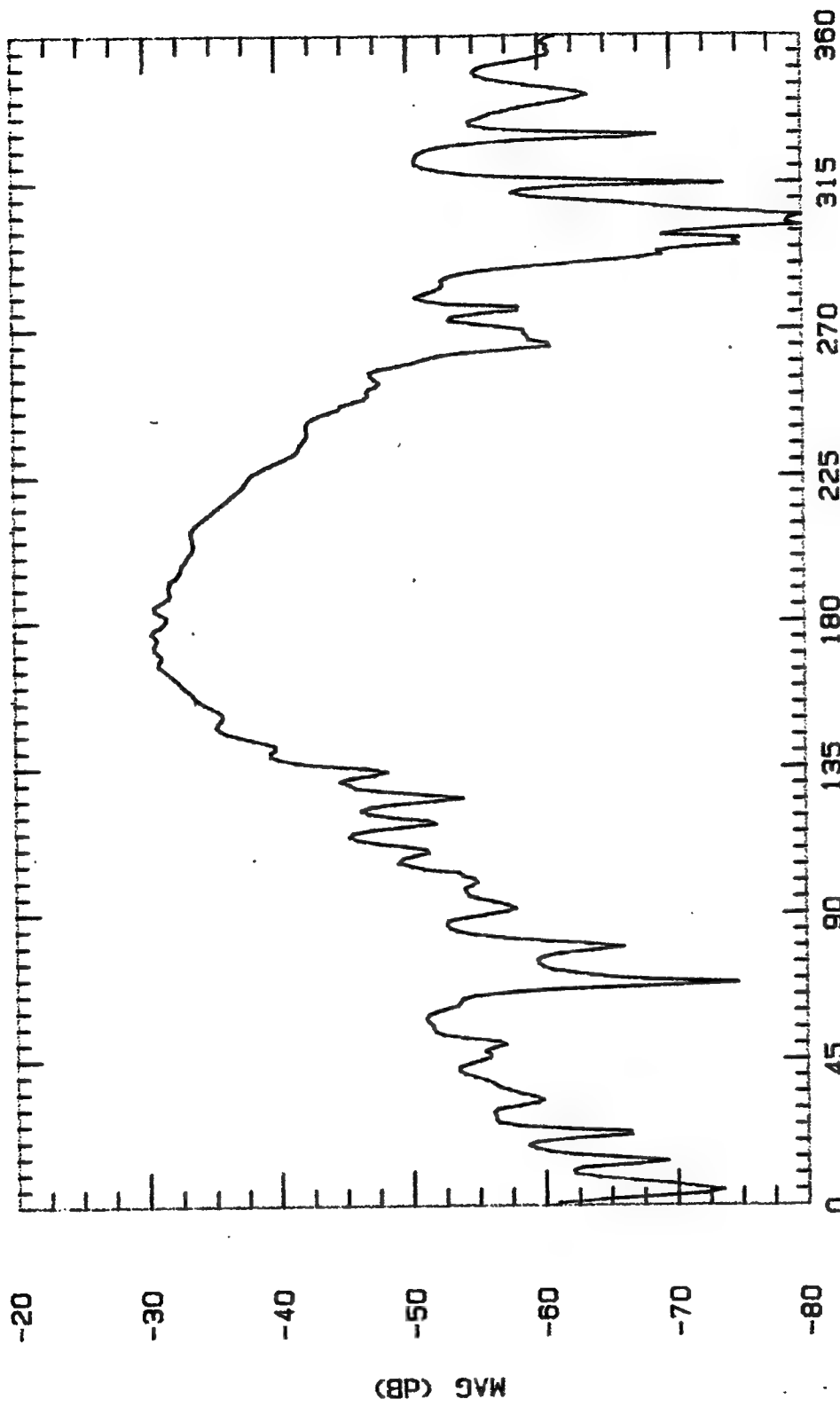


File Name	Frequency	Pattern Type	Date
BLPL650	8.5 GHz	E-PLANE	25 OCT

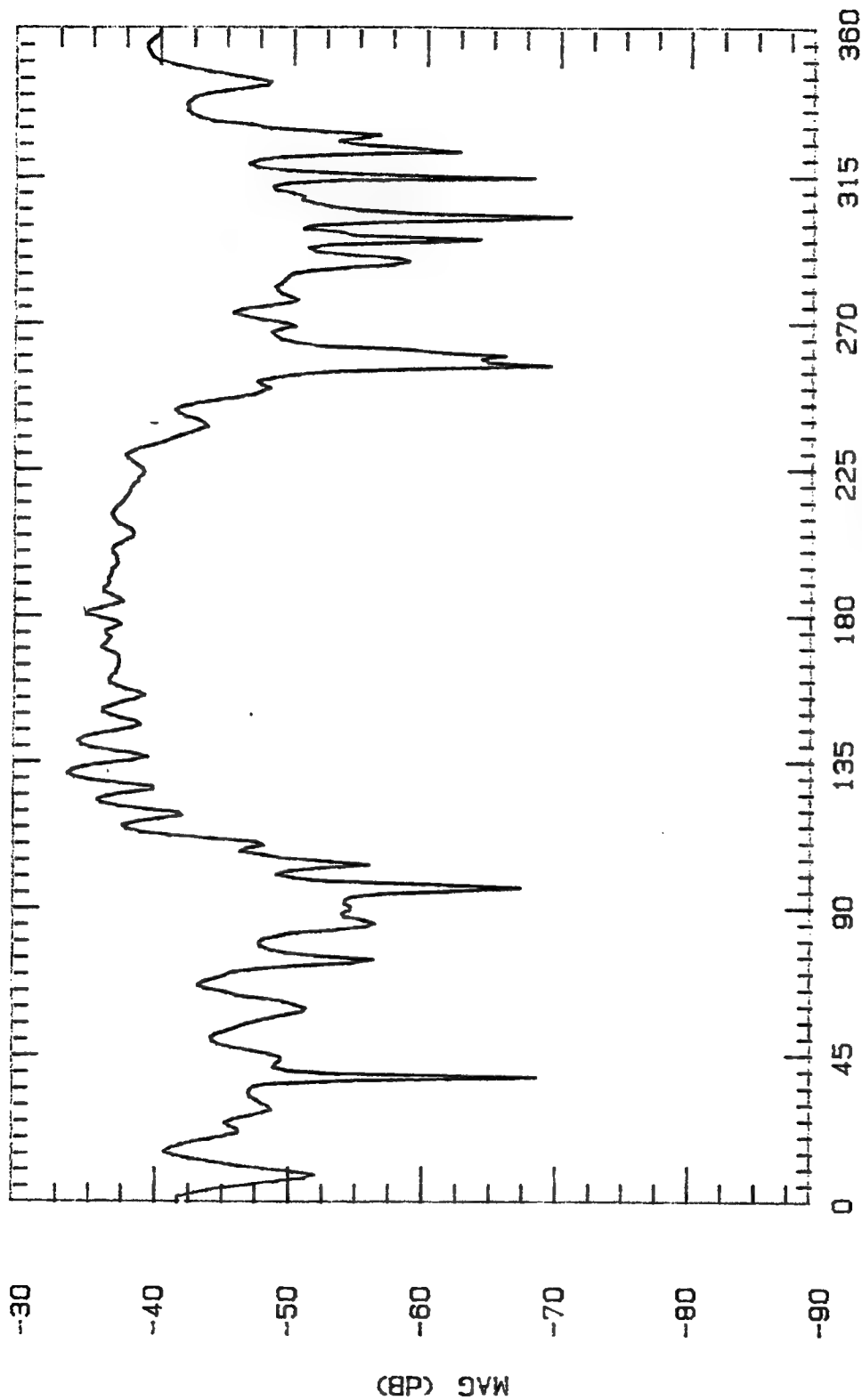


ASPECT ANGLE (DEGREES)

File Name	Frequency	Pattern Type	Date
BLPL670	6.7 GHz	E-PLANE	25 OCT

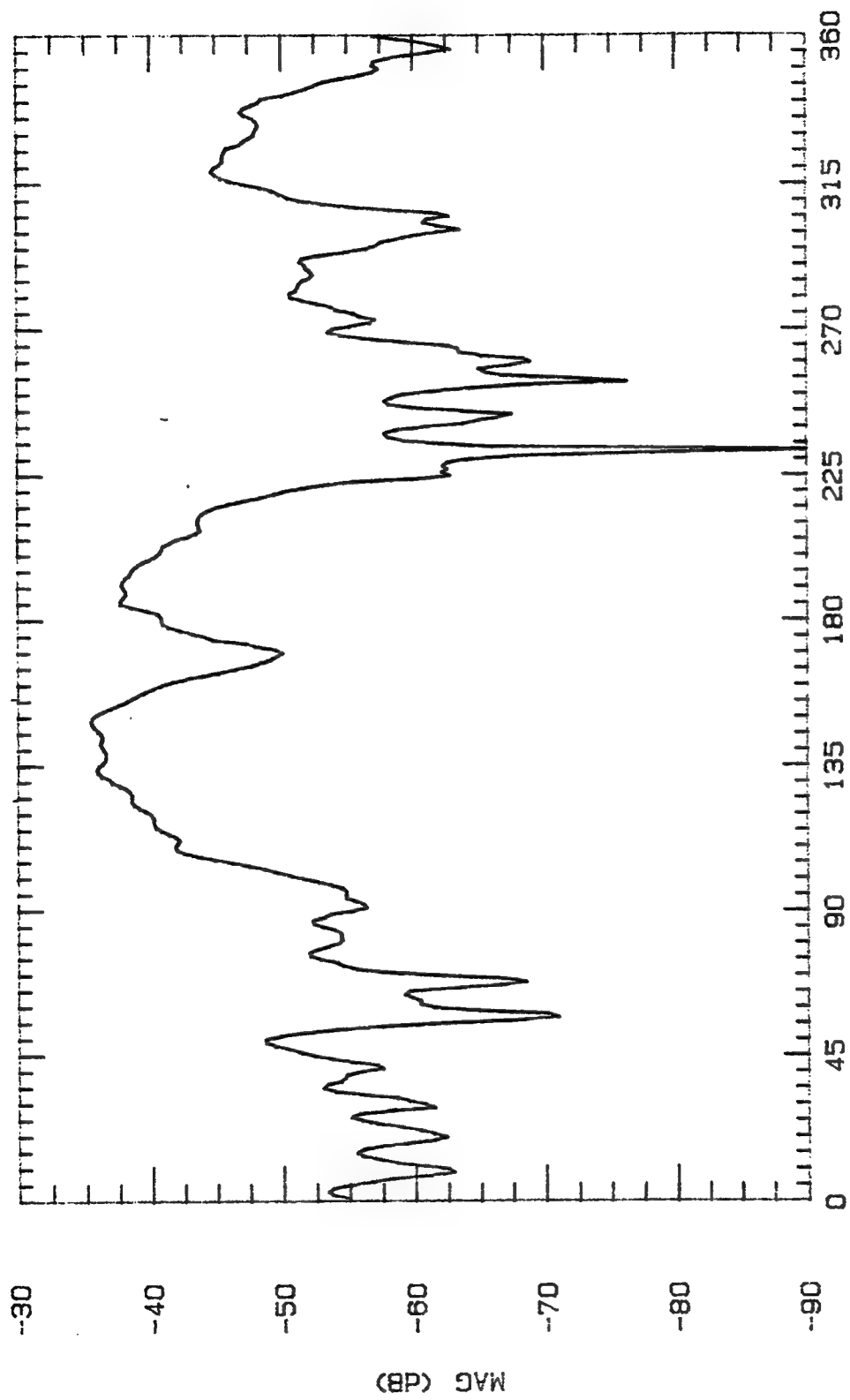


File Name	Frequency	Pattern Type	Date
BLPL700	7 GHz	E-PLANE	25 OCT



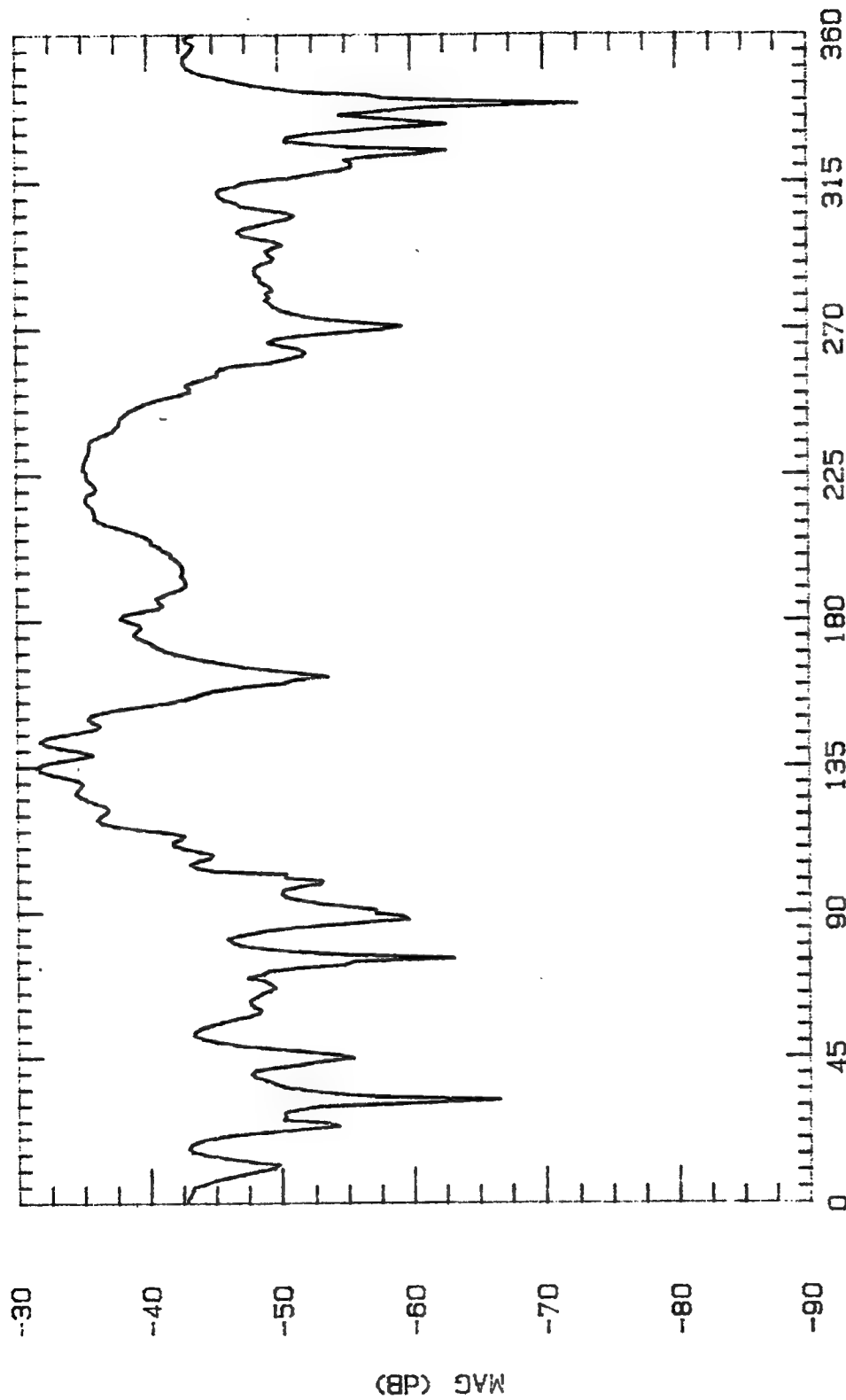
ASPECT ANGLE (DEGREES)

File Name	Frequency	Pattern Type	Date
BLPL725	7.25 GHz	E-PLANE	28 OCT 94

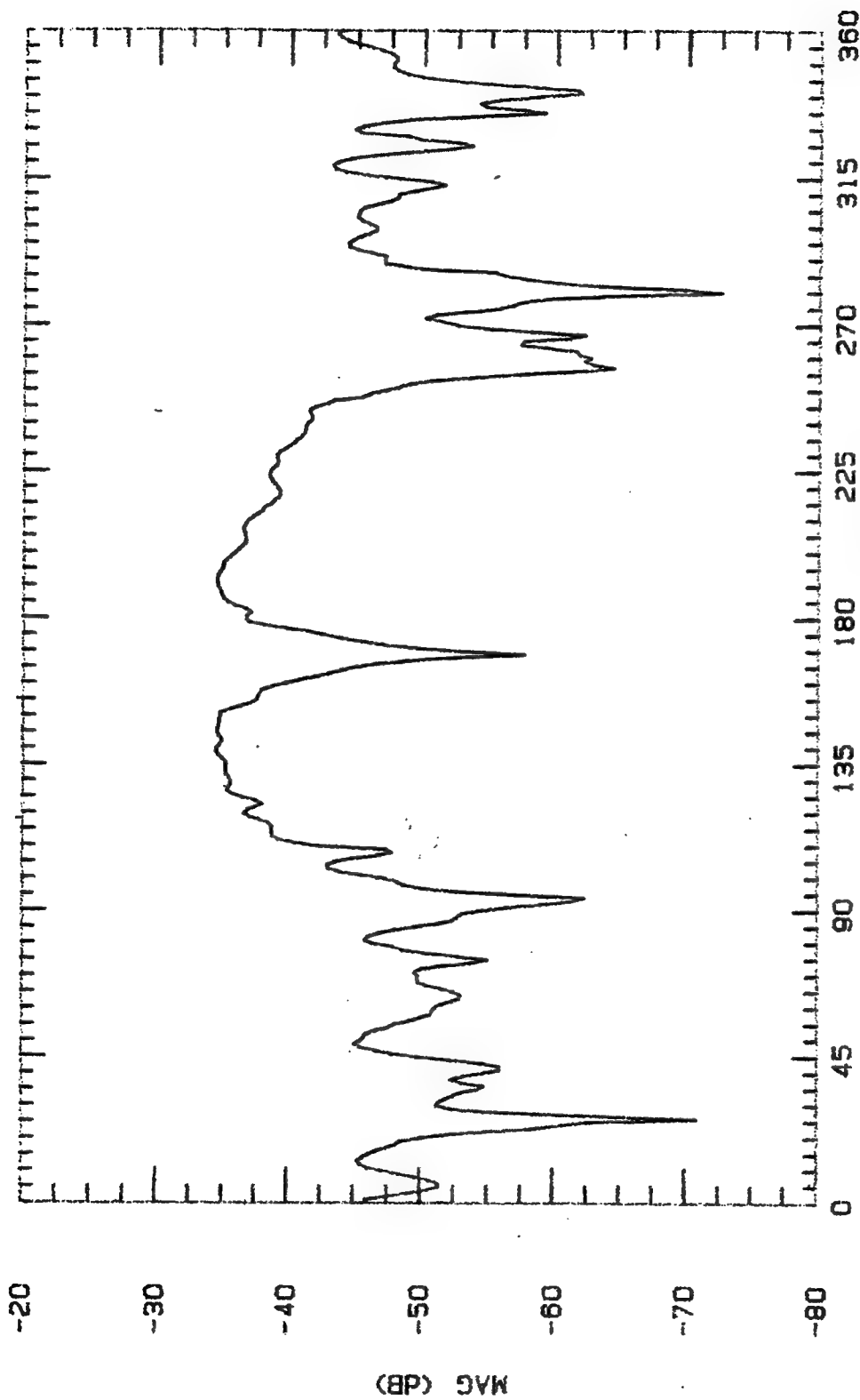


ASPECT ANGLE (DEGREES)

File Name	Frequency	Pattern Type	Date
BLPL750	7.5 GHz	E-PLANE	28 OCT 94

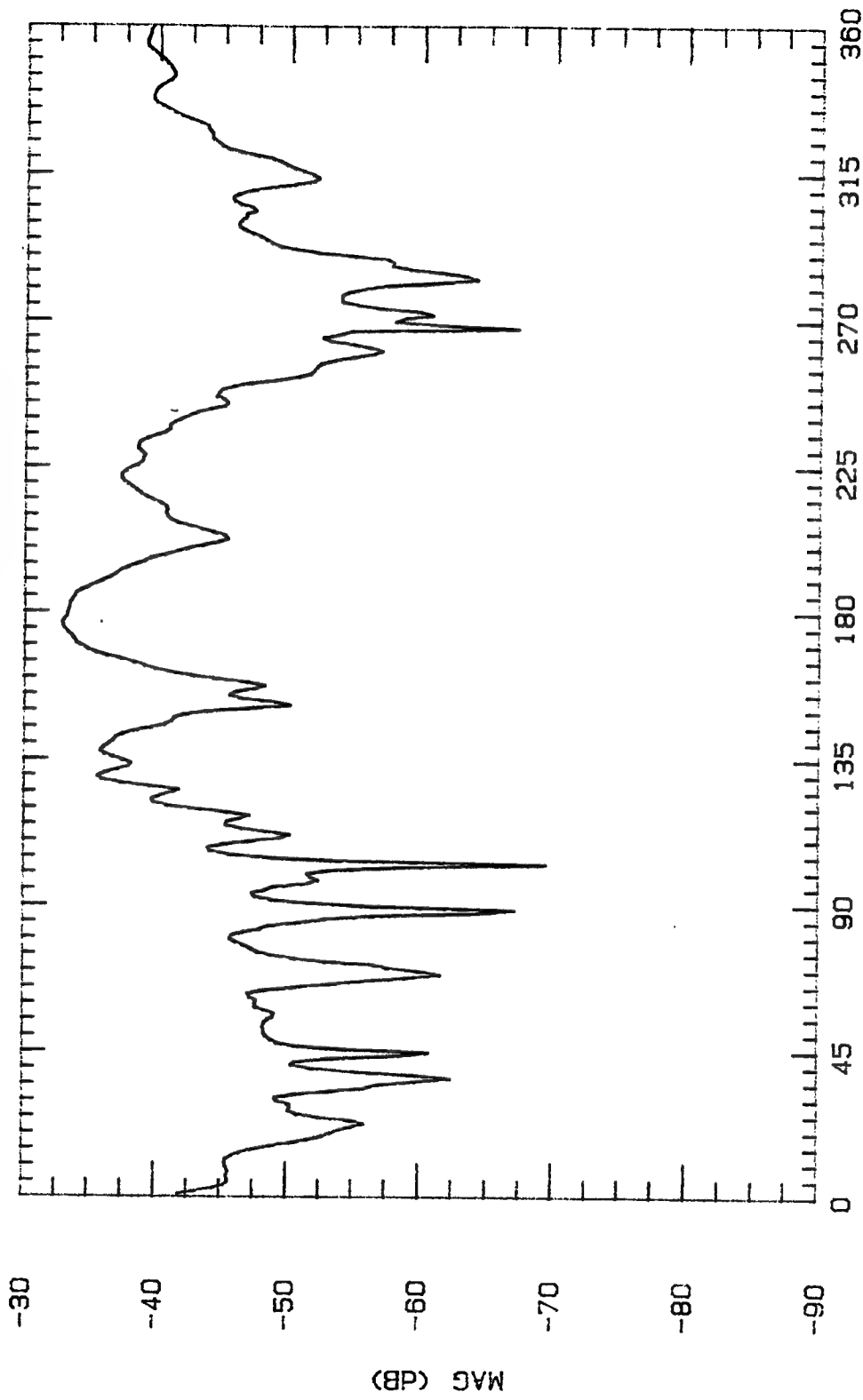


File Name	Frequency	Pattern Type	Date
BLPL775	7.75 GHz	E-PLANE	28 OCT

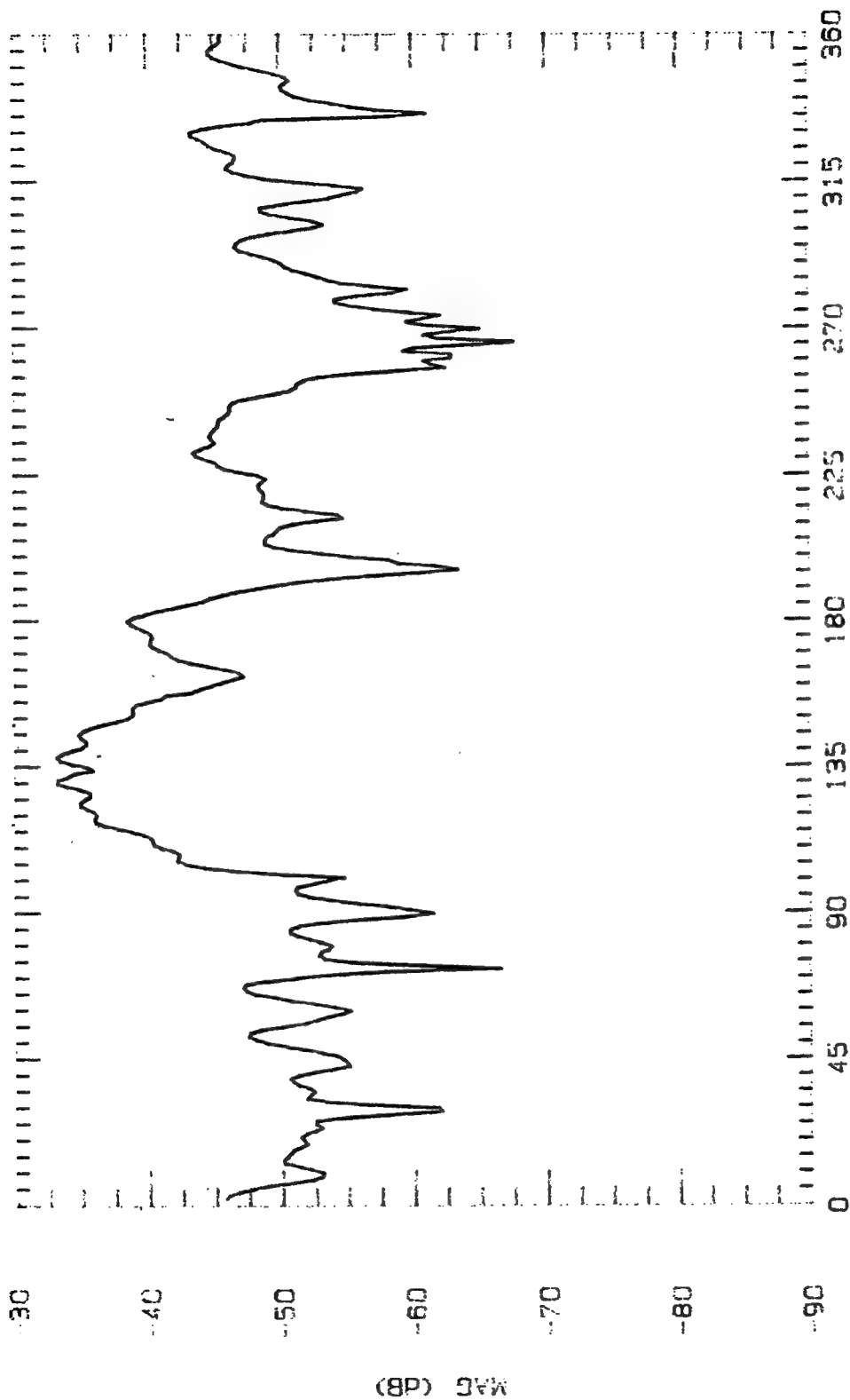


ASPECT ANGLE (DEGREES)

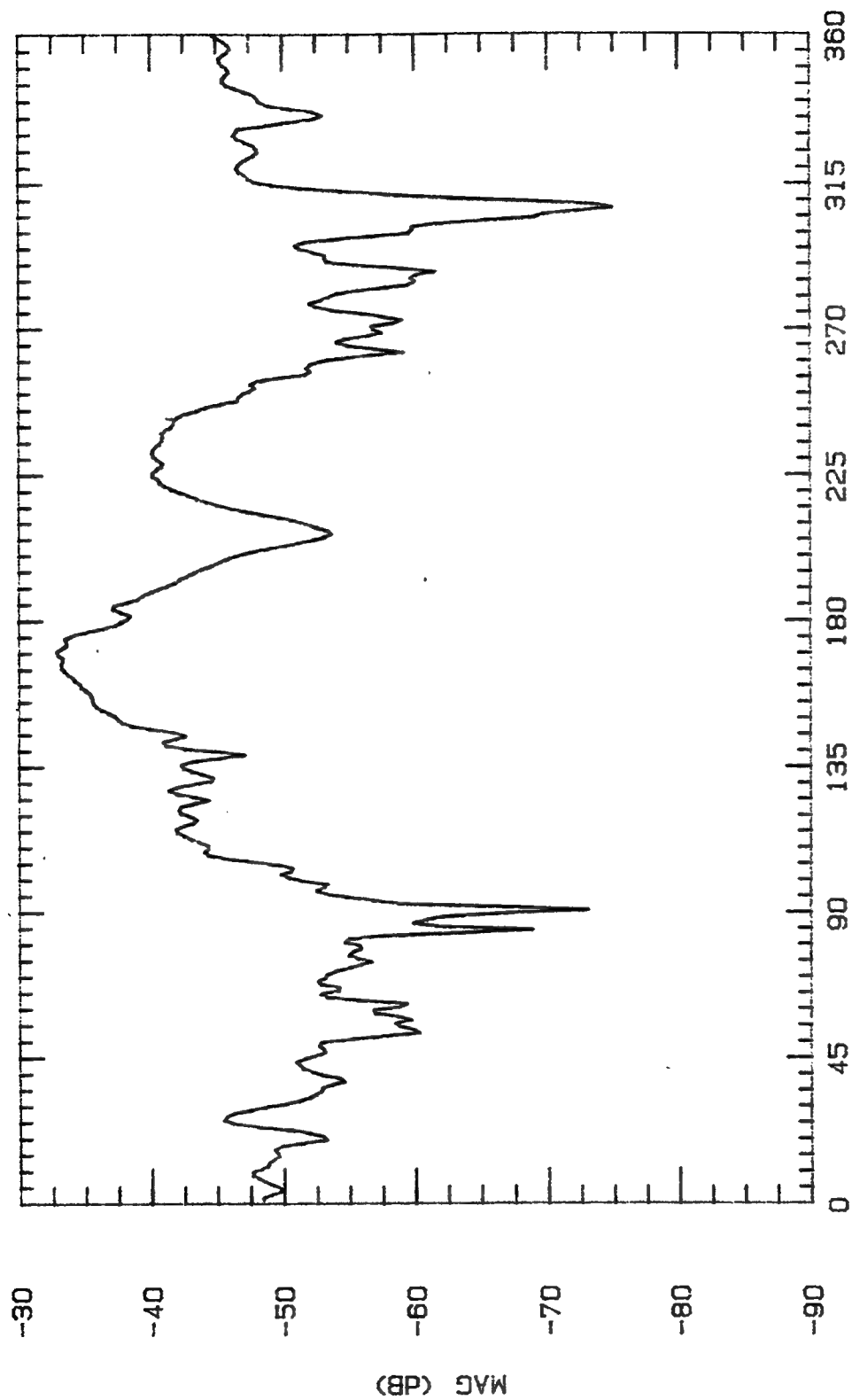
File Name	Frequency	Pattern Type	Date
BLPL800	8 GHz	E-PLANE	25 OCT



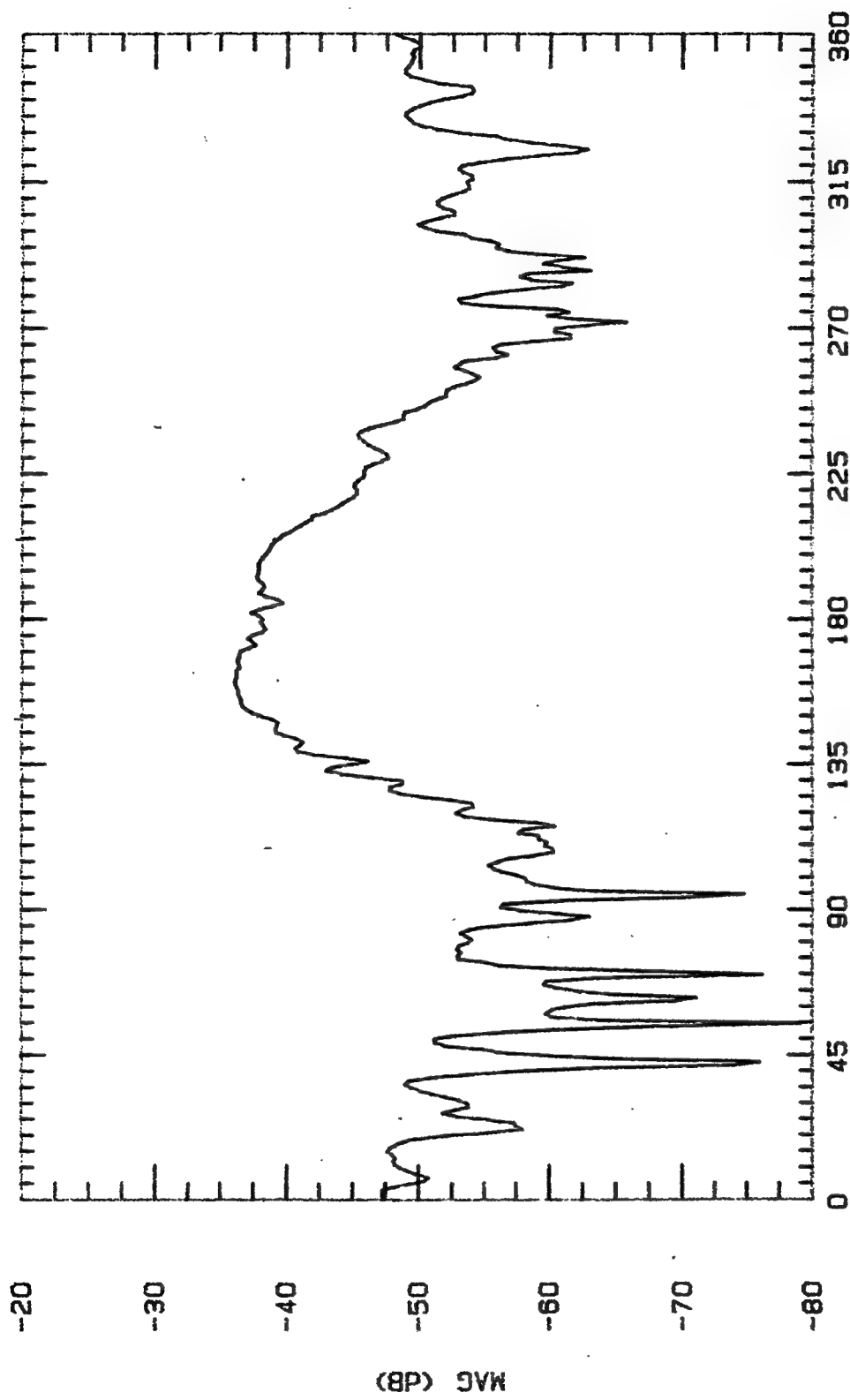
File Name	Frequency	Pattern Type	Date
BLPL825	8.25 GHz	E-PLANE	28 OCT



File Name	Frequency	Pattern Type	Date
BLPL850	8.5 GHz	E-PLANE	28 OCT

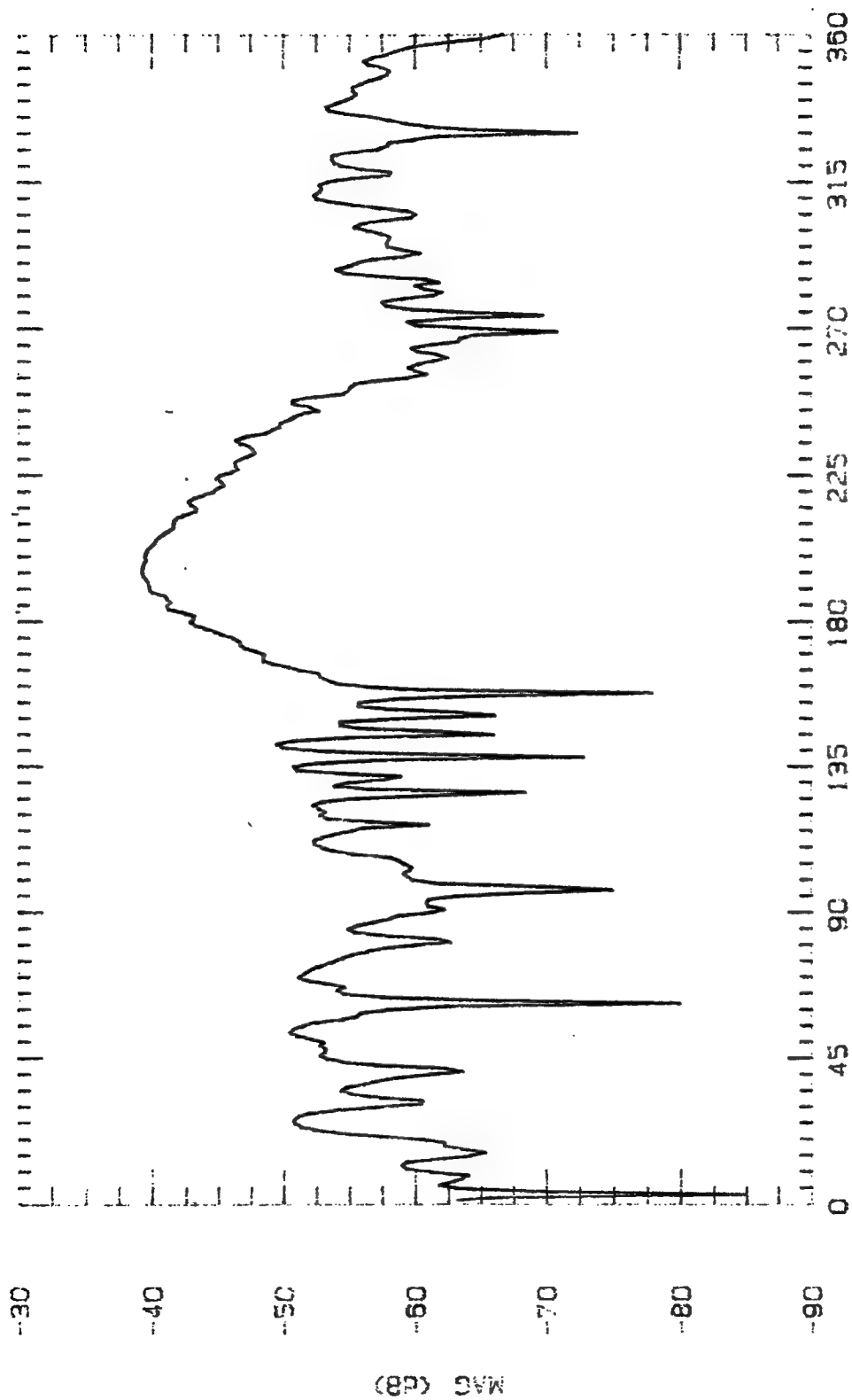


File Name	Frequency	Pattern Type	Date
BLPL075	8.75 GHz	E-PLANE	28 OCT

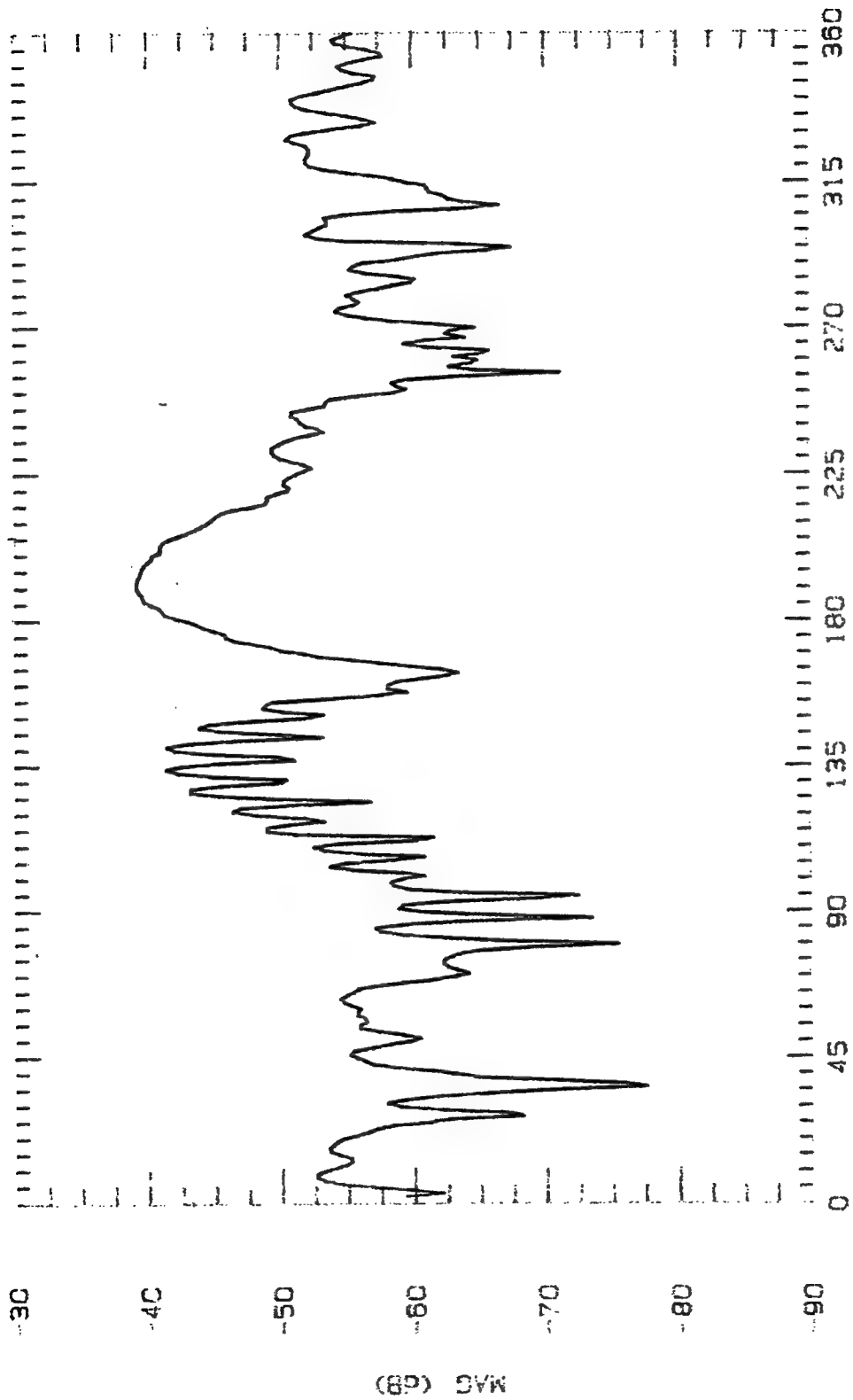


ASPECT ANGLE (DEGREES)

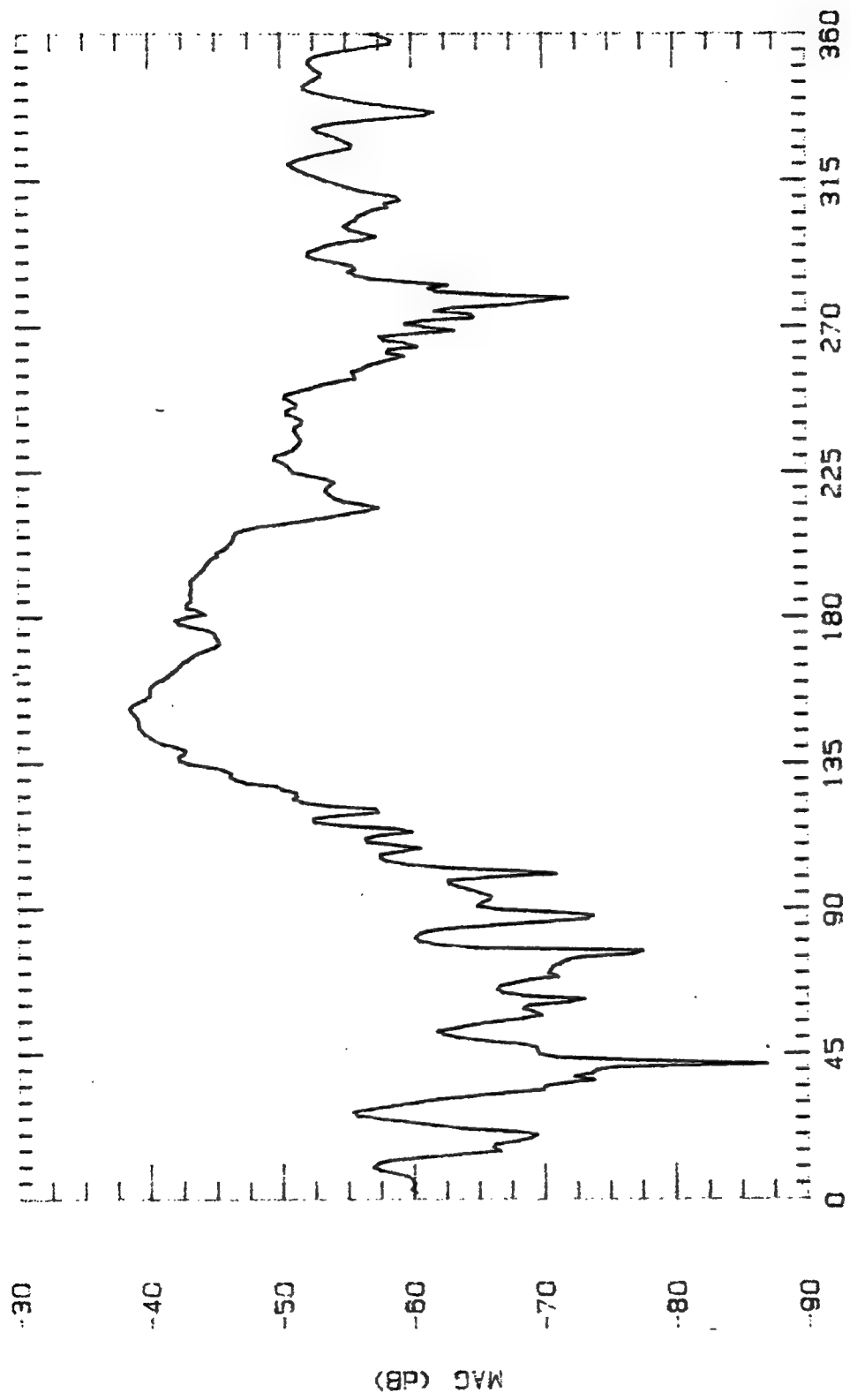
File Name	Frequency	Pattern Type	Date
BLPL900	9 GHz	E-PLANE	25 OCT



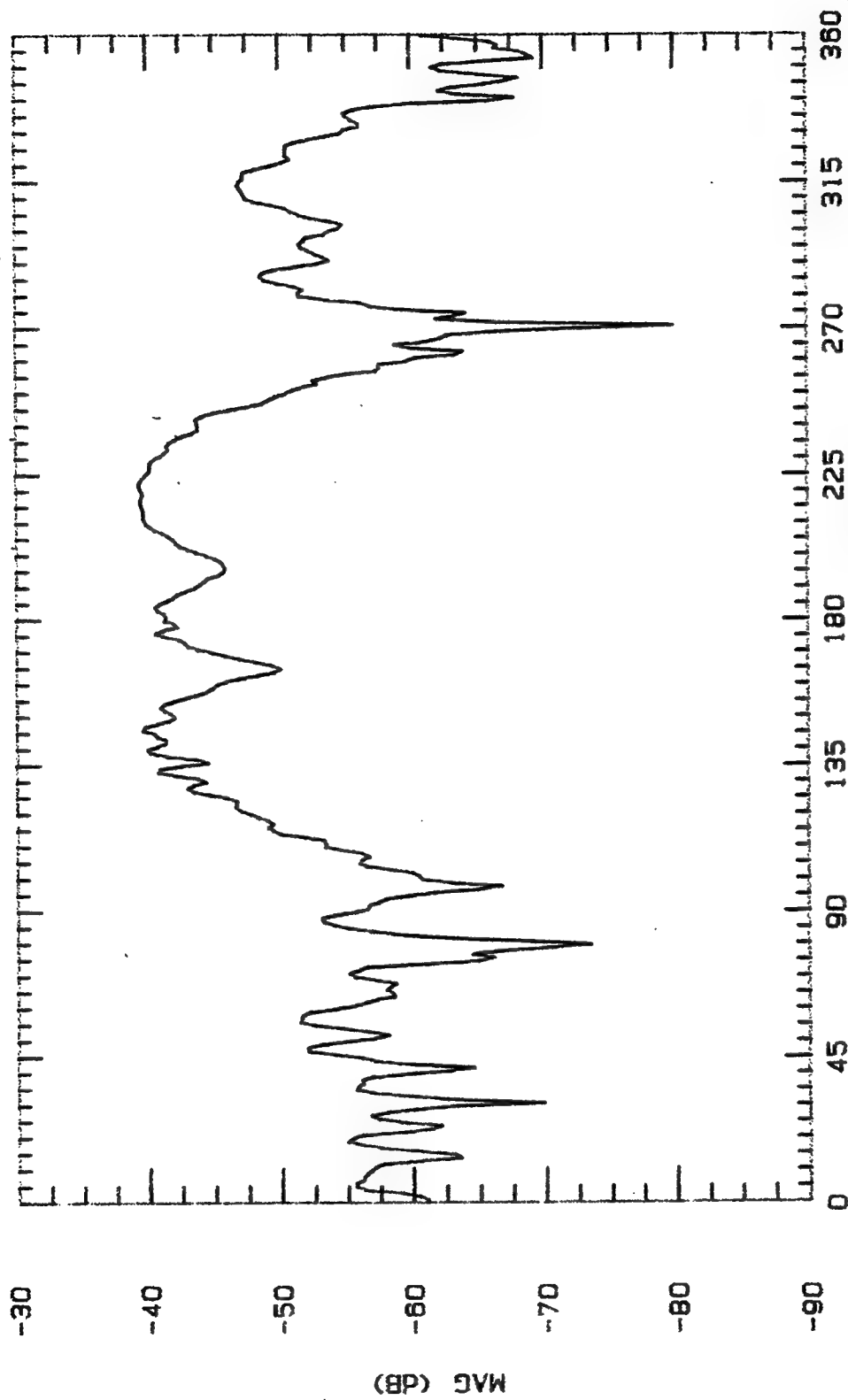
File Name	Frequency	Pattern Type	Date
BLPL925	9.25 GHz	E-PLANE	28 OCT



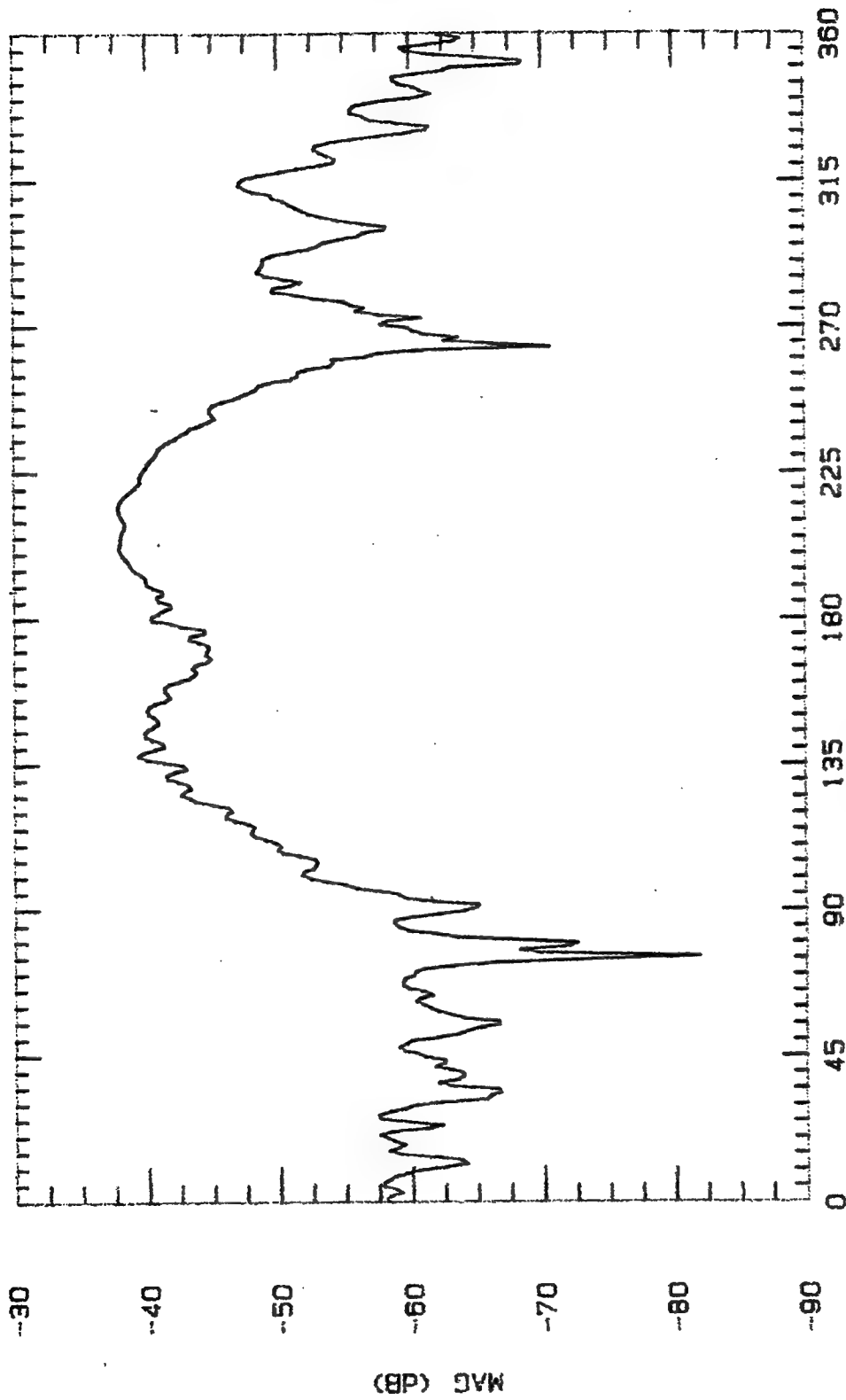
File Name	Frequency	Pattern Type	Date
BLPL950	9.5 GHz	E-PLANE	28 OCT



File Name	Frequency	Pattern Type	Date
BLPL975	9.75 GHz	E-PLANE	28 OCT

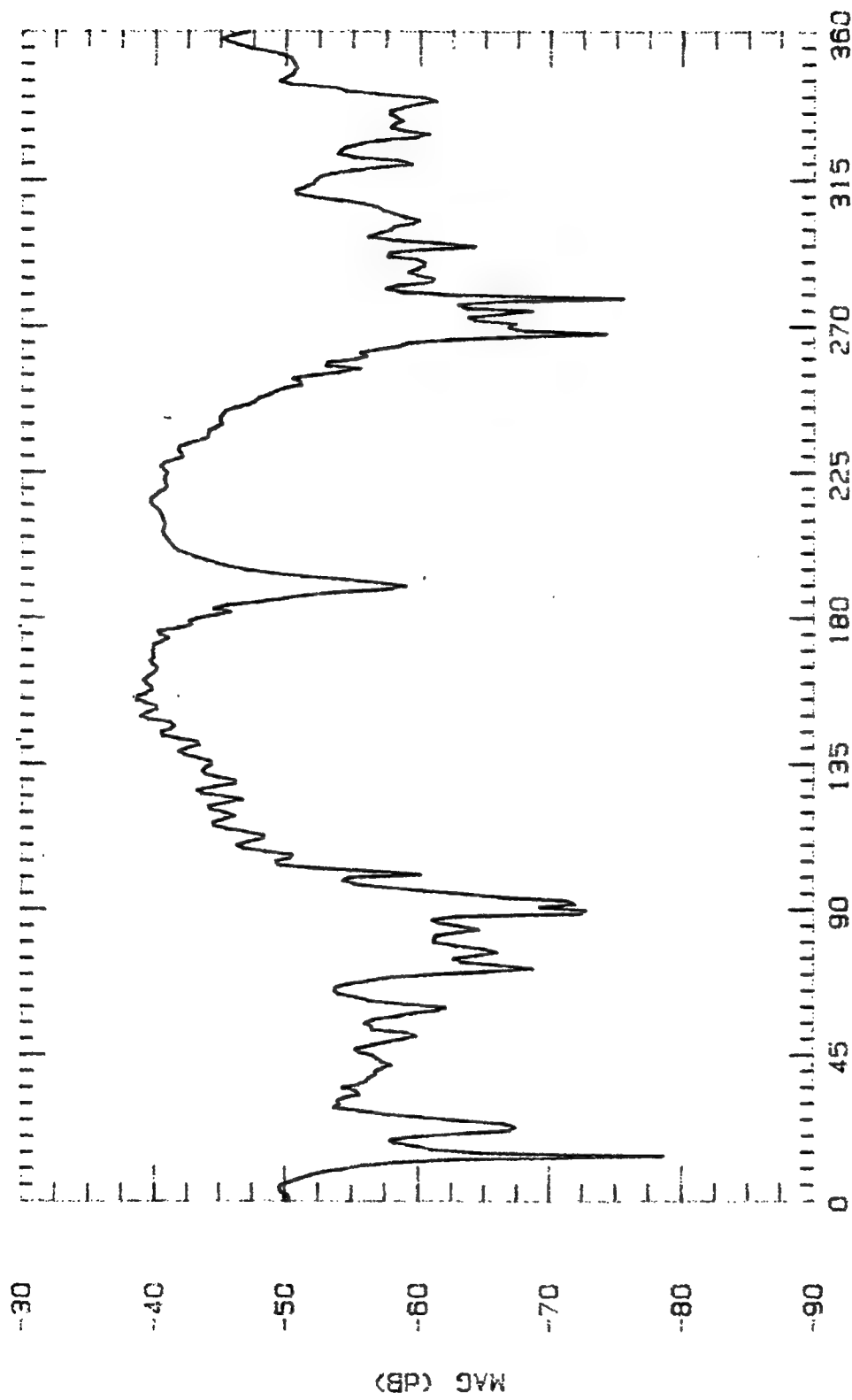


File Name	Frequency	Pattern Type	Date
BLPL1000	10 GHz	E-PLANE	25 OCT

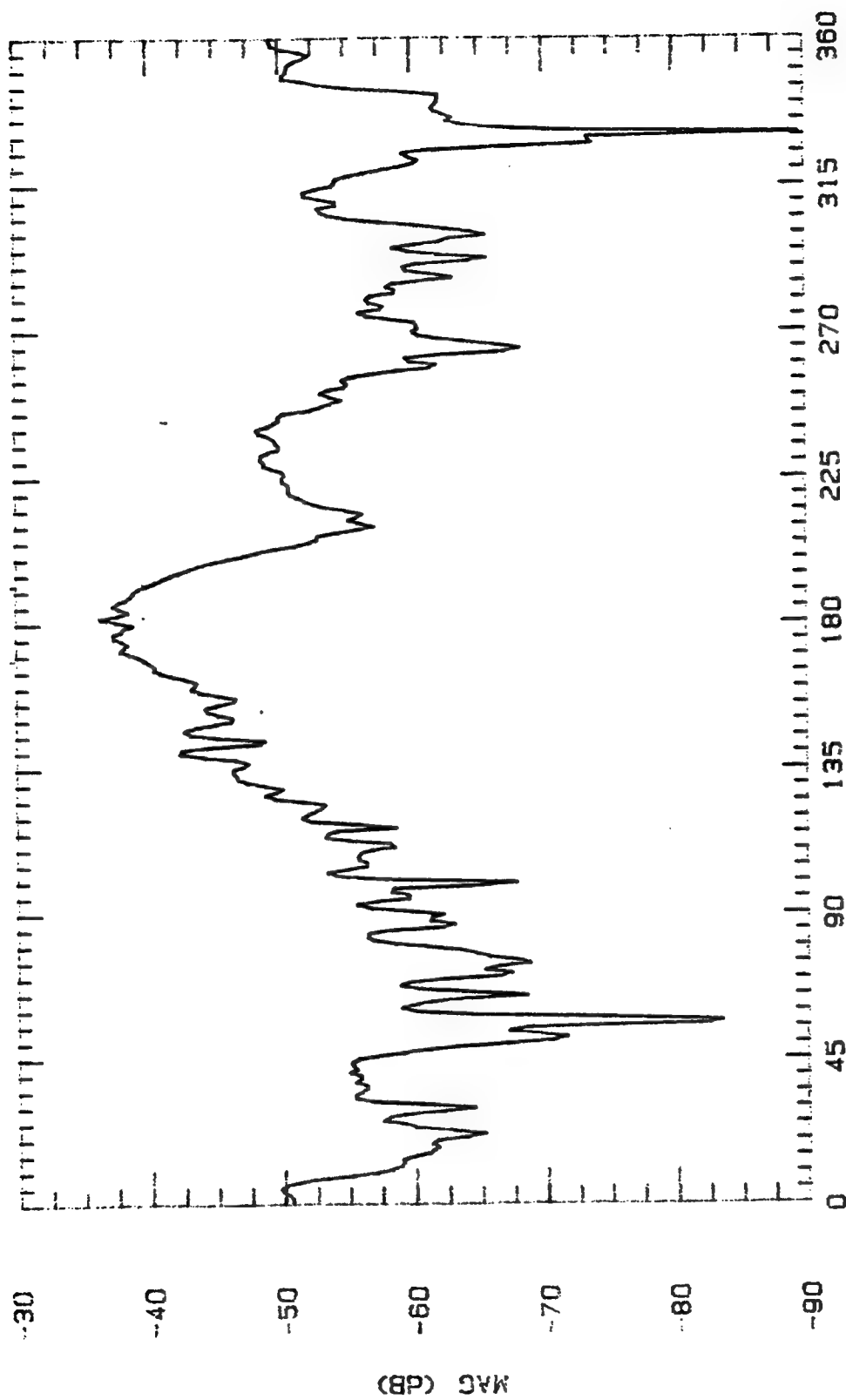


ASPECT ANGLE (DEGREES)

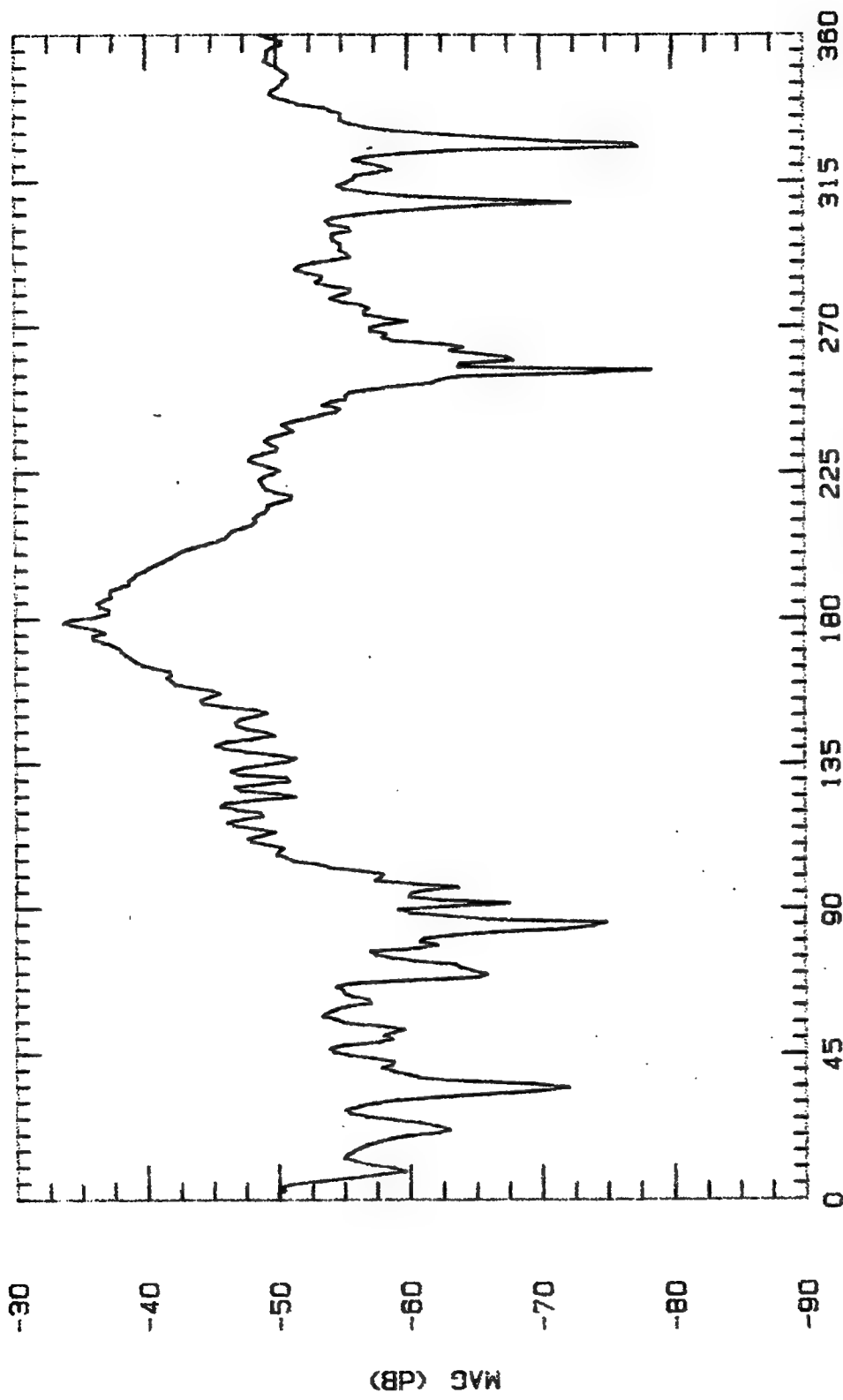
File Name	Frequency	Pattern Type	Date
BLPL1025	10.25 GHz	E-PLANE	25 OCT



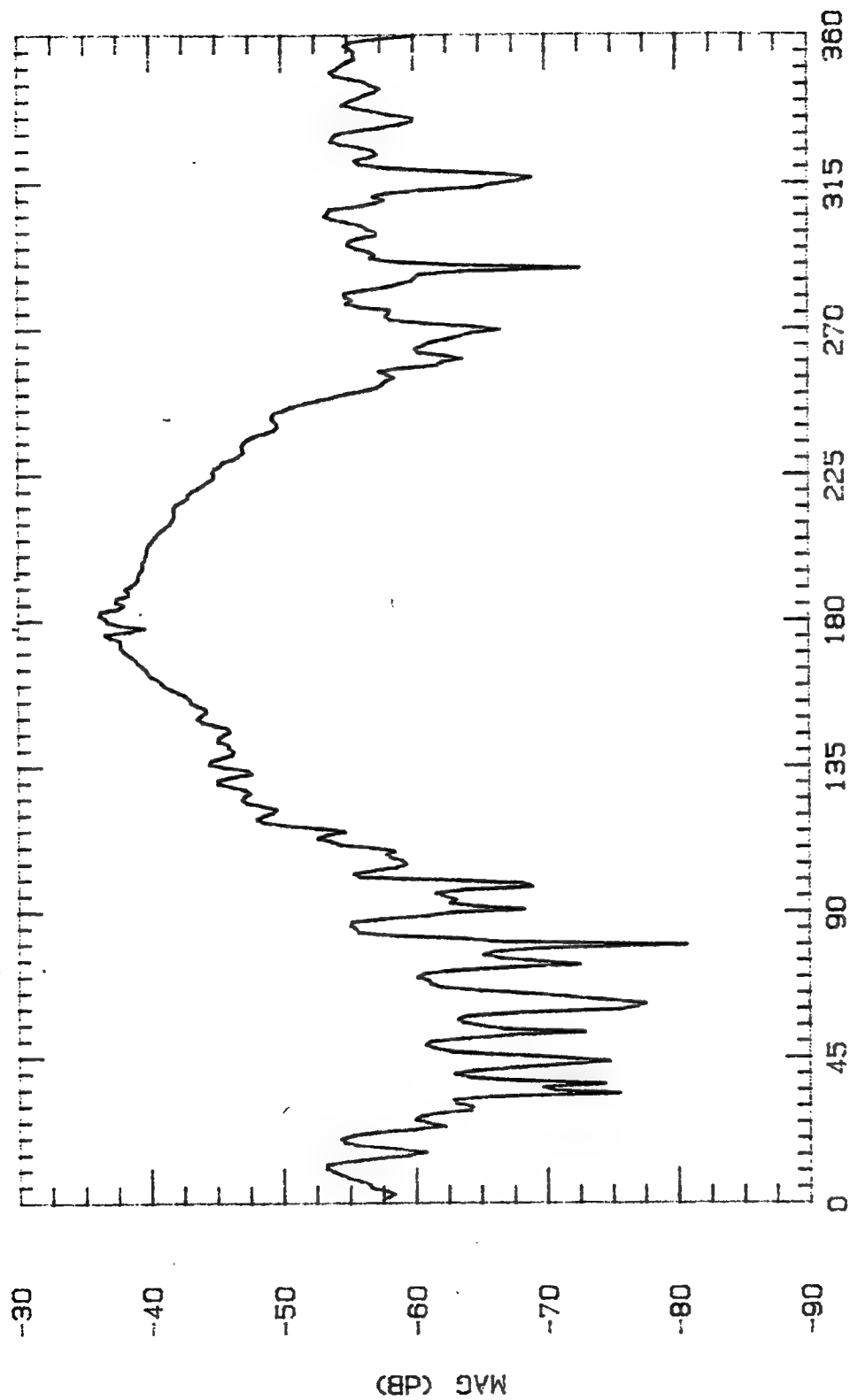
File Name	Frequency	Pattern Type	Date
BLPL1050	10.5 GHz	E-PLANE	28 OCT



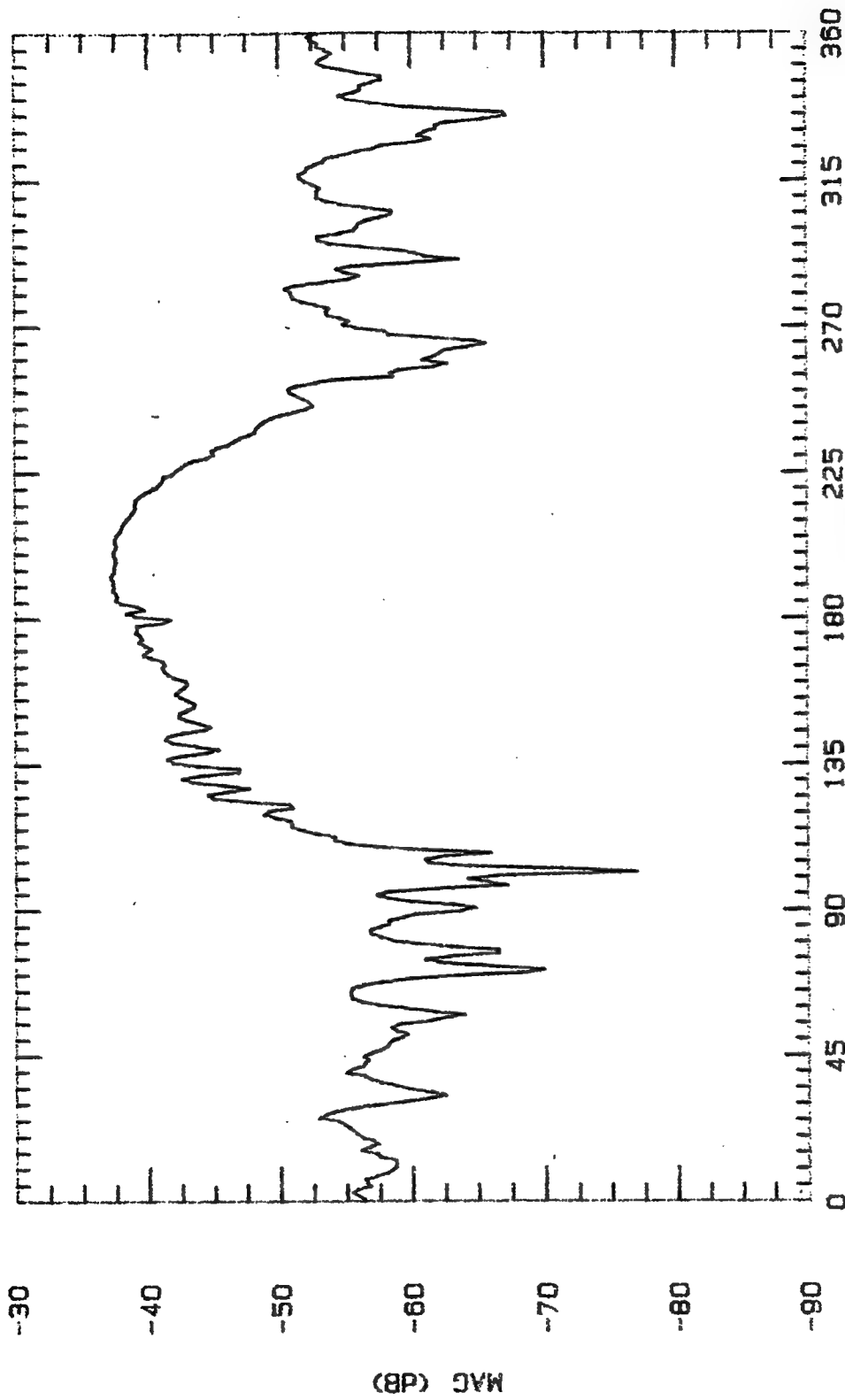
File Name	Frequency	Pattern Type	Date
BLPL1075	10.75 GHz	E-PLANE	28 OCT



File Name	Frequency	Pattern Type	Date
BLPL1100	11 GHz	E-PLANE	25 OCT

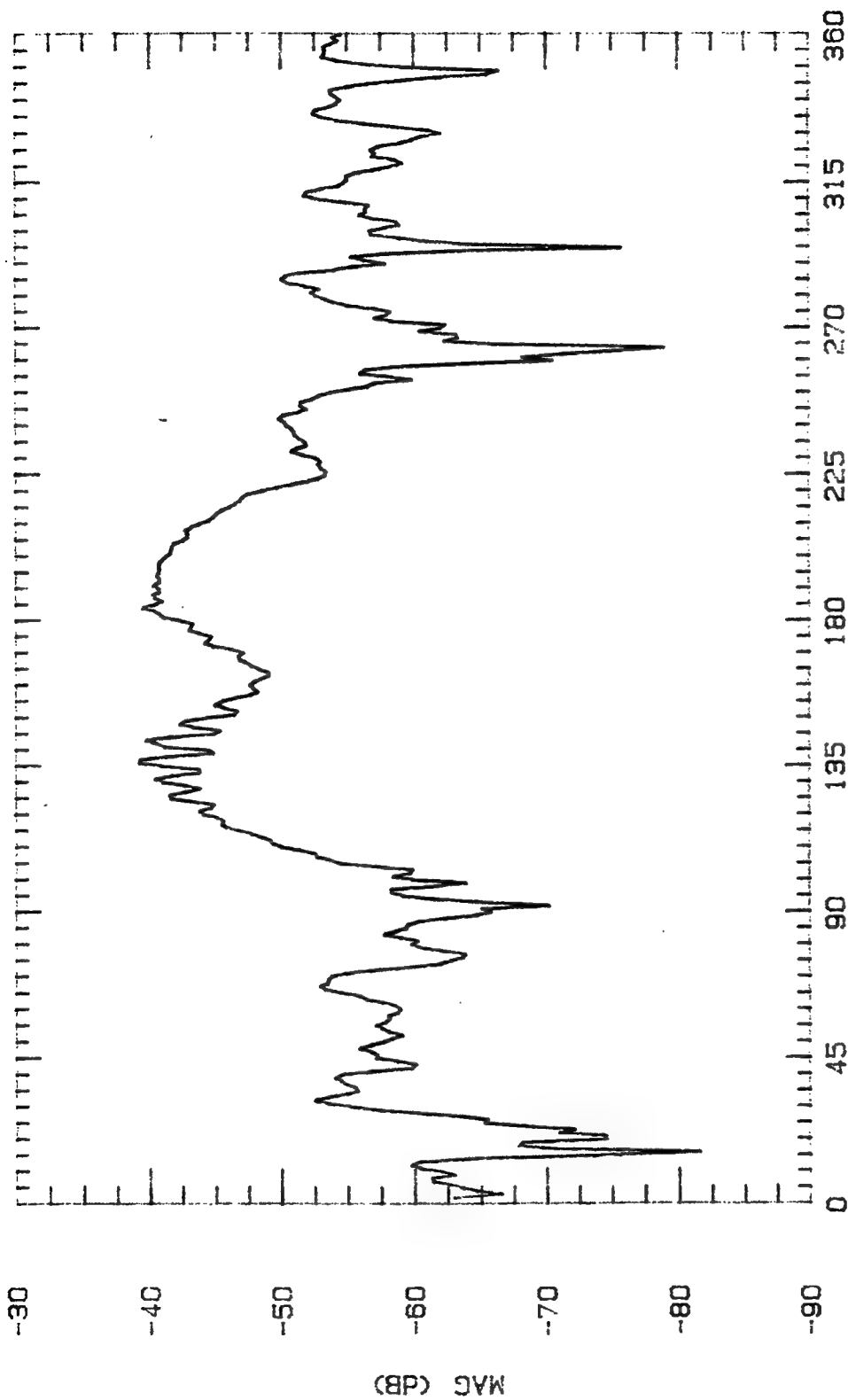


File Name	Frequency	Pattern Type	Date
BLPL1125	11.25 GHz	E-PLANE	28 OCT

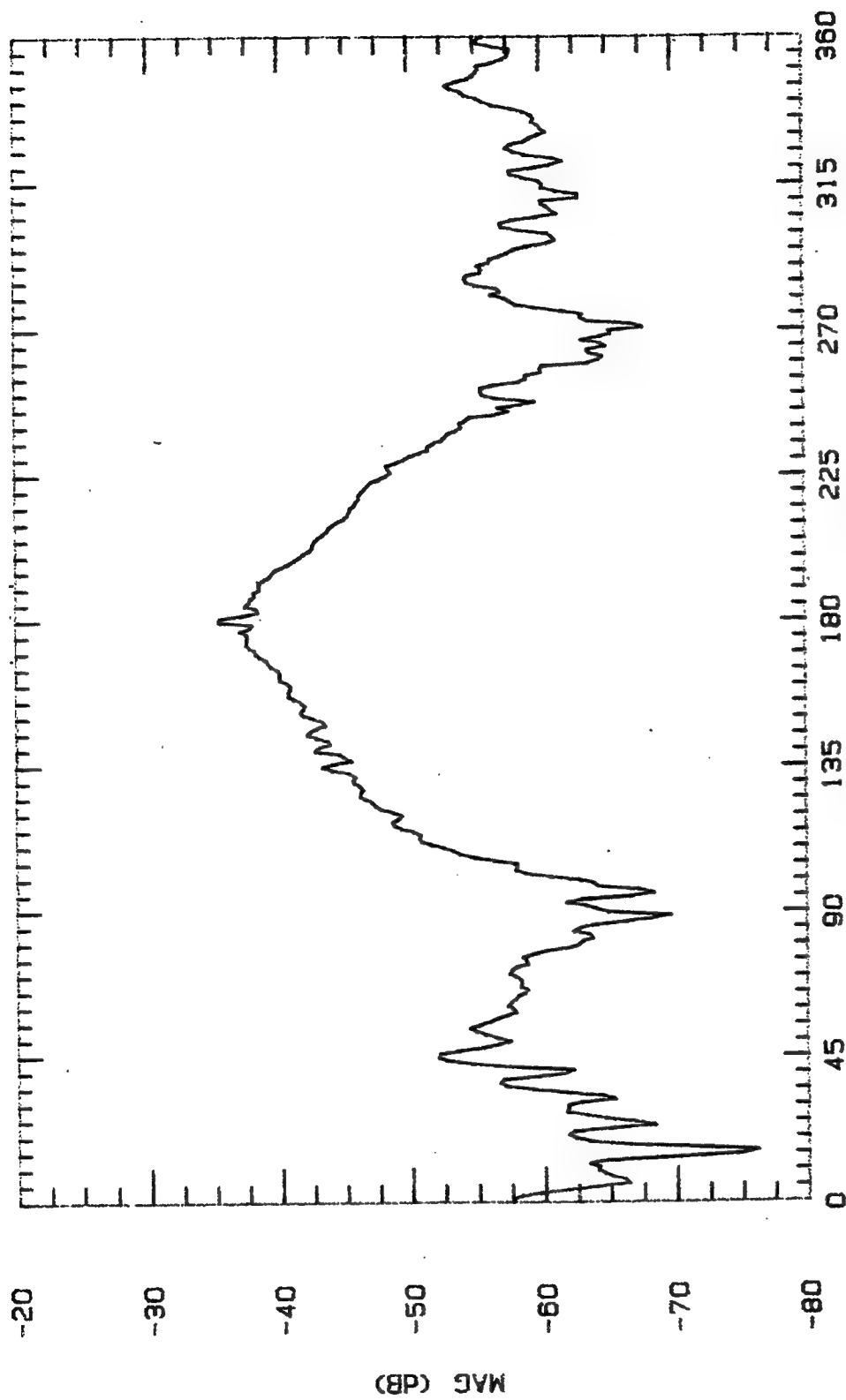


ASPECT ANGLE (DEGREES)

File Name	Frequency	Pattern Type	Date
BLPL1155	11.55 GHz	E-PLANE	25 OCT

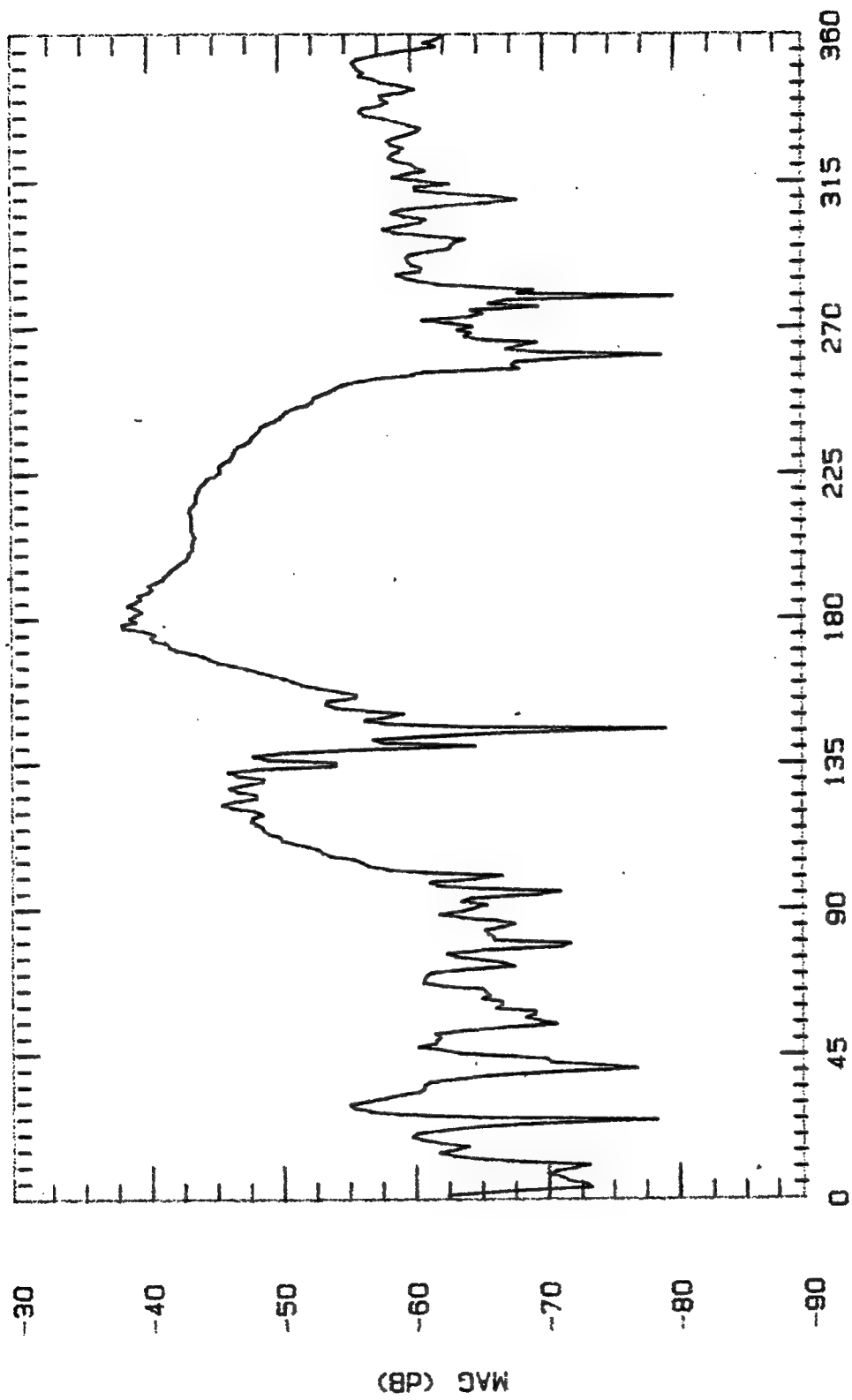


File Name	Frequency	Pattern Type	Date
BLPL1175	11.75 GHz	E-PLANE	28 OCT



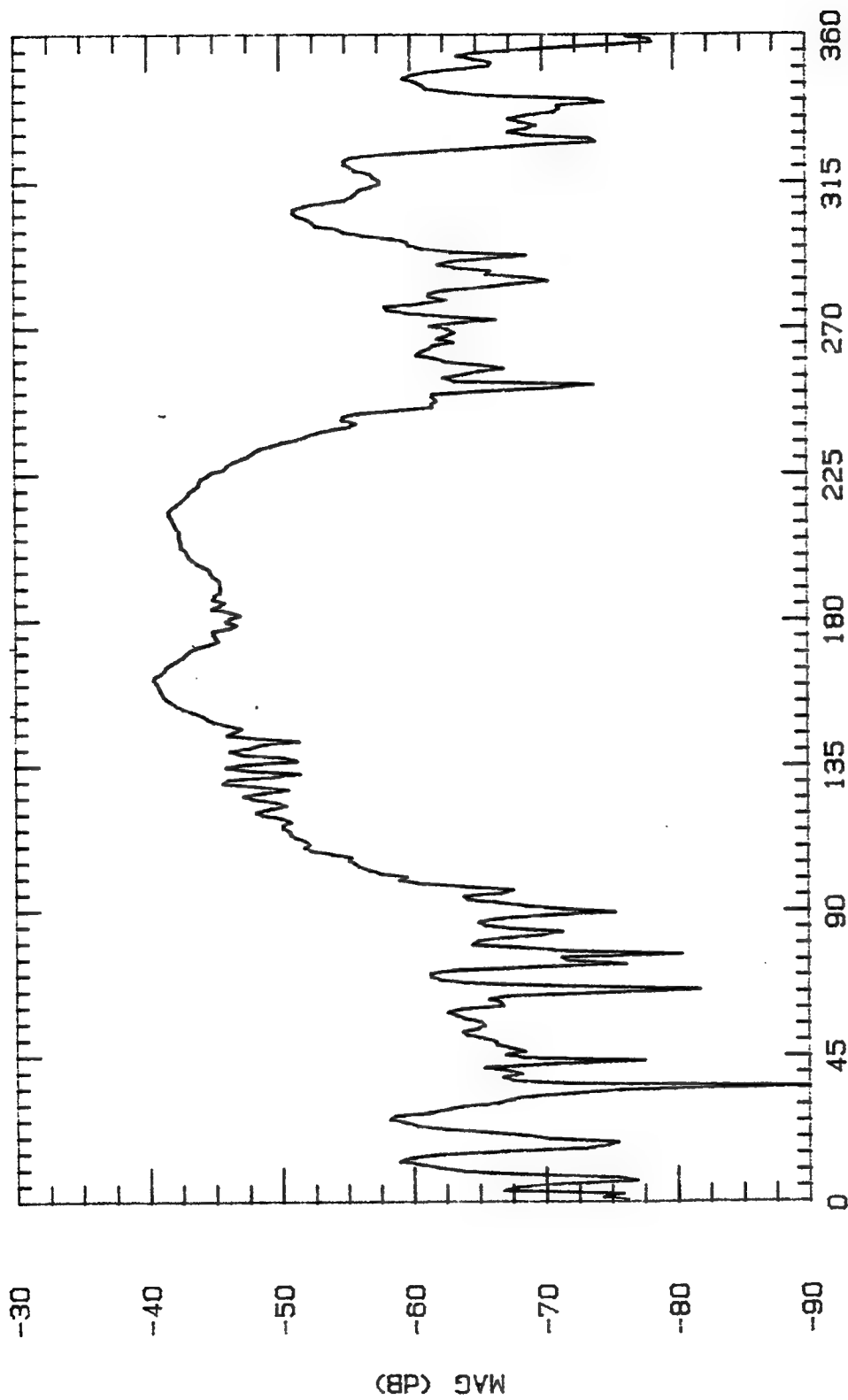
ASPECT ANGLE (DEGREES)

File Name	Frequency	Pattern Type	Date
BLPL1200	12 GHz	E-PLANE	25 OCT



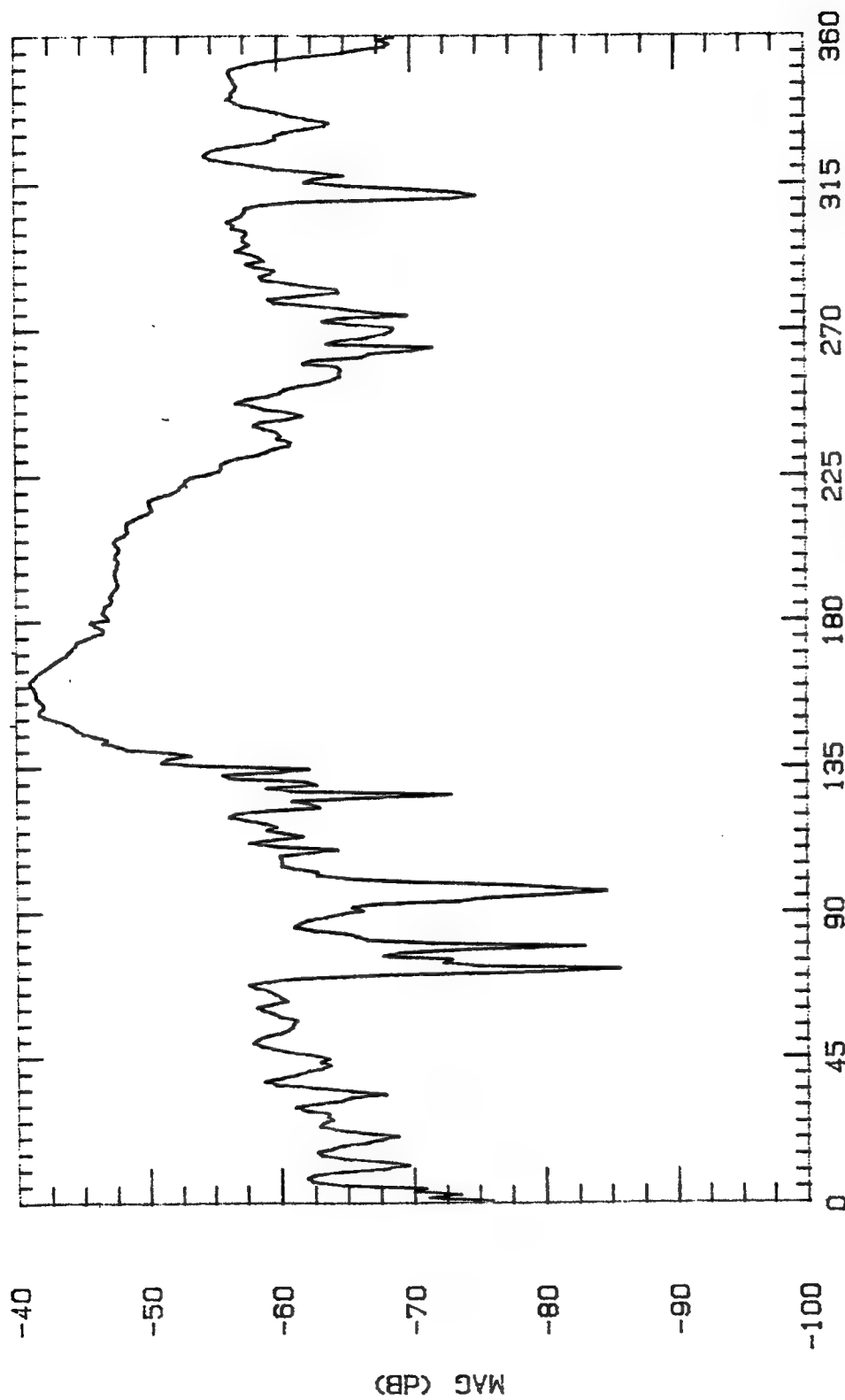
ASPECT ANGLE (DEGREES)

File Name	Frequency	Pattern Type	Date
BLPL1240	12.4 GHz	E-PLANE	25 OCT



ASPECT ANGLE (DEGREES)

File Name	Frequency	Pattern Type	Date
BLPL1275	12.75 GHz	E-PLANE	28 OCT



ASPECT ANGLE (DEGREES)

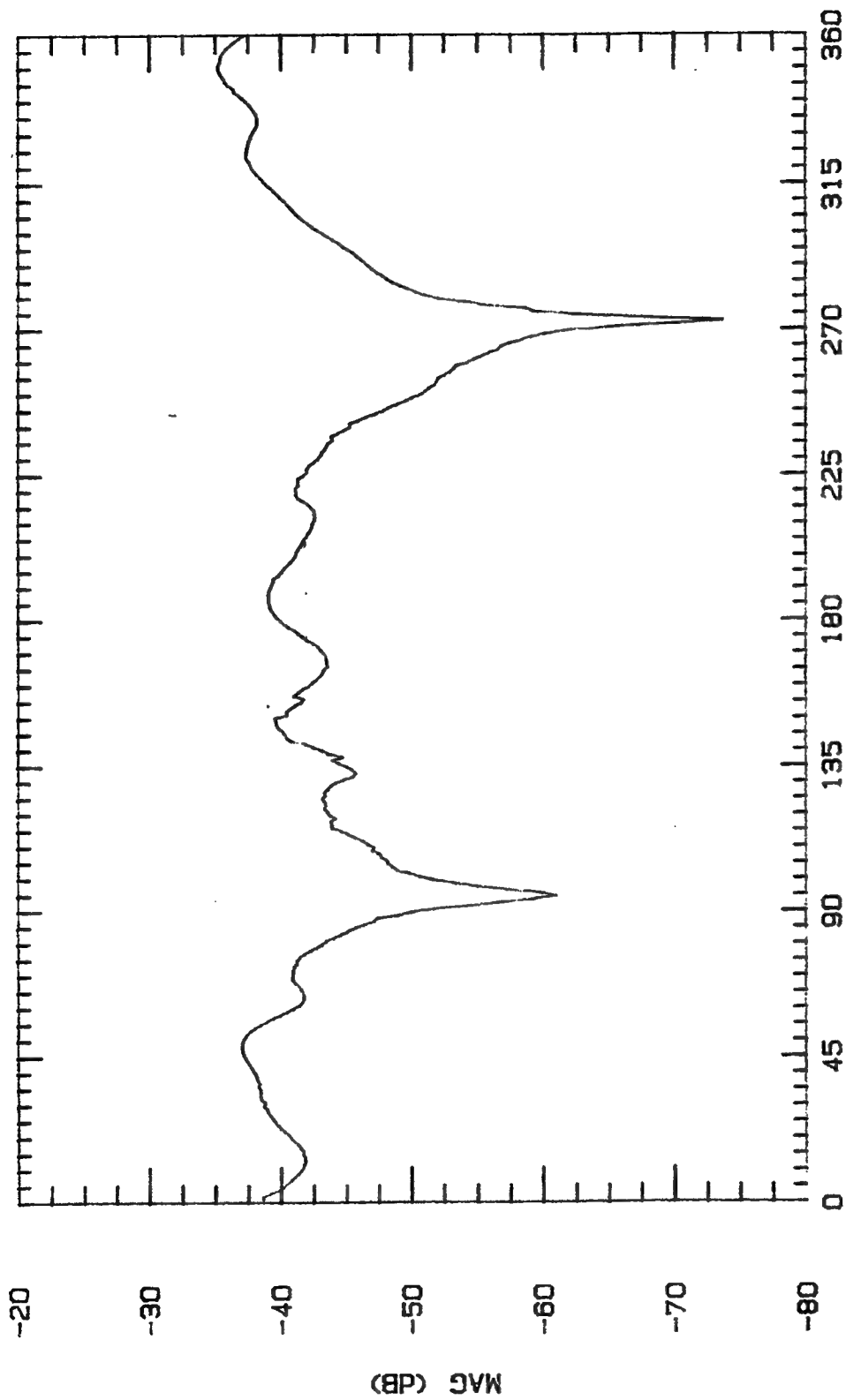
File Name	Frequency	Pattern Type	Date
8LPL1300	13 GHz	E-PLANE	28 OCT 84

APPENDIX L: Antenna Pattern Cuts For 12.4, 7.4, & 3.1 GHz Three Layer Design
(2B, 1S (1 array), 1B, 1S (5 arrays), 6B, 1S (7 arrays), 5B)

Freq (GHz)	Normal Gain (dBi)	Max Gain (dBi)	Squint (deg)	Beamwidth (-3dBi to -3dBi) (deg)
-----	-----	-----	-----	-----
2.00	-24.5	-22.5	7	30
2.25	-19.5	-17.7	3	27
2.50	3.3	3.3	0	65
2.75	1.5	3.4	8	62
3.00	5.6	5.6	0	55
3.25	-5.6	-4.5	20	63
3.50	-15.1	-6.1	-34	42
3.75	0.1	0.1	0	35
4.00	-2.8	-1.3	9	56
4.25	-7.2	-6.1	3	35
4.50	5.7	5.7	0	52
4.75	1.6	2.1	-8	45
5.00	1.3	1.4	0	75
5.25	-3.2	-2.2	-5	90
5.50	-0.9	3.7	-5	57
5.75	4.8	5.1	-3	55
6.00	1.1	1.4	-7	68
6.25	-1.9	1.3	-3	44
6.50	-0.6	1.1	22	75
6.75	3.1	3.5	-10	60
7.00	-3.5	1.8	-36	37
7.25	-4.8	-0.1	-40	33
7.50	-12.5	3.2	45	35
7.75	-3.2	-1.5	2	45
8.00	-2.6	-1.6	25	57
8.25	-4.6	-3.6	-5	58
8.50	0.4	0.4	0	45
8.75	-3.4	-0.4	5	47
9.00	-9.3	-3.3	17	30
9.25	6.9	7.4	5	32
9.50	-0.2	0.8	2	41
9.75	-0.3	0.7	17	27
10.00	-2.4	1.1	20	38
10.25	8.7	-1.8	25	27
10.50	-0.1	0.2	2	18
10.75	-5.6	-2.1	50	86
11.00	-0.6	-0.6	0	22

APPENDIX L (Continued)

11.25	-4.2	-2.5	2	60
11.50	-4.6	-0.6	20	38
11.75	-13.2	-4.4	38	18
12.00	1.7	1.7	0	56
12.25	4.0	5.3	-27	58
12.50	-5.2	-2.0	-27	23
12.75	1.1	2.1	4	25
13.00	2.0	2.0	0	22



File Name

Frequency

Pattern Type

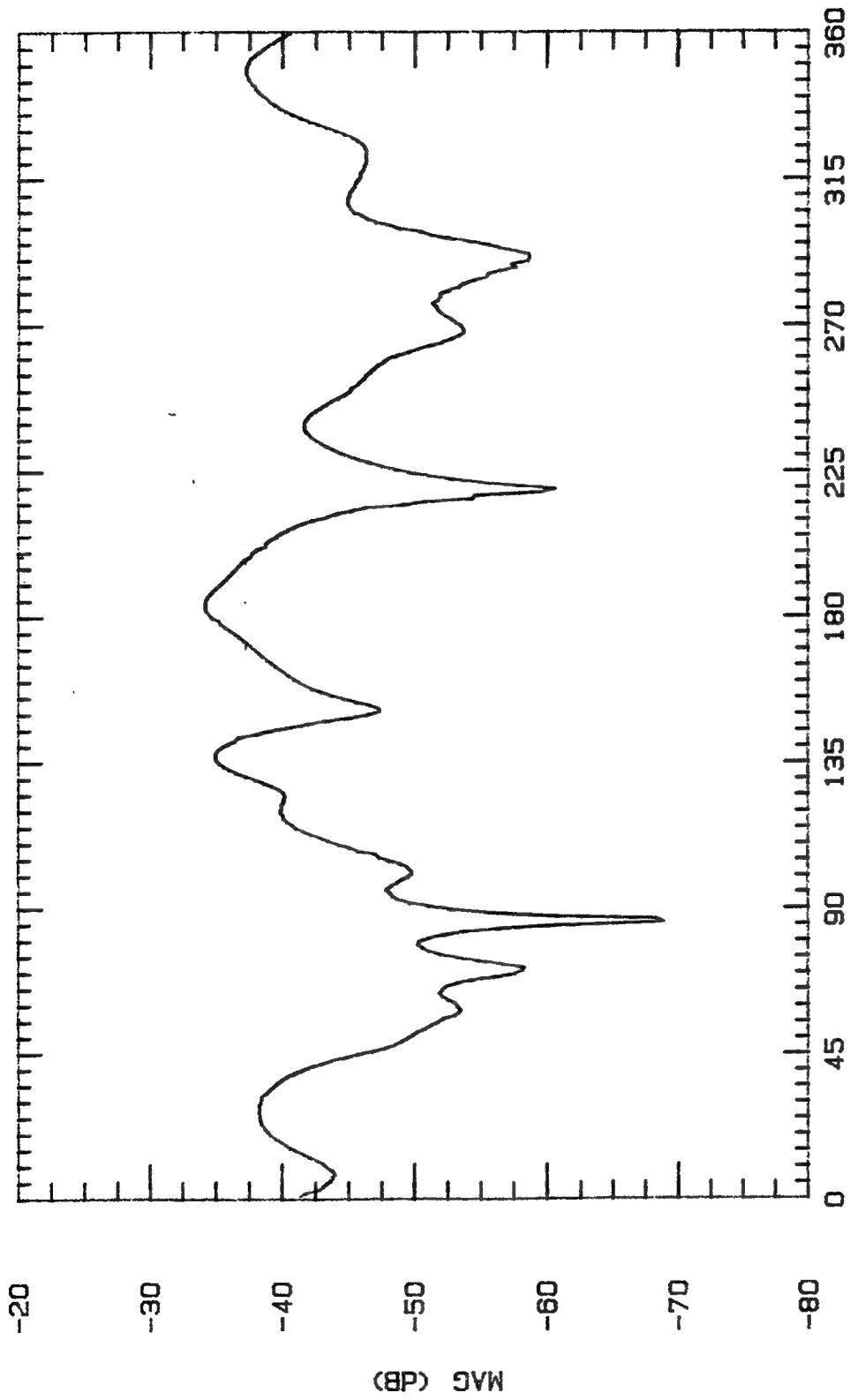
Date

3ALPL200

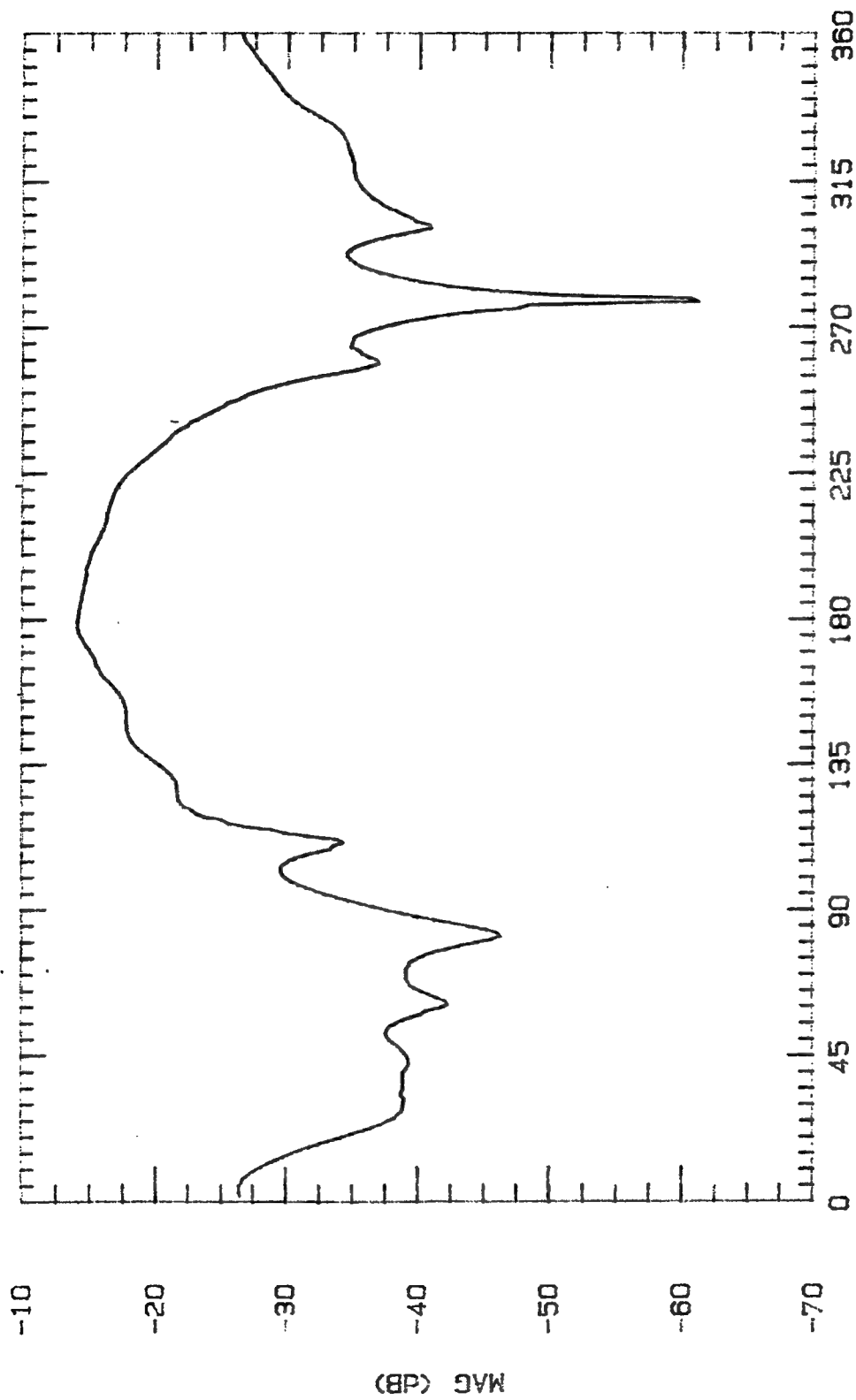
2 GHz

E-PLANE

29 OCT 94

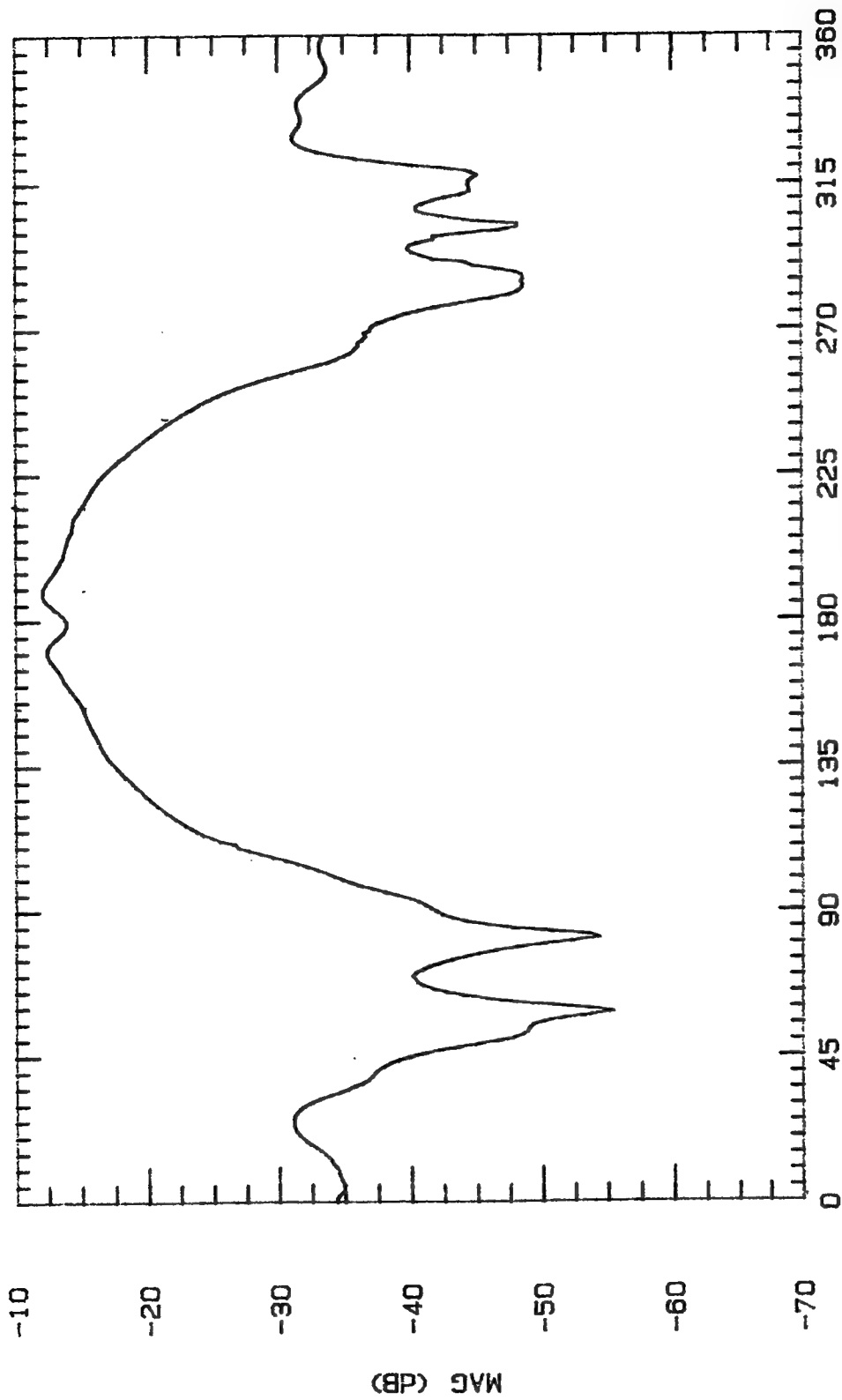


File Name	Frequency	Pattern Type	Date
3ALPL225	2.25 GHz	E-PLANE	28 OCT 94

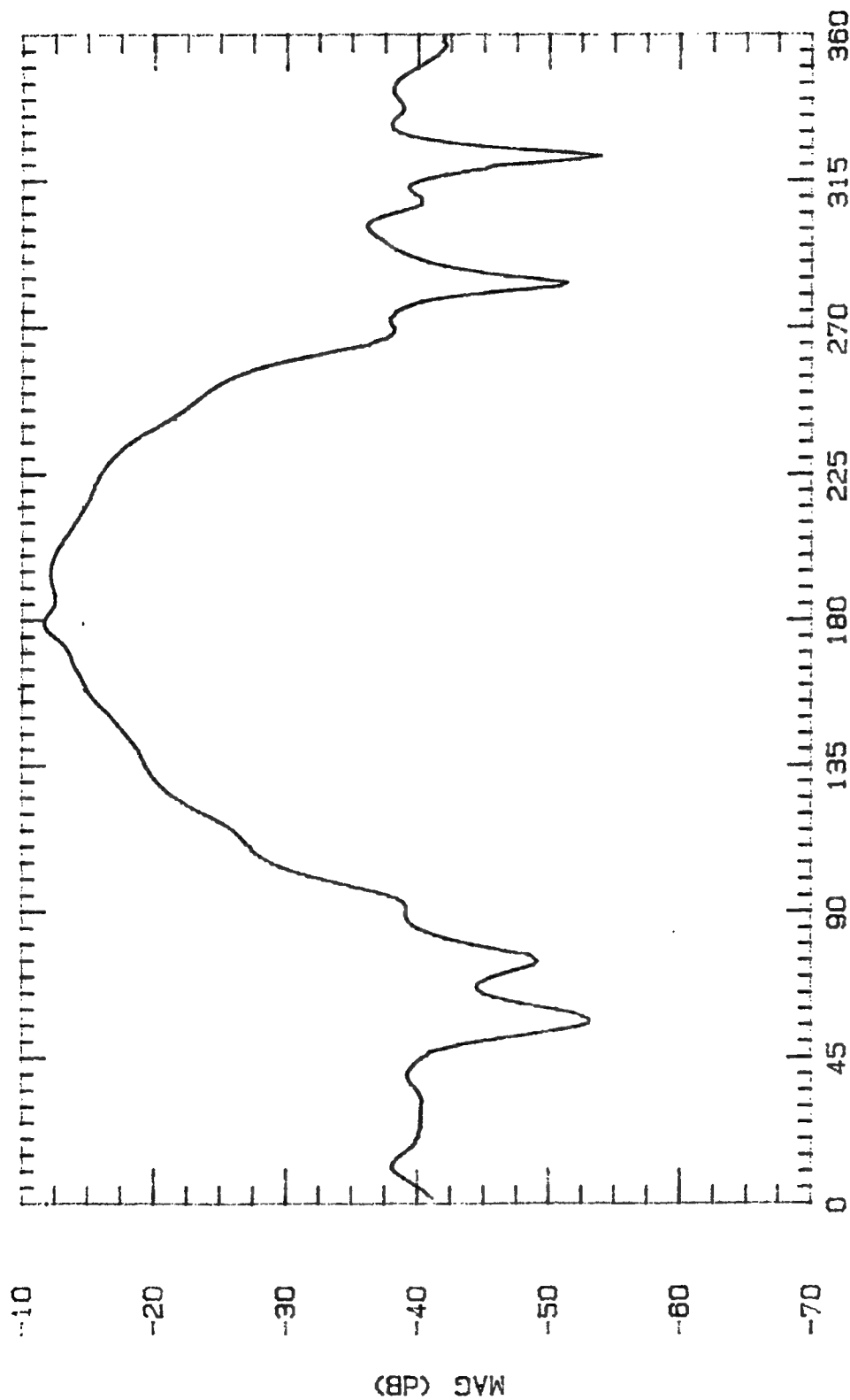


ASPECT ANGLE (DEGREES)

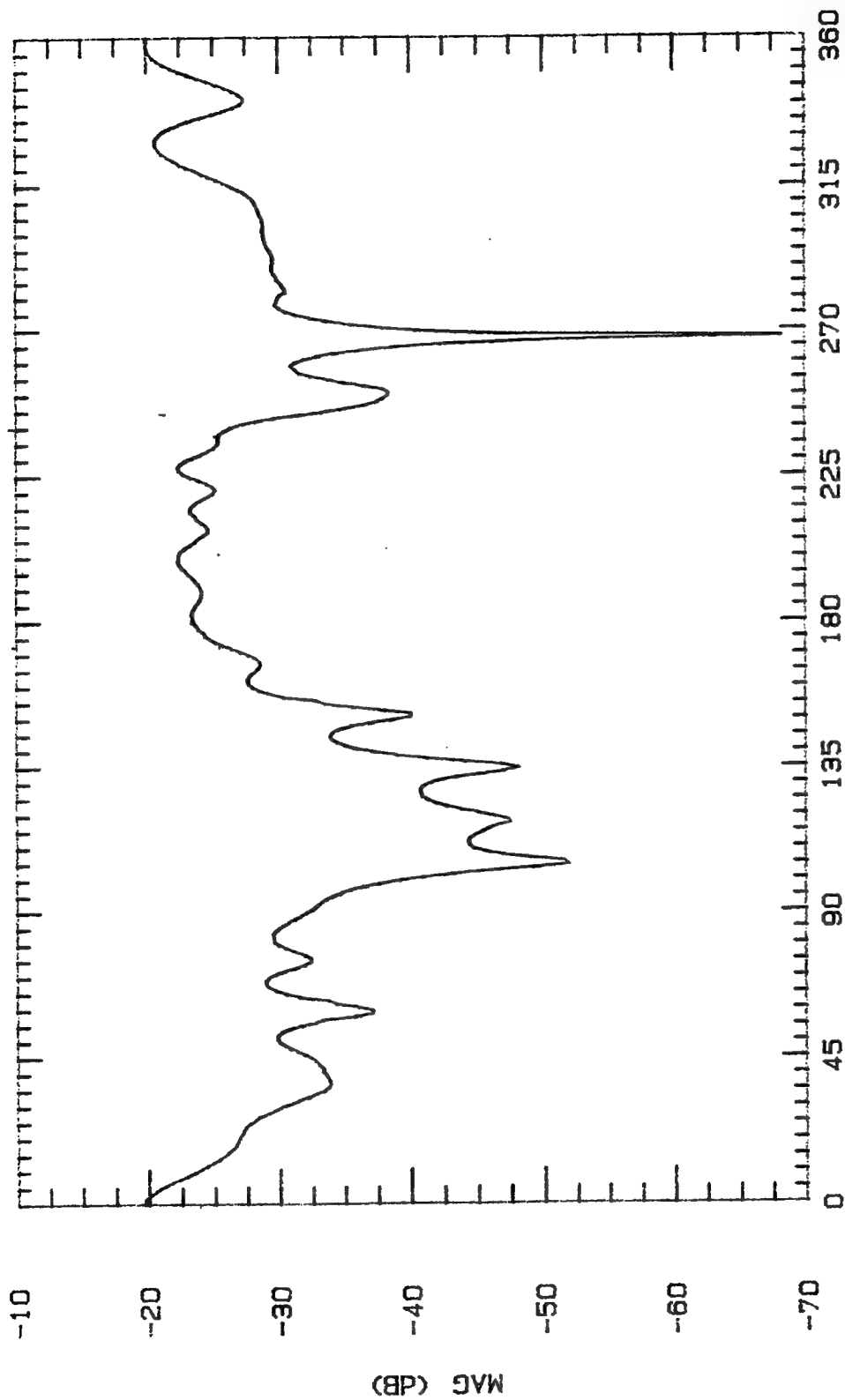
File Name	Frequency	Pattern Type	Date
3ALPL250	2.5 GHz	L-PLANE	29 OCT 94



File Name	Frequency	Pattern Type	Date
3ALPL275	2.75 GHz	E-PLANE	28 OCT 84

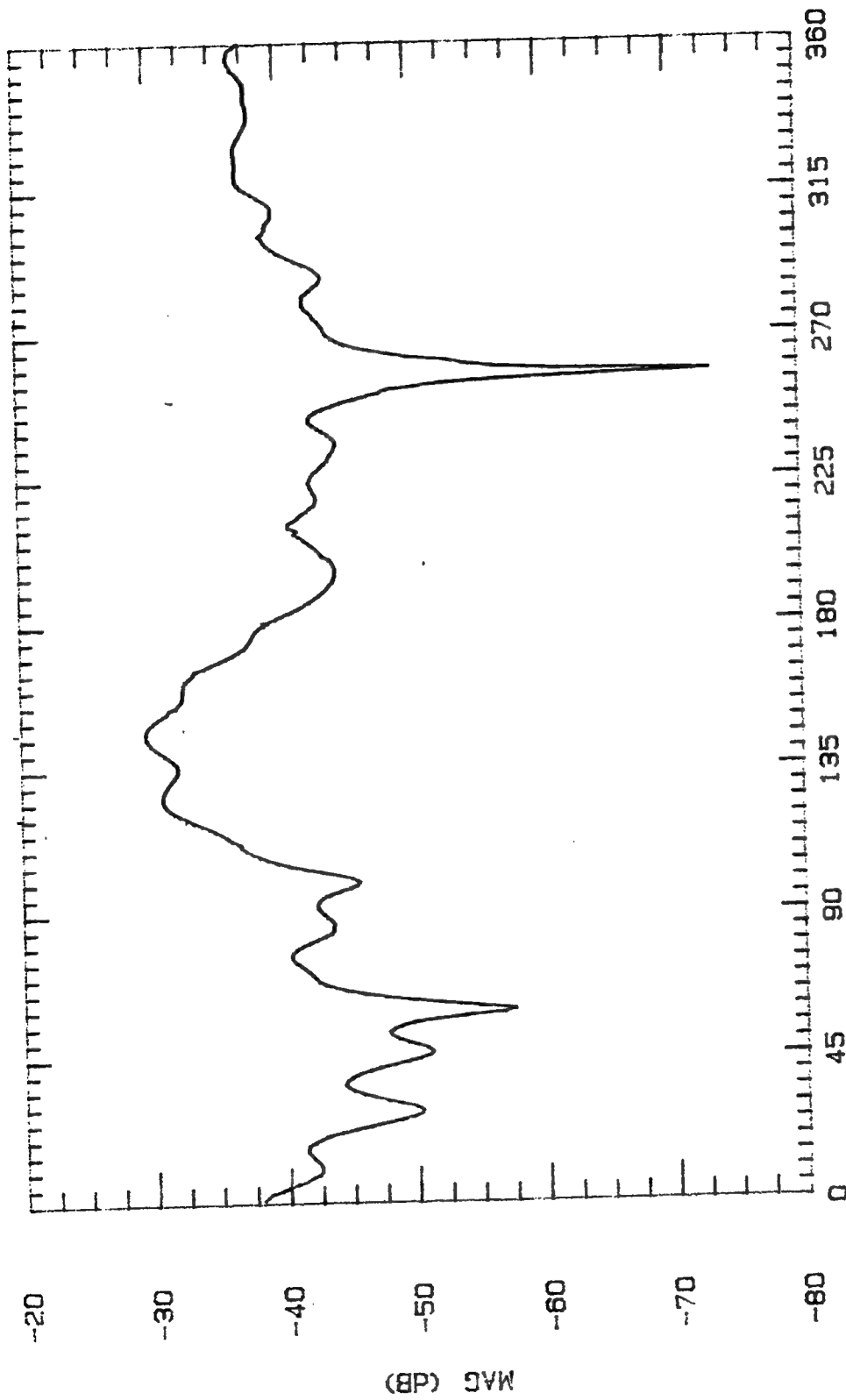


File Name	Frequency	Pattern Type	Date
3ALPL300	3 GHz	E-PLANE	29 OCT 94

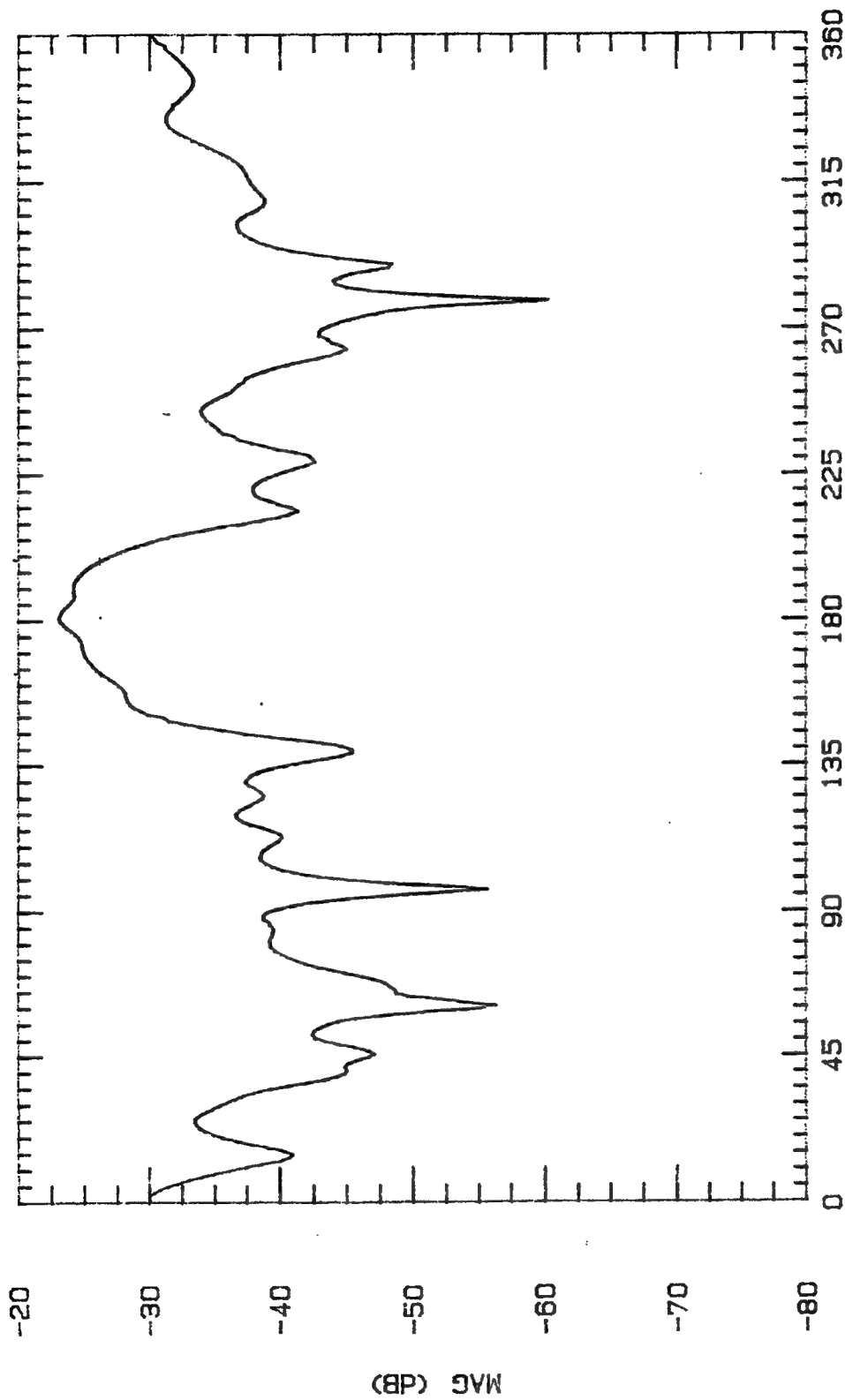


ASPECT ANGLE (DEGREES)

File Name	Frequency	Pattern Type	Date
3ALPL325	3.25 GHz	E-PLANE	28 OCT 94

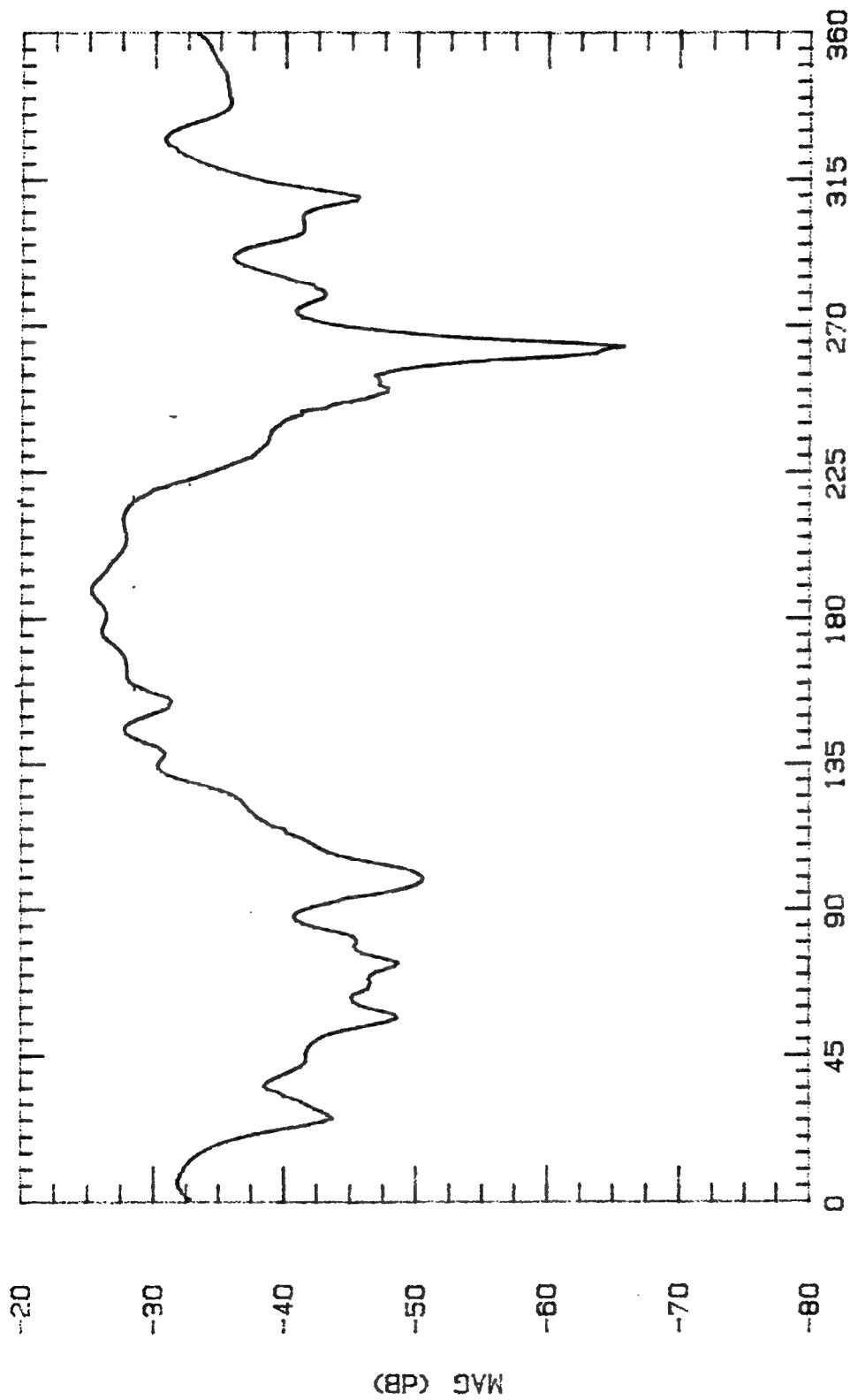


File Name	Frequency	Pattern Type	Date
9ALPL350	3.5 GHz	E-PLANE	28 OCT 94



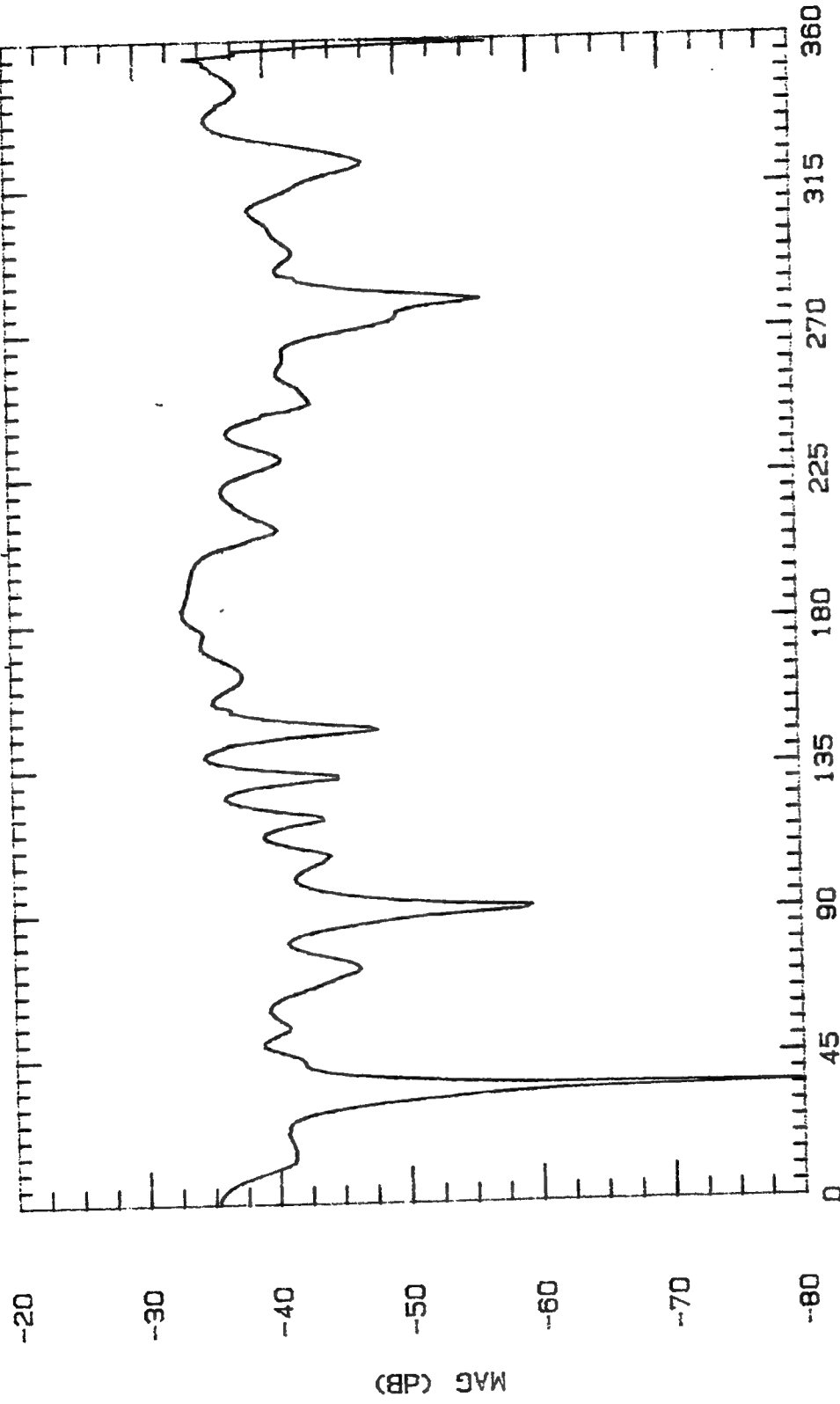
ASPECT ANGLE (DEGREES)

File Name	Frequency	Pattern Type	Date
3ALPL375	3.75 GHz	E-PLANE	28 OCT 94



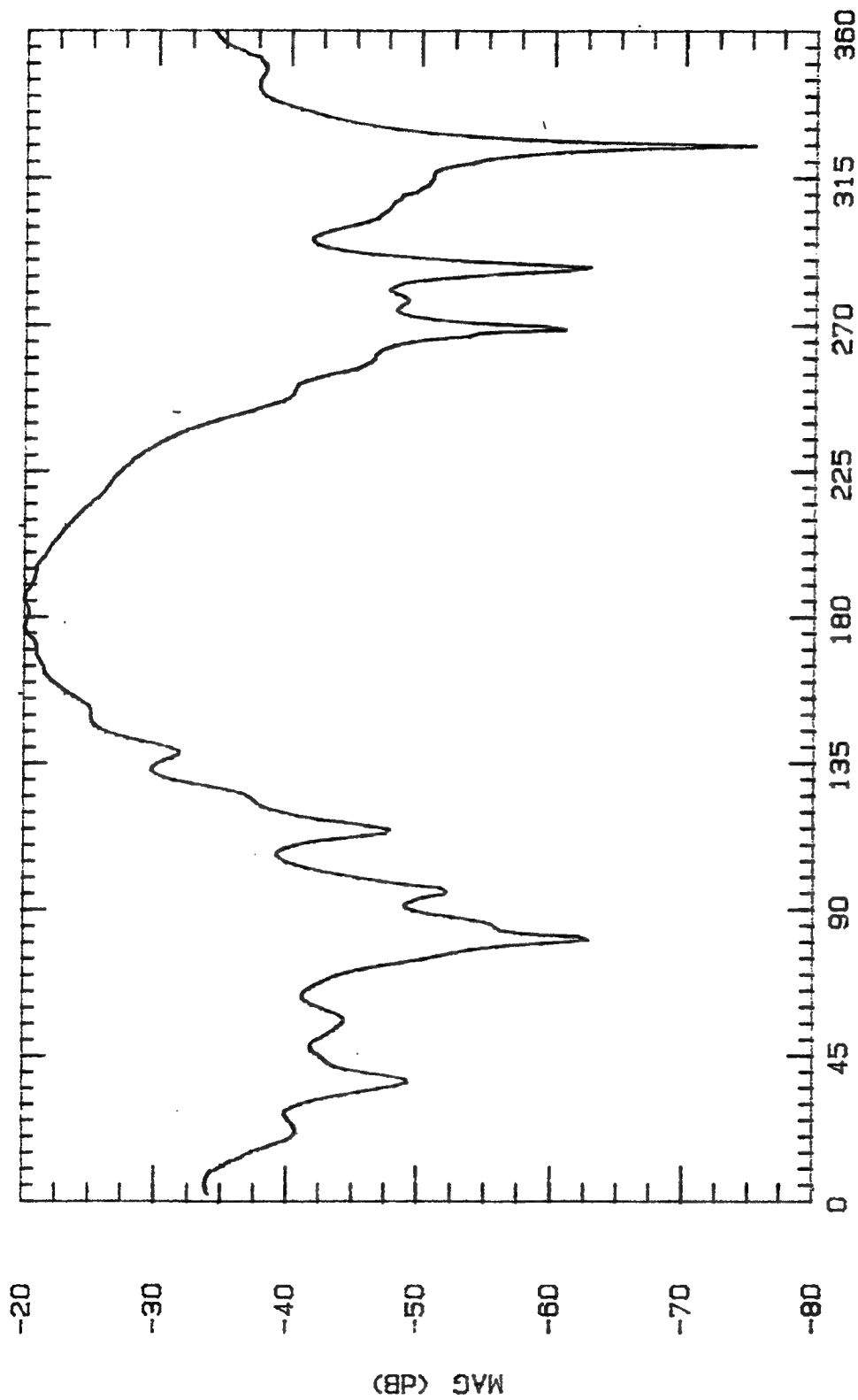
ASPECT ANGLE (DEGREES)

File Name	Frequency	Pattern Type	Date
3ALPL400	4 GHz	E-PLANE	29 OCT 94



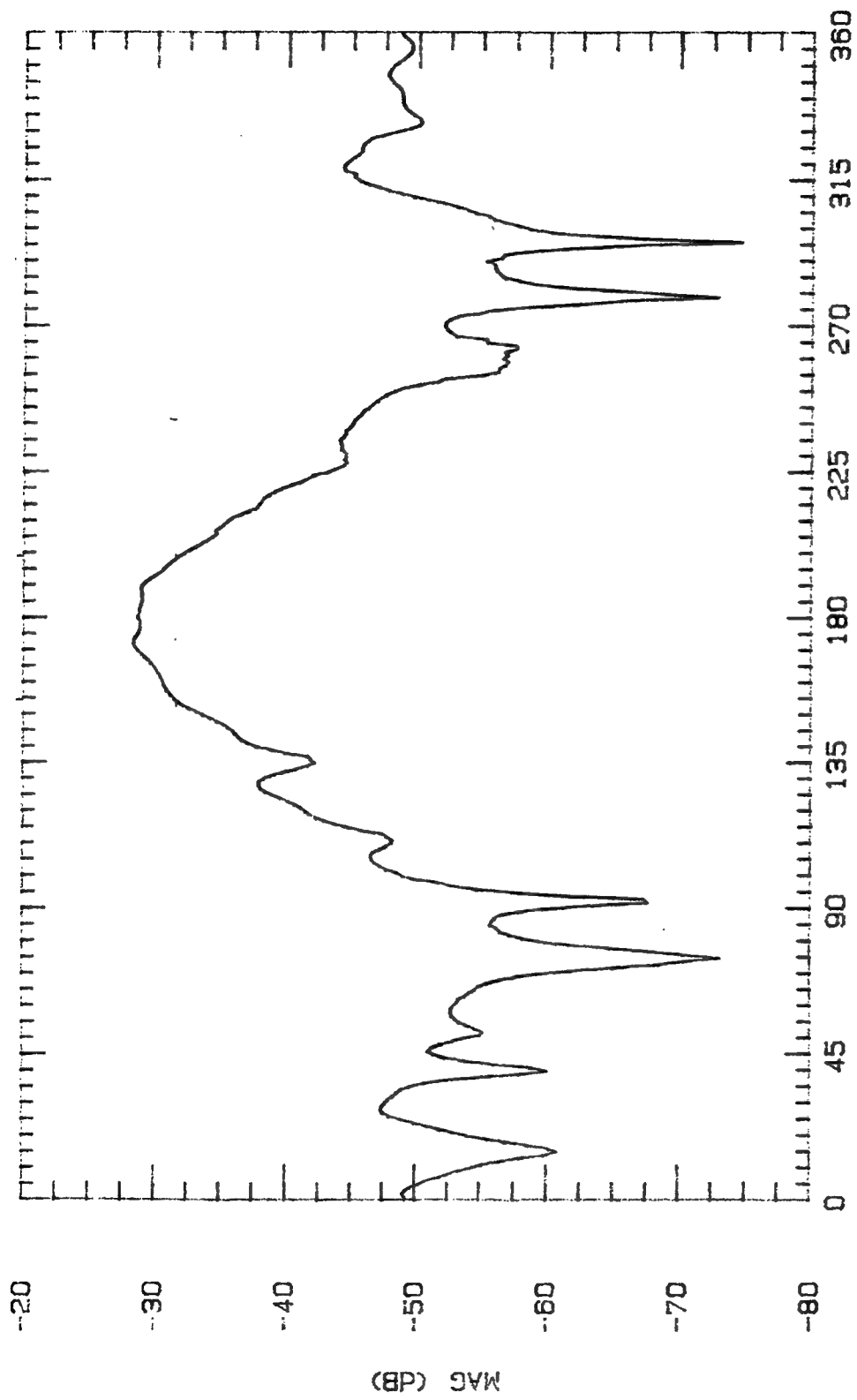
ASPECT ANGLE (DEGREES)

File Name	Frequency	Pattern Type	Date
3ALPL425	4.25 GHz	E-PLANE	28 OCT 94



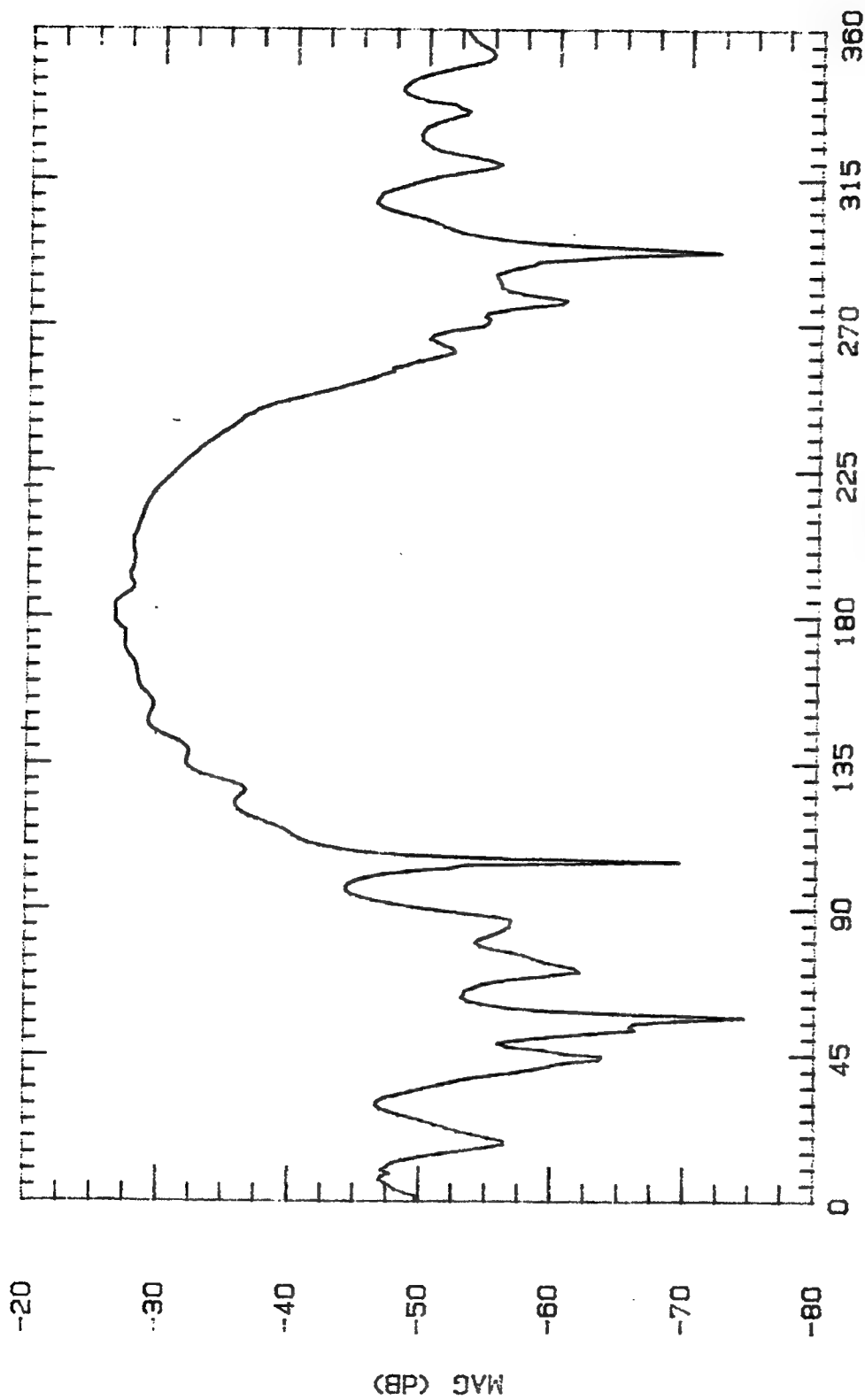
ASPECT ANGLE (DEGREES)

File Name	Frequency	Pattern Type	Date
3ALPL450	4.5 GHz	E-PLANE	27 OCT



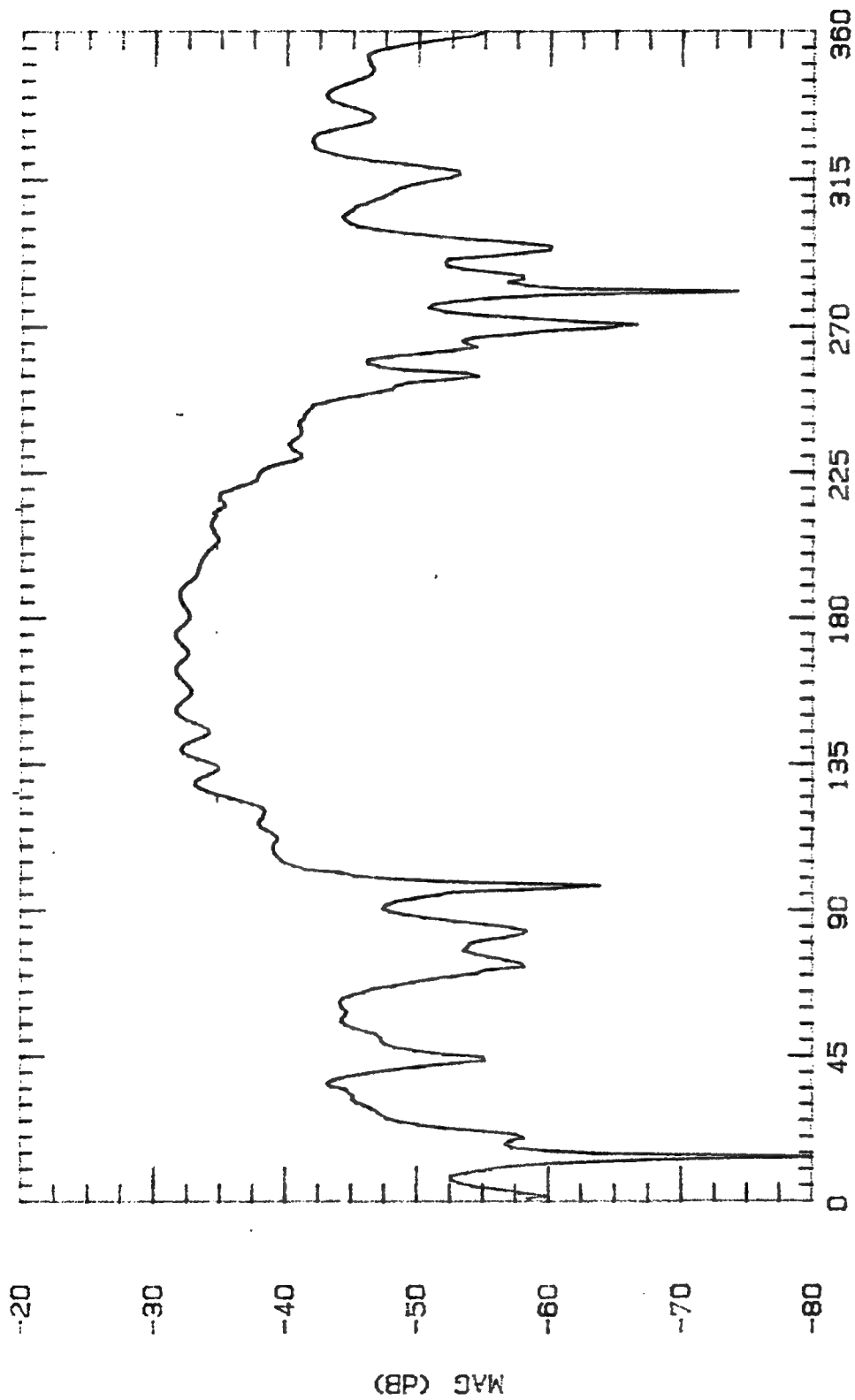
ASPECT ANGLE (DEGREES)

File Name	Frequency	Pattern Type	Date
3ALPL475	4.75 GHz	E-PLANE	28 OCT 94



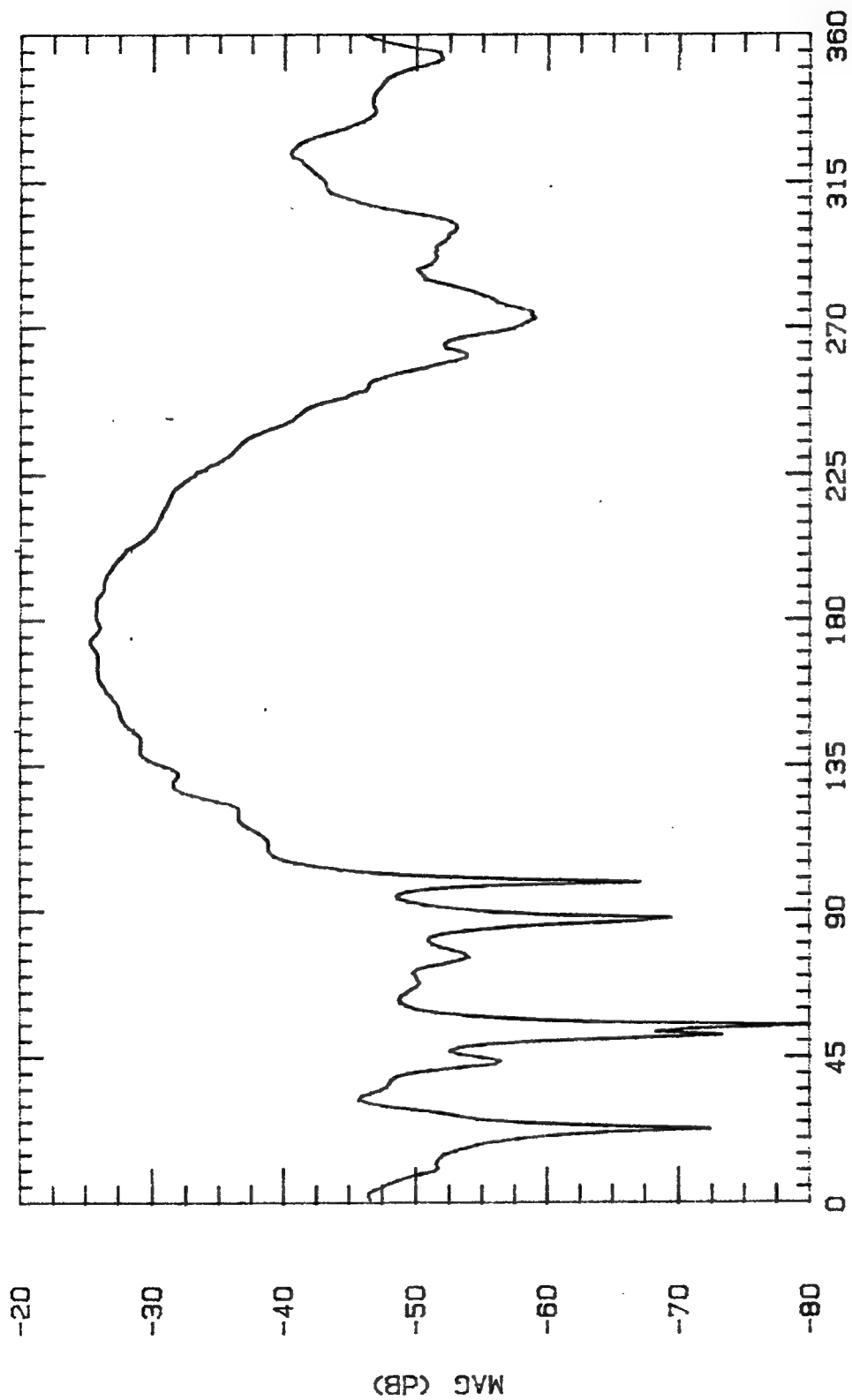
ASPECT ANGLE (DEGREES)

File Name	Frequency	Pattern Type	Date
3ALPL500	5 GHz	E-PLANE	29 OCT 94

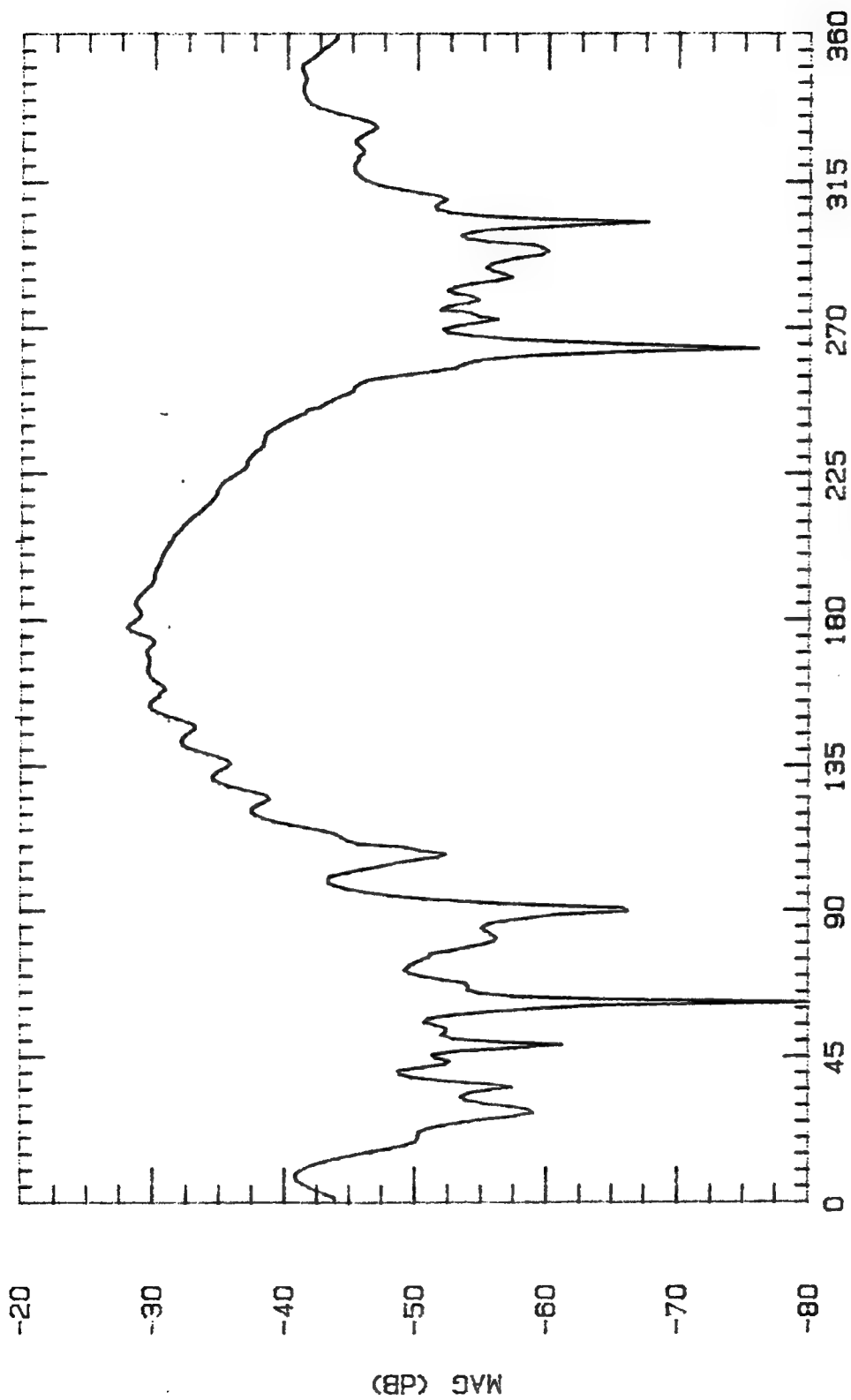


ASPECT ANGLE (DEGREES)

File Name	Frequency	Pattern Type	Date
3ALPL525	5.25 GHz	E-PLANE	28 OCT 94

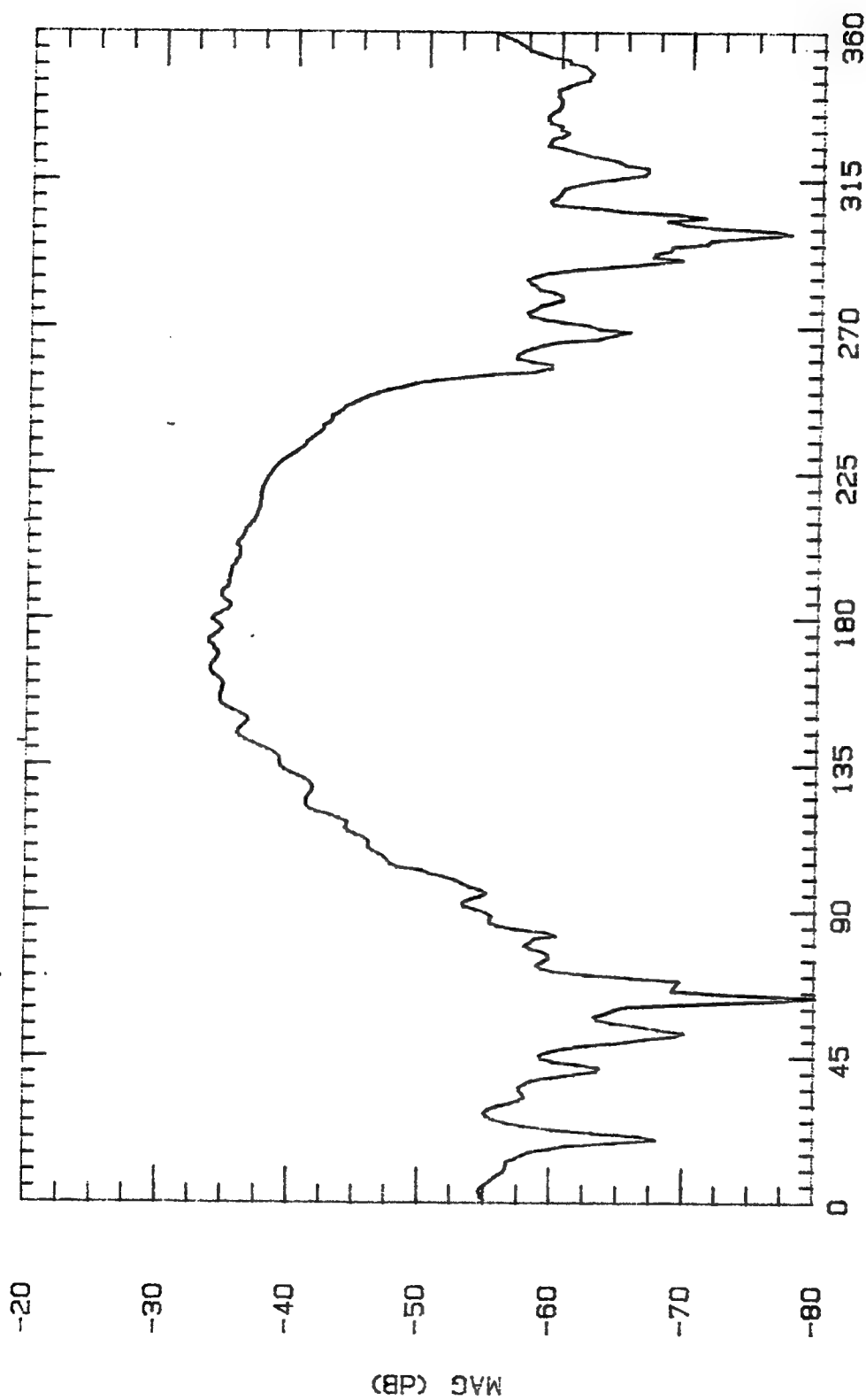


File Name	Frequency	Pattern Type	Date
3ALPL550	5.5 GHz	E-PLANE	27 OCT



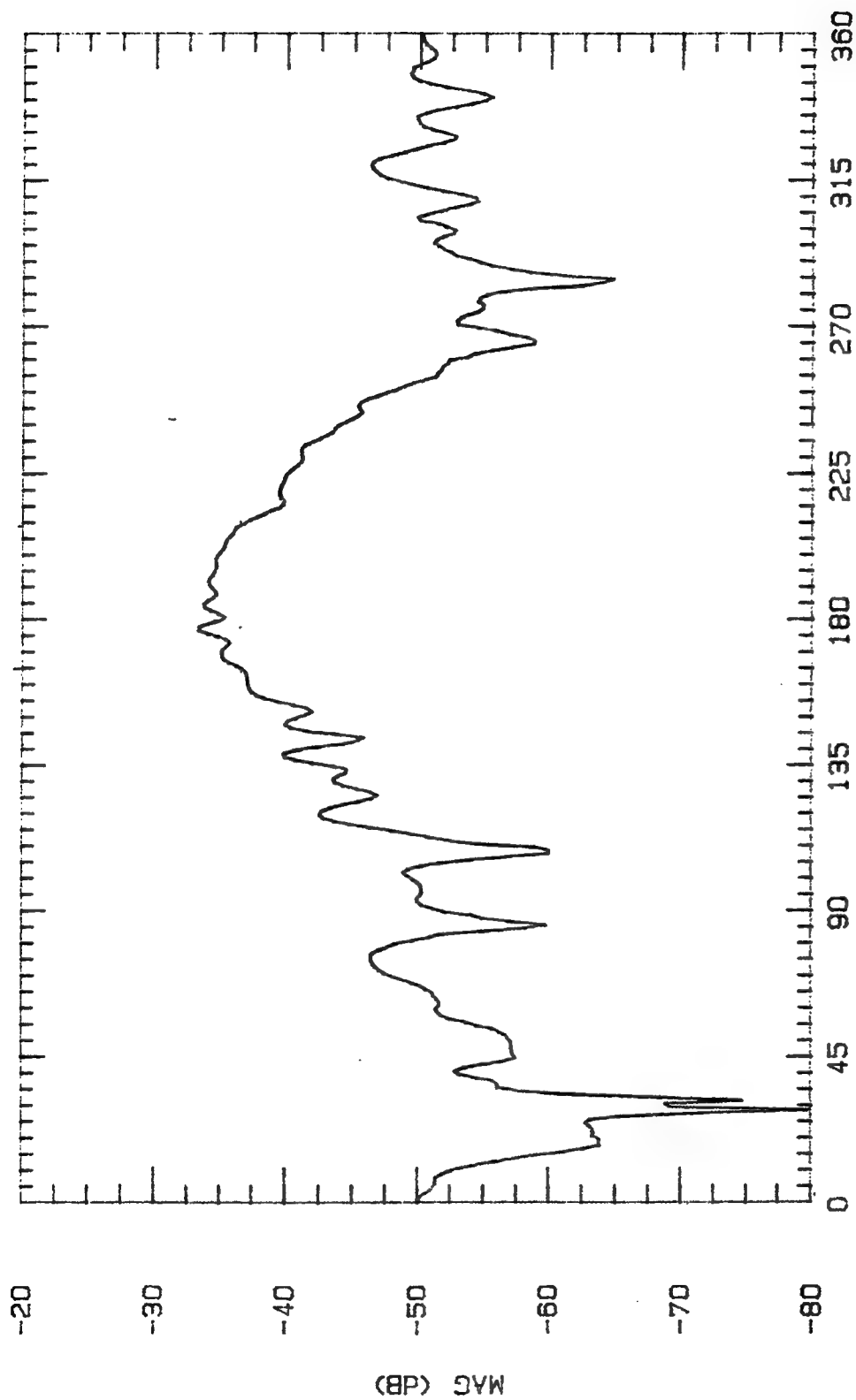
ASPECT ANGLE (DEGREES)

File Name	Frequency	Pattern Type	Data
3ALPL575	5.75 GHz	E-PLANE	28 OCT 84



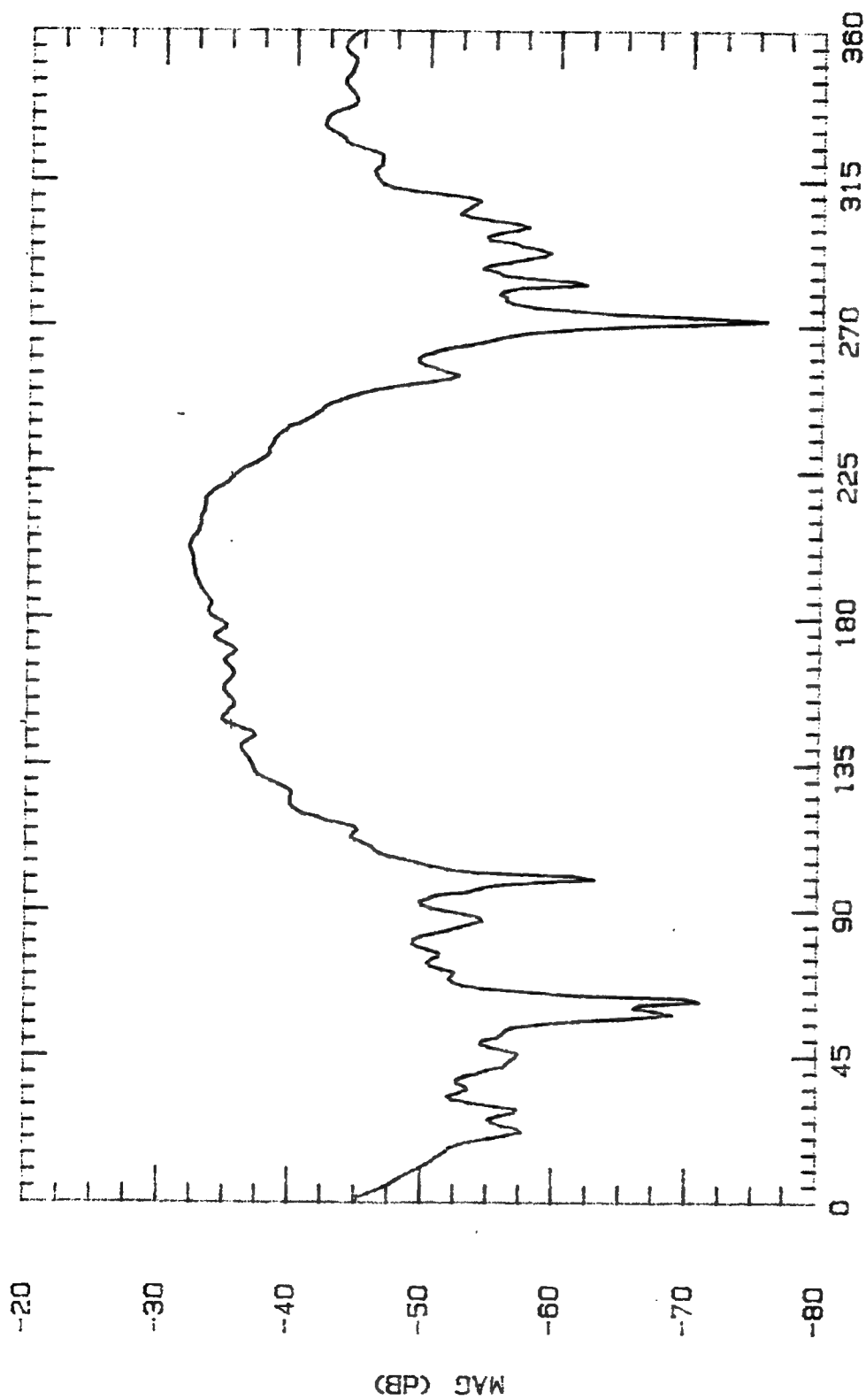
ASPECT ANGLE (DEGREES)

File Name	Frequency	Pattern Type	Data
3ALPL800	6 CH2	L-PLANE	29 OCT 94



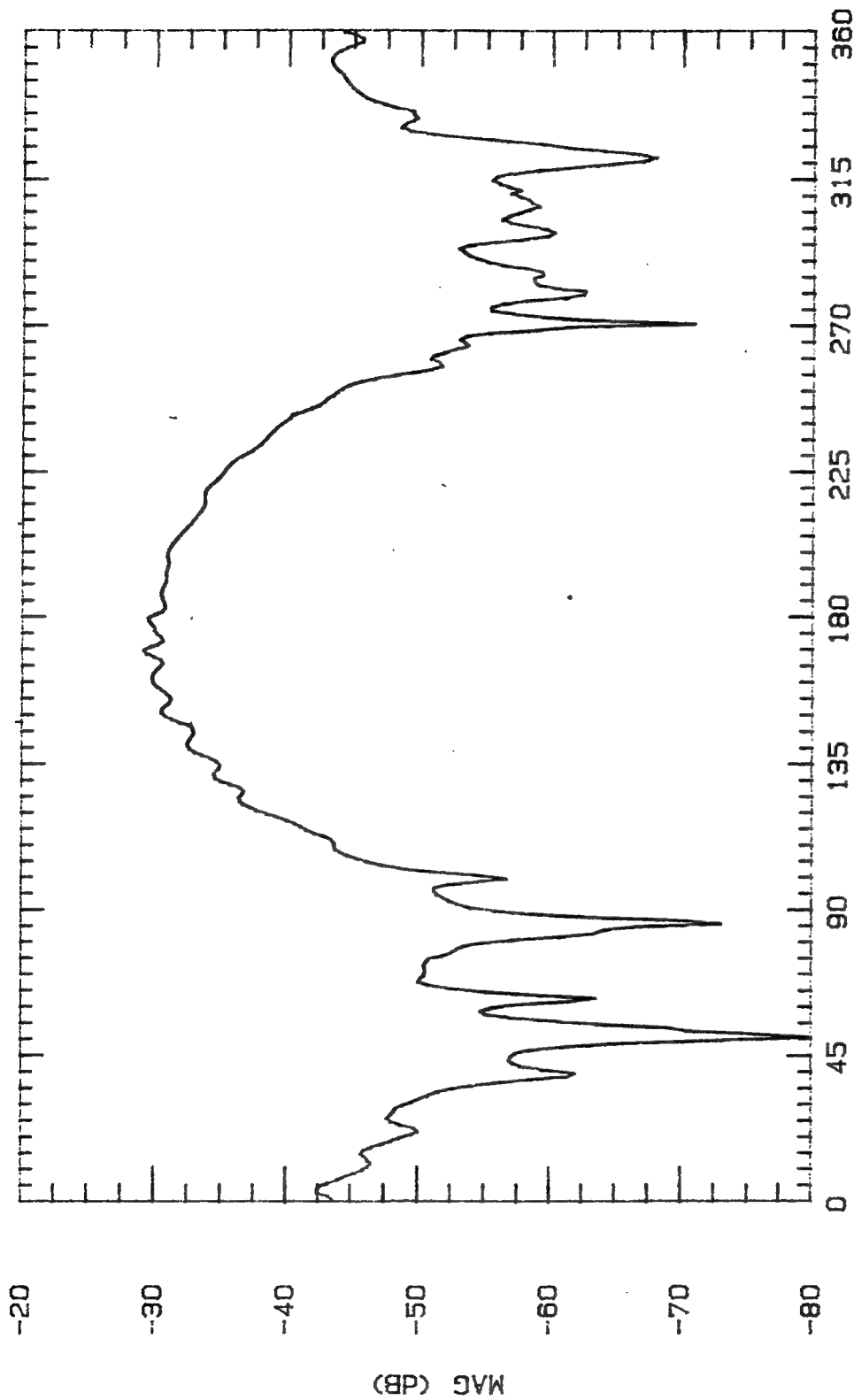
ASPECT ANGLE (DEGREES)

File Name	Frequency	Pattern Type	Date
3ALPL625	8.25 GHz	E-PLANE	28 OCT 94



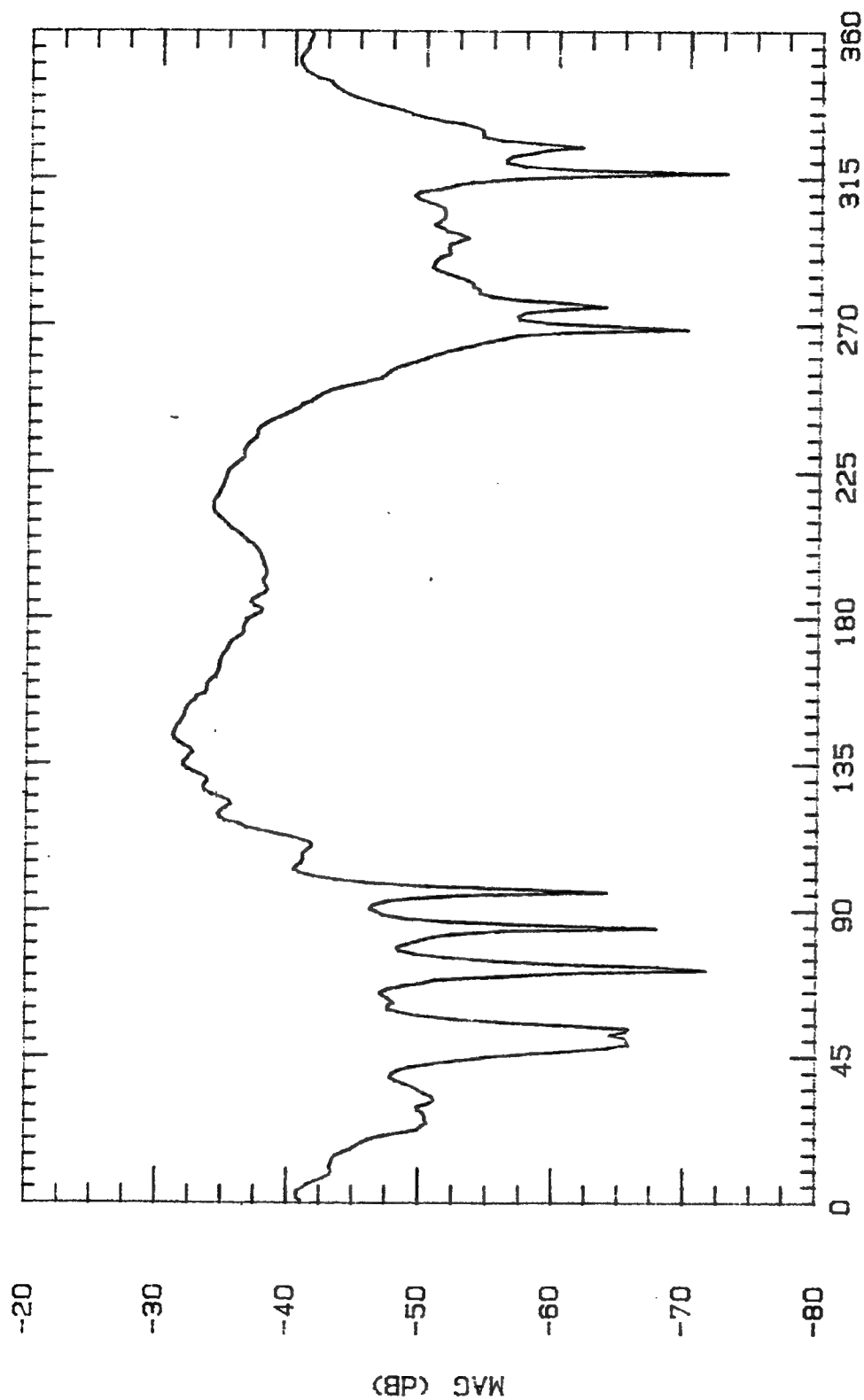
ASPECT ANGLE (DEGREES)

File Name	Frequency	Pattern Type	Date
3ALPL850	8.5 GHz	E-PLANE	28 OCT 94



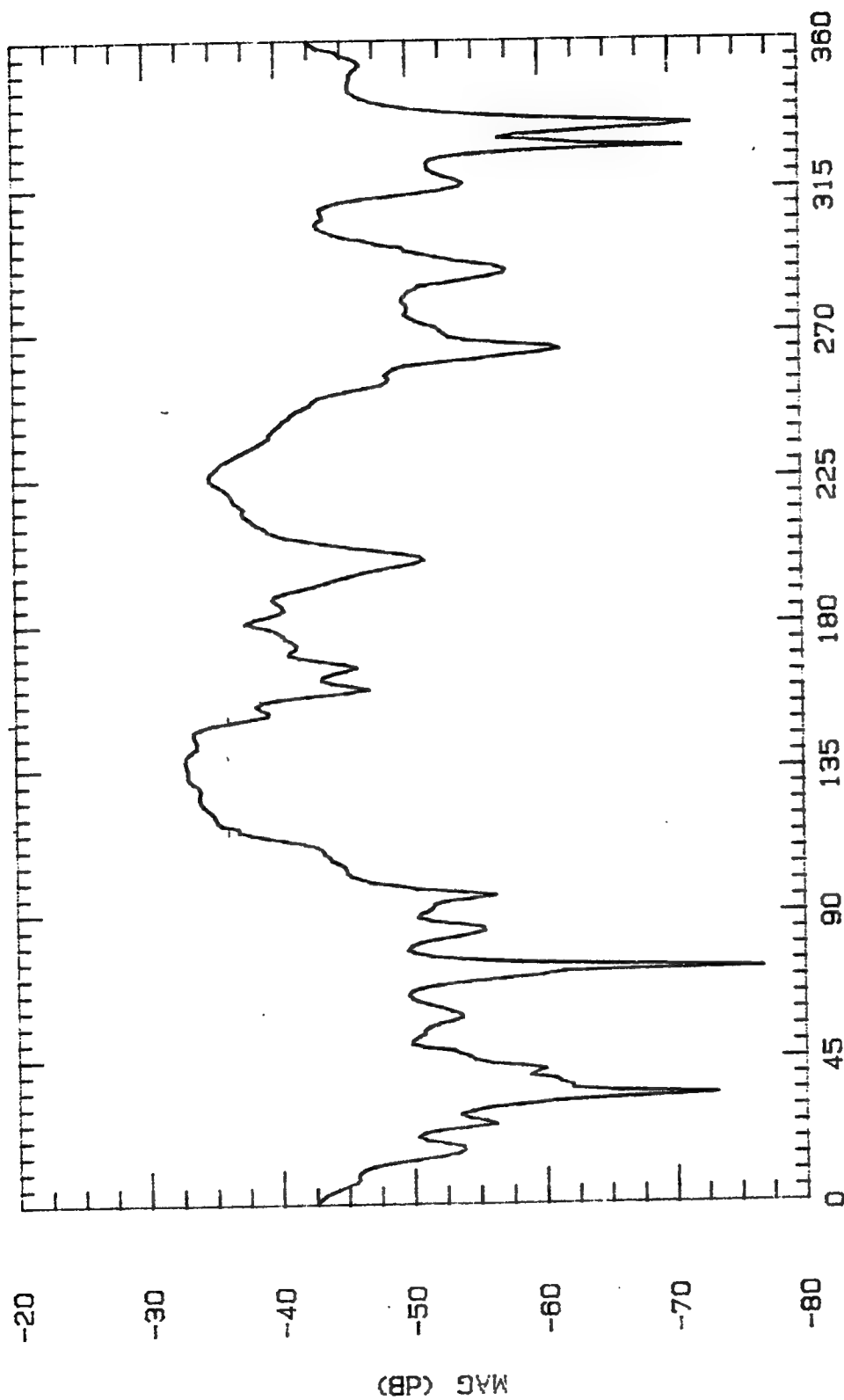
ASPECT ANGLE (DEGREES)

File Name	Frequency	Pattern Type	Date
3ALPL675	8.75 GHz	E-PLANE	28 OCT 94



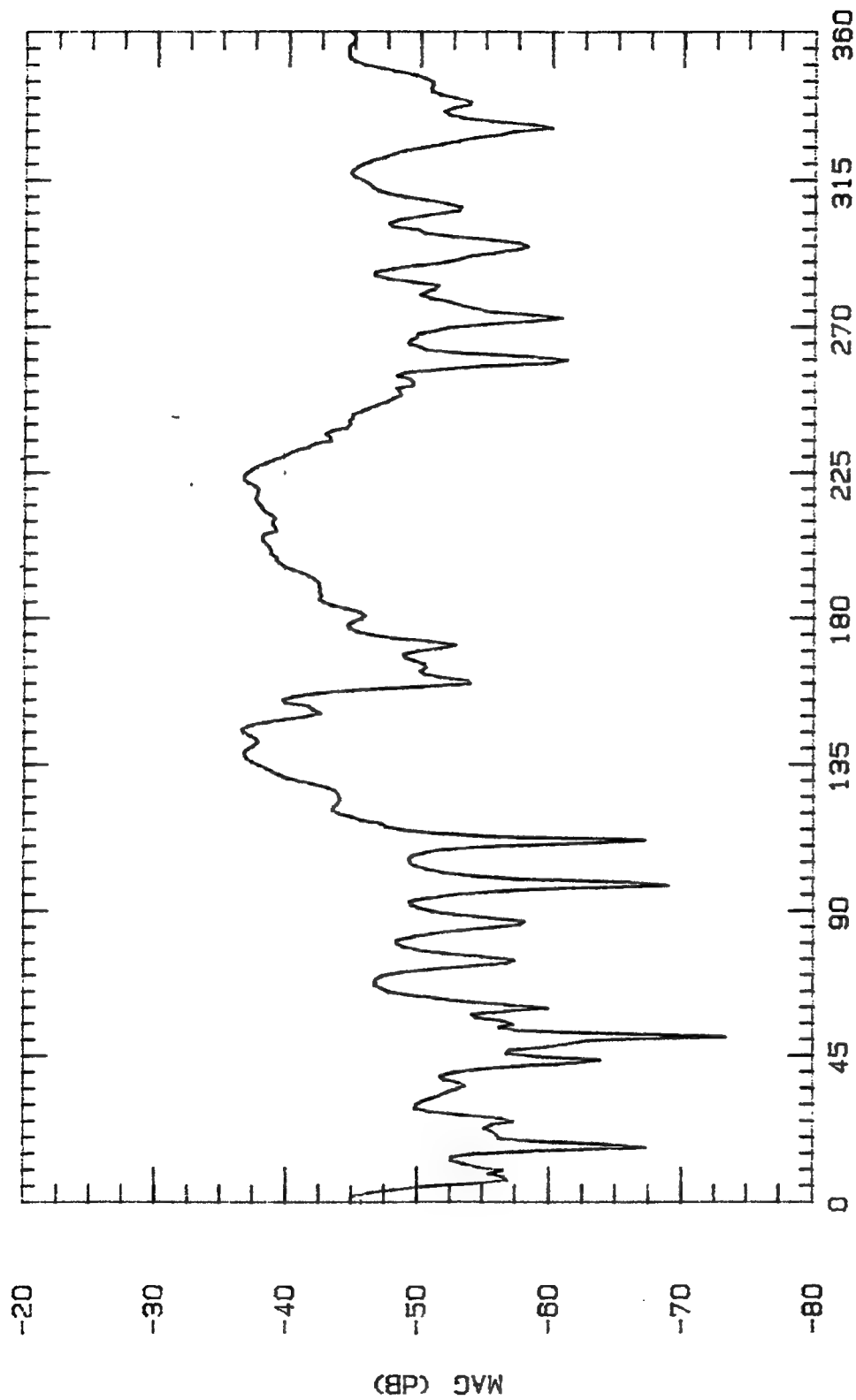
ASPECT ANGLE (DEGREES)

File Name	Frequency	Pattern Type	Date
3ALPL700	7 GHz	E-PLANE	29 OCT 84



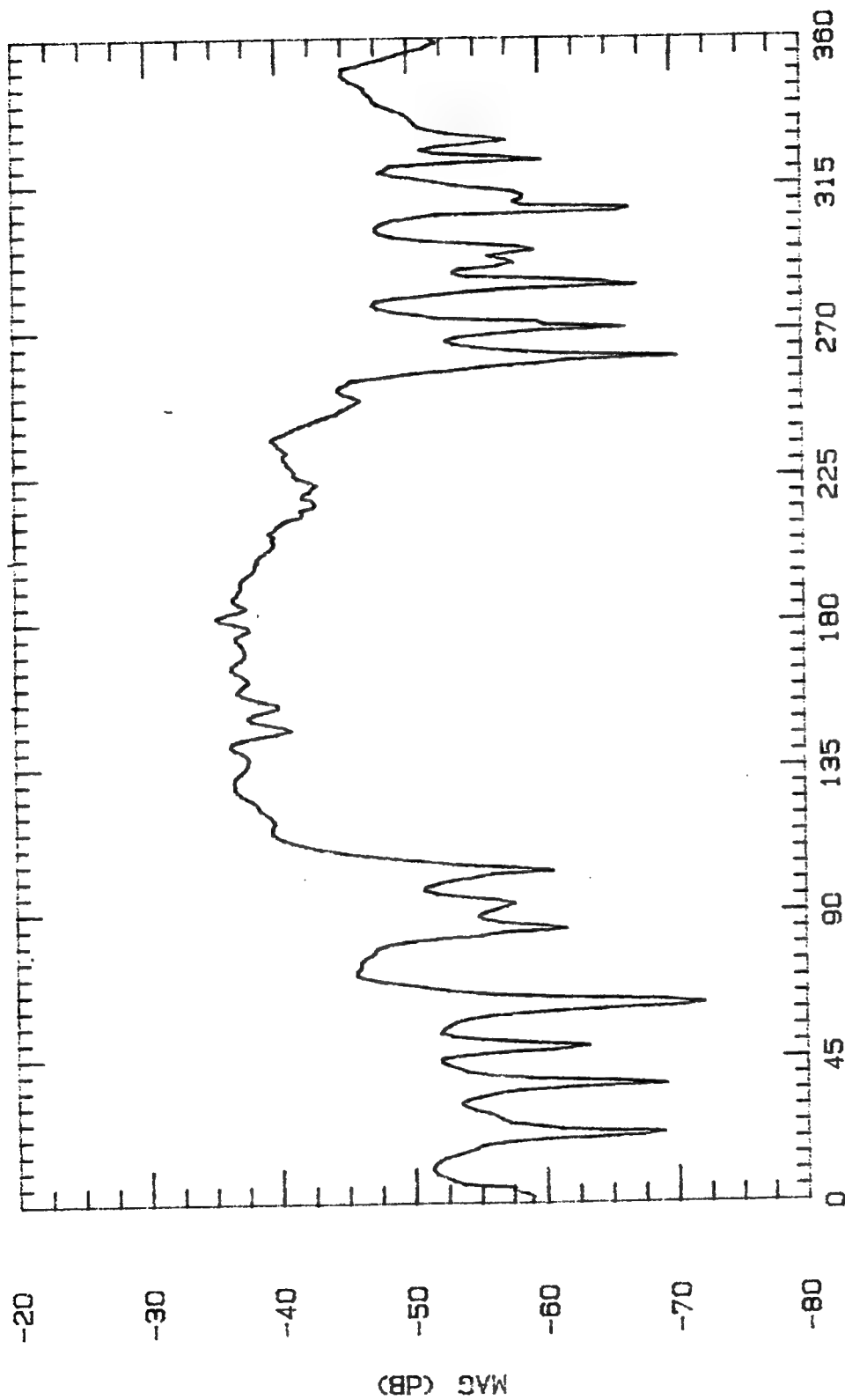
ASPECT ANGLE (DEGREES)

File Name	Frequency	Pattern Type	Date
3ALPL725	7.25 GHz	E-PLANE	28 OCT 94
3ALPL725	7.25 GHz	E-PLANE	28 OCT 94



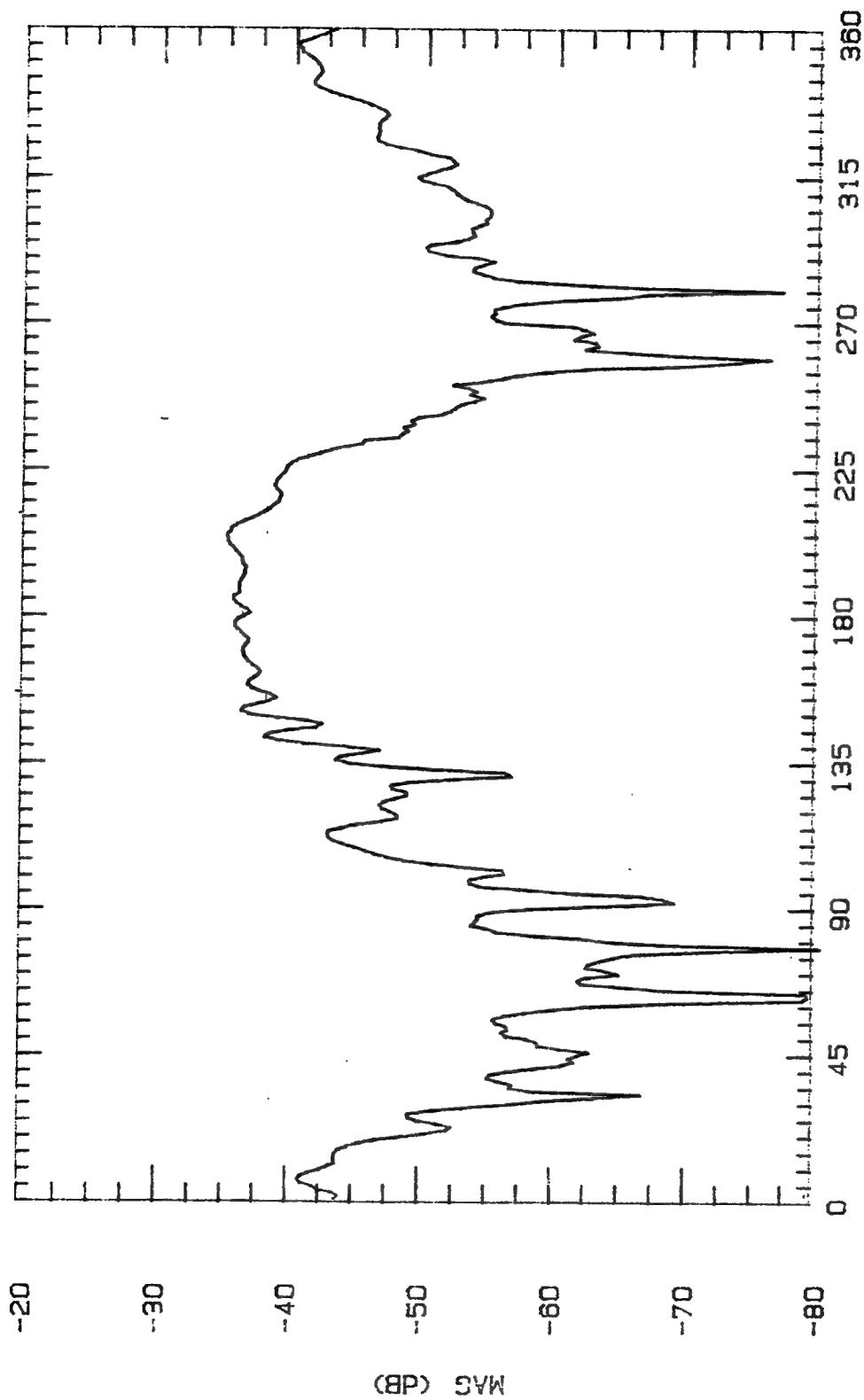
ASPECT ANGLE (DEGREES)

File Name	Frequency	Pattern Type	Date
3ALPL750	7.5 GHz	E-PLANE	28 OCT 84



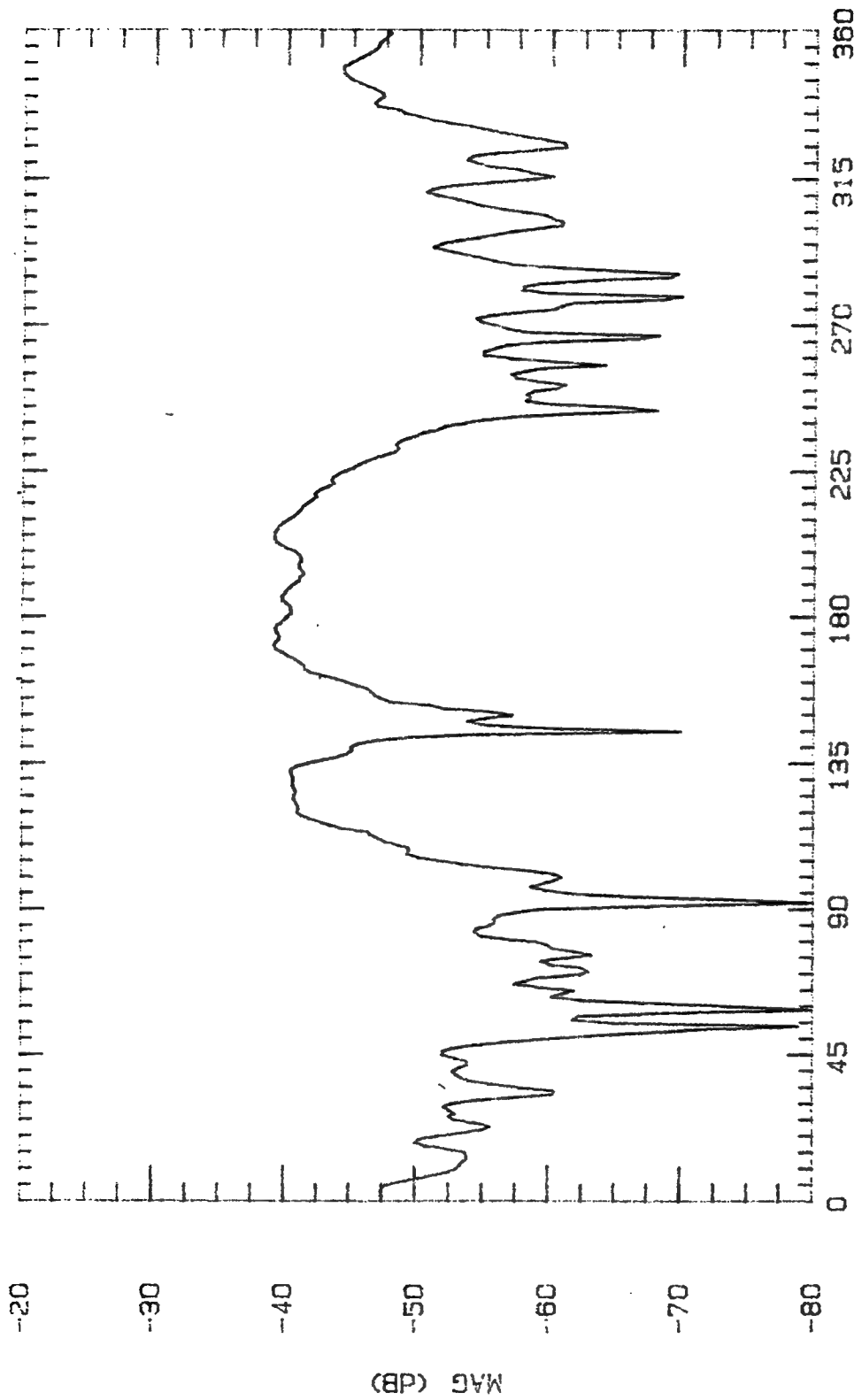
ASPECT ANGLE (DEGREES)

File Name	Frequency	Pattern Type	Date
3ALPL775	7.75 GHz	E-PLANE	28 OCT 94



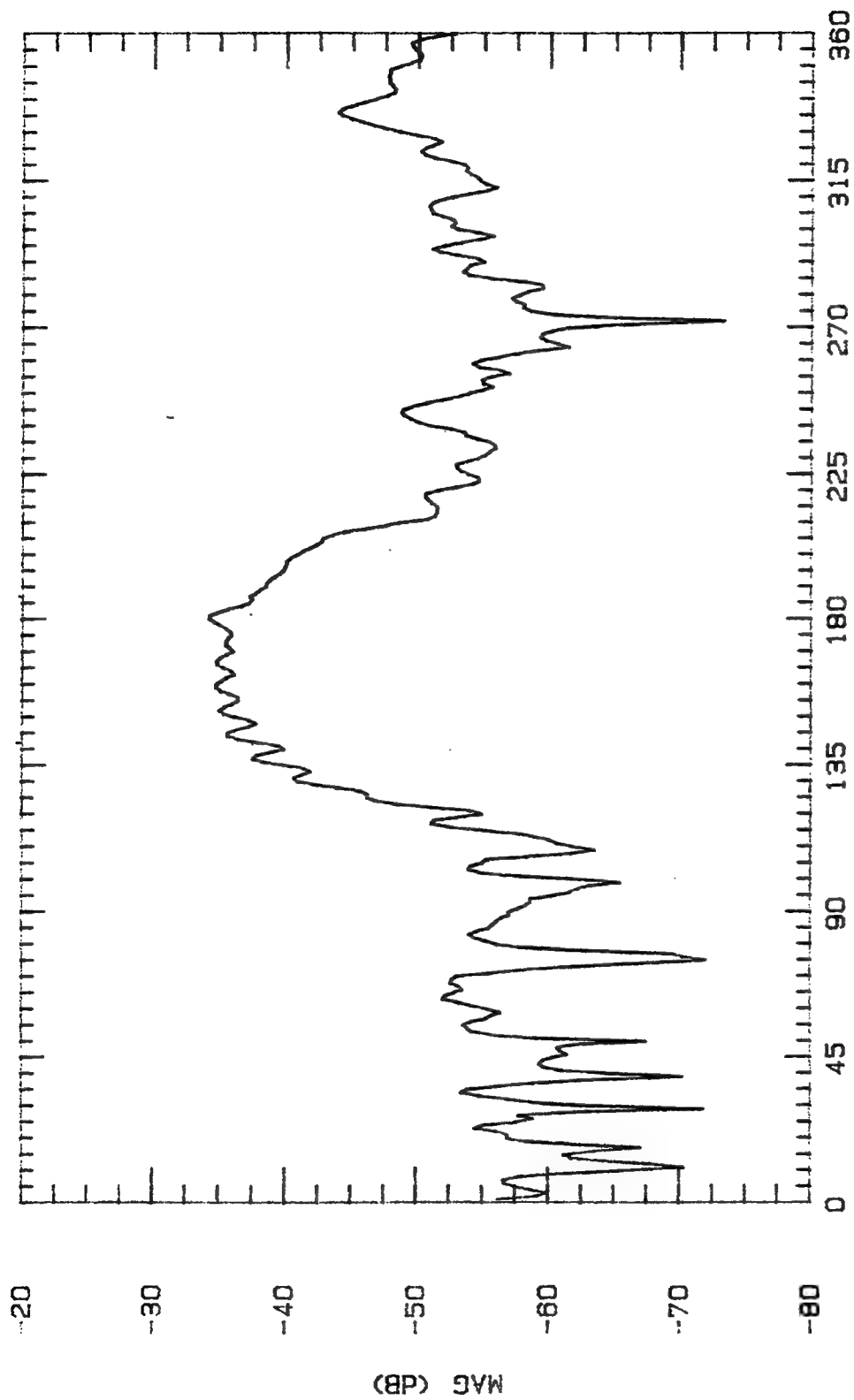
ASPECT ANGLE (DEGREES)

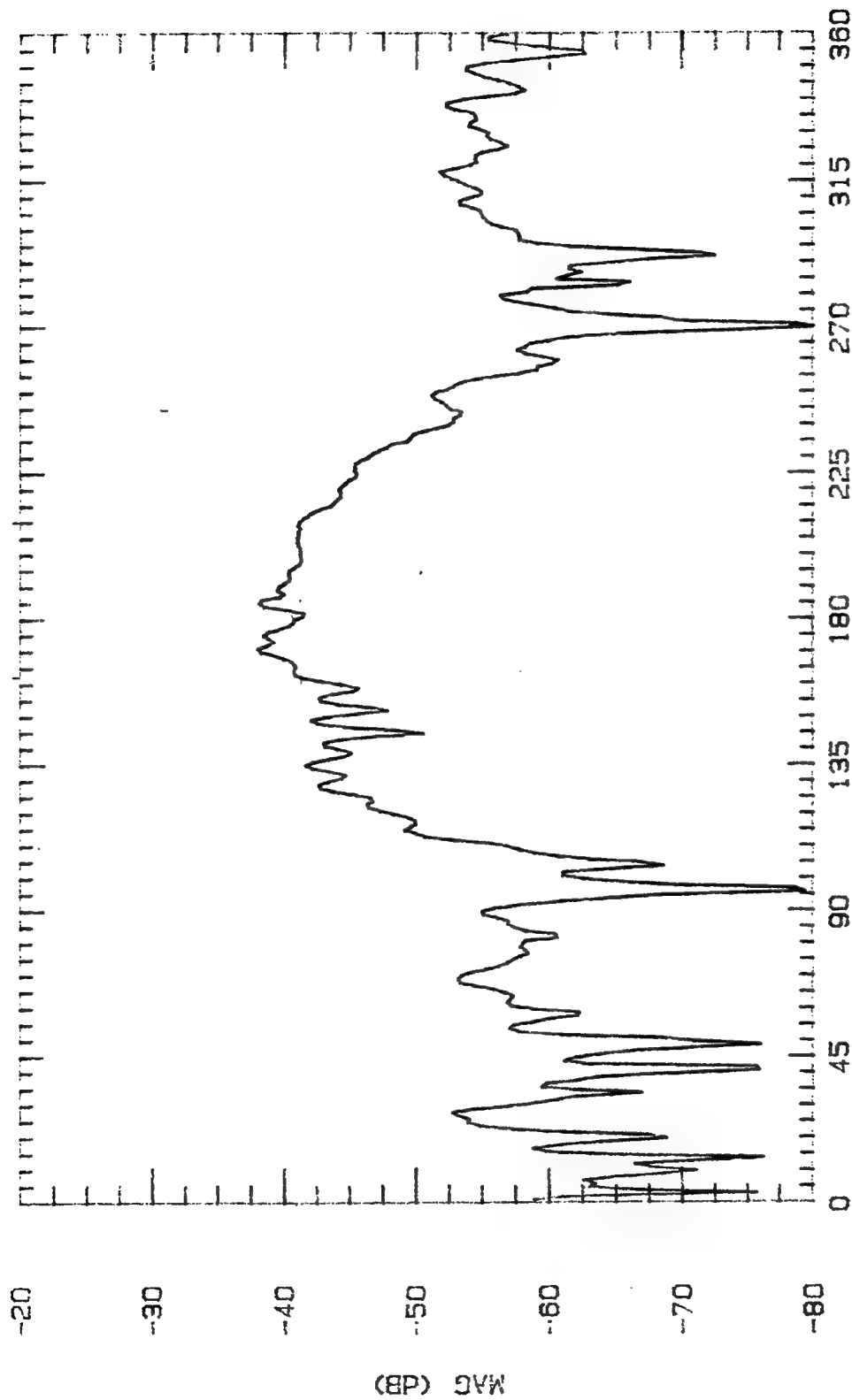
File Name	Frequency	Pattern Type	Date
3ALPL800	8 GHz	E-PLANE	29 OCT 94



ASPECT ANGLE (DEGREES)

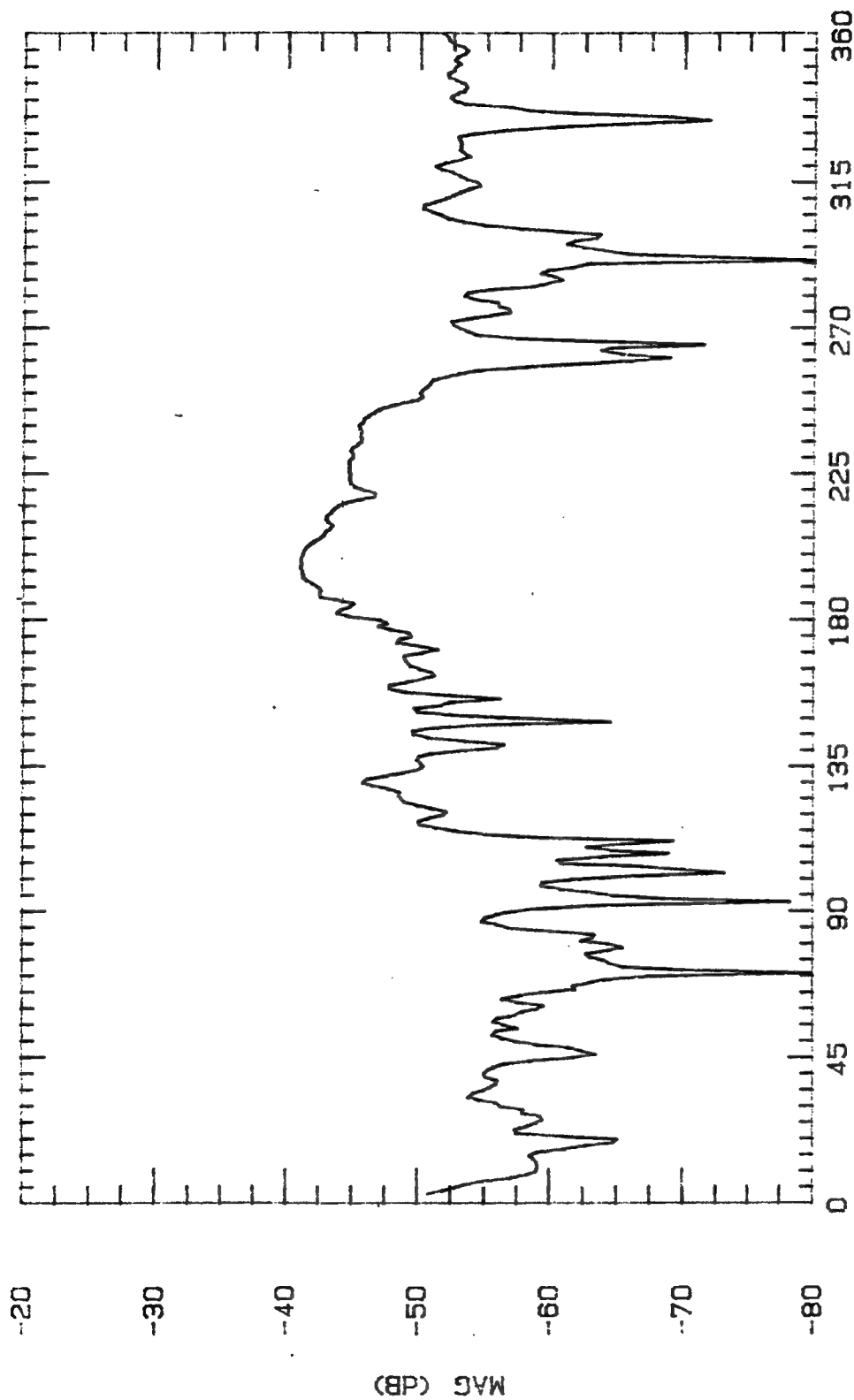
File Name	Frequency	Pattern Type	Date
3ALPL825	8.25 GHz	E-PLANE	31 OCT 94



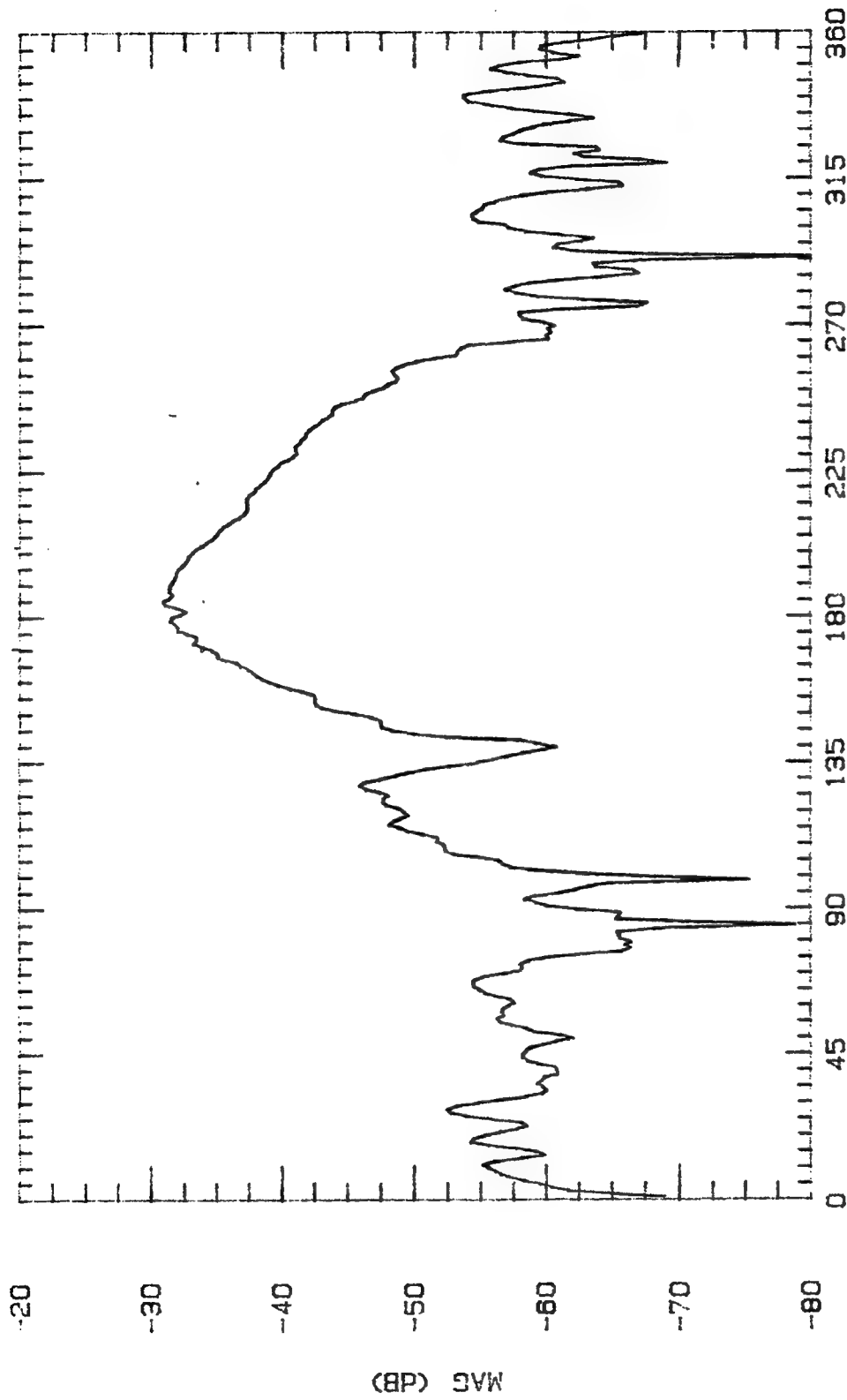


ASPECT ANGLE (DEGREES)

File Name	Frequency	Pattern Type	Date
3ALPL875	8.75 GHz	E-PLANE	28 OCT 94

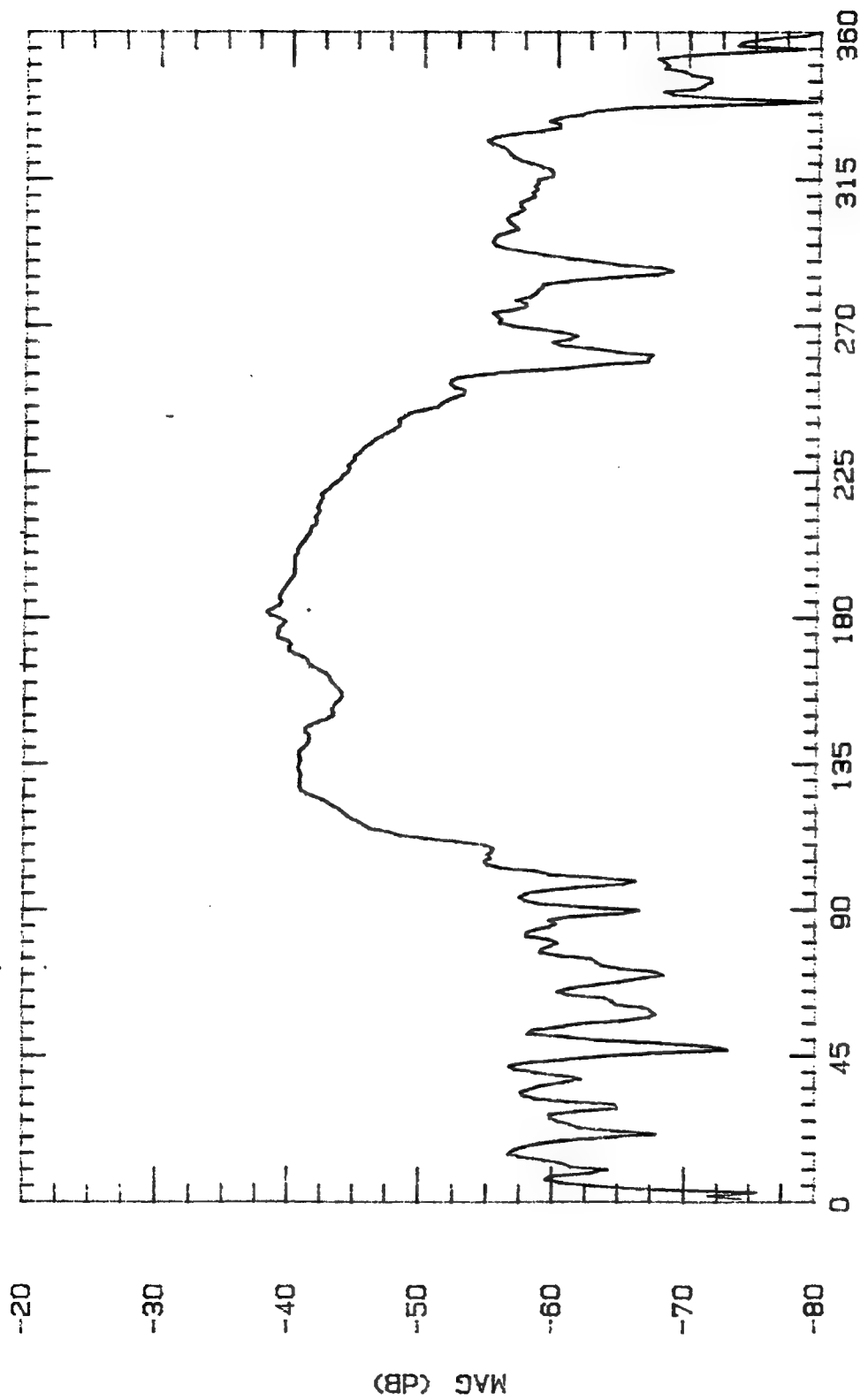


File Name	Frequency	Pattern Type	Date
3ALPL800	9 GHz	E-PLANE	29 OCT 94



ASPECT ANGLE (DEGREES)

File Name	Frequency	Pattern Type	Date
3ALPL925	9.25 GHz	E-PLANE	28 OCT 94



ASPECT ANGLE (DEGREES)

Date

28 OCT 94

File Name

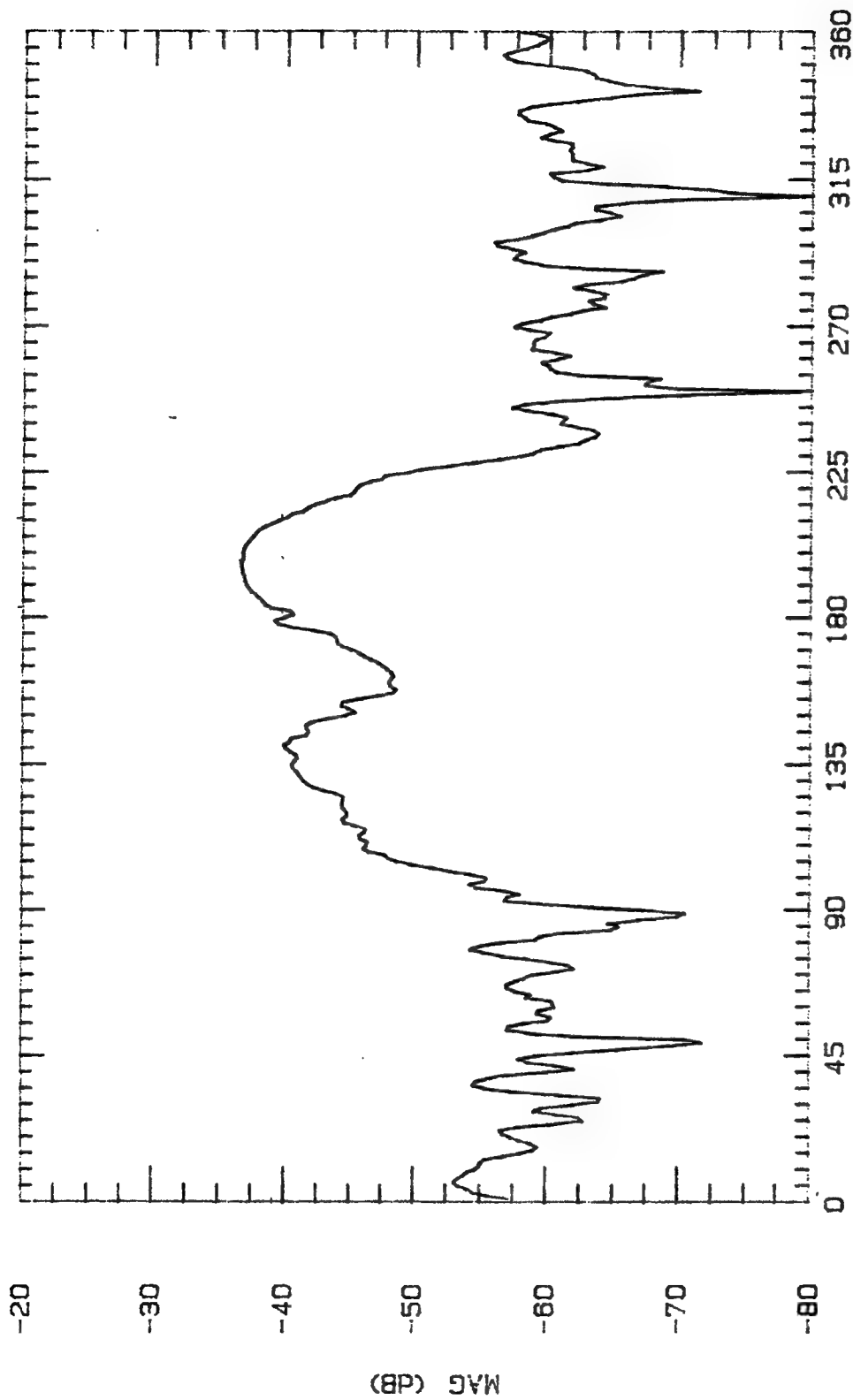
3ALPL950

Frequency

9.5 GHz

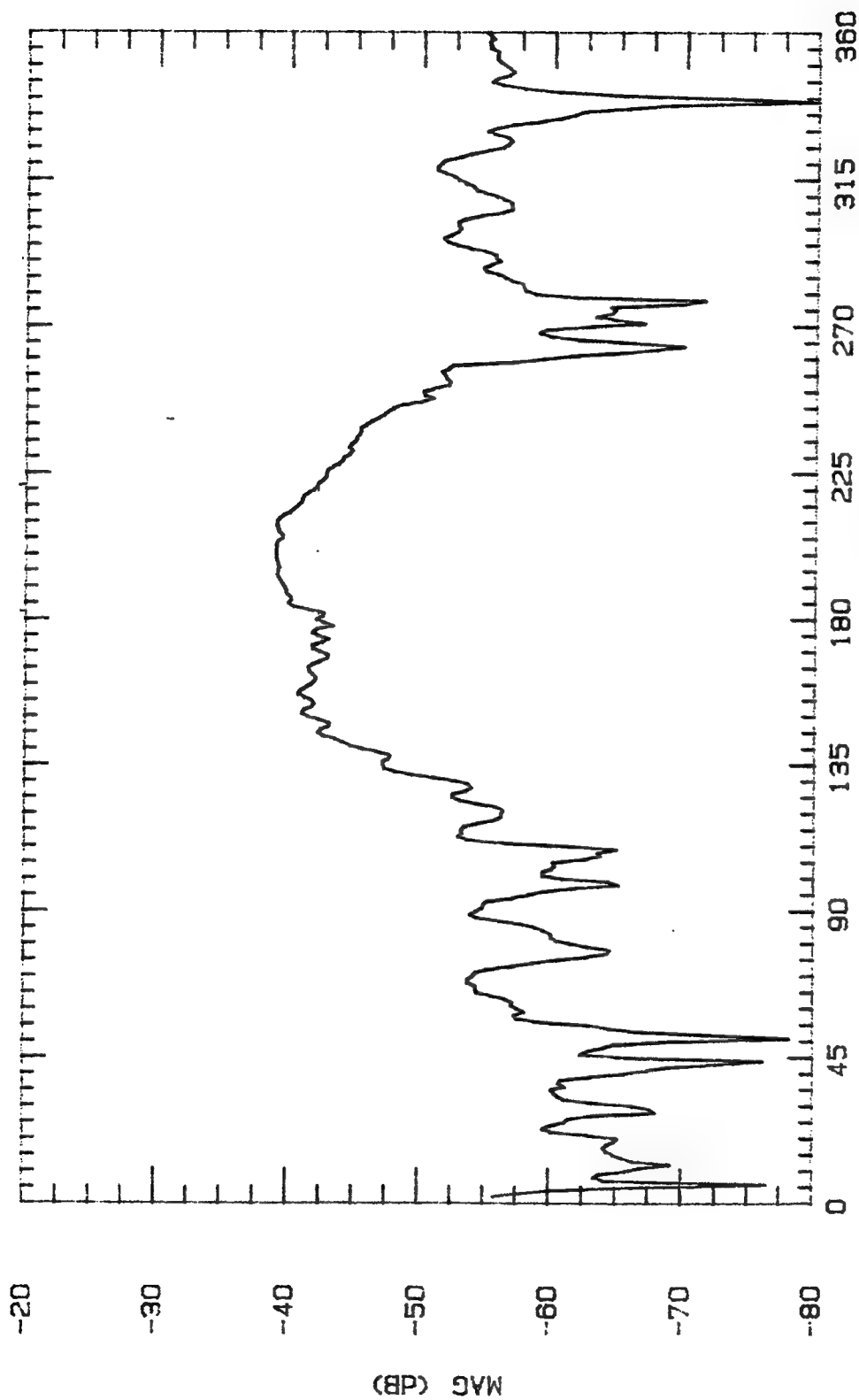
Pattern Type

E-PLANE



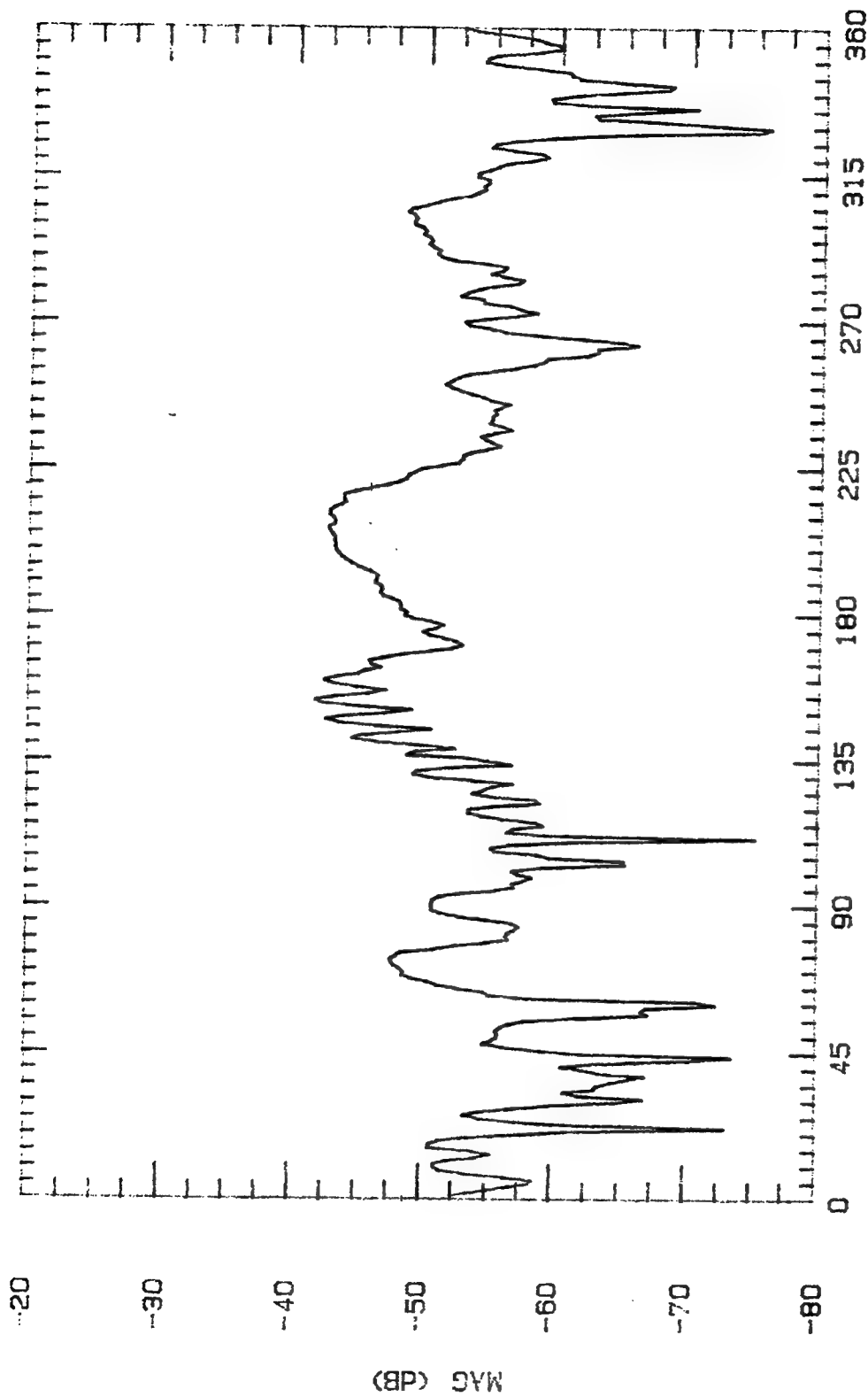
ASPECT ANGLE (DEGREES)

File Name	Frequency	Pattern Type	Date
3ALPL975	9.75 GHz	E-PLANE	28 OCT 94



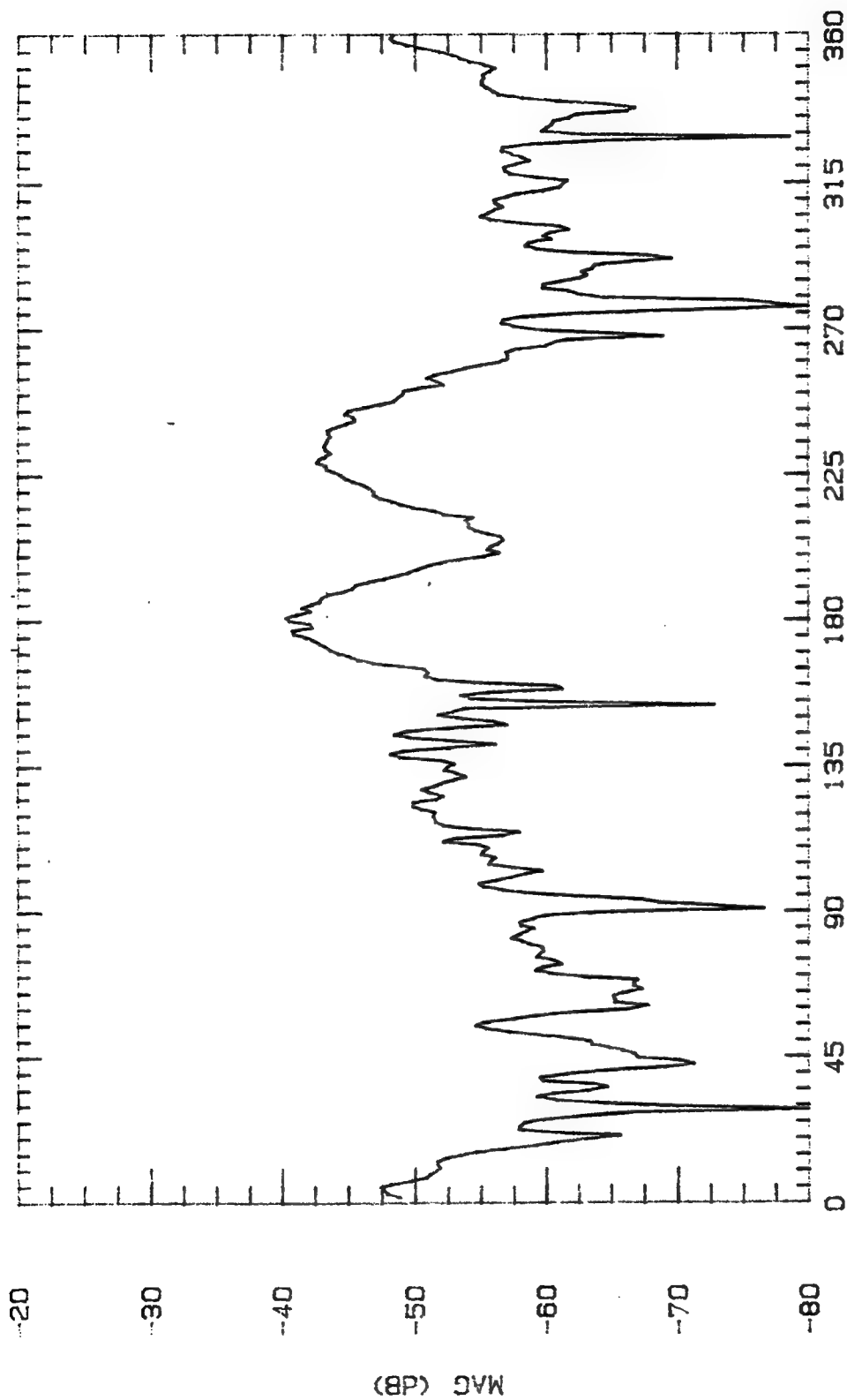
ASPECT ANGLE (DEGREES)

File Name	Frequency	Pattern Type	Date
3ALPL1000	10 GHz	E-PLANE	29 OCT 94

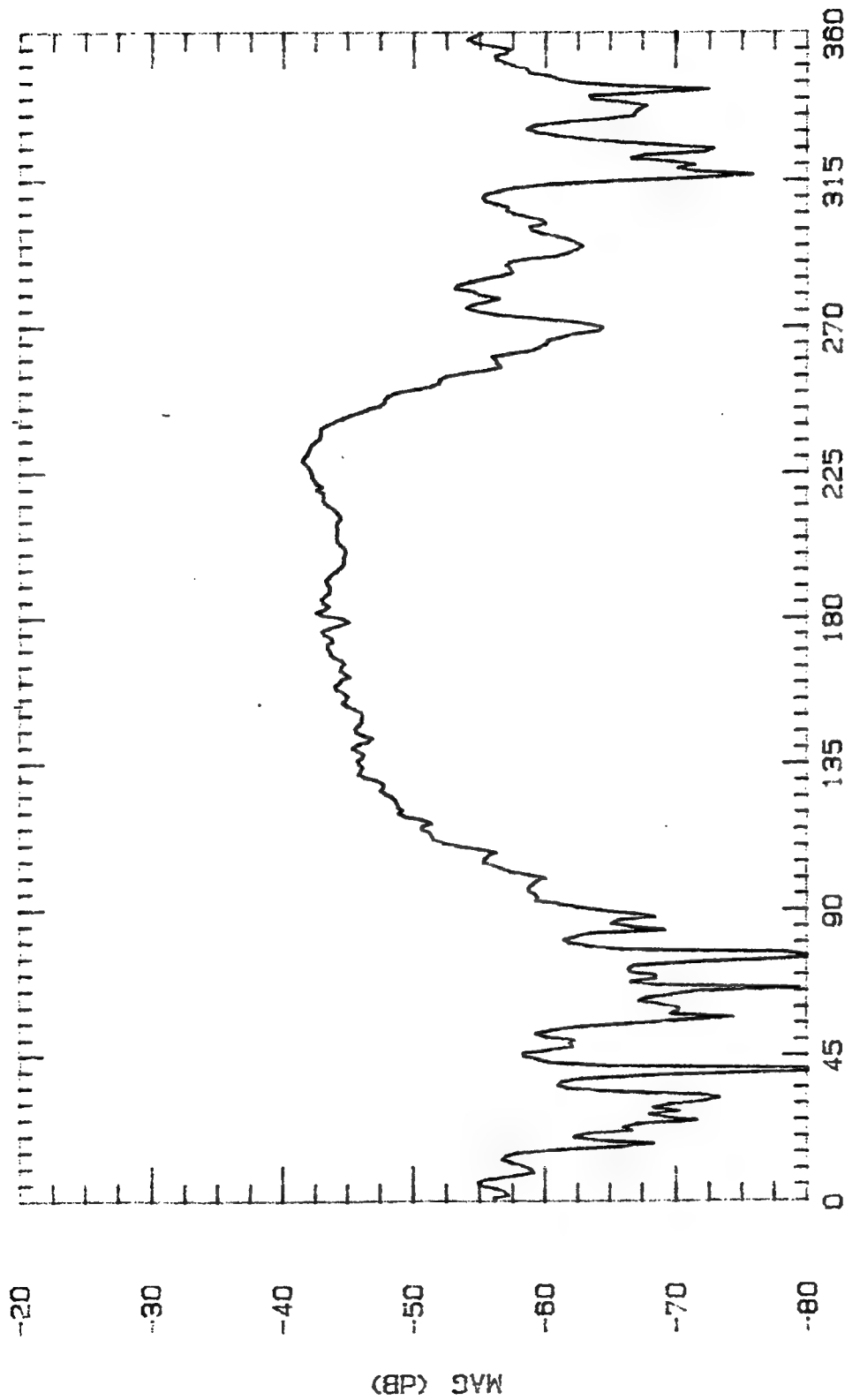


ASPECT ANGLE (DEGREES)

File Name	Frequency	Pattern Type	Date
3ALPL1025	10.25 GHz	E-PLANE	28 OCT 94

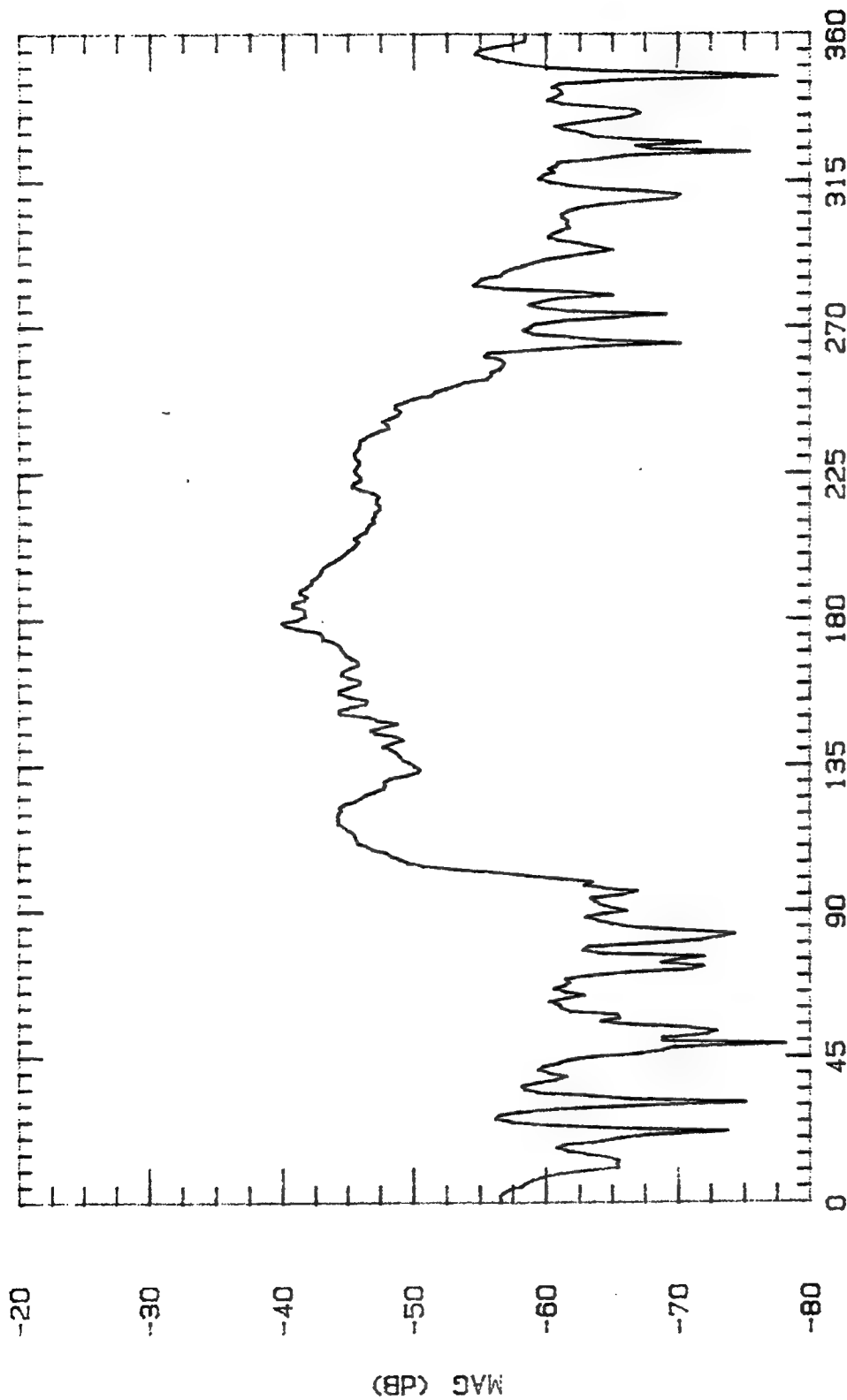


File Name	Frequency	Pattern Type	Date
3ALPL1050	10.5 GHz	L-PLANE	28 OCT 94



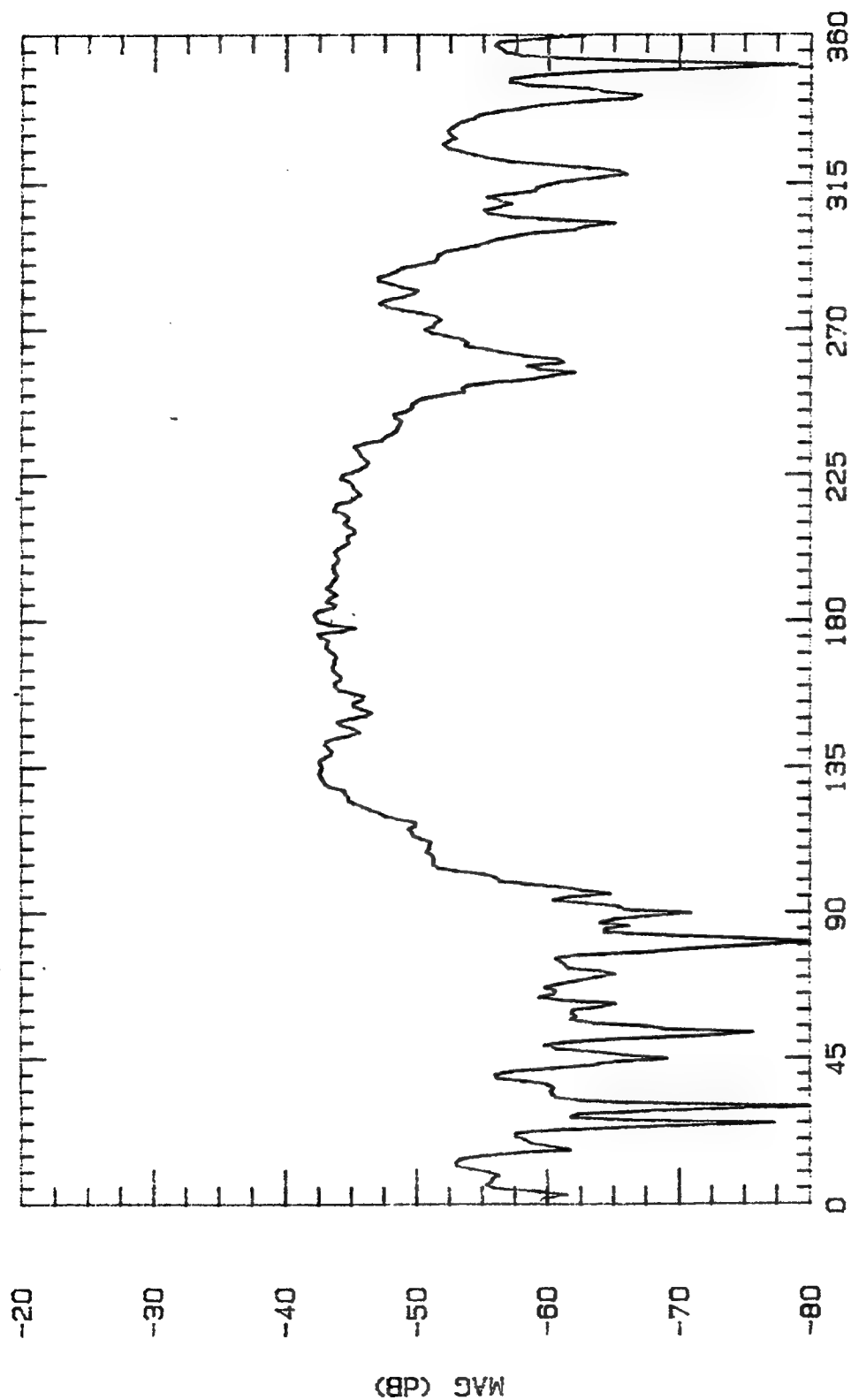
ASPECT ANGLE (DEGREES)

File Name	Frequency	Pattern Type	Date
3ALPL1075	10.75 GHz	E-PLANE	28 OCT 94



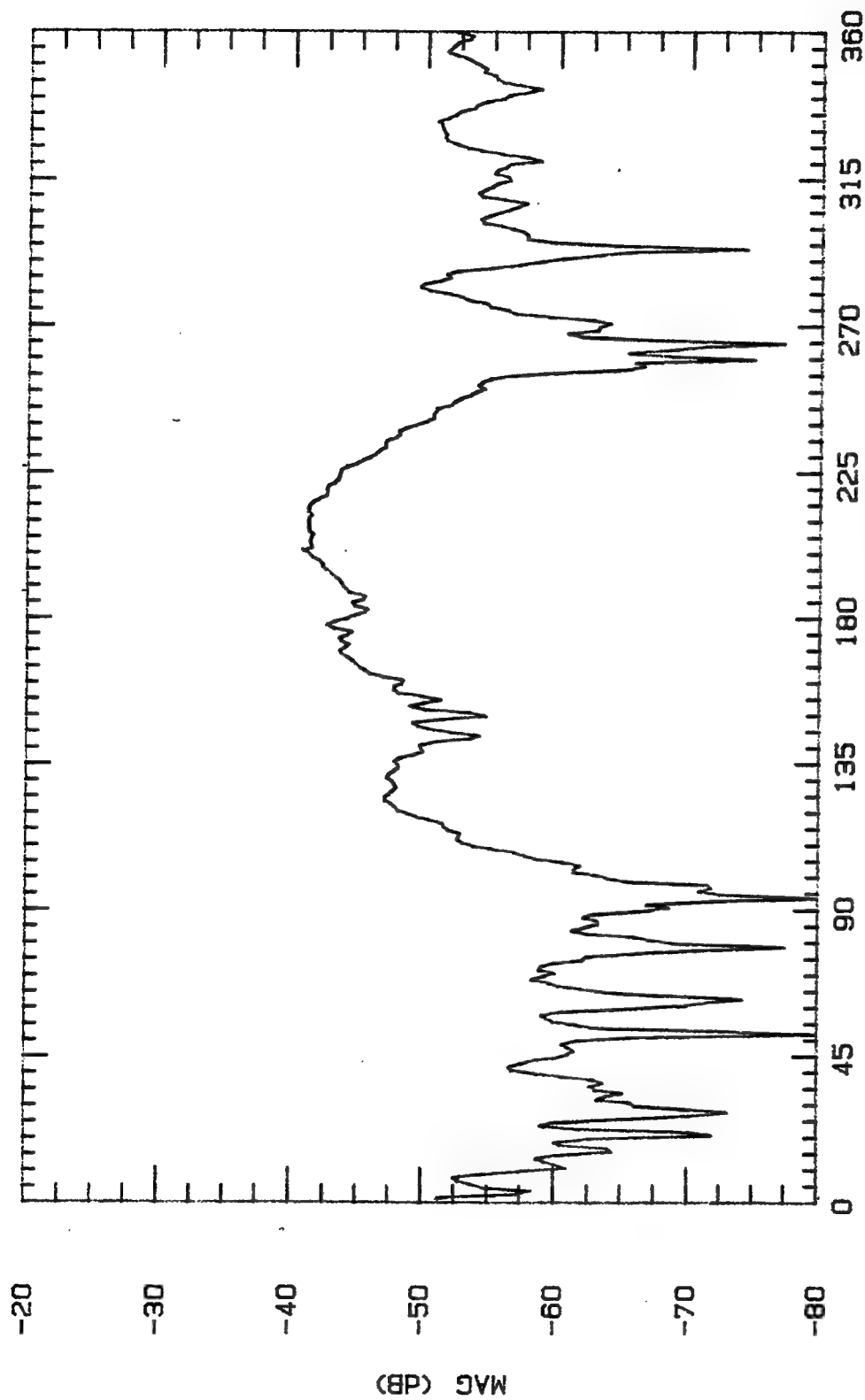
ASPECT ANGLE (DEGREES)

File Name	Frequency	Pattern Type	Date
3ALPL1100	11 GHz	E-PLANE	29 OCT 94

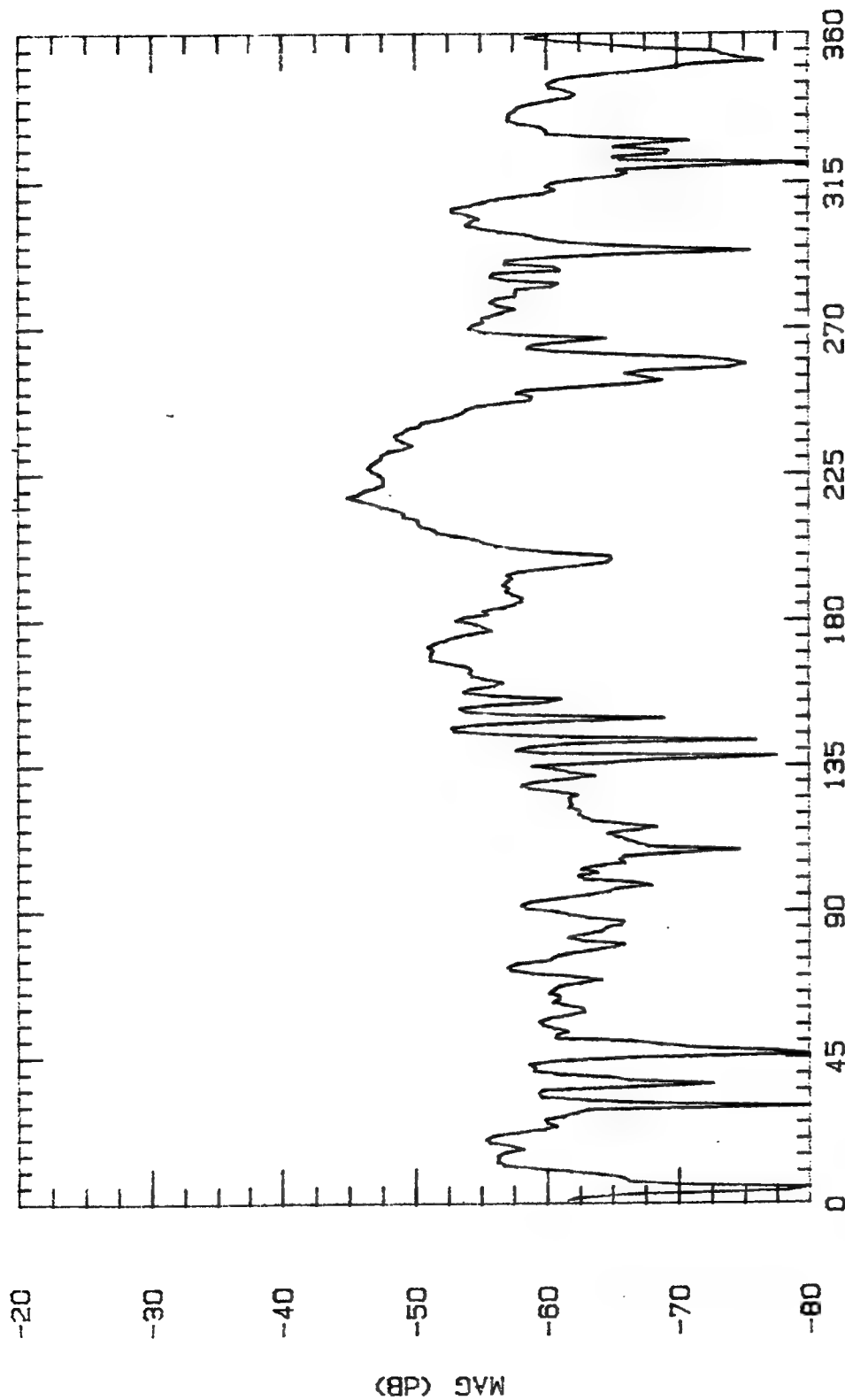


ASPECT ANGLE (DEGREES)

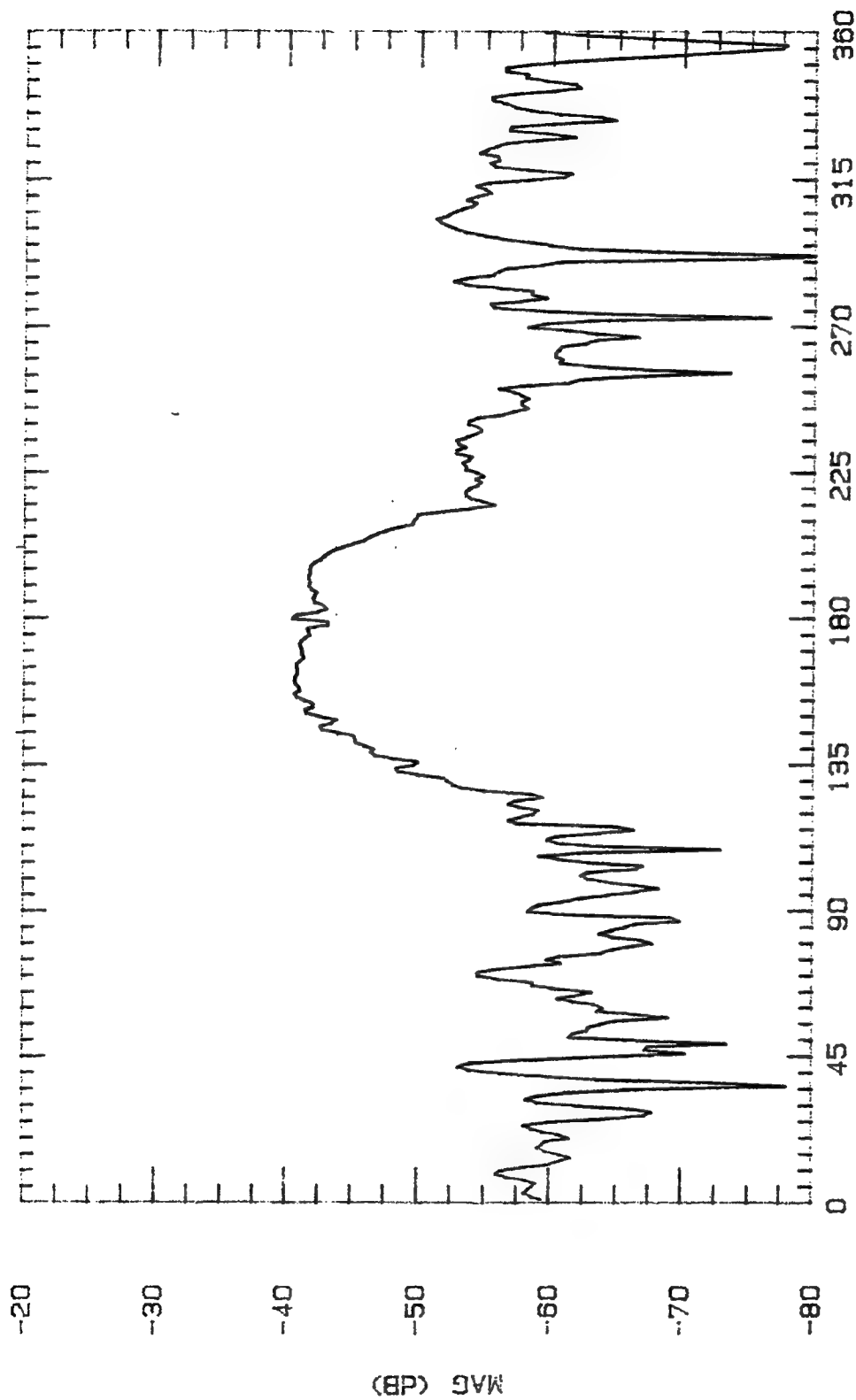
File Name	Frequency	Pattern Type	Date
3ALPL1125	11.25 GHz	E-PLANE	31 OCT 94



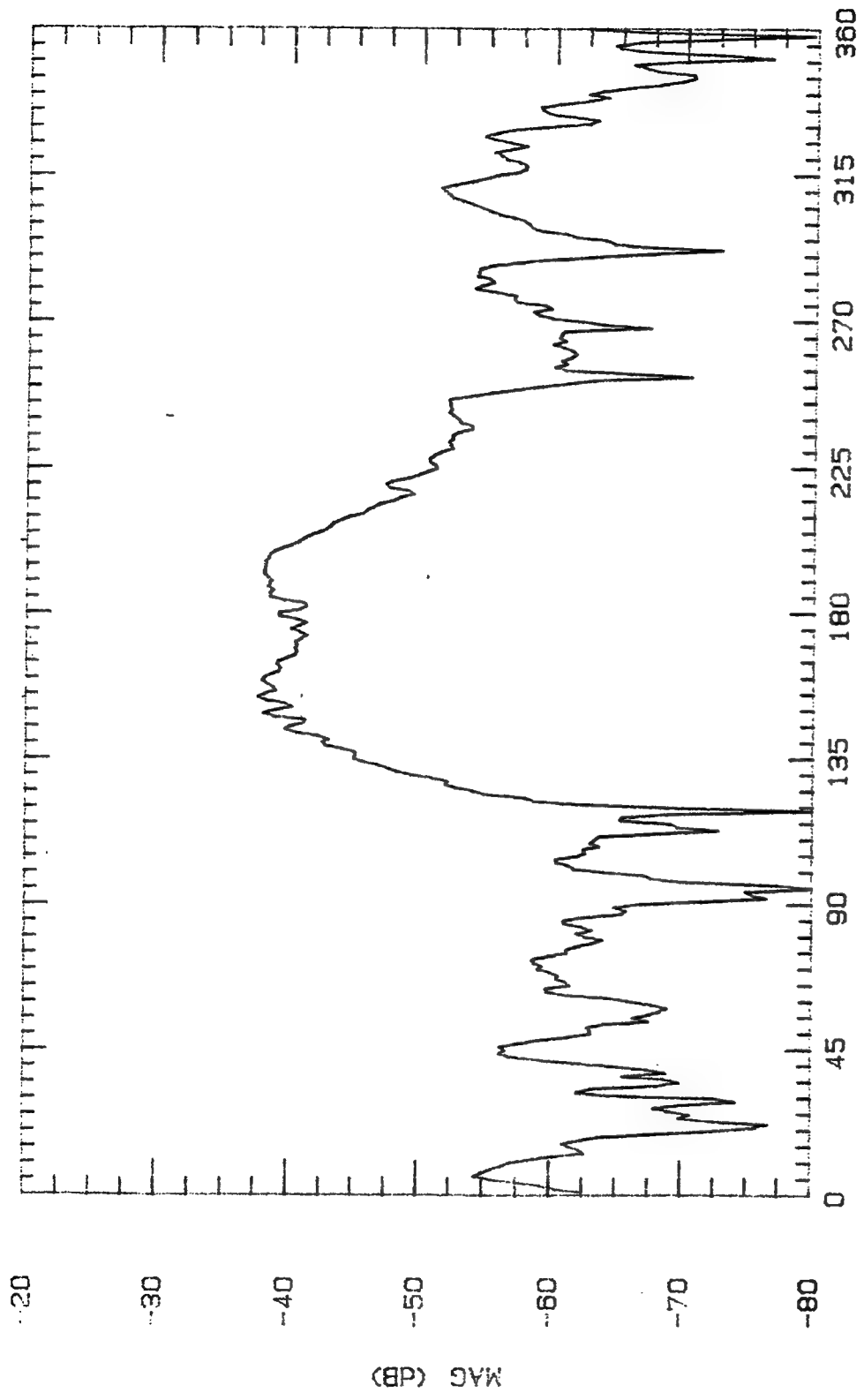
File Name	Frequency	Pattern Type	Date
9ALPL1150	11.5 GHz	E-PLANE	28 OCT 94



File Name	Frequency	Pattern Type	Date
3ALPL1175	11.75 GHz	E-PLANE	31 OCT 94

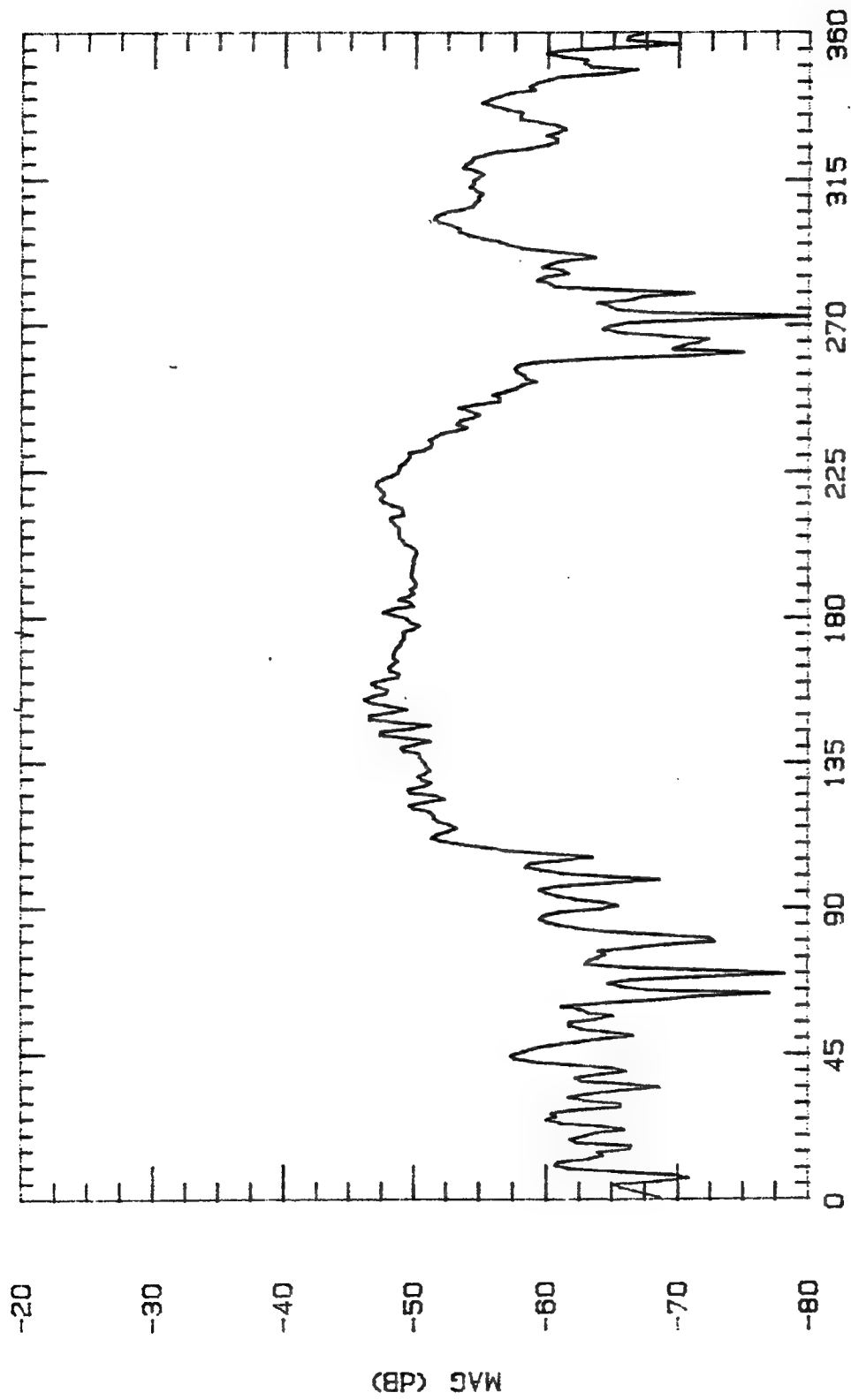


File Name	Frequency	Pattern Type	Date
3ALPL1200	12 CHz	E-PLANE	29 OCT 94

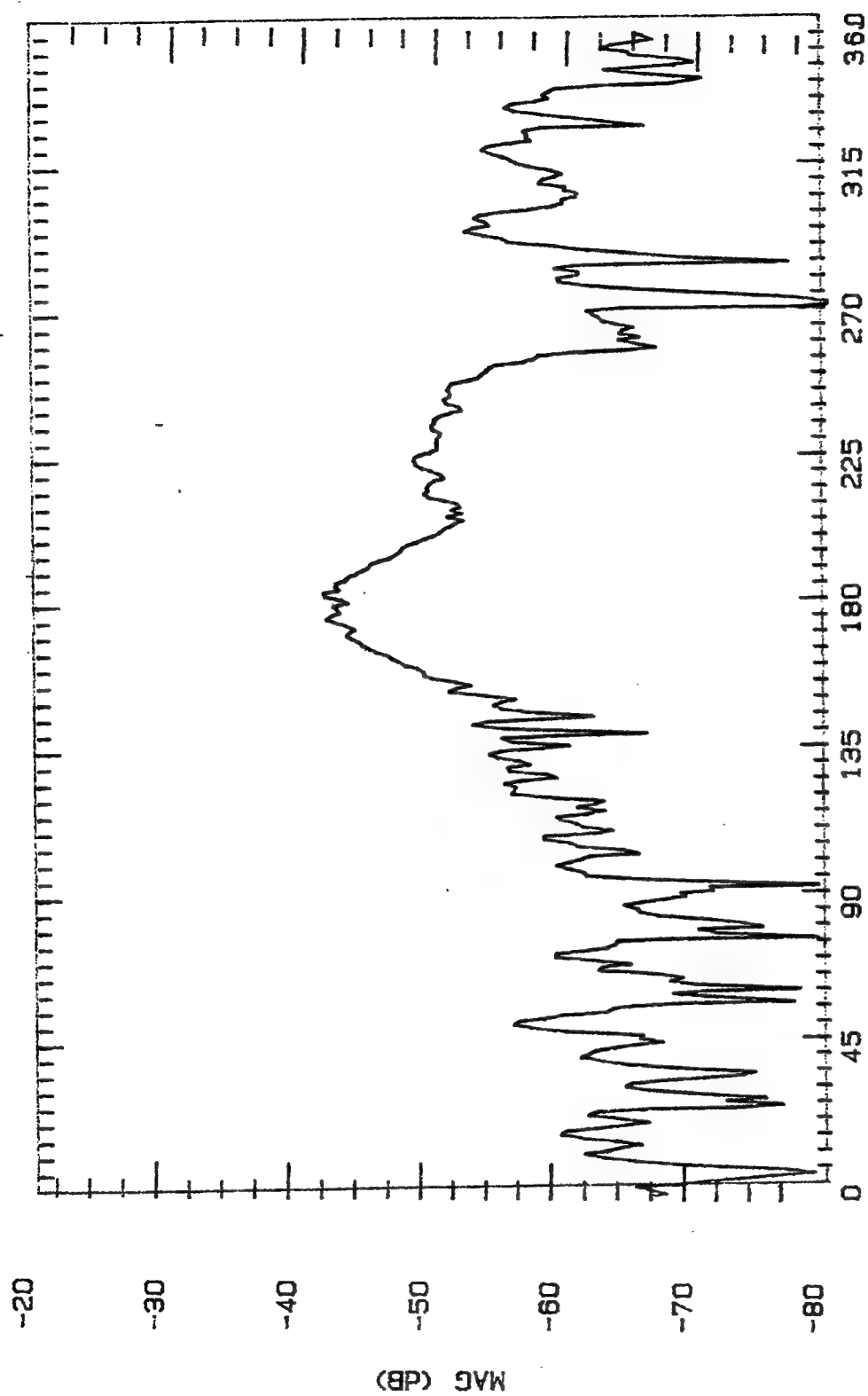


ASPECT ANGLE (DEGREES)

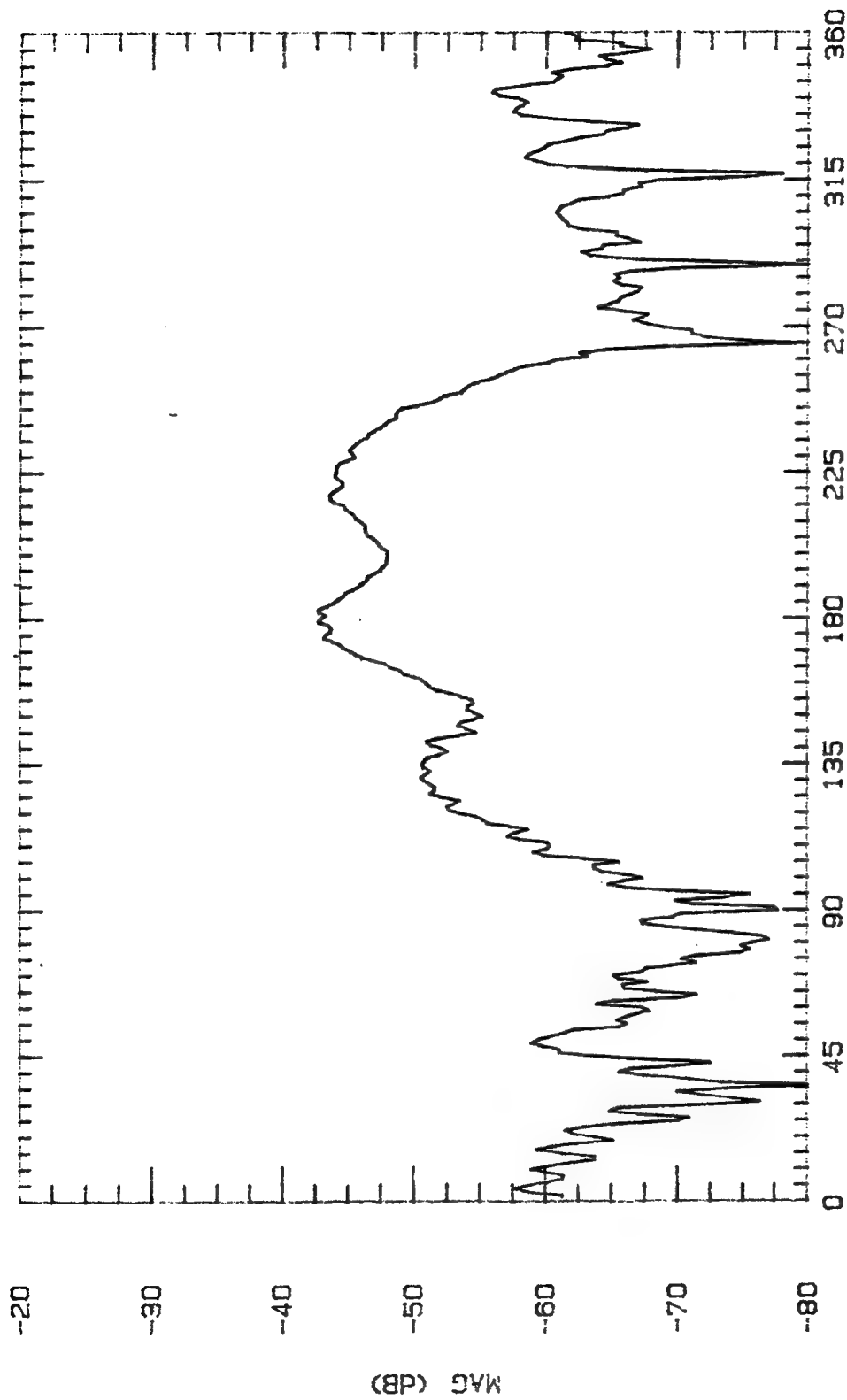
File Name	Frequency	Pattern Type	Date
3ALPL1225	12.25 CHz	E-PLANE	31 OCT 94



File Name	Frequency	Pattern Type	Data
3ALPL1250	12.5 GHz	E-PLANE	28 OCT 94



File Name	Frequency	Pattern Type	Date
9ALPL1275	12.75 GHz	E-PLANE	31 OCT 94



ASPECT ANGLE (DEGREES)

Date

Pattern Type

Frequency

File Name

29 OCT 94

L-PLANE

19 GHz

3ALPL1900

Bibliography

1. Balanis, Constantine A. Antenna Theory: Analysis and Design. New York: John Wiley & Sons, 1982.
2. Curtis, Walter. "Spiral Antennas," IRE Transactions on Antennas and Propagation. 298-306, May 1960.
3. Dyson, John D. "The Equiangular Spiral Antenna," IRE Transactions on Antennas and Propagation, Vol 7. 181-187, April 1959.
4. Foster, Ronald M. "A Reactance Theorem," The Bell System Technical Journal, Vol 3, 1924.
5. Harrington, R. F. Time-Harmonic Electromagnetic Fields. New York: McGraw-Hill, 1961.
6. Henderson, Lee. "The Periodic Moment Method Code," Version 3.0, Computer Software. Ohio, circa 1990.
7. Holzheimer, T. R. and J. C. Holloway. "Investigation of Spiral Performance Over Tightly Spaced Ground Planes," IEEE Transactions on Antennas and Propagation. 454-457, 1993.
8. Howell, James E. "Missile-Borne Tracking Antenna," DTIC Report, RG-TR-63-20, 1963.
9. Hughes, Jeff. "The Hoser Code," Computer Software. Ohio, circa 1990.
10. Knott, Eugene F., John F. Shaeffer and Michael T. Tuley. Radar Cross Section. Boston: Artech House, 426-429, 1993.
11. Kraft, U. R. "Optimization of Circular Polarization Performance For Four Arm Planar Spiral Antenna with Non-Perfect Excitation Networks," IEEE Proceedings, Vol 137. Pt H, No. 1. 45-50, Feb 1990.
12. Laxtapi, S. R. and R. Mittra, "Characteristics of Excited Planar-equiangular-spiral antennas." Proceedings of the IEE, Vol 114, No.3. 352-359, March 1967.
13. Mayes, P.E. and John D. Dyson, "Multi-Arm Logarithmic Spiral Antennas," Proceedings from the 10th Annual Symposium on USAF Antenna Research & Development Program. 67-70, Oct. 1960.

14. Milligan, Thomas A. Modern Antenna Design. New York: McGraw Hill, 372-376, 1985.
15. Morgan, T. E. "K-Band Spiral Antenna," Conference Proceedings on Multi-Octave Active and Passive Components and Antennas. 1-10, 1987.
16. Morgan, T. E. "Reduced Size Spiral Antenna," Work done under contract K/LR12a/452 by Marconi Space & Defense Systems Ltd. England, 1-4, 1975.
17. Munk B. A. and S. W. Schneider, "On Edge Absorbers In General," Technical Report 724988-1, The Ohio State University ElectroScience Laboratory, under Contract EY7090VB1S for TRW Avionics & Surveillance Group. San Diego, Oct. 1992.
18. Munk, B. A. "Periodic Surface For Large Scan Angles," United States Patent Number 3789404, 1974.
19. Nakano, Hisamatsu and others. "A Spiral Antenna Backed by a Conducting Plane Reflector," IEEE Transactions On Antennas and Propagation, Vol AP-34, No. 6. 791-796, June 86.
20. Penney, Christopher W. and Raymond J. Luebbers. "Input Impedance, Radiation Pattern, and Radar Cross Section of Spiral Antennas Using FDTD," Conference Proceedings for the 10th Annual Review of Progress in Applied Computational Electromagnetics. 468-472, 1994.
21. Ransom. "An Experimental Investigation Into the Four Arm Spiral Antenna," Technical Report for Air Force Avionics Lab. 1-18, May 1965.
22. Rudge, A. W., K. Milne, A. D. Olver and P. Knight. Handbook of Antenna Design, Vol 2. London: Peter Peregrinus Press, 920-924, 1983.
23. Stutzman, Warren L. and Gary A. Thiele. Antenna Theory and Design. New York: John Wiley & Sons, 281-287, 1981.
24. Wheeler, Harold A. "Antenna System Having a Reflector With A Substantially Open Construction," United States Patent Number 3836977, 1974.

Vita

Capt Joe Zaren was born in Philadelphia in 1965. He received his commission in the Air Force through the ROTC program at Duke University, where he majored in Electrical Engineering. His first assignment was with Material Command at Los Angeles Air Force Base where he worked in the Air Force Satellite Control Network (AFSCN) SPO. He was initially responsible for testing ground support software that was used to control different satellites. Later, he was responsible for ensuring AFSCN capabilities were satisfied to support the Milstar Satellite Program's launch requirements. While stationed in Los Angeles, he obtained his Professional Engineer's License. AFIT was his second assignment. He completed SOS by correspondence shortly after arriving at AFIT in June 1993. His follow-on assignment will be at Wright Laboratory.

Permanent Address:

147 N. Main St.
Yardley, PA 19067

REPORT DOCUMENTATION PAGE				Form Approved OMB No. 0704-0188	
Public reporting burden for this collection of information is estimated to average 1 hour per response, including the time for reviewing instructions, searching existing data sources, gathering and maintaining the data needed, and completing and reviewing the collection of information. Send comments regarding this burden estimate or any other aspect of this collection of information, including suggestions for reducing this burden, to Washington Headquarters Services, Directorate for Information Operations and Reports, 1215 Jefferson Davis Highway, Suite 1204, Arlington, VA 22202-4302, and to the Office of Management and Budget, Paperwork Reduction Project (0704-0188), Washington, DC 20503.					
1. AGENCY USE ONLY (Leave blank)		2. REPORT DATE Dec 94		3. REPORT TYPE AND DATES COVERED Final, Apr-Dec 94	
4. TITLE AND SUBTITLE Improving The Performance Of Spiral Antennas By Using Passive Scatterers				5. FUNDING NUMBERS	
6. AUTHOR(S) Capt Joseph S. Zaren					
7. PERFORMING ORGANIZATION NAME(S) AND ADDRESS(ES) Air Force Institute Of Technology Wright Patterson AFB OH 45433-6583				8. PERFORMING ORGANIZATION REPORT NUMBER AFIT/GE/ENG/94D-34	
9. SPONSORING / MONITORING AGENCY NAME(S) AND ADDRESS(ES) WL/AAWW-1 Bldg 620 2241 Avionics Circle Suite 16 Wright Patterson AFB OH 45433-7318				10. SPONSORING / MONITORING AGENCY REPORT NUMBER	
11. SUPPLEMENTARY NOTES					
12a. DISTRIBUTION / AVAILABILITY STATEMENT Approved for public release; distribution unlimited				12b. DISTRIBUTION CODE	
13. ABSTRACT (Maximum 200 words) The purpose of this study was to explore the viability of improving the performance of cavity-backed antennas. Traditionally antenna cavities are filled with electromagnetic absorber to mitigate interference effects that would otherwise cause the antenna radiation pattern to vary widely at different frequencies. The approach used in this research was to replace the absorber with dielectric slabs, some of which contained arrays of dipoles. These dipole arrays were modeled as frequency selective surfaces using two periodic moment method based computer programs and one transmission line program. A systematic study was performed that identified the effect of changing the dipole array parameters on prospective cavity designs. Seven different cavity configurations were tested using a log periodic trapezoid wire antenna system designed to support 2.3 - 12.4 GHz. Cavity configurations using one, two, and three layers of dipole arrays were tested and compared to both absorber-filled and dielectric-filled cavity configurations. The results were inconclusive because even though some two layer designs and one three layer design had better gain almost entirely throughout the 2 - 12 GHz region, the gain of the baseline absorber-filled and dielectric-filled cavities varied widely over this bandwidth. No cavity configuration provided an extended 3 dB bandwidth. Additional research is recommended.					
14. SUBJECT TERMS Cavity-backed antennas, frequency selective surfaces				15. NUMBER OF PAGES 346	
				16. PRICE CODE	
17. SECURITY CLASSIFICATION OF REPORT UNCLASSIFIED	18. SECURITY CLASSIFICATION OF THIS PAGE UNCLASSIFIED	19. SECURITY CLASSIFICATION OF ABSTRACT UNCLASSIFIED	20. LIMITATION OF ABSTRACT		